Fountain Clocks

CLUB E

Monday, July 22 2013, 10:30 am - 12:00 pm

Chair: **Krzysztof Szymaniec**
NPL

IFCS-EFTF3-A1-1

Contributing to the International Atomic Time Using an Atomic ^{87}Rb Fountain Clock

J. Guéna, M. Abgrall, A. Clairon, S. Bize

LNE-SYRTE, Observatoire de Paris, UMR CNRS 8630, UPMC, Paris, France

Email: jocelyne.guena@obspm.fr

The second of the International System of Units (SI) is defined using the ground state hyperfine transition of the caesium 133 atom. Today the accuracy of the widely used international atomic time (TAI) is provided by an ensemble of atomic caesium fountains worldwide used as primary frequency standards (PFS), which give the most accurate realization of the SI second. In 2001, considering the development of new frequency standards, the Consultative Committee for Time and Frequency (CCTF) of the Comité International des Poids et Mesures recommended that a list of secondary representations of the second (SRS) be established to eventually be used in a new definition of the second. In 2004, a first SRS, the ^{87}Rb ground state hyperfine transition, was proposed. In 2012, CCTF established a list of 11 recommended transitions.

In the last years, the FO2-Rb fountain frequency standard, part of the dual Rb/Cs fountain FO2[1] at LNE-SYRTE, has reached performances in terms of precision, reproducibility and reliability, equivalent to that of the PFSs[2]. The frequency measurements of a H-maser with FO2-Rb, in an almost continuous Rb/Cs comparison over the years 2010-2012, are already worth of more than 22 monthly calibrations of TAI. Therefore it was interesting to go throughout the process of contributing to TAI with a SRS, to explore implications in terms of both procedures and science.

We will report the first contribution to TAI based on a SRS, here ^{87}Rb using the FO2-Rb measurements. We present the process from end-to-end. Asides from the fountain and its performances, we describe how it is connected to time scales. We report on measurements of this frequency standard against LNE-SYRTE primary frequency standards, down to a fractional uncertainty of 4.4×10^{-16}, and on the establishment of the recommended value for the ^{87}Rb hyperfine transition frequency. We describe the procedure used to incorporate this secondary representation into *Circular T* and demonstrate the link of FO2-Rb to the TAI ensemble with a statistical uncertainty of $\sim1.3\times10^{-16}$. This work is an experimentation of what could be done with optical frequency standards in the prospect of a redefinition of the SI second.

This work with FO2-Rb, and more generally with the PFSs, benefits now also to the new realization of UTC(OP), the prediction of UTC for France, which is based on a H-maser steered by the SYRTE fountains.

---

[1] J. Guéna *et al.*, "Demonstration of a Dual Alkali Rb/Cs Fountain Clock", IEEE Trans. Ultrason. Ferroelectr. Freq. Control, vol. 57, no.3, p. 647–653, 2010.

[2] J. Guéna *et al.*, "Progress in atomic fountains at LNE-SYRTE", IEEE Trans. Ultrason. Ferroelectr. Freq. Control, vol. 59, no.3, p. 391-410, 2012.

IFCS-EFTF3-A1-2

Ramsey pulling in fountain clocks

V. Gerginov, N. Nemitz, S. Weyers

Time and Frequency Department, Physikalisch-Technische Bundesanstalt, Braunschweig, Germany

Email: Stefan.Weyers@ptb.de

The frequency shifting effect of Ramsey pulling[3], which is caused by asymmetric hyperfine σ-transitions ($\Delta F = 1$, $\Delta m_F = \pm 1$) in the Ramsey cavity, usually plays a minor role in the overall uncertainty budget of fountain clocks. The reason is that due to the employed state selection technique most of the atoms are in an $m_F = 0$ clock ground state and the neighbouring $m_F \neq 0$ ground states are essentially emptied. Moreover, the remaining $m_F \neq 0$ state populations are usually quite symmetrically distributed among the $\pm m_F$ states. However some peculiarities of fountain clocks can give reason for refreshed consideration.

Recently we have revisited frequency shifts in caesium fountains due to Ramsey pulling, both theoretically and experimentally. Extending the work of Cutler *et al.*[1], Zeeman ground state coherences which are created *before* the first Ramsey interaction during the state selection process have been taken into account in the calculations. The role of such initial Zeeman ground state coherences for Ramsey pulling has been already investigated for thermal beam clocks, where the state selection is effectuated by optical pumping[4]. Here we included initial Zeeman ground state coherences in a six-level density matrix model to take into account the effects of the microwave pulse of the state selection process in a fountain clock. Solving numerically the von Neumann equation for this system we find similarly to the work of Lee *et al.*[2] that in the presence of initial coherences frequency shifts due to Ramsey pulling are largely enhanced and can become significant under certain conditions. In contrast to the perturbative approach of previous work, the numerical approach enables us to take into account the phase variation of π of the transverse rf cavity fields along the flight path of the atoms and to perform Monte Carlo simulations for realistic atom cloud geometries and trajectories including cloud position offsets from the fountain axis.

We also experimentally explored the effects of Ramsey pulling in the PTB fountain CSF1[5]. This fountain is a suitable choice, because its state selection cavity is located just below the Ramsey cavity within the magnetically shielded C-field region. Therefore the phases of the coherences created during the state selection process do no average out and can result in detectable frequency shifts. For the generation of significant asymmetric coherent superpositions of the ground state components ($F = 3, 0$) and ($F = 3, \pm 1$), the microwave frequency in the state selection cavity was intentionally detuned from the clock transition frequency. Additionally, the excitation of hyperfine σ-transitions ($\Delta F = \pm 1$, $\Delta m_F = \pm 1$) was enhanced in both cavities by operating the state selection cavity at 9π and the Ramsey cavity at $7\pi/2$ microwave pulse areas. As a result, we observed frequency shifts up to $\pm 3 \times 10^{-14}$ at state selection frequency detunings of ±120 Hz. For a range of detunings and magnetic field strengths in the cavity region the observed frequency shifts match well the predictions of the model.

[3] L. S. Cutler *et al.*, Journal of Applied Physics 69, 2780 (1991)

[4] H. S. Lee *et al.*, Metrologia 40, 224 (2003)

[5] S. Weyers *et al.*, Metrologia 38, 343 (2001); S. Weyers *et al.*, Proc. 6th SFSM, St. Andrews 2001, 64–71

IFCS-EFTF3-A1-3

Scattering of Cold Atom Coherences by Hot Atoms: Background Gas Collision Shifts of Primary Fountain Clocks

Kurt Gibble[1]

[1]Department of Physics, The Pennsylvania State University, University Park, PA, USA

Email: kgibble@psu.edu

Several primary cesium fountain frequency standards report an uncertainty of 1×10^{-16} for the frequency shift due to background gas collisions[6-8]. It contributes noticeably to a number of overall uncertainty budgets, as low as 2.1×10^{-16},[8] and can be the largest single contribution in the uncertainty budget. These uncertainties are estimated using the measured pressure shift for H_2 in room-temperature Cs cell clocks[9]. This is not justified since any momentum transferred to a cold atom almost always prevents it from being detected. We theoretically analyze the quantum scattering and show that H_2 room-temperature measurements produce frequency shifts with the opposite sign and overestimate the cold-atom background-gas shift by an order of magnitude. Highly polarizable gases, including background Cs vapor, produce similar shifts for cold atoms as H_2. We also show that general considerations allow the background shift to bounded by measuring the loss in Ramsey fringe contrast due to background gas collisions. Measuring the contrast or using the calculated shifts for cold atoms can significantly reduce the background gas shift in uncertainty budgets so that it no longer contributes significantly.

[6] S. Weyers, U. Hübner, R. Schröder, "Uncertainty evaluation of the atomic caesium fountain CSF1 of the PTB," Chr. Tamm, and A. Bauch, Metrologia vol. 38, p. 343-352, 2001.

[7] R. Li, K. Gibble and K. Szymaniec, "Improved accuracy of the NPL-CsF2 primary frequency standard: evaluation of distributed cavity phase and microwave lensing frequency shifts," Metrologia vol. 48, p. 283-289, 2011.

[8] J. Guéna, M. Abgrall, D. Rovera, P. Laurent, B. Chupin, M. Lours, G. Santarelli, P. Rosenbusch, M. E. Tobar, R. Li, K. Gibble, A. Clairon, and S. Bize, "Progress in Atomic Fountains at LNE-SYRTE," IEEE Trans. Ultrasonics, Ferroelectrics, and Freq. Control, vol. 59, p. 391-410, 2012.

[9] C. W. Beer and R. A. Bernheim, "Hyperfine pressure shift of ^{133}Cs atoms in noble and molecular buffer gases," Phys. Rev. A vol. 13, p. 1052-1057, 1976.

IFCS-EFTF3-A1-4

Accuracy evaluation of IT CsF2

Filippo Levi[1], Giovanni A. Costanzo[2], Claudio E. Calosso[1], Davide Calonico[1],

Steven R. Jefferts[3], Thomas P. Heavner[3]

[1]Optic Division, INRIM, Torino, Italy
[2]Electronic Department, Politecnico di Torino, Torino, Italy
[3]Time and Frequency Division, NIST, Boulder, Co, USA

Email: f.levi@inrim.it

At INRIM we have realized and characterized a nitrogen cooled Cs fountain, the new Italian primary frequency standard. Our fountain is the result of a fruitful collaboration with NIST Time and Frequency Division, where the physical package of two twin fountains NIST F2 and ITCsF2 was realized.

The fountain accuracy was evaluated with respect to the following frequency shift: atom density, blackbody radiation, Zeeman effect, gravitational potential, microwave leakage, distributed cavity phase and other minor effects. Thanks to nitrogen cooling, low atomic density and particular care in the physical structure design, we could reduce significantly important sources of uncertainty. The accuracy budget of IT CsF2 combine to a total type B uncertainty of 1.8×10^{-16}, and a similar statistical uncertainty over a twenty day measurement evaluation (density shift is accounted for in the type A uncertainty).

Preliminary comparisons between ITCsF2, NIST F1 and NIST F2 have shown an agreement better than 5×10^{-16}.

The most relevant contribution to the uncertainty budget are summarized in the following table.

ITCsF2 Accuracy Budget		
Effect	Bias (10^{-16})	Uncertainty (10^{-16})
Blackbody Radiation	-1.5	0.5
Zeeman Effect	1103	1.0
Gavitation	261.2	0.1
Microwave	-3.5	1.4
Total Type B		*1.8*
Atomic Density	-3.2	2.1
Dead Time	-	1.2
Total Type A		*2.4*
Total	**1356**	**3.0**

IFCS-EFTF3-A1-5

Preliminary Results on the KRISS-F1 Primary Atomic Fountain Frequency Standard

Sang Eon Park[1], Myoung-Sun Heo[1], Sang-Bum Lee[1], Kurt Gibble[2], Dai-Hyuk Yu[1], Chang Yong Park[1], Won-Kyu Lee[1], Taeg Yong Kwon[1]

[1]Division of Physical Metrology, Korea Research Institute of Standards and Science, Daejeon 305-340, Korea

[2]Department of Physics, The Pennsylvania State University, University Park, PA 16802, USA

Email: parkse@kriss.re.kr

We present preliminary results of the primary fountain frequency standard KRISS-F1. Figure 1 is a 3D drawing of the KRISS-F1 physics package. Previously we have observed Ramsey fringes with ^{133}Cs atoms using a test interrogation cavity. The linewidth of the central fringe was 1 Hz, and the signal-to-noise ratio about 600[10]. With ^{133}Cs and ^{87}Rb interrogation cavities, KRISS-F1 can be operated as a ^{133}Cs and ^{87}Rb fountain[11]. Since the distributed cavity phase shift error (DCP) gives one of the largest uncertainties of atomic fountain primary frequency standards, new Cs and Rb cavities that are designed to minimize DCP[12] are about to be installed.

Our atomic sources are two 150 mg ^{133}Cs and one 100 mg ^{87}Rb getters (Alvasource). With the getter sources we can control atomic vapor pressure by adjusting getter currents, choosing to evaporate only the atom that we want to use.

We use two fiber port clusters (two-to-three) to distribute cooling laser beams for Cs (852 nm) and Rb (780 nm) with same splitting ratios. The outputs of fiber port clusters are connected to fiber collimators with PM fibers. Six fiber collimators are directly connected to the surfaces of trap chamber ports to avoid beam misalignments. Each fiber collimator contains monitor photodiodes. Of order 10^7 and 10^6 Cs atoms are trapped and cooled with MOT and optical molasses, respectively. An accuracy evaluation will be carried out after installing the new cavities. Our conference paper will update our progress towards the KRISS-F1 accuracy evaluation.

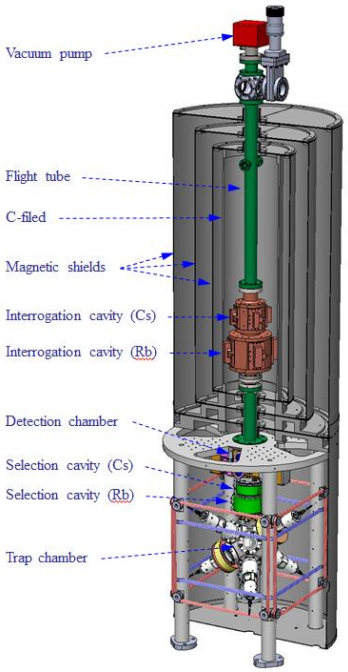

Fig. 1: 3D model of the KRISS-F1 physics package.

[10] S. E. Park, L. Z. Li, S.-B. Lee, D.-H. Yu, C. Y. Park, W.-K. Lee, T. Y. Kwon, "KRISS atomic fountain clock: Current status," *CPEM 2012 Conf. Digest*, pp. 608-609, July 2012.

[11] J. Guena, P. Rosenbusch, P. Laurent, M. Abgrall, D. Rovera, G. Santarelli, M.E. Tobar, S. Bize, A. Clairon, "Demonstration of a dual alkali Rb/Cs fountain clock," *IEEE Trans. Ultrason. Ferroelectr. Freq. Control*, vol. 57, no.3, pp. 647-653, 2010.

[12] R. Li and K. Gibble, "Evaluating and minimizing distributed cavity pase errors in atomic clocks," *Metrologia*, vol. 47, no. 5, pp. 534-551, 2010.

Opto-Electronic Oscillators

CLUB H

Monday, July 22 2013, 10:30 am - 12:00 pm

Chair: **Gilles Cibiel**
CNES

Widely Tunable Opto-Electronic Oscillator

D. Eliyahu, W. Liang, E. Dale, A. Savchenkov,

V. Ilchenko, A. B. Matsko*, D. Seidel, and L. Maleki

OEwaves Inc., 465 North Halstead Street, Suite 140, Pasadena, CA 91107, USA

*Email: andrey.matsko@oewaves.com

We describe a novel photonic oscillator based on an optical whispering gallery mode (WGM) microresonator. The oscillator features low phase noise (better than -100 dBc/Hz at 10 kHz), low power consumption, compact size, and wideband tunability (1.6-15.6 GHz, limited by the bandwidth of the RF amplifier). Performance parameters of the oscillator are superior to existing free running tunable electronic oscillators and synthesizers operating in the frequency band, with the close-in phase noise at least 10 dB lower than what is currently achieved. The oscillator is projected to have low acceleration sensitivity. The successful fabrication of the device supports the development of novel ultra-wideband receivers for communications and radar applications.

The oscillator takes advantage of the opto-electronic oscillator (OEO) architecture. The OEO is based on an opto-electronic feedback loop that directly converts light energy to spectrally pure microwave or RF oscillation, and has been described in detail in the literature. The oscillator is driven with a continuous wave laser that acts as a source of energy. Additional RF amplification might be needed if the optical power is insufficient for the oscillation to start. An important feature of the OEO architecture is that the phase noise does not degrade with increasing oscillation frequency, in contrast to electronic based oscillators.

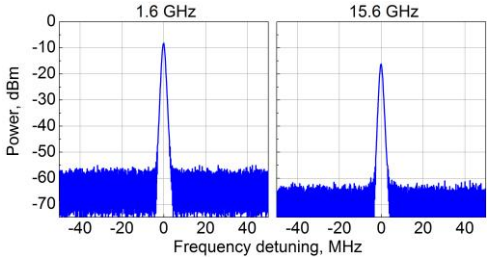

Fig. 2: Example of spectra of the RF signal generated by the tunable oscillator.

The novel tunable OEO operates as follows. Light from an agile tunable semiconductor laser is fed into a broadband phase modulator, then to an ultra-high-Q optical WGM microresonator, and then to a fast photodiode, to produce an electric signal. A comparably short fiber link (100-300 m or shorter) can be inserted at the front of the photodiode to improve the phase noise of the oscillator. The signal from the photodiode is amplified before being fed back to the phase modulator to complete the OEO loop. Self-sustained oscillation starts when amplification in this feedback loop exceeds the loss. The narrow optical bandwidth of the resonator (10 MHz) provides the filter function required for the loop. The change in the laser frequency provides the tunability of the oscillator. The spectral purity depends on the Q of the optical part of the circuit circuit ensured by the optical WGM microresonator. This configuration eliminates supermodes in the noise spectra associated with fiber OEOs.

The device does not require the laser light to pass through the ultra-high-Q optical resonator, as was required in all previous implementations of resonator-based OEOs. Only one modulation sideband passes the resonator mode. Aside from simplification of the architecture, this feature allows improving the linearity of the optical part of the opto-electronic loop. Moreover, it allows reducing the resonator size leading to reduction of the vibration sensitivity of the system.

IFCS-EFTF2-A2-2

Kerr Frequency Comb-Based K_a-band RF Photonic Oscillator

V. Ilchenko, J. Byrd, A. Savchenkov, D. Eliyahu,

W. Liang, A. B. Matsko*, D. Seidel, and L. Maleki

OEwaves Inc., 465 North Halstead Street, Suite 140, Pasadena, CA 91107, USA

*Email: andrey.matsko@oewaves.com

We report on the realization of a packaged RF photonic oscillator based on Kerr optical frequency comb generated in an ultra-high Q crystalline whispering gallery mode (WGM) resonator. The oscillator produces spectrally pure RF signals in K_a frequency band, characterized with single sideband phase noise of -110 dBc/Hz at 10 kHz (see Fig. 1). The stability of the free running oscillator is characterized with Allan deviation of 10^{-10} at 1s. We show that self-injection locking of the laser frequency to an optical WGM is important for the stable operation of the device.

The optical Kerr frequency comb is a product of cubic optical nonlinearity of the material of which the resonator is made, and is generated by pumping one of the resonator modes with a continuous wave coherent light. Kerr frequency comb generation is a unitary process, and can occur in a resonator where the only losses are related to coupling to the external world. In such a case the repetition frequency of the comb does not depend on either frequency or power of the pump light, and the comb becomes an ideal oscillator that does not require any stabilization. The phase noise of the repetition rate of such a comb is given by Leeson formula with oscillator bandwidth coinciding with the bandwidth of the optical modes of the nonlinear resonator and the phase noise has only f^{-2} and f^0 spectral frequency components.

In practice, contact of the resonator with the environment as well as finite absorption in the resonator host material spoil the stability conditions, and the repetition rate of the comb becomes dependent on parameters of the pump light. To regain the stability, locking the laser to the resonator mode becomes necessary.

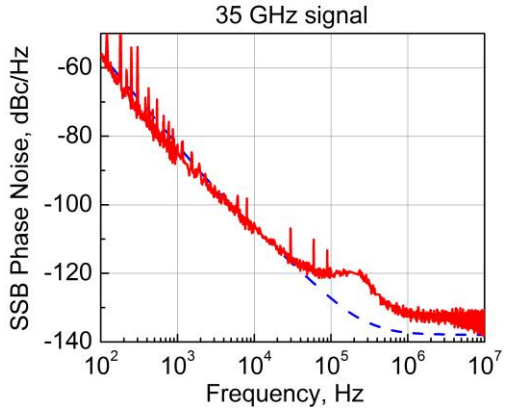

Fig. 3: Example of spectra of the RF signal generated by the Kerr frequency comb-based RF photonic oscillator (red line). The hump around 200 kHz results from the noise of the x4 divider utilized to reduce the oscillation frequency to be able to measure it with OEwaves phase noise measurement system. The theoretical curve for the phase noise of the particular oscillator is shown by blue dashed line.

An important feature of the Kerr comb is that it is enough to stabilize only a single point in its frequency spectrum to obtain its stable operation. Since the frequency of one comb line coincides with the frequency of the pump laser, and the comb repetition rate is fixed by the properties of the monolithic resonator generating the comb, the entire Kerr comb is stabilized once the frequency of the pump laser is stabilized to an external reference. There is no need to generate an octave spanning Kerr comb to stabilize it. We discuss our progress in experimental realization of the frequency stabilization scheme.

IFCS-EFTF2-A2-3

Fiber ring resonators with Q factors in excess of 10^{10} for Time and Frequency Applications

K. Saleh*, A. Fernandez*, O. Llopis*, Gilles Cibiel+

* CNRS ; LAAS ; Université de Toulouse ; 7 av. du Colonel Roche, 31077 Toulouse, France
+ CNES, 18 avenue Edouard Belin, F-31410 Toulouse, France

Email: llopis@laas.fr

Recent work has shown the capability of fiber ring resonators (FRRs) of featuring very high optical quality factors (Q_{Opt})[13].These FRRs are compact and easy to use. However, their high quality factor, combined with significant intra-cavity power enhancement factor, lead to the generation of nonlinear optical effects inside the resonator, especially Rayleigh and Brillouin scattering. When the FRR is used to stabilize the frequency of an optoelectronic oscillator (OEO), these nonlinear optical effects degrade the OEO phase noise[14]. In order to eliminate a great part of these effects, an optical isolator has been inserted inside a 100 m-long FRR that featured a Q_{Opt} of $2.1x10^9$. The use of this FRR to stabilize the frequency of a 10 GHz OEO has resulted in a phase noise level as low as -50 dBc/Hz at 10 Hz offset frequency[1]. This result establishes the state-of-the-art phase noise level obtained in a passive optical resonator based OEO.

Since this aforementioned work, different studies have been performed to increase the FRR's quality factor above 10^{10}. We have recently measured an ultra-high Q_{Opt} of $1.25x10^{10}$ in a 120 m-long FRR (see Fig. 1), but without an isolator inside the fiber loop. When this FRR has been included in the OEO setup, the use of a very low optical power at the resonator's input was mandatory to prevent the nonlinear optical effects from being generated efficiently. This has of course degraded the noise to carrier ratio at the resonator output, resulting in an excess phase noise of the OEO. Indeed, we have measured a -40 dBc/Hz phase noise level at 10 Hz offset frequency from a 10 GHz RF carrier (see Fig. 1) in spite of the ultra-high Q. Currently, we are designing a new 1 km-long immunized and optimized FRR. This resonator will include a low loss isolator and the simulated Q_{Opt} is $1.5x10^{10}$. The use of this Brillouin-immunized 1 km-long FRR in an OEO setup may lead to a much lower phase noise level than the one obtained with the 120 m-long FRR. Results on this new device will be presented at the conference.

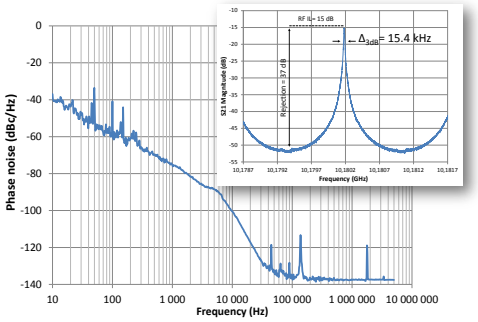

Fig. 4: Phase noise spectrum of a 10 GHz optoelectronic oscillator based on a 120m-long FRR featuring a $1.25x10^{10}$ Q_{Opt} factor. The noise measurement was performed at very low injected

[13] K. SALEH, P.H. MERRER, O. LLOPIS, and G. CIBIEL, "Optoelectronic oscillator based on fiber ring resonator: overall system optimization and phase noise reduction", 2012 IEEE International Frequency Control Symposium (IFCS), 21-24 may 2012.

[14] K. SALEH, O. LLOPIS, and G. CIBIEL, "Optical Scattering Induced Noise in Fiber Ring Resonators and Optoelectronic Oscillators", to be published in Journal of Lightwave Technology, (2013).

IFCS-EFTF2-A2-4

Experimental characterization of optoelectronic oscillators based on optical mini-resonators

Rémi Henriet, Aurélien Coillet, Patrice Salzenstein, Khaldoun Saleh, Laurent Larger, Yanne K. Chembo

Franche Comté Electronique Mécanique Optique Thermique Sciences et Technologies (FEMTO-ST), Centre National de la Recherche Scientifique (CNRS), Besançon, France

Email: patrice.salzenstein@femto-st.fr

We develop an optoelectronic resonator[15] (OEO) based on intensity modulation and a high-Q disk resonator. In this OEO, the resonant element is a 5 mm diameter crystalline whispering-gallery-mode resonator[16] (WGM). It selects the microwave oscillating frequency as an optical storage energy element. This resonator also filters the microwave modulation signal. The generated oscillating frequency corresponds to the free spectral range of the mini-resonator in the range 10–11 GHz[17]. Therefore no delay-induced spurious peaks are present in the spectrum, in contrast to the case of the classical optoelectronic oscillator where the storage element consists of an optical fiber delay line[18,19]. This resonator has a high quality factor which can be characterized by the cavity ring-down method[20]. Another advantage of our system resides in its compactness allowing for efficient control of the temperature. We present experimental results related to the temporal dynamics and phase noise performance of WGM-based OEO. The analysis proceeds by matching the theoretical and experimental results[21]. Power spectrum is given and the generated microwave signal stands 50 dB above the filtered noise of the RF amplifier. We evaluate the phase noise performance[22] of this OEO, and also provide a discussion relatively to its main features.

---

15 L. Maleki, "The optoelectronic oscillator," Nature Photonics, 5(12), 728–730 (2011).

16 V. S. Ilchenko, X. S. Yao, L. Maleki, "High-Q microsphere cavity for laser stabilization and optoelectronic microwave oscillator," Proceedings of SPIE, 3611, 190–198 (1999).

17 K. Volyanskiy, P. Salzenstein, H. Tavernier, M. Pogurmirskiy, Y. K. Chembo, L. Larger, "Compact Optoelectronic Microwave Oscillators using Ultra-High Q Whispering Gallery Mode Disk-Resonators and Phase Modulation," Optics Express, 18(21), 22358–22363 (2010).

18 X. S. Yao, L. Maleki, "High frequency optical subcarrier generator," Electronics Letters, 30(18), 1525–1526 (1994).

19 K. Volyanskiy, J. Cussey, H. Tavernier, P. Salzenstein, G. Sauvage, L. Larger, E. Rubiola, "Applications of the optical fiber to the generation and to the measurement of low-phase-noise microwave signals," J. Opt. Soc. Am. B, 25(12), 2140-2150 (2008).

20 Y. Dumeige, S. Trebaol, L. Ghisa, Thi Kim Ngan Nguyen, H. Tavernier, P. Féron, "Determination of coupling regime of high-Q resonators and optical gain of highly selective amplifiers," J. Opt. Soc. Am. B 25(12), 2073–2080 (2008).

21 Y. K. Chembo, K. Volyanskiy, L. Larger, E. Rubiola and P. Colet, "Determination of phase noise spectra in optoelectronic microwave oscillators: a Langevin approach," IEEE J. of Quantum Electron., 45, 178–186 (2009).

22 P. Salzenstein, E. Pavlyuchenko, A. Hmima, N. Cholley, M. Zarubin, S. Galliou, Y. K. Chembo and L. Larger, "Estimation of the uncertainty for a phase noise optoelectronic metrology system", Physica Scripta, 2012(T149), 014025 (2012).

IFCS-EFTF2-A2-5

High spectral purity microwave and terahertz oscillator

Gwennaël Danion[1], Goulc'hen Loas[1], Ludovic Frein[1], Cyril Hamel[1], Anthony Carré[1], Steve Bouhier[1], Marc Vallet[1], Marc Brunel[1], Antoine Rolland[1], Mehdi Alouini[1], François Bondu[1], Alain Brillet[2], Jean-Pierre Coulon[2], Frédéric Cleva[2], Mourad Merzougui[2], Alexandre Beck[3], Guillaume Ducournau[3], Jean-François Lampin[3], Mohamed Zaknoune[3], Christophe Coinon[3], Xavier Wallart[3], Emilien Peytavit[3], Tahsin Akalin[3], Grégoire Pillet[4], Loïc Morvan[4], Ghaya Baili[4] and Jérôme Bourderionnet[4]

[1]Departement Optique et Photonique, IPR, Université Rennes1 CNRS, Rennes, France

[2]ARTEMIS, Observatoire de la côte d'Azur, Nice, France

[3]Groupe Photonique/THz, IEMN, Université de Lille CNRS,Villeuneuve d'Ascq, France

[4]Thales Research and Technology, Palaiseau, France

Email: gwennael.danion@univ-rennes1.fr

We present a microwave/THz oscillator project (2012-2014) excepted to show below -150 dB rad^2/Hz phase noise at an offset frequency of 10 kHz for a 30 GHz carrier frequency as well as 18 GHz, 100 GHz, 400 GHz, 1 THz. The microwave/THz signal is obtained by mixing two optical frequencies with a photomixer.

A dual-axis two frequency cross polarization laser will be stabilized onto two resonances of one Fabry-Perot cavity. The two frequencies sense the same cavity length fluctuations so that the best possible relative stability of the beat note is limited by the relative dimensional stability of the cavity. This cavity spacer is made with an ultra low expansion ceramic (ULE) placed in vacuum. A 75% fraction of the beam transmitted by the cavity is used to stabilize the amplitude of the laser, and a 25% fraction is sent on a polarizer and a photomixer for optical to millimetre wave conversion. The AM/PM conversion, especially the opto-thermal conversion in the cavity i.e. the absorbed power fluctuations, is negligible at a 1 Hz frequency offset by stabilization of the optical carrier at the 8.10^{-9}/Hz$^{1/2}$ level.

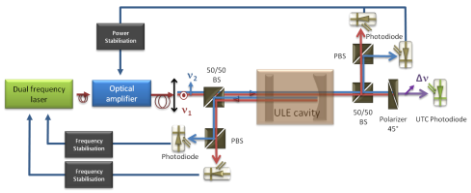

Fig. 5: One microwave/THz oscillator

This oscillator is based on a dual frequency laser system whose beat note frequency is continuously tunable from DC to 600 GHz. An Erbium/Ytterbium solid-state two-axis dual-frequency laser system followed by amplifier stage has been developed. Each polarization frequencies is independently tunable by 1.7 GHz steps by tilting its etalon and continuously with an electro-optic crystal. We have chosen two lithium tantalate (LiTaO3) crystals; thermo-optic (600MHz/°C) and electro-optic (1.1MHz/V) effects enable to lock each frequency on the resonance of a 1.5 GHz free spectral range Fabry Perot cavity. Each polarization light beam is amplified by a fiber system. Our system amplifier is composed of an erbium doped fiber amplifier (EDFA) and a semiconductor optical amplifier (SOA) per polarization axis. This amplifier system permits to deliver 18 dBm power, to stabilize the power fluctuations and to reduce the relative intensity noise by 20 dB, especially the relaxation oscillation.

IFCS-EFTF2-A2-6

Inverse Relationship between OEO *Q*-factor and *g*-sensitivity

James P. Cahill[1,2], Justin Pritchett[1], Ryan Sorensen[1], Morris Berman[1], Olukayode Okusaga[1], Weimin Zhou[1], Gary M. Carter[2], Curtis R. Menyuk[2]

[1]U.S. Army Research Laboratory, Adelphi, MD
[2]University of Maryland: Baltimore County, Baltimore, MD

Email: james.p.cahill.ctr@us.army.mil

We present evidence that the vibration (*g*-) sensitivity of a fiber-based OEO decreases as the fiber length wound to a single spool increases. This is the result of two effects. First, the magnitude of the vibration-induced perturbation remains constant with increasing fiber length because of diminishing mechanical coupling between the outer layers of fiber and the spool. Second, the power spectral density (PSD) of the phase noise induced by a constant magnitude perturbation decreases as the *Q* factor (i.e. fiber length) of the cavity increases. This is an oscillator filtering effect. We can exploit these effects to construct fiber-based OEOs with lower *g*-sensitivity.

A sinusoidal vibration induces a peak in the OEO phase noise at the vibration frequency with PSD proportional to $(\Delta l/l)^2$, where Δl is the vibration-induced change in length of the fiber delay, and l is the length of the total fiber delay.[i] We use t^{his} sideband to characterize both the filter effect and the mechanical coupling between fiber and spool. In order to maintain consistency we use identical spools in all tests.

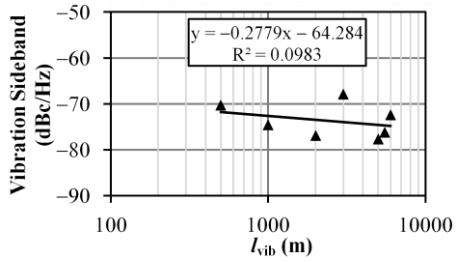

Figure 1. PSD of the vibration-induced phase noise peak as a function of the length of fiber exposed to vibration. Total OEO delay is fixed.

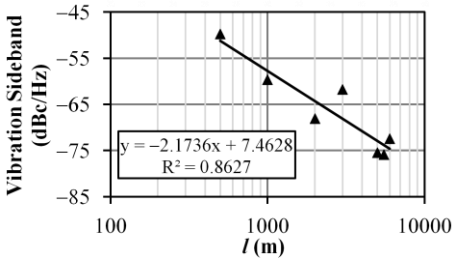

Figure 2. PSD of the vibration-induced phase noise peak as a function of total OEO fiber delay length. The entire delay is exposed to vibration.

To demonstrate the diminished coupling between fiber and spool, we keep the total fiber delay of the OEO at a constant length while exposing only a portion, l_{vib}, of the fiber delay to a sinusoidal vibration. Fig. 1 plots the PSD of the vibrational sideband as a function of l_{vib}. Because we hold all relevant parameters constant, the PSD of the vibrational sideband will be proportional to Δl^2. Yet fig. 1 shows that the PSD is independent of l_{vib}. Thus, the mechanical coupling between the fiber and spool has effectively saturated, and Δl is independent of the fiber length.

To demonstrate the oscillator filtering effect, we expose the entire fiber delay of the OEO to a sinusoidal vibration. Fig. 2 plots the PSD of the vibration-induced sideband as a function of the total delay length, l. The PSD of the sideband decreases approximately quadratically as fiber length increases. Thus, as the OEO Q increases, the vibrational noise is effectively filtered out.

Micro- Nano- Devices

CLUB D

Monday, July 22 2013, 10:30 am - 12:00 pm

Chair: **Ashwin Seshia**
University of Cambridge

IFCS-EFTF4-A3-1

Nanoscale Resonant Sensors and Transducers with 1D and 2D Carbon Nanostructures

Max Zenghui Wang[1]

[1]Electrical Engineering, Case Western Reserve University, Cleveland, OH 44106, USA

Email: zenghui.wang@case.edu

Carbon-based nanostructures, such as graphene and carbon nanotubes, have outstanding mechanical properties and can be implemented as novel nanomechanical devices. Such devices, owing to their miniature sizes and the unique physical properties of the materials, make excellent candidates for physical and chemical sensors. In particular, nanomechanical resonators based on carbon nanotubes and graphene have demonstrated exceptional sensitivities to various processes. On the other hand, the unique geometries of these miniature devices allow the mechanical motion of the carbon nanostructure to be excited, detected, and tuned both optically and electrically, making them nanoscale mechanical transducers.

In this paper, we will focus on the state-of-the-art nanomechanical resonators made of carbon nanotubes and graphene, and evaluate their potential as ultra-sensitive sensors and the ultimate limits on their sensitivities. Specifically, we will describe nanotube resonator mass sensors with the best ones achieving single-atom mass sensitivity, a graphene resonant penta-cene sensor, and a nanotube resonant sensor for surface processes such as adsorption and phase transition[ii]. In addition, we will briefly discuss the ultimate limits for these resonators for physical sensing, identify the key unresolved issues, and propose the future possibilities and directions of technical efforts[iii].

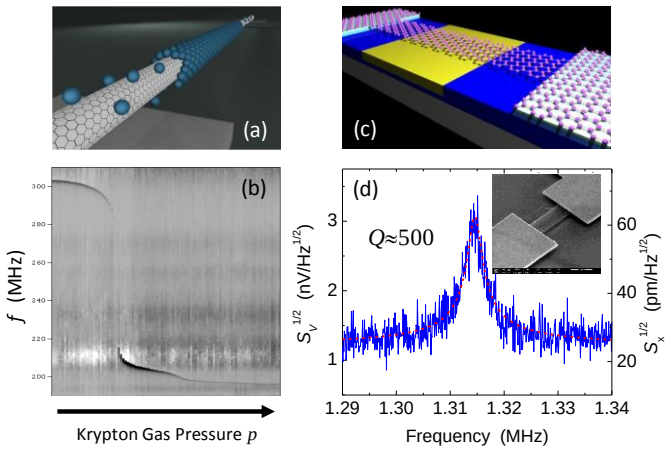

Fig. 6: Nanomechanical resonator devices based on 1D and 2D carbon nanomaterials. (a) Enhanced illustration of Krypton atoms adsorbed on a single-walled carbon nanotube resonator, forming an atomic layer of commensurate solid. (b) Resonance frequency of a carbon resonator decreases as background Kr pressure increases at 77K, revealing the condensation of an adsorbed Kr layer on the nanotube surface. (c) Enhanced illustration of a doubly-clamped graphene resonator with local gate electrode. (d) Thermomechanical resonance from a 1.315MHz graphene resonator, and calibration of the noise floor and quality (*Q*) factor. *Inset*: SEM image of the device. Right axis shows scale in displacement spectral density.

IFCS-EFTF4-A3-2

NANOMECHANICAL MASS SPECTROMETRY FOR THE CHARACTERIZATION OF HIGH MASS NANOPARTICLES

E. Sage[1], A. Brenac[2], R. Morel[2], C. Dupré[1], C. Marcoux[1], H. Blanc[1], M. S. Hanay[3], S. Kelber[3], M.L. Roukes[3], E. Colinet[1], L. Duraffourg[1] and S. Hentz[1]

[1]CEA, LETI, MINATEC campus, 17 rue des martyrs, 38054 GRENOBLE Cedex 9, France.
[2]INAC/SP2M and Université Joseph Fourier, CEA Grenoble, 38054 Grenoble, France.
[3]Kavli Nanoscience Institute and Departments of Physics, Applied Physics, and Bioengineering, California Institute of Technology, MC 149-33, Pasadena, California 91125 USA.
Email: eric.sage@cea.fr

Nano Electro Mechanical Systems (NEMS)-based Mass Spectrometry (MS) holds great promise for point of care applications[23] or air quality monitoring. Real-time, single protein MS has recently been demonstrated with top-down silicon resonators[24]. These devices operate in a mostly unexplored mass range where particles display a wide mass distribution and where there is no mass standard. A direct comparison of NEMS-MS and reference MS measurement (here conventional Time-Of-Flight (TOF) MS) is therefore crucial and is presented for the first time in this paper. The NEMS device is fabricated on a 200mm SOI wafer with VLSI process. It is a 160nm thick doubly clamped beam, electrostatically actuated, with heterodyne piezoresistive detection[25]. Its first two resonance frequencies are simultaneously tracked with Phase Locked Loops.

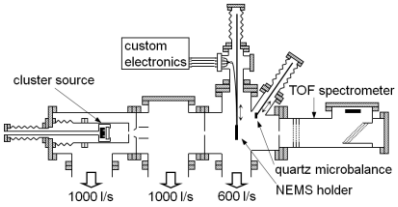

Figure 1: Schematic of the mass deposition setup

The NEMS device is inserted in the deposition chamber of a custom sputtering-gas aggregation setup able to produce nanometric metallic clusters with tunable deposition rate and diameter[26] (see Figure 1). First the NEMS experimental mass sensitivity is calculated by varying the deposition rate, measured with a Quartz Crystal Microbalance (QCM). In a second step, tantalum clusters were projected onto the surface of the NEMS with a flux rate allowing for individual particle measurement. Figure 2 shows preliminary mass distributions obtained with both NEMS-MS and TOF-MS: the distribution shape is reproduced with fidelity (widths at half maximum 352kDa and 408kDa respectively) and the mean masses are very close. NEMS-MS displays a resolving power similar to TOF-MS in this mass range, and even better at higher mass ranges. This demonstrates all the potential of NEMS-MS in this mass range. The mass offset as well various mass distributions are under investigation.

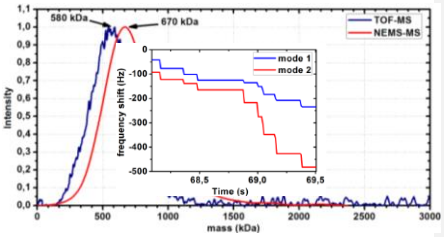

Figure 2: TOF-MS and NEMS-MS mass spectra of tantalum clusters. (1 Da=1.66 × 10^{-27} kg). Inset: frequency jumps induced by individual landing events

[23] A. Boisen, *Nature Nanotechnology*, vol. 4, pp. 404-405, 2009.

[24] M. S. Hanay et al, *Nature Nanotechnology*, vol. 7, pp. 602-608, 2012.

[25] E. Mile et al, *Nanotechnology*, vol. 21, pp. 165504, 2010.

[26] R. Morel et al, *Eur. Phys. J. D*, 24, pp. 287-290, 2003.

IFCS-EFTF4-A3-3

Micro-electro-mechanical resonant tilt sensor with 250 nano-radian resolution

Xudong Zou, Pradyumna Thiruvenkatanathan and Ashwin A. Seshia

Nanoscience Centre, Department of Engineering, University of Cambridge, United Kingdom

Email: xz280@cam.ac.uk

This paper reports on a high-resolution frequency-output MEMS tilt sensor based on resonant sensing principles[1]. The tilt sensor measures orientation by sensing the component of gravitational acceleration along a specified input axis (Fig. 1). The devices consist of a suspended proof mass connected to two double-ended tuning fork (DETF) resonators at each end through a lever arrangement. When subjected to a tilt with respect to the gravitational axis, the tuning forks respond through a shift in their resonant frequency and the differential frequency shift can be then calibrated with respect to the tilt angle. Prototype devices are fabricated in a foundry SOI-MEMS process and optical micrographs of the device are shown in Fig.2. The microfabricated chips are mounted onto standard chip carriers and then vacuum packaged using a custom process. A combination of design enhancements enables significantly higher sensitivity for this device as compared to previously reported prototype sensors[1].

The vacuum packaged sensor chip is co-integrated with oscillator circuits on a PCB and mounted on a manual tilt table. Figure 3 depicts the tilt test set-up and Fig. 4 shows the output frequency variation of DETF_1 (see Fig. 1) observed in a 0^o-90^o tilt test. The tilt test results indicate that the new sensor provides a relatively linear response in the range of $\pm 20^o$ with a scale factor of approximately 50.06 Hz/degree. Fig. 5 shows the results of a measurement on the output stability of the device as determined by Modified Allan Deviation measurements. The resolution of the resonant tilt sensor is found to be approximately 250 nano-radian for an integration time of 0.8 s, which is over an order of magnitude better than previously reported results[27]. The impact of polarization voltage induced noise and drift is also seen by comparing the two plots in Fig. 5.

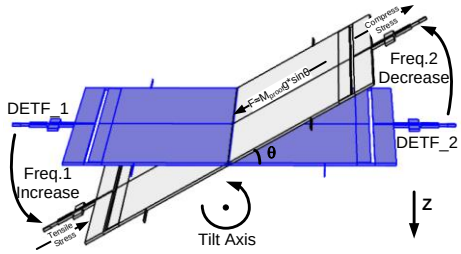

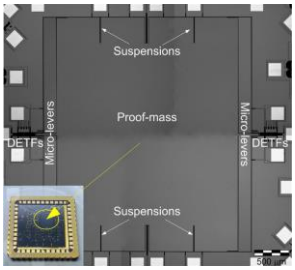

Fig.1: Tilt sensor operation principle. Fig.2: Optical micrograph of sensor (inset: vacuum packaged device).

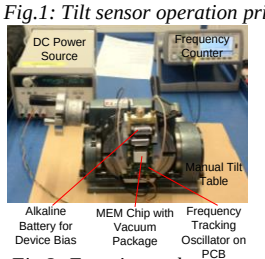

Fig.3: Experimental set- up.

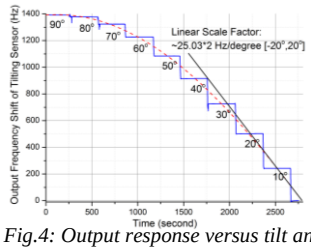

Fig.4: Output response versus tilt angle.

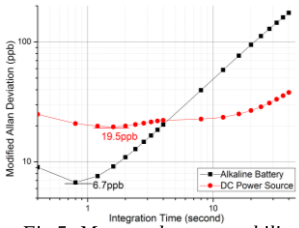

Fig.5: Measured output stability.

[27] X.Zou, et al., "Micro-electro-mechanical resonant tilt sensor," Frequency Control Symposium (FCS), 2012 IEEE International, 21-24 May 2012.

IFCS-EFTF4-A3-4

Two-Dimensional (2D) Semiconducting Crystal Nanomechanical Resonators with Frequency Scaling

Jaesung Lee[1*], Zenghui Wang[1], Keliang He[2], Jie Shan[2], and Philip X.-L. Feng[1*]

[1]Department of Electrical Engineering & Computer Science, [2]Department of Physics
Case Western Reserve University, Cleveland, OH 44016, USA

Email: jaesung.lee@case.edu, philip.feng@case.edu

We report the first demonstration of resonant nanoelectromechanical systems (NEMS) based on ultrathin molybdenum disulfide (MoS_2) crystals down to only a few atomic layers, with measurements of resonances in the HF/VHF bands, and studies of frequency scaling pathways toward the UHF/microwave regimes. Atomically-thin 2D crystals have recently shown interesting promises for enabling new nanoelectronic and optoelectronic devices[iv]. The unique mechanical properties of these 2D crystals, including excellent elastic modulus (~0.2–1TPa) and extremely high strain limits (~10^2–10^3 times higher than in 3D crystals), also make them attractive for 2D NEMS[v,vi]. Atomically-thin MoS_2, successfully isolated from the bulk only recently, is the first direct-bandgap semiconducting crystal in 2D form. The extensive measurements and analysis in this work with many devices establish MoS_2 as a new material for frequency-scalable NEMS resonators and transducers. Our study opens up possibilities for new types of NEMS, where the mechanical properties of 2D MoS_2 can be coupled to its semiconducting attributes.

We fabricate our devices using mechanical exfoliation and characterize them with optical microscope, SEM, and AFM. Nanomechanical resonances of the suspended MoS_2 devices are detected with a sensitive laser interferometer. Figure 1a shows the characteristics of a typical device. We have studied >20 devices with diameters of d~1.5 to ~6μm, and thicknesses t~10–100 layers. Combining data with modeling, we clearly identify the different elastic regimes (Fig. 1b). The full paper will present our experiments in detail, including the full analysis with quantitative design rules and scaling laws for engineering UHF devices.

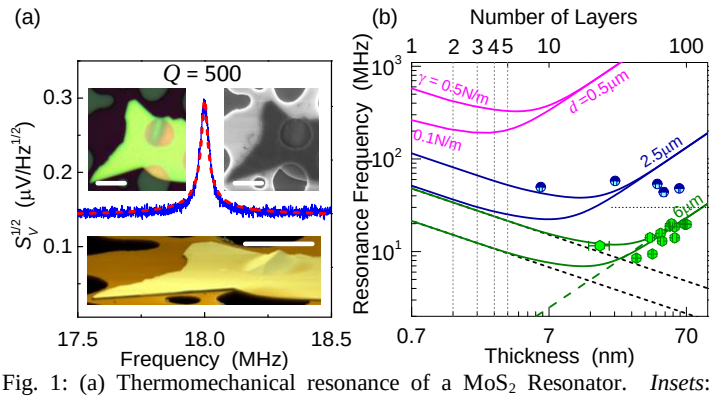

Fig. 1: (a) Thermomechanical resonance of a MoS_2 Resonator. *Insets*: Device images from optical microscope (top left), SEM (top right), and AFM (bottom). (b) Calculated resonance frequency versus MoS_2 thickness for three different device diameters, each with 0.1 and 0.5N/m built-in tension. Dashed slopes indicate the plate and membrane limits. Horizontal dashed line indicates the onset of VHF band. Measured resonance frequencies from devices with different sizes are shown with different

IFCS-EFTF4-A3-5

Aluminum Nitride Nano-Plate Resonant Infrared Sensor with Self-Sustained CMOS Oscillator for Nano-Watts Range Power Detection

Yu Hui and Matteo Rinaldi

Department of Electrical and Computer Engineering, Northeastern University, Boston, MA/USA

Email: hui.y@husky.neu.edu, rinaldi@ece.neu.edu

This paper presents, for the first time, a fast (thermal time constant of 1.3 ms) and sensitive (responsitivity of 267 Hz/µW) Infrared (IR) detector based on a MEMS-CMOS oscillator consisting of an Aluminum Nitride (AlN) nano-plate resonator (NPR) connected to a compact and low power CMOS self-sustained oscillator (fabricated in the AMIS 0.5 µm CMOS process) as a direct frequency readout. A high performance (quality factor Q = 1433 and electromechanical coupling coefficient k_t^2 = 1.56%) MEMS resonant structure based on a thin AlN (250 nm thick) NPR coated with Si_3N_4 (100 nm thick) as IR absorber was fabricated and tested, showing a measured temperature coefficient of frequency (TCF) of -30 ppm/K and FEM simulated temperature rise factor of 72.5 mK/µW. Thanks to the high electromechanical performance of the MEMS resonator, a compact and low power (2.3 mW) self-sustained CMOS oscillator circuit was used as a direct frequency readout, enabling the demonstration of a novel uncooled IR detector with a low Noise Equivalent Power (NEP) of 18 nW/Hz$^{1/2}$.

High performance MEMS resonant IR detectors based on gallium nitride[28] and Y-cut quartz[29] have been previously demonstrated, showing high sensitivity and low detection limit, however, none of them have been interfaced with CMOS readout circuits. This work takes the advantages of excellent piezoelectric transduction and unique scaling properties of AlN (which, differently from gallium nitride and quartz, can be deposited directly on silicon substrate with a low temperature sputtering process), enabling the use of a self-sustained CMOS oscillator circuit, which drastically reduces the size, complexity, power and noise performance of the frequency read-out and paves the way for the implementation of a new generation of NEMS uncooled, compact, fast, sensitive and low power IR focal plane arrays.

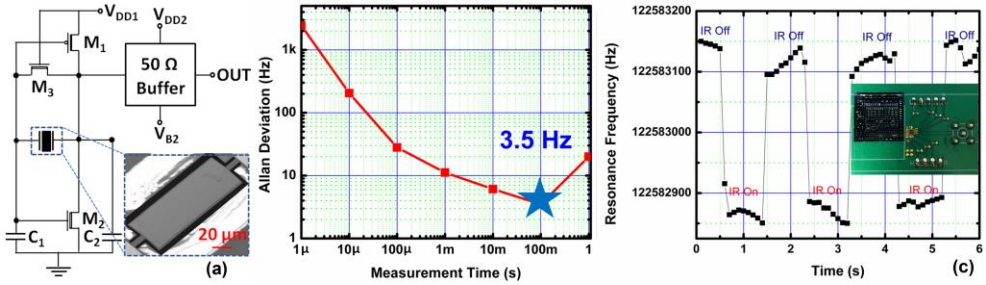

Figure 1: (a) The fabricated AlN nano-plate IR sensor connected to a self-sustained CMOS oscillator circuit for direct frequency readout. (b) Measured Allan Deviation of the sensor output signal showing an ultra-low noise induced frequency fluctuation of only ~28 ppb (3.5 Hz/122.6 MHz). (c) Sensor response for IR absorbed power of ~1 µW. The inset shows the AlN NPRs chip bonded to the CMOS readout chip fabricated in the AMIS 0.5 µm CMOS process.

[28] V. J. Gokhale, J. Roberts, and M. Rais-Zadeh, Hilton Head 2012, pp. 46-49, 2012.

[29] M. B. Pisani, K. L. Ren, P. Kao, and S. Tadigadapa, J. Microelectromech. Syst. Vol. 20, pp. 288, 2011.

Optical Fiber T+F Transfer I

CLUB E

Monday, July 22 2013, 02:00 pm - 03:30 pm

Chair: **Ronald Holzwarth**
Menlo Systems

White Rabbit for Time Transfer

Erik van der Bij, Maciej Lipiński, Javier Serrano

CERN, Geneva, Switzerland

Email: Erik.van.der.Bij@cern.ch

White Rabbit[30] (WR) is a protocol developed to synchronize nodes in a packet-based network with sub-ns accuracy. The protocol results from the combination of IEEE1588-2008 (PTP) with two further requirements: precise knowledge of the link delay and clock syntonization over the physical layer with Synchronous Ethernet.

The master node in a WR link uses a clock derived from a reference (e.g, a 10 MHz from a Cs clock or GPS) to encode data over the physical layer, while the slave recovers this clock (syntonization) and bases its timekeeping on it. Absolute time synchronization between master and slave is achieved by adjusting the clock phase and offset of the slave to that of the master. The phase and offset adjustment is done through the two-way exchange of PTP sync messages that are time-stamped to achieve sub-ns accuracy thanks to dedicated hardware support.

In White Rabbit, the precise knowledge of the link delay is obtained by accurate hardware timestamps and calculation of the delay asymmetry supported by knowledge of delays introduced by the hardware. Multi-link WR networks can be made by chaining WR links forming a hierarchical topology of master and slave nodes. The protocol allows the use of redundant links, thereby making the network more robust to link failures.

Although originally specified to transfer time with accuracy better than 1 ns on a network of up to 2000 nodes over a distance up to 10 km, tests show that better results and longer distances can be obtained. Work is underway to integrate the WR protocol into the next revisions of the IEEE1588 standard.

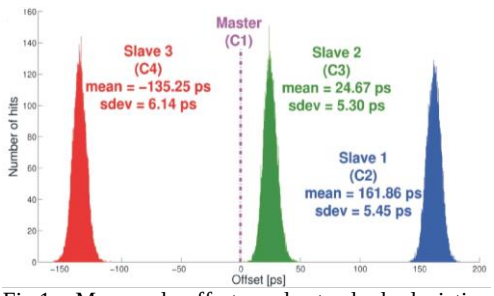

Fig.1: Measured offset and standard deviation between the Pulse-Per-Second output of the reference switch (Master) and each of the three cascaded switches (Slaves 1, 2 and 3), connected through 5 km of single mode fiber (total of 15 km from the Master to the Slave 3 switch).

The complete electronics and firmware designs of WR interfaces and switches are published under the CERN Open Hardware Licence; therefore anyone can study the implementation and contribute to improve the performance and functionality. At the same time this hardware is commercially available from engineering companies who can provide support.

White Rabbit is currently being tested for applications in control systems of particle accelerators, telescope arrays and for long distance accurate time transfer.

[30] White Rabbit. http://www.ohwr.org/projects/white-rabbit

Towards a Large-Scale, Optical Timing Distribution System with Sub-Femtosecond Residual Timing Jitter

Michael Y. Peng[1], Patrick T. Callahan[1], Amir H. Nejadmalayeri[1], Stefano Valente[2,3], Kemal Ahmed[2], Ming Xin[2], Eric Monberg[4], Man Yan[4], Lars Grüner-Nielsen[4], John M. Fini[4], Tony D. Roberts[5], Philip Battle[5] and Franz X. Kärtner[1,2]

[1]Department of EECS and Research Laboratory for Electronics, Massachusetts Institute of Technology, Cambridge, MA, USA
[2]Center for Free-Electron Laser Science, Deutsches Elektronen-Synchrotron, Hamburg, Germany
[3]Department of Electrical Engineering and Computer Science, University of L'Aquila, L'Aquila, Italy
[4]OFS Laboratories, Somerset, NJ, USA and [5]AdvR, Inc., Bozeman, MT, USA

Email: mypeng@mit.edu

Over the past 10 years, we have developed a pulsed optical timing distribution system[31] for large-scale, long-term synchronization of radio-frequency and optical sources in X-ray laser facilities, which may extend over several kilometers. The system consists of a femtosecond laser tightly locked to a microwave reference and fiber links stabilized via compact, single-crystal balanced optical cross-correlators (BOCs). Sub-10-fs performance over days of operation has been achieved[32] but is limited mainly by polarization mode dispersion in standard single-mode fiber. In the near future, it is necessary to improve timing distribution down to sub-femtosecond precision; current facilities, such as LCLS at Stanford, can already produce X-ray pulses shorter than 10 fs and concepts for sub-fs X-ray pulse generation are already in place. In the past two years, we have developed key components and characterized commercial femtosecond lasers suitable for realizing the next-generation, sub-femtosecond, fiber-based timing distribution system.

As demonstrated by Kim et al.[33], BOCs can be used to characterize the timing jitter of mode locked lasers with attosecond precision. We used this technique to characterize the jitter of two identical, commercially-available femtosecond lasers (OneFive-ORIGAMI) and confirmed that their high-frequency jitter for frequencies higher than 1 kHz is less than 70 as (Fig.1a). These lasers therefore have sufficiently low noise to serve as master oscillators for sub-fs timing distribution. Second, to eliminate slow drifts induced by polarization mode dispersion, we implemented a 1.2-km polarization-maintaining fiber link using 1 km of standard PM fiber and 0.2 km of novel dispersion-compensating PM fiber from OFS. Link operation for 16 days showed only 0.9 fs RMS timing drift and during a 3-day interval only 0.2 fs drift (Fig.1b). Lastly, we present a hybrid integrated BOC fabricated by AdvR using PPKTP waveguides[34] (Fig.1c). We seek to solve long-term drift issues by eliminating alignment drifts in free-space BOCs and to reduce the required optical power by a factor of 10-100 while achieving similar signal-to-noise levels as those from bulk-crystal BOCs. With further development, these components can soon be interfaced to realize a completely fiber-coupled, sub-femtosecond optical timing distribution system.

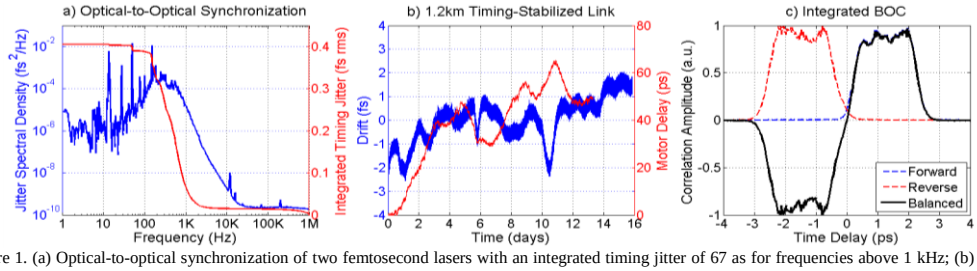

Figure 1. (a) Optical-to-optical synchronization of two femtosecond lasers with an integrated timing jitter of 67 as for frequencies above 1 kHz; (b) 1.2-km timing-stabilized PM fiber link with uninterrupted operation for 16 days with ~0.9 fs RMS timing drift and 3 days with ~0.2 fs drift; (c) Effective timing sensitivity curve for an integrated PPKTP waveguide operated as a double-pass, balanced optical correlator.

[31] J. Kim et al., "Drift-free femtosecond timing synchronization of remote optical and microwave sources," Nature Photon., 2: 12, 733–736, 2008.
[32] M. Ferianis et al., "All-optical Femtosecond Timing System for the Fermi@ Elettra FEL," Proc. FEL., Vol 11, 2011.
[33] J. Kim et al., "Attosecond-resolution timing jitter characterization of free-running mode-locked lasers," Opt. Lett., 32: 24, 3519–3521, 2007.
[34] A. Nejadmalayeri et al., "Guided wave optics in periodically poled KTP," Opt. Lett., 34, 2522-2524, 2009.

IFCS-EFTF5-B1-3

Local ties control in application of laser time transfer

Jan Kodet, Ulrich Schreiber, Johann Eckl[#], Ivan Prochazka*, Petr Panek[+]

Technische Universität München, Wettzell Observatory, 93444 Bad Koetzting, Germany
[#]Bundesamt für Kartographie und Geodäsie, Geodätisches Observatorium Wettzell, Germany
*Czech Technical University in Prague, Brehova 7, 115 19 Prague 1, Czech Republic
[+]Institute of Photonics and Electronics, Chaberska 57, 182 51, Prague, Czech Republic

kodet@fs.wettzell.de

In many fundamental physical experiments time plays an important role. The standard way for the comparison of time and frequency is the application of GNSS signals and the Two-Way Satellite Time and Frequency Transfer - TWSTFT. This technique is based on radiofrequency signal transmission. Recently, there is a rapid increase of optical time comparison development, which uses the Satellite Laser Ranging network (SLR). Currently the French project T2L2 is in operation on board Jason 2 and the European Space Agency project ELT in support of the Atomic Clock Ensemble in Space (ACES) is under development. The goal of both projects is the time synchronization with a precision below 40 ps rms and an absolute error well below 100 ps. Comparing the results of the optical time transfer with the GNSS time comparison requires unprecedented control of the local ties between the different observation techniques. One of the possible methods is the application of the Two Way Time Transfer (TWTT) on a single coaxial cable. Such a system can be implemented using two or more event timers, which are interconnected by a standard coaxial cable. The event timers are exchanging pulses between each other and time tagging them. Out of the measured result one can evaluate the difference of time scale represented by the event timers. It was shown that such a technique can be used for time transfer with a precision of a few picoseconds of rms and an absolute error below 20 ps for distances reaching several hundreds of meters.

We have implemented this technique for establishing and monitoring the absolute time delays between the SLR system and the time laboratory on the Geodetic Observatory in Wettzell. The event timers were developed at the Czech Technical University. The measurement principal is based on a SAW filter excitation. The Event Timers were located in different buildings 50 meters apart and with the help of the TWTT technique, the delay between them was measured. The second input sockets of the event timers were used to monitor the respective local timescale.

IFCS-EFTF5-B1-4

Single Photons Optical Two Way Time Transfer Providing Picosecond Accuracy

Ivan Prochazka[1], Josef Blazej[1], Jan Kodet[1,2], Petr Panek[3]

[1]Czech Technical University in Prague, Brehova 7, 115 19 Prague, Czech Republic
[2]Technical University Munich, Station Wettzell, 93444 Koetzting, Germany
[3]Institute of Photonics and Electronics, ASCR, Chaberska 57, 182 51 Prague, Czech Rep.

Email: prochazk@cesnet.cz

We are reporting on a new approach to an optical Two Way Time Transfer (TWTT) which is based on optical signals of individual photons. This approach enables to reach extreme timing stabilities and minimal systematic errors using existing electro-optic technologies.

The two way time transfer is an effective way to synchronize two independent time scales with high precision and accuracy independently on the variations of the interconnecting channel[35]. In our previous work we have demonstrated electronic circuits for two-way time transfer via a single coaxial cable with picosecond accuracy and precision[36]. This technique may be effectively applied in configurations, where the sites may be interconnected by a broad bandwidth coaxial cable. Considering the performance of the top quality coaxial cables available, the picosecond performance may be accomplished over distances up to 2 km maximum. For longer distances the optical approach may be considered.

We have designed and tested the optical analogy of the two way time transfer using a common optical channel. To minimize the systematic error sources the photon counting approach has been applied. The pilot experiment has been completed in our lab. The test pulses were generated by laser diodes in a form of short pulses. The signal may be propagated either in a single mode optical fiber or in a free space. Thanks to photon counting approach the optical loses on the line is not a critical issue, one way losses of 90 dB may be tolerated. The optical signals are detected by solid state photon counters, the timing is accomplished by sub-ps timing systems NPET[37]. The experiment proved the capability of this technique to maintain picosecond stability of TWTT over the periods of seconds to days. The systematic errors are expected to be of the order of units of picoseconds. The experiment results will be presented.

35 J. Levine, "A review of time and frequency transfer methods," Metrologia, vol. 45, p. S162 - S174, 2008.

36 I. Prochazka, J.Kodet, and P.Panek, "Electronic circuit for two-way time transfer via a single coaxial cable with picosecond accuracy and precision," Rev. of Sci. Instruments, vol 83 (11), 116104, 2012.

37 I. Prochazka, J. Blazej, J. Kodet, "New technologies for time transfer with picoseconds precision and accuracy," In 2012 International Frequency Control Symposium Proceedings, Baltimore, MD, USA, 2012 IEEE International, pp. 298 - 304, May 21 - 24 2012, doi: 10.1109/FCS.2012.6243610

IFCS-EFTF5-B1-5

Implementing a nationwide robust time- and frequency distribution

Per Olof Hedekvist, Sven-Christian Ebenhag, Carsten Rieck, Kenneth Jaldehag[1], Jonatan Walck, Patrik Fältström[2], Peter Löthberg[3],Ove Landberg, Håkan Swedenborg[4]

[1]SP Technical Research Institute of Sweden, Borås, Sweden
[2]Netnod Internet Exchange, Stockholm, Sweden
[3]Stupi, Los Altos, CA/USA
[4]PTS, Swedish Post and Telecom Agency, Stockholm, Sweden

Email: per.olof.hedekvist@sp.se

There is an increasing need for accurate and reliable time information in digital communication, including network timing, data time stamping, smart grid surveillance and control, cyber forensics, etc. The efforts have to a wide extent being focused on accuracy, precision and authentication, to assure that the given time and frequency signals are accurate and reliable. In addition to this, the implementation in Sweden has worked on the robustness of the time keeping, and the access to reliable signals from a network of spatially distributed redundant clock sites.

The Swedish UTC-realization, UTC(SP), is managed by SP, the National Metrology Institute of Sweden, and located in Borås in the SW part of Sweden. UTC(SP) is based on an H-maser corrected to an ensemble of atomic clocks located in their own facilities, and at two other locations. In the new distributed system, two redundant timescales are also implemented at a new location in Stockholm. Each of these timescales will be based on an H-maser, and constantly managed and adjusted using the data from all other available atomic clocks in the network as well as the UTC-data from SP. If any of the clocks are disconnected, each timescale will automatically make a best estimate based on the data from the remaining clocks. In addition, 4 distribution points operated by Netnod in Stockholm, Gothenburg, Malmo and Sundsvall will be upgraded with two Cs clocks at each site, also reporting data for the time scales. Each distribution point is right at the Internet exchanges, synchronized to UTC(SP) using time transfer links, and offers 2 independent NTP-servers to the general public adding robustness to the time system at large and bringing time synchronization services closer to the Internet community.

Fig. 7: National distribution of atomic clocks, for a robust access to reliable time and frequency signals

The time is made available to network users through NTP, both IPv4 and IPv6, and one server implemented for the distribution of authenticated ntp. Furthermore, the access to stable E1 frequency is offered at the Netnod locations, and the SP sites can be used as references for GNSS time transfer. The time and frequency data, including uncertainties and accessibility, is logged and published online for free evaluation.

Micro-Scale Oscillators

CLUB D

Monday, July 22 2013, 02:00 pm - 03:30 pm

Chair: **Dan Stevens**
Consultant

IFCS-EFTF1-B2-1

UHF Quartz MEMS Oscillators for Dynamics-Based System Enhancements

R.L. Kubena, D.J. Kirby, Yook-Kong Yong*, D.T. Chang, F.P. Stratton, H.D. Nguyen, R.J. Joyce, R. Perahia, H.P Moyer, & R.G. Nagele
HRL Laboratories, LLC, Malibu, CA., 90265 USA
*Rutgers Univ., Piscataway, New Jersey

Email: rlkubena@hrl.com

Processes for fabricating full wafers of UHF quartz MEMS oscillators bonded to Si have been developed at HRL over the past several years. These devices have shown state-of-the-art noise and stability[38] along with extremely small vacuum packaged die size of less than 3 mm^2. An interesting by-product of the high frequency, small size, and wafer-scale fabrication of these devices is that several novel dynamics-based enhancements can be considered. These include the reduction of the phase noise contributions of the amplifier by driving the resonator into a non-linear state with a high phase slope versus frequency.[39,40] In addition, large enhancements of the Q through nonlinear modal coupling of the fundamental and third overtone have been predicted.[41] By adding control electrodes on the Si substrate and in the capping wafer and capacitive electrodes on the quartz, dynamic force rebalancing can be utilized to reduce the vibration sensitivity using low voltages. Finally, co-integration of these devices with other sensors on a chip, such as a microgyro, becomes possible and allows active frequency-locking schemes to be implemented in a small ovenized housing for improved inertial bias stability. These features may provide important performance enhancements for future mobile communication systems.

An example of the phase noise enhancements that are possible with these techniques is shown in Fig. 1. An 804-MHz fundamental-mode AT-cut oscillator circuit was configured with a variable gain amplifier, phase shifter, and admittance measurement probes to allow sweeping the phase (frequency) across the resonator at different known applied AC voltages. As the drive level approaches the bifurcation point (>150 mV), a sharp drop in the phase noise is observed near the highest phase slope. We believe this is the first time such a sharp drop in phase noise has been observed near the critical point for nonlinearly operated quartz oscillators. For 200 mV of applied voltage, the true phase noise reduction was masked due to limited gain from the amplifier in the loop. For automated start-up, a phase dither in the loop in conjunction with an AGC circuit can be used to adjust the operating point for locating the highest phase slope conditions. Since the quartz plate is only about 2-µm thick, the required voltages for bifurcation are within CMOS levels.

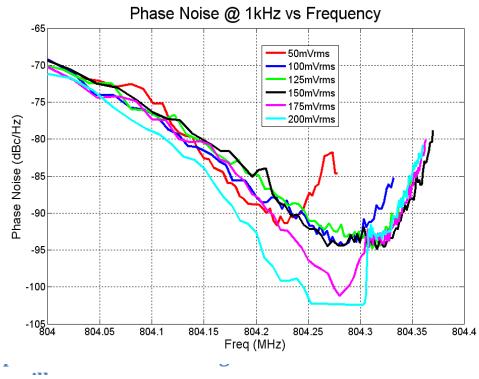

COMSOL models have been developed to enable the modeling of stress propagation from the mounts into the active resonator and the effect on the f/T curves. Controlling and minimizing these stresses in small quartz resonators is critical for maintaining high stability while concurrently implementing these new concepts. In this paper, we will review these concepts and describe our recent modeling and experimental work for implementing them.

---

[38] R.L. Kubena, et. al., "Next Generation Quartz Oscillators and Filters for VHF-UHF Systems," Proc. 2006 IEEE International Microwave Symposium, San Francisco, Ca., June 11-16, 2006.

[39] B. Yurke, et. al., " Theory of amplifier-noise evasion in an oscillator employing a nonlinear resonator," *Phys. Rev. A*, vol. 51, no. 5, pp. 4211-4229, May 1995.

[40] H.P. Moyer, et. al., "Nonlinear Behavior of an UHF Quartz Resonator in an Oscillating System," 2012 IEEE IFCS, May 21-24, 2012.

[41] Yook-Kong Yong, "Resonator Q Increase and Noise Reduction in Third Overtone Thickness Shear Resonators by the Nonlinear Characteristics of their Fundamental Thickness Shear Mode," Proc. 2012 IEEE IFCS, May 21-24, 2012.

IFCS-EFTF1-B2-2

Nonlinear Dynamics in Aluminum Nitride Contour-Mode Resonators

Nicholas Miller, Gianluca Piazza

Department of Electrical and Computer Engineering, Carnegie Mellon University, Pittsburgh, Pennsylvania, USA

Email: njmiller@andrew.cmu.edu

Aluminum nitride (AlN) contour-mode resonators (CMRs), see figure 1 right, have previously been shown to exhibit a softening nonlinearity due to self-heating[1,2]. In previous analysis[2] the resonator was modeled quasi-statically leading to a Duffing resonator model. In this work we show that the slow dynamics of the resonator amplitude and phase are described by the model

$$\dot{u} = -(1 + i\sigma)u - (\delta + i)u\tau + \nu, \qquad \dot{\tau} = -\frac{1}{\gamma}\tau + |u|^2,$$

where u is the resonator's normalized complex amplitude and τ is the normalized resonator temperature deviation from ambient. The resonator admittance, Y, is a linear function of u. The fixed points ($\dot{u} = \dot{\tau} = 0$) of this model agree with that of the Duffing resonator model with nonlinear damping. However, the dynamics differ due to thermal relaxation over the time scale γ. This is typically in the millisecond range for AlN CMRs. Accordingly, the difference between the self-heating model and the Duffing model can be revealed during fast frequency sweeps using a vector network analyzer, see figure 1 left. This has important ramifications for applications of resonator nonlinearity, for example the evasion of amplifier noise in oscillators[3].

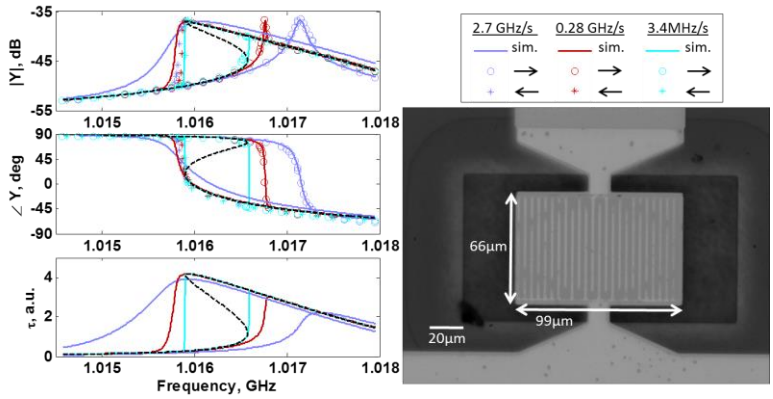

Fig. 8: (Left) Admittance, Y, and temperature, τ, response to a frequency sweep. The model prediction is shown with solid curves and the measured sweeps up and down with markers. The black dashed line shows the fixed points of the above resonator model. (Right) Microscope image of AlN CMR.

[1] A. Tazzoli *et al.*, "Experimental investigation of thermally induced nonlinearities in aluminum nitride contour-mode mems resonators." *IEEE Electron Device Letters*, vol. 33, p.724-726, 2012.

[2] J. Segovia-Fernandez and G. Piazza, "Thermal nonlinearities in AlN contour mode resonators", in review, 2013.

[3] L.G. Villanueva *et al.*, "Surpassing fundamental limits of oscillator using nonlinear resonators", *arXiv:1210.8075[cond-mat.mes-hall]*, 2012.

Comment [GP1]: Fix label on Y axis of first plot as you have Y^2…(it should be Y).

Any chance we could make the lines a bit thicker or somehow more easily viewable?

The definition of fixed points is not very clear….what exactly do you mean in this case?

Finally, how about sticking in an SEM of the resonator?…just in case some reviewer only look at the title and figure.

Comment [GP2]: Maybe add a reference here…

IFCS-EFTF1-B2-3

Close-in Phase Noise Reduction in an Oscillator based on 222 MHz Non-Linear Contour Mode AlN Resonators

J. Segovia-Fernandez, C. Cassella, G. Piazza

Electrical and Computer Engineering, Carnegie Mellon University, Pittsburgh, PA, USA

Email: jsegovia@andrew.cmu.edu

Phase Noise (PN) reduction in oscillators has been traditionally accomplished by using low noise amplifiers or high quality factor (Q) resonators, in accordance with Lesson theory[42]. However, previous work on nonlinearly driven resonators has suggested that locking the device into a particular nonlinear state (so-called bifurcation) can help evading the amplifier noise[43]. AlN Contour Mode Resonators (CMRs) are an emerging class of piezoelectric MEMS devices exhibiting high Q and low motional resistance at high frequencies (f_{res}). Because of their micron-scale size the AlN CMRs have revealed a nonlinear behavior induced by self-heating when driven with relatively high power[44]. In this work, we show a substantial improvement of the PN close-in (-20dBc/Hz @ 100Hz) of a 222 MHz oscillator that incorporates a nonlinearly driven AlN CMR.

The oscillator circuit presented here was built using coaxial electronic components (Fig. 1). The experiments were carried out by setting the DC bias of the amplifier to 6V, therefore ensuring enough gain to both sustain oscillations and drive the resonator nonlinearly. The phase shifter was manually tuned in steps of 5° to increase the circuit delay and, hence, lock the oscillator at different frequencies (f_{osc}) on the non-linear resonance curve of the 222 MHz AlN CMR device. Fig. 2 depicts PN (dBc/Hz) versus offset frequency (f_{off}) for different phase delays. A dramatic change of slope in the PN close-in (f_{off}<1kHz) is observed when $f_{osc}<f_{res}$ (f_{res} is indicated on the plot). This frequency corresponds to the device operating past bifurcation, as we can infer by measuring the resonator admittance in open loop for the same output power. The data highlight that for particular phase shifts >15°, the PN curve experiences a significant reduction in slope (from $1/f^4$ to $1/f^2$). Furthermore, the experimental results show that the AlN CMR thermal time constant (τ_{TH})[3] limits the maximum f_{off} for which a PN improvement can be recorded.

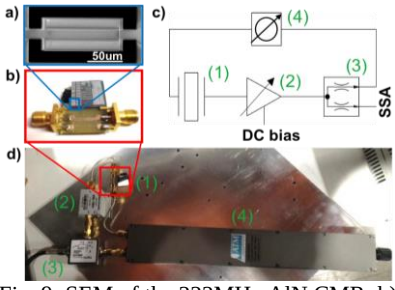

Fig. 9: SEM of the 222MHz AlN CMR; b) wirebonded AlN CMR on a PCB; and both c) schematics and d) actual oscillator setup including (1) AlN CMR, (2) amplifier, (3) power splitter, and (4) phase shifter.

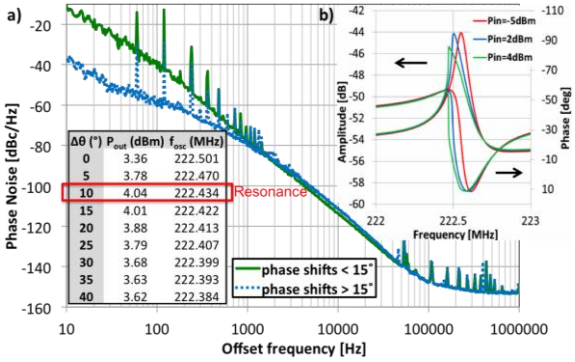

Fig. 10: a) *PN* vs f_{off} at DC bias=6V and different phase shifts ($\Delta\theta$). b) Open loop amplitude and phase of AlN CMR admittance for various input powers.

[42] D. B. Leeson, "A simple model of feedback oscillator noises spectrum," Proc. IEEE, vol. 54, pp. 329–330, 1966.

[43] B. Yurke, D.S. Greywall, A.N. Pargellis, and P.A Busch, "Theory of amplifier-noise evasion in an oscillator employing a nonlinear resonator," Phys. Rev. A, vol. 51, pp. 4211-4229, 1995.

[44] J. Segovia-Fernandez, A. Tazzoli, M. Rinaldi, G. Piazza, "Nonlinear lumped electrical model for contour mode AlN resonators," *IEEE Int. Ultrasonics Symp.*, pp.1846-1849, 2011

IFCS-EFTF1-B2-4

MEMS-based mechanical AGC for oscillator circuits

Andreja Erbes[1], Xueyong Wei[2], Ashwin A. Seshia[1]

[1]Engineering Department, University of Cambridge, Cambridge, United Kingdom
[2]School of Mechanical Engineering, Xi'An Jiaotong University, Xi'An, China

Email: ae279@cam.ac.uk

This paper investigates a nonlinear amplitude saturation behavior in an electrostatically transduced, Si MEMS disk resonator (Fig. 1), operating in its secondary elliptical bulk-mode (*2EBM*) at 3.932 MHz towards its implementation as an all-mechanical automatic gain control (AGC) element. The nonlinear vibration behavior of the *2EBM* mode is experimentally observed in open-loop testing (Fig. 2) such that above a threshold small signal drive v_{ac} = 1.22 Vp-p at a polarization voltage of V_{DC} = 100 V, the vibration amplitude of the mode saturates. Such nonlinear clamping behaviors have been reported in other MEMS resonators[45, 46].We also study this nonlinearity in an oscillator circuit (Fig. 3) designed such that the driving power level at the resonator input (v_{ac}) is manually tuned as the circuit operates and the oscillation amplitude is recorded (v_{output}), for different V_{DC}. Fig. 4 shows a clear transition of the oscillator amplitude from the linear to the nonlinear saturation region as the driving power increases. This transition point is consistent with the behavior measured in open-loop testing. Short-term frequency stability measurements were also conducted for different v_{ac} and the resulting Allan deviation plots (Fig. 5) show an improvement in the short-term stability (0.5s averaging time) from 1.4 ppb in the linear region (v_{ac} = 1.2 Vp-p) to 0.4 ppb for operation in the amplitude saturation region (v_{ac} = 1.6-2.4 Vp-p). These results indicate that the amplitude clamping effect in nonlinear microresonators can be applied in MEMS based oscillator circuits as a mechanical AGC to simplify the circuit configuration as well as retain excellent short term frequency stability.

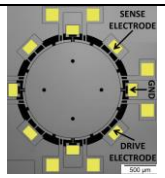

Fig. 1: Optical micrograph of the 3.932 MHz disk resonator

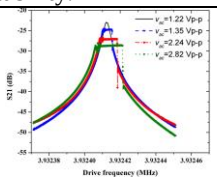

Fig. 2: Measured *S21* parameter at the *2EBM* mode for different drive v_{ac} and V_{DC}=100 V.

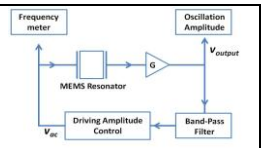

Fig. 3: Schematic of the oscillator circuit using the disk resonator

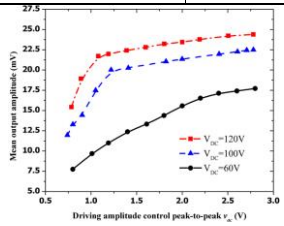

Fig. 4: Oscillation amplitude v_{output} for different drive v_{ac} in the closed loop configuration of Fig. 3.

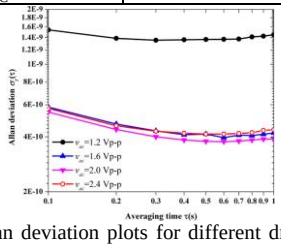

Fig. 5: Allan deviation plots for different drive v_{ac} and V_{DC}=120V.

[45]C. van der Avoort et al., "Amplitude saturation of MEMS resonators explained by autoparametric resonance", *J. Micromech. Microeng.*, vol. 20, no. 10, 2010.
[46]L. Lipiäinen *et al.*, "Nonlinear excitation of a rotational mode in a piezoelectrically excited square-extensional mode resonator", *Appl. Physics Lett.*, vol. 100, no. 153508, 2010.

IFCS-EFTF1-B2-5

A 1 GHz SAW oscillator on epitaxial GaN/Si substrate: toward co-integrated frequency sources

Marc Faucher[1], Gilles Martin[2], Jean-Michel Friedt[2], Sylvain Ballandras[3,4]

[1]IEMN UMR CNRS 8520, Villeneuve d'Ascq, France

[2]FEMTO-ST, UMR 6174 CNRS-UFC-ENSMM-UTBM, Besançon France

[3]SENSeOR SAS, TEMIS Innovation, Besançon France

[4]frec|n|sys SAS, Besançon France

Email: marc.faucher@iemn.univ-lille1.fr

Motivation :

SAW-resonator based oscillators are fabricated for embedded applications such as Radar and local oscillator for space missions requiring frequency transposition for telecommunications. Although rather compact, these discrete devices contribute to on-board charge and are currently poorly suited to co-integration. The possibility for providing ultimately compact sources able to operate on the same board than most radio-frequency circuits would yield a major advance for integrated time-frequency systems.

Achieved work :

We investigated the use of GaN/Si(111) epilayers for fabrication of SAW oscillators. Devices have been designed on 1.8µm thick GaN. Tank to the analysis of the obtained results, a set of elastic constants has been fitted. Comparison between experimental and theoretical transfer functions has been also exploited to refine the estimation of the wave characteristics. An oscillator has been finally built using the obtained resonators to assess the interest of this material for this kind of application.

Results:

SAW resonators have been processed using E-beam lithography with a 2 µm period, yielding resonators operating near 1 GHz with Q factor close to 2000 and insertion losses better than 12 dB. Two port resonators were inserted in a feed-back loop oscillator based on a low-noise HX2400 amplifier, enabling short term measurements as well as phase noise extraction. A short term stability of 10^{-7} per second has been measured, clearly penalized by the temperature sensitivity of the SAW (near -30 ppm.K^{-1}). A phase noise figure of -115 dBc/Hz was found at 10 kHz from the carrier and a flour of -165 dBc/Hz was finally measured (Fig. 1). Although these figures are not the best achievable using this material, they are really promising as High Electron Mobility Transistors (HEMTs) are currently manufactured on the same substrate, allowing for future development of co-integrated SAW oscillators.

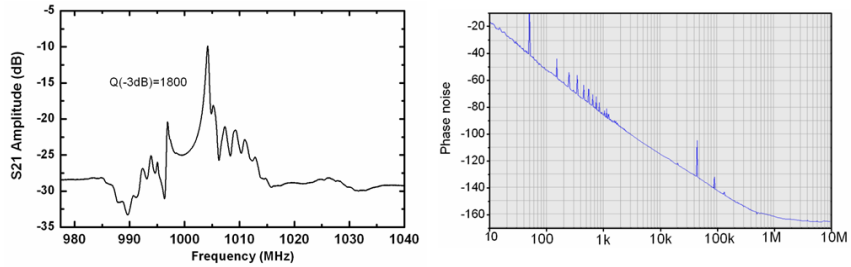

Fig. 11: Measured response of the GaN resonator (left) and phase noise measurement (right)

Lattice Clocks I

CLUB H

Monday, July 22 2013, 02:00 pm - 03:30 pm

Chair: **Tetsuya Ido**
NICT

IFCS-EFTF6-B3-1

Strontium lattice clocks with reduced BBR uncertainty

Stephan Falke, Nathan Lemke, Stefan Vogt, Uwe Sterr, Christian Lisdat

Physikalisch-Technische Bundesanstalt (PTB), Braunschweig, Germany

Email: stephan.falke@ptb.de

The leading contribution to the uncertainty of state-of-the-art optical lattice clocks is related to the blackbody radiation (BBR) emitted by the surfaces surrounding the atoms that are interrogated while being held in an optical lattice. In strontium and ytterbium optical lattice clocks relative frequency corrections of several 10^{-15} are applied to account for an ac Stark frequency shift due to the BBR of the apparatus at room temperature. Its uncertainty causes the leading contribution to the uncertainty budget of the clock of a few times 10^{-17}.

Both, the environmental temperature and the correction coefficient need to be known precisely to reduce this uncertainty contribution. We will present work that improved significantly the knowledge of the correction coefficient for strontium lattice clocks. We measured the differential dc polarizabilty of the clock states to a high precision. This quantity was used along with other available data, such as the magic wavelength or oscillator strengths of atomic transitions, to model the ac polarizability of the clock states. It is then possible to integrate the ac Stark shift of the clock transition over the temperature dependent BBR spectrum. We used Monte-Carlo simulations to determine the uncertainty of the correction.[47] (See related work on ytterbium.[48]) Now, the uncertainty of the BBR correction coefficient limits the uncertainty at room temperature to a few 10^{-18} fractional frequency uncertainty. Absolute temperature measurements of the environment of better than 0.05 K will be required at room temperature to fully exploit the improved correction coefficient. At present, despite a reduction of thermal gradients across our vacuum chamber, the associated temperature uncertainty of 0.4 K translates to an uncertainty due to blackbody radiation of 3×10^{-17}.

To target sub-10^{-17} relative frequency uncertainty with optical lattice clocks, the design of the setup must allow for a precise description of the BBR field. We follow two approaches:

(a) a more homogeneous temperature of the vacuum chamber and

(b) shuttling the atoms into an environment providing a cryogenic blackbody radiation field.[49]

With the improved blackbody radiation correction the systematic uncertainty of lattice clocks is already significantly below even the best cesium fountain clocks. Moreover, their instabilities are typically orders of magnitude below those of microwave clocks.[50] Direct comparisons between two or more optical clocks are becoming the method of choice. At PTB the strontium optical lattice clock is compared to an ytterbium single ion clock[51] for studies of systematic frequency shifts and direct frequency ratio measurements evaluating the clocks with respect to a possible re-definition of the Second.

---

[47] T. Middelmann *et al.*, Phys. Rev. Lett. **109**, 263004 (2012).

[48] J. Sherman *et al.*, Phys. Rev. Lett. **108**, 153002 (2012), K. Beloy *et al.*, Phys. Rev A **86**, 051404 (2012).

[49] T. Middelmann *et al.*, IEEE Trans. Instrum. Meas. **60**, 2550 (2011), T. Middelmann *et al.*, New. J. Phys. **14** 073020 (2012).

[50] C. Hagemann, IEEE Trans. Instrum. Meas., DOI: 10.1109/TIM.2013.2242597 (2013).

[51] N. Huntemann et al., Phys. Rev. Lett. **108**, 090801 (2011).

IFCS-EFTF6-B3-2

Characterizing the blackbody shift in a lattice clock to $1x10^{-18}$

A. D. Ludlow[1], K. Beloy[1], J. A. Sherman[1], N. Hinkley[1,2],
N. Phillips[1], N. D. Lemke[1], M. Schioppo[1], C. W. Oates[1]

[1]Time & Frequency Division, National Institute of Standards and Technology,
Boulder, Colorado USA
[2]Department of Physics, University of Colorado, Boulder, Colorado USA

Email: ludlow@boulder.nist.gov

The optical lattice clock promises frequency uncertainty and instability at fractional levels of 10^{-18}. To achieve such performance, several key advances are first required and research with this focus is being undertaken worldwide. Perhaps the most formidable obstacle to be overcome is controlling the blackbody radiation (BBR) shift at the 10^{-18} level.

Characterization of the BBR shift first requires accurate knowledge of the atomic sensitivity to thermal radiation, rooted in the details of the electronic structure. Because of the low-frequency nature of room-temperature blackbody emission, this atomic sensitivity can be neatly divided into two terms: the static polarizability and a small dynamic correction accounting for time-dependent aspects of the thermal radiation field with the corresponding atomic response. We report a high accuracy measurement of the differential static polarizability of the clock transition in a Yb lattice clock, yielding an uncertainty in the static atomic sensitivity which corresponds to $< 1x10^{-19}$ clock uncertainty[52]. Furthermore, we report two independent determinations of the dynamic correction[53], which consequently contributes to a BBR shift uncertainty of $1x10^{-18}$ at room temperature.

To realize a total BBR shift uncertainty at such a level, the thermal radiation environment bathing the atoms must be known to high accuracy. To date, imperfect knowledge of this environment has led to clock uncertainties of $3x10^{-17}$ or higher. We describe here in detail a radiation enclosure surrounding the lattice trapped atoms designed to constrain the thermal environment sufficiently well to achieve $1x10^{-18}$ clock uncertainty. The shield is designed for operation at either room or cryogenic temperatures.

Finally, we will present early results from comparative measurements between two Yb lattice clocks. Exploiting an ultra-stable laser for clock interrogation[54], both systems have demonstrated measurement instability at or better than $5x10^{-16}/\tau^{1/2}$. Using this measurement capability, we further characterize light shifts originating from the optical lattice confinement.

---

[52] J. A. Sherman et al., "High-Accuracy Measurement of Atomic Polarizability in an Optical Lattice Clock", Phys. Rev. Lett., vol. 108, 153002, 2012.

[53] K. Beloy et al., "Determination of the 5d6s $^3D_1$ state lifetime and blackbody-radiation clock shifts in Yb", Phys. Rev. A., vol. 86, 051404(R), 2012.

[54] Y. Y. Jiang et al., "Making optical atomic clocks more stable with 10^{-16}-level laser stabilization", Nat. Photonics, vol. 5, p. 158-161, 2011.

IFCS-EFTF6-B3-3

First spectroscopy of the $^1S_0$ – $^3P_0$ transition in Lamb-Dicke confined magnesium atoms

André Kulosa, Steffen Rühmann, Dominika Fim, Klaus Zipfel, Wolfgang Ertmer, Ernst M. Rasel

Institut für Quantenoptik, Leibniz Universität Hannover, Hannover, Germany

Email: kulosa@iqo.uni-hannover.de

We report on the status of the magnesium optical clock experiment in Hannover. Recently, we demonstrated the first spectroscopy of the spin-forbidden $^1S_0$ – $^3P_0$ clock transition in µK cold magnesium atoms that were trapped in an optical lattice at the predicted magic wavelength of 469 nm.

Due to the lack of sub-Doppler cooling techniques, we prepare our atoms using a continuous loading scheme for an optical dipole trap at 1064 nm[55]: Atoms with milli-Kelvin temperature are continuously transferred to the dipole trap by creating a loss channel for $^3P_0$ atoms. The coldest among them can be captured by the optical potential for subsequent transfer into the optical lattice.

Applying an external homogeneous magnetic field creates a mixture of the $^3P_0$ and $^3P_1$ states weakly allowing the $^1S_0$ – $^3P_0$ transition[56]. Performing such a magnetic field-induced spectroscopy, we have been able to de-excite 25% of $^3P_0$ atoms on the 458 nm intercombination transition to the $^1S_0$ ground state.

The interrogation laser for the ultra-narrow clock transition is a frequency doubled diode laser at 916 nm stabilized to a vibration insensitive optical cavity. The laser system shows a fractional frequency instability of $\sigma_y(\tau = 1\ \mathrm{s}) = 5 \times 10^{-16}$.

As a next step, we will experimentally investigate the magic wavelength for magnesium.

[55] M. Riedmann, et al., Phys. Rev. A **86**, 043416 (2012)

[56] A. V. Taichenachev, et al., Phys. Rev. Lett. **96**, 083001 (2006)

IFCS-EFTF6-B3-4

Mercury optical lattice clock at LNE-SYRTE

R. Tyumenev, Z. Xu, J. J. McFerran and S. Bize.
SYRTE, 61 avenue de l'Observatoire, 75014 Paris, France
Email: sebastien.bize@obspm.fr

An ensemble of atomic clocks is being developed at LNE-SYRTE, comprising Cs and Rb atomic fountains, two Sr optical lattice clocks, and a Mercury (Hg) optical lattice clock. Hg is a very interesting candidate for making an optical lattice clock, due to several favorable atomic properties. The $^1S_0$ – $^3P_0$ clock transition in Hg has very low blackbody radiation shift. For instance blackbody radiation sensitivity in Hg is a factor of ~34 less than in Sr. Hg has a high vapor pressure at room temperature, which allows eliminating large temperature gradients in the experimental setup due to heating systems. Hg atoms can be laser-cooled to rather low temperature of 30 μK with a single stage magneto optical trap (MOT), performed on $^1S_0$ – $^3P_1$ transition, and directly loaded in the optical lattice.

In this poster, we describe our experimental setup and the latest results that we obtained with it. Atoms are confined in a vertically orientated optical lattice with depth about 20 recoils energy at 362 nm. Atoms are loaded in optical lattice from a MOT with cooling light at 253.7 nm. Once atoms are trapped in optical lattice, we apply Rabi light pulse at 265.6 nm, delivered from ultra-stable laser source connected to the LNE-SYRTE primary reference signal via optical frequency combs. High precision spectroscopy experiments allowed us to determine magic wavelength for Hg with precision up to 10^{-3} nm [1]. We demonstrated atomic quality factors as high as 10^{14} (11 Hz at 1128 THz), locked an ultra-stable laser to the ultra-narrow $^1S_0$ – $^3P_0$ clock transition and demonstrated a fractional frequency instability of $5.4 \times 10^{-15}/\sqrt{\tau}$ for $\tau \leq 400$ s [2]. We performed a preliminary study of systematic shifts and a series of absolute frequency measurements with an uncertainty of 5.7 parts in 10^{15} [3].

In future, we are planning to improve our cooling light source and have more power in MOT light beams, increase trap depth in our 1D optical lattice trap, which is a significant challenge given the magic wavelength in the UV range. This will help us to increase the atom number by more than one order of magnitude, to improve the signal to noise ratio in the clock transition spectroscopy, to determine the magic wavelength with increased precision, and to study systematic frequency shifts down to the 10^{-16} level, as a first step before seeking the limits of the Hg system which are expected in the low 10^{-18} range, at room temperature.

[1] J. J. McFerran et al., PRL 108, 183004 (2012).

[2] J. J. McFerran et al., Optics Letters, 37, 3477 (2012).

[3] J. J. McFerran et al., Oral presentation at the 2012 EFTF.

GNSS and Services

CLUB E

Monday, July 22 2013, 04:30 pm - 06:00 pm

Chair: **Alexander Kuna**
Institute of Photonics and Electronics

IFCS-EFTF5-C1-1

Technical Status of Galileo Development

Alexander Mudrak[1], Joerg Hahn[1], Daniel Blonski [1]

[1]Galileo Project Office, European Space Agency, Noordwijk, The Netherlands

Email: alexander.mudrak@esa.int

Galileo is Europe's own global navigation satellite system, providing a highly accurate global positioning service under civilian control. It is inter-operable with GPS and Glonass, the US and Russian global satellite navigation systems.

By offering dual frequencies as standard, Galileo will deliver real-time positioning accuracy down to the metre range. Galileo will also disseminate UTC with the accuracy of 30 ns.

Experimental satellites GIOVE-A and GIOVE-B were launched in 2005 and 2008 respectively, serving to test critical Galileo technologies, while also the securing of the Galileo frequencies within the International Telecommunications Union.

On 21 October 2011 the first two of four operational satellites have been successfully launched, two additional satellites followed on 12 October 2012. Those satellites have been developed together with the necessary ground infrastructure to validate the Galileo concepts in orbit. This In-Orbit Validation (IOV) phase will be executed during the early summer this year.

The four operational satellites launched so far - the basic minimum for satellite navigation in principle - serve to validate the Galileo concept with both segments: space and related ground infrastructure. The satellites are carrying 2 passive Hydrogen masers and 2 RAFS each.

The IOV satellites form part of the final constellation of satellites and will be followed by additional satellite launches to reach Initial Operational Capability (IOC) by mid-decade.

At this stage, The Open Service, Search and Rescue and Public Regulated Service will be available with initial performances. A range of Galileo services will be extended as the system is built up from IOC to reach the Full Operational Capability (FOC) by this decade's end.

Two Galileo Control Centres (GCCs) have been implemented on European ground to provide for the control of the satellites and to perform the navigation mission management.

IFCS-EFTF5-C1-2

Absolute Timing Calibration of a GPS/Galileo Combined Receiver

Blair Fonville[1], Edward Powers[1]

Alexander Mudrak[2], Joerg Hahn[2], Pierluigi De Simone[2], Rigas Ioannides[2]

[1]U.S. Naval Observatory, Washington, United States
[2]Galileo Project Office, European Space Agency, Noordwijk, The Netherlands

Email: blair.fonville@usno.navy.mil

Future GNSS navigation users will benefit from multiple satellite constellations, with improved satellite visibility, reduced dilution of precision (DOP), and better multipath mitigation, among others benefits. In order to utilize multiple navigation systems, receivers must establish within themselves a common system time reference. Therefore, GPS and Galileo will broadcast GPS-to-Galileo Time Offset (GGTO), which will enhance the system interoperability.

Through GGTO Subgroup of EU-US WG-A, USNO (representing GPS) and ESA (for Galileo) have agreed on the methods to compute and coordinate the GGTO values. During the initial stages of the coordination, and throughout Galileo's IOV campaign, the different methods will provide validation to the GGTO computations, ensuring the most accurate results.

One of the techniques to be employed for GGTO determination will utilize a GPS/Galileo combined receiver. For its proper application, the receiver must be precisely calibrated to account for its internal time delays among all of the GPS and Galileo channels, which would result in errors in the GGTO computation. In September of 2012, the USNO team visited the European Space Research and Technology Centre (ESTEC) in Noordwijk, the Netherlands, to jointly conduct the initial absolute receiver calibration. Afterwards, the receiver calibration procedure has been consolidated and the final calibration has been executed in May 2013 for both USNO and ESTEC receivers (commercial off-the-shelf models).

This paper described the consolidated procedures and the results of the calibration.

IFCS-EFTF5-C1-3

Research and Compare of Timing Methods for Compass Satellite Navigation System

H. Sha[1], J.W. Zhan[1],J.H. Wang, G.Z. Zhang[1], G. Ou[1]

[1]Satellite Navigation R&D Center, National Univ. of Defense Technology, Changsha 410073, China

Email: sandhai@163.com

The timing method for the COMPASS system, its full coverage, all-weather, high precision timing, has been widely used in China's electric power, communications, finance and other industries. However, taking into account national security and economic stability, and the COMPASS system timing products must to be used in the important foundation network relationship to the national economy. Currently, the COMPASS system timing methods are including the RDSS two-way timing, RDSS one-way timing and RNSS timing, totaling three methods. There into RDSS two-way timing is active timing mode, has high timing accuracy, but the limited number of users; the RDSS one-way timing needs to be known location of the user, has lower timing accuracy; The RNSS timing can be produced the positioning and clock error data at the same time. This paper first analyzes the system composition and working principle of the three timing methods, and explores the various sources of error in timing methods. Then through the budget of the sources of error, the precision on various timing methods is drawn. Finally, it is detailed comparison of the three timing methods of performance, features, functions, summed up the direction of various timing application, and its future development prospects.

IFCS-EFTF5-C1-4

Performances of EGNOS Network Time : an update

Delporte Jérôme[1], Suard Norbert[1], Uhrich Pierre[2]

[1]CNES, French Space Agency, Toulouse, France
[2]LNE-SYRTE, Observatoire de Paris, Paris, France

Email: jerome.delporte@cnes.fr

EGNOS (European Geostationary Navigation Overlay Service) is the European Satellite Based GPS Augmentation System. It generates its own system time scale ENT (EGNOS Network Time) that is steered by EGNOS ground control segment to GPS time (GPST). The time offset between ENT and UTC is broadcast in EGNOS navigation message. To compute that offset, an EGNOS ground station was set up in Observatoire de Paris and is connected to UTC(OP), the local realization of UTC at LNE-SYRTE in Observatoire de Paris.

Applying EGNOS corrections on GPS measurements provides a precise time and navigation solution referenced to ENT. Therefore the assessment of the time difference between ENT and UTC is a key issue for time users. We previously described the EGNOS ground station in Observatoire de Paris and its connection to UTC(OP)[57] and more recently the timing performances of ENT with respect to GPST and UTC[58]. We also described a method used to validate the EGNOS Message Type #12 that contains ENT – UTC(OP). This method is using another dual-frequency GPS time receiver (OPMT) connected to UTC(OP).

In this paper, we provide an update on:

- the status of the EGNOS operational service
- the performances of ENT with respect to GPST and UTC using more than 5 years of broadcast data
- the performances of the broadcast ENT – UTC(OP) using more than 4 years of real data of OPMT receiver.

The latter provides interesting indications on the timing stability of the internal delays of both the EGNOS ground station at OP and the OPMT reception chain used for validation.

Finally, LNE-SYRTE has improved the performances of UTC(OP) since October 2012[59]. The impact for EGNOS and its time users is discussed.

[57] P. Uhrich et al., "The French Time Reference UTC(OP) and the Connection of the EGNOS Network Time", Proc. of EFTF 2005, pp. 539-544

[58] J. Delporte et al., "EGNOS Network Time and its relationships to UTC and GPS time", proc. of PTTI 2009.

[59] G.D. Rovera et al., "The new UTC(OP) based on LNE-SYRTE atomic fountains", abstract submitted to this conference.

IFCS-EFTF5-C1-5

Exponential Degrading of NTP Synchronization with Number of Network Hops

Akihiko Machizawa, Tsukasa Iwama

National Institute of Information and Communications Technology, Tokyo, Japan

Email: machi@nict.go.jp

The Network Time Protocol (NTP) is a standard for time synchronization in IP-based network. There are hundreds of public NTP servers in the world. Conventional client software select a peer / server using statistics of packet delay jitters for some manually listed servers, even though it is often said that the nearest NTP server should be used. What is "nearest"? There are two metrics for network distance[60]. One is delay time and another is hop-count. The hop-count tells the number of routers on the network path. The communication quality is degraded due to the hop-count, because most of jitters and packet losses occurred at routers. Although it is known that packet delay jitters are proportional to the square root of hop-count[61], it has not yet suggested how much degrading increasing hops affect NTP synchronization. In this article, we show the client accuracy degrading with the hop-count in a quantitative way. We also propose a nearest NTP server detection method using Round Trip Hop-counts (RTH). RTH is the total number of hops on the path from a client to a server (forward path) and the backward path.

Fig. 1 plots the standard deviation of one-way delay between our NTP server, ntp.nict.jp, and some client along the estimated RTH on a semi-log scale. The one-way delay represents the client synchronization, because it is sum of the clock offset and network delay. The accuracy of time synchronization of clients degrades exponentially with the hop-counts. An IPv4 header has a Time-to-Live (TTL) field and an IPv6 header has a Hop Limit (HL) field. Since each router subtracts one count from these fields, the hop-count can be estimated with the fields. The estimation of RTH is twice of estimated one-way hop-count from clients to the server.

The forward path and the backward path may be different. We propose TTL/HL reflecting method at servers to measure the RTH. This method copies the TTL/HL values of in-coming request packets at the servers into the field of the out-going NTP server response packets. The TTL/HL values are decreased successively through forward and backward path. The clients can select the nearest NTP server among listed servers with this method.

Selecting the nearest server will lead, (1) to improve client accuracy, (2) to reduce network traffic, and (3) to reduce power consumption. We implemented the TTL/HL reflecting function on the servers associated with ntp.nict.jp (this NTP server is a multiple IP address host).

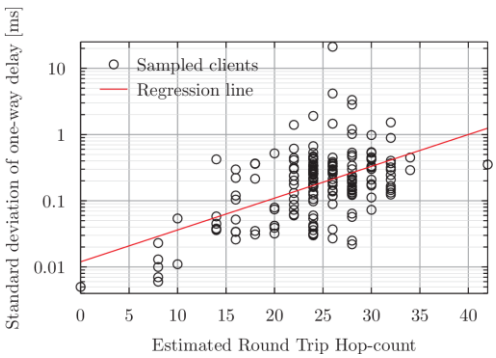

Fig. 12: Client accuracy degrading with Round Trip Hop-count. The standard deviation of one-way delay from clients to ntp.nict.jp rises exponentially with increasing of network distance (RTH).

60 V. Paxson et al. :"Framework for IP performance metrics," IETF, RFC 2330 (1998)

61 C. Barry et al. :"Synchronization in Packet Networks: Timing Metrics and Monitoring ," Proc. PTTI 2008

Emerging Sensors

CLUB D

Monday, July 22 2013, 04:30 pm - 06:00 pm

Chair: **Mauricio Pereira da Cunha**
University of Maine

IFCS-EFTF4-C2-1
Bernard Legrand[1], Marc Faucher[1], Lionel Buchaillot[1], Estelle Mairiaux[1], Benjamin Walter[1], Zhuang Xiong[1]
[1]*NAM6, IEMN CNRS, Villeneuve d'Ascq, France*

Silicon MEMS resonators: a story from signal processing devices to Atomic Force Microscopy sensors

Bernard Legrand, Marc Faucher, Lionel Buchaillot,
Estelle Mairiaux, Benjamin Walter, Zhuang Xiong

IEMN – UMR 8520 CNRS, NAM6 group, Villeneuve d'Ascq, France

Email: bernard.legrand@isen.iemn.univ-lille1.fr

Electromechanical micro-resonators (MEMS resonators) are devices that give access in the electrical domain to the properties of a mechanical resonance thanks to electromechanical transducers. They have benefited since the 1980's from surface micromachining processes compatible with silicon integrated circuit technologies. Many academic and industrial research works have been carried out especially in the field of signal processing, e.g. filters or time references, but also in the field of sensors. In particular, MEMS resonators can be used as Atomic Force Microscopy (AFM) probes, taking advantage of higher resonance frequencies and quality factors than those of standard AFM probes based on cantilevers.

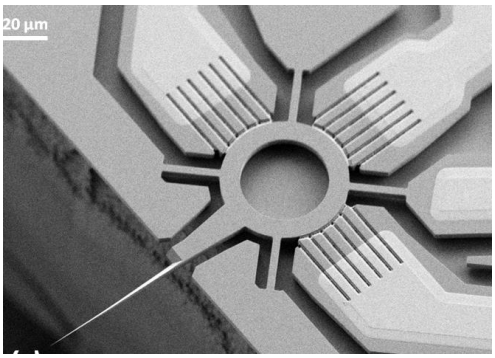

Fig. 13: Atomic Force Microscopy probe based on MEMS ring resonator. Resonance frequency is 12 MHz. Capacitive transduction is used to drive and sense the device vibration.

AFM systems have been widely used for 20 years in academic and industrial work. They give access to microscopy images at the nanoscale. Many labs are currently trying to use the oscillating mode of AFM to probe biological nanosystems and their dynamics in a liquid environment. However, AFM performances are limited by the AFM oscillator itself. It is typically made of a tip supported by a cantilever beam whose oscillating properties are drastically degraded once placed in a liquid. Our approach consists in changing the overall AFM oscillator and choosing an in-plane vibration mode in the 10-100 MHz range that reduces the hydrodynamic damping. This new generation of high sensitivity AFM force sensor is expected to be an unprecedented tool for imaging biological and chemical systems at the nanoscale and the possibility of kinetic spectroscopy in liquids.

The presentation will focus on our recent development of MEMS based AFM probes that make use of vibrating rings in the range of 10 to 20 MHz with capacitive transducers (Fig. 1). Integration of such force sensors in a commercial AFM set-up will be described as well as the imaging capabilities obtained on DNA origamis samples. Force resolution is currently in the range of a few picoNewtons.

The Optoelectronic Oscillator as an Acoustic Sensor

Olukayode Okusaga,[1] James P. Cahill,[1,2] Justin Pritchett,[1] Ryan Sorenson,[1] Weimin Zhou,[1]
Morris Berman,[1] Gary M. Carter,[2] Curtis R. Menyuk[2]

[1]U.S. Army Research Laboratory, Adelphi, MD
[2]University of Maryland: Baltimore County, Baltimore, MD

Email: olukayode.k.okusaga.civ@mail.mil

In this work, we present a novel fiber-optic acoustic sensor based on a high-*Q* optoelectronic oscillator (OEO) and a fiber delay-line interferometer. Fig. 1 shows a schematic diagram of our acoustic sensor. The OEO fiber loop acts as the transducer: converting pressure waves into phase fluctuations on the OEO's RF signal. Fiber-based sensors typically have greater dynamic range than other high-performance sensors. In addition, the low loss-per-unit-length of optical fiber allows for the use of fiber spools that over 100 m long: increasing acoustic sensitivity and range. However, optical scattering in fibers tends to distort the measured signal spectrum.[62] By detecting phase fluctuations – not on the laser carrier – but on the OEO's RF signal, we have constructed a long-fiber-loop acoustic sensor with both high sensitivity and spectral resolution.

At offset frequencies that are relevant for acoustic sensing – <1 Hz to 100 kHz – the OEO's phase noise is over 60 dB lower than that of a typical laser

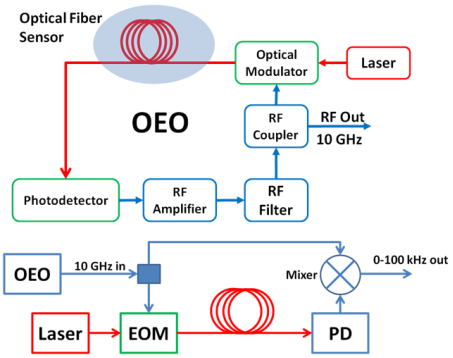

Fig. 14: A schematic diagram of our OEO-based acoustic sensor.

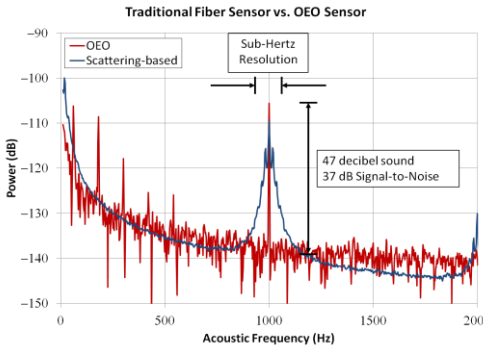

Fig. 2: Plots of the measured acoustic signal from the OEO-based and a conventional fiber sensor.

used in sensing applications. In addition, by suppressing optical scattering[63] in the OEO's fiber spool, we suppress the effects of fiber-induced noise on the detected acoustic spectrum. The result, as shown in Fig. 2, is an acoustic sensor with both high sensitivity and frequency resolution. Our OEO-based sensor can detect a 10 dBa signal with sub-Hertz resolution. In Fig. 2, we have included data measured using a conventional fiber-optic interferometer to measure the same 1 kHz acoustic source for comparison.

---

[62] O. Okusaga, J. Cahill, W. Zhou, A. Docherty, G. M. Carter, C. R. Menyuk, "Optical scattering induced noise in RF-photonic systems," *Frequency Control Symposium (FCS), 2011 IEEE International*, pp. 1–6, 2011.

[63] O. Okusaga, W. Zhou, J. Cahill, A. Docherty, C. R. Menyuk, "Fiber-induced degradation in RF-over-fiber links," *Frequency Control Symposium (FCS), 2012 IEEE International*, pp.1-5, 21-24 May 2012.

IFCS-EFTF4-C2-3

TOWARDS A SAW BASED PHONONIC CRYSTAL SENSOR PLATFORM

R. Lucklum[1], M. Zubtsov[1], M.-P. Schmidt[2], A. Oseev[1], S. Hirsch[2], Falk Hagemann[3]

[1]Institute of Micro and Sensor Systems, Otto von Guericke University Magdeburg, Germany
[2] Teprosa GmbH, Magdeburg, Germany
[3]SAW Components Dresden GmbH, Germany

Email: ralf.lucklum@ovgu.de

A sensor platform based on phononic crystals specifically attractive for biosensing will be introduced. The unique feature of this sensor concept is the determination of volumetric properties of analytes at volume as low as 1 nl and less. The sensor platform has the capability paving the way to study biomaterials directly in their physiological environment without any label.

Phononic Crystals (PnC's) belong to the group of metamaterials. These artificial materials are engineered to have properties that have not been found in nature. The typical structure consists of periodically arranged scattering centers with properties different to a homogeneous matrix. Sensors are designed in a way that the PnC offers specific mini transmission bands realized with certain defect structures. The material of interest constitutes one component of the phononic crystal, e.g., a liquid in a fluidic channel as part of the PnC[64]. Meeting the typical dimensions of microfluidic systems requires frequencies in the range of several MHz to several 100 MHz. Higher frequencies contribute to enhanced sensitivity. The key difference to acoustic or micromechanical resonators is that the resonance frequency of the PnC cavity is strongly governed by the group velocity of sound of the confined liquid or related parameters, not by properties of a sensitive film immobilized on the surface of the resonator (although this version is another way of exploiting the sensor platform).

The challenge to access higher frequencies is threefold: Devices providing good electromechanical coupling and low insertion loss at MHz frequencies, design of the PnC with appropriate band gaps, technology to realize the structure. Most appropriate for acoustic waves in the mid-MHz range are piezoelectric surface acoustic wave (SAW) devices. It has been shown previously that phononic crystal designs exist featuring a full band gap for SAW[65]. However, significant extension of the models is required to incorporate a liquid into the structure. Numerical simulations (Comsol Multiphysics) deal with finding the desired design to achieve a band gap overlapping with the transmission region of the SAW device. Unfortunately, etching technology is far less developed for piezoelectric materials compared to Si. We will present our theoretical and experimental results achieved with quartz-based wafers. Figure 1 shows exemplarily an array of etched holes as required for different SAW frequencies.

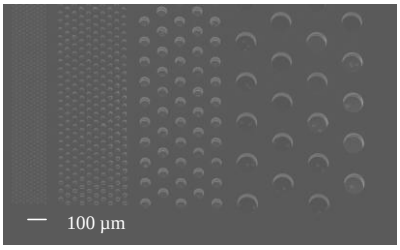

Fig. 1: SEM picture of a set of hole arrays etched into a quartz crystal.

[64] R. Lucklum, M. Ke, M. Zubtsov, Sensors Actuators B 171-172, 271-277 (2012).

[65] V. Laude, M. Wilm, S. Benchabane, A. Khelif, Phys. Rev. E 71, 036607 (2005).

Absolute phase and amplitude mapping of surface acoustic wave fields

Damien Teyssieux, Thomas Baron, Jean-Michel Friedt and Pascal Vairac

FEMTO-ST, UMR CNRS 6174, 32 Avenue de l'Observatoire, F-25044 Besançon, France

Email: damien.teyssieux@femto-st.fr

Energy confinement in acoustic transducers is a significant parameter since it is closely related to the quality factor of the device. Thus, mapping acoustic energy at the surface of bulk and surface acoustic devices is of significant interest in validating design parameters and identifying sources of energy leakage. In this context, a scanning heterodyne interferometer is presented for acoustic wave acoustic energy mapping with the measurement of the absolute phase and out-of-plane vibration amplitude in the [5-1200] MHz range. The flexible experimental setup allows for a vibration detection limit of 10 pm and the frequency range can be increased up to 4.5 GHz by only improving the photo-detector bandwidth.

We consider the acoustic energy mapping and a complementary analysis to the classical electrical S-parameters characterization since the latter is insufficient for a good acoustic phenomena comprehension. Consequently, several optical setups have been developed in order to measure the surface acoustic vibration[viviiiix]

The presented interferometer is based on a double-pass structure which presents several advantages compared with the classical structure: simplicity (fewer components) and ease of alignment. A dedicated high frequency demodulator is used in order to detect the absolute phase of the vibration, with obsolute amplitude obtained without calibration due to the heterodyne structure. The scanning speed depends on the amplitude of the vibration and can be around >50000 points per hour (for a vibration of 100 pm). Phase unwrapping demonstrates consistent slope with the expected acoustic velocity in the mirrors of a resonator and the standing wave is observed in the acoustic cavity.

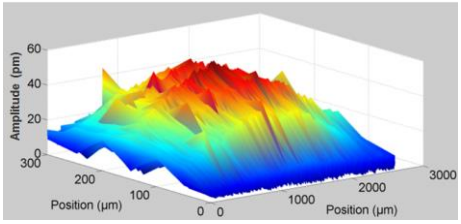

Fig. 15: Vibration amplitude (pm)

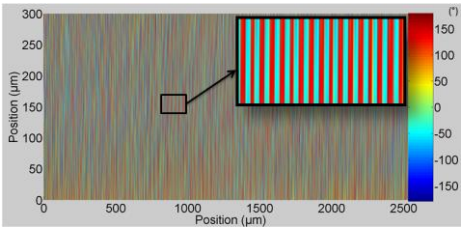

Fig. 16 : Vibration phase (°)

Acoustic energy distribution on a single-port quartz SAW operating @ 392 MHz.

IFCS-EFTF4-C2-5

Mapping Thermomechanical Vibrations and Mode Shapes in High Frequency SiC-on-Insulator Nanoscale Resonators

Jaesung Lee[1*], Zenghui Wang[1], Mehran Mehregany[1], Philip X.-L. Feng[1*]

[1]Electrical Engineering, Case Western Reserve University, Cleveland, OH 44106, USA

Email: jaesung.lee@case.edu, philip.feng@case.edu

We report on experimental demonstration of multi-mode radio-frequency nanomechanical disk resonators in a novel 500nm SiC-on-insulator (SiCOI) technology, and on measurements of directly mapping the mode shapes of the multiple resonances with high spatial resolution. By employing and engineering ultrasensitive optical interferometric techniques, we measure the lowest possible levels of vibrations, *i.e.*, the undriven thermomechanical resonances arising from the intrinsic Brownian motions, in these SiCOI disk resonators. Spatially mapping the resonant mode shapes of multi-mode nanomechanical resonators can greatly facilitate understanding and harnessing these multiple modes for sensing and frequency control applications.

Our resonant devices (500nm-thick poly-SiC disks anchored on SiO_2 center pedestals) feature a uniform optical cavity (depth=500nm) with the underneath Si substrate. We use an optical interferometer with fm/Hz$^{1/2}$-level displacement sensitivity[66,67,] to transduce the thermomechanical motion of the device into electrical signals. The ~1μm laser spot enables spatially mapping the different resonance modes.

Figure 1 shows measured noise spectral density of five mechanical resonance modes. The peak amplitude of the mode strongly depends on the laser spot position (see insets). In the center of the disk (position (a)), no measurable motion signal is observed. In the positions (b) and (c), we detect 5 and 4 resonance modes, respectively. Measured resonance frequencies and spatial maps of the mode shapes (center row insets) agree very well with COMSOL simulation results (bottom row insets). We also observe interesting effects such as the off-center position of the pedestal lifting the frequency degeneracy between the first two modes and breaking the azimuthal symmetry in the mode shape of the third resonance mode, as well as electronically tuning the resonances, which we will report in detail in the full paper.

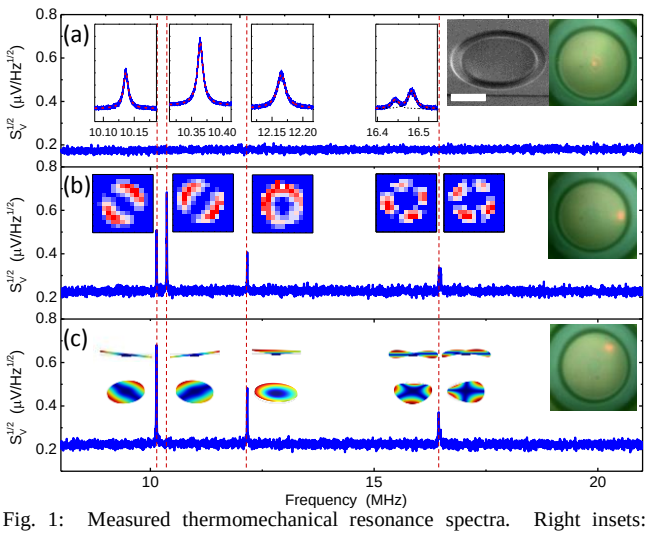

Fig. 1: Measured thermomechanical resonance spectra. Right insets: optical images showing the exact actual positions of the laser spot. Top insets: plots of resonances with fit (same *y* axis and scale as in main plots). Middle insets: spatial intensity map for each mode. Bottom insets: COMSOL simulation of the mode shapes. Top right: SEM image (scale

[66] W. K. Hiebert, D. Vick, V. Sauer, M. R. Freeman, *J. Micromech. Microeng.* **20**, 115038 (2010).
[67] J. Lee, P. X.-L. Feng, *Proc. IEEE Inter. Freq. Contr. Symp. (IFCS2012)*, DOI: 10.1109/FCS.2012.6243742.

Optical Combs I

CLUB H

Monday, July 22 2013, 04:30 pm - 06:00 pm

Chair: **Jason Jones**
University of Arizona

IFCS-EFTF6-C3-1
Tobias Kippenberg[1]
[1]*EPFL, Switzerland*

Soliton mode-locking in optical microresonators

T. Herr[1], V. Brasch[1], J.D. Jost[1], C.Y. Wang[1], N.M. Kondratiev[2], M.L. Gorodetsky[2], T.J. Kippenberg[1,3]
[1]*École Polytechnique Fédérale de Lausanne (EPFL), 1015 Lausanne, Switzerland*
[2]*Faculty of Physics, Moscow State University, Moscow 119991, Russia*
[3]*Max-Planck-Institut für Quantenoptik, 85748 Garching, Germany*

Abstract: We demonstrate soliton mode-locking in continuously pumped, non-linear optical MgF_2 microresonators, resulting in low noise frequency comb spectra and ultra-short pulses of 200 fs duration with a repetition rate of 35.2 GHz.
OCIS codes: (140.3945) Microcavities; (190.4380) Nonlinear optics, four-wave mixing; (060.5530) Pulse propagation and temporal solitons; (140.4050) mode-locked lasers; (140.7090) Ultrafast lasers; (190.7110) Ultrafast nonlinear optics

The discovery of passive mode-locking via saturable absorbers has led to optical femto-second pulses with applications ranging from eye-surgery to the analysis of chemical reactions on ultra-short timescales. In the frequency domain a train of such optical pulses corresponds to a frequency comb (equidistant optical laser lines spaced by the pulse repetition rate), which finds use in precision spectroscopy and optical frequency metrology. Not relying on mode-locking, and without the formation of pulses, frequency combs can also be generated in continuously driven, high quality-factor, Kerr-nonlinear optical microresonators via cascaded four-wave mixing. Applying a pulse-shaping mode-locking mechanism to such microresonator based frequency combs could enable compact and robust femto-second pulse generators. However, saturable absorbers are challenging to apply to microresonators as they affect the high quality factor essential to nonlinear frequency conversion.

Here, we demonstrate passive mode-locking of a microresonators comb via soliton formation without saturable absorber. Indeed solitons are stable and attractive states of the system and a saturable absorber, as required for stability in soliton mode-locked lasers, is not necessary. The formation of solitons is enabled by the balance between anomalous resonator dispersion and Kerr-nonlinearity. The employed crystalline MgF_2 resonator, has a coupled resonance width of 450 kHz and a free-spectral range of 35.2 GHz. Frequency combs can be generated when coupling a continuous wave pump laser (10-100 mW, 1553 nm) to the resonator via a tapered fiber. The transitions to and between different soliton mode-locked states manifest themselves as discrete steps in the transmission signal when scanning the pump laser over a resonance. These steps deviate markedly from the expected triangular, non-linear resonance shape (cf. Fig. 1b). Each step corresponds to a change of state, namely the number of solitons propagating inside the resonator. When tuning the pump laser into a soliton mode-locked state, we observe the generation of pulses with 200 fs duration (detected by frequency resolved optical gating, FROG). The generated optical spectra are low noise as evidenced by the narrow repetition rate beatnote at a frequency of 35.2 GHz. In the single soliton case the frequency comb spectrum shows very little line-to-line power variation, as required for broadband telecom and spectroscopy applications. Numerical simulations based on coupled, non-linear mode equations reproduce the step features and the formation of multiple and single cavity solitons. These simulations are also in excellent agreement with an analytical model of solitons on a weak continuous wave background. In addition, we verify that the solitons in the microresonator can be analytically described by the solutions of the driven, damped non-linear Schroedinger equation.

The presented results open the route towards compact microresonator based femto-second sources, where the parametric gain in principle gives access to pulse center wavelength that are difficult to access using conventional mode-locked lasers, such as the mid-infrared. Our observations apply equally to other microresonator comb platforms. In this context, we note that independent research has very

recently reported on femto-second pulse generation and mode-locking in Si_3N_4 microresonators. The smooth optical soliton spectra are essential for frequency domain applications such as channel generators in advanced telecommunication or in fundamental studies such as astrophysical spectrometer calibration. Moreover, femto-second pulses in conjunction with external broadening provide a viable route to a microresonator based RF-to-optical links.

Low-noise 1-micron optical frequency comb based on diode-pumped solid-state laser technology

S. Kundermann, Erwin Portuondo-Campa, Jonathan Bennès, Steve Lecomte

Time & Frequency, Centre Suisse d'Electronique et de Microtechnique, Neuchâtel, Switzerland

Email: steve.lecomte@csem.ch

Optical frequency combs (OFCs) have revolutionized the way optical frequency metrology can be done since more than 10 years and are a key component in optical atomic clocks. Initially demonstrated with Ti:Sapphire lasers, optical frequency combs have been generated with several other laser technologies. Fiber laser technology at wavelengths of 1 micron and 1.55 microns has been the object of many efforts for improving their performances and in particular the noise properties. OFCs based on passively mode-locked diode-pumped solid-state lasers (DPSSLs) have been less studied while offering excellent prospects for low-noise high-performance operation due to the low-loss low-gain laser configuration. A 1.55-microns DPSSL has been self-referenced and characterized in Ref. [68] while in Ref. [69] a self-referenced 1-micron Yb:KYW has demonstrated state-of-the-art low phase-noise microwave generation. Here we present a passively mode-locked diode-pumped Yb:glass laser that has been self-referenced.

The laser is mode-locked via a saturable absorber mirror and delivers 111 fs transform limited soliton pulses with an average output power of 205 mW at a repetition rate of 100 MHz. After propagation in a highly nonlinear optical fiber, the laser pulses generate an octave spanning supercontinuum amounting 110 mW of average power which is then sent into an f-2f Michelson interferometer for carrier-envelope offset frequency (f_0) detection. No external optical amplifier is needed. A signal-to-noise ratio of up to 40 dB for f_0 (at an instrument resolution bandwidth of 91 kHz) has been detected. Using standard locking electronics and feedback to the pump diode injection current, f_0 was phase locked to an H-maser referenced microwave synthesizer. The in-loop integrated phase noise amounts 736 mrad when integrated from 1 Hz to 1 MHz for a measured f_0 frequency of 274 MHz (see Fig. 1). The achieved integrated phase noise is comparable to the best fiber lasers. The f_0 phase-locking is very robust and lasts for days. The relative intensity noise (RIN) of the laser has been measured. For a free-running laser, at offset frequencies above the laser pump modulation bandwidth (100 kHz), shot-noise limited RIN is achieved with a level of -154 dBc/Hz.

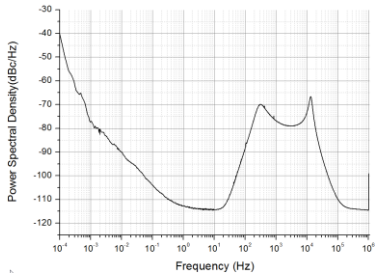

Fig. 17: Phase-noise power spectrum density of the divided by 16 274-MHz carrier-envelope offset frequency

In conclusion we have demonstrated a robust and low-noise self-referenced passively mode-locked diode-pumped Yb:glass solid-state laser. The authors would like to thank the Canton de Neuchâtel for financial support and Scott Diddams and Stephanie Meyer for helpful discussions.

[68] S. Schilt et al., "Fully stabilized optical frequency comb with sub-radian CEO phase noise from a SESAM-modelocked 1.5-μm solid-state laser" Opt. Expr. Vol. 24, p. 2471-24181, 2011

[69] S. Meyer, T. M. Fortier, S. Lecomte, S. A. Diddams, "A frequency-stabilized Yb :KYW femtosecond laser frequency comb and its application to low-phase noise microwave generation", submitted to Appl. Phys. B

IFCS-EFTF6-C3-3

Terahertz activities based on an optical frequency comb

Motohiro Kumagai, Shigeo Nagano, Hiroyuki Ito, Masatoshi Kajita, Yuko Hanado

Space-time Standards Laboratory
National Institute of Information and Communications Technology (NICT), Tokyo, JAPAN

Email: mkumagai@nict.go.jp

Research at Terahertz (THz) frequencies is very active in applications such as material analysis, wireless communication, remote sensing, and biological imaging. However, no accurate frequency standard exists in THz region. This has led NICT start research to establish a new frequency standard in the THz region.

Firstly we address the absolute frequency measurement of a THz frequency continuous wave (CW.) Our measurement system is based on a femto-second (fs) pulse fiber laser comb and a photoconductive antenna (PCA). Pulsed light from the fs fiber laser is focused onto the antenna gap of the PCA. In the antenna, a time-varying photocarrier is created and its Fourier expansion forms a comb structure. The comb structure mode extends to THz region, resulting in the generation of frequency grids in the THz region, which we call "THz comb". By mixing the THz comb and the CW-THz, an absolute frequency measurement is possible. In a measurement of a 300GHz wave, we have confirmed that the measurement system has a fractional instability at the 10^{-16} level at averaging time of over 1000 seconds. The present resolution is limited by the electronic noise of the current-to-voltage conversion amplifier used at the output of the PCA. The photocarrier THz comb can be used for not only microwave-to-THz conversion but also THz-to-microwave conversion. We have demonstrated a generation of low-phase-noise microwave signal synthesized from a 0.3 THz radiation. The phase information of the 0.3 THz signal was copied to the 1GHz signal without degradation. This technique potentially transfers the phase information of THz radiation into accessible microwave region.

THz CW generation by photomixing of two optical lasers whose frequencies have a THz-level separation is capable of providing an accurate frequency reference. One candidate for such a technique is the use of two optical modes of a mode-locked laser whose repetition frequency is well-stabilized. However, it is difficult to extract only two modes from the mode-locked laser with a conventional optical bandpass filter (a bandwidth of about 10 GHz) because the repetition frequency of the laser is normally less than 1GHz. By applying ultra-narrow optical filtering based on stimulated Brillouin scattering to the fs fiber comb we have successfully extracted only two optical modes and generated a highly accurate and high contrast 100GHz wave using an uni-travelling carrier photo detector.

IFCS-EFTF6-C3-4

Robust, frequency-stable and accurate mid-IR laser spectrometer based on frequency comb metrology of quantum cascade lasers up-converted in orientation-patterned GaAs

S. Schiller[1], M. Hansen[1], I. Ernsting[1], S. Vasilyev[1], A. Nevsky[1]

A. Grisard[2], E. Lallier[2], B. Gerard[2]

[1] Heinrich-Heine-Universität Düsseldorf, Germany

[2] Thales Research and Technology / III-V Lab, Campus Polytech., 91767 Palaiseau, France

Email: step.schiller@uni-duesseldorf.de

The mid-infrared spectral range (12 µm > λ > 4.5 µm) is of interest in both applied and fundamental spectroscopy. Approaches pursued for enabling mid-IR spectroscopy are based on generating the desired radiation by down-conversion, either of frequency combs or of cw near-IR sources. Such downconverted sources, however, typically have low spectral power density. Upconversion of the mid-IR radiation to the near-IR range provides a way to take advantage of the frequency measurement capabilities of the standard Erbium-fiber frequency comb. In this work we present a simple and robust solution applicable to the whole mid-IR spectral range, based on the use of quantum cascade lasers (QCL) as the source of spectroscopic radiation.

Orientation-patterned gallium arsenide is used as the nonlinear material to generate the sum-frequency wave of a QCL with a standard high-power cw Erbium fiber laser. The sum-frequency wave is further amplified by a semiconductor amplifier. Continuous measurements of this wave's and the fiber laser's frequency by a standard Erbium fiber frequency comb provide sinals allowing frequency control of the MIR laser. The proof of principle is performed with a quantum cascade laser at 5.4 µm, which is upconverted to 1.2 µm. Both the QCL and the cw fiber laser are stabilized to the frequency comb using feedback control. At the same time, the absolute QCL frequency is determined relative to an atomic frequency reference. We achieved a frequency instability at the sub-10 kHz-level and also long-term stability and controlled frequency tuning.

With its current performance and its ease of use, this type of spectrometer could be used e.g. for photoacoustic spectroscopy, multipass-cell spectroscopy, integrated cavity output spectroscopy, or Lamb-dip spectroscopy.

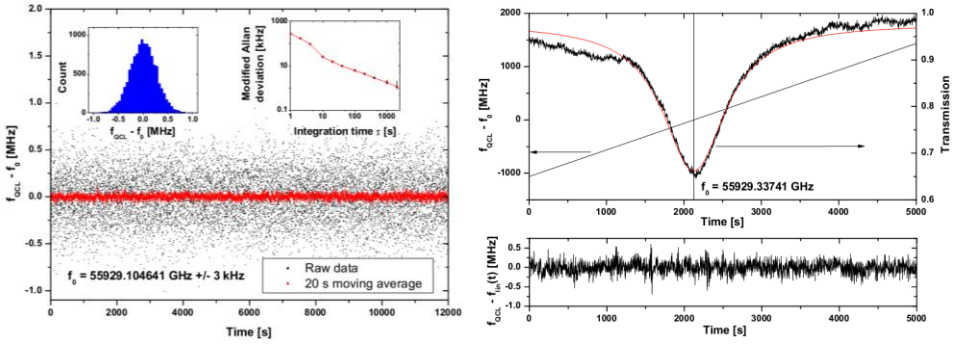

Fig. 1 Left: Long-term frequency stability of the QCL. Right: Spectrometer frequency scan over a range of 2.5 GHz, performed by scanning the repetition rate of the frequency comb. An absorption line of N_2O was recorded simultaneously. Bottom: QCL frequency linear fit residuals.

IFCS-EFTF6-C3-5

Long distance phase-coherent link between near- and mid-infrared frequencies

B. Argence[1], B. Chanteau[1], O. Lopez[1], D. Nicolodi[2], G. Santarelli[2,3], C. Chardonnet[1], C. Daussy[1], B. Darquié[1], Y. Le Coq[2], A. Amy-Klein[1]

[1]Laboratoire de Physique des Lasers, Université Paris 13, Sorbonne Paris Cité, CNRS, Villetaneuse, France

[2]LNE-SYRTE, Observatoire de Paris, CNRS, UPMC, Paris, France

[3]Laboratoire Photonique, Numérique et Nanosciences, Université de Bordeaux 1, Institut d'Optique and CNRS, Talence, France

Email: berengere.argence@univ-paris13.fr

Ultra-high-resolution spectroscopy enables to test fundamental physics with molecules as for instance the non conservation of parity[70] or the stability of the electron-to-proton mass ratio[71]. However many of these tests rely on the availability of ultrastable and accurate laser sources emitting in the mid-infrared (IR) where molecules exhibit rovibrational transitions. It is thus very challenging to develop a frequency stabilization scheme in the mid-IR with performance similar to the visible and near-infrared domain.

For that purpose, we have built a frequency chain which enables to transfer coherently the stability and accuracy of an ultrastable laser emitting at 1.54 µm to the mid-IR spectral region (Fig. 1). This ultrastable signal is generated at LNE-SYRTE where its frequency is measured against a set of primary standards using an optical frequency comb. It is transferred from LNE-SYRTE to LPL through an optical link[72]. A second optical frequency comb is phase-locked to this signal and, using sum-frequency generation in a non-linear crystal[73], the mid-IR frequency is compared to a high-harmonic of the comb repetition rate.

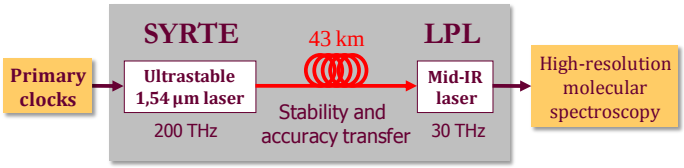

Fig. 18: Principle of the mid-IR frequency stabilization

With this set-up, we stabilized a CO_2 laser and obtained a relative frequency stability at the state-of-the art[74]. We are now progressing towards the extension of this stabilization scheme to Quantum Cascade Lasers.

[70] B. Darquié et al, "Progress toward a first observation of parity violation in chiral molecules by high-resolution laser spectroscopy", Chirality, vol. 22, pp. 870-884, 2010.
[71] A. Shelkovnikov et al, "Stability of the Proton-to-Electron mass ratio", Phys. Rev. Lett., vol. 100, p. 150801-150803, 2008.
[72] O. Lopez et al., "Cascaded multiplexed optical link on a telecommunication network for frequency dissemination," Opt. Expr., vol. 18, p. 16849-16857, 2010.
[73] A. Amy-Klein et al, "Absolute frequency measurement of an SF6 two-photon line using a femtosecond optical comb and sum-frequency generation", Opt. Lett., vol. 30, p. 3320-3322, 2005.
[74] V. Bernard et al, "CO_2 laser stabilization to 0.1-Hz level using external electrooptic modulation", IEEE J. of Quant. Electr., vol. 33, pp. 1282-1287, 1997.

IFCS-EFTF Group 1 poster session 1

Forum Hall

Monday & Tuesday, July 22-23, 2013, 01:00 pm - 02:00 pm and 3:30 pm - 4:30 pm

Chair: **Derek Puccio**
Quartzdyne

IFCS-EFTF1-PAB1-1

Improving frequency Control of Temperature Compensated Surface Acoustic Wave Devices

Sergey Mishin
Advanced Modular Systems, Inc
Goleta, CA/USA
smishin@amssb.com

Michael Gutkin
Advanced Modular Systems, Inc
Goleta, CA/USA
mgutkin@amssb.com

A. Bizyukov
School of Physics and Technologies
Karazin Kharkiv National University. Kharkiv, Ukraine

Vladimir Sleptsov
Moscow State Aviation Technological University
Moscow, Russia

Abstract— In this paper, we demonstrated improvement of frequency uniformity for Temperature Compensated Surface Acoustic Wave (SAW) devices. SiO_2 has been used to obtain low Temperature Coefficient (TempCo) in SAW devices for more than three decades [1]. One of the big issues is that SAW devices have to be processed at temperatures below 300C. When low temperature SiO_2 is exposed to the ambient environment, it interacts with ambient humidity [2], [3], [5], [6]. Such interactions can change frequency of the SAW devices and can make frequency trimming with a focused Ion Beam [7], [8] extremely challenging. UV and steam treatment of SiO_2 improved trimming rate stability on the first trimming [4] and [9], but was not sufficient to provide tight frequency control required for SAW devices after the second trimming. Using silicon nitride (Si_3N_4) capping layer on top of SiO_2 showed some improvement in frequency control after trimming process. Most improvement was obtained using aluminum nitride (AlN) capping layer on top of SiO_2 followed by two trimming steps.

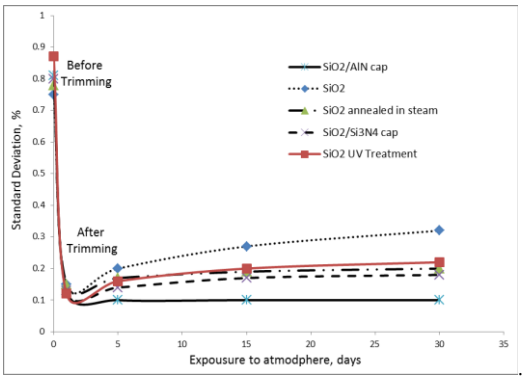

Figure 2. Cross wafer Frequency variation as a function of time exposure to atmosphere for different methods of SiO_2 treatments and capping processes

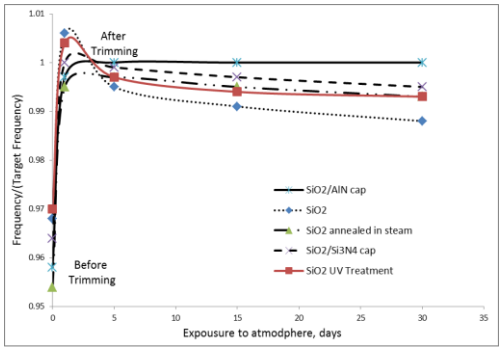

Figure 1. Average Frequency as a function of time exposure to atmosphere for different methods of SiO_2 treatments and capping processes

REFERENCES

[1] Willingham, C.B., et.al., "Temperature Compensated Surface Wave Devices", United States Patent #3965444I. S. Jacobs and C. P. Bean, "Fine particles, thin films and exchange anisotropy," in Magnetism, vol. III, G. T. Rado and H. Suhl, Eds. New York: Academic, 1963, pp. 271–350.

[2] H.A.Naseem, et.al., "Stress and bonding characterization of PECVD silicon dioxide films",Electrochemical Society, Vol.97-10, pp.217-226,4-9 May,1997

[3] Leplan H., "Ressidual stresses in evaporated silicon dioxide thin films: Correlation with deposition parameters and aging behavior", Journal of Applied Physics, pp.962-968, 1995

[4] M.S. Haque, et.al., "Post-deposition processing of low temperature PECVD silicon dioxide films for enhanced stress stability", Thin Solid Films, Volumes 308-309, 1997, pp. 68-73

[5] Leplan H., "Kinetics of residual stress evolution in evaporated silicon dioxide films exposed to room air", Journal of Applied Physics, pp.6926-6931, 1996

[6] Parada E. G., "Aging of photochemical vapor deposited silicon oxide thin films", Journal of Vacuum Science &Technology, Volume 14, pp.436-440

[7] Quiang Zou, et.al., "High Coupling Coefficient Temperature Compensated FBAR Rsonator for Oscillator Apllication with wide Pulling Range", 2010 IEEE International Frequency Control Symposium, pp. 646-650

[8] S. Mishin, "Improving Manufacturability of Bulk Acoustic Wave and Surface Acoustic Wave Devices", SPAWDA 2011, IEEE

[9] S. Mishin, et.al., "Production Issues in Using Silicon Dioxide Films for Temperature Compensated Bulk and Surface Acoustic Wave Devices", 2012 IEEE International Frequency Control Symposium

IFCS-EFTF1-PAB1-2

Investigation of the electrode coating influence on the frequency temperature characteristics of the resonators operating at the rotated Y-cut $Ca_3TaGa_3Si_2O_{14}$ single crystals

Andrey Medvedev, Aleksey Zabelin, Svetlana Bazalevskaya, Oleg Buzanov, Sergey Sakharov

OAO «Fomos - Materials», Moscow, Russia

medvedev@newpiezo.com

[INTRODUCTION] More stringent requirements for temperature stability of piezoelectric devices have encouraged the development of new materials for use in resonators and filters operating on bulk acoustic waves. $Ca_3TaGa_3Si_2O_{14}$ (CTGS) single crystal is of special interest. CTGS has small frequency deviation in the temperature range (temperature frequency coefficient of the second order ($TFC^{(2)}$) is about −0.026 ppm/($°C^{-2}$) [1], −0.039 ppm/($°C^{-2}$) [2]). In this work, the influence of electrode materials and sizes on frequency temperature characteristics of CTGS resonators operating at TS-mode was investigated.

[EXPERIMENTAL] Piezoelectric resonators were made from CTGS crystals grown by CZ method. The plates of six cuts (YZw)–25°, (YZw)–22°20', (YZw)–21°20', (YZw)–21°, (YZw)–20°30', (YZw)–20° were produced. The fundamental frequency of TS-mode was about 10.8 kHz. Electrodes of different sizes and from diverse metals (Al, Ag and Au) were deposited. The thickness of the electrodes was 200 um. The measurements of the temperature frequency characteristics were performed in the S&A W2200B Temperature Test System. The attenuation characteristics of the CTGS resonators were measured using Agilent E5061A specter analyzer.

[RESULTS AND DISCUSSION] The frequency temperature characteristic of the CTGS resonators operating at rotated Y- cuts is represented by a parabola. The dependences of turnover temperature as functions of angle cuts for different diameters of Ag electrodes are given in fig.1. $TFC^{(2)}$ for −21°20' angle cut is −0.022 ppm/ ($°C^{-2}$). Also, for this angle, the ratio of the electrode diameter to the plate thickness (Bechmann's number) has been obtained (fig.2) below which there is only one discrete eigenmode. The investigation results of the frequency temperature and amplitude frequency characteristics of CTGS resonators with Al and Au electrodes will be shown at the conference.

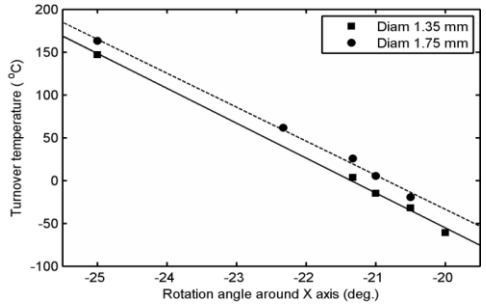

Fig. 1: Turnover temperature vs. rotation angle for Ag electrodes.

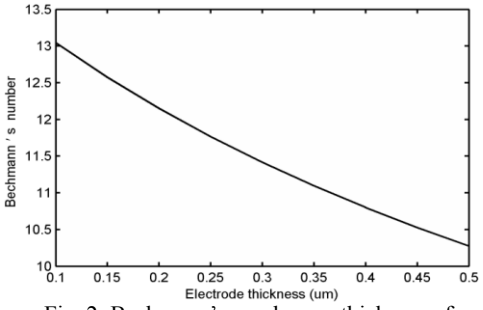

Fig. 2: Bechmann's number vs. thickness of Ag electrodes.

[1] Shen Jen *et al.*:2002 IEEE Int. Freq. Con. Symp., p.307-310
[2] Fapeng Yu *et al.*:J. Appl. Phys. 109,114103 (2011)

IFCS-EFTF1-PAB1-3

IR-reflectance assessment of the tilt angle of AlN-wurtzite films for shear mode resonators

Jimena Olivares[1], Mario de Miguel-Ramos[1], Enrique Iborra[1], Marta Clement[1], Milena Moreira[2], Ilia Katardjiev[2]

[1]GMME-CEMDATIC-ETSIT, Universidad Politécnica de Madrid, Madrid, Spain
[2]Department of Solid State Electronics, Uppsala University, Uppsala, Sweden

Email: eiborra@etsit.upm.es

Shear mode resonators are becoming increasingly interesting as biochemical sensors due to their capacity to operate in liquid media. Previous studies show that, unlike longitudinal mode resonators, the quality factor and the electromechanical coupling factor of shear resonators do not diminish as much when operating in liquid media. Transverse electric fields can excite shear modes in AlN films exhibiting a nonzero c-axis mean tilt with respect to the normal through the component of the field normal to the c-axis and the piezoelectric coefficient d_{15}. Assessment of the c-axis tilt of AlN microcrystals is usually performed by x-ray diffraction, by scanning the ψ axis when θ is fixed at the value of the (00·2) direction. However, such a measurement is time-consuming and difficult to implement in-line. Infrared characterization is a fast and reliable alternative to XRD. In this communication we assess the angle between the c-axis of AlN microcrystals and the substrate surface by evaluating the wavenumber of the longitudinal optical (LO) vibrational mode absorption band obtained from the IR reflectance spectrum of the film surface.

AlN films with tilted grains were deposited by off-axis sputtering of an target in Ar/N_2 mixtures on oxidized wafers covered with a metallic layer. θ/2θ patterns and the dispersion in the of the (00·2) AlN reflection were measured along the wafer in several positions. Infrared reflectance spectra provided the local thickness of the AlN and the structure of the A1-E1 combined absorption LO mode, which related to the tilt of the c-axis of AlN figure). Bow measurements done by profilometry gave the local in-plane Atomic force microscopy was used to the surface topography of the films.

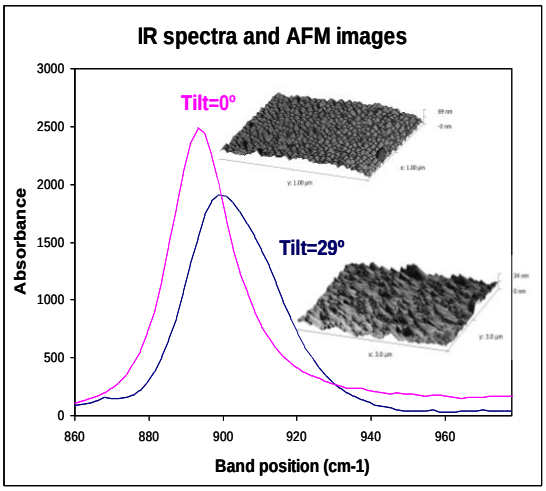

Al silicon XRD ψ axis film is (see stress. assess

The tilt angle of the c-axis oriented AlN microcrystals measured by XRD varied from 0° at the center of a 100 mm-wafer to 34° at its edge. This was correlated with the position of the band of A1-E1 mixed LO mode, which was shifted towards greater wavelengths as the tilt angle increased. The influence of stress on the position of the IR band was negligible compared to the shift associated to the increasing tilt of the grains. IR reflectance measurements offer a straightforward non-destructive diagnostic method for the assessment of tilted grains in AlN films.

IFCS-EFTF1-PAB1-4

Measurement of independent piezoelectric constants of a lanthanumgallium silicate family crystals by x-ray diffraction method

Buzanov Oleg[1], Irzhak Dmitrii[2], Roshchupkin Dmitry[2]

[1]OAO Fomos materials, Moscow, Russsia
[2]Institute of Microelectronics Technology and High-Purity Materials RAS, Chernogolovka, Russia

Email: irzhak@iptm.ru

This work presents results of measurements of piezoelectric tensor components for a lanthanum gallosilicate family crystals with x-ray diffraction technique using. For crystal of this family (point group 32, space group *P*321) the piezomodulus tensor has only two independent components d_{11} and d_{14}.

The method used to measure piezoelectric constants of the studied material is based on the phenomenon of reverse piezoelectric effect. The effect consists in that a piezoelectric crystal undergoes deformation when external electric field is applied to it. In certain crystallographic directions, the applied external electric field would cause compression or tension of the crystal lattice (diagonal components of the deformation tensor). It should be noted that diagonal components of deformation tensor are nothing short of the interplanar spacing changing in corresponding direction. Changes of the interplanar spacing in the crystal can be measured by x-ray diffractometry through following the changes of the Bragg peak position. Experimental rocking curves demonstrated this phenomenon are shown on Fig. 1.

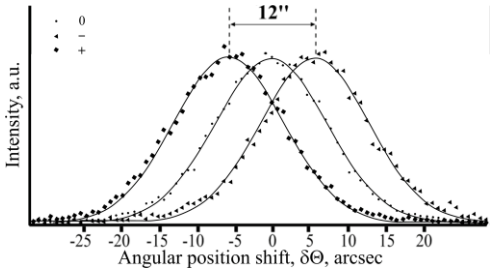

Fig. 19: Rocking curves measured on (440) reflection of calcium-tantalum gallosilicate crystal under applied voltage: “+” +1900 V, “-” -1900 V, “0” 0 V.

It should be noted that single-crystal X-cut plate is sufficient for the measurement of both piezoelectric constants d_{11} and d_{14}. In this case reflection and transmission geometries of Bragg diffraction should be used.

IFCS-EFTF1-PAB1-5

Method of controlling coupling coefficient in sputtered Aluminum Scandium Nitride for high volume production.

Sergey Mishin[1], Michael Gutkin[1], Alexander Bizyukov[2] , Vladimir Sleptsov[3]

[1] Advanced Modular Systems, Inc, Goleta, CA/USA, smishin@amssb.com

[2] Karazin Kharkiv National University, Kharkiv, Ukraine

[3] Moscow State Aviation Technological University Moscow, Russia

Email: smishin@amssb.com; mgutkin@amssb.com

Abstract— In this paper, we studied the effect of stress of Aluminum Nitride film containing various concentrations of Scandium (Sc). Coupling coefficient (kt2) was measured across wafer and wafer to wafer as a function of stress and Sc content of the film. Previous studies demonstrate a considerable increase in kt2 as a function of Sc content of the film [1], [2], [4], [5]. Unfortunately, when deposited on 200mm wafers we observed that kt2 varies significantly more than that of standard Aluminum Nitride (AlN). Both stress and concentration of Sc must be controlled across a wafer to achieve uniform kt2 acceptable for production of Bulk Acoustic Resonator (BAW) devices [3], [6], [7]. We were able to control kt2 across a wafer and wafer-to-wafer by adjusting magnetic fields in our magnetron as well as adjusting concentration of Sc in our two sputtering targets.

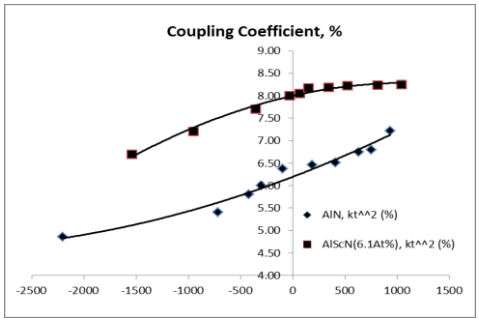

Figure 1. Variation of kt2 as a function of stress for AlN and AlScN films

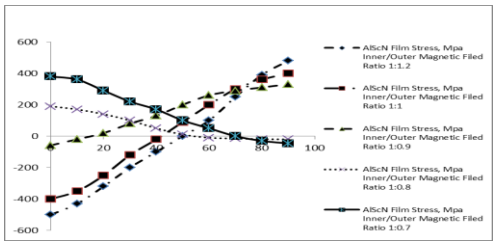

Figure 2. Stress variation across a wafer as a function of the ratio of inner and outer target magnetic field

REFERENCES

[1]Milena Moeira, et.al., "Aluminum scandium nitride thin-film bulk acoustic resonators for wide band applications", Vacuum, July 2011, Issue 1, pp. 23-26

[2]Morito Akiyama, "Influence of temperature and scandium concentration on piezoelectic response of scandium aluminum nitride alloy thin films", Applied Physics Letters, Oct. 2009, Vol.95, Iss. 16, pp. 2107-2107-3

[3]H.P.Lobl, et.al.. "Piezoelectric materials for BAW resonator and filters", 2001 IEEE International Ultrasonics Symposium, Atlanta, GA, Oct. 7-10,pp.807-811.

[4]Pau Muralt, et.al.. "Electromechanical properties of AlScN thin films evaluated at 2.5 GJz film bulk acoustic resonators", Applied Physics Letters 99, 2011

[5]Keiichi Umeda1, et.al.. "Piezolecetric properties of ScAlN thin films for piezo-MEMS devices", MEMS 2013, Taipei, Taiwan, January 20 – 24, 2013

IFCS-EFTF1-PAB1-6

High temperature perovskite-structured $BiFeO_3$-$PbTiO_3$-$Bi(Zn_{1/2}Ti_{1/2})O_3$ piezoelectric ceramics

Jian Yu and Xianbo Hou

Functional Materials Research Laboratory, Tongji University, Shanghai 200092, China

Email: jyu@tongji.edu.cn

High temperature and high performance ferroelectric piezoelectric ceramics are striking strongly for emerging high temperature applications of piezoelectric filters, sensors and actuators. Lead Zirconate-Titanate (PZT) near the morphotropic phase boundary (MPB) dominates commercial piezoceramics but has relatively low Curie temperature (T_C) below 386°C. The $BiFeO_3$-$PbTiO_3$ (BF-PT) system was reported to have T_C ~ 632°C at its coexistent phase boundary (CPB) with around 32 at.% $PbTiO_3$ content. Nevertheless, poor mechanical and insulating properties limit their piezoelectric characterizations and applications in the form of ceramics.

In this presentation, the authors demonstrated experimentally that adding $Bi(Zn_{1/2}Ti_{1/2})O_3$ (BZT) into $BiFeO_3$-$PbTiO_3$ system makes their ceramics mechanically robust, owing to reduced negative thermal expansion coefficient. Perovskite-structured BF-PT-BZT ternary solid solution keeps the CPB feature but T_C increases up to about 700°C. Systematical investigations showed that the CPB position, T_C and piezoelectric properties of BF-PT-BZT are closely dependent on the ceramic grain size, resulting from different processing and thermal treatments. A maximum piezoelectric property of T_C = 560°C, d_{33} = 30 pC/N, $\varepsilon_{33}^T/\varepsilon_0$ = 302, and $\tan\delta$ = 0.02 was obtained here for the CPB 0.53BF-0.32PT-0.15BZT ceramics with average grain size about 0.3μm, which is better than that of commercial K-15 piezoceramics: T_C ~ 610°C, d_{33} = 18 pC/N, $\varepsilon_{33}^T/\varepsilon_0$ = 140, and $\tan\delta$ ~ 0.03.

The La substitution effect on the lattice structure and piezoelectric properties of tetragonal 0.50BF-0.35PT-0.15BZT ceramics was also studied. It was observed that the tetragonality of *c/a* ratio and T_C decrease but the piezoelectric properties increase with increasing La substitution. The enhanced piezoelectric performance with La substitution was preferably attributed to the structural phase transition from tetragonal into coexistent tetragonal and rhombohedral. For the CPB $Pb_{0.35}Bi_{0.625}La_{0.025}(Ti_{0.425}Zn_{0.075}Fe_{0.5})O_3$ ceramics poled at 140°C with 5 kV/mm DC electric field, a good piezoelectric property of T_C = 497°C, $\varepsilon_{33}^T/\varepsilon_0$ = 367 and d_{33} = 43 pC/N was obtained, which is comparable with the commercial MLT piezoceramics with T_C = 495°C, $\varepsilon_{33}^T/\varepsilon_0$ = 170 and d_{33} = 51 pC/N.

Our experimental studies demonstrate that BF-PT-BZT ceramics exhibit not only good high temperature piezoelectric properties but also better mechanical properties. In contrast to MLT and K-15 commercial piezoceramics, BLF-PT-BZT provides a big space like the PZT to adjust piezoelectric performance and temperature stabilities by changing composition near the CPB for applications of high temperature filters and sensors. Our essay is anticipated to excite new designs of high temperature and high performance perovskite-structured ferroelectric piezoceramics and extend their application fields of piezoelectric transducers and sensors.

IFCS-EFTF1-PAB1-7

Optimization of tether geometry to achieve low anchor loss in Lamé mode resonators

Vikram Thakar[1] and Mina Rais-Zadeh[1, 2]

[1] Department of Mechanical Engineering, University of Michigan, Ann Arbor, USA
[2]Department of Electrical Engineering, University of Michigan, Ann Arbor, USA

Email: thakar@umich.edu

The quality factor (*Q*) of micromachined resonators in the sub-GHz regime is most often limited by the anchor loss (design dependent) rather than the fundamental material limitations[1]. In this work we study the fundamental cause of anchor dissipation in Lamé or wineglass mode resonators and show that by optimizing the resonator tether geometry, low anchor losses can be achieved[76]; thus, making it possible to reach the intrinsic frequency×*Q* (*f*×*Q*) limit of the resonator.

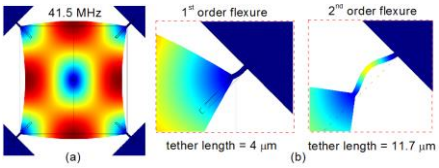

Fig. 1:(a) Resonator mode shape. (b) First two flexural modes of the tether. Tether width is 2 μm for both.

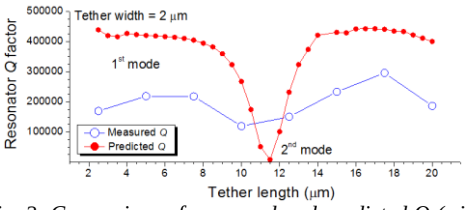

Fig. 2: Comparison of measured and predicted Q (with anchor and phonon loss[75] limit) as a function of tether length for a tether width of 2 μm.

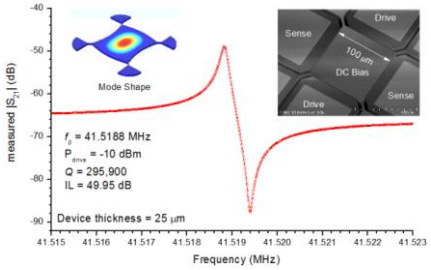

Fig. 3: Measured response and a SEM image of a Lamé mode resonator (tether width 2 μm, length 17.5 μm).

In order to support the Lamé mode resonance, the tethers are required to undergo forced flexural vibrations. As a consequence the anchor loss in such resonators is strongly dictated by the resonance frequency of the tether. When the tether resonance frequency is close to the frequency of the Lamé mode, the resonator *Q* is reduced due to the larger amount of energy lost from the tethers (*Fig. 1*). On the other hand, tether geometries having resonances far from the Lamé mode frequency show a higher anchor *Q*. To verify this hypothesis, finite element analysis of the structures is performed using COMSOL with anchor loss estimated using the Perfectly Matched Layer (PML) approach (*Fig. 2*)[77]. For experimental characterization, devices are fabricated on a low-resistivity SOI substrate with 1 μm actuation gaps and released using backside DRIE. Both the simulation and measurement results for the fundamental Lamé mode are found to corroborate the presented hypothesis (*Fig. 2*). Using such an optimization technique, a high-*Q* Lamé mode resonator operating in its fundamental mode at 41.5 MHz is demonstrated with a *Q* of 296,000 (in vacuum, at room temperature and 300V bias). The *f*×*Q* of the resonator is 1.23×10^{13}, which is close to the fundamental limit for silicon (*Fig. 3*)[1]. Note that the required bias voltage can be reduced by reducing the actuation gap.

[75] R. Tabrizian, M. Rais-Zadeh and F. Ayazi, *Transducers*, 2009.

[76] L Khine and M. Palaniapan, *J. Micromech. Microeng.*, vol. 19, pp. 015017, 2009.

[77] D. Bindel and S. Govindjee, *Int. J Numer. Meth. Eng.*, vol. 64, pp. 789-818, 2005.

Mechanically Coupled SOI Lamé-Mode Resonator-Arrays: Synchronized Oscillations with High Q Factors of 1 Million

Yuanjie Xu and Joshua E.-Y. Lee

Department of Electronic Engineering, City University of Hong Kong, Hong Kong SAR

Email: joshua.lee@cityu.edu.hk

In this work, we present the first demonstration of synchronized oscillations in an SOI resonator array with Q's of 10^6 through mechanical coupling. Our experimental results indicate that even as the length of the array is expanded, Q is maintained at 10^6 (*f*-*Q* of 1.3×10^{13}); close to that of a single Lamé resonator. These results in turn suggest that mechanical coupling can be extended to even yet longer arrays for improved transduction and power handling without diminishing Q.

Mechanically coupling resonators into arrays for synchronized oscillation has been demonstrated previously in CMOS MEMS[78] and PolySi[79] to achieve reduced motional resistance and increased power handling. However, till now no mechanical-coupled array approaching the *f*-*Q* limit of Si has been demonstrated. Here we apply mechanical coupling to the isochoric Lamé mode where thermoelastic damping is insignificant relative to anchor and Akhiezer effect loss.

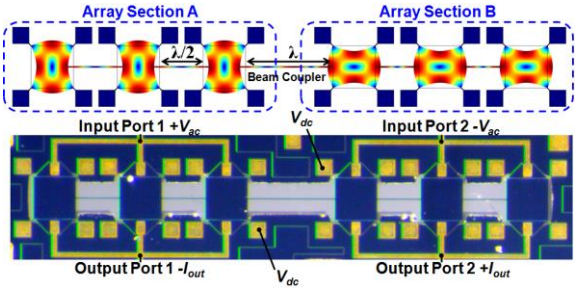

Fig. 20: FE simulation and micrograph (showing also the transduction configuration) of a coupled 6-resonator array

An array of up to 6 resonators (each $320\times320\mu m^2$) was fabricated using a standard SOI MEMS process. To allow fully-differential capacitive transduction, the array is divided into 2 sections (Fig 1). The 3 resonators in each section are designed to resonate in phase using half-wavelength (λ/2) beam couplers. Between the 2 sections, the vibration-combination is anti-phase through a full wavelength (λ) beam coupler.

The devices were measured in vacuum using a DC bias voltage V_{dc} of 50V and RF source power of 0dBm. Fig. 2 shows the measured electrical transmission of arrays of 6 and 4 resonators, including a single Lamé resonator (360μm). Q is the same between the two arrays, and just slightly lower compared to the single Lamé (1.2 million). An increase in the nonlinear bifurcation point could be observed when increasing the array length.

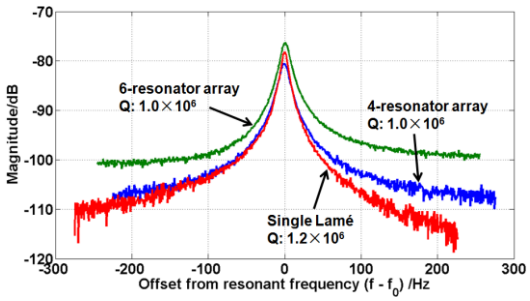

Fig. 2: Measured transmission of a 6-resonator relative to a 4-resonator array and single Lamé resonator

[78] M.-H. Li, W.-C. Chen, S.-S. Li, "Mechanically coupled CMOS-MEMS free-free beam resonator arrays with enhanced power handling capability," IEEE Trans. Ultrason. Ferroelectr. Freq. Control, vol. 59, no. 3, pp. 346-357, Mar. 2012.

[79] Y.-W. Lin, S.-S. Li, Z. Ren, C. T.-C. Nguyen, "Low phase noise array-composite micromechanical wine-glass disk oscillator," Tech. Dig. IEEE Int. Electron Devices Mtg., Washington, DC, Dec. 5-7, 2005, pp. 287-290.

A Parallel-Class Thermally-Actuated Micromechanical Filter with Tunable Center Frequency and Bandwidth

Cheng Tu, Joshua E.-Y Lee

Department of Electronic Engineering, City University of Hong Kong, Hong Kong

Email: mems305@gmail.com

In this paper, we report the very first thermally-actuated micromechanical filter. As a proof of concept, the filter has a modest center frequency of 64 MHz, which in principle can be scaled to yet higher frequencies. Resonators using thermal actuation and piezoresistive readout (thermal-piezoresistive resonators) have attracted much interest owing to a promising frequency-scaling characteristic in terms of electromechanical transduction and the simplicity in fabrication[80]; but they also suffer from substantial direct resistive coupling between the input and output ports. By using a parallel-class configuration[81] applied to a pair of these resonators, feedthrough cancellation can be achieved while simultaneously realizing a 2nd-order high stopband rejection filter.

Fig. 1 shows SEMs of a pair of dog-bone shaped twin resonators fabricated side-by-side on the same die using a standard SOI MEMS process. Also shown is the circuit schematic to realize a parallel-class filter. Both resonators are electro-thermally excited by the same AC drive voltage, but their output motional currents are sensed differentially. A slight mismatch between their resonant frequencies results in a bandpass filter frequency response. Since the resonant frequencies of each resonator can be can be tuned by adjusting the bias voltage due to the Joule heating effect, their separation and thus the bandwidth of the filter can be tuned as shown in Fig. 2 (from 0.004% to 0.002%). The center frequency of the filter is also tunable by the same effect (72.2ppm tuning range achieved so far). The out-of-band rejection is more than 10dB. It should be noted that the response shown in Fig. 2 was measured without proper termination, but still showing very little ripple in the passband (<1dB). These results further highlight the applicability of thermal actuation to high frequency applications to now also include even filtering.

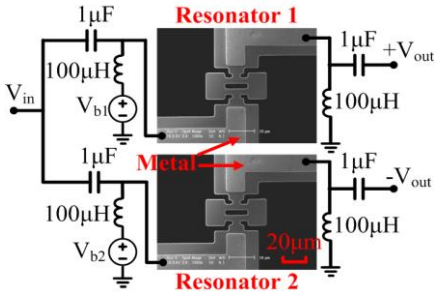

Fig. 21: Circuit schematic for the parallel class filter with SEMs of two 64MHz 10-μm-thick dog-bone resonators fabricated using a standard SOI MEMS process.

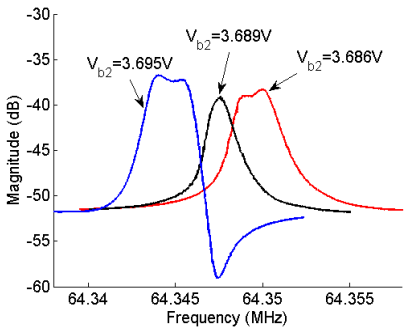

Fig. 2: Measured electrical transmission of the filter. V_{b2} is varied to demonstrate tuning of the bandwidth while V_{b1} is kept constant at 3.52V.

[80] A. Rahafrooz, S. Pourkamali, "High-frequency thermally actuated electromechanical resonators with piezoresistive readout", IEEE Trans. Electron Devices, vol. 58, p. 1205-1214, 2011.

[81] S.-S. Li, Y.-W. Lin, Z. Ren, C. T.-C. Nguyen, "A micromechanical parallel-class disk-array filter", Proceedings of 2006 IEEE Int. Frequency Control Symp., Geneva, Switzerland, May 29-June 1, 2007, pp. 1356-1361.

IFCS-EFTF1-PAB1-10

Anomalous DC-Current-Induced Attenuation of Q Factor in a Silicon Contour Mode Micromechanical Resonator

Haoshen Zhu, Cheng Tu and Joshua Lee

Department of Electronic Engineering, City University of Hong Kong, Hong Kong

Email: haoshezhu2-c@my.cityu.edu.hk

Micromachined silicon resonators have the advantage of employing intrinsic gain in the form of piezoresistive sensing[82] or a resonant body transistor[83] to enhance electromechanical transduction. This entails applying a DC bias current through the resonator. In this paper, we show that simply applying a DC current for such a purpose could significantly reduce the quality factor (Q) given the right combination of conditions such that the thermal and elastic eigenmodes overlap.

We applied a DC bias current ranging from 1mA to 20 mA through a single-crystal-silicon square plate resonator vibrating in the square extensional (SE) mode for piezoresistive sensing with capacitive drive. Self-heating due to the bias current causes the resonant frequency to shift, which we have modeled using finite element simulation. Unreported elsewhere, Q was found to drop by more than half around a precise bias current level as shown in Fig. 1. By fine tuning the bias current around 15mA, it is found that the peak height decreases while the -3dB bandwidth notably widens as the bias current is tuned closer to a precise bias point given by 15.246mA. This effect appears to be symmetric about this biasing (Fig 2). It can be further noted that the original single peak splits to two peaks at this bias point.

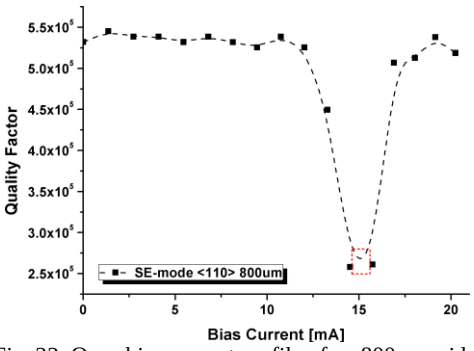

Fig. 22: Q vs. bias current profile of an 800μm wide SE-mode resonator aligned along the <110> crystal axis. Significant Q drop is detected around 15mA.

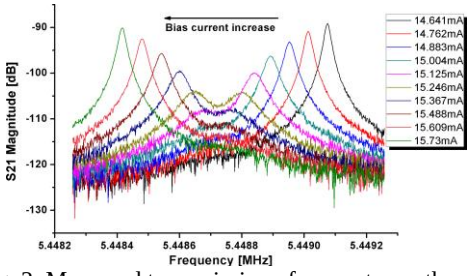

Fig. 2: Measured transmission of resonator as the bias current is fine-tuned around 15mA (highlighted by red box in Fig. 1), showing the transition of Q.

To rule out its causal relation to piezoresistive electromechanical coupling, we have repeated multiple measurements using capacitive sensing with a heating current through the device. Resonators of different dimensions and orientations were also measured, all confirming the same trends. This effect is believed to arise from thermo-elastic coupling. Due to the temperature dependence of silicon's elasticity, self-heating due to bias current causes the mechanical frequency to shift. As the elastic and thermal modes overlap, thermo-elastic damping[84] is magnified, thus leading to a significant drop in Q.

[82] J. T. M. van Beek, et al., IEEE IEDM 2007, pp. 411–414.

[83] D. Grogg, et al., IEEE IEDM 2008, pp.1-4.

[84] A. Duwel, et al., JMEMS, vol. 15, no. 6, pp. 1437-1445, 2006.

IFCS-EFTF1-PAB1-11

Multimode Characteristics in Mechanically-Coupled Silicon Carbide (SiC) Nanowire Array Resonators

Rui Yang[1*], Jaesung Lee[1], Zenghui Wang[1], Philip X.-L. Feng[1*]

[1]Electrical Engineering, Case Western Reserve University, Cleveland, OH 44106, USA

Email: rui.yang@case.edu, philip.feng@case.edu

We report measurements and modeling of arrays of mechanically-coupled very thin SiC nanowire (SiC NW) nanomechanical resonators. The exceptional mechanical properties and very attractive optical properties of SiC make it highly interesting for nanoelectromechanical systems (NEMS) and optomechanical devices, with resonant modes operating at high frequencies that can be exploited for resonance-based signal processing and sensing applications. In this work, we demonstrate arrays consisting of SiC NWs as narrow as 50nm (patterned by electron beam lithography on a ~50nm SiC epilayer) and investigate the multimode resonances in mechanically coupled arrays.

Figure 1a shows measured multimode response from an array of 10 SiC NWs with individual dimensions $L \times w \times t \approx 10\mu m \times 50nm \times 50nm$. Sensitive detection of mechanical displacement down to the levels of Brownian motions of the devices is achieved by using a laser interferometer with ~1μm spot size and pm/√Hz displacement sensitivity (on SiC NWs). We directly map the mode shapes with high spatial resolution, and compare the results with finite element modeling (COMSOL, Fig. 1). Mechanical coupling (via the clamping plate) suppresses the natural modes of each individual NWs, while enabling the system to exhibit new collective resonances. Probing the characteristics the coupled modes and degeneracy allows us to determine and further engineer the coupling strength, toward higher performance SiC NEMS arrays for specific applications[85,86,87]. By carefully examining the resonance characteristics their scaling laws with array size (N, number of NWs), we advance this SiC device technology as platform, with sensitive optomechanical transduction, for studying new phenomena in large-N systems, from chaos to synchronization.

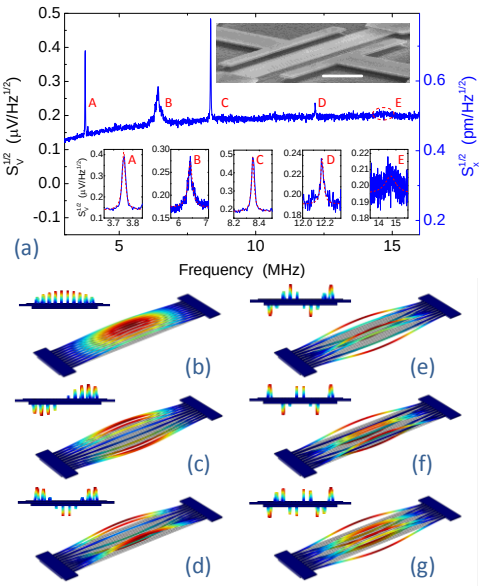

Fig. 1: (a) Resonance spectrum measured from a SiC NW array of N=10. *Insets*: first 5 measured resonances (A-E) with fitting indicated by the red dashed line. (b)-(g): COMSOL simulation of the first 6 coupled modes of the array of 10 SiC NWs. *Insets*:

[85] S. Lee, C.T.-C. Nguyen, "Mechanically-coupled micromechanical resonator arrays for improved phase noise", *Proc. IEEE Int. Freq. Contr. Symp. (IFCS 2004)*, pp. 144-150 (2004).

[86] D. Weinstein, *et al.*, "Mechanical coupling of 2D resonator arrays for MEMS filter applications", *Proc. IEEE Int. Freq. Contr. Symp. & Euro. Freq. & Time Forum (IFCS-EFTF 2007)*, pp. 1362-1365 (2007).

[87] G.K. Ho, R. Abdolvand, F. Ayazi, "Through-support-coupled micromechanical filter array", *Proc. 17th IEEE Int. Conf. on MEMS (MEMS 2004)*, pp. 769-772 (2004).

IFCS-EFTF Group 2 poster session 1

Forum Hall

Monday & Tuesday, July 22-23, 2013, 01:00 pm - 02:00 pm and 3:30 pm - 4:30 pm

Chair: **Fabrice STHAL**
FEMTO-ST

IFCS-EFTF2-PAB2-1

Study of Phase Noise in VCXO with Inversion-Mode Varactors

Yao Huang Kao and Teh Chau Liau

Department of Communication Engineering, Chung Hua University, Hsinchu Taiwan

Email: yhkao@chu.edu.tw

Voltage controlled crystal oscillators (VCXO) play an essential role in modern communication as reference sources in local oscillators. In this application the stringent request of phase noise and wide tuning are needed. The VCXO is normally built by CMOS process due to low cost and the capability of total integration. For simplicity, the MOS varactor in inversion mode is often employed to change the frequency. However, the capacitance measured in small-signal approach appears a step-like shape, which is not obvious for wide tuning application. In this abstract, the tuning behavior and related phase noise in large-signal operation is investigated.

According to the Leeson's model, phase noise is inversely proportional to signal power. In our design, the signal magnitude is maximized to have rail to rail swing. The dimension of varactor is traded off between tuning ratio and quality factor. Under TSMC standard 0.35um mixed-mode process with 2P4M and Polycide, the dimensions of width W, channel length L, and finger number m are chosen as $W \times L \times m = 30\mu \times 1\mu \times 40$, respectively. The varactor encounters different modes of strong inversion and depletion. The partition depends on the tuning voltage. The value of capacitance is predicted from Fourier analysis of I-V waveform. The wiring and C-V characteristic of inversion mode are shown in Fig. 1a and Fig. 1b, respectively. The slope is steep at small swing and becomes slanted as the swing is increased.

The performances of tuning capability in the typical Pierce oscillator with power supply V_{DD}=3V are shown in Fig. 2a. The linear tuning range is obtained from zero to 1.8V with deviation is from -30 to +20ppm, respectively. Above 1.8V the tuning is saturated. The slope is maximized at 0.8V with roughly equal duration in inversion and depletion. The corresponding phase noises are also illustrated in Fig. 2b. The worst case -80dBc@10Hz offset occurs at the point with maximal tuning slope. At both ends with smaller slopes the phase noises becomes better -90~-100 dBc@10Hz offset. The measured tuning capability matches well with the prediction under large-signal swing.

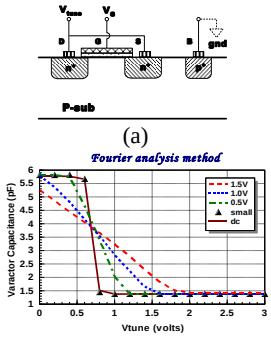

(a) (b)

Fig. 1 NMOS varactor in (a) Inversion mode and (b) C-V curves

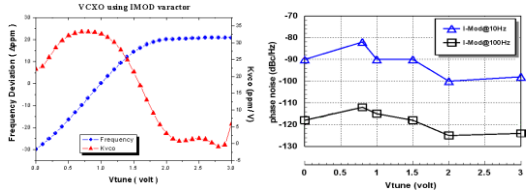

(a) (b)

Fig. 2 (a) Measured frequency deviation and slope and (b) phase noises at offset 10 and 100Hz

A low-phase-noise 4.72-5.58-GHz LC-VCO design

Yung-Hsiang Ho[1] and Chia-Yu Yao[2]

Department of Electrical Engineering, NTUST, Taipei, Taiwan

Email: [1]D9807403@mail.ntust.edu.tw, [2]chyao@mail.ntust.edu.tw

For the application requiring a high frequency and good phase noise performance, the LC-tank VCO is popular in VCO design. In order to have a small VCO gain, the LC-tank VCO usually has a capacitor array across the VCO's differential outputs as the coarse-tuning stage for the band selection.

Fig.1 shows the proposed LC-tank VCO schematic. It uses a PMOS cross-coupled pair to mimic a negative resistor. The varactors C_{j1}-C_{j2}, two shunt capacitors C_{f1}-C_{f2}, the capacitor array, and the inductor L form the resonator of the VCO. The current on R_c contains even-order harmonics. These harmonics mixing with the VCO's output produces an in-band noise. This in-band noise makes the VCO's phase noise even worse. The proposed VCO utilizes a capacitor C_c across R_c to suppress the harmonics. In addition, we use two capacitors C_{f1} and C_{f2} across M_1 and M_2, respectively, to serve as a filter to reduce the amplitude of the harmonics. Let $v_1 = v_{com} + v_m \sin \omega t$ and $v_2 = v_{com} - v_m \sin \omega t$. We can obtain

$$\begin{cases} I_1 = \frac{k'}{2}\frac{W}{L}[(v_{com} - v_m \sin \omega t - v_s) - v_t]^2 \\ I_2 = \frac{k'}{2}\frac{W}{L}[(v_{com} + v_m \sin \omega t - v_s) - v_t]^2 \end{cases}$$

$$\begin{cases} I_1 = \frac{k'}{2}\frac{W}{L}[(V_{dc} - v_s)^2 - 2V_{dc}v_m \sin \omega t + v_m \sin^2 \omega t] \\ I_2 = \frac{k'}{2}\frac{W}{L}[(V_{dc} - v_s)^2 + 2V_{dc}v_m \sin \omega t + v_m \sin^2 \omega t] \end{cases}$$

$$I_c = I_1 + I_2 = \frac{k'}{2}\frac{W}{L}\left[2(V_{dc} - v_s)^2 + 2{v_m}^2\left(\frac{1 - \cos 2\omega t}{2}\right)\right]$$

where $V_{dc} = v_{com} - v_t$. Fig. 2 shows the small-signal circuit model of the VCO's upper part where $Zc = R_c \,//\, C_c$. The capacitors C_{f1} and C_{f2} in parallel with Zc serve as a filter for the even-order harmonic signals at v_s.

The VCO was realized in TSMC 0.18 μm CMOS process. Fig. 3 shows the measured phase noise of the VCO output tuned at 5.17 GHz. The phase noise is –137.12 dBc/Hz at 10-kHz offset frequency. The measured rms jitter is 2.072 ps at 5.428-GHz output. The power consumption is 10 mW at 1.8-V supply voltage.

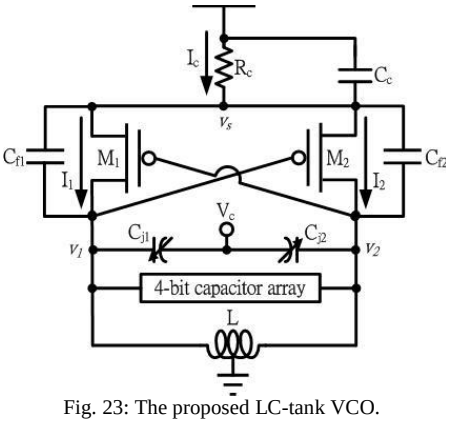

Fig. 23: The proposed LC-tank VCO.

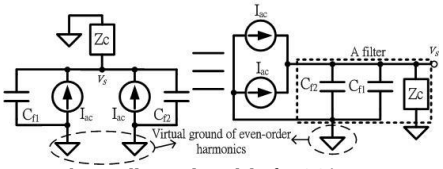

Fig. 2: The small-signal model of VCO's upper part.

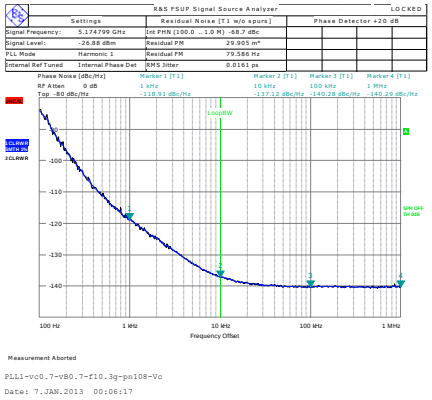

Fig. 3: Measured phase noise at 5.17 GHz.

This work is partially supported by the National Science Council of Taiwan under grant NSC 101-2221-E-011-

IFCS-EFTF2-PAB2-3

Using 2-Bit Counter to Predict the Starting SAR Bit for a Fast-Locking Wide-Range All-Digital DLL

Yung-Hsiang Ho[1] and Chia-Yu Yao [2]

Department of Electrical Engineering, NTUST, Taipei, Taiwan

Email: [1]D9807403@mail.ntust.edu.tw, [2]chyao@mail.ntust.edu.tw

Among various digital delay-locked loops (DLLs), the successive approximation register (SAR)-based DLL is promising because it provides better tradeoff among hardware area, delay resolution, and lock time.

Assume that the time delay introduced by the digital controlled delay line (DCDL) is linearly varied with the SAR code. If a SAR bit is set to high, the delay of the DCDL will increase by a half of the delay amount corresponding to the previous significant bit. Thus, if we can estimate the current delay of the DCDL, we can predict the starting bit from which the SAR search can begin with to shorten the lock time of the DLL.

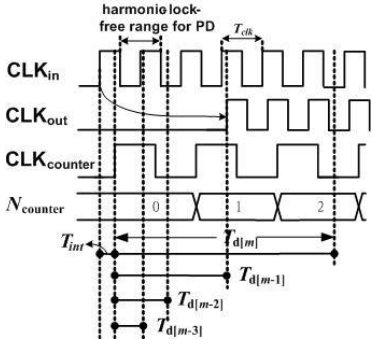

Fig. 24: A timing example when SSARBP starts form the (M-1)th bit.

In order to explain the proposed starting SAR-bit prediction (SSARBP) method, some notations are shown in Fig. 1. Let T_{clk} denote one clock cycle, T_{int} represent the intrinsic delay of the delay line, and $T_{d[m]}$, $m = 0, 1, \ldots, M$, represent the excess delay of the delay line caused by setting the mth bit of the control code to logic high. As mentioned before, $T_{d[m]} = 2T_{d[m-1]}$. In this paper, we assume that the control code for the DCDL has $M + 1$ bits.

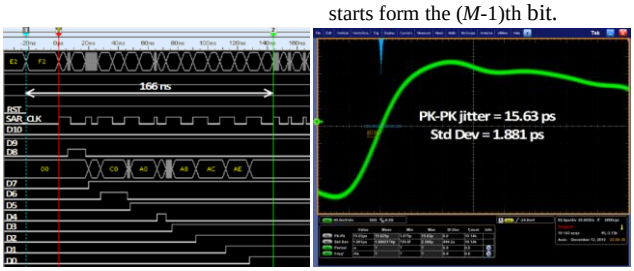

(a) (b)

Fig. 2: (a) The measured SAR code in the lock-in process for a 120-MHz input clock. (b) The measured jitter for a 1-GHz input clock.

In the proposed DLL, we divide the input clock (CLK_{in}) frequency by two as the clock signal ($CLK_{counter}$) for the counter. Fig. 1 shows an example timing diagram. In the beginning of an SSARBP cycle, we reset the DCDL first. After T_{int}, the counter starts to count. We then monitor the DCDL output signal CLK_{out}. When the rising edge of CLK_{out} is observed, the counter value at that moment gives the DCDL delay information. We can use the information to adjust the SAR code. The DLL circuit was implemented in TSMC 0.18 μm CMOS process. The measured results show that the proposed circuit can operate from 66 MHz to 1 GHz. The lock time is within 17-23 clock cycles. Fig. 2(a) shows that the lock time is 20 clock cycles for a 120-MHz input clock. Fig. 2(b) shows that the rms jitter is 1.881 ps for a 1-GHz input clock.

This work is partially supported by the National Science Council of Taiwan under grant NSC 101-2221-E-011-168.

IFCS-EFTF2-PAB2-4

Low phase noise microwave analog optical link performance study for high dynamic environment platform

Jean-Marc LESAGE[1], Mathieu LE PIPEC[1]

[1]DGA – Information Superiority, DGA French MoD, Bruz, France

Email: jean-marc.lesage@dga.defense.gouv.fr

Distribution of very low phase noise and low spurious microwave Local Oscillator (LO) is needed for most of the radar or electronic warfare applications. In this paper we study the capability to optically carry low phase noise LO, thanks to a directly-modulated optical link[1], while subjected to severe environmental conditions. First the optical link is compared to a coaxial cable link in terms of additive phase noise subsequently the absolute amplitude and phase noise under random vibration are compared. Firstly, it should be noticed that even in case of a wide band optical link, the phase noise floor difference between optical and coaxial cable is small even for short distance links. Secondly, the absolute amplitude and phase noise of the optical and coaxial cable link are measured with the entire optical link or only with some piece component of the link (10 GHz LO, optical fiber, laser and photodiode) under random vibration. The phase noise degradation is almost the same when the optical or the coaxial link is under vibration and the main degradation is always due to the Local Oscillator whatever the technology is (OEO : Opto-Electronic Oscillator, quartz,…; some ways of improvement of optical link g-sensitivity that can be useful for OEO[2] will be discussed). Thanks to recent experimentations done by DGA, it has been shown that very low phase noise microwave LO signals can be carried on optical link without any phase noise degradation due to the link while subjected to random vibration.

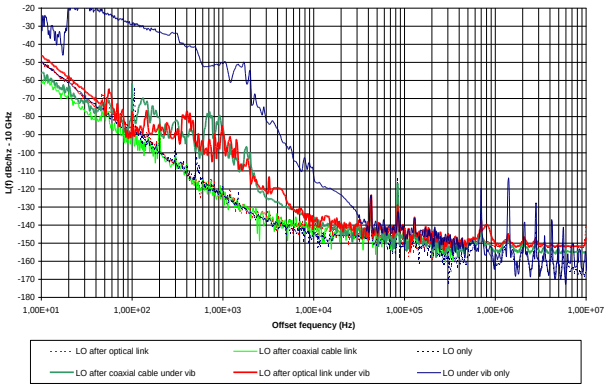

Fig. 25: Phase noise of the optical and coaxial cable links with all the links or only part of them under random vibration

[1] M.Chtioui *et al* "Analog microwave photonic link based on a high power directly modulated laser, a high power photodiode and passive impedance matching", Microwave Photonics 2012.

[2] D. A. Howe *et al* "Active Vibration-induced PM Noise Control in Optical Fibers: Preliminary Studies", IEEE 2007

Acknowledgements: The directly modulated optical link, designed by TSA in the frame of the DGA-funded project ORGE, use semiconductor DFB laser diode and MUTC photo-diode, designed by 3-5 Lab and packaged by 3S Photonics.

IFCS-EFTF2-PAB2-5

Evaluation of the accuracy of the method for measuring state-of-the-art ultra-high stability quartz crystal oscillators

Patrice Salzenstein[1], Alexander Kuna[2], Frédéric Lefebvre[3]

[1]Franche Comté Electronique Mécanique Optique Thermique Sciences et Technologies (FEMTO-ST), Centre National de la Recherche Scientifique (CNRS), Besançon, France
[2]Intitute of Photonics and Electronics (IPE), Academy of Sciences, Prague, Czech Republic
[3]Oscilloquartz, Neuchâtel, Switzerland

Email: patrice.salzenstein@femto-st.fr and kuna@ufe.cz

The best frequency stability ever measured on a quartz crystal oscillator was recently obtained. This new *Boitiers à Vieillissement Amélioré* (BVA) oscillator has an estimated flicker frequency modulation (FFM) floor as lower as 2.5×10^{-14} at 5 MHz[88,89]. It leads to a significant step. To achieve such a low FFM floor, we assume that best resonators are fully characterized[90] and packed. It was obtained using a double rotated SC-cut quartz with low phase noise, good aging characteristics and low sensitivity to drive level dependency placed in appropriate thermostat in the first prototype of a double oven-controlled crystal oscillator (OCXO) realized in Switzerland by Oscilloquartz company. We checked that the ultra-stable signal delivered by such a BVA oscillator can be distributed without any degradation of its short term stability[91]. It has to be underlined that precise measurements on oscillators were carefully performed at the Time and Frequency department in Prague in very favorable environmental conditions and deduced by three cornered hat analysis[92,93,94,95] on a dedicated system[96]. Our process for short term is analogous to what occurs for long term frequency stability characterization, but could provide questionably a precise determination of FFM floor. The analysis proceeds by matching the theoretical and the best experimental curves not exactly simultaneously. In this paper we discuss the accuracy of our method.

---

88 P. Salzenstein, A. Kuna, L. Šojdr and J. Chauvin J., "Significant step in ultra high stability quartz crystal oscillators", Electronics Letters, 46(21), 1433–1434, (2010).

89 A. Kuna, J. Cermak, L. Šojdr, P. Salzenstein and F. Lefebvre, "Lowest Flicker-Frequency Floor Measured on BVA Oscillators", IEEE Trans. on UFFC 57(3), 548-551 (2010).

90 P. Salzenstein, A. Kuna, L. Šojdr, F. Sthal, N. Cholley and F. Lefebvre, "Frequency stability measurements of ultra-stable BVA resonators and oscillators", Electronics Letters, 46(10), 686-688 (2010).

91 P. Salzenstein, N. Cholley, A. Kuna, P. Abbé, F. Lardet-Vieudrin, L. Šojdr and J. Chauvin, "Distributed amplified ultra-stable signal quartz oscillator based", Measurement, 45(7), 1937–1939 (2012).

92 J. E. Gray and D. W. Allan, "A Method for Estimating the Frequency Stability of an Individual Oscillator," Proc. of the 28th Ann. Symp. on Freq. Contr., May 1974, pp. 243-246 (1974).

93 D. W. Allan, "Time and frequency (time domain) characterization, estimation, and prediction of precision clocks and oscillators," IEEE Trans. on UFFC, 34(6), 647–654 (1987).

94 P. Tavella and A. Premoli, "Estimation of Instabilities of N Clocks by Measuring Differences of their Readings", Metrologia, 30(5), 479-486 (1993).

95 F. Vernotte, M. Addouche, M. Delporte and M. Brunet, "The three cornered hat method: an attempt to identify some clock correlations", IEEE Freq. Contr. Symp., 23-27 Aug. 2004, pp. 482- 488 (2004).

96 G. Brida, "High resolution frequency stability measurement system," Rev. Sci. Instrum., 73(5), 2171–2174 (2002).

IFCS-EFTF2-PAB2-6

Measurements of Intrinsic Phase Fluctuations in a Cryogenic Microwave Amplifier

Romain Bara-Maillet[1], Stephen R. Parker[1], Eugene N. Ivanov[1], Jean-Michel Le Floch[1], Michael E. Tobar[1]

[1]ARC Centre of Excellence for Engineered Quantum Systems, School of Physics, The University of Western Australia, Crawley, WA/Australia

Email: barar01@student.uwa.edu.au

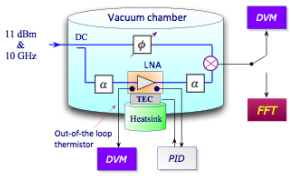

Fig. 26: Experimental setup.

There has been a continuous interest in the development of cryogenic microwave amplifiers with low level of phase noise and power dissipation for fundamental physics experiments. For example, such amplifiers have enabled accurate characterization of electromagnetic properties of ultra-high Q electromagnetic resonators at single photon energies[97]. They are also crucial for experiments on the coherent manipulation of spin qubits with implications to quantum computing[2]. We studied the phase noise properties of a low noise X-band cryogenic amplifier (LNF LNA7-10) both at room and cryogenic temperature. The amplifier was placed in a temperature-stabilized environment to minimize the influence of ambient temperature on the phase delay of the transmitted signal. By utilizing both the time and frequency domain techniques we measured amplifier phase noise spectra at Fourier frequencies from tens of μHz to 1 MHz. At room temperature, the noise measurements were conducted with a mixer-based phase bridge, Fig. 1. The bridge was placed on a temperature-stabilized plate inside a vacuum chamber, Curve 1 in Fig. 2 shows the phase noise floor of the thermally isolated phase bridge as a function of Fourier frequency F. It can be closely approximated by $4\ 10^{-13} / F + 2\ 10^{-18} / F^3$ (rad^2/Hz). The cubic term in the above fit dominates the noise floor at F<1 mHz. It reflects the residual effect of ambient temperature fluctuations on the spectral resolution of the phase bridge. For comparison, the noise floor of the "exposed" phase bridge is limited by ambient temperature fluctuations at F<1 Hz. Curve 2 in Fig. 2 shows the phase noise spectrum of the LNA at 9 GHz with -34 dBm input power. It has a rather unusual $1/F^{1/2}$ dependence in the frequency range 20mHz<F<200Hz. At F<1 mHz, amplifier phase noise is proportional to $1/F^3$, which can be attributed to fluctuations of the ambient temperature. The discussion on phase noise properties of the above amplifier at 5 Kelvin is beyond the scope of this Abstract and will be presented at the Symposium.

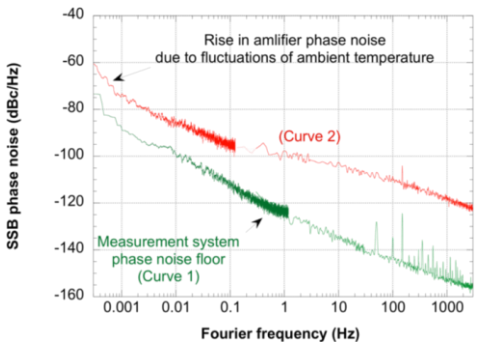

Fig. 2: Phase noise spectra at ambient temperature

[1] D. Reilly and J. Colless, "Cryogenic high-frequency readout and control platform for spin qubits", Rev. Sci. Instrum. 83, 023902 (2012); doi: 10.1063/1.3681195

[2] D. Creedon, Y. Reshitnyk, W. Farr, J. Martinis, T. Duty and M. Tobar, "High Q-factor sapphire whispering gallery mode microwave resonator at single photon energies and millikelvin temperatures", Appl. Phys. Lett. **98**, 222903 (2011)

IFCS-EFTF2-PAB2-7

VERY LOW POWER CONSUMPTION, ULTRA LOW PHASE MOISE, MINIATURE CONVENTIONAL OCXO

R. Boroditsky, J. Gomez,

NEL Frequency Controls, 357 Beloit Street, Burlington, WI 53105

Battery powered equipment, whether instrumentation, underwater exploration, or military require high performance frequency sources with very low power consumption for obvious reason. Current state of the art in the area of very low power consumption OCXO [1], [2] employs evacuation of the entire (or almost entire) electronic circuit with crystal resonator in metal enclosure and internally heating the content. Although achieving the goal of significant reduction in power consumption (60 – 80 %), this approach has some serious drawbacks. The phase noise performance of one of the implementations is average at best, of another - is outright poor. Evacuation of the entire OCXO requires very complex and tedious processes, since any minute contamination can destroy deep vacuum, needed for device to operate. The availability of die semiconductor components, a necessity for inside the vacuum, is very limited. The devices are susceptible to exposure of elevated temperatures, which might induce internal outgassing and deterioration of vacuum level. The goal of this work was to create a device, which would eliminate above mentioned drawbacks i.e. employ conventional heating technique, use off-the shelf widely available components, have comparable to evacuated devices power consumption and size, and exhibit superior phase noise performance. The goal was achieved by implementing special thermal insulation technique, and NELs ULPN technology in 20x20x10 mm package. While the steady state power consumption at room temperature is less than 250 mW, the phase noise at 10 Hz offset at <-145 dBc/Hz is better by 20 to 45 dBc than published specifications, and at -174 dBc/Hz, by 10 to 30 dBc on the floor.

IFCS-EFTF2-PAB2-8

Phase Group Characteristic Based Frequency Measurement Method with Wide Band and Fast Response

Shaofeng Dong, Wei Zhou, Wei Hu, Jinsong Zhan

Department of Measurement and Instrument, Xidian University, Xi'an, China

Email: shaofengdong@126.com

As the rapid development of frequency standard, the need arises to measure frequency in a wide band with a high resolution. Restricted by the influence of ± 1 counting error, the resolution of the existing frequency measurement method is hard to improve.

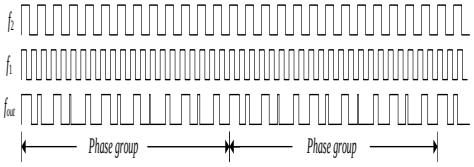

Fig. 1: Variation rule of phase group.

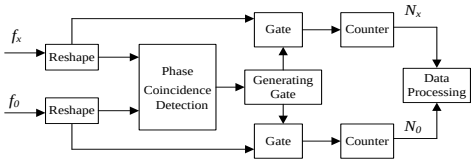

Fig. 2: Wide-band frequency measurement method.

By analyzing the phase variation rule between every two periodic signals with different frequency, as shown in Fig. 1, the phase group characteristics, such as phase group synchronization, are revealed in the paper. With these characteristics, the direct measurement and comparison of periodic signals with different frequencies in a wide band with a high resolution can be realized.

In this method, as shown in Fig. 2, two adjacent phase coincidence points of the reference frequency f_0 and the measured frequency f_x are used to generate the measurement gate. Because f_0 and f_x are synchronized strictly with the start and stop signals of the gate, ± 1 counting error can be eliminated. In gate time, the counting numbers of f_x and f_0 are N_x and N_0, respectively, thus the measured frequency $f_x = f_0 \times \frac{N_x}{N_0}$. If there is a multiple relationship between f_0 and f_x, it takes a long time to generate the measurement gate. Fine phase shift is used on the reference frequency to shorten the measurement time.

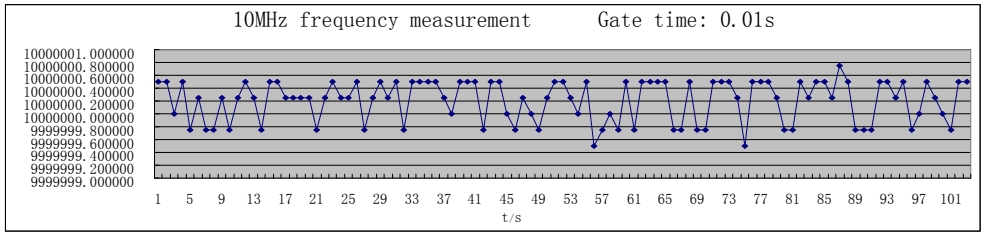

Fig. 3: Experiment of frequency measurement at 10MHz.

Experiment results show, the method achieves a precision higher than 1×10^{-13}/s in frequency comparison, as shown in Fig. 3, the typical precision of signal from 30 kHz to100MHz achieve $6\sim8\times10^{-12}$/s. With the improvement of phase coincidence detection resolution, phase shift precision and component response speed, the precision of this method can be further improved.

Supported by the Fundamental Research Funds for the Central Universities No. K5051204003, the National Natural Science Foundation of China under Grant No. 10978017.

IFCS-EFTF2-PAB2-9

Event Timing Device Providing Subpicosecond Precision

Petr Panek[1], Jan Kodet[2,3], Ivan Prochazka[2]

[1] Institute of Photonics and Electronics, AS CR, Chaberska 57, 182 51 Prague, Czech Republic
[2] Czech Technical University in Prague, Brehova 7, 115 19 Prague, Czech Republic
[3] Technische Universität München, Station *Wettzell*, 93444 Kötzting, Germany

Email: panek@ufe.cz

We are reporting on the latest experimental results achieved with an event timing device using a surface acoustic wave filter as a time interpolator[98]. During tests of the first prototype, the dominant source of the measurement error was identified to be caused by noise of the filter excitation[99]. Therefore a new concept of the excitation for the next version of the device was designed. The exciter is activated just for a very short period keeping the energy of the noise at the input of the filter as low as possible. This solution led to considerable improvement of the device performance.

It results from the experimental measurements that the single shot precision is repeatedly lower than 500 fs RMS when time marks generated synchronously with the time base are measured. The behavior of the observed fluctuations can be well described as white noise with Gaussian distribution. Resulting precision is in an agreement with the error budget based on the theoretical analysis.

When asynchronous time marks are split into two event timers and the resulting time difference is measured, the single shot precision is below 700 fs RMS per channel. In this case the measurement is affected not only by random errors, but also by non-linearity of the time interpolation. Harmonic distortion in the analog-to-digital converter has been identified as the main source of this additional error. The time interpolation error is a periodic function of the time mark position. This dependence oscillates very quickly in comparison to the clock period[100].

The temperature dependence is below 0.1 ps/K. Operating the device in a common laboratory environment without temperature stabilization, the stability TDEV better than 3 fs has been routinely achieved for range of averaging intervals from 10 s to several hours.

The event timers are capable of stand-alone operation or they can create a net of timing units distributed in an area where unified time is kept using optional Two-Way Time Transfer modules[101].

---

[98] P. Panek, "Time-interval measurement based on SAW filter excitation", IEEE Trans. Instrum. Meas., vol. 57, p. 2582-2588, 2008

[99] P. Panek, I. Prochazka, "Time interval measurement device based on surface acoustic wave filter excitation, providing 1 ps precision and stability", Rev. Sci. Instrum., vol. 78, p. 094701-4, 2007

[100] I. Prochazka, P. Panek, "Nonlinear effects in the time measurement device based on surface acoustic wave filter excitation", Rev. Sci. Instrum., vol. 80, p. 0761021-3, 2009

[101] P. Panek, J. Kodet, I. Prochazka, "Accuracy of two-way time transfer via a single coaxial cable", Metrologia, vol. 50, p. 60-65, 2013

Background, Motivation and Objective:

Today, millions of FBAR Filters and Duplexers are sold into cell phones every year. The all-silicon package used to package these filters (providing both package integrity and hermeticity) has been utilized for the past 10 years and, to date, no part has been returned for compromised integrity or hermeticity failures. The lid wafer in the all-silicon package has, until recently, only been used to provide through-Si vias from the FBAR filter to the outside pads. The addition of circuitry to the lid enables a host of new applications. Examples include the integration of SOI switches for advanced filter switch modules, or the integration of SiGe LNAs with filters to provide extremely compact filter/amplifier functionality. Our first application, however, is the integration of oscillator circuitry with a temperature-compensated FBAR resonator. The resulting chip-scale oscillator produces a single, well-defined frequency, and is highly sensitive (on the parts-per-million level) to package hermeticity. This allows for the design and optimization of a robust package for yield and performance, and for the testing of new markets not dominated by filtering.

Statement of Contribution and Methods:

We present a fourth- design generation Free Running Oscillator and Voltage Controlled Oscillator using integrated bipolar circuitry in the lid wafer with a temperature-compensated FBAR resonator in the base wafer. The goal is to produce a high frequency, low-noise oscillator. Because there are over 15,000 oscillators per wafer, we can develop very sensitive testing procedures to study the oscillator behavior. We have determined our frequency measurement accuracy and precision to be ~ 0.2 parts-per-million, and our phase sensitivity floor to be less than -175 dBc/Hz. Tests of package hermeticity completed to date suggest that the oscillators behave with the same level of integrity as our standard FBAR filters.

Results/Discussion:

The goal of this program is to demonstrate a robust, repeatable, chip-scale oscillator with superior performance. We have measured tens of thousands of oscillators and observe a mean jitter performance between 12kHz and 20MHz of 7.5 femto seconds. Output power is 2.4 dBm and the output drives 100 Ω differential. The mean phase noise of the 2608 MHz oscillator at 800 kHz offset is -158 dBc/Hz and the mean at 10 kHz offset is -118 dBc/Hz. The device draws 18.8 mA at 3.3V, and the phase noise at all frequency offsets stays within 1 dB over the temperature range from -40 to 120°C. We see a 1 to 1 correlation between resonator Q improvement and close-in phase noise: a 15% improvement in Q between two wafer lots improves close-in phase noise by 1.2 dB. Far from carrier noise is set by the power delivered to the resonator. Due to the ability of the resonator to remain linear at high powers, we have seen far-from-carrier phase noise as low as -174 dBc/Hz. The sensitivity to acceleration of these oscillators is on the order of 1 ppB/g and the start up time is measured to be less than 10 μsec.

IFCS-EFTF2-PAB2-11

The Measurement of Transient Stability With High Resolution

Lina Bai, Wei Zhou, Zongqiang Xuan, Qinglan Zhang
Dept.of Measurement and Instrument, Xidian University. Xi'an, 710071, P.R.China

Measuring transient noise and short-term stability of signals with the digital counting methods is very difficult. Transient stability plays an important part in the characterization of phase noise of signal with high resolution.

With counting measuring method, the measuring gate is usually formed from 1ms until 10s. Gate resolution was significantly lower in shorter gate. However, the possibly short measurement gate such as corresponding to the measured signal period is important to reflect the phase noise condition of the frequency source using time domain method intuitively.

Phase coincidence detection technology plays a key role in the measurement of periodic signals such as frequency with high resolution, which can detect the same information about their phases between two detected signals with identical or different nominal frequencies. It is always difficult to reach "absolute" coincidence in the implementation of phase coincidence. Thus there becomes the threshold of phase coincidence detection sensitivity, which is the value representing the phase coincidence when the signal phase difference is less than it. In addition, there also exists the stability of the threshold.

Measuring and adjusting the phase difference between standard frequency signals can make it fixed at the threshold of phase coincidence detection circuit sensitivity. Technologically speaking, the coincidence detection sensitivity can not be particularly high, which is often fixed in the order of ns or hundreds of ps. If there is no effect of noise, it can still keep positive continuous coincidence information. However, when the phase difference of the two signals is adjusted to the verge of coincidence detection sensitivity, the output can also be detected if there is no noise. But if there is noise, the phase variation will be between the inner and outer of the verge, thus the information of phase coincidence will not always exist. So we can judge the phase instability of signals accurately from the continuity and discontinuity of the coincidence information. This is our continuous and discontinuous condition according to coincidence information to accurately judge the signal phase instability. The fastest response time can reach nominal period of the signal. Oscillators with low phase noise and high stability have apparent continuity of coincidence status, while the ones with relatively poor phase noise and stability will have apparent discontinuity of coincidence and the width of the discontinuity will be relatively large.

Thus the transient frequency stability can be identified from the unstable state of interrupted, disability of coincidence detection circuit and the measurement result of the phase difference. The measurement resolution depends on disability of 5ps of the coincidence detection circuit.

The formula for calculating is derived from the formula of Allen variance:

$$\sigma_y(\tau) = \frac{1}{\tau}\sqrt{\sum_{i=1}^{m}\frac{(\Delta T_{i+1} - \Delta T_i)^2}{2m}}$$

Where Δ T represents the phase difference, and τ the duration of the corresponding period time.

Continuous coincidence detection based on the periodic of the signals can realize the stability measurement. For example, 10 MHz can reach the measurement of 100 ns of the stability response time. At the same time, when we started the stability measurement of 1 μs, 10 μs and 100 μs, we should take the total coincidence variation in 10, 100 and 1000 periods into account. The emphasis should be put on the analysis of the width of discontinuity coincidence point which can be converted into phase amplitude information.

IFCS-EFTF2-PAB2-12

Phase noises of GaN-based surface acoustic wave oscillator

Rimantas Miškinis[1], Emilis Urba[1], Dmitrij Smirnov[1], Albertas Sereika[2], Romualdas Rimeika[2], Daumantas Čiplys[2]

[1]Metrology Department, Center for Physical Sciences and Technology, Vilnius, Lithuania
[2]Radiophysics Department, Faculty of Physics, Vilnius University, Vilnius, Lithuania

Email: miskinis@pfi.lt

The phase noise is one of the most important characteristics of oscillators determining its application possibilities. Gallium nitride is a material of interest with respect to electronics[1]. Our aim is to investigate the phase noise features of a GaN-based surface acoustic wave oscillator as well as to reveal the possibilities for employing such a device as a sensor of ultraviolet radiation. We use a structure similar to that described in the paper[102]. The GaN layers were grown by low-pressure metalorganic chemical vapor deposition on (0001) sapphire substrates. A pair of Al interdigital transducers was deposited on the GaN layer surface. Several samples with layer thicknesses in the range from 1.4 to 2.4 μm and transducer period of 24 μm were used. The corresponding resonant transducer frequencies ranged from 200 to 310 MHz. The distance between the transducers was 11 mm. This two-port SAW delay line was connected to a feedback loop of a wide-band amplifier. The output signal of the SAW oscillator was fed to a frequency counter.

The time base of the SR 620 frequency counter was disciplined to the 10 MHz signal of the Lithuanian national time and frequency standard HP5071A. With the measurement results being saved every second, we obtained the two series for each structure – one in the darkness and another with UV illumination. We used a 15 W lamp of the BLB type with the maximum at about 365 nm as a source of UV radiation. Both series were longer than 48 hours. Further, we discuss the results obtained with one of the structures. Average frequency generated in the darkness was 238.38 MHz, while that in illumination 222.64 MHz. Fig. 1 shows the power spectrum density $S_y(f)$ of the relative frequency deviation of the output signal for both series calculated following the instructions of the standard[103]. It is seen that the signal obtained with UV illumination features generally higher noise level, with some irregularly spaced peaks on the PSD graph. Noise level shall be taken into account while designing frequency shift-based UV sensors to make sure that the frequency shift obtained has not been overwhelmed by the phase noise.

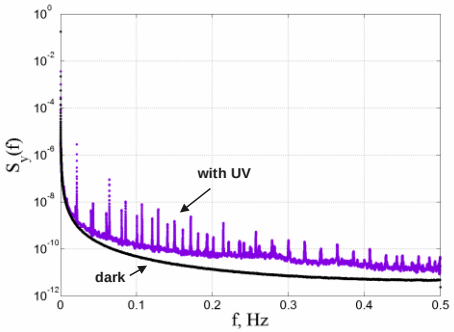

Fig. 27: Power spectrum density (PSD) of the output signal obtained with and without UV illumination

[102] D. Ciplys et al, "Visible–blind photoresponse of GaN-based surface acoustic wave oscillator", Appl. Phys. Lett., vol. 80, No. 11, p. 2020- 2022, 2002.

[103] IEEE Standard Definitions of Physical Quantities for Fundamental Frequency and Time Metrology – Random instabilities, IEEE Standard 1139 (July 1999).

IFCS-EFTF2-PAB2-13

Balanced SAW Oscillator in Composite Configuration with Colpitts and Cross-Coupled Pair

Yao Huang Kao and I-Jhih Wu

Department of Communication Engineering, Chung Hua University, Hsinchu Taiwan

Email: yhkao@chu.edu.tw

The oscillators with high quality-factor resonators in balanced configurations have received much attention. [104] These have the advantages of reduced noise, good power supply rejection ratio, and direct matching to the inputs of preceded stages. Recently two balanced SAW oscillators with two parallel Colpitts and with cross-coupled pair have been presented. [105] As compared, the former has better phase noise but suffers from the long transition due to the lack of phase inversion in initial growing. On the contrary, the latter has the opposite results. In this study a modified Colpitts architecture embedded with cross-coupled pair is investigated. The circuit is implemented under TSMC 0.18um CMOS process. The inherent feature of phase inversion needed for the parallel Colpitts can be easily provided by the cross-coupled pair. With the enhanced pair, the waveform transition speed is raised and thus, the start up and phase noise is improved. Actually, the cross-coupled pair also acts as latching in digital circuit. Here, the design of the pair size is carefully traded between latching and phase noise as shown in Fig. 1. The performances in cross coupled oscillators w/o Colpitts are summarized in the table I. The composite one indeed behaves better performance in terms of figure of merit (FOM).

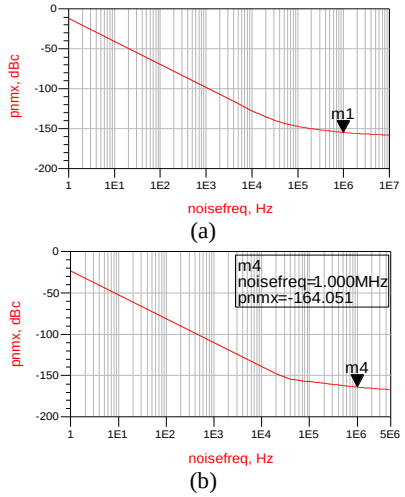

Fig. 28: Calculated Phase Noises in (a) cross-coupled CMOS oscillator and (b) composite oscillator with Colpitts and cross coupled pair.

Table I Performance List

Oscillator	Cross-Coupled Pair	Cross-Coupled Pair & Colpitts
CMOS Process	0.18um	0.18um
Power Supply(V)	1.6(V)	1.6(V)
Total Current(mA)	3.05(mA)	4.45 (mA)
Total Power Dissipation (mW)	4.88(mW)	7.12 (mW)
Oscillator Frequency(MHz)	622.642(MHz)	622.7 MHz
Phase Noise(dBc/Hz@1MHz)	- 153.59 dBc/Hz	- 164 dBc/Hz
Output Power(dBm)	- 4.44(dBm)	4.47(dBm)
Chip size(mm2)	0.545*0.510 (mm2)	0.68*0.585 (mm2)
$FOM = 10\log\left[\left(\frac{\omega}{\Delta\omega}\right)^2 \times \frac{1}{L(\Delta\omega)\cdot P}\right]$	202	211

[104] M. Aissi, E. Tournier, M.A. Dubois, C. Billard, H. Ziad, and R. Plana, IEEE RFIC Sym., 2006 , 24– 28.

[2] Y. H. Kao and I. J. Wu, IEEE NEWCAS, 2011, p. 995-998.

IFCS-EFTF2-PAB2-14

Integrating performance and production oriented design of satellite oscillators

Eskelinen Harri[1], Eskelinen Pekka[2],

[1]Lappeenranta University of Technology / School of Mechanical Engineering / Finland
[2]Aalto University / School of Electrical Engineering, Helsinki / Finland

Email: harri.eskelinen@lut.fi

This paper continues the research[106], in which the manufacturability analysis was carried out for of an oscillator made for the 5 GHz satellite and radar bands. The electronic circuit uses two cascaded bipolar microwave transistors in a emitter feedback amplifier configuration which is combined with a cylindrical dielectric resonator. Three miniature coupling loops are included to it, one for amplifier input, one for amplifier output via a Wilkinson power divider and another for the optional tuning varactor diode.

We have set two research questions: Firstly, how much is it possible to increase the Q-value of the resonator by improving the manufacturing quality of its milled geometries? Secondly, is it possible to describe the required manufacturing accuracy with the Q-value added to the PDM (Product Data Management) data set? The scope of this paper focuses on the multidisciplinary aspects of integrated performance and productive oriented design of satellite oscillators. For the first time the quality characteristic (Q-value) could be utilized directly in oscillator's mechanical PDM data to guide production.

Experimental evaluations of the effects of dimensional uncertainties were analyzed by constructing three resonators with different coupling loops. EdgeCAM simulations were used to evaluate the required PDM data for guiding the milling tools. Laboratory tests were conducted to measure the achievable surface quality and dimensional and geometric tolerances of the milled cavities.

A scalar network analyzer system was utilized and resonator center frequency, insertion loss, and quality factor were measured with different vertical and horizontal disc positions. The wide-band spectral response of each resonator was established. Based on the results the ceramic resonator disc alignment or its position in the cavity was not critical compared to the circular symmetry requirement of the cavity.

When analyzing the effects of non-circular cavity cross section, it was noticed that e.g. 0.1 mm deflection, which covers 90 degrees of the circumference of the cavity, causes the center frequency to rise to 5.1206 GHz, meanwhile the insertion loss was 10.60 dB and the Q-value dropped to 8533. These kinds of tests were repeated to collect and construct the corresponding PDM data set, which illustrates the relationships between the values of circularity and dimensional inaccuracy of cavities and the corresponding changes of the Q-values and the center frequencies.

[106] Eskelinen H., Montonen M., Performance-Integrated DFMA Analysis of a Satellite Oscillator, Advanced approaches to analytical and systematic DFMA analysis, Edited by Harri Eskelinen, Acta Universitatis Lappeenrantaensis 509, ISBN 978-952-265-366-6, Finland, 2012.

IFCS-EFTF2-PAB2-15

Redundant Frequency Source with Seamless Switchover

Shi Shaohua[1], Li Xiaohui[2], Tang Sheng[3]

[1]National Time Service Center, Chinese Academy of Sciences, Xi`an, Shaanxi, China
[2]Key Lab. Of Time & Frequency Primary Standards, CAS, Xi`an, Shaanxi, China
[3]Northwest University, Xi`an, Shaanxi, China

Email: ssh@ntsc.ac.cn

This paper describes a redundant frequency source system with seamless switchover that produces a stable and continuous output frequency signal. This system has primary and backup frequency produce links to generate the reference frequency. It has the ability to monitor the integrity of frequency produce links and switchover seamlessly between the primary and the backup links. By use intermediate oscillator of the measurement system as a third party criterion, the autonomous monitor integrity of frequency produce links was achieved without external reference signal. The excellent short-term stability characteristics of intermediate oscillator improves the accuracy and real-time for the monitoring of sudden failure and the degradation of performance. Seamless switchover was defined as the maintenance of both output phase and frequency continuity while and after the switcher from the primary to the backup links. It was initiated when system detects a degradation of the integrity of primary links. The experiment result has been presented showing that there were no detectable change in phase and frequency after the switchover, and the jump of frequency was less than 2e-13, the change of phase less than 100ps[107].

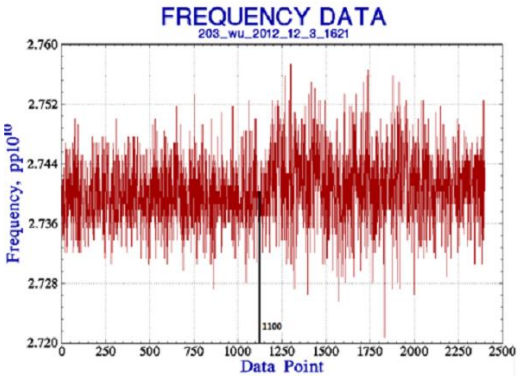

Fig. 1 Frequency change during and after switchover

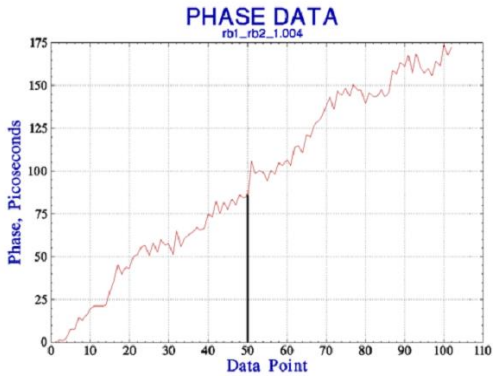

Fig. 2 Phase change during and after switchover

[107] Supported by National Natural Science Foundation of China

IFCS-EFTF2-PAB2-16

Programmable Delay Controller Allowing Frequency Synthesis and Arbitrary Binary Waveform Generation

Marek Peca, Michael Vacek, Vojtěch Michálek

Výzkumný a zkušební letecký ústav, a. s., Beranových 130, Praha – Letňany, Czech Republic
České vysoké učení technické v Praze, Břehová 7, 115 19 Praha 1, Czech Republic

Email: peca@vzlu.cz

Design of a programmable delay controller (PDC) within an ordinary space-compatible field-programmable gate array (FPGA) fabric is presented. Although PDC is a common digital block nowadays[108,109,110], the possibility to use it for low-jitter arbitrary frequency generation constrained only by minimum edge-to-edge time still seems to be uncovered. The PDC being presented may be able to replace current building blocks such as direct digital synthesizer (DDS), phase-locked loop (PLL) or various modulators; all within purely digital circuit (i.e., FPGA). Typical PDC based on a digital circuitry consists of fixed-length delay elements (transmission lines, gates) composed into signal path by electronic switches (multiplexers).

The novel idea of the developed PDC is seamless line delay switching at sampling frequency f_s close to the generated output frequency f_o unleashing the possibility of arbitrary binary waveform (frequency) generation constrained only by $f_o \leq f_s$ (*~100MHz*). Glitch-free operation with no unintentional edges is employed for proper PDC control signal switching.

The overall output signal (f_o) jitter is composed solely of the jitter of input signal and propagation jitter of the delay elements. For the selected delay line configuration, jitter (random component), non-linearity and resolution are presented. The overall signal path delay is continuously measured and calibrated using time-to-digit converter[111] (TDC) and/or phase meter circuits, both synthesized within the same FPGA fabric.

Preliminary single shot jitter measured for various signal path delays, using pulse generator being synchronous with TDC system/sampling clock, is about σ*=10ps* (Fig. 1) for the given space-compatible FPGA fabric.

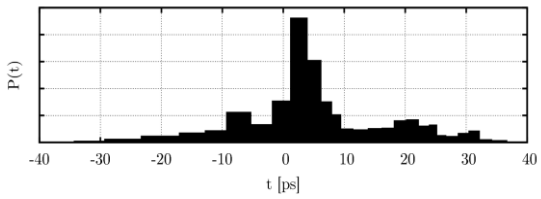

Fig. 29: PDC single shot jitter.

[108] D. C. Auth Z. L. M. Li, J.and Zheng and S. Wu, "Dynamic range accurate digitally programmable delay line with 250-ps resolution," in 8th International Conference on Signal Processing, 2006.

[109] A. de Castro and E. Todorovich, "High resolution fpga dpwm based on variable clock phase shifting," IEEE Transactions on Power Electronics, vol. 25, pp. 1115–1119, 2010.

[110] NB6L295: Dual Channel Programmable Delay Line with LVPECL Output, ON Semiconductor. [Online]. Available: http://www.onsemi.com.

[111] M. Peca, M. Vacek, and V. Michalek, "Time-to-digit converter based on radiationtolerant fpga," in 26th European Frequency and Time Forum, 2012, pp. 286–289.

IFCS-EFTF2-PAB2-17

An Efficient Room Temperature Only (RTO) Trimming Solution for an Accurate Self-Compensated Oscillator (SCO)

A. Elkholy, A. Ahmed, M. Shadoufa, M. Sakr, A. El-Sayed, M. Yousef, A. Helmy, M. Essam, N. Sinoussi

Timing Products Division, Si-Ware Systems, Cairo, Egypt

Email: nabil.sinoussi@si-ware.com

Driven by the continuous need for integration and cost reduction, research is eager to find a proper CMOS compatible replacement for quartz crystal oscillators (XOs). In a previous work[112], a self-compensated CMOS LC oscillator (SCO) based on LC tank temperature null (TNULL) phenomenon was introduced. The SCO forces the LC tank to operate at its specific TNULL phase (φ_{NULL}) where the oscillator exhibits a frequency deviation of few tens of ppms across a given temperature range. However, process variations affect the value of φ_{NULL}. Thus, trimming is required to compensate for these variations. Since it can degrade the overall cost and accuracy of the solution, trimming is one of the major challenges in having a highly accurate and fully-integrated LC-based reference clock generator.

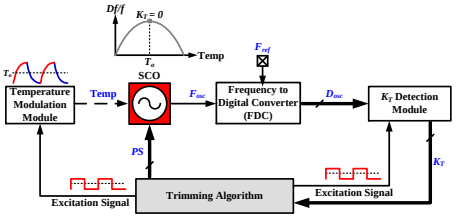

Fig. 30: Block diagram of RTO infrastructure.

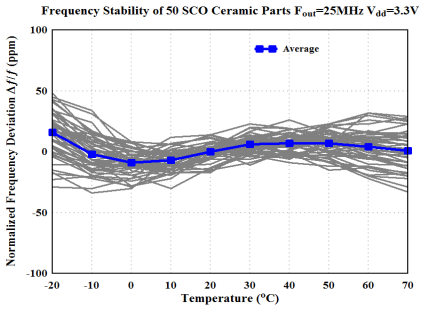

Fig. 31: The frequency deviation across temperature of 50 parts trimmed using the RTO to produce 25MHz CMOS output.

This work presents a new on-chip room temperature only (RTO) trimming solution for a highly accurate SCO with minimum testing overhead. The main objective of the trimming procedure is to search for the optimum phase setting (PS_{opt}) which adjusts oscillator phase to φ_{NULL}. Fig. 1 shows the block diagram of the RTO trimming infrastructure. It utilizes on-chip heaters to modulate the oscillator thermally. The oscillator output becomes a frequency modulated (FM) signal whose modulation depth depends on the frequency sensitivity to temperature (K_T). Using a frequency-to-digital converter (FDC) referred to an external reference frequency (F_{ref}), the oscillator FM signal is demodulated; hence, K_T is extracted. An intelligent trimming algorithm is used to search for PS_{opt} by adjusting the SCO K_T around room temperature to be approximately zero; hence, obtain the optimum SCO temperature dependence.

The SCO is implemented with the fully-integrated RTO trimming infrastructure on a standard CMOS 0.18µm technology. The RTO is utilized to trim 50 parts to produce 25MHz CMOS output. The parts are trimmed in parallel such that the average trimming time consumed per part is less than 1s. Fig. 31 shows the measured frequency deviation versus temperature of the 50 parts. The SCO achieves ±50ppm frequency stability across temperature from -20°C to 70°C.

[112] A. Ahmed *et al.*, "A Highly Stable CMOS Self-Compensated Oscillator (SCO) Based on an LC Tank Temperature Null Concept," Proc. IEEE FCS-EFTF, May 2011, pp. 443 – 447.

GRAIL USOs; Another In-Flight Quartz Radiation Experiment

Weaver Gregory[1], Asmar Sami, Oudrhiri Kamal[2]

[1]Space Department, Johns Hopkins University Applied Physics Laboratory, Laurel, MD/USA
[2]Radio Science Systems Group, NASA Jet Propulsion Laboratory, Pasadena, CA/USA

Email: gregory.weaver@jhuapl.edu

The Gravity Recovery and Interior Laboratory (GRAIL) mission successfully ended on Dec. 17th, 2012 after an extended science phase of over 280 days mapping the gravitation field gradient of the Moon with a precision of better than 50 E-6 g's over the entire lunar surface. The mission was performed by two tandem flying spacecraft named Ebb and Flow, both of which carried a JPL Microwave Dual One-way Ranging (DOWR) instrument that together formed a highly precise relative measure of the distance between the two spacecraft as they orbited the Moon.

The precision of the radio link maintained by the DOWR instruments was derived from the high frequency stability of the JHU/APL ultra-stable oscillators USO on-board each spacecraft. D. G. Enzer, et. al. describe the rare ability to extract the individual frequency stability of both in-flight GRAIL USOs without consideration of atmospheric propagation or the use of ground-clock comparison.[113] The opportunity to observe the USOs frequency throughout the GRAIL mission provides a record of not only the intrinsic performance of the oscillators, but their behavior during exposure to space conditions.

Reaction of quartz resonators (such as used in the GRAIL USOs) to ionizing radiation is well known. In 2003, an analysis of the Milstar FLT-1 on-board oscillator's frequency behavior during exposure to solar flares, described as a *space experiment*, was performed using space-weather data accumulated by the GOES.[114] In our paper, we will follow with another 'space experiment' analysis of the frequency effect of the March 7th, 2012 X5.4 level solar flare on the GRAIL USOs, which were in lunar orbit at that time. Fig. 1 shows the intensity of the March 7th proton flux detected by GOES 13. We will discuss the impact of this radiation exposure, and the asymmetric behavior of two space-oscillators coincidentally perturbed by the same space-weather event.

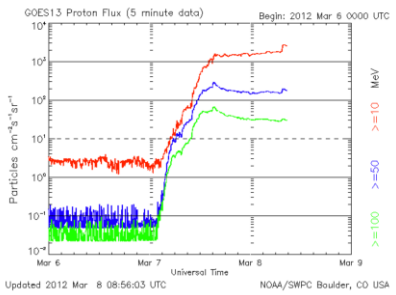

Fig. 32: Proton flux data collected from the Geosynchronous Operational Environmental Satellite GOES 13 during the ingress of ionizing radiation from the X5.4 solar flare of Mar 7th, 2012.

[113] D. G. Enzer, R. T. Wang, K. Oudrhiri, W. M. Klipstein, "In situ measurements of USO performance in space using the twin GRAIL spacecraft", 2012 IEEE IFCS Proc., p. 533-537

[114] S. D. LaLumondiere, S. C. Moss, J. C. Camparo, "A "space experiment" examining the response of a geosynchronous quartz crystal oscillator to various levels of solar activity," IEEE Trans. UFFC, vol.50, no.3, pp.210-213, March 2003

IFCS-EFTF2-PAB2-19

Long-Term Stability of a MEMS Disk Oscillator

Tristan O. Rocheleau, Thura Lin Naing, and Clark T.-C. Nguyen

University of California at Berkeley, Berkeley, CA, USA

Email: Tristan@eecs.berkeley.edu

A low phase noise oscillator referenced to a wine-glass disk MEMS resonator, hermetically vacuum packaged, and measured in a double-oven system, *cf.* Fig.1, has provided a first long-term measurement of a MEMS oscillator over 6 months. After an initial burn-in period, the frequency can be seen to stabilize to within the short-term measurement variation of ±300 ppb over a period of months, a significant improvement from previous studies on other MEMS resonator types[115,2], where frequency fluctuations were ±3.1 ppm[1] and ±1.2 ppm[2] over similar time scales. Including burn-in, the total observed aging of 9 ppm is now on par with many consumer quartz oscillators[3] designed for timing applications.

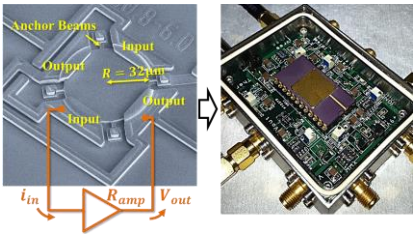

Fig.1: The 61-MHz wineglass disk oscillator. The circuit on left is hermetically sealed in the package and double oven on the right for temperature-stable measurements.

Wine-glass disk oscillators are known to exhibit exceptional short-term stability, having met the challenging GSM phase noise spec. some time ago[2], but long-term stability has until now been unpublished. To remedy this, Fig.1 presents the measured MEMS oscillator, comprised of a wine-glass disk resonator bond-wired to a custom transimpedance amplifier and hermetically packaged in a custom-built vacuum-packaging system capable of maintaining μtorr pressures. A double-oven system maintains a constant oscillator temperature at 34°C with less than 0.001°C deviation, a key improvement over previous long-term studies[1].

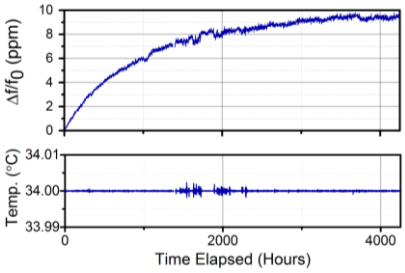

Fig.2: Measured frequency drift and temperature stability of the MEMS oscillator. Frequency measurements were made using an Agilent 53230A frequency counter with a 100s measurement time.

Fig.2 presents measured oscillator frequency versus time data over a half year aging period, exhibiting the same logarithmic decay behavior typical for quartz oscillators[3]. The increasing frequency suggests stress relaxation over mass loading or package leaks as the aging mechanism—no great surprise as both bondwires and high-temp glue adhering the die to package would be expected to produce strain. Despite this, performance is good, on par even with low-cost quartz oscillators. This is not unexpected for such wine-glass devices, for which supports attached to quasi-nodal points on the resonant disk structure greatly isolate the disk from the substrate and its associated stress changes.

---

[115] B. Kim et al., "Frequency Stability of Wafer-Scale…", *Sensors and Actuators A*, vol. 136, p. 125-131, 2007

[2] R. Tabrizian et al., "A 27 MHz Temperature Compensated MEMS Oscillator…", *Proc. MEMS* 2012, p. 23-26

[3] J. R. Vig and T. R. Meeker, "The Aging of Bulk Acoustic…", *Proc. IFCS* 1991, p. 77-101

[4] Y.-W. Lin et al., "Series-Resonant VHF…", *JSSC*, Vol. 39, No. 12, p. 2477-2491, 2004

IFCS-EFTF2-PAB2-20

All-Digital Frequency Synthesis based on Single-Bit Nyquist-Rate Sinewave Quantization with IID Random Dithering

Paul P. Sotiriadis[1], Natalia Miliou[1],
[1]Department of ECE, National Technical University of Athens, Greece
Email: miliou@ieee.org

The interest in all-digital frequency synthesis (FS) has been intensified in the R.F.I.C. industry over the past few years due to the challenge in the design and the extra cost of fabrication of R.F. analog and mixed-signal I.C. versus standard digital ones in modern nano-scale I.C. technologies. Efforts towards all-digital FS can be traced at least thirty years back[116]. This paper proposes single-bit dithered Nyquist-rate quantization of a sinewave as a method for all-digital FS.

The concept is illustrated in Fig. 1 where a random sequence $\{\mathbf{u}_k\}$ (dither) is subtracted from the sinewave and the result is quantized producing signal $\mathbf{x}_k = \mathrm{sgn}(\cos(\Omega k) - \mathbf{u}_k)$. Here $T_s = 1/f_S$ is the sampling period. Since $\cos(\Omega k)$ can be generated with very high precision using a LUT, the single-bit quantization is by far the dominant source of spurs and noise. In this sense Fig. 1 is a classical DDS with high resolution LUT, amplitude dithering and a 1-BIT DAC (i.e. an MSB truncator). We consider independent and identically distributed dithering sequences with continuous Cumulative Distribution Function (CDF) $G:[-1,1]\to[0,1]$ which we express as a series of Chebyshev polynomials of the first kind, i.e., $G(u) = \frac{1}{2} + \frac{1}{2}\sum_{j=0}^{\infty} \alpha_j T_j(u)$. Using the coefficients α_j we derive the power spectral density (PSD) of the output $\mathbf{x}(t)$ to be:

$$S_x(f) = \mathrm{sinc}^2(fT_S)\cdot\left[\sum_{j=1}^{\infty}\frac{\alpha_j^2}{4}\sum_{k=-\infty}^{\infty}\delta\left(f - \frac{k}{T_S} \pm \frac{j\Omega}{2\pi T_S}\right) + T_S\left(1 - a_0^2 - \frac{1}{2}\sum_{j=1}^{\infty}a_j^2\right) + a_0^2\cdot\delta(f)\right]$$

where the first term (sum) in the brackets is the desirable frequency component at $\Omega/(2\pi T_S)$ along with all harmonics present (modulo f_S), the second term is the continuous noise floor and the third one is the DC component of the output. We define the dynamic range (DR) as the ratio of the power of the frequency component at $\Omega/(2\pi T_S)$ over the noise's PSD at the same frequency and derive: $\mathrm{DR} = 10\log_{10}\left(\sum_{r=-\infty}^{\infty} a_{|1+qr|}^2 \Big/ \left[2 - 2a_0^2 - \left(\sum_{j=1}^{\infty} a_j^2\right)\right]\right) + 10\log_{10}(f_S) - 3.01$. The paper also presents necessary and sufficient conditions for spurs-free output, like that in Fig. 2 (without the $\mathrm{sinc}^2(fT_S)$ factor) and CDFs

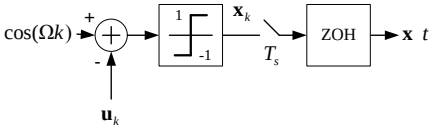

Fig. 33: Dithered single-bit sinewave quantization

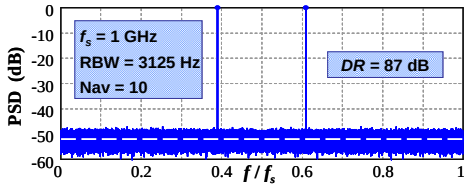

Fig. 2: Normalized PSD ($f_S = 1\,GHz$) resulting in a variety of DR values and spectra.

[116] V.S. Reinhardt, "Direct digital synthesizers", Technical Report, Hughes Aircraft Co, L.A., CA, Dec. 1985.

IFCS-EFTF Group 3 poster session 1

Forum Hall

Monday & Tuesday, July 22-23, 2013, 01:00 pm - 02:00 pm and 3:30 pm - 4:30 pm

Chair: **Elizabeth Donley**
NIST

IFCS-EFTF3-PAB3-1

Comparative Performance of Compact Schemes of Atomic Beam Longitudinal Deceleration Designed for Space-Based Frequency Standards

Vadim Zholnerov[1], AntonVershovskii[2], Yuri Rozhdestvenskiy[1]

[1]Russian Institute of Radionavigation and Time, St.-Petersburg, Russia
[2]Ioffe Phys.-Tech. Institute of Russian Academy of Science, St.-Petersburg, Russia
Email: zholnerov@mail.ru

Space-based frequency standards are probably the most important parts of any global navigation system. Optical frequency standards demonstrating the unique stability are extremely promising for space applications. Nevertheless, the stringent requirements to these applications force us to look for simpler technical solutions; among these, the radiofrequency standards using cold atom beams seem to have the greatest potential, and one of the solutions involves the use of CPT-Ramzey resonance optical detection[117].

Since the sensitivity of any scheme of registration of radio-optical resonance in an atomic beam is limited by the longitudinal velocity of the atoms, the velocity of the order of 1 m/s and registration area length of at least 0.5 m are required for obtaining stability of 10^{-15}. The combination of these requirements, in turn, limits the allowable transverse velocity of the atoms in the beam.

The optical preparation of the atomic beam characterized by the longitudinal velocity of 1 m/s and a divergence of 0.05 rad is a difficult task due to the limitations of the existing slowing schemes. There are two types of these schemes – so-called "laser chirping", and "Zeeman slowing"; the latter allows a continuous beam of cold atoms to be obtained, which is considered an advantage. In practice, however, none of these schemes in their classic versions provide a longitudinal deceleration of atoms below $10 \div 20$ m/s because of the significant time needed for slowing of atoms from the initial thermal distribution to a narrow velocity peak.

Therefore it was proposed[1] to significantly reduce the upper limit v_0 of the initial velocities of the atoms that interact with the laser radiation. In this case, the time of longitudinal deceleration dramatically decreases, which gives hope for obtaining the number of atoms with velocities ≤ 1 m/s sufficient for registration. The operating mode of such a slower is pulsed; some loss of intensity of the atomic beam occurs in this scenario, since only the slowest part of the thermal beam interacts with the cooling light. Thus, at a speed v_0 corresponding to one-half of the average thermal velocity, about 2% of a thermal beam are effectively used; this is compensated by shorter time (and hence the shorter slowdown length and less required power), and smaller transverse dimensions of the beam of atoms in the registration area..

In the present report, we numerically simulate the process of longitudinal cooling of the atomic beam in two slowing schemes, varying the initial velocity range and comparing the characteristics of the laser chirping and Zeeman slowing methods. We also examine the effectiveness of modifications of these methods implying use of a multimode cooling light. Estimates of the number of cold atoms required to obtain a stable CPT-Ramzey resonance signal are presented.

---

[117]V. S. Zholnerov, A. K. Vershovskiy, Yu. V. Rozhdestvenskiy, "Project of a Satellite Slow Beam Atomic Clock with CPT-Ramsey Registration", Proc. EFTF-2012, Gothenburg, Sweden, p.320-322, 2012.

Medium- to Long-Term Frequency Stability of High-Performance CW Double-Resonance Rb standard

Thejesh Bandi[1], Christoph Affolderbach[1], Camillo Stefanucci[2], Francesco Merli[2,3], Anja K. Skrivervik[2], Gaetano Mileti[1]

[1]Laboratory of Time & Frequency (LTF), University of Neuchâtel, Neuchâtel, Switzerland
[2]Laboratory of Electromagnetics and Acoustics (LEMA), EPFL, Lausanne, Switzerland
[3]Present address: RF Division, HUBER+SUHNER AG, Herisau, Switzerland

Email: thejesh.bandi@unine.ch

We have developed a compact high-performance laser-pumped Rb cell frequency standard suitable in particular as onboard GNSS oscillator[118]. It has a volume (physics package and laser head) $V < 3$ dm^3, mass < 2 kg and power consumption < 18 W. The clock exploits an enlarged magnetron-type microwave cavity[119] having TE_{011}-like mode that can hold the vapor cell of 25 mm diameter. A preliminary short-term frequency instability exhibiting $<1.4\times10^{-13}\ \tau^{-1/2}$ was reported[120].

In this communication we present detailed short-term noise budget analysis. A systematic metrological characterization of perturbing physical effects influencing the medium- to long-term clock frequency instability, such as the 2nd-order Zeeman shift, light-shifts, microwave power shift, cavity pulling, spin-exchange shift, and the temperature coefficient shifts will be presented.

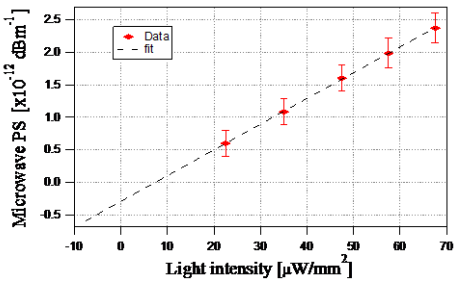

Fig. 34: Microwave power shift dependence on the pump light intensity. The laser frequency is stabilized close to the center of the optical transition in the clock cell.

We measure intensity light-shift coefficient (α) of $-2.85(2)\times10^{-12}$ mm^2/μW. At this condition of reduced α, we study the microwave power shift, and observe that the magnitude of microwave PS depends on the interrogating laser light intensity as shown in Fig. 1. For instance, at an input laser intensity of 8 μW/mm^2, one can nullify the effect of microwave power shift. We also present the frequency light-shift coefficient (β) and show its dependence on the input laser intensity.

These studies are of relevance for improving the medium- to long-term frequency stability of portable Rb cell standards, by compensating for the light-shift coefficients (α and β), microwave power shift, cavity pulling, second-order Zeeman shift and vapor cell temperature coefficients.

Acknowledgements: This work was supported by the SNSF (grant no. 140712) and the ESA. We thank C. E. Calosso (INRIM, Italy) for the microwave synthesizer (LO). We thank F. Gruet, M. Pellaton, P. Scherler and M. Dürrenberger (all LTF) for technical support.

---

[118] T. Bandi et al., "Laser-pumped high-performance compact gas-cell Rb standard with $< 3\times10^{-13}\ \tau^{-1/2}$ stability", Proc. of European Frequency and Time Forum (EFTF), Gothenburg, Sweden, April 24-26, 2012, pp. 494-496.

[119] C. Stefanucci, T. Bandi, F. Merli, M. Pellaton, C. Affolderbach, G. Mileti, A. K. Skrivervik, "Compact microwave cavity for high performance rubidium frequency standards", Rev. Sci. Instrum., vol. 83, 104706, 2012.

[120] T. Bandi et al., "Double-resonance in alkali vapor cells for high performance and miniature atomic clocks", Proc. of IEEE International Frequency Control Symposium, Baltimore, USA, May 21-25, 2012, pp. 686-691.

IFCS-EFTF3-PAB3-3

Dynamic Stark Effect in the Rubidium End Resonance with Laser Pumping

A.A.Baranov, S.V. Ermak, V.V. Semenov

Department of Quantum electronics, Saint-Petersburg State Polytechnic University, Saint-Petersburg, Russia

Email: lexusbar@gmail.com

In a work[121] a novel end resonance technique based on the optical orientation of the working atoms was suggested. This technique implementation decrease spin-exchange broadening of the resonance line in comparison to the magnetic-independent 0-0 resonance. However, light and orientation frequency shift inaccuracies weren't taken into account, whereas they inevitably lead to resonance frequency instability[122]. In this work we present analytical and experimental studies on the light shift component in the case of 1 degree uncertainty of the angle between magnetic field and optical axis directions. The results were carried out for Rb^{87} atoms pumped by a circular polarized laser beam of 100 μW/cm^2 intensity and 100 MHz linewidth. Table 1 contains the calculated results of the research. Light shift curves for $m_f = 0 \rightarrow 0$ and $m_f = 1 \rightarrow 2$ resonances in relation to the short-wave component of the D_1 line are sown on Figure 1. Experimental data has a good matching with the analytical estimates.

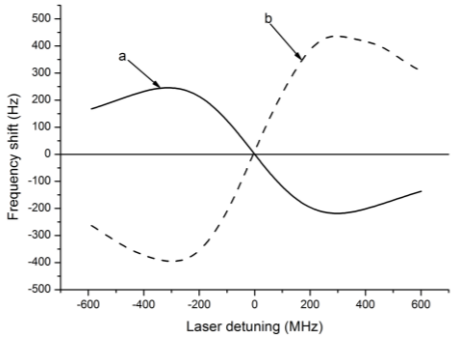

Fig. 35: Light shift curves for $m_f = 0 \rightarrow 0$ (a) and $m_f = 1 \rightarrow 2$ (b) transitions with laser tuned to Rb^{87} D_1 line, F=1 level.

Table 1.

	D_1				*D_2*			
Hyperfine level	*F = 1*		*F = 2*		*F = 1*		*F = 2*	
Light polarization	σ^+	σ^-	σ^+	σ^-	σ^+	σ^-	σ^+	σ^-
Light shift curve toughness (Hz / MHz)	3	−8	5	−1	5	-10	10	3
Orientation inaccuracy (1° C-field variation)	$4\cdot10^{-13}$	$3\cdot10^{-13}$	$4\cdot10^{-12}$	$3\cdot10^{-12}$	$3\cdot10^{-13}$	$7\cdot10^{-13}$	$3\cdot10^{-12}$	$4\cdot10^{-13}$

[121] Y-Y Yau, A.B.Post, N.N.Kuzma, A.M.Braun, M.V.Romalis, W.Happer .- Intens, Narrow Atomic-Clock Resonances, Physical Review Letters, v.92, №11, P.110801-110801-4, 2004.

[122] A.A. Baranov, S.V. Ermak, V.V. Semenov Orientation Frequency Shift of 0-0 Hyperfine Resonance in Rb^{87} Vapor with Selective Optical Pumping.- Optics and Spectroscopy, 2013, Vol. 114, No. 3, pp. 337–339. © Pleiades Publishing, Ltd., 2013.

IFCS-EFTF3-PAB3-4

2^{nd}-Harmonic Signals in Vapor-Cell Clocks as a Measure of Error-Signal Quality

James Camparo and Gilda Fathi
james.c.camparo@aero.org
Physical Sciences Laboratories
The Aerospace Corporation, 2310 E. El Segundo Blvd., El Segundo, CA, 90245, USA

In the standard frequency-feedback loop of atomic clocks, a field's frequency is modulated at f_m, and the atomic dynamics are detected and demodulated at the fundamental frequency (i.e., the 1^{st} harmonic). This 1^{st}-harmonic signal, S_1, is used to generate a correction for the clock's voltage-controlled crystal oscillator (VCXO), locking its output frequency to the atomic system. An intuitive understanding of this process is typically obtained by viewing the atomic dynamics in terms of the quantum system's *static* response to a resonant field: the 1^{st} harmonic atomic dynamics are taken as proportional to the 1^{st} derivative of the static resonance lineshape, the 2^{nd} harmonic dynamics proportional to the 2^{nd} derivative, etc. This *quasi-static approximation* suggests that the 2^{nd} harmonic signal, S_2, can be used to assess the atomic signal's quality for frequency stabilization purposes. Specifically, since the 2^{nd} derivative of the lineshape is proportional to the *slope* of the 1^{st} derivative, the quasi-static approximation suggests that one can take S_2 as a measure of the atoms' frequency-discrimination capability: $S_2 \sim dS_1/d\Delta$, where Δ is the frequency detuning of the VCXO's (multiplied) output frequency from the atomic resonance.

The problem with this logic, however, is that in order to obtain large signal-to-noise ratios and narrow atomic linewidths it is typical for atomic clocks to operate under conditions where $f_m \sim \Omega \sim \gamma$, with Ω and γ the Rabi frequency and relaxation rate, respectively. This regime of operation is neither quasi-static (large γ), adiabatic (large Ω), nor sudden (large f_m). Consequently, none of the standard approximations of quantum dynamics legitimately apply, notably the quasi-static approximation.

In order to develop a better *intuitive* understanding of atomic dynamics in the regime of clock operation, and in particular the nature of the atoms' 2^{nd} harmonic response to a frequency modulated field, we have begun a series of experiments investigating 2^{nd} harmonic signals as they appear in rubidium atomic clocks. In this presentation we will first discuss our experimental 2^{nd} harmonic testbed, which employs a diode laser for Rb^{87} optical pumping instead of an rf-discharge lamp to allow better experimental control over the light shift. Following this, we will discuss our initial results comparing S_2 with $dS_1/d\Delta$ for different modulation frequencies, and how well these results agree with a Quasi-Static Approximation (QSA) theory and a Small Modulation-Signal (SMS) theory. (Both of these theories yield closed-form expressions for S_2 and $dS_1/d\Delta$, as opposed to non-intuitive tables of numbers.) In brief, we find that the SMS theory is much better at predicting the relationship between S_2 and $dS_1/d\Delta$ than the QSA theory. This has relevance for atomic clocks, because at present engineers use empirical relationships between S_2 and $dS_1/d\Delta$ to set the optimum microwave power-level for their clock's operation (i.e., the optimum power-level for $dS_1/d\Delta$). Should the SMS theory's validity continue to be substantiated, it will give engineers a better understanding of the basic atomic physics that underpins their empirical relationships.

IFCS-EFTF3-PAB3-5

Higher-order Sideband Excitation for Pulsed CPT Atomic Clocks

Shigeyoshi Goka, Yuichiro Yano

Graduate School of Science and Engineering, Tokyo Metropolitan University,
Hachioji, Tokyo 1920397, Japan

Email: goka@tmu.ac.jp

A higher-order sideband excitation method combined with a pulse excitation is proposed to reduce power consumption of coherent population trapping (CPT) atomic clocks. Since the higher-order sideband excitation enables reduction of RF frequency, our method can significantly reduce switching power loss of a RF generator and its peripheral circuits. In the previous work[1], we reported the CPT-Ramsey resonances using a liquid crystal modulator for low power operation, therefore, our method can be applied to chip-scale atomic clocks (CSACs).

A 895 nm vertical-cavity surface-emitting laser (VCSEL) was used to excite Cs at the D_1 line. The Cs gas cell had a optical length of 20 mm and contained ^{133}Cs atoms and 4.0 kPa of Ne buffer gas at a controlled temperature of 42 ºC. The linearly polarized (lin || lin) laser beam was intensity-modulated by an acousto-optical modulator (AOM) to excite a CPT-Ramsey resonance. The pulsed laser light field with the 1.0 kHz switching frequency was generated by the AOM. The modulation RF frequency f_{RF} was set as $f_{RF} = f_{hfs} / 2n$. Here, f_{hfs} is the hyperfine-splitting frequency and n is the sideband order. Since switching power loss of RF is proportional to its frequency, lower f_{RF} can reduce power loss of a RF generator and its peripheral circuits. The measured CPT characteristics excited by the continuous and pulse method are shown in Table 1.

The experimental results show that the 3rd-order sideband excitation can lead to narrow fringe width and high contrast compared with the conventional continuous excitation (n = 1). The relative figure of merit was 2.3 and the relative light shift was less than one-third that with the conventional excitation. These results indicate that our method can reduce RF switching power loss and improve frequency stability.

Table 1 Measurement values with higher-order sideband pairs under continuous and pulse excitation.

Excitation Method	Sideband Order	f_{RF} [GHz]	Contrast [%]	FWHM	Q value (f_{RF}/ FWHM)	Relative Light Shift [10^{-12}/(μW/cm^2)]	Figure of Merit (Q value × Contrast)	Relative Figure of Merit
Continuous	n = 1	4.596 325	3.3	2.32 kHz	1.98×10^6	18.6	6.5×10^6	1.0
	n = 2	2.298 162	0.7	1.09 kHz	2.11×10^6	115	1.5×10^6	0.23
	n = 3	1.532 108	0.8	700 Hz	2.19×10^6	118	1.8×10^6	0.27
Pulse	n = 1	4.596 325	5.3	406 Hz	1.13×10^7	0.602	6.0×10^7	9.2
	n = 2	2.298 162	1.8	216 Hz	1.06×10^7	3.82	1.9×10^7	2.9
	n = 3	1.532 108	1.4	142 Hz	1.08×10^7	5.86	1.5×10^7	2.3

[1] "Pulse Excitation Method of Coherent-Population-Trapping Suitable For Chip-Scale Atomic Clock," Yuichiro Yano, Shigeyoshi Goka, Jpn. J. Appl. Phys. **51** (122401) 2012

IFCS-EFTF3-PAB3-6

The NPL Primary Frequency Standard System

K. Szymaniec, S. N. Lea, K. Liu*, P. B. Whibberley

National Physical Laboratory, Teddington, UK
*National Institute of Metrology, Beijing, China

Email: ks1@npl.co.uk

At the National Physical Laboratory, a system of primary frequency standards (PFS) is being developed with the aims of quasi continuous calibration of the duration of the step interval of the international time scales UTC and TAI, provision of stable reference and steering parameters for the local representation of UTC maintained by NPL, and absolute frequency measurements of atomic frequency standards being developed as secondary representations of the second.

This PFS system will consist of two caesium fountains. A microwave synthesizer based on an optical frequency comb referenced to an ultra-stable laser is being developed to replace the existing quartz local oscillator. One caesium fountain, NPL-CsF2, has been fully operational since 2009; following an initial accuracy evaluation in 2010 a reduced type B uncertainty of 2.3×10^{-16} was published in 2011, taking into account improved evaluation of the distributed cavity phase (DCP) shift[123]. A second fountain, similar to NPL-CsF2 in design and expected performance, is currently being assembled and preliminary operation is planned for summer 2013.

The design of NPL-CsF2 is relatively simple, with a single stage magneto-optical trap (MOT) with cooling beams in the (0,0,1) configuration. The small size of the atomic cloud released from the MOT is an advantage for cancellation of the collisional frequency shift[124]. An additional optical pumping stage accumulates the atomic population in the $m_F = 0$ clock state, resulting in a five-fold increase in the detected atomic signal[125]. This also enables the fountain to be operated at a higher densities of atoms, further reducing the uncertainty in extrapolation to zero density. The new fountain, NPL-CsF3, will incorporate many features of NPL-CsF2. The major novelty is a new microwave cavity designed to minimize the DCP shift[126].

NPL-CsF2 has been producing data almost continuously since early 2009. Unintentional breaks occur on average less than once in 33 days. Intentional interruptions are scheduled for system and lab maintenance. To date, 37 UTC evaluations have been reported to BIPM, covering 780 days, with typical total uncertainty (including frequency transfer uncertainty) of 4×10^{-16}. Since February 2011 a pilot scheme has been run to enhance the generation of the UTC(NPL) time scale. The setup consists of a free running hydrogen maser with its frequency shifted in an external offset generator according to measurements made by the fountain.

Highlights of our design and details of operation will be presented, together with discussion of long-term performance and results of calibrations of UTC and of UTC(NPL).

---

[123] R. Li, K. Gibble, K. Szymaniec, "Improved accuracy of the NPL-CsF2 primary frequency standard: evaluation of distributed cavity phase and microwave lensing frequency shifts", Metrologia, vol. 48, p. 283–289, 2011.

[124] K. Szymaniec, W. Chalupczak, E. Tiesinga, C. J. Williams, S. Weyers, R. Wynands, "Cancellation of the collisional frequency shift in caesium fountain clocks", Phys. Rev. Lett, vol.98, p.153002-1, 2007.

[125] K. Szymaniec, H-R. Noh, S. E. Park, A. Takamizawa, "Spin polarisation in a freely evolving sample of cold atoms", Appl. Phys. B, (in press).

[126] K. Gibble, S. N. Lea, K. Szymaniec, "A microwave cavity designed to minimize distributed cavity phase errors in a primary cesium frequency standard", Conference on Precision Electromagnetic Measurements (CPEM), p. 700–701, 2012.

IFCS-EFTF3-PAB3-7

Reducing the Blackbody Radiation Shift in the NIM new fountain design

Fang Fang*, Xiaoke Yan, Weiliang Chen, Kun Liu, Nianfeng Liu, Rui Suo, and Tianchu Li
Time and Frequency Division, National Institute of Metrology,
Beijing, P. R. China
*E-mail: fangf@nim.ac.cn

We are developing a new Cs fountain frequency standard in NIM, and shooting for the frequency uncertainty of a few parts in 10^{16}. The new fountain will run in a lab with the temperature fluctuation of 0.3K, and no active temperature control system will be added outside the flight tube of the fountain. Instead, an annular glass-water heat pipe will be used as an isothermal liner surrounding the flight tube to attenuate the temperature variations and improve temperature uniformity. The thermal conductivity of a glass isothermal liner is about 10 times higher than that of coppers. According to the working principle of heat pipe, it also works like a low pass filter, and reduces the temperature fluctuations of the system. The advantage of using an isothermal liner is to make the temperature of the whole interrogation region more uniform and stable. With precision standard platinum resistance thermometers measuring the temperatures of a few locations of the flight tube, the averaged temperature uncertainty is less than 50 mK. The frequency shift due to the blackbody radiation can be calculated according to the equation: $\Delta\nu=\beta(T/300)\text{^}4[1+\varepsilon(T/300)\text{^}2]^x$. With the coefficient of $\beta=-1.572(6)\text{E-}4$ and $\varepsilon=1.3(1)\text{E-}2$[xi,xii], the black body radiation shift can reach down to 8.5E-17 of this new fountain clock design.

IFCS-EFTF3-PAB3-8

Improvements of the atomic fountain clock at SIOM

Yuan-bo Du[1,2], Rong Wei[1], Ri-chang Dong[1,2], and Yu-zhu Wang[1]

[1]*Key Lab for Quantum Optics, Shanghai Institute of Optics and Fine Mechanics, Chinese Academy of Sciences, Shanghai, China, 201800;*

[2]*University of Chinese Academy of Sciences, Beijing, China, 100049*

A compact ^{87}Rb atomic fountain clock has been evaluated in Shanghai Institute of Optics and Fine Mechanics, Chinese Academy of Sciences, comparing with a H-maser, the stability of the clock has been measured and expressed as $\sigma(\tau)=5E\text{-}13\tau^{-1/2}$ at the time range of 3.5s to 40 000s, which reached 2.6E-15 at the average time of 40000 seconds, and degenerated at longer time due to the frequency drift of the H-maser, and the type-B uncertainty of the clock has been evaluated with the value of 2.4E-15. Several improvements have been realized on the clock, one was using an oven controlled crystal oscillator as its local oscillator and locking the clock by directly feeding the error signal to the oscillator, so as to let the clock have standard frequency signal outputs, in the research, we have demonstrated that the residual frequency drift of local oscillator was at the level of 10^{-16}-10^{-17}, which would affect the frequency shift and uncertainty, as well as given the method of correction, and which should be an universal effect for periodically running primary clocks. Another improvement was pointing out a method named as "self comparing" to evaluating the distributed cavity phase shift, collision shift, and light shift, by comparing the errors of atomic fountain clock when which was alternately running in two different states, the method evaluated the effects independently, not requiring any other comparing device, which the measuring precision of better than the uncertainty of the clock.

IFCS-EFTF3-PAB3-9

Design and realization of a low phase gradient microwave cavity for a continuous atomic fountain clock

Laurent Devenoges[1], Gianni Di Domenico[2], André Stefanov[3], Pierre Thomann, Laurent-Guy Bernier[1], Jacques Morel[1]

[1]Federal Institute of Metrology METAS, Bern, Switzerland
[2]Laboratoire Temps-Fréquence, Université de Neuchâtel, Neuchâtel, Switzerland
[3]Institute of Applied Physics, University of Bern, Bern, Switzerland

Email: laurent.devenoges@metas.ch

Last year we presented measurements of the microwave phase gradients in the coaxial cavity of the continuous fountain clock FOCS-2 and we pointed out that the excitation of higher-order cavity modes[127] limited the performance of the clock at the level of 10^{-14}.
We report here on the design, realization and performances of a low phase gradient microwave cavity with two interaction zones. The resonator is composed of a ring waveguide of rectangular cross-section with two independent feeds equidistant from the two interaction zones (see Fig 1(a)).
We fully characterized the amplitude and phase of the electromagnetic field in the microwave cavity

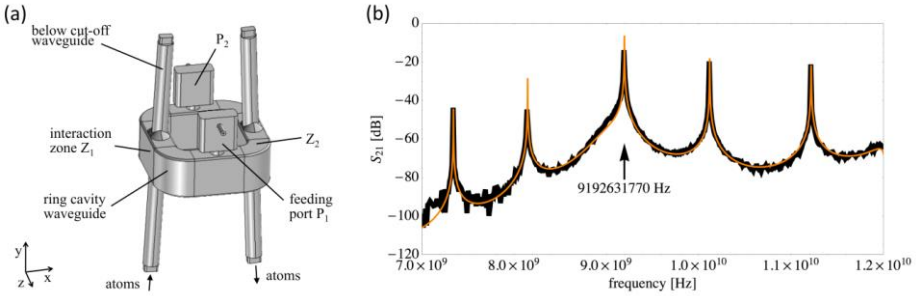

Fig. 36: (a) Scheme of the microwave cavity. The resonator is composed of a ring waveguide with two interaction zones Z_1 and Z_2 equidistant from the feeding ports P_1 and P_2. (b) Cavity transmission spectrum: measurement (black curve) is compared to finite element simulations (orange curve).

with the help of three-dimensional finite element simulations and analytical modeling. We predicted that spatial phase variations of 30×10^{-6} rad may be reached over each interaction zone by balancing power feeds[128]. To guarantee the phase homogeneity, the cavity has been machined with ultra-precision diamond milling, providing tolerances of a few micrometers for dimensions of the ring waveguide with an excellent surface roughness of 15 nm. The effect of mechanical imperfections on phase gradients has been extensively characterized with numerical simulations. After cavity assembly and tuning, measurements of the microwave spectrum (Fig. 1(b)) and the quality factor (Q_0=14'000) showed an excellent agreement with finite element numerical simulations. Latest results and future perspectives of the cavity performances will be presented.

[127] A. Stefanov et al., "Finite element method evaluation of the phase gradient in a coaxial microwave cavity", in preparation, 2013.

[128] G. Di Domenico et al., "Low phase gradient microwave cavity with two interaction zones for a continuous atomic fountain clock", submitted to IEEE UFFC, 2012.

IFCS-EFTF3-PAB3-10

Preliminary Results of the Microwave Frequency Standard based on $^{113}Cd^{+}$ Ions

Jianwei Zhang[1,2], Shiguang Wang[1,3], Kai Miao[1,2], Zhengbo Wang[1,2], Lijun Wang[1,2,3]

[1]NIM-THU Joint Institute for Measurement Science (JMI), Tsinghua University, Beijing (100084), People's Republic of China
[2]Department of Precision Instruments, Tsinghua University, Beijing (100084), People's Republic of China
[3]Department of Physics, Tsinghua University, Beijing (100084), People's Republic of China

Email: zhangjw@tsinghua.edu.cn

In the past decades, frequency standards based on trapped ions have been widely investigated. A project aimed at a microwave atomic clock based on the laser-cooled $^{113}Cd^{+}$ ions has been carried out since 2010 in our laboratory. This cadmium ion clock is expected to apply in the comparison between the clocks located in different places.

A linear quadruple ion trap and the technique of laser cooling are applied in this clock. The used laser system is a frequency-quadrupled diode laser system from Topitca Inc. To stabilize the frequency of the laser to MHz level, the 858 nm seed laser of this laser system is stabilized by comparing the frequency with an 852nm laser stabilized to the cesium lines via a transfer cavity[129]. By the laser cooling, the ions can be cooled down to crystallization state. In our experiments, it is demonstrated that approximately 10^4 ions are cooled to 16 mK by laser cooling[130]. Meanwhile, the frequency of the clock transition, the ground-state hyperfine splitting of $^{113}Cd^{+}$ ions, is measured[131], and the result is 15. 199 862 854 96(12) GHz.

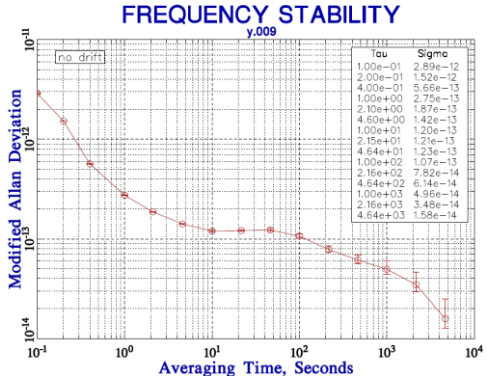

Fig. 37: Modified Allan deviation of the measured data. The period of measurement time is approximately 6 hours and the linear frequency drift

Recently, the preliminary stability of this clock is measured by the close-loop operation. Figure 1 shows the modified Allan deviation of the measurement where the linear frequency drift is removed. Because the loop time constant here is about 100 s, the stability at the averaging time less than 100 s is from the local oscillator. The stability from 100 s to 4000 s is approximately $1.5\times10^{-12}\ \tau^{-1/2}$. A series of upgrading of the experimental setup are planned, and an improved result is expected in the next phase.

---

[129] S.G. Wang, J.W. Zhang, Z.B. Wang, B. Wang, W.X. Liu, Y.Y. Zhao, L.J. Wang, "Frequency stabilization of a 214.5 nm ultraviolet laser", Chin. Opt. Lett., vol. 11, p.031401, 2013

[130] S.G. Wang, J.W. Zhang, K. Miao, Z.B. Wang, L.J. Wang, "Cooling and crystallization of trapped $^{113}Cd^{+}$ ions for atomic clock", Chin. Phys. Lett., vol. 30, p.013703, 2013

[131] J.W. Zhang, Z.B. Wang, S.G. Wang, K. Miao, B. Wang, L.J.Wang, "High-resolution laser microwave double-resonance spectroscopy of hyperfine splitting of trapped 113Cd+ and 111Cd+ ions", Phys. Rev. A, vol. 86, p.022523, 2012

IFCS-EFTF3-PAB3-11

Sub-mm scale optical fiber guided deep ultra-violet optical source for trapped mercury ion clocks

Lin Yi, Eric A. Burt, Shouhua Huang, and Robert L. Tjoelker

Jet Propulsion Laboratory, California Institute of Technology, Pasadena, USA

Email: Lin.Yi@jpl.nasa.gov

Mercury ion based atomic frequency standards provide practical advantages for spacecraft and ground applications requiring reliable, stable and/or compact atomic clocks [1-5]. In these standards, the size and geometry of the mercury RF discharge lamp used to generate 194 nm light and the related optical design to deliver the light to the confined ion cloud are one of the key challenges towards simplification and product commercialization.

In this paper, we demonstrate the functionality of a mercury capillary lamp with a diameter in the sub-mm range and Deep Ultra-Violet (DUV) radiation delivery via an optical fiber integrated with the capillary. DUV spectrum control is observed by varying the manufacturing parameters such as buffer gas type and pressure, capillary diameter, electrical resonator design, and temperature.

We will also show data for clock operation of the $^{199}Hg^{+}$ hyperfine transition at 40.5GHz when applying the above lamp and optical design. This new approach towards a more practical UV optics interface could benefit ion clock commercialization and trapped ion clock developments for deep space and GNSS.

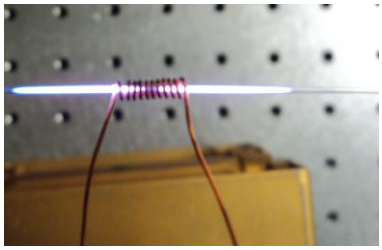

Fig. 38: DUV discharge plasma generated in a 0.45mm capillary tube. The capillary tube is fused

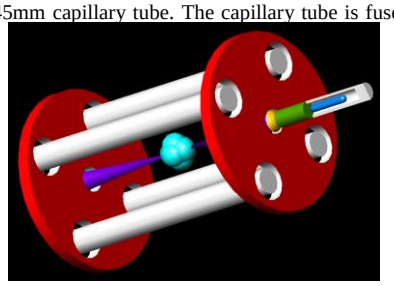

Fig. 2: Linear ion trap incorporating an integrated capillary lamp and fiber optic light delivery. Mercury ions (light blue) are trapped along the node created by the rods (grey) and endcaps (red). The capillary lamp at the right is integrated with the fiber (green) delivering DUV light (violet cones) to the ion cloud through a small lens (yellow).

IFCS-EFTF3-PAB3-12

Real Time Monitoring of the LNE-SYRTE Clock and Oscillator Ensemble and Applications

M. Abgrall, B. Chupin, D. G. Rovera, J. Guéna, S. Bize, P. Rosenbusch, M. Lours, Ph. Laurent, A. Clairon

LNE-SYRTE, Observatoire de Paris, UMR CNRS 8630, UPMC, Paris, France

Email: michel.abgrall@obspm.fr

The current LNE-SYRTE metrological ensemble includes an ultrastable frequency reference based on a cryogenic sapphire oscillator (CSO) slowly phase locked on an H-maser. We have improved the reliability of our maser ensemble with the set up of two new ones. Three phase comparators continuously measure the differences between our five H-masers.

The ultrastable reference is distributed to the other experiments located in laboratories a few 100 meters distant from the CSO through compensated fiber links. The signal is transmitted to the three fountains FO1, FO2 and FOM, and to the femtosecond lasers that allow connecting the strontium and mercury optical lattice clocks to the primary frequency standards.

In this poster, we will present the data processing that we have implemented to monitor this clock ensemble. Dedicated softwares hourly analyze the CSO loop and the fiber links data, to produce plots and files of interval to be rejected due to abnormal behaviors. The fountain data are also processed every hour. The raw data and parameters are uploaded from the fountain's computers in order to estimate and apply the frequency shift corrections for each clock cycle. We then apply an averaging over 0.1 d periods and a 3 σ filtering before computing the differences between the fountains on their synchronous operation periods. Besides, using the masers comparisons, we also get the calibration of each maser against the fountains. These processes including plots and alarm email generation facilitates the continuous survey of the operation of the clock ensemble and the detection of anomalies, necessary in the framework of the PHARAO/ACES space mission. The processed data will also serve in the future for the generation of a redundant UTC(OP) based on two different masers steered by the fountains.

IFCS-EFTF3-PAB3-13

Physics of systematic frequency drift of active hydrogen masers with autonomous cavity auto tuning

Vasilyev V. I., Gavrilov V. V., Gorelov A. G .

Institute of Electronic Measurements KVARZ, Nizhny Novgorod, Russia

Email: nnipi_kvarz@sinn.ru

Systematic frequency change of a signal (drift) is one of the primary metrological characteristics of hydrogen maser, but hypotheses about the drift nature so far have either qualitative or statistical and descriptive property. The analysis of evolution is based on research of an asymptotics of relaxation processes in quantum system[132]. As a first approximation the solution of the hydrogen maser differential equations in a «steady-state» approximation is used. The physical model of frequency drift is created; the principles of drift minimization are discussed.

The results of theoretical research are compared with results of experiments and long-term practical observations over drift of a hydrogen maser[133]. One of research conclusions is the statement that drift can change the value and a sign.

The importance of correct work of autonomous cavity auto tuning system is theoretically and experimentally proved. In Fig. 1 data on long-term measurements of frequency of our new CH1-75B Active Hydrogen Maser model are shown. This model can to tune the cavity with controlled accuracy. In the figure evolution of frequency of CH1-75B with the microwave cavity tuned and detuned by +40 Hz are presented. After cavity detuning the frequency of a maser was compensated by $\Delta f / f = -1\times10^{-12}$. After cavity detuning drift increased by 1.5 times from $+1.3\times10^{-15}$ to $+1.9\times10^{-15}$ per day. Microwave cavity was again tuned 38 days later. Frequency drift thus returned to its previous value.

The offered theoretical model allows to predict further behavior of maser frequency with the help of maser parameters monitoring.

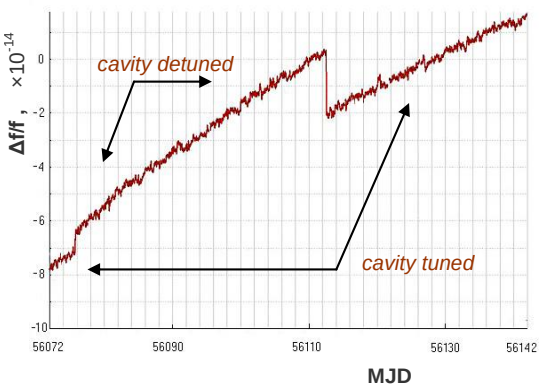

Fig. 39: H-Maser CH1-75B – secondary standard of unit of frequency VET1-20 (Institute of Electronic Measurements KVARZ) difference frequency. H-Maser with the microwave cavity tuned and detuned by +40 Hz.

132 Pestov E.N. Stability of relaxation processes in a quantum system as a main factor for achieving the long-term frequency stability of a standard.// – Proc. of the joint conference IFCS/EFTF. – USA, San Francisco. –2011, pp. 623-627.

133 Vasilyev V.I., Gavrilov V.V. Investigation of systematic frequency drift of active hydrogen frequency standards // Proc. of the 6th International Symposium "Metrology of Time and Space". – Russia, Moscow. –2012, pp. 151-154.

IFCS-EFTF3-PAB3-14

Active H-maser with increase power of the output signal

To improve short-time stability the amplification of the hydrogen maser output signal due to using the single-state selection and cooling the source cell is theoretically discussed. The results of the numeric calculation active H-maser power versus magnet parameters of specific selective system and source temperature are obtained. Particularly, the effect of increase maser power in 1.8 times due to amplification and elongation of selective system magnets is quantitatively calculated. Moreover, the output power is increased in 1.3 times due to cooling the source cell to the room temperature. The quantitatively comprasion between efficiency four-polar and six-polar magnets is done. In conclusion, the theoretic prototype of maser, that has a short-time stability achieved 2.48x10(-14) for one second, is represented.

IFCS-EFTF3-PAB3-15

A Waveguide Cavity for Miniature Rb Atomic Clock

Thomas Cao[1], Leiji Liu[2], Lin Yang[3], Xingshi Zheng[4]

[1]Spaceon Company, Chengdu, China

Email: sccyh@163.com

Rb atomic clock as a frequency standard is popularly used in the aspect of telecoms, electronic instruments, etc., although Chip-Scale Atomic Clock (CSAC) based Coherent Population Trap (CPT) has been manufactured two years ago. CSAC has tiny size and very low power dissipation, but the disadvantages of high costs and lack of batch engineer applications in CSAC can not been surpassed in short term. Alternatively, Rb atomic clock with traditional gas-cell has the advantages in costs and in power dissipation, and has got improvements in reducing profile recent year. The means to reduce Rb clock dimension is mostly to design kinds of cavity, and some progress has been made in recent year. Nowadays, introducing waveguide to the Rb clock cavity design, we have realized a novel miniature waveguide cavity, and Rb clock with the cavity is lowered by three folders.

In order to stimulate clock transition in Rb clock, the H-component of the 6.8Ghz microwave signal must be parallel to the quantum axes by C-field, and the level of the signal must be enough high. Except for resonant cavity, a kind of circular tube waveguide with one cirque cover made by Efratom was actually used in miniature Rb clock. But in this cavity, there is a difficult to tune its coupling ring which is soldered with Step-Recovery-Diode (SRD), and the coupling efficiency is very low by electronic vector. While designing our waveguide cavity, we specially set a screw slot to tune the cavity, and coupling ring made with semicircular figure can transfer microwave by magnetic vector. In this way, the screw slot acts as a relay-race to pass the microwave signal to Rb cell. Therefore, the size of the cavity can be reduced at large extent, and microwave coupling efficiency can get enough high simultaneously. With help of software simulation, the design has been approved. According to the data, in the waveguide cavity, the efficiency climax is 6.8 GHz, and magnetic component is parallel to the quantum axes, which satisfy the design requirements. Especially, the high coupling efficiency is from coordination between the semicircular ring and the tuning screw, which is the shinning point in the design.

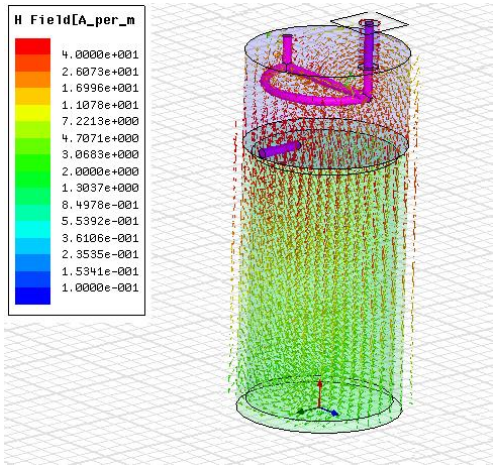

Fig. 40: the structure and the simulation of the miniature waveguide cavity. 6.8 GHz signal inputs into the cavity, and a special traveling wave model is shaped, the parallel H-component is enough high.

Instead of traditional cavity, the waveguide cavity was used in a typical Rb clock, and the similar Allan deviation of the clock has achieved. It means the novel waveguide cavity with lower size than resonant cavity can be used in Rb clock. Recently, the traditional Rb clock compatible with OCXO has been made with the cavity.

IFCS-EFTF3-PAB3-16

Experimental study on mutual injection locked VCSELs

Bozhong Tan[1], Jiehua Chen[2], and Sihong Gu[1,2]

[1] School of Physics, Huazhong University of Science and Technology,
Wuhan, People's Republic of China
[2] Key Laboratory of Atomic Frequency Standards, Wuhan Institute of Physics and Mathematics,
Chinese Academy of Sciences, Wuhan, People's Republic of China
Email: shgu@wipm.ac.cn

To exploit the better light source for the CPT atomic clock, we have developed a lin⊥lin quasi-bichromatic laser.[134] Whereas the realized laser generator still does not suit for a practical package atomic clock as a bulky optical isolator is used. Recently we have further explored a scheme that two VCSELs are frequency mutual injection locked, and which does not need the optical isolator.[135] However, there exist cavity modes problem as the two VCSELs form an optical cavity. We have systematically studied the influence of cavity modes on the quality of the produced lin⊥lin quasi-bichromatic laser, and our experimental results reveal that with proper parameters the influence of cavity modes can be well depressed, typical optical spectrum recorded under different parameters are present in Fig.1(a) and Fig.1(b). We have applied the lin⊥lin quasi-bichromatic laser of Fig.1(a) in CPT resonance experiment and obtained high quality CPT resonance signal. It is promising to realize a package lin⊥lin quasi-bichromatic laser generator and apply it in the package CPT atomic clock.

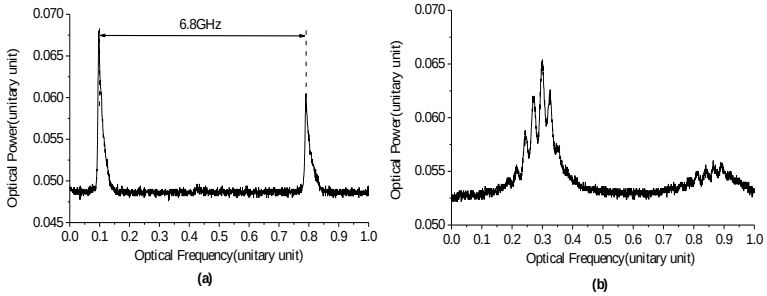

Fig. 41: The optical spectrum of two VCSELs' ouput recorded by Fabry-Perot interferometer. The injection ratio is (a) 0.5% , (b) 2.2%.

[134] Peter Yun, Bozhong Tan, Wei Deng, Jing Yang and Sihong Gu, "Quasi-bichromatic laser for lin⊥lin coherent population trapping clock produced by vertical-cavity surface-emitting lasers", Rev. Sci. Instrum. vol.83, p.093111, 2012.

135 Bozhong Tan, Peter Yun, Jing Yang, Yuan Tian, Sihong Gu, "A chip scale lin⊥lin quasi-bichromatic laser scheme", submit.

IFCS-EFTF3-PAB3-17

Effect of the coherent population trapping on saturated absorption resonances in Cs vapor

Ersoy Şahin[1], Ramiz Hamid[1] and Azad Ch. Izmailov[2]
[1]National Metrology Institute of Turkey, Gebze, Kocaeli, TURKEY
[2]Institute of Physics, Azerbaijan National Academy of Sciences, H. Javid av. 33, Baku, Az-1143, AZERBAIJAN
Email: ersoy.sahin@ume.tubitak.gov.tr

We have detected and analyzed sub-Doppler resonances in absorption of the monochromatic probe light wave interacting with the counterpropagating bichromatic laser beam in the rarefied Cs vapor. Given photoprocesses were realized on resonant 3-level Λ-systems formed by spectral components of the Doppler broadened D_2 line of cesium atoms.

The scheme of our setup is shown in Fig.1. The diode laser generates the monochromatic laser beam with the scanned frequency ω_1. The second coherent radiation component (with the frequency ω_2) was obtained from the initial beam by the electro-optical modulator. The frequency difference $(\omega_1 - \omega_2)$ was stabilized near the microwave interval $\Delta \approx 9192.6$ MHz between hyperfine sublevels of the Cs ground term.

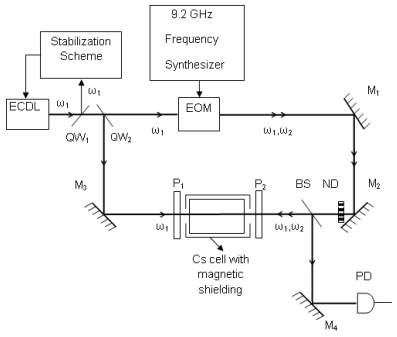

Fig.1. Scheme of the experimental setup, which includes external cavity diode laser (ECDL), electro-optical modulator (EOM), beam splitter (BS), mirrors (M_1, M_2, M_3, M_4), polarizers (P_1, P_2), quartz windows (QW_1, QW_2), neutral density fitler (ND), photodiode (PD) and the Cs cell with the magnetic shielding

Sub-Doppler saturated absorption resonances of the probe beam were recorded versus the scanned laser frequency ω_1 at various fixed values of the frequency difference $(\omega_1 - \omega_2)$ and intensity of the bichromatic pumping beam (having the same parallel linear polarization). By this applied method, we have established the essential dependence of given sub-Doppler resonances on the frequency difference $(\omega_1 - \omega_2)$ in its narrow interval (<1MHz) around the hyperfine splitting $\Delta \approx 9192.6$ MHz. According to our analysis, given interesting features are caused by displays of the coherent population trapping[1] on resonant 3-level Λ-systems interacting with counterpropagating pumping and probe beams. Obtained results of this work may be used for optimization of laser frequencies stabilization on atomic transitions.

[1] E. Arimondo, "Coherent Population Trapping in Laser Spectroscopy", Progress in Optics (Elsevier, New York, 1996), Vol. 35, 257-354.

IFCS-EFTF Group 4 poster session 1

Forum Hall

Monday & Tuesday, July 22-23, 2013, 01:00 pm - 02:00 pm and 3:30 pm - 4:30 pm

Chair: **Paul Muralt**
EPFL

IFCS-EFTF4-PAB4-1

Wireless temperature sensing of fast rotating objects

R. Fachberger*, C. Werner*

*Sensideon, Wels, Upper Austria/Austria

Email: funk@sensideon.com

A surface acoustic wave (SAW) transponder system was developed to measure the temperature and optimize the heat flow within a continuously variable transmission (CVT) gearing of a combustion engine. Though no external trigger is used, temperature measurements on the rotating parts have been realized up to a rotational speed of 8.000 rpm.

Temperature sensing of fast rotating objects is needed to optimize temperature critical parts or to find the operational limit of certain components within high speed engines. SAW transponder systems are well suited for such sensing applications, as they can be interrogated wirelessly[136].

In the paper a SAW sensing system for temperature measurement of fast rotating objects is described. The system was developed to measure the disk temperature of a CVT gearing. This temperature is critical due to possible heat transfer to the gear belt. The systems works without an external trigger and can be attached with minimal effort. The temperature of the disk was measured up to a rotational speed of the CVT disk of 8.000 rpm (Fig. 1). In the laboratory temperature measurements have been realized up to a rotational speed of more than 30.000 rpm.

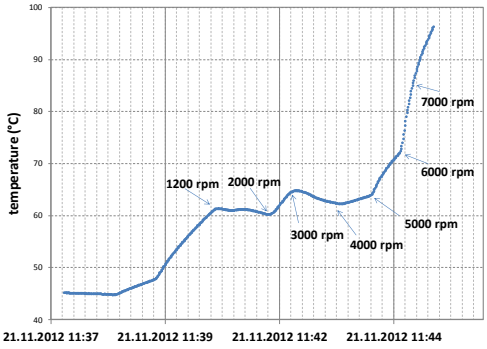

Fig. 42: Measured temperature of the fast rotating CVT disk

For a good thermal coupling the SAW sensor was directly attached to the CVT disk. Via a coaxial cable the radio frequency signal was transmitted from the SAW device to the transponder antenna, screwed onto the CVT gearing. All transponder parts have been locked with an epoxy adhesive, to ensure a good bond to the fast rotating gearing. A specialized transponder antenna was designed and matched to the metal surrounding and the SAW device to achieve a good sensor signal. Aspects of the system design and the measurement results are presented.

[136] A. Binder, R. Fachberger, "Wireless SAW temperature sensor system for high-speed high-voltage motors," IEEE Sensors Journal, vol. 11/4, pp 996 – 970, 2011

IFCS-EFTF4-PAB4-2

Packageless temperature sensor based on AlN/IDT/ZnO/Silicon layered structure

Ouarda Legrani[1], Omar Elmazria[1], Meriem Elhosni[1], Sergei Zhgoon[2], Ausrine Bartasyte[1] and Philippe Pigeat[1]

[1] Institut Jean Lamour, UMR 7198 Université de Lorraine – CNRS, France
[2] Moscow Power Engineering Institute, 14 Krasnokazarmennaja, 111250 Moscow, Russia

Email: ouarda.legrani@ijl.nancy-universite.fr

In previous works we have shown theoretically and experimentally [1], [2] the possibility to generate simultaneously Surface Acoustic Wave (SAW) and Waveguiding layer acoustic wave (WLAW) in layered structures AlN/ZnO/diamond [1] and AlN/ZnO/Silicon [2]. Such structures are of great interest because of their potential applications as packageless resonators, filters or sensors, based on WLAW, and as thermally compensated gas or liquid sensors, based on the combination of both SAW and WLAW. The aim of this work is to evidence the potential of the AlN/ZnO/Silicon structure as low cost, CMOS compatible and packageless temperature sensor able to operate at harsh environments.

2µm thick ZnO films were deposited on (100) Si by RF magnetron sputtering. IDTs were fabricated on ZnO/Si surface by sputtering aluminum followed by photolithography and wet etching processes. The AlN protection layer of 30 µm thick, deposited by RF magnetron sputtering, was optimized in order to avoid the AlN film cracking. A delay line operating at 525 MHz was obtained and tested versus temperature in air and in contact with liquid. Experimental characterization was compared to modeling with commercial software (COMSOL Multiphysics). The full sized delay line was simulated and the liquid was modeled by an additional layer on the top of AlN film. The effective confinement of the wave was shown by deposition of water's micro drop on the device and confirm by modeling.

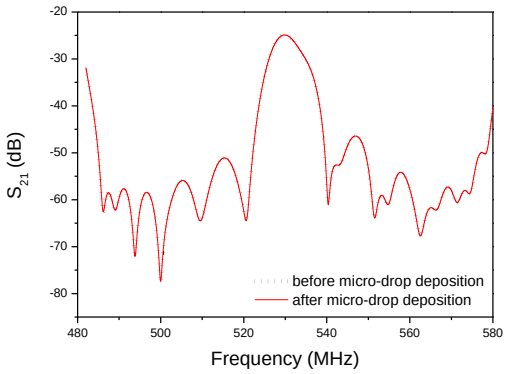

Fig. 1: Test of the wave confinement by the deposition of a water micro-drop on the AlN/ IDT/ZnO/Si structure.

Frequency-Temperature characteristic shows a very good linearity and a TCF value of -19ppm/°C in air and in contact with liquid. One can also observe that there is no change in transmission responses (S_{21}) collected in both conditions (Fig. 1). These results prove the total confinement of the wave in the AlN/IDT/ZnO/Si structure which is confirmed by 2D FEM modeling. Note that a Rayleigh wave on open surface is partially or completely attenuated. This study confirmed the feasibility of the AlN/IDT/ ZnO/Si structure as packageless sensor sensitive to temperature with the ability to protect itself from undesired environment effects such as humidity, gas corrosif or not, liquid, ...

[1] O. Elmazria et al., Applied Physics Letters, vol. 95, p. 233503, 2009.

[2] O. Legrani et al. ; IEEE sensor Journal, vol. 13, p. 487-491, 2013.

IFCS-EFTF4-PAB4-3

Piezoelectric and electroacoustic properties of V-doped and Ta-doped AlN thin films

E. Iborra[1], V. Felmestger[2], M. Mikhov[2], J. Capilla[1], J. Olivares[1], M. Clement[1]
[1]GMME-CEMDATIC-ETSIT, Universidad Politécnica de Madrid, Madrid, Spain
[2]OEMGroup Inc., Gilbert, AZ, USA

Email: eiborra@etsit.upm.es

New piezoelectric thin films for electroacoustic applications are being currently developed. AlN-based ternary compounds are expected to possess better properties than conventional AlN, such as larger piezoelectric activity, thermal stability of frequency and temperature resistance. The effect of adding Cr, Sc, Mg, Ti and B to AlN films has been previously investigated. Tantalum and vanadium are transition elements that can fit the oxidation level to substitute Al in the wurtzite AlN structure; their different ionic radii allow predicting changes in the AlN lattice structure and thus in the piezoelectric properties. In this communication we investigate the properties of $Al_{(1-x)}V_xN$ and $Al_{(1-x)}Ta_xN$ compounds for electroacoustic device applications.

1 µm-thick Al-X-N films (X = V or Ta) were reactively sputtered on 150 mm-Si (100) wafers using a dual target ac (40 kHz) powered S-gun magnetron. For this study, the two concentrically-nested ring-shaped targets were made of pure Al and pure X material. The power applied to each target could be controlled separately. The Si wafers were placed directly above the target array, which provided Al-X-N films with a gentle radial gradient of the X concentration. For electroacoustic test devices a very simple acoustic mirror made of a SiO_2/Mo/Al stack was used under a Mo/Al-X-N/Mo piezoelectric sandwich. The wafers were cut radially into 75 mm-strips, which were characterized at different points each 1 cm. The properties of the films were investigated as a function of their composition, measured by Rutherford backscattering spectrometry. The microstructure and morphology films were assessed by X-ray diffraction and infrared reflectance. Their electroacoustic properties and dielectric constant were derived from the frequency response of BAW test resonators built along the strip and separated by 1 mm.

The piezoelectric characterization through the test resonators reveals that all the samples investigated exhibit a significant decrease of the piezoelectric activity as compared to pure AlN films. Only the films containing the smallest amounts of V showed piezoelectric activity, although they hardly reach values of the electromechanical coupling factor k_{eff}^2 of 2.4%. XRD measurements suggest that V does not incorporate homogeneously in the AlN lattice and a slight variation of the c lattice constant has been detected. Films with the highest V content (around 5% atomic) exhibit an increase of the electrical conductivity. As for Ta doped films, the larger k_{eff}^2 of 4% corresponds to the film with the lowest Ta content. The decrease of k_{eff}^2 is accompanied by a reduction in the sound velocity of the longitudinal mode and an increase of the dielectric constant ranging from 10% to 20%. Structural characterization reveals that Ta distributes homogeneously in the AlN lattice and increases its c lattice constant up to 25%. The poor piezoelectric activity of Al-X-N films cannot be justified only by the presence of small amounts of impurities. The appearance of shear resonances as we move towards the edges of the wafers, along with the presence of a disordered layer developed during the early stages of growth revealed by XRD, suggest the presence of tilted grains in the films, which is more pronounced in Al-V-N films. This has been previously associated to growth of grains with opposite polar orientation, which would account for the lowering of the piezoelectric response. Further sputter process optimization is required to address the technological aspects of the film crystallinity and enhance the piezoresponse.

IFCS-EFTF4-PAB4-4

Evaluation of the acoustical properties of adhesive-free dual layer piezoelectric PVDF copolymer Transducer

Adit Decharat, Sanat Wagle and Frank Melandsø

Department of Physics and Technology, The University of Tromsø, N-9037 Tromsø, Norway

Email: adit.decharat@uit.no

Multiple layer of piezoelectric copolymer transducer has been deployed to improve the performance of transducers since their mechanical coupling efficiency are relatively low compare to ceramic transducer. Traditionally, to fabricate multilayer polymer transducers from pre-polarized film, adhesive layers are used for increasing their stack layers, which require mechanically attaching process where the desired and consistent thickness of each adhesive layer are difficult to achieve. Such condition, consequently, caused reduction of overall acoustic response signal[137]. As far as we know, only one group has previously produced an adhesive-free multilayer transducer with few publications[138]. Therefore, there is a need for comparative evaluations on the modeling with experimental result of an adhesive-free transducer.

In this study, we present the simulation and experimental results of the adhesive-free dual layer ultrasonic transducer. Using copolymer polyvinylidene fluoride trifluoro ethylene P(VDF-TrFE) in the fluid form together with commercial fabrication processes like spin coating, mask lithography and chemical etching etc., the dual layer transducer stacks were fabricated directly onto a Polyethyleneimine (PEI) backing unit. A FEM software (COMSOL Multiphysics) was employed to simulate the acoustical properties of the transducer. To characterize the transducer, the acoustic backscattering measurement from the backing-air interface was performed by exciting the transducer with ultra-wideband pulse (UWB) with various pulse widths. Transducer electrical impedance as function of frequency was also obtained by using an impedance analyzer.

The amplitude of the acoustical response from the backscattering measurements was for most cases significantly higher, when the transducer was excited and received signals from the both layers compared to a single one as shown in Fig. 1. Moreover, smooth broad-band acoustic signals were also measured. The simulated pulse echo response of the dual layer transducer under various pulse width excitation signals were calculated and compared from the experimental results, which showed good agreements. The simulation and fabrication processes were found to be beneficiary for the further analysis of multiple stacking of PVDF copolymer to enhance the acoustical performance.

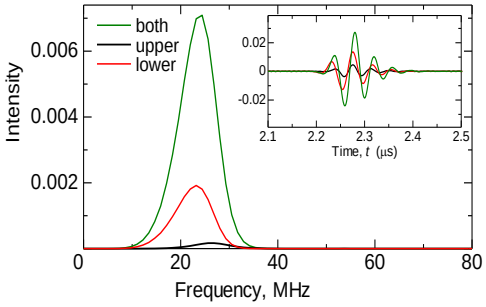

Fig.1: Acoustic reflection from backside of PEI backing (small window) and corresponding frequency spectrum.

[137] Q. Zhang , P. A. Lewin and B. P. E. "PVDF transducers - A performance comparison of single layer and multilayer structures", IEEE Trans. Ultrason., Ferroelect., Freq. Contr., vol. 44, pp.1148 -1156, 1997.

[138] T. Lilliehorn, T. Blom, U. Simu, S. Johansson, M. Nilsson, M. Almqvist, "Multilayer piezoelectric copolymer transducers", Proc. of 2005 IEEE Ultrasonics Symposium 3 (2005) 1618 – 1620.

Software Defined Radio for Passive Sensor Interrogation

J.R. Humphries and D.C. Malocha

Department of Electrical Engineering and Computer Science
University of Central Florida, Orlando, FL, USA

Email: James.Humphries@knights.ucf.edu

The software defined radio (SDR) provides a unique platform for interrogating passive, wireless SAW sensors. We have explored a commercially available SDR, the universal software radio peripheral (USRP), developed by Ettus Research. The highly versatile USRP platform defines many interrogator functions in software rather than hardware. The system provides a cost effective manner to develop a prototype transceiver (passive tag reader), and allows both internal FPGA programming and custom post processing software by the user.

This SDR design approach uses the N200 USRP and WBX daughterboard, providing center frequency tuning between 50MHz and 2.2GHz with +20dBm output power. The USRP hardware driver (UHD) is utilized to provide the software interface between the host computer and N200. GNU Radio, an open-source DSP and software radio library, is also employed for signal generation and post processing. The system allows the user to define the desired center frequency and sensor interrogation signal (chirp or other) of the transceiver. This information is passed to the USRP, which handles the transmission of the signal samples as well as acquiring the sensor responses. The data is returned to the host PC for post processing and data extraction.

The USRP capabilities are demonstrated by interrogating multiple orthogonal frequency coded (OFC)[139] SAW temperature sensors at 915MHz. Since OFC is a spread spectrum coding technique (>20MHz bandwidth) and since synchronization is required for passive sensor signal averaging, the USRP FPGA code was modified to handle the TX and RX independently from the host computer. This is in contrast to the default operation where signal sampling is accomplished over Ethernet. Characterization of the system is given with respect to SNR, output power, minimum detectable signal, and noise figure. Sensor range measurement experiments are also provided to characterize output power and signal averaging efficiency.

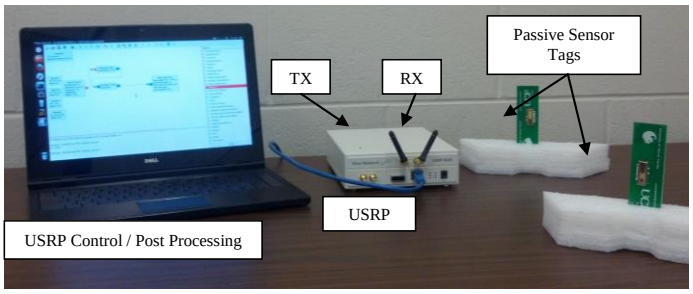

Figure 43: The N200 USRP (Center) is utilized to interrogate passive, wireless sensor tags (right). The center frequency and bandwidth of the transmitted output signal is defined by the user on the host computer (left). The USRP then independently handles transmitting the interrogation signal and receiving the sensor responses. Post processing of the data on the PC allows for signal averaging and data extraction.

[139] Malocha, D.C.; Puccio, D.; Gallagher, D., "Orthogonal Frequency Coding for SAW Device Applications," *Ultrasonics Symposium, 2004 IEEE* , pp. 1082- 1085 Vol.2, 23-27 Aug. 2004

IFCS-EFTF4-PAB4-6

Induced surface roughness to promote the growth of tilted AlN films for shear mode resonators

Mario de Miguel-Ramos, Marta Clement, Jimena Olivares, Jose Capilla, Jesús Sangrador, Enrique Iborra
GMME-CEMDATIC-ETSIT, Universidad Politécnica de Madrid, Madrid, Spain

Email: eiborra@etsit.upm.es

A serious drawback of biochemical sensors based on piezoelectric resonators is the requirement of operating in liquid environments. This can be overcome by exciting shear modes that exhibit less attenuation in liquid media than longitudinal modes. Shear modes can be excited in AlN-based resonators as long as that the films exhibit grains tilted with respect to the surface normal. These are commonly achieved by off-axis sputter deposition on rough substrates, since AlN microcrystals tend to grow normal to the surface whatever its topography. To achieve the desired tilt, a good control of the slopes of the substrate topography is required. The required roughness can be developed either in the underlying layers before the growth of the AlN film, or directly in the AlN deposition process by carrying out its growth under high pressure during the first stages, thus promoting the development of a thin layer of randomly oriented grains, which are the seed for the growth of the tilted AlN microcrystals. In this communication we analyze the influence of the substrate surface structure and the deposition parameters on the crystalline orientation of the AlN films and, hence, on the frequency response of shear mode resonators.

AlN films were deposited at 350°C in an UHV sputtering system on silicon substrates covered with Bragg mirrors composed of Mo and porous-SiO_2 layers. The first set of AlN films with tilted-grains was achieved by adjusting the roughness of the uppermost SiO_2 layer by varying the deposition conditions. SiO_2 layers were assessed by AFM and covered afterwards with a Mo or Ir bottom electrode before growing the AlN film. The second set of films was achieved by depositing at high pressure a non-oriented AlN seed layer on the bottom electrodes. In this case, the Bragg mirrors had been previously polished to remove the influence of their roughness.

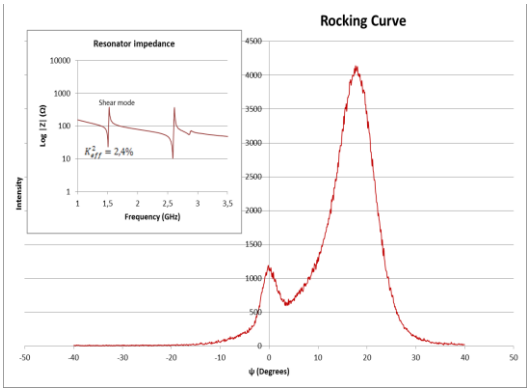

X-ray diffraction, infrared reflectance, AFM and electrical characterization were used to assess the influence of the seed layer structure and the deposition parameters on the tilt angle, the crystal quality and the shear mode frequency response of the AlN-based resonators. Depending on the roughness and nature of the seed layer, a controlled tilt varying from 0º to 30º was achieved. The frequency variation of the electrical impedance was fitted using Mason's model for both longitudinal and shear modes, which allowed us to derive the electromechanical coupling coefficient k_s^2 of the shear mode and its acoustic velocity. Values of k_s^2 as high as 2.4 % and an acoustic velocity of 6450 m/s were obtained in AlN films with 20° tilted grains deposited on rough SiO_2 substrates (see figure). Rough AlN seed layers provided values of k_s^2 up to 2% with great reproducibility. Preliminary in-liquid tests are also presented.

IFCS-EFTF4-PAB4-7

GNURadio as a digital signal processing environment: application to acoustic wireless sensor measurement and time & frequency analysis of periodic signals

J.-M Friedt[1]

[1] SENSeOR, c/o FEMTO-ST Time & Frequency, UMR CNRS 6174, Besançon, France

Email: jmfriedt@femto-st.fr

Digital signal processing has gained growing interest with respect to analog processing due to its reconfigurability, stability and flexibility. Thanks to these properties, a given hardware operating condition can be tuned as a function of operating mode (initialization, continuous mode or standby), whatever the environmental conditions (as opposed to resistor value dependence with temperature or capacitance with moisture levels) or as a function of the targeted application at the prototyping stage. Software Defined Radio is interested in the application of digital signal processing methods to radiofrequency signals, amongst which lie the frequency range of the devices of interest to the time and frequency community.

Although dedicated hardware and software has been demonstrated as functional for phase noise characterization of stable oscillators, no general purpose toolbox has been provided towards the time & frequency community for digital processing of the recorded signal in real time. In this presentation, we consider the GNURadio software environment as a suitable tool both for teaching and getting acquainted with the basics of digital signal processing applied to time & frequency characterization of periodic signals, but also as a framework for efficiently recycling the implemented algorithm on a wide range of hardware and thus on a wide range of frequencies. Indeed, the signal source supported by GNURadio range from the audio frequency sound card (<100 kHz signals) to the 100-MHz UHD provided by Ettus Research, to the Digital Video Broadcast (DVB) receiver USB dongles compatible with the low cost requirements of teaching. Most significantly, this opensource framework allows any interested user to add his own source and sink as peripherals whose data flow then become compatible with the processing flow already implemented.

In this presentation, we introduce the basic concepts of GNURadio, first from a user perspective with either the programming of signal processing chains written in the Python language or generated using the graphical user interface GNURadioCompanion. Then, we demonstrate how dedicated signal processing blocks, first prototyped in an interpreted language (GNU Octave or Matlab), are included within the GNURadio framework. We are interested in using existing GNURadio processing blocks for real time control and processing signals recorded from an implementation of a 2.45-GHz FMCW RADAR[140] used for probing acoustic delay lines acting as passive sensors interrogated through a wireless link, and for providing basic signal processing tools such as frequency counting and phase noise spectra. We demonstrate consistency between measurements from digital implementations of these algorithms and the classical measurement obtained with analog tools.

[140] inspired from MIT's Small Radar System course at http://ocw.mit.edu/resources/#LincolnLaboratory

IFCS-EFTF4-PAB4-8

Modeling and Analysis of a Liquid-Level Sensor Utilizing an Evanescent Field of a Trapped-Energy Vibrator

Ken Yamada, Tatsuya Ishioka, Naoki Aita

Department of Electronic Engineering, Tohoku Gakuin University,
Tagajo, Miyagi, Japan

Email: k-yamada@tjcc.tohoku-gakuin.ac.jp

A novel approach for detecting a small-scale variation in liquid level that employs a piezoelectric thickness vibrator operating in a trapped-energy mode has been studied by the authors[141,142,143]. In a trapped-energy resonator, an evanescent field is created in the surrounding (unelectroded) region in which the vibration amplitude decays exponentially. If the evanescent region is dipped in a liquid, a depth-dependent leakage of vibration energy will occur and this causes the deterioration in the mechanical quality factor Q_m and/or the electric conductance G. Because the liquid level is detected by observing variation in G of the resonator, it is desirable for simulating its operation that the sensing device should be modeled by an equivalent electric network.

In this study, the sensor is modeled by modifying an equivalent electric network proposed by Nakamura *et al*. which could represent the propagation of a thickness-vibration mode along the piezoelectric plate. Figure 1 shows the network model[144] for the sensing vibrator with a thickness of 2H. The central electroded region is composed of a transmission line (length: 2l, characteristic impedance: Z_0, wave number: γ) which is related to the electric terminal via some additional elements including a damped capacitance C_0. The section between the electrode edge and the liquid surface is expressed by a transmission line representing the unelectroded portion of length 2d, wave number γ_D and characteristic impedance Z_{0D}. The outermost regions are supposed to have an infinite length and are therefore expressed by the characteristic impedance Z_{0D}. To take the radiation loss into account, a phase angle $-\delta$ is applied to Z_{0D} for the portion dipped in a liquid. The variation in the electric properties with the dipping depth is evaluated for several geometry of the sensor by varying the ratio d/H.

Figure 2 shows an example of the variations in G with the liquid level d/H at the resonance frequency of the fundamental and inharmonic overtone modes. The ratio l/H is 9, and the admittance characteristic computed for the unloaded plate is shown in the inset. It is shown that the sensing property varies depending on which one of the fundamental and overtone mode is used.

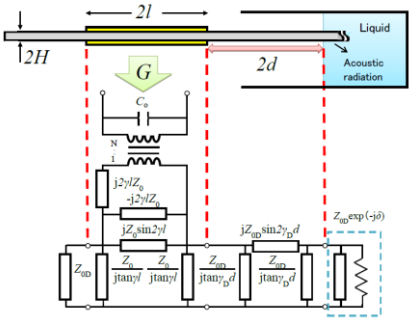

Fig. 1 Liquid-level sensor and network model

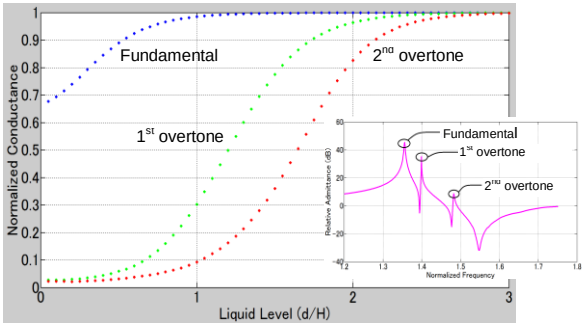

Fig. 2 Variations in G with the liquid level at resonance

[141] K. Yamada, H. Honda, S. Horiuchi, and T. Kinai: Jpn. J. Appl. Phys. **48** (2009) 07GB08.
[142] K. Yamada, S. Horiuchi, H. Honda, and T. Kinai: Proc. 2009 IEEE Ultrason. Symp., p.2508.
[143] K. Yamada and S. Seto, and S. Horiuchi: Proc. 2011 IEEE Ultrason. Symp., p.1522.
[144] K. Yamada, T. Koyama, and S. Seto: Jpn. J. Appl. Phys. **51** (2012) 07GC04.

IFCS-EFTF4-PAB4-9

THE $GaPO_4$ BIOSENSOR´S AFFINITY AND ITS ELECTRONIC EVALUATION

Milan Kolář and Jaroslav Nosek
Technical University of Liberec
Faculty of Mechatronics, Informatics and Interdisciplinary Studies
Studentska 2, CZ-461 17 Liberec, Czech republic

Abstract - This paper deals with the formation of the ASC immunocomplex at the surface of the Y-cut $GaPO_4$ resonator vibrating in thickness-shear mode. The three different orientations YXl (0.0°), YXl (-11.0°), and YXl (-16.4°), with the tolerance on the rotation angle $\pm$ 0.1° of the samples, are used in this study. The relevant GaPO4 material constants were calculated.
The biochemical affinity process can be characterized by association and dissociation kinetic rate constants, by binding between a covalently immobilized small molecule and its relative antibodies. The binding curves of series resonance frequency f_s vs. time t were measured and discussed. The following tasks were considered: activation by the cystamine, glutaraldehyde, and albumine as bioactive buffer, ASC antibody solution with phosphate buffer, and regeneration of the biosensor.
Standard frequency response of a new biosensor was evaluated by the analyzer Agilent E5100A. However, the newly developed digital processing techniques are used to precise the measurement and to evaluate the frequency changes. The Field Programmable Gate Array circuits (FPGA) open the field of digital signal processing. Our solution used the digital down converter (DDC) for evaluation of frequency changes. The DDC consists of three components: reference complex oscillator, low-pass filter and down sampler. Complex (quadrature) oscillator works on principle of direct digital synthesis and it provides a pair orthogonal sine and cosine waveform. The complex multiplier works as mixer, its output includes images centered at the sum and difference of input frequencies. The low-pass filter is digital FIR filter and it passes the difference frequency. The down sampler reduces the sampling rate of a signal.
The digital solution gives important advantages – digital stability, controllability and small size, that allow to realize the biosensor controller unit in a smaller volume. This solution reduces the cost of the biosensor unit and bringing it closer to the solutions "lab on chip". However, a resolution of the biosensor was maintained.

Keywords: GaPO4 biosensor, ASC formation, FPGA circuits, evaluation of frequency changes

IFCS-EFTF Group 5 poster session 1

Forum Hall

Monday & Tuesday, July 22-23, 2013, 01:00 pm - 02:00 pm and 3:30 pm - 4:30 pm

Chair: **Philip Tuckey**
LNE-SYRTE, Paris Observatory

IFCS-EFTF5-PAB5-1

Frequency Stability Estimation of Compass On-Board Clock Based on Smoothed Broadcast Ephemeris

Hang Gong[1], Wenke Yang[1], Zengjun Liu, Xiangwei Zhu[1], Feixue Wang[1]

[1] Satellite Navigation R&D Center, School of Electronic Science and Engineering, National University of Defense Technology, Changsha, Hunan 410073, China

Email: gonghang@nudt.edu.cn

Short-term frequency stability of on-board clocks is of paramount importance to GNSS applications, such as clock modeling and clock offset prediction. The ODTS method, which is well-known and commonly used, needs continuous observation from large monitoring networks and complex algorithms. BeiDou Navigation Satellite System (BDS/Compass) and Galileo are in their early stage of construction and do not have worldwide observation networks to track the satellite continuously. In addition, limited access permission has also restricted the common users from obtaining precise on-board clock parameters.

Based on the analysis of single station estimation method of satellite on-board clock stability, this paper proposed a simple estimation method based on smoothed broadcast ephemeris (namely SBE method), which only needs observation from one single receiver. The principle of this method is discussed, followed by performance evaluation using GPS data. Compared to IGS final clock product and other two methods namely PE and BE method, the performance of this method is validated (Fig.1). We conclude that the relative estimation error of this method is less than 10% for the average time of 1~800 seconds, which is consistent with the results of PE method using precise ephemeris.

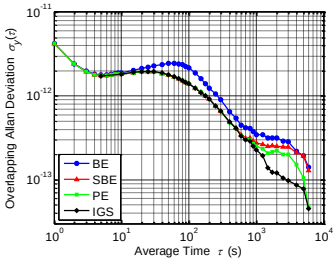

Fig. 44: Frequency stability of GPS PRN14 estimation result comparison among BE, PE and SBE Method

Finally, the short-term stability of all the current Compass on-board clocks (until December 2012) are estimated by the proposed method (Fig.2), the results show that the stability of all the satellite clocks are consistent and agree well with ODTS results. The short-term stability of current Compass on-board clocks is approximately 6×10^{-12}(τ=1s), 2×10^{-12}(τ=10s), 5×10^{-13}(τ=100s), 2×10^{-13}(τ=1000s).

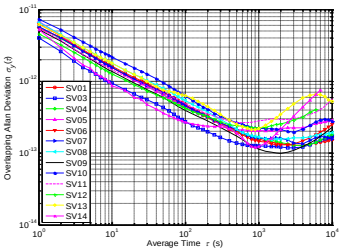

Fig. 2: Frequency stability of all the current Compass on-board clocks estimated by SBE Method

This proposed method in this paper provided some meaningful suggestions of short-term frequency stability estimation and simulation of on-board clock for Compass and Galileo civil users. When the satellite on-board clock stability is better than receiver clock, the method also provides a receiver clock stability estimation approach. In addition, since the method could calculate the short-term stability of the satellite clock in real-time directly using broadcast ephemeris and monitoring receiver's observation, it is also valuable for integrity monitoring and online performance assessment of satellite on-board clock.

IFCS-EFTF5-PAB5-2

The Test and Evaluation of GPS On-board Clock

Yongliang XU[1,2], Wei LI[1,2]

[1]National Time Service Center, Xi'an, China

[2]Key Lab of Time and Frequency Standard of the Chinese Academy of Sciences

Email:xuyl@ntsc.ac.cn

Abstract: In satellite navigation system, the mainly time-frequency equipment of space segment is on-board clock, and its performance directly related to the pseudo code ranging and doppler effect observation precision, then affects the satellite navigation system orientation, velocity measurement and time service, so the test and evaluation of the on-board clock attach much importance. The on-board clock performance evaluation experiment had been done many times in the GPS, GALILEO and GLONASS satellite navigation systems. The similar research and experiment are carrying out in Chinese satellite navigation system.

This paper studies the indicators used to evaluate the on-board clock, including the definition and calculation model of accuracy and stability. The performance of GPS on-board clock is evaluated based on the GPS on-board clock time difference data released by the IGS. Using Hadamard variance to evaluate the stability, the results show that the stability a day of most GPS on-board rubidium atomic clocks can reach 2×10^{-14}, in the time interval of 5 days, the stability reaches the highest level.

Keywords: On-board clock, evaluation, accuracy, stability

IFCS-EFTF5-PAB5-3

An FPGA implementation of the Distributed RF over White Rabbit

Pedro Moreira[1], Javier Serrano[2], Pablo Sanchez[2], Tomaz Wlostowski[2], Izzat Darwazeh[1]

[1] Electronic & Electrical Engineering, UCL, London, United Kingdom
[2] BE/CO/HT, CERN, Geneva, Switzerland

Email: pedro.moreira.09@ucl.ac.uk

Previous works have demonstrated modeling verification of the signal acquisition and processing blocks implemented by the distributed RF over White Rabbit (WR) system architecture and their effect on the SNR and Phase-Noise of the distributed RF signal[xiii]. This novel architecture relies on the White Rabbit network (an Ethernet based network with sub-nanosecond timing accuracy specification) to distribute an RF signal over distances that can reach 10 km using relatively low network bandwidth. Thus, the remaining network's bandwidth can be employed to transmit other control or non-control data.

To validate its real performance in a realistic scenario, this paper describes an FPGA implementation of the distributed RF scheme. In addition, characterization the reconstructed RF is given by showing measurements of the reconstructed RF signal phase-noise spectrum and Allan deviation. The paper continues with a description of the frequency drift and offset between the original and reconstructed RF signal.

Figure 1 and 2 shows the block diagram of the hardware implementation for the transmitter and receiver nodes of the distributed RF architecture.

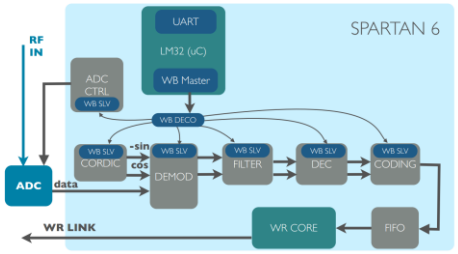

Figure 45 - Transmitter Architecture

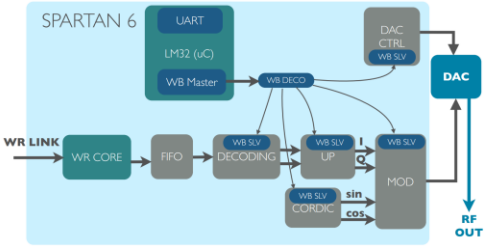

Figure 46 - Receiver Architecture

The results obtained from the presented FPGA system implementation confirm that the proposed distributed RF architecture is a low cost solution suitable for the distribution of RF signals. The RF signal can be distributed over relatively large distance using non-dedicated links and still reach the required SNR and phase-noise performance.

IFCS-EFTF5-PAB5-4

Calibration System For Stopwatches

A. Sahar[1,3], E.F. Dierikx[2], R.P. van Bemmelen[2], R.P. van Otterloo[2], M. Fauzi [3], M. Nasir[1]

[1]NML, SIRIM Berhad, Bandar Baru Salak Tinggi, 43900 Sepang, Malaysia

[2]VSL, Thijsseweg 11, NL-2629 JA, Delft, Netherlands

[3]Faculty of Electrical Engineering, University Technology of Malaysia, 81310 Skudai, Johor, Malaysia

Email: ahmads@sirim.my

Stopwatches and other similar timing display devices can be calibrated using three methods: the direct comparison, the totalize method and the time base method[1]. In the time base method, the frequency of the time base of the stopwatch, typically a quartz oscillator is measured directly. The time base method has a smaller measurement uncertainty than the other two methods.

In 2012, NML, SIRIM Berhad has developed an in-house designed calibration system for timing devices with displays that have digital seven segment characters on its display. The new system developed is based on an optical sensor and a dual counter.

An optical sensor (Fig.1) is directed to one of the seven segment characters of the LCD timing display of the stopwatch. When the stopwatch is free running, the counters will read the segments and take turns on counting the pulses of the 10 kHz reference frequency. The counted pulses are displayed in seconds.

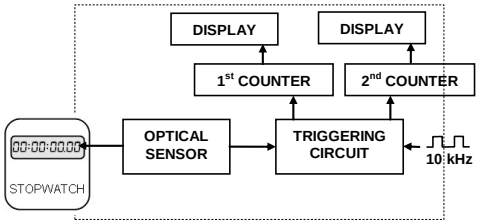

Fig. 1. Stopwatch calibration setup at NML, SIRIM

To evaluate the performance of the NML's calibration system, method used and technical competence, a bilateral comparison was organized with the national metrology institute from the Netherlands, VSL. The comparison protocol, traveling standards and evaluation results were prepared by the VSL.

VSL uses a commercial instrument based on the time base method. The sensor of the stopwatch calibrator (Fig.2) is sensitive to radiation that is commonly emitted from stopwatches. This radiation can be 32.768 kHz (internal oscillator), 32 Hz (LCD display) or 1 Hz (motor). The calibrator is calibrated by applying a known frequency signal derived from a reference frequency standard.

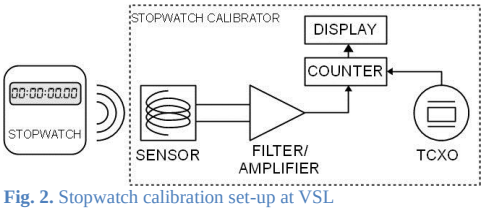

Fig. 2. Stopwatch calibration set-up at VSL

The transfer standards used in the comparison were an electronic stopwatch with LCD display and an electronic wristwatch with LCD display.

The results of the comparison show that there is a good agreement between the two laboratories within the combined relative uncertainty of 0.3 μs/s for a time interval of 1 day.

---

[1] Jeff C. Gust, Robert M. Graham and Michael A. Lombardi, "Stopwatch and Timer Calibration (2009 edition),"NIST Special Publication 960-12, 66 pages, January 2009

IFCS-EFTF5-PAB5-5

Analysis of the Sagnac Effect on the Accuracy of the Long Haul Optical Fiber Time Transfer System

Yu Longqiang , Lu Lin, Wang Rong, Jing Jisong, Wu Chuanxin, Zhu Yong, Zhang Baofu

PLA University of Science and Technology, Nanjing, China

Email: nj_lulin@163.com

In recent years, time transfer on long-haul optic fiber is proposed to compare two geographically separated clocks with high accuracy, on condition that the propagation time between two clocks is reciprocal or the unequal propagation time can be accurately measured and compensated [1][2]. In this paper, to the best of our knowledge, the influence of Sagnac effect in time transferring system over optical fiber is discovered and analyzed for the first time.

The Sagnac effect[3] in optic fiber time transferring system can be illustrated as Fig1. A and B are two points on the earth. The dashed line AB denotes the original optical fiber link between A and B. Simultaneous propagation processes are separated into two sequential processes to explain the phenomena more clearly as following: In time t, an optical signal is sent out from the A and it arrives at B in time t_1. Then, the signal starts in the opposite direction from B to A and reaches A in time t_2. So the actual bidirectional paths are A-B_1 and B_1-A_2 instead of A-B since the optical fiber is moving with the earth rotation. It is evident that bidirectional propagation times between two stations are unequal due to Sagnac effect, so calculation and compensation are needed to achieve accurate synchronization.

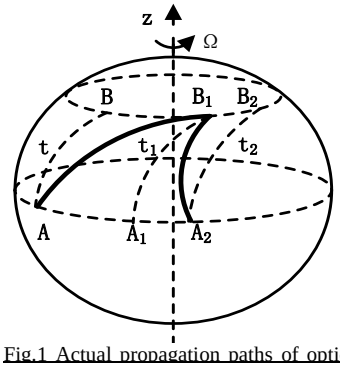

Fig.1 Actual propagation paths of optical

City	Distance(km)	Offset(ns)
London	1024.1	-3.2903
Rome	1189.3	-0.6357
Moscow	1667.3	4.7355
Stockholm	1054.3	0.6856

Table.1 Time deviation from Prague to other cities due to Sagnac effect

Infinitesimal of the fiber link and Lorentz-Einstein transformation are used to deduce the equation (1) which can calculate the Sagnac induced time deviation. The curve L_{AB} denotes an arbitrary fiber link illustrated in Fig.1. θ is azimuth angular and φ is polar angular in spherical coordinates through the fiber link. R is the mean radius of the earth, Ω is the earth angular velocity and c is the speed of light in vacuum.

$$\Delta T = \int_{L_{AB}} (R\sin\varphi)^2 \Omega / c^2 d\theta \qquad (1)$$

Table.1 shows Sagnac time deviations calculated by equation (1) when time is transferred from Prague to other four Europe cities with different directions through spherical circumference fiber links. It is showed that the Sagnac deviation may reach 10^{-9}s when the transfer distance is longer than hundreds of kilometers and it is also decided by practical route of the fiber links. So accurate time compensation or calibration concerning Sagnac effect should be committed for the purpose of reaching sub-nanosecond accuracy in long-haul optical fiber time transferring system.

[1] S. -C. Ebenhag, et al.. "Time transfer over a 560km fiber link ". Proc. 22nd EFTF, p.23~25, 2008.

[2] V. Smotalacha et al.. "Time transfer in optical network ", 42nd PTTI Meeting, p.427~436, 2010.

[3] R. Wang *et al*.. "Modified sagnac experiment for measuring travel-time difference between counter-propagating light beams in a uniformly moving fiber". *Physcs Letters A*, vol .**312**(2),p.7~10, 2003.

IFCS-EFTF5-PAB5-6

Interlaboratory Comparisons for Frequency Calibration: A First Two-Year Campaign in Italy

Franco Cordara[1], Diego Orgiazzi[1], Valerio Pettiti[2]

[1]Calibration Laboratories Department, ACCREDIA, Torino, Italy
[2]Optics Division, Istituto Nazionale di Ricerca Metrologica (INRIM), Torino, Italy

Email: diego.orgiazzi@tiscali.it

In 2011 and 2012 the Calibration Laboratories Department of ACCREDIA, the Italian Accreditation Body, together with the Time and Frequency Laboratory of the Optics Division of INRIM, the Italian NMI, organized two Interlaboratory Comparisons (ILC) for frequency calibration. The ILCs were directed towards most of the Italian Accredited Calibration Laboratories (ACLs) aiming to experimentally assess their metrological capabilities, as requested by ACCREDIA rules and according to the ISO/IEC 17025:2005[146]. More than 85% of all the Italian ACLs for frequency calibration were involved in the two ILCs - 8 in 2011, 10 in 2012 - which represents the first successful national campaign in this field and maybe the first in Europe.

Both ILCs implemented a multilateral scheme having INRIM as the pilot laboratory and fulfilled the EA requirements[147]. A set of instruments, preliminarily calibrated by the pilot laboratory, was circulated among the ACLs. Each ACL hosted the instruments for one week while performing all the measurements requested by the calibration protocol, before sending them to the next ACL. During each circulation, lasting from 5 to 6 months, the instruments were sent back once to INRIM for an intermediate calibration. A closure calibration was performed by the pilot laboratory at the end of each campaign in order to assess the consistency of the instruments performances in terms of stability and repeatability.

The set of travelling instruments included a GPS Disciplined Oscillator (GPSDO) with a 10 MHz output frequency used as reference standard for the ILC. A signal splitter allowed for connecting the GPSDO to the same antenna already used in the ACL for its local GPSDO-based frequency reference. Moreover, a netbook was used to collect relevant internal data for remote monitoring of the travelling standard. In the 2011 campaign, a low frequency function generator up to 15 MHz and a high frequency synthesizer up to 3 GHz – both externally referenced by the travelling GPSDO - were used to generate the signals to be measured by the ACLs. In the 2012 campaign, the two generators were replaced with the internal synthesizer of the GPSDO providing signals in the 1 Hz to 20 MHz range. Every ACL was asked to estimate the normalized frequency deviation of the 10 MHz provided by the travelling GPSDO versus the frequency standard of the laboratory, applying its accredited calibration procedures. Both direct frequency and time interval measurements were performed. Some decadic frequency values were also measured. The calibration measurement capabilities at 10 MHz of the ACLs ranged from 10^{-9} to 10^{-12}.

The paper will report all technical and logistic details of these ILCs (e.g., specification of travelling instruments, measurements requested by the protocol, problems faced and lessons learnt), together with an evaluation of the normalized errors E_n. An overall critical assessment of the whole experiment will be also provided and suggestions on possible improvements for future exercises will be discussed.

[146] ISO/IEC 17025:2005 "General requirements for the competence of testing and calibration laboratories"

[147] EA-2/14 M:2008 "Procedure for Regional Calibration ILCs in Support of the EA MLA"

IFCS-EFTF5-PAB5-7

Dual-Mixer Time-Difference Measurement system using Discrete Fourier Transformation

Shinya Yanagimachi, Akifumi Takamizawa, Takehiko Tanabe, Ken Hagimoto, Takeshi Ikegami

National Metrology Institute of Japan (NMIJ), AIST, Tsukuba, Ibaraki 305-8563, Japan

Email: s.yanagimachi@aist.go.jp

Precise oscillator have been contributing to the development of modern science and technology, such as the establishment of high-speed communications, navigation systems, and fundamental physics. Atomic clocks play an important role in the reliable implementation of time and frequency standards. The Dual-Mixer Time-Difference(DMTD) is the most appropriate way to measure the time difference between precise oscillators with a typical standard reference signals of 5, 10, and 100MHz.[148,2]

For the past decade, owing to the development of digital signal processing(DSP), it is proposed that low-speed analog-to digital converters(ADCs) are employed to deal with the beat signals instead of the time interval counter(TIC)[3]. This technique has an advantage that the measurement system has fewer components than the conventional DMTD, as there is no need for Sinusoidal-pulsed converters(SPCs) and zero cross detectors(ZCDs) in the TIC. Recently, for the DMTD using low-speed ADCs, we proposed the usage of discrete Fourier transformation (DFT) as a DSP technique (Fig.1),[4] and clarified the condition where the truncation error affect the accuracy to determine time difference and frequency difference between two oscillators. The truncation error occurs because of the disagreement between the real signals and suppositional signals based on the DFT.

In the conference, we will discuss the truncation error limiting the accuracy to determine the clock parameters, the realization of the measurement system(Fig.2), and the extensibility for multichannel DMTD system.

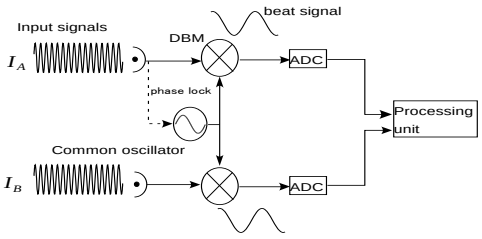

Fig. 47: Configuration of DMTD using DFT. Contrast to a conventional DMTD, SPCs and TICs is not required Instead, an ADC and a processing unit for the DFT are used.

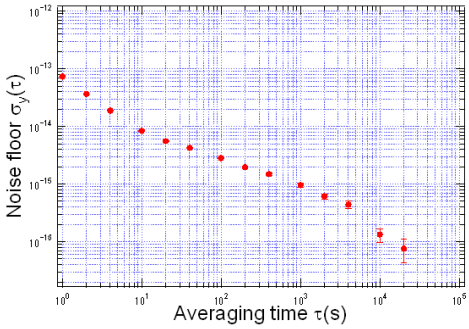

Fig. 2: System noise floor expressed in terms of Allan deviation as a function of the averaging time with the carrier frequency of the oscillator 10 MHz.

[148]D. W. Allan, and Herman Daams: Proc. 29th Annual Frequency Control Symp., 1975, p. 404.

[2]S. Stein, D. Glaze, J. Levine, J. Gray, D. Hilliard, D. Howe, and A. Erb: IEEE Trans. Instrum. Meas. **32** (1983) 227.

[3]M. Uchino, and K. Mochizuki: Electron. Commun. Jpn. **87** (2004) 21.

[4]S. Yanagimachi, K. Hagimoto, and T. Ikegami: JJAP, 52(2013) to be published.

IFCS-EFTF5-PAB5-8

Frequency reference transfer via optical fiber based on RF photonic phase shifter

Jianguo Shen, Guiling Wu, Lingdong Wang, Weiwen Zou, Jianping Chen

State Key Laboratory of Advanced Optical Communication Systems and Networks, Shanghai Jiao Tong University, Shanghai 200240, China

Email: wuguiling@sjtu.edu.cn

Frequency reference transfer via optical fiber is considered to be a promising method and has attracted an intensive research[149]. In this paper, a novel scheme of optical fiber frequency transfer, where a linear and stable RF photonic phase shifter (RFPPS) is designed and used as the transmitter and phase compensator at the same time, is proposed and validated experimentally.

Fig.1 shows the schematic of the proposed scheme. The RFPPS is implemented by a dual parallel Mach-Zehnder modulator and optical filter[150]. When a frequency reference signal is applied to the RFPPS, two subcarriers separated by the frequency of the reference signal are generated. Since the phase difference of two subcarriers depends on the bias voltage with the relation: $\theta = (V/V_\pi)\pi$, the phase shift of the recovered reference signal on the PD can be tuning linearly and fast by the bias voltage of the modulator. Therefore, the phase noise induced by the optical fiber link can be cancelled by simply controlling the bias voltage of the modulator with the phase error obtained by detecting the round trip phase fluctuation.

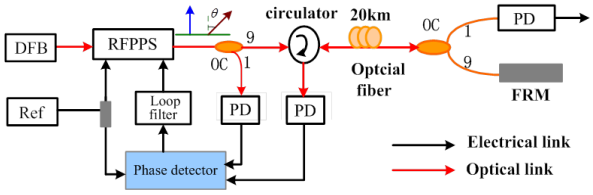

Fig. 1. The schematic of the propose frequency transfer system. FRM: Farlady rotation mirror.

Figure 2 shows the measured timing drifts in open and closed loop condition at receiver end over 20km optical link. Compared to open loop, the timing drift is suppressed from 130ps to less than 1ps in closed loop.

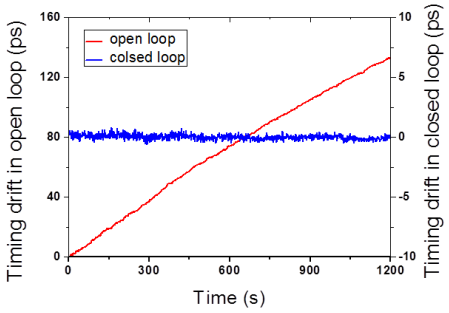

Fig. 2. Timing drifts in open and closed loop

[149] S. M. Foreman, K. W. Holma, K. W. Hudson, D. D. Jones, J. Ye, "Remote transfer of ultrastable frequency references via fiber networks" Rev. Sci. Instrum, vol.78, P. 021101, 2007.

[150] J.G. Shen, G. L. Wu, W. W. Zuo, J. P. Chen, "A photonic RF phase shifter based on a dual-parallel Mach-Zehnder modulator and an optical filter", Appl. Phys. Express, vol. 5, p. 072502, 2012.

IFCS-EFTF5-PAB5-9

Evaluation of a High Performance Continuous Time Interval Analyzer for Measuring Phase Stability

Glenn Bideberg[1], Sven-Christian Ebenhag[1], Per Olof Hedekvist[1], Freddy Ben-Zeev[2] and Ron Sigura[2]

[1]SP Technical Research Institute of Sweden, Boras, Sweden
[2]GuideTech, Mountain View, CA USA

Email: glenn.bideberg@sp.se

With an increased need for time interval precision in fiber frequency measurements within the framework of the National Metrology Institute for Time and Frequency in Sweden, an evaluation of a commercially available high performance "CTIA" Continuous Time Interval Analyzer on PCI card has been made.
The device under test was GT668PXI CTIA "Continuous Time Interval Analyzer" from GuideTech Inc. This is a device that currently is used for applications worldwide ranging from Satellite Tracking, Semiconductor- and Optical Testing, to monitoring of atomic clocks. It has a specified 2ps resolution which corresponds to the performance found in premium high-end Bench-Top Scopes.

The used methods for making clock frequency and phase measurements using a GT668PXI CTIA along with the Stable32 stability analysis software package will be presented together with the experimental results. The measurements will be performed in a controlled laboratory environment. The device is evaluated by direct frequency measurement using the device under test as a high-resolution CTIA, and by 1pps time interval measurements using a pair of dividers to produce reference and measurement signals and measuring their time difference.

Based on the results, an analysis of the suitability for the fiber-based measurements is performed by SP, in comparison to alternative techniques such as phase comparators.

IFCS-EFTF5-PAB5-10

OPTIME – time and frequency dissemination system based on fiber optical network – PIONIER

W. Adamowicz[4], A. Binczewski[5], W. Bogacki[5], A. Czubla[3], P. Dunst[2], J. Igalson[4], J. Kołodziej[1], P. Krehlik[1], D. Lemański[2], M. Lipiński[1], J. Nawrocki[2], P. Nogaś[2], P. Ostapowicz[5], T. Pawszak[4], J. Pieczerak[4], M. Stroiński[5], Ł. Śliwczyński[1], K. Turza[5]

[1]AGH University of Science and Technology (AGH), Krakow, Poland

[2] Astrogeodynamic Observatory (AOS), Borowiec, Poland

[3] Central Office of Measures (GUM), Warsaw, Poland

[4] Orange Poland (TPSA), Warsaw, Poland

[5] Poznan Supercomputing and Networking Center (PSNC), Poznan, Poland

Email: mlipinsk@agh.edu.pl, nawrocki@cbk.poznan.pl, a.czubla@gum.gov.pl, Janusz.Pieczerak@orange.com, wojbor@man.poznan.pl,

We describe the current stage and perspectives concerning using the optical network for time and frequency dissemination in Poland. In the first part we summarize an over-a-year continuous operation of 420 km-long connection between GUM in Warsaw and AOS in Borowiec near Poznan[151]. The link is based on the fiber optic system for time and frequency dissemination, developed at AGH[152,153]. Herein, for the first time, we are reporting over a year comparison of UTC(PL) and UTC(AOS) atomic timescales with this system, and we refer it to the results of comparisons performed by GPS-based methods, and we also address some practical aspects of maintaining time and frequency dissemination over fiber optical network.

In the second part we describe the OPTIME project (national time and frequency distribution system) which is based on the experience gained on the connection between GUM and AOS using fibers provided by PSNC (PIONIER) and TPSA, and on our other experiments[154]. We focus on general architecture created in OPTIME project.

In the last part we present the first phase of development of OPTIME system with two reference laboratories: GUM – Warsaw and AOS – Borowiec, with local repositories in PSNC – Poznan and Torun, and with the first end-users in FAMO – Torun.

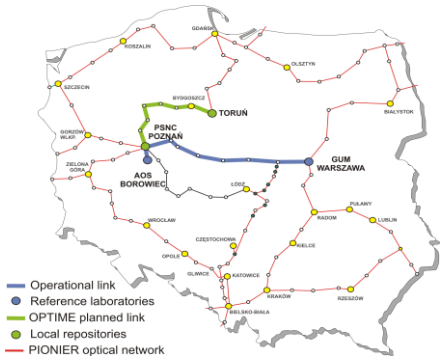

Fig. 48: National time and frequency distribution system – first phase.

Acknowledgement: Project OPTIME (no. PBS1/A3/13/2012) is co-founded by The National Centre for Research and Development – Poland.

[151] Ł. Śliwczyński, P. Krehlik, A. Czubla, Ł. Buczek and M. Lipiński, "Dissemination of time and RF frequency via a stabilized fibre optic link over a distance of 420 km", Metrologia 50, 133-145, 2013.

[152] P. Krehlik, Ł. Śliwczyński, Ł. Buczek and M. Lipiński, "Fiber optic joint time and frequency transfer with active stabilization of the propagation delay", IEEE Trans. Instrum. Meas. vol. pp.61 2844–51, 2012.

[153] Ł. Śliwczyński, P. Krehlik, Ł. Buczek, M. Lipiński, "Frequency transfer in electronically stabilized fiber optic link exploiting bidirectional optical amplifiers", IEEE Transaction on Instrumentation and Measurement, vol. 61, no. 9, pp. 2573-2580, 2012.

[154] P. Krehlik, Ł. Śliwczyński, Ł. Buczek, M. Lipiński, "Multipoint dissemination of RF frequency in fiber optic link with stabilized propagation delay", paper submitted to IEEE Trans. UFFC, 2013.

IFCS-EFTF5-PAB5-11

Interpolating time counter with a multi-edge coding

Ryszard Szplet, Dominik Sondej, Grzegorz Grzęda

Faculty of Electronics, Military University of Technology, Warsaw, Poland

Email: rszplet@wat.edu.pl

Precise integrated time-to-digital converters (TDC) are typically based on discrete delay lines built as chains of buffers[155]. Due to technological spread and changes in ambient conditions the delays of buffers involved are non-uniform. It manifests in different widths of quantization steps of TDC transfer function and ultimately deteriorates the resolution and linearity of conversion. The ultra-wide steps, especially observed in FPGA-based TDCs, may be reduced in the process of conversion by detecting not a single but a multiple signal transitions in a delay line[156]. The latter is further called a multi-edge coding.

In this paper we present the design, operation and test results of an interpolating time counter with a multi-edge coding principle applied in the second stage of interpolation. The counter is implemented in an FPGA device Spartan-6 (*Xilinx*) and provides a 2.6 ps resolution, 8 ps precision and 1 s measurement range. The development of such a high performance instrument needs to solve several design problems. The main of them are an implementation of a pattern generator and elimination of bubble errors. The aim of the pattern generator is to produce and launch a model square signal with a certain amount of edges and possibly minimal delays between them. We designed and tested two pattern generators based respectively on look-up tables and on a carry chain. The former one is simpler for implementation while the latter allows to control parameters of the model signal. This is important feature for the quality of T/D conversion that depends, among others, on the complexity of the model signal. We tested three variants of TDC with coding of three rising, three falling and six alternated edges.

With the increase in resolution of precise TDC, some invalid bits in the output thermometer code (bubble errors) may be observed. It happens due to many reasons, for example, signal jitter, device mismatch or supply voltage noise. In the TDC based on the coding of a single edge this error can be easily eliminated by the virtual rearranging of delay line outputs. However, if both, rising and falling, signal edges are coded additional hardware solutions are needed. In the designed time counter the bubble errors are eliminated with the use of a fast asynchronous encoder.

Tests of the time counter reveal also the look-ahead effect in the carry chains built in the FPGA device. This effect may cause loss of monotonicity of TDC transfer function. To avoid it, the order of delay cells is again virtually changed by a dedicated priority encoder.

The further research on this method includes the use of the multi-edge coding described here in the recently developed independent time coding lines[157] that should lead to higher resolution and precision as well as to smaller chip area.

---

[155] J. Kalisz, "Review of methods for time interval measurements with picosecond resolution", Metrologia, vol. 41, pp. 35–51, 2004

[156] J. Wu, Z. Shi, "The l0-ps Wave Union TDC: Improving FPGA TDC Resolution Beyond Its Cell Delay", IEEE Nuclear Science Symp. Conf. Record, pp. 3440–3446, 2008

[157] R. Szplet, Z. Jachna, P. Kwiatkowski, K. Rozyc, "A 2.9 ps equivalent resolution interpolating time counter based on multiple independent coding lines", Meas. Sci. Technol. 24 (2013) 035904 (15pp)

IFCS-EFTF5-PAB5-12

Managment and monitoring layer of optical network for time and frequency transfer

W. Bogacki[2], J. Kołodziej[1], J.Stępień[1], K. Turza[2]

[1] AGH University of Science and Technology, Mickiewicza 30, 30-057 Krakow, Poland
[2] Poznan Supercomputing and Networking Center, Noskowskiego 12/14, 61-704 Poznan, Poland

Email: jacek.kolodziej@agh.edu.pl

We describe requirements analysis and basic hardware solutions of optical network management and monitoring layer addressed to precise time and frequency transfer. We present current stage and perspectives of supervising time transfer fiber link. The work is based on experience coming from an over-a-year continuous operation of 420 km-long connection between Central Office of Measures (GUM) in Warsaw, and Astrogeodynamic Observatory (AOS) in Borowiec near Poznan. The link is based on the fiber optic system for time and frequency dissemination, developed at AGH[158,159,160]. The proposed solution will be used in OPTIME project.

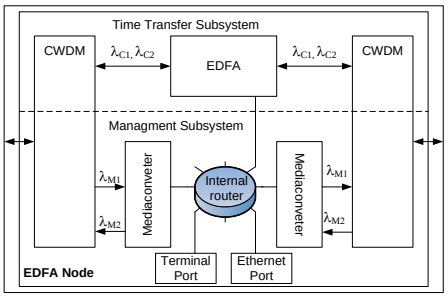

Fig. 49. Node of fiber optic system for time and frequency transfer with management subsystem.

We present specific requirements for monitoring, calibration and management the transmission lines to ensure high functionality, safety, and quality of the time and the frequency dissemination. The whole system must deliver information for providers, end-users, and equipment producers. One part of the paper contains a description of the essential elements of the system and communication methods, which are based on the standard protocols like SNMP or SSH.

The second part includes proposed hardware solution of optic system for time and frequency transfer with management subsystem which use multiplex data and management signals between devices (IN and OUT of Band). The block diagram in Fig. 1 shows typical node of the system. Control and status data coming from dedicated EDFA (Erbium Doped Fiber Amplifier) are formatted into Ethernet packet and distributed according routing table by internal router to 2 media converters or local external Ethernet port. The CWDM module combines two control link (with λ_{M1} and λ_{M2} wavelengths) with time transfer carrier (λ_{C1} and λ_{C2} wavelengths) in one common fiber. In summary we present preliminary results of transmission in couple of network configuration scenarios, showing data flow of managements packets.

Acknowledgement: Project OPTIME (no. PBS1/A3/13/2012) is co-founded by The National Centre for Research and Development – Poland.

[158] P. Krehlik, Ł. Śliwczyński, Ł. Buczek and M. Lipiński, "Fiber optic joint time and frequency transfer with active stabilization of the propagation delay", IEEE Trans. Instrum. Meas. vol. pp.61 2844–51, 2012.

[159] Ł Śliwczyński, P. Krehlik, A. Czubla, Ł. Buczek and M. Lipiński, "Dissemination of time and RF frequency via a stabilized fibre optic link over a distance of 420 km", Metrologia vol. 50, doi:10.1088/0026-1394/50/2/133, 2013.

[160] Ł. Śliwczyński, J. Kołodziej, „ Bidirectional optical amplification in long-distance two-way fiber optic time and frequency transfer systems", IEEE Transactions on Instrumentation and Measurement, in press.

IFCS-EFTF5-PAB5-13

Precision Time-Transfer over Optical Fiber Using an FPGA-based Time-Transfer Modem

Michael J. Wouters, Magnus T.L. Hsu

National Measurement Institute, Sydney, Australia

Email: Michael.Wouters@measurement.gov.au

Precise frequency transfer over optical fiber has been an active area of research for a number of years and attention has recently turned to precise time-transfer. Time-transfer differs from frequency transfer in that the propagation delay of the signal needs to be measured continuously. Five techniques have been reported: using a digital pulse[161]; using time-transfer modems designed for two-way satellite time-transfer[162]; using data framing information that is present on communications network traffic[163]; using RF-modulated lasers at two different optical frequencies[164]; and a refinement of the Precise Time Protocol[165].

The work reported here is a Field Programmable Gate Array (FPGA) based implementation of a time-transfer modem, using off-the-shelf hardware. The goal is to integrate the time-transfer modem with the digital radio-frequency transfer technique that we have previously reported[166]. Eventually, the system should be implementable on relatively low-cost hardware.

The current version of the modem measures the signal delay via pseudo-random noise (PRN) ranging using standard GPS PRN codes. One attractive feature of implementing the modem on an FPGA is that different codes and interpolation schemes can be easily tried, since only changes to software are required.

The modem has been benchtop-tested by inserting fixed delays in the signal path. These tests indicate a delay measurement accuracy better than 100 ps, with the measurement limited by the calibration of the fixed delays. Measured delays show stability at the 1 ps level over periods of a week.

We are presently working on testing the modem on a number of optical fiber links that we have available, and will be reporting the results of these experiments at the conference.

---

[161] Wang, *et al.*, "Precise and Continuous Time and Frequency Synchronisation at the 5×10^{-19} Accuracy Level", Sci. Rep., vol. 2, Article 556, 2012.

[162] Dirk Piester, *et al.*, "Time transfer through optical fibers (TTTOF): first results of calibrated clock comparisons", Proc. 41st PTTI, p. 89-99, 2009.

[163] Sven-Christian Ebenhag, *et al.*,"Time Transfer between UTC(SP) and UTC(MIKE) Using Frame Detection in Fiber-Optical Communication Networks", Proc. 43rd PTTI, p. 431-41, 2011.

[164] Sven-Christian Ebenhag, *et al.*, "Single way fiber based time transfer with active detection of time transfer variations", Proc. 42nd PTTI, p. 413-25, 2010.

[165] Pedro Moreira, *et al.*, "White Rabbit: Sub-Nanosecond Timing Distribution over Ethernet", ISPCS, 2009.

[166] M. T. L. Hsu, *et al.*, "All-Digital Radio-Frequency Signal Distribution Via Optical Fibers", IEEE Phot. Tech. Lett, vol. 24 , p. 1015-17, 2012.

IFCS-EFTF5-PAB5-14

Fiber-optic Time and Frequency Transfer based on RF Carrier Phase and Pseudorandom Noise Code

Wenke Yang[1], Hang Gong[1], Long Huang[1], Xiangwei Zhu[1], Guangfu Sun[1]

[1] School of Electronic Science and Engineering, National University of Defense Technology, Changsha, Hunan 410073, China

Email: ywk@nudt.edu.cn

Many literatures have been reported on stable frequency transfer via optical fibers (both in optical and RF domains). As to time transfer over fibers, frame detection in SDH or SONET network, timing code including 1PPS signal transferred using two-way Dense Wavelength Division Multiplexing (DWDM)and two-way time transfer over fiber link based on commercial modems have been reported.

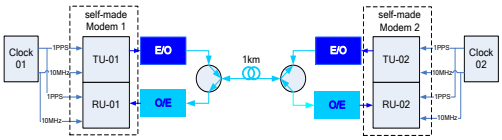

Fig. 50: The two-way fiber-optic time and frequency transfer system with self-made modems and 1km spooled-fiber

In this paper, the experiment based on self-made modems and off-the-shelf fiber-optic devices aiming at achieving precise fiber-optic time and frequency transfer technique based on radio frequency (RF) carrier phase tracking and pseudorandom noise code correlation is demonstrated. It is different from the previous work on time transfer over fibers, for that the RF carrier phase information and the pseudorandom noise code are both used through the fiber-optic link in the two-way mode. It works like two-way satellite time and frequency transfer (TWSTFT), but the signal propagation path is replaced with optical fiber and the up and down frequency converting process for satellite transmit is replaced by the intensity modulation and the corresponding direct detect of the optical wave. The RF carriers modulated by different pseudorandom noise codes are transmitted by the fiber-optic link with intensity modulation and direct detect of 1550nm optical wave in two-way mode. At both ends, the one-way delay including time difference of both end clocks are measured by pseudorandom noise code correlation and RF carrier tracking. With the assumption of two-way transfer symmetry, the time difference of both end clocks can be calculated.

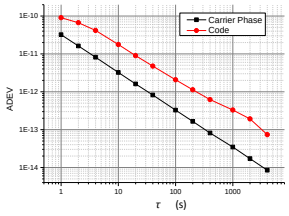

Fig. 51: The measurement noise shown as ADEV with carrier phase and code respectively

The two-way transfer asymmetry caused by the different optical wavelengths for both directions, which is the case in DWDM system, is avoided by the Code Division Multiple Access (CDMA) system here. The demonstration system is with the 66MHz carrier and 1km spooled-fiber. The experiment shows that the two-way fiber-optic time and frequency transfer system with self-made modems and 1km spooled-fiber is of the measurement noise with Allan deviation (ADEV) of $3.2\times10^{-11}\tau^{-1}$ with carrier phase information and $9.1\times10^{-11}\tau^{-1}$ with pseudorandom noise code correlation.

IFCS-EFTF5-PAB5-15

Study on the Method of Measuring and Estimating the Time Synchronization Accuracy under Constellations Autonomous Operation based on the Ground Testing System

Ren Xiaoqian[1,2,3], Qin weijin[1,2,3], Wu Haitao[1,2] Hua Yu[1,2]

[1]National Time Service Center, China Academy of Sciences, Xi'an, Shannxi/China
[2]Key Laboratory of Precision Navigation and Timing Technology, CAS, Xi'an, China
[3]University of Chinese Academy of Sciences, Beijing, China

Email: renxq@ntsc.ac.cn

With the development of satellite navigation systems and navigation warfare concepts proposed, the capability of autonomous survival and operation of the satellite navigation system has become an important part of the research in the field. Making the inter-satellite link to achieve the autonomous function of constellation is one of the primary means to improve the viability of the satellite navigation system. The study of measuring and estimating constellations autonomous operation time synchronization's accuracy in condition of the satellite navigation system operate normally is so little.

This paper discusses the importance of testing and verification for diffident working mode, it provides one kinds of method of measuring and estimating the time synchronization accuracy under constellations autonomous operation based on the ground testing system. In the paper, it gives the basic principle and the computational model, verifying and analysing the method by simulation data.

The method of measuring and estimating the time synchronization accuracy under constellations autonomous operation based on the ground testing system is worked under the mode of transmitting and receiving signal itself. It transmits signal to the all satellites on the visible range by the same carrier frequency, and transmits to the same satellite ground station by satellite transponder, and trigger satellite local time to broadcast signal by the special carrier frequency (to make a difference from the transponder signal). The ground station receive broadcast signal and transponder signal. It can determine the deviation between the satellite time and ground standard time by comparing the deviation between the receive broadcast signal and transponder signal. Thereby, it can measure and estimate the time synchronization accuracy under constellations autonomous operation. The figure of working principle is shown in figure 1.

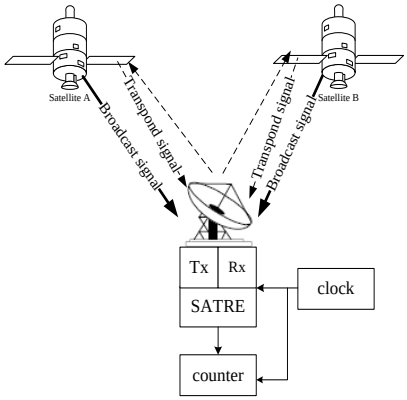

Figure1 The figure of working principle

This method provides technical support for building global satellite navigation system 's inter-satellite link.

IFCS-EFTF5-PAB5-16

Ultra-Short Term Clock Offset Prediction for Two-Way Satellite Time Synchronization

Zhang Shengkang[1,2], Zhang Li[1,2], Yang Yujie[1]

[1] Beijing Institute of Metrology and Measurement, Beijing, China
[2] Science and Technology on Metrology and Calibration Laboratory, Beijing, China

Email: Zhangsk@126.com

Based on the principle of two way satellite time transfer, a time synchronization system with master-slave structures is established. In the system, slave sites compare their clocks time with the master clock by two way satellite time transfer system in turn. After a period of comparison, the time offset, fractional frequency offset or even fractional frequency drift of the slave clock are estimated with respect to the master clock. Then, the time offsets between the two clocks are predicted in the next period of time, when the two way link is switched to another slave site. The time offset prediction error of the slave clock is a main error source in the synchronization system. Three offset prediction algorithms called linear fitting prediction, quadratic polynomial prediction and grey system model prediction are investigated.

In order to evaluate the performance of the above-mentioned clock offset predicting algorithms, four groups TWSTT data are selected randomly, each of them is 40min length. The previous 10min data is used to estimate the fractional clock parameters, and to predicting the next 30min clock offset. The later 30min TWSTT data is used to validate the performance of the algorithms. Fig. 1 shows two groups of the predicting results of the three algorithms. Tab. 1 lists the quantitative analyzing the predicting performance. The results show the linear fitting algorithm has an obvious good performance in ultra-short term prediction than quadratic polynomial method, And it's quite simple than grey system model algorithm. The time synchronization system use the linear fitting algorithm for clock offset prediction in practice and has a good practical effect.

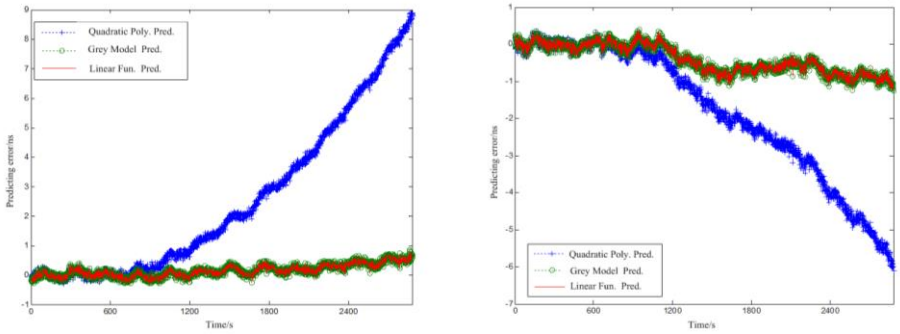

Fig. 52: Comparison of the predicting performance of the three algorithms

Tab. 1 Predicting error of the three algorithms

Alg. / Seq.	Quadratic polynomial			Grey system Model			Linear fitting		
	Avg.	Std.	Max.	Avg.	Std.	Max.	Avg.	Std.	Max.
1	2.503	2.640	8.887	0.147	0.209	0.833	0.144	0.207	0.826
2	-1.804	1.790	6.099	-0.410	0.387	1.251	-0.406	0.384	1.242

IFCS-EFTF5-PAB5-17

A Measurement Method of the GEO Satellite Local Oscillator Error

Jing Wenfang[1,2,3], Lu Xiaochun[1,2], Wang Danni[1,2], Zhang Fuchen[1,3]

1. National Time Service Center, Chinese Academy Of Sciences, XiAn Lintong710600, China
2. Key Laboratory for Precise Navigation, Positioning and Timing of the Chinese Academy of Sciences, Xi'an 710600, China;
3. Graduate University of the Chinese Academy of Sciences, Beijing100039, China)

Email: jingwenf@126.com

Abstract: The Two-Way Satellite Time and Frequency Transfer (TWSTFT) method has, in recent years, been accredited as the most effective and high precision system. But as the frequency stabilities of today's sophisticated atomic-level clocks improve, so must the stability of a Two-Way system's method of time and frequency transfer. Carrier-phase information holds the promise of improving the stabilities of TWSTFT measurements, because of the great precision at which frequency transfers can be achieved. Many years ago, some scientists try to use carrier-phase in TWSTFT, in the trial of time and frequency transferring between USNO and NIST station, some excited results proved the theory and showed the promise of carrier-phase measurement. But because of the poor stability of telecommunications GEO satellite and some other factors, the result didn't review in other trial station. Then no further research reference was published.

Recently, COMPASS system of china has launched several GEO satellite with high quality local oscillator, which brought some brighter shining light for the carrier-phase application in TWSTFT. And a COMPASS GEO satellite has transponder as well as satellite direct transmitter. So, a method based on direct transmitter signal to model the satellite local Oscillator and forecast its changing trend is presented. Then, the satellite clock bias at each moment can be obtained. According to the bias, the TWSTFT transmitter baseband can pre-adjust the transmitter clock to relief the clock bias error to enhance the TWSTFT precision.

The purpose of this paper is to discuss this recent work, with emphasis on the Kalman forecast model to calculate the satellite local Oscillator bias. And the method of making use of dual frequency to get the satellite local Oscillator changing trend is introduced. The simulation and measurement trial is on the going, results will be revealed in the text.

IFCS-EFTF5-PAB5-18

Research on Calibration of TWSTFT Link by GPS

Zhiqiang Yang, Kun Liang, Qinghua Xu, Aimin Zhang

National Institute of Metrology, Beijing, China

Email: yangzq@nim.ac.cn

Two-way satellite time and frequency transfer (TWSTFT) is one of the most precise techniques of time and frequency transfer between laboratories. At present, TWSTFT is performed operationally in at least two laboratories in the United States, twelve in Europe, and seven in the Asia Pacific region. The cooperation is organized by the CCTF Working Group on TWSTFT.

The NIM01 TWSTFT earth station was established in year 2008, and participate the Europe-Asia TWSTFT link now. After October of year 2012, NIM has participated the UTC calculate by both GPS and TWSTFT. But the TWSTFT system of NIM is not be calibrated, so the calibration of NIM TWSTFT Link is extremely urgent.

We research on the calibration technique of NIM TWSTFT Link by GPS. The time and frequency transfer GPS receiver and transfer link are calibrated. We did time and frequency transfer experiment between PTB and NIM use both TWSTFT and GPS time transfer system, process the experiment data of both system and get the time difference of them, so the TWSTFT Link is calibrated by GPS at NIM. The calibration result is shown in Fig 1, the time difference of TWSTFT and GPS is about 1648ns, the calibration uncertainty is 5ns.

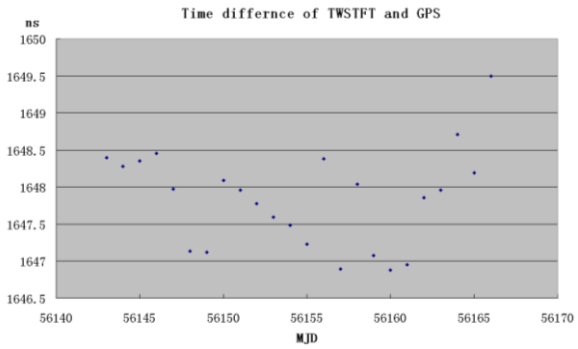

Fig. 53: Time difference of TWSTFT and GPS, the experiment laboratory is NIM and PTB, the period is from MJD56143 to MJD56166

IFCS-EFTF5-PAB5-19

Precision Analysis of Non-continuous Two-way Satellite Time Comparison

Wei Pei [1,2,3], Yang Xu-hai[1,2], Guo Ji[1,2], Li Zhi-gang[1,2], Qin Wei-jin[1,2]

[1]National Time Service Centre, Chinese Academy of Sciences, Xi'an, China
[2]Key Laboratory of Precision Navigation and Timing Technology,
Chinese Academy of Sciences, Xi'an, China
[3]University of Chinese Academy of Sciences, Beijing, China

Email: weipei@ntsc.ac.cn

As one of the high accuracy time comparison methods, Two-way Satellite Time and Frequency Transfer (TWSTFT) is one of the important methods for Bureau International des Poids et Mesures (BIPM) to organize international comparison, calculation of the International Atomic Time (TAI) and Coordinated Universal Time (UTC). Due to the interference of emitting device of TWSTFT to co-located devices of Very Long Baseline Interferometry (VLBI) or International GNSS Service (IGS) and the limitation of satellite transponder resources, the comparison is not proceed continuously. Ten consecutive days of data from C-band TWSTFT Network of National Time Service Center (NTSC) was used for analyzing the precision of non-continuous TWSTFT. The raw data of non-continuous TWSTFT was dealt with linear interpolation method. Then the result was compared with the result of continuous TWSTFT which was seen as the true value. Finally, the influence of interval time to the precision of non-continuous TWSTFT was analyzed. The comparison shows that: when the interval time is less than 2.5 days, the RMS of the difference between non-continuous and continuous TWSTFT is better than 1ns; when the interval time is 0.5 day, the RMS is better than 0.5ns.

IFCS-EFTF5-PAB5-20

The building algorithm of system time of auto-navigation constellation

Qin Weijin[1,2,3], Sun Baoqi[1,2], Yang Xuhai [1,2], Guo Ji[1,2], Wei Pei[1,2,3]
[1]National Time Service Centre, Chinese Academy of Sciences, Xi'an, China
[2]Key Laboratory of Precision Navigation and Timing Technology,
Chinese Academy of Sciences, Xi'an, China
[3]University of Chinese Academy of Sciences, Beijing, China

Email: qwj@ntsc.ac.cn

The building algorithm of system time is one of the research focus of auto-navigation constellation. This paper is on the basis of classic algos algorithm, which based on centralized processing mode of auto-timekeeping constellation, gives a kind of building algorithm of system-time of which modified determination weight and prediction clock velocity: the choose of determination of on-board clock 's weight and selection of clock velocity 's prediction are determinated by the on-board clock quantity which referring to the computation and the aim of building system time . Lacking of longly on-board clock data, it can not be used the method of determination weight of ground clock, while velocity change of on-board clock can reflect frequency change of on-board clock all the same, so it uses clock velocity insteading of clock frequency for determinating weight; in the classic algos algorithm, the clock velocity of former one month as clock velocity prediction of this month, this algorithm uses two kinds of method of predicting clock velocity: a. with the former two epochs each satellite of each day predict many days' velocity, b. with the former two epochs each satellite of first day predict many days' velocity. Choosing the on-board clock of best hour-stability as the main clock, ccording to defined sample interval, getting all the available on-board clock error relative to the main clock. The system time is built by the following modified algos algorithm, finally, we get all the on-board clock error of this system time. This paper gives the computation model of building of system time, and with 60 days data of IGS precise clock error to test the algorithm(system time is IGST).

The result shows: comparing to the equal weighted algorithm, the algos weighted algorithm has better stability. Adding prediction has a significant improvement on the system time's stability. The stability of clock error of method a and method b both improves obviously on the raw clock error. The system time of method a is better than method b, 60 days later, the difference of autonomous system time which relative to IGST(International GNSS Service Time), method a is about 30ns, method b is about 70ns. It can be used for the building algorithm of system time of auto-navigation constellation.

IFCS-EFTF5-PAB5-21

Research On Technology of Pseudo-range measurement based on CMMB

Changjiang Huang[1,2,3], Yu Hua [1,2], Yonghui Hu[1,2], Yu Xiang[1,2,3],

1. National Time Service Center, the Chinese Academy of sciences, Xi'An , China
2. Key Laboratory of Precision Navigation and Timing Technology, NTSC,CAS, Xi'an , China
3. University of the Chinese Academy of Sciences, Beijing ,China

The technology of China Mobile Multimedia Broadcasting (CMMB), which has been the multimedia broadcasting standard of small-size portable electronic equipments, has won favor of more and more users. Many research institutes and their staff in china are focusing on the technology of mobile location based on CMMB signal. CMMB, which is an Orthogonal Frequency Division Multiplexing (OFDM) modulation system, can improve largely the precision of location because of its favorable anti-multipath performance.

In signal structure of CMMB, both same thoroughly synchronization signals inserted in every beach and the continual pilots in all OFDM symbols can be used to capture and track the received signal. In the process of Pseudo-range measurement, united symbol synchronization from rough symbol synchronization in time field and accurate symbol synchronization in frequency field is executed at first, then the fraction and integer part of frequency offset are respectively estimated and revised. At last, with tracking in real time of sampling frequency offset and rectifying of the synchronization sampling clock frequency of VCXO, the frequency offset from Doppler effects is decreased effectively. After symbol and frequency synchronization, one of both consecutive same synchronization signals is selected and is demodulated by means of FFT algorithm. After getting the Pseudo-random sequence from the synchronization signal, we can achieve the cross correlation between the pseudo-random sequence and local corresponding pseudo-random sequence in receiver. At the same time, we track accurately the pseudo-random sequence using code tracking loop and achieve the time difference and pseudo-range between the station and the receiver once the cross correlation peak value appears.

In this paper, we present and analyze a technique for pseudo-range measurement in CMMB receiver. The symbol synchronization, the rectification of carrier frequency offset and the pseudo-range measurement are simulated based on the sampled datum. The simulation result shows that the error of carrier frequency offset is less than 10^{-13} and the precision of pseudo-range measurement is less than 6 meters when the sampling rate is 60 MHz.

IFCS-EFTF5-PAB5-22

Satellite Clock Modelling and Multi-GNSS Solutions

Etienne Orliac[1], Rolf Dach[1], Kan Wang[2], Markus Rothacher[2], Urs Hugentobler[3],

and Drazen Svehla[4]

[1]Astronomical Institute, University of Bern, Bern, Switzerland
[2]Institute of Geodesy and Photogrammetry, Swiss Federal Institute of Technology, Zurich, Switzerland
[3] Institut für Astronomische und Physikalische Geodäsie, Technische Universität München, Munich, Germany
[4]European Space Operations Centre, European Space Agency, Darmstadt, Germany

Email: etienne.orliac@aiub.unibe.ch

In traditional GNSS processing, an independent set of clock parameters is estimated every processed epoch. It represents a huge number of parameters which highly correlate with station height and troposphere parameters. However, no use is made from the fact that the most stable clocks (on the ground and in space) could be modeled, and in turn, help stabilizing the overall GNSS solution.

Based on data from the Multi-GNSS EXperiment (MGEX) from the International GNSS Service (IGS), we first analyze the performances of the GPS Block IIF and Galileo IOV satellites from the clock time series as computed by CODE (Center for Orbit Determination in Europe) over carefully selected periods where, among other criteria, IOV satellites had their H-Maser clock active. This CODE MGEX solution bases on the rigorous combination of GPS, GLONASS, and Galileo data, hence gives the possibility to investigate the (receiver dependent) inter-system biases (ISB) between the different GNSS. A special emphasis is put on the GPS-Galileo ISB and recommendations for operational processing are given.

Still using MGEX data, we investigate the impact of clock modelling and solar radiation pressure models on the determination of orbits and clock parameters for the IOV satellites. Kinematic orbit determination with stochastic clock modelling is also investigated for all GNSS satellites carrying highly stable clocks and results are compared.

Finally, MGEX data from a regional network is used to investigate the impact of deterministic and stochastic satellite clock modelling on parameters with a high resolution in time, such as kinematic coordinates or troposphere parameters. The various solutions based on deterministic and stochastic clock modelling are compared to the traditional solution were clock parameters are estimated independently every epoch.

IFCS-EFTF5-PAB5-23

Real-Time Remote Calibration (RTRC) System for Time and Frequency

LIANG Kun[1], ZUO Fei[2], PEI Chao[2], ZHANG Side[3]

[1]Division of Time and Frequency Metrology, National Institute of Metrology, Beijing, China
[2]School of Electronics and Information Engineering, Beijing JiaoTong University, Beijing, China
[3]Beijing Trust GPS Science&Technology Development Co., Ltd, Beijing, China

Email: liangk@nim.ac.cn

Abstract: The time and frequency transfer receiver NIMTFGNSS-1[1] has been developed since 2011. Based on it, real-time and remote calibration by GNSS code based time and frequency transfer has been studied, and one new type of real-time remote calibration system named RTRC has been designed and implemented. The users who should be authorized by the administrator of the system can use one NIMTFGNSS-1 receiver to check and get real-time (16-minute interval) remote calibration of their time scales and frequency standards for time and frequency on the web by the internet. As well, the user could check and get the calibration results using any longer period historical data. For the user who has no any time scale or frequency standard and needs either or both of them which time or frequency should be traced to UTC(NIM), National Time and Frequency Primary Standard of China, NIM can provide one low-cost Rubidium clock as the accessory of the receiver that makes up one time scale disciplined by UTC(NIM) in real time (UTC(NIM) Disciplined Oscillator, NIMDO) together with the receiver. NIMDO has the legal and direct traceability to UTC(NIM); its time and frequency accuracy has been improved thanks to the high level reference time scale and time scale algorithm; its long stability has been ameliorated due to the real-time and short latency steering to UTC(NIM). For the verification and demonstration of RTRC system, five receivers have been laid up at the two campuses of NIM and hereinto two of them have the accessories of Rubidium clock. About 10 ns and 2e-13 calibration uncertainty separately for time and frequency could be acquired. Referenced to UTC(NIM), we can acquired preliminarily that the time and frequency accuracy of NIMDO could separately be better than 10 ns and 1e-13 averaging one day, and the time and frequency stability averaging one day could separately be better than 5 ns and 1e-13. Soon we would improve the steering algorithm and lay up five NIMTFGNSS-1 receivers at four different cities (Shenyang, Guiyang, Shanghai, and Beijing) in China to verify longer baseline effects. In the near future, using GNSS real-time or near real-time precise ephemeris products, GNSS carrier phase time and frequency transfer will be studied and applied in RTRC and NIMDO to improve their performances.

References:

1. LIANG Kun, ZHANG Aimin, GAO Xiaoxun,WANG Weibo, NING Dayu, ZHANG Side, “Study and Development of a New GNSS Receiver for Time and Frequency Transfer,” Proc. of EFTF 2012, pp. 529-536, 2012.

IFCS-EFTF5-PAB5-24

The Application of VRS in Common-View Based One-Way Timing Method

Xu Longxia[1,2], Guo Meijun[1,3], Li Xiaohui[1,2], Zhang Huijun[1,2], Liu Yinhua[1,2]

[1]NTSC, CAS, Xi'an, China
[2] Key Lab of Precision Navigation and Timing Technology, NTSC, Xi'an, China
[3]University of Chinese Academy of Sciences, Beijing, China

Email: xulongxia@ntsc.ac.cn

The concept of Common-View based One-way Timing Method (CV-OWTM) is proposed by the author in the IFCS conference last year[167]. This method provides users a way to acquire the standard time with the accuracy of about 5ns by observing navigation satellites[168]. However, the CV-OWTM performs a same deficiency like the common view time transfer, that is, the timing accuracy decrease with the increase of distance between users and the reference stations. In order to solve this problem, the Virtual Reference Station (VRS) technique that used in RTK is improved and applied to CV-OWTM.

The VRS in CV-OWTM is different from that in RTK in several aspects. The improved VRS operates on the pseudo-range observations. Therefore, it has a wider work range and isn't sensitive to the movement of user positions. Moreover, the VRS correction is calculated by users not by the data processing center which simplifies the communication between user and the data processing center.

The right figure shows the principle of VRS. Based on a reference stations network in China, this paper will discuss the optimal virtual correction algorithm for users. The number of reference stations that users adopted and the weights of involved stations both are key factors that determine the generation of VRS correction. Based on the selected two different kinds of user positions, combinations of different number of stations and two methods of determining weights are experimented.

The research results indicate that the VRS technique can supply a gap of CV-OWTM for sure. The optimal number of reference stations for users' application is one or three. And the distance between the user and reference station decide the weight of timing observation of this station. All in all, the application of VRS can guarantee CV-OWTM provides the timing accuracy of 5ns.

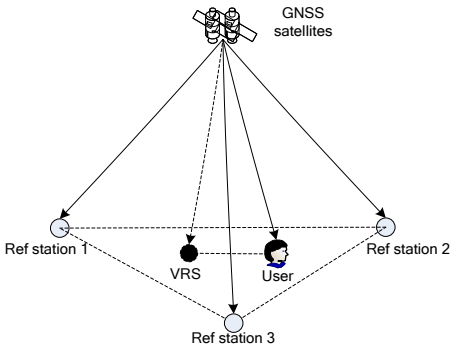

Fig. 54: The principle of VRS. According to the positions of reference station, the user selects data of appropriate reference stations and computes the timing data of a virtual station near the user. Then the timing data from the nonexistent station is applied to correct the output of the user receiver. As the timing data is relative to the standard time, the user can obtain the standard time information ultimately.

[167] Xu L X, "A new timing method based on common-view", 2012 IFCS Proceedings, p. 181-184, 2012.

[168] Xu L X, "Study of a new one-way timing method", Sci China: Phys Mech &Astron, vol. 55, p. 2476-2481, 2012.

IFCS-EFTF5-PAB5-25

Precise Point Positioning with integer ambiguities in the Atomium software

Mari Carmen Martínez-Belda[1], [2]Pascale Defraigne

[1]Applied Mathematics Department, University of Alicante, Spain
[2]Royal Observatory of Belgium, Brussels, Belgium

Email: carmen.martinez@ua.es

The time-transfer technique based on Precise Point Positioning (PPP) has proved to be a very effective technique allowing the comparison of atomic clocks with a precision of a hundred picoseconds. However, one limitation for the accuracy of the solutions comes from the fact that the ambiguous inherent term (integer number of cycles) of the carrier phases cannot, in a PPP approach, be solved as an integer number; only float value (which includes remaining un-calibrated hardware satellite and receiver biases) can be determined. Nevertheless, since 2007, several studies have demonstrated the possibility to resolve ambiguities at the un-differenced level[169,170]. The IGS analysis center CLS now distributes satellite clock biases[171] which allow to solve for integer ambiguities in a single-station PPP computation. This paper will present the recent developments introduced in the Atomium software to produce an integer ambiguity PPP solution, and the first results obtained for the UTC(k) comparisons.

[169] D. Laurichesse and F. Mercier, « Integer ambiguity resolution on undifferenced GPS phase measurements and its application to PPP », ION-GNSS 2007, Fort Worth, Texas.

[170] P. Collins, « Isolating and estimating undifferenced GPS integer ambiguities », ION NTM 2008, San Diego, California.

[171] S. Loyer, F. Perosanz, F. Mercier, H. Capdeville, and J.C. Marty, « Zero-difference GPS ambiguity resolution at CNES-CLS IGS Analysis Center », J. Geod., vol. 86(11), p. 991-1003, 2012.

IFCS-EFTF5-PAB5-26

A Detection Algorithm of Frequency Jumps for GNSS Satellite Clocks

X.M. Huang[1], H. Sha[1], H. Gong[1], X.W. Zhu[1], G. Ou[1]

[1]Satellite Navigation R&D Center, National Univ. of Defense Technology, Changsha 410073, China

Email: huangxinming_2007@163.com

As the frequency and time reference of space satellites, satellite clock has a direct influence on GNSS service performance. Any anomaly of the atomic clock behavior on board the satellites causes errors for user position. Therefore, it is necessary to detect clock anomaly. Frequency jumps are one of the most common anomalies in atomic clocks of on-board satellites, which appear due to space radiation, temperature change and other factors. In this paper, Original measurement data are pre-whetted by exponential filter, and real-time satellite clock frequency residuals are obtained by least squares estimation, and a novel sum test statistic based on residuals is constructed. Optimal detector and energy detector based on frequency residuals are proposed in order to evaluate performance of the new detector constructed. Performance of the new algorithm is analyzed and verified by simulation. The results show that the new algorithm has a perfect performance of detecting frequency jump. The detection algorithm of frequency jumps for satellite clocks proposed in this paper is helpful to GNSS satellite clock autonomous integrity monitoring.

IFCS-EFTF5-PAB5-27

Combination of T2L2 and GPS-CP data : Towards an improvement of Time Transfer Accuracy

Ph. Guillemot[1], P. Exertier[2], E. Samain[2],
M. Laas-Bourez[2], J. Delporte[1]
[1]*CNES –French Space Agency, Toulouse, France*
[2]*OCA – Observatoire de la Côte d'Azur, Caussol, France*

philippe.guillemot@cnes.fr

Abstract

The Time Transfer by Laser Link (T2L2) experiment, developed by both OCA and CNES, performs ground to ground time transfer up to intercontinental distances in non common views. The principle is derived from laser telemetry technology with dedicated space equipment designed to record arrival time of laser pulses at the satellite. Using laser pulses instead of radio frequency signals, T2L2 permits to realize some links between distant clocks with expected time stability of a few picoseconds and accuracy better than 100 ps.

On the one hand, several T2L2 experiments demonstrated the capability of the system to perform time transfer with an accuracy in the 100 ps range[172]. Nevertheless laser operations are weather dependent and do not allow continuous comparison of remote clocks. On the other hand GPS time transfer is a worldwide, all weather, fully operational system. GPS data processing has been widely improved since the first common view / single satellite time transfer and GPS Carrier Phase techniques now allow continuous comparison with an accuracy in the nanosecond range. However, carrier phase data are ambiguous and several methods were developed in order to overcome this problem. Performance of these methods[173] are widely demonstrated for frequency transfer and with continuous data. But some ambiguities remain when there are gaps in the data and for accurate time transfer.

This work investigates the possibility to combine GPS-CP time transfer using single-difference (and zero-difference) integer ambiguity resolution[174] and T2L2 data in order to improve the resolution of the remaining GPS-CP ambiguities, in case of interruption in the data, and the accuracy of the time transfer. First we introduce the method and then we present some first results for common view time transfer between European stations.

[172] E. Samain et al, "T2L2: Ground to Ground Time Transfer", EFTF 2012, Goteborg, Sweden, 23-37 may 2012.

[173] D. Laurichesse et al, "Integer Ambiguity Resolution on Undifferenced GPS Phase Measurements and Its Application to PPP and Satellite Precise Orbit Determination", Journal of the Institute Of Navigation, pp 135-149, Vol. 56 N° 2, 2009

[174] J. Delporte et al., "GPS Carrier-Phase Time Transfer Using Single-Difference Integer Ambiguity Resolution", International Journal of Navigation and Observation, Volume 2008 (2008), Article ID 273785, doi:10.1155/2008/273785

IFCS-EFTF5-PAB5-28

The STE-QUEST Mission: Objectives and Mission Design, Spacecraft, Science Payload and Time & Frequency Links

Hess MP, Hechenblaikner G

Astrium Space Transportation, Friedrichshafen, Germany

Email: Marc-Peter.Hess@astrium.eads.net

Space-Time-Explorer-Quantum Equivalence Principle Space Test (STE-QUEST) is an M-class mission candidate for launch in 2022/2024 in the ESA Cosmic Vision programme. It was selected by the European Space Agency for an assessment study until mid-2013, which started with an ESA-internal assessment, followed by ongoing mission assessment studies performed by competitive industrial teams.

The principle aim of STE-QUEST is to study the cornerstones of Einstein's Equivalence Principle, pushing the limits of measurement accuracy by several orders of magnitude compared to what is currently achievable in ground based experiments. On one hand experiments are performed to measure the gravitational red-shift experienced by highly accurate atomic clocks in the gravitational fields of earth or sun. On the other hand differential accelerations of atomic clouds are measured with an atom interferometer to test the universality of free fall and the Weak Equivalence Principle.

The spacecraft accommodate an atom interferometer as well as a highly accurate space atomic clock based on the ACES PHARAO clock. Time and frequency links in the microwave and optical domain compare the on-board clock to ground clocks, each equipped with microwave antennae and optical terminals. The ground stations are distributed over three continents in Boulder, Torino, and Tokyo. In order to maximize the signal, i.e. the frequency difference between the two clocks, a highly elliptical orbit with perigee altitude of 700 km and apogee altitude of approx. 50 000 km is chosen.

We report on preliminary results of the mission assessment under the lead of EADS Astrium. Some basic features of the mission design are discussed and the design concepts of the spacecraft, science payload and time and frequency links are briefly reviewed.

IFCS-EFTF5-PAB5-29

BDS Satellite Orbit Determination Based on Inter-satellite and Satellite-to-station Ranging

Donghui Wang, Shaowei Yong

Navigation R&D Center, School of Electronic Science and Engineering, National University of Defense Technology, Changsha 410073, China

Email: wdhhawk@gmail.com

The ground stations of BDS are all distributed in China. The distribution is so concentrated that the visible arcs of MEO satellites are only less than 30% and the orbit determination accuracy is restricted. Inter-satellite ranging to increase useful observation data is a very effective method to improve orbit determination accuracy.

In the paper, a new TDMA frame structure is proposed as inter-satellite ranging work mode. The structure is shown in figure 1. It consists of 15 minutes master frames repeated over time. The master frame consists of two frames, the first is ranging frame, the second is communication and data processing frame. Ranging frame is divided into N TDMA slots of 9 seconds each. Each satellite is allocated one slot. In order to increase inter-satellite ranges, each slot is divided into 3 ranging units of 3 seconds each.

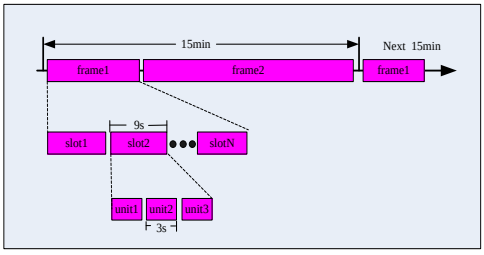

Fig. 1. TDMA Frame structure

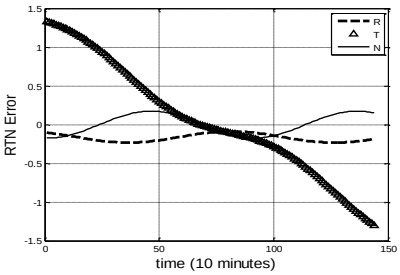

Fig. 2. Orbit determination result with 0.3m inter-satellite ranging error, 15 minutes ranging interval and 12 inter-satellite ranging links

Under the new inter-satellite work structure, some simulations are carried on with different number of inter-satellite ranging links, different ranging interval and different ranging errors.

Simulation results show that when the system ranging error of satellite-to-state is 0.6m, and random ranging error is 0.3m, the 3D satellite orbit determination accuracy is 14.5m(RMS), and the URE of 2 hours prediction is 1.0m if inter-satellite link is not available. After adding the inter-satellite link system, the orbit determination accuracy is improved greatly. When the inter-satellite ranging errors are the same as satellite-to-station ranging errors, and the ranging interval is 15 minutes, the largest improvement of orbit determination accuracy is 68.0%, and when system error reduced to 0.3m, the largest improvement of orbit determination accuracy is 73.2%, and when system error reduced to 0.1m, the largest improvement of orbit determination accuracy is 76.1%. The satellite orbit determination accuracy under different ranging intervals and link numbers are also given. An example result is shown in figure 2. From the simulation results, the optimized inter-satellite ranging mode can be summarized.

IFCS-EFTF Group 6 poster session 1

Forum Hall

Monday & Tuesday, July 22-23, 2013, 01:00 pm - 02:00 pm and 3:30 pm - 4:30 pm

Chair: **Sébastien Bize**
SYRTE-Observatoire de Paris

IFCS-EFTF6-PAB6-1

Optically trapping of magnesium for a lattice based frequency standard

Klaus Zipfel[1], André Kulosa[1], Dominika Fim[1], André Kulosa[1],Steffen Rühmann[1],

Wolfgang Ertmer[1], Ernst Rasel[1]

[1]Leibniz Universität Hannover, Institut für Quantenoptik, Hannover, Germany

Email: zipfel@iqo.uni-hannover.de

State-of-the-art optical clocks with neutral atoms probe a narrow transition of atoms which are tightly confined in an optical lattice at the "magic wavelength"[175]. A promising candidate for such a frequency standard is bosonic ^{24}Mg because of its low sensitivity to black body radiation (BBR) and simple electronic structure.

With this contribution we present the setup of the optical traps and report on the latest results. For magnesium, loading the optical lattice directly from a magneto optical trap (MOT) is not efficient because of density limitations, high temperatures in the milli-Kelvin regime and the lack of adequate sub-Doppler-cooling methods. We therefore transfer our atoms via the $^1S_0$ - $^3P_1$ transition to the triplet manifold where we operate a second MOT and introduce a loss channel to the $^3P_0$ state. Operating both MOTs and the transfer laser simultaneously creates a flux of $^3P_0$ atoms which can be used to continuously load a dipole trap, acting as an energy filter for only the coldest atoms[176]. Since the light at the predicted "magic wavelength" of 469 nm ionizes the atoms in the upper ^3D_j states of the second MOT, we first load a dipole trap at 1064 nm where we accumulate up to 10^5 atoms at 50 µK. With the subsequent transfer to the optical lattice we end up with up to 10^4 atoms at about 10 µK which can be used for spectroscopy.

[175] M. Takamoto et al., "An optical lattice clock", Nature, vol. 435, p. 321-324, 2005.

[176] M. Riedmann, "Beating the density limit by continuously loading a dipole trap from millikelvin-hot magnesium atoms", Phys. Rev. A, vol. 86, 2012.

IFCS-EFTF6-PAB6-2

Towards one single highly stable master laser for the interrogation of SYRTE's Sr and Hg optical lattice clocks

Predehl Katharina, Nicolodi Daniele, Eismann Ulrich, Le Targat Rodolphe, Lodewyck Jérôme, Shi Chunyan, Tyumenev Rinat, Bize Sebastien, Le Coq Yann

LNE-SYRTE, Observatoire de Paris, CNRS, UPMC, 61 avenue de l'Observatoire, Paris, France
Email: katharina.predehl@obspm.fr

Optical atomic clocks have reached a level of performance that allows us to sensitively probe the concepts of fundamental physics in table-top experiments. Moreover, it is widely accepted that optical clocks will constitute a future reference for the SI time and frequency units due to their very high stability and accuracy[177]. For instance, neutral atom optical clocks have been proposed to have a fundamental *Quantum Projection Noise* (QPN) residual instability below 10^{-17} after 1s of integration time[178]. However, this level of performance is currently covered by frequency fluctuations of the clock interrogation laser that are aliased directly onto the measured atomic line (*optical Dick effect*). Towards QPN limited clock operation, large effort has been spent to optimize the widely employed laser systems stabilized to high-finesse Fabry-Pérot etalons that can currently reach residual instabilities as low as a few 10^{-16} [179]. However, cavity length changes due to the thermal motion of the mirror atoms pose a severe limit to this performance.

At the *Laboratoire National de métrologie et d'Essais - Système de Référence Temps Espace* (LNE-SYRTE) we pursue a different approach that has recently been demonstrated to potentially achieve tenfold higher laser stabilities[180] [181]. Using this technique, the frequency discriminator to stabilize the laser is generated by spectrally burning transmission lines into the inhomogeneously broadened spectrum of rare-earth ions doped into a crystal matrix. At cryogenic temperatures, these ions are well shielded within the host and the transition is widely decoupled from thermo-mechanical noise. This allows for transmission line-widths of less than 1 kHz at short integration times and low residual frequency drifts.

Based on this spectral hole-burning technique we propose to develop a laser system with a fractional short term stability of less than 10^{-16} and a residual drift of less than 10 mHz/s. This includes the systematic exploration of different matrix structures and mounting geometries in order to achieve optimized performance. This laser will serve as a master for the interrogation lasers of three different optical clocks. In particular, this comprises two strontium optical clock systems at 430 THz (698 nm) and one mercury optical clock system at 1.2 PHz (266 nm)[182] [183]. The phase stability of the master at 258 THz (1160 nm) will be transferred to the different clock wavelengths by means of an optical femtosecond frequency comb. Recent experiments conducted at LNE-SYRTE show that the frequency conversion preserves the master's spectral purity. This also includes the fiber-based frequency dissemination between the different laboratories.

---

[177] P. *Gill,* F. *Riehle,* "On secondary representations of the Second", Proc. of EFTF 2006, Braunschweig 2006.
[178] M. Takamoto et al., " An optical lattice clock" Nature 435, 321, 2005
[179] T. Kessler et al., "A sub-40-mHz-linewidth laser based on a silicon single-crystal cavity", Nat. Phot. 6, 687, 2012.
[180] M.J. Thorpe et al., "Frequency-stabilization to 6×10-16 via spectral-hole burning", Nat. Phot. 5, 688, 2011.
[181] O-F Chen et al., "Spectrally Narrow, Long-Term Stable Optical Frequency Reference Based on a Eu3+:Y2SiO5 Crystal at Cryogenic Temperature", Phys. Rev. Lett. 107, 223202, 2011.
[182] J. J. McFerran et al.,"Neutral atom frequency reference in the deep ultraviolet with a fractional uncertainty of 5.7×10^{-15}", Phys. Rev. Lett. 108, 183004, 2012.
[183] R. Le Targat et al., "Accurate Optical Lattice Clock with 87Sr Atoms", Phys. Rev. Lett. 97, 13081, 2006.
(see also arXiv:1301.6046)

IFCS-EFTF6-PAB6-3

Transportable Strontium optical lattice clock

Nicola Poli[1], Soroosh Alighanbari[2], Geoffrey Barwood[3], Qun-Feng Chen[2], Ingo Ernsting[2], Patrick Gill[3], Alexander Nevsky[2], Stephan Schiller[2], Marco Schioppo[1], Lyndsie Smith[4], Denis Sutyrin[1], Guglielmo M. Tino[1], Stephan Vogt[5] *and the SOC2 team*[6]

[1]Dipartimento di Fisica e Astronomia e LENS, Universita' di Firenze, INFN sezione di Firenze, Via Sansone, 1 - 50019 Sesto Fiorentino (FI)- Italy
[2]Heinrich- Heine-Universität Düsseldorf, Germany
[3]National Physical Laboratory Teddington, the United Kingdom
[4]University of Birmingham the United Kingdom
[5]Physikalisch-Technische-Bundesanstalt,Germany
[6]Leibniz Universität Hannover, German; Observatoire de Paris, France; University of Birmingham,; TOPTICA Photonics AG, Germany; EADS Astrium Friedrichshafen, Germany; Menlo Systems GmbH, Germany; Kayser Italia S.r.l.,Italy; Centre Suisse d'Electronique et de Microtechnique SA, Switzerland; Kayser-Threde GmbH, Germany University of Neuchatel; Istituto Nazionale di Ricerca Metrologica, Italy

Email: nicola.poli@unifi.it

We report on the status of the research project SOC2: "Towards Neutral-atom Space Optical Clocks" funded by the EU 7th framework programme (grant agreement #263500) with the main aim of developing demonstrators of transportable lattice clocks with ~10^{-17} relative frequency accuracy [1]. Novel design solutions allowed us to reduce size, weight and power consumption with respect to traditional apparatus for laser cooling [2,3]. At the same time a high degree of operation reliability has been ensured by a modular architecture.

Recently the laser-cooling atomic source developed in Firenze [2] has been integrated with compact subsystems developed by the consortium and the clock is now fully operational. Compact laser sources developed by PTB and University of Hannover have been stabilized through compact frequency stabilization system (FSS) developed by National Physical Laboratory and University of Düsseldorf. First tests demonstrated continuous operation of the clock for more than 4 hours.

Results on high resolution spectroscopy of the $^1S_0$-$^3P_0$ clock transition on Sr isotopes will be reported together with a systematic uncertainty budget. Moreover, prospects for performing absolute frequency measurements with Italian mw primary references (ITCsF1 and ITCsF2) and Yb optical frequency reference through a 650 km-long optical fiber link will be discussed [4].

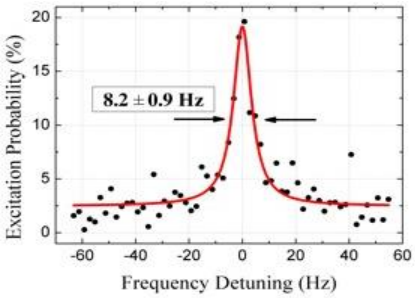

Fig. 55: Lattice spectroscopy on $^1S_0$-$^3P_0$ transition on bosonic ^{88}Sr atoms with SOC2 apparatus.

References

[1] S. Schiller et al. "*Let's embrace space",* volume II, **45**, 452-463 (2012). ISBN 978-92-79-22207-8

[2] M. Schioppo, et al., Proceedings of EFTF 2010 ESA- ESTEC

[3] M. Schioppo et al. Rev. Sci. Instrum. **83**, 103101 (2012)

[4] F. Levi et al. Proceedings of 2013 IEEE—UFFC joint symposia (2013)

IFCS-EFTF6-PAB6-4

Comparison of Sr optical lattice clocks

Chunyan Shi[1], Ulrich Eismann[1], M. Gurov[1], Rodolphe Le Targat[1], Jérôme Lodewyck[1]

[1]LNE-SYRTE, Observatoire de Paris, CNRS, UPMC, Paris, France

Email: chunyan.shi@obspm.fr

We present a set of high resolution comparisons between two state-of-the-art optical lattice clocks using strontium atoms. With a statistical resolution of 2×10^{-17}, we measure a relative frequency difference of 1.1×10^{-16} between the two apparatuses, in agreement with the combined accuracy budget of 1.6×10^{-16}. This comparison, beating the level of uncertainty that can be resolved by comparing different optical clocks to microwave references, corroborates the established accuracy budget for optical lattice clocks, and show that they are competitive for a possible redefinition of the second with optical references[1].

In addition, we present the ongoing development of a new vacuum system that will enable further improvement of the accuracy budget. A fine estimation of the temperature of the environment surrounding the atoms will enable to decrease the contribution of the black body radiation shift in the low 10^{-17} range without degrading the cycle time. Furthermore, the optical cavity used to generate the optical lattice in which the atoms are trapped is doubly resonant for the lattice light and the $^1S_0 - {}^1P_1$ light (461 nm). With this cavity, the number of atoms in the fundamental clock state can be detected in a non destructive way by dispersive interaction between the atoms and the 461 nm light. Such a detection yields an improved signal to noise ratio with respect to previous work[2]. Here, we discuss heterodyne detection strategies to reach the optimal detectivity, as well as progress in implementing these schemes.

[1] R. Le Targat *et al.*, "Experimenting an optical second with strontium lattice clocks", arXiv:1301.6046 (2013)

[2] J. Lodewyck *et al*, "Nondestructive measurement of the transition probability in a Sr optical lattice clock" Phys. Rev. A 79, 061401(R) (2009).

IFCS-EFTF6-PAB6-5

A transportable optical lattice clock using ^{171}Yb

Gregor Mura, Charbel Abou Jaoudeh, Tobias Franzen, Axel Görlitz, Heiko Luckmann, Ingo Ernsting, Alexander Nevsky, Stephan Schiller *and the SOC2 team*[2]

[1] Institut für Experimentalphysik, Heinrich- Heine-Universität Düsseldorf, Germany

[2]Physikalisch-Technische-Bundesanstalt Braunschweig, Germany; Leibniz Universität Hannover, Germany; Observatoire de Paris, France; Universita' di Firenze, Italy; Istituto Nazionale di Ricerca Metrologica, Torino, Italy; National Physical Laboratory Teddington, United Kingdom; University of Birmingham, United Kingdom; TOPTICA Photonics AG, Germany; EADS Astrium Friedrichshafen, Germany; Menlo Systems GmbH, Germany; Kayser Italia S.r.l., Italy; Centre Suisse d'Electronique et de Microtechnique SA, Switzerland ; University of Neuchatel, Switzerland ;

E-Mail: axel.goerlitz@uni-duesseldorf.de

Optical lattice clocks based on elements with two valence electrons are strong competitors in the quest for next generation time and frequency standards. While promising results have already been obtained on several stationary setups using Sr, Hg, Mg and Yb, transportable clocks are desirable for both performance evaluation and applications.

In the framework of the SOC2 project [1], we are developing a transportable Yb lattice clock demonstrator. Our setup is based on compact diode lasers (399 nm, 1156 nm followed by waveguide SHG, 759 nm) and a fiber laser (1111 nm followed by waveguide SHG), and features an intra-vacuum enhancement resonator to allow the formation of a large-volume 1-dimensional optical lattice using moderate laser power.

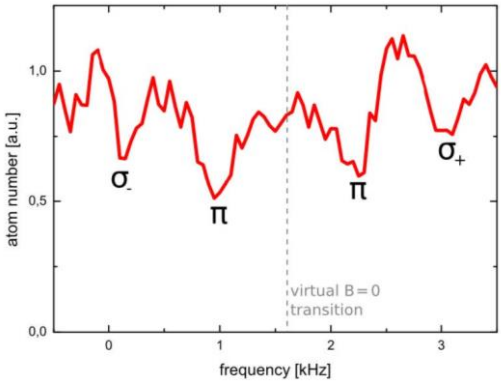

Fig. 56: Spectroscopy of the $^1S_0 \rightarrow {}^3P_0$ clock transition in an unpolarized sample of ^{171}Yb trapped in an optical lattice in the presence of a magnetic bias field.

Here we present first results of spectroscopy of the $^1S_0 \rightarrow {}^3P_0$ transition at 578 nm in ^{171}Yb confined in a one-dimensional optical lattice. We have observed linewidths below 200 Hz which were limited by saturation broadening. Currently the system is being improved towards competitive clock operation as well as more compact and robust subsystems.

The research leading to these results has received funding from the European Union Seventh Framework Programme (FP7/2007-2013) under grant agreement n. 263500.

References

[1] www.soc2.eu; S. Schiller et al. "Towards Neutral-atom Space Optical Clocks (SOC2): Development of high-performance transportable and breadboard optical clocks and advanced subsystems" on "*Let's embrace space, volume II*" **45**, 452-463 (2012). ISBN 978-92-79-22207-8

IFCS-EFTF6-PAB6-6

Improved set-up for the Ytterbium Optical Clock at INRiM

Marco Pizzocaro[1,2], Luca Lorini[1], Davide Calonico[1], Giovanni A. Costanzo[2], Filippo Levi[1]

[1]Istituto Nazionale di Ricerca Metrologica, Torino, Italy
[2]Politecnico di Torino, Torino, Italy

Email: m.pizzocaro@inrim.it

We present an upgraded setup for cooling and trapping of ytterbium atoms in the optical clock experiment developed at Istituto Nazionale di Ricerca Metrologica (INRIM). The experiment aims to cool and trap ytterbium atoms in a two stage magneto-optical trap (MOT) (at 399 nm and 556 nm for the first and second stage, respectively) and to probe the narrow-line clock transition at 578 nm in an optical lattice at the magic wavelength (759 nm).

We obtain blue light at 399 nm by second harmonic generation of a Ti:sapphire laser at 798 nm with a linewidth < 20 kHz. A lithium triborate (LBO) non-linear crystal in an enhancing cavity allows to obtain up to 0.6 W at 399 nm starting with 1.1 W of infrared light. To cope for the long term frequency drift, the laser is locked to the atomic resonance by transverse spectroscopy on a ytterbium beam.

The green 556 nm radiation is obtained by second harmonic generation of an amplified 1112 nm Yb-doped fiber laser using a periodically-poled potassium titanyl-phosphate (PPKTP) crystal in single pass. Up to 12 mW of 556 nm light has been obtained starting from 1.1 W of 1112 nm light. The laser is frequency stabilized on a ultra-stable cavity.

The lattice laser is a Ti:sapphire laser with an output power of 3.2 W at 759 nm and has a linewidth < 20 kHz. This source is able to provide large trap depths both for 1D and multidimensional lattice configurations.

A new physic package is designed, including the vacuum chamber, the MOT coils and the atomic source. The new vacuum chamber is made in aluminum and it has indium-sealed viewports with high-performance anti-reflection coating for wide optical access and flexible lattice geometries. The target vacuum pressure in the trapping region is better than 1×10^{-9} mbar, which allows the atom lifetime in lattice required by the optical clock operation. A high efficiency atomic oven source allows a high number of trappable atoms. Atoms can be slowed using a counter-propagating beam at 399 nm without a dedicated Zeeman slower, exploiting the leaking field of the MOT coils.

IFCS-EFTF6-PAB6-7

An Improved Single-Ion End-Cap Trap for Optical Clocks

P.B.R. Nisbet-Jones, S.A. King, R.M. Godun, H.A. Klein, P.Gill

National Physical Laboratory (NPL), Teddington, UK

Email: peter.nisbet-jones@npl.co.uk

Recent advances in the field of single-ion frequency standards have resulted in optical atomic clocks with systematic uncertainties in the 10^{-16}- 10^{-18} range, beyond that of the best caesium fountains. At this level of precision, frequency shifts caused by the trap environment start to limit the achievable performance of the standard.

One of the most significant shifts is the dc-Stark shift caused by blackbody emission from the trap electrodes. As end-cap ion traps[1] typically operate with RF electric fields in the range of 10^6 V/m, dielectric heating of the trap structure can cause a temperature rise of up to hundreds of degrees if thermal performance is not considered in the design. In the case of Yb^+ [2,3], for example, the mid-IR radiation emitted will cause a frequency shift on the order of 10^{-17} per degree.

By building a trap from materials with high thermal conductivity, and by minimizing the intrinsic rf-heating of the trap structure itself, this temperature rise can be minimized. Combining good thermal design of the trap structure with accurate *in situ* measurements of the trap temperature, the black-body frequency shift can be more accurately constrained. One of the methods to reduce the blackbody shift is by mechanically polishing the electrodes, thus reducing their emissivity. An added benefit of this is a reduction in the anomalous (phonon) heating of the ion. With the $^{171}Yb^+$ octupole transition in particular, as it has an excited state decay rate on the order of nHz[4], there is significant scope for reducing the Fourier limited linewidth if the phonon heating rate of the trap can be reduced. This is predominantly achieved by using a large electrode spacing (0.75mm) and utilizing the $\sim d^{-4}$ scaling of the anomalous heating rate.

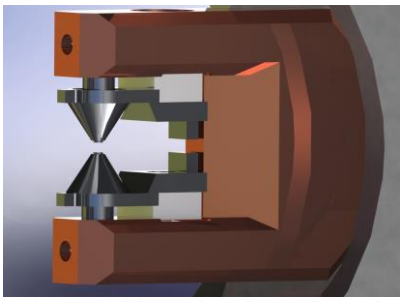

RF is applied to molybdenum electrodes via a heat sunk copper mount with large ceramic spacers to reduce dielectric heating.

This work is supported by the UK National Measurement System and the European Metrology Research Programme (EMRP) and is performed alongside groups at NPL, PTB, CMI and MIKES. The EMRP is jointly funded be the EMRP participating countries within EURAMET and the European Union.

[1] C.A. Schrama, Optics. Coms., vol. 101, 32-36, 1993.
[2] N. Huntemann, PRL, vol. 108, 090801, 2012.
[3] S.A. King, N. J. Phys., vol. 14, 013045, 2012
[4] M. Roberts, PRA, vol. 62, 020501, 2000

IFCS-EFTF6-PAB6-8

Progress report of an $^{27}Al^{+}$ ion optical clock

Ke Deng, Zetian Xu, Wenhao Yuan, Jie Zhang, Zehuang Lu, and Jun Luo

MOE Key Laboratory of Fundamental Quantities Measurement, School of Physics,

Huazhong University of Science and Technology, Wuhan, P.R. China

Email: zehuanglu@mail.hust.edu.cn

The $^{1}S_0$-$^{3}P_0$ transition of $^{27}Al^{+}$ at 267.4 nm has long been recognized as an excellent optical clock transition candidate. Here we give a progress report of our project to build an $^{27}Al^{+}$ ion optical clock. The first stage design goals for the $^{27}Al^{+}$ ion optical clock are an inaccuracy level of 10^{-17} and stability of 10^{-16} in one second. The implementation of the $^{27}Al^{+}$ ion optical clock will be through quantum logic spectroscopy (QLS)[184], as first proposed by NIST. A single $^{25}Mg^{+}$ ion will be trapped together with a single $^{27}Al^{+}$ ion. The $^{25}Mg^{+}$ ion acts as the logic ion and is used for sympathetic cooling and internal state detection of the $^{27}Al^{+}$ ion.

In the planned experiment, a 285 nm FHG laser is used for photo-ionization of Mg atoms, and a single 280 nm laser system will be used to cool and detect the $^{25}Mg^{+}$ ion. The 280 nm laser is derived from an 1120 nm laser. Its SHG at 560 nm is locked to the transition of molecular I_2. An electro-optic modulator is placed between the SHG and FHG in the laser system to generate 9.2 GHz sidebands[185]. The FHG stage of the laser is designed to be double resonant with both carrier and sidebands. One sideband of the 280 nm laser is used for Doppler cooling and detection, while the carrier of the 280 nm laser is further used for Raman sideband cooling of $^{25}Mg^{+}$ ion. A linear ion trap is placed in the center of a UHV vacuum chamber, which is made of titanium to reduce the magnetic field influence. Fig. 1 shows the whole experimental setup. The linear ion trap is also made of titanium, and coated with gold.

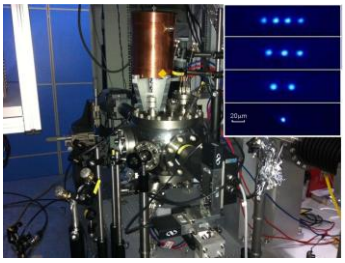

Fig. 57: Experimental setup showing vacuum chamber and lasers for ion experiment. Inset shows pictures of crystallized Mg ions.

At the moment, both 285 nm laser and 280 nm laser have been successfully frequency locked. The oscillator of 285 nm at 1140 nm was digitally locked to a high precision Toptica wavemeter. With this laser, Mg atoms have been photo-ionized. Mg ions have been trapped and laser cooled with 280 nm laser, and crystallization of Mg ions has been observed. The inset of Fig. 1 shows pictures of crystallized Mg ions. One single Mg ion has been trapped. Through micromotion compensation and trapping parameters optimization, the temperature of this single trapped ion is lowered to around 8 mK, close to Doppler cooling limit. Further experimental progress in Raman sideband cooling of a single Mg ion will be presented.

[184] P. O. Schmidt, T. Rosenband, C. Langer, W. M. Itano, J. C. Bergquist, and D. J. Wineland, "Spectroscopy using quantum logic," Science, vol. 309, p. 749, 2005.

[185] B. Hemmerling, F. Gebert, Y. Wan, D. Nigg, I. V. Sherstov, and P. O. Schmidt, "A single laser system for ground-state cooling of $^{25}Mg^{+}$," Appl. Phys. B, vol. 104, p. 583, 2011.

IFCS-EFTF6-PAB6-9

Progress Report on the Development of Ultra-stable Lasers for Al^+ Optical Clocks

Yingxin Luo, Bing Ouyang, Xiaoyi Zeng, Jie Zhang, Zehuang Lu, and Jun Luo

MOE Key Laboratory of Fundamental Quantities Measurement, School of Physics, Huazhong University of Science and Technology, Wuhan, P.R. China

Email: jie.zhang@mail.hust.edu.cn

The recent progress of ultra-narrow linewidth lasers used for Al^+ optical frequency standards will be presented. Two diode lasers are phase stabilized to ultra-stable ULE cavities, whose 4th harmonics will be used as the de-shelving laser and the clock laser for Al^+ clock transition respectively.

Al^+ clock transition requires ultra-narrow linewidth laser as the clock laser with sub-hertz linewidth. To develop this clock laser, a diode laser with wavelength of about 1070 nm is phase stabilized to two independent cavities through two stages of Pound-Drever-Hall (PDH) locking. The output of the clock laser is amplified, and then frequency quadrupled to generate the 4th harmonic ultraviolet output at 267.4 nm. To facilitate fast detection of the clock transition, a de-shelving laser with linewidth of sub-100 Hz level at 267.0 nm is needed, thus another diode laser with wavelength of 1068 nm is phase stabilized to another cavity (Fig. 1(a)) and then frequency quadrupled to generate the ultraviolet output. The ultra-stable cavities are made of ULE materials with the zero-crossing temperature of CTE (coefficient of thermal expansion) near 25 °C, and are installed inside vacuum chambers (Fig. 1(b)).

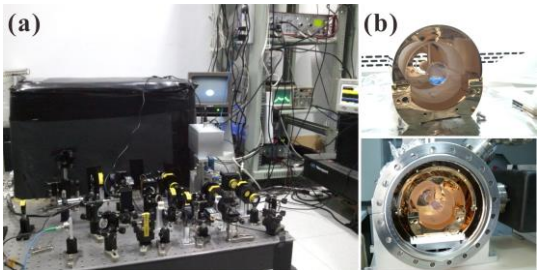

Fig. 58: Experimental schemes (a) for PDH stabilization of a diode laser with one of the ultra-stable ULE cavities; (b) the design of the cavity is optimized by FEA simulations, and is installed inside a vacuum chamber.

Cavities with notched structures are normally optimized for smallest vibration sensitivity through quasi-static Finite Element Analysis (FEA) simulations[186]. Since quasi-static analysis does not consider the inertia and damping effects, the calculated vibration sensitivity might not reflect the real results. Here we present FEA dynamic analysis of the notched cavities steady state response under dynamically changing loads. With the calculated results, and measured ground vibration spectral density curve, we can more realistically predict the cavity length variations due to ground vibration. This dynamic analysis can also be used for estimation of the acoustic noise influence on the cavity stability.

Latest results of the lasers, including static and dynamic FEA simulation results, characterization of the locking systems performance, and laser linewidths and long-term stabilities measurement, will be presented.

[186] S. A. Webster, M. Oxborrow, and P. Gill, "Vibration insensitive optical cavity", Phys. Rev. A, vol. 75, p. 011801, 2007.

IFCS-EFTF6-PAB6-10

An ultrastable optical oscillator for a magnesium lattice clock

Dominika Fim, André Kulosa, Steffen Rühmann, Klaus Zipfel, Wolfgang Ertmer, Ernst M. Rasel

Institut für Quantenoptik, Leibniz Universität Hannover, Hannover, Germany

Email: fim@iqo.uni-hannover.de

Spectroscopy of the strictly forbidden $^1S_0 \rightarrow {}^3P_0$ transitions in alkaline- earth elements are today performed in the sub-Hertz regime. In order to observe this transition in lattice-trapped magnesium atoms, a frequency doubled diode laser system, generating 458 nm, is stabilized to a horizontally mounted high finesse resonator (F = 600.000) at the fundamental wavelength of 916 nm. The resonator is made of ULE and fused silica mirrors. With this setup a fractional instability of $5x10^{-16}$ in 1 s at 916 nm could be achieved. This is only factor of two higher than the calculated thermal noise floor of the resonator. We also studied the phase noise introduced by the SHG stage contributing with an instability of $2x10^{-16}$ for 1s. We will give an overview of this system and will report on our results.

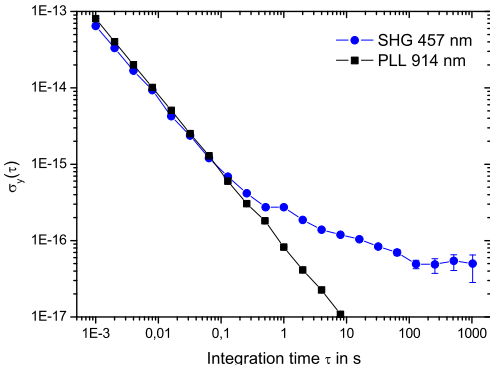

Fig. 59: Allan deviation of the second harmonic process and the phase lock loop performance

.

IFCS-EFTF6-PAB6-11

External Cavity Diode Laser at 420 nm Wavelength for Atomic Spectroscopy

Xi Zeng[1] and Dmitri L Boïko[1]

[1]Centre Suisse d'Électronique et de Microtechnique, Jaquet-Droz 1, 2002 Neuchâtel, Switzerland

Email: xi.zeng@csem.ch, dmitri.boiko@csem.ch

Wavelength tunable diode lasers with narrow linewidths are vital for many applications in atomic physics and spectroscopy. Specifications of these lasers are well established for probing alkali vapor absorption lines in the near infrared (NIR) spectrum[187]. In the blue-violet wavelength range, there are a few commercial models available, but they often lack information vital for atomic spectroscopy such as relative intensity noise (RIN) and frequency noise spectra. Here, we report on our realization of an external cavity diode laser (ECDL) suitable for interrogation of Rb vapor in the $5^2S_{1/2}$-$6^2P_{3/2}$ (420.2 nm wavelength) and $5^2S_{1/2}$-$6^2P_{1/2}$ (421.5 nm) atomic lines as well as of Sr+ ions in the $2S_{1/2}$-$2P_{1/2}$ cooling transitions (421.6 nm).

The semiconductor gain chip used for the ECDL is a commercial InGaN/GaN Fabry-Perot laser with lasing wavelength around 420 nm. No specific provision for antireflection coating of the cleaved facet was made, but we benefit from GaN-based lasers having naturally smaller facet reflectivity at ~17% than the 32-34% found in conventional GaAs-based lasers used for NIR spectroscopy. External cavity feedback is provided by an optical grating with 1800 grooves per mm installed in Littrow configuration. Challenges for single mode laser operation and uniform wavelength tuning originate from the mode-clustering effect typical for GaN-based laser diodes. Nevertheless, our preliminary results demonstrate efficient mode filtering by the external cavity and large tuning range of the lasing wavelength. Figure 1(a) shows the L-I curves of the laser diode without external feedback (lasing threshold ~40 mA) and in ECDL configuration (lasing threshold ~31 mA). The ripples in the ECDL's L-I curve are caused by mode hopping effects. The ECDL can achieve output power greater than 4.6 mW with injection current of 110 mA. The wavelength tuning range is almost 7 nm while maintaining single lasing mode in the optical spectrum as seen in Fig 1(b). The mode hop free tuning range is 57.7 GHz, which is more than sufficient for envisioned atomic spectroscopy applications. Figure 3(c) contains the ECDL's preliminary RIN measurement results (the RIN limited by photocurrent shot noise is 3×10^{-14} Hz^{-1}). Measurements on frequency noise and laser linewidth are ongoing.

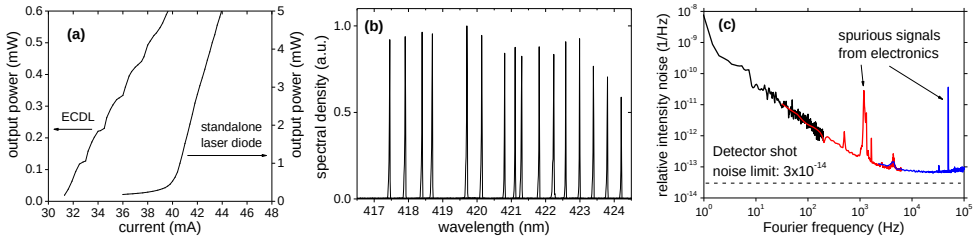

Fig. 1. (a) L-I curves of the laser diode without external feedback and in ECDL configuration. (b) Example lasing wavelengths by the ECDL at 60 mA. (c) The ECDL's relative intensity noise at 59 mA.

[187] C. Affolderbach and G. Mileti, "A compact laser head with high-frequency stability for Rb atomic clocks and optical instrumentation", Review of Scientific Instruments, vol. 76, p. 073108-1 - 073108-5, 2005.

IFCS-EFTF6-PAB6-12

Stable frequency comparison of different optical clocks

Christian Grebing, Burghard Lipphardt, Stephan Falke, Nils Huntemann, Nathan Lemke, Thomas Legero, Christian Hagemann, Uwe Sterr, Christian Tamm, Ekkehard Peik, Christian Lisdat, and Harald Schnatz

Physikalisch-Technische Bundesanstalt, Braunschweig, Germany

Email: christian.grebing@ptb.de

Frequency standards based on ultra-narrow optical transitions of single ions or ensembles of atoms have reached a level of stability and reproducibility that surpassed those of primary clocks in the microwave region. Currently at PTB, several types of optical clocks are investigated: ion clocks based on a single Yb^+ and Al^+ ion and an optical lattice clock based on neutral Sr atoms[188,189]. Since the individual clocks work at different wavelengths an optical network based on frequency combs that connect different spectral regions is needed for clock comparisons and frequency measurements

Commercially available frequency combs for metrology typically employ a common oscillator that feeds multiple Er^+-doped fiber amplifiers (EDFA) followed by short pieces of highly non-linear fibers to provide high-power output at wavelengths according to customers' needs. On the one hand this makes these combs a handy and comfortable tool but on the other hand any noise generated in the EDFA branches will bias measurements between different output ports of the comb system. We investigated this differential noise by measuring the frequency ratio of two cavity-stabilized lasers in the visible and infrared spectral range with two independent multi-port frequency comb systems[190] (see Fig. 1). The Allan deviation shows an instability plateau of $\sigma_y(\tau) = 2 \cdot 10^{-16}$ between τ = 1...100 s, which is attributed to environmental perturbations acting on the unstabilized fiber inside the EDFA paths. This instability plateau can be further reduced by measuring and compensating the differential noise. For longer averaging times the instability averages down to $\sigma_y(\tau) < 1 \cdot 10^{-18}$ for $\tau > 1 \cdot 10^4$ s. The long-term instability is an order of magnitude smaller than what is currently achievable with the most advanced optical atomic clocks.

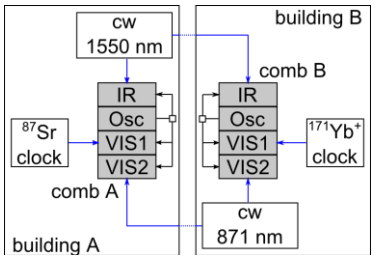

Fig. 1: Measurement setup: The lines indicate fiber links between the elements. The blue ones are equipped with a fiber noise cancellation.

This measurement is a first step for determining the ratio of PTB's $^{171}Yb^+$ ion clock and ^{87}Sr lattice clock frequencies, which is currently under investigation, with minimum uncertainty contribution from the frequency comb system.

---

[188] N. Huntemann et al.,"High-accuracy optical clock based on the octupole transition in $^{171}Yb^+$", *Phys. Rev. Lett.*, vol. 108, p. 090801, 2012

[189] St. Falke et al.,"The ^{87}Sr optical frequency standard at PTB", *Metrologia*, vol. 48, p. 399 - 407, 2011

[190] C. Hagemann et al.,"Providing 10^{-16} short-term stability of a 1.5-µm laser to optical clocks", to appear in *IEEE Instrum. Meas.*, vol. 62 (preprint: arXiv:1208.1634)

IFCS-EFTF6-PAB6-13

Compact and Dual Ti: Sapphire Comb Lasers Pumped by Single Fiber Laser

Tze-Wei Liu[1], Chien-Ming Wu[2], Shinn-Yan Lin[3], Wang-Yau Cheng[4]

[1]Department of Physics, National Taiwan University, Taipei, Taiwan
[2]Institute of Photonics Technologies, National Tsing-Hua University, Hsinchu, Taiwan
[3]National Standard Time and Frequency Laboratory, Telecommunication Laboratories, Chunghwa Telecom, Taoyuan, Taiwan
[4]Department of Physics, National Central University, Chun-Li, Taiwan

Email: sylin@cht.com.tw

Ti:sapphire crystal is a commonly used gain medium both for continuous wave (CW) and mode-locked (ML) pulsed lasers in the near infrared (IR) region. Optical frequency combs are especially sensitive to power instability, because pump power fluctuations directly affect the repetition rate and the carrier-envelope phase. Improvements in IR fiber laser technology made possible to have sufficient optical pump power in the visible region[191] using second-harmonic generation in quasi-phase-matched ferroelectric materials such as MgO-doped periodically poled stoichiometric lithium tantalate (PP-MgO:SLT)[192]. Compared to the conventional diode pump solid-state laser pump sources, fiber laser based pumps have the advantages of being more compact, lower cost, and consuming less energy.

We demonstrated each femtosecond Ti:sapphire comb laser pumped by 4.5W continuous-wave 532nm light generated by frequency doubling a 1064nm ytterbium fiber laser. The laser repetition rates were set to be 1GHz and the average power of the plus is about 700mW. Absolute mode frequency of laser was directly monitored by a cesium two-photon stabilized diode laser. In order to make the system small, we develop the hand size cesium two-photon stabilized diode laser (HS-CTSDL)[193] to be the frequency standard of the absolute mode frequency. The instability of the HS-CTSDL frequency is about 100Hz at 400s sampling time. A maximum frequency discrepancy of 3.5kHz during 16 days shows the high reproducibility of the HS-CTSDL. We lock the repetition rate to the synthesizer, and lock the absolute frequency to the HS-CTDSL. The line width of the repetition rate reduces to about 2Hz after lock. The standard deviation of the absolute frequency is about 15.791kHz with 0.1 second get-time, and it will become about 6.072kHz with 1s sampling time. The Allan deviation of the beat frequency shows that the absolute frequency instability was estimated as 5×10^{-12} at 10s sampling time.

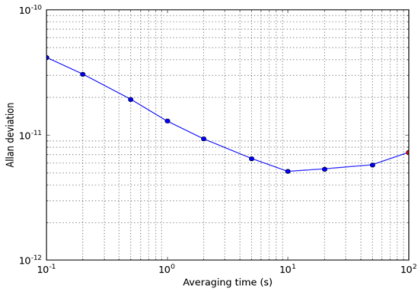

Fig. 60: After lock the comb laser, we measure the beat note of one comb mode and cesium two-photon stabilized diode laser. Allan deviation of the beat frequency shows that the absolute frequency instability was estimated as 5×10^{-12} at 10s sampling

[191] G. K. Samanta, S. Chaitanya Kumar, and M. Ebrahim-Zadeh, Opt. Lett. 34, 1561 (2009).

[192] H. Furuya, A. Morikawa, K. Mizuuchi, and K. Yamamoto, Jpn. J. Appl. Phys. Part 1 45, 6704 (2006)

[193] Y-H Chen, T-W Liu, C-M Wu, C-C Lee, C-K Lee, and W-Y Cheng, Opt. Lett. 36, 76 (2011)

IFCS-EFTF6-PAB6-14

Optical Frequency Measurement Comparison Using Fiber Laser Combs between CMS and NMIJ

Jin-Long Peng[1], Ren-Huei Shu[1], Tze-An Liu[1], Hajime Inaba[2], Kazumoto Hosaka[2], Masami Yasuda[2], Daisuke Akamatsu[2], Atsushi Onae[2], and Feng-Lei Hong[2]

[1]Center for Measurement Standards, Industrial Technology Research Institute, Hsinchu, Taiwan
[2]National Metrology Institute of Japan, National Institute of Advanced Industrial Science and Technology, Tsukuba, Japan

Email: jlpeng@itri.org.tw

An Er-fiber laser comb made by the Center for Measurement Standards (CMS), Taiwan was shipped to the National Metrology Institute of Japan (NMIJ) to compare with the NMIJ fiber laser comb by simultaneously measuring the frequency of a reference-cavity-stabilized Nd:YAG laser at 1064 nm. The measured frequency difference is 32 mHz, which corresponds to a relative difference of 1.1×10^{-16}. Furthermore, method for determining the comb mode number using two combs with large difference of repetition rate is proposed.

Both the CMS and NMIJ fiber laser combs are home-made Er-doped ring fiber laser mode-locked by nonlinear polarization rotation (NPR)[194, 2]. The laser head of the CMS fiber laser comb is only about an A3 paper size with 7-mm thick, which is very compact and easy for transportation. The repetition rates are 250 MHz and 87.6 MHz for the CMS and NMJ comb, respectively. The repetition and offset frequencies of both combs are phase locked to the RF references synthesized from an H-maser linked to the Coordinated Universal Time (UTC, NMIJ). The two combs are beating with the Nd:YAG laser, which has frequency instability of less than 1×10^{-14} at 1 s. The two beat signals and their divided-by-10 signals are measured with four counters simultaneously to check cycle-slip from the counters. If the counting of the beat signal does not match with that from the 1/10 of the beat signal, cycle-slip has happened and that data point is deleted. The measured frequency differences are shown in Fig. 1. The averaged frequency difference is only 32 mHz, which is limited by the measurement time.

An NMIJ fiber comb had also been shipped to the National Metrology Institute, Australia to compare the frequency measurement of an iodine-stabilized He-Ne laser at 633 nm in 2006. The measured frequency difference was 38 mHz[2]. The comparison results validate the measurement capability of the CMS fiber laser comb.

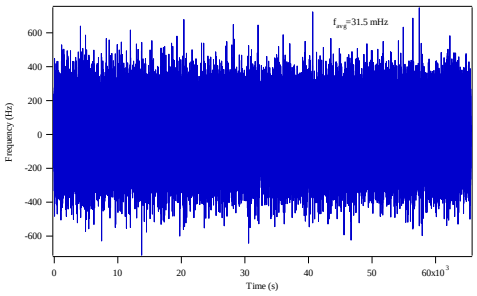

Fig. 61: Measured frequency differences between the CMS and NMIJ fiber laser comb.

[194] J.-L. Peng, T.-A Liu, and R.-H. Shu, "Self-referenced Er-fiber laser comb with 300 MHz comb spacing," Proc. 2009 Joint Meeting of the IEEE International Frequency Control Symp. and the EFTF Conf. p.344-346.

[2] H. Inaba, Y. Nakajima, F.-L. Hong, K. Minoshima, J. Ishikawa, A. Onae, H. Matsumoto, M. Wouters, B. Warrington, and N. Brown, "Frequency measurement capability of a fiber-based frequency comb at 633 nm," IEEE Trans. Instru. Meas. vol. 58, p.1234-1240, 2009.

IFCS-EFTF6-PAB6-15

Experimental Setup of Cs Active Optical Clock

Z. Xu, Y. Wang, D. Wang, X. Zhang, X. Xue, D. Pan, W. Zhuang, J. Chen

School of Electronics Engineering and Computer Science,
Peking University, Beijing 100871, China

Email: jbchen@pku.edu.cn

To push the linewidth of optical clock from Hz to mHz is a main topic for clock development[195].

Active optical clocks[2,3,4] theoretically have the potential of mHz linewidth, thus expected will provide much better stability than that of passive optical clocks. In a three-level configuration[5,6], the pumping laser directly affects the frequency of clock transition. In order to greatly reduce the light shift of clock transition caused by pumping laser, we are setting up an experiment to investigate active optical clock in 4-level configuration with Cesium atoms.

The melting temperatures of alkali atoms, like Cs and Rb, are very low, and the laser diode for related wavelength of atomic transitions are commercially available, thus Cs or Rb active optical clock experiment with thermal cell or magneto-optical trap is economic.

A homemade external-cavity diode laser at 455 nm is employed as the pumping laser. Saturated absorption spectrum of cesium between $6S_{1/2}$ (F=4) and $7P_{3/2}$ (F'=3,4,5) is observed. The population inversion between $7S_{1/2}$ state and $6P_{3/2}$ state in a thermal cesium cell has been experimentally established.

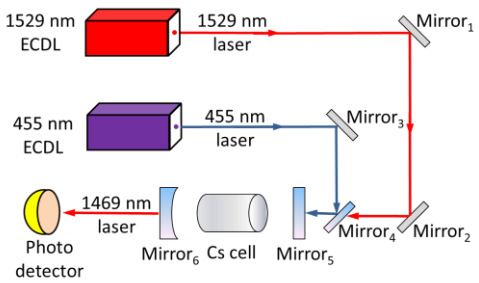

Fig. 62: Experimental setup of cesium active optical clock in four-level configuration. $Mirror_1$, $Mirror_2$ and $Mirror_3$ are highly reflecting mirrors at 1529 nm. $Mirror_4$ is coated with 1529 nm anti-reflection and 455 nm high-reflection coating. $Mirror_5$ is coated with 455 nm anti-reflection and 1469 nm high-reflection coating. $Mirror_6$ is coated with 455.5 nm high-reflection and the reflectivity of 1469 nm is 68.5%.

The experimental setup of cesium active optical clock is shown in Fig. 1. The cavity is composed of a planar mirror ($Mirror_5$) and a concave mirror ($Mirror_6$). $Mirror_5$ is coated with 455 nm anti-reflection and 1469 nm high-reflection coating. $Mirror_6$ is coated with 455.5 nm high-reflection and the reflectivity of 1469 nm is 68.5%. A 1529 nm external-cavity diode laser is used to calibrate the cavity. The 455 nm pumping laser is introduced into the cavity to generate active optical clock laser output at 1469 nm. The experimental results will be reported.

---

[195] D. Yu and J. Chen, "Optical Clock with Millihertz Linewidth Based on a Phase-Matching Effect", Phys. Rev. Lett.., vol. 98, p. 050801, 2007.

[2] J. Chen, "Active Optical clock," Chinese Science Bulletin, vol. 54, p. 348, 2009.

[3] Y. Wang, "Optical clocks based on stimulated emission radiation," Chinese Science Bulletin, vol. 54, p.347, 2009.

[4] D. Yu and J. Chen, "Laser theory with finite atom-field interacting time," Phys. Rev. A, vol. 78, p. 013846, 2008.

[5] D. Meiser et al., "Prospects for a millihertz-linewidth laser," Phys. Rev. Lett., vol. 102, p. 163601, 2009.

[6] J. Chen and X. Chen,"Optical lattice laser," 2005 IEEE Freq. Contr. Symp., p. 608, 2005.

IFCS-EFTF6-PAB6-16

Dispersion Detection of Optical Clock Transition in Thermal Atomic Beam

Xiaogang Zhang, Xiaobo Xue, Duo Pan, Wei Zhuang, Jingbiao Chen

School of Electronics Engineering and Computer Science,
Peking University, Beijing 100871, China

Email: jbchen@pku.edu.cn

In order to develop small optical clock for various transportable applications with better stability and accuracy than that of commercial small Cs clock and H-maser clock, our group has proposed a small Ca atomic beam clock scheme with electron-shelving detection[196,2]. Its potential stability was experimentally demonstrated recently[3].

However, the residual ground state atom after the clock laser interrogation attributes very large background of detected clock signal. One way to avoid this difficulty is to transfer most of ground state atoms to $^3P_1$ state in advance[2] via adiabatic passage[4]. Here, we present dispersive detection of optical clock transition in thermal Ca atomic beam, and this alternative detection method can effectively reduce the background light contribution due to the residual ground state atom after the clock laser interrogation to clock signal.

The experimental setup of Ca atomic beam optical clock with dispersive detection is shown in Fig. 1. We will discuss two experimental schemes of dispersive detection. One is to apply dispersive detection on 657 nm clock transition of Ca atoms directly, but the signal amplitude is limited by atomic flux and low spontaneous decay rate. The second scheme is to apply dispersive detection on Ca atoms in the electron shelving transition with a 423 nm laser after conventional clock laser interrogation. The experimental results will be reported.

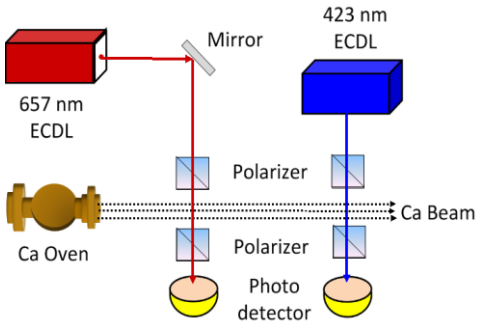

Fig. 63: Experimental setup of dispersion detection of optical clock transition in thermal Ca atomic beam

[1]Huang Kaikai, Zhang Jianwei, Yu Deshui, Chen Zhenhui, Zhuang Wei, Chen, Jingbiao, "Application of electron-shelving detection via 423 nm transition in Calcium-beam optical frequency standard", Chin. Phys. Lett., Vol. 23 p319,2006.

[2] Kaikai Huang, Donghai Yang, Jingbiao Chen "Small compact Calcium-beam optical frequency standard in Peking university and its new scheme", Proc. of 20th EFTF, pp376-378, 2006, 27-30 March 2006, Braunschweig Germany.

[3] John J. McFerran and Andre N. Luiten, "Fractional frequency instability in the 10^{-14} range with a thermal beam optical frequency reference", JOSA B, Vol. 27, p. 277, 2010.

[4] Xie Xiaopeng, Zhuang Wei, Chen Jingbiao, "Adiabatic passage based on the Calcium active optical clock", Chin. Phys. Lett., 27(7), 074202, (2010).

IFCS-EFTF6-PAB6-17

Testing Polish Optical Clock Calibration Procedures: Absolute Frequency Measurement of Rubidium 5S-7S Two-Photon Transitions

Michal Zawada[1], Piotr Ablewski[1], Wojciech Gawlik[2], Rafal Gartman[1], Piotr Maslowski[1], Piotr Morzynski[1], Bartlomiej Nagorny[1], Filip Ozimek[3], Czeslaw Radzewicz[3], Piotr Wcislo[1], Marcin Witkowski[1,4], Roman Ciurylo[1]

[1]Institute of Physics, Nicolaus Copernicus University, Torun, Poland
[2]Institute of Physics, Jagiellonian University, Krakow, Poland
[3]Institute of Experimental Physics, Faculty of Physics, University of Warsaw, Warsaw, Poland
[4]Institute of Physics, University of Opole, Opole, Poland

Email: zawada@fizyka.umk.pl

We report the absolute frequency measurements of rubidium 5S-7S two-photon transitions with an optical frequency comb. The digital lock to the transition, the procedures of evaluating the accuracy budget and measurements of the frequency with the optical frequency comb, which are prepared for the system of two optical lattice clocks with strontium atoms, are tested with much simpler setup. The narrow 760-nm Rb 5S–7S two-photon transitions, insensitive to a magnetic field, are particularly interesting as a frequency standard. The similar line, the 778-nm Rb 5S–5D transition has been recommended as the realization of the SI length unit meter[197]. As a result of this test, we obtained higher accuracy of the transition measurement than any previously reported[198] thanks to the very good long term stability of our experimental setup.

[197] Bureau International des Poids et Mesures (BIPM), in Report of the 86th Meeting of the Comité International des Poids et Mesures (CIPM), (BIPM, Sèvres, France, 1997)

[198] Ming-Sheng Ko and Yi-Wei Liu, Opt. Lett., **29**, 1799 (2004), A. Marian et al., Phys. Rev. Lett. **95**, 023001 (2005), K. Pandey et al., Opt. Lett., **33**, 1675 (2008)

IFCS-EFTF6-PAB6-18

Compact Methane Based OFS with $3 \cdot 10^{-15}$ short term stability

Gubin M., Kireev A., Lasarev V.*) Pnev A.*), Shelkovnikov A., Tyurikov D.
P.N. Lebedev Physical Institute, Moscow, Russia
*) N.E. Bauman Moscow State Technical University, *Moscow, Russia*
mgubin@okb.lpi.troitsk.ru

A compact optical frequency standard (OFS) with a short term stability at the level of 10^{-15} is needed for precise time-frequency measurements, navigation etc. One of the important applications of such OFS is use as a source of interrogative signal for laser cooled ions and atoms in electromagnetic traps. In present work we developed a new generation of two-mode He-Ne/CH_4 OFS stabilized over narrow saturated dispersion (SD) resonance at traditional F_2^2 line (ν_3 vibrational-rotational band of methane, 3.39μm) [1]. This device will be used for repetition rate stabilization of a Er fiber femtosecond laser as in [2].
Essential improvements were introduced into regular design of this type of OFS with internal absorption cell. The optical resonator was built as a zerodur monoblock unit without mechanical adjustments (except PZT elements); optical losses of the mirrors and internal windows separating active and passive media were minimized, so that total losses per round trip are estimated as 5-6 %. Special attention was paid to avoid parasitic back reflections from any optical element in the resonator. As a result the device combines high passive stability with a good quality quantum reference. Obvious advantage as compared to widely used lasers stabilized over high-Q cavities is much slower frequency drift. Also the interrogative oscillator based on He-Ne/CH_4 OFS does not require cryogenic equipment as microwave generators based on sapphire whispering gallery resonators do.

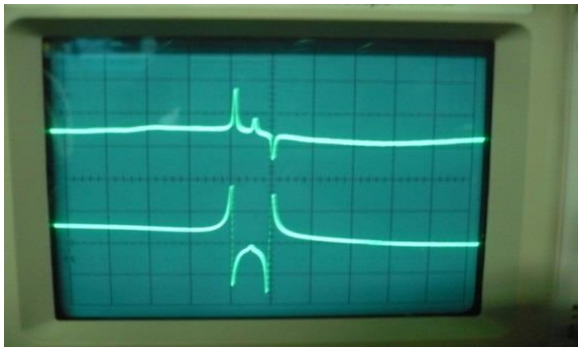

Fig 1. Resonances of SD (lower trace) and SA (upper trace) observed at the monoblock two-mode He-Ne/CH_4 OFS.

The parameters which determine Allan deviation of a frequency stabilized device are the beat frequency spectral density fluctuations of a free-running He-Ne/CH_4 OFS and a slope of the SD resonance at its center. At present the free running monoblock He-Ne/CH_4 OFS demonstrates spectral density of a beat frequency noise at the level ~ 0.1 Hz/$Hz^{1/2}$ (for typical laser output power ~ 0.1 mW) mainly determined by spontaneous emission (Shawlow-Townes limit). The slope of the SD methane resonance at its center (the 1st derivative) is ~ 0.3 Hz/Hz (Fig.1, lower trace).

It means that the frequency stability of a compact monoblock He-Ne/CH_4 OFS can reach $3 \cdot 10^{-15}$ at 1s. Direct comparison of two identical monoblock OFS is in progress and results will be discussed at the Conference.

---

[1] M.A. Gubin, E.D. Protsenko, "Laser frequency standards based on saturated-dispersion lines of methane", Quantum Electron, 1997, **27** (12), 1048–1062.

[2] M.A. Gubin, A.N. Kireev, A.V. Konyashchenko, P.G. Kryukov, A.S. Shelkovnikov, A.V. Tausenev, D.A. Tyurikov, «Femtosecond fiber laser based methane optical clock», Appl. Phys. B (2009) 95: 661–666.

IFCS-EFTF6-PAB6-19

IODINE STABILIZED IR LASER SOURCES

N. Chiodo[1], N. Castagna[1], M. Lours[1], D. Holleville[1], Y. Le Coq[1], F. Du-Burck[2], and O. Acef [1]

[1]LNE-SYRTE, Observatoire de Paris / CNRS-UMR 8630 / UPMC Paris 6, Paris, France
[2]LPL/ CNRS-UMR 7538 / Univ. Paris 13 - Sorbonne Paris Cité, Villetaneuse, France

e-mail: ouali.acef@obspm.fr

Solid state lasers emitting in the IR, such as Nd: YAG or fiber lasers offer attracting possibilities for development of compact and ultrastable setups, regarding to their low intrinsic phase noise, strong output powers and robustness. On the other hand, iodine lines in the green range of the visible domain exhibit high quality factor and strong signal-to-noise ratio yielding to confer to those lasers frequency stability in the 10^{-14} range at 1s. Nowadays, high efficiency non linear crystals permit to link in simple way the IR to visible range.

These couples of "IR laser/Iodine hyperfine line" are very promising for various terrestrial and/or space applications such as transportable optical clock, ultrastable frequency references for space interferometers, satellite laser links, long distance measurements, etc …

We report on iodine frequency stabilization of various IR laser sources on iodine hyperfine transitions in the green range. Different harmonic generation processes based on several designs of Periodically Poled Lithium Niobate non linear crystals (PPLN) are used to link the IR emission to the green region.

We have developed and tested various compact experimental setups using both multi-pass or intra-cavity short cells, in order to meet transportable/spatial requirements. Narrow hyperfine iodine lines below 500 kHz width are detected in the 514 nm/532 nm range and used for the IR sources stabilization.

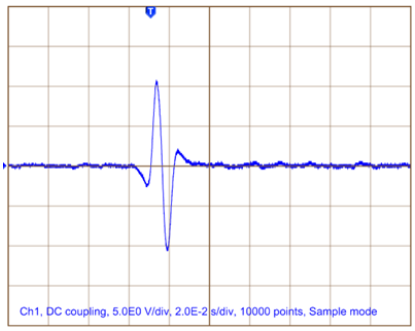

Record of the a_{10} hyperfine component of the
P 46 (44-0) line at $\lambda \sim 514.5$ nm
(Time constant 1 ms)

The details of these developments and the results will be presented at the conference.

This work is supported by CNES, DGA-ANR (Contract 11-ASTR 001-01).

IFCS-EFTF Student Poster Competition

Forum Hall

Monday & Tuesday, July 22-23, 2013, 01:00 pm - 02:00 pm and 3:30 pm - 4:30 pm

Chair: **Leonhard Reindl**
University of Freiburg

IFCS-EFTF-SPC-1

An Integrated SAW Sensor with Direct Write Antenna

Mark W. Gallagher[1], William Smith[2], Donald C. Malocha[1]

[1]Deparment of Electrical Engineering and Computer Science,
University of Central Florida, Orlando, FL 32816
[2]MesoScribe Technologies Inc., St. James, New York 11780

Email: MGallagher@knights.ucf.edu

This paper presents a wafer-level integrated SAW sensor using conventional thin-film fabrication for the SAW, and the direct write of a thicker dissimilar metal for the antenna. Previous proof-of-concept results using thin antenna films demonstrated the feasibility of planar device integration, but had limited interrogation range.[199] For the first time, a direct write process is utilized to deposit the antenna conductor onto the SAW substrate, providing ease of fabrication, optimal film thickness, and superior adhesion. Shown in Figure 64, the automated thermal spray process selectively deposits conductive or dielectric films onto a CAD defined area for rapid, conformal fabrication, allowing sensor integration on a range of surfaces. Results presented will show an increase in range, compared to previous work, through an improved low loss design.

Using the direct write process, shown in Figure 64, 15 μm thick copper is 'written' onto lithium niobate without a mask. Thick antenna traces lower antenna resistive losses, because of increases in conductivity and decreased skin depth effects. The traces adhere well to the 80 nm aluminum SAW transducer pads that are patterned previously by a traditional photolithographic process. The process allows multiple metal levels, trenching, and trimming, for optimum design and fabrication of research or a commercial product. The updated design yields three devices on a 76 mm wafer and requires no mechanical bonds; bond free devices are ideal for demanding environmental sensors.

Antenna gain and bandwidth trade-offs must be made to the integrated design to meet device size and system performance requirements. The design of a 915 MHz meandered dipole antenna with low mismatch loss and maximized radiation efficiency over an 8% SAW fractional bandwidth is demonstrated. Experimental performance results of antennas fabricated on standard FR4 and on-wafer by electroplating or direct write process will be contrasted. Temperature sensors are fabricated on YZ-$LiNbO_3$ and simultaneous operation, over temperature, in a multi-sensor system will be demonstrated wirelessly at several meters. The integration of SAW and direct write technology offers a multitude of opportunities for new sensor and communication system embodiments.

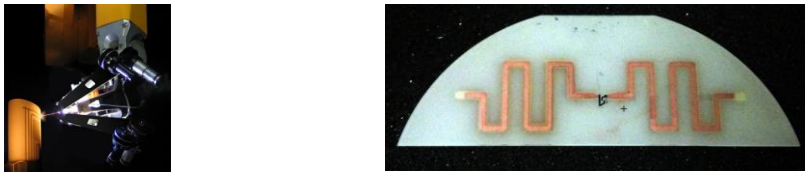

(a) (b)

Figure 64: (a) The automated direct write robot printing to a part. (b) An example of a 915 MHz SAW sensor and direct write dipole antenna integrated onto a 76 mm Y-cut lithium niobate wafer.

[199] M. W. Gallagher, B. C. Santos and D. C. Malocha, "Wireless wideband SAW sensor - antenna design," in *IEEE Int. Frequency Control Symp.*, Newport Beach, CA, 2010, pp.291-296.

NANOMECHANICAL MASS SPECTROMETRY FOR THE CHARACTERIZATION OF HIGH MASS NANOPARTICLES

E. Sage[1], A. Brenac[2], R. Morel[2], C. Dupré[1], C. Marcoux[1], H. Blanc[1], M. S. Hanay[3], S. Kelber[3], M.L. Roukes[3], E. Colinet[1], L. Duraffourg[1] and S. Hentz[1]

[1]CEA, LETI, MINATEC campus, 17 rue des martyrs, 38054 GRENOBLE Cedex 9, France.
[2]INAC/SP2M and Université Joseph Fourier, CEA Grenoble, 38054 Grenoble, France.
[3]Kavli Nanoscience Institute and Departments of Physics, Applied Physics, and Bioengineering, California Institute of Technology, MC 149-33, Pasadena, California 91125 USA.
Email: eric.sage@cea.fr

Nano Electro Mechanical Systems (NEMS)-based Mass Spectrometry (MS) holds great promise for point of care applications[200] or air quality monitoring. Real-time, single protein MS has recently been demonstrated with top-down silicon resonators[201]. These devices operate in a mostly unexplored mass range where particles display a wide mass distribution and where there is no mass standard. A direct comparison of NEMS-MS and reference MS measurement (here conventional Time-Of-Flight (TOF) MS) is therefore crucial and is presented for the first time in this paper. The NEMS device is fabricated on a 200mm SOI wafer with VLSI process. It is a 160nm thick doubly clamped beam, electrostatically actuated, with heterodyne piezoresistive detection[202]. Its first two resonance frequencies are simultaneously tracked with Phase Locked Loops.

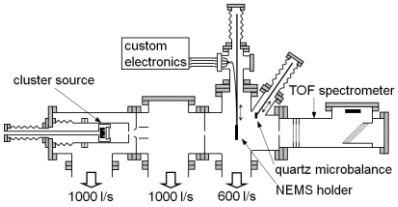

Figure 1: Schematic of the mass deposition setup

The NEMS device is inserted in the deposition chamber of a custom sputtering-gas aggregation setup able to produce nanometric metallic clusters with tunable deposition rate and diameter[203] (see Figure 1). First the NEMS experimental mass sensitivity is calculated by varying the deposition rate, measured with a Quartz Crystal Microbalance (QCM). In a second step, tantalum clusters were projected onto the surface of the NEMS with a flux rate allowing for individual particle measurement. Figure 2 shows preliminary mass distributions obtained with both NEMS-MS and TOF-MS: the distribution shape is reproduced with fidelity (widths at half maximum 352kDa and 408kDa respectively) and the mean masses are very close. NEMS-MS displays a resolving power similar to TOF-MS in this mass range, and even better at higher mass ranges. This demonstrates all the potential of NEMS-MS in this mass range. The offset as well various mass distributions are under investigation.

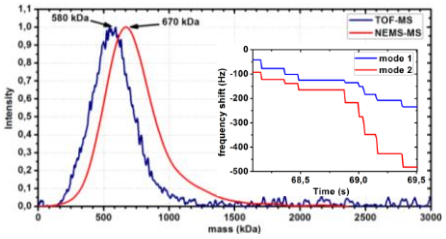

Figure 2: TOF-MS and NEMS-MS mass spectra of tantalum clusters. (1 Da=1.66 × 10^{-27} kg). Inset: frequency jumps induced by individual landing events

[200] A. Boisen, *Nature Nanotechnology*, vol. 4, pp. 404-405, 2009.

[201] M. S. Hanay et al, *Nature Nanotechnology*, vol. 7, pp. 602-608, 2012.

[202] E. Mile et al, *Nanotechnology*, vol. 21, pp. 165504, 2010.

[203] R. Morel et al, *Eur. Phys. J. D*, 24, pp. 287-290, 2003.

IFCS-EFTF-SPC-3

Micro-electro-mechanical resonant tilt sensor with 250 nano-radian resolution

Xudong Zou, Pradyumna Thiruvenkatanathan and Ashwin A. Seshia

Nanoscience Centre, Department of Engineering, University of Cambridge, United Kingdom

Email: xz280@cam.ac.uk

This paper reports on a high-resolution frequency-output MEMS tilt sensor based on resonant sensing principles[1]. The tilt sensor measures orientation by sensing the component of gravitational acceleration along a specified input axis (Fig. 1). The devices consist of a suspended proof mass connected to two double-ended tuning fork (DETF) resonators at each end through a lever arrangement. When subjected to a tilt with respect to the gravitational axis, the tuning forks respond through a shift in their resonant frequency and the differential frequency shift can be then calibrated with respect to the tilt angle. Prototype devices are fabricated in a foundry SOI-MEMS process and optical micrographs of the device are shown in Fig.2. The microfabricated chips are mounted onto standard chip carriers and then vacuum packaged using a custom process. A combination of design enhancements enables significantly higher sensitivity for this device as compared to previously reported prototype sensors[1].

The vacuum packaged sensor chip is co-integrated with oscillator circuits on a PCB and mounted on a manual tilt table. Figure 3 depicts the tilt test set-up and Fig. 4 shows the output frequency variation of DETF_1 (see Fig. 1) observed in a 0^o-90^o tilt test. The tilt test results indicate that the new sensor provides a relatively linear response in the range of $\pm 20^o$ with a scale factor of approximately 50.06 Hz/degree. Fig. 5 shows the results of a measurement on the output stability of the device as determined by Modified Allan Deviation measurements. The resolution of the resonant tilt sensor is found to be approximately 250 nano-radian for an integration time of 0.8 s, which is over an order of magnitude better than previously reported results[204]. The impact of polarization voltage induced noise and drift is also seen by comparing the two plots in Fig. 5.

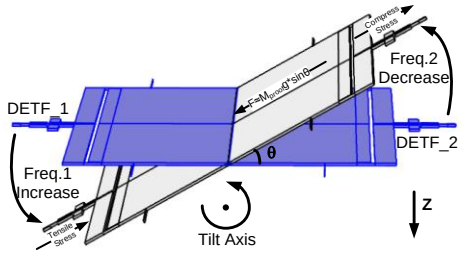

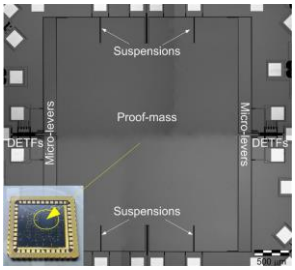

Fig.1: Tilt sensor operation principle. Fig.2: Optical micrograph of sensor (inset: vacuum packaged device).

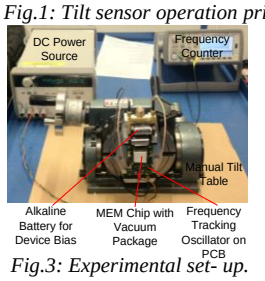

Fig.3: Experimental set- up.

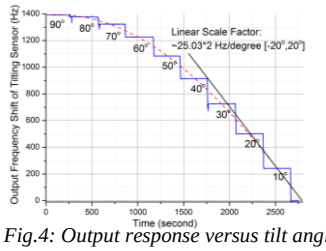

Fig.4: Output response versus tilt angle.

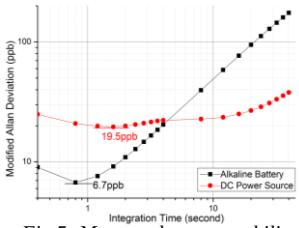

Fig.5: Measured output stability.

[204]X.Zou, et al., "Micro-electro-mechanical resonant tilt sensor," Frequency Control Symposium (FCS), 2012 IEEE International, 21-24 May 2012.

Mapping Thermomechanical Vibrations and Mode Shapes in High Frequency SiC-on-Insulator Nanoscale Resonators

Jaesung Lee[1*], Zenghui Wang[1], Mehran Mehregany[1], Philip X.-L. Feng[1*]

[1]Electrical Engineering, Case Western Reserve University, Cleveland, OH 44106, USA

Email: jaesung.lee@case.edu, philip.feng@case.edu

We report on experimental demonstration of multi-mode radio-frequency nanomechanical disk resonators in a novel 500nm SiC-on-insulator (SiCOI) technology, and on measurements of directly mapping the mode shapes of the multiple resonances with high spatial resolution. By employing and engineering ultrasensitive optical interferometric techniques, we measure the lowest possible levels of vibrations, *i.e.*, the undriven thermomechanical resonances arising from the intrinsic Brownian motions, in these SiCOI disk resonators. Spatially mapping the resonant mode shapes of multi-mode nanomechanical resonators can greatly facilitate understanding and harnessing these multiple modes for sensing and frequency control applications.

Our resonant devices (500nm-thick poly-SiC disks anchored on SiO_2 center pedestals) feature a uniform optical cavity (depth=500nm) with the underneath Si substrate. We use an optical interferometer with fm/Hz$^{1/2}$-level displacement sensitivity[205,206,] to transduce the thermomechanical motion of the device into electrical signals. The ~1μm laser spot enables spatially mapping the different resonance modes.

Figure 1 shows measured noise spectral density of five mechanical resonance modes. The peak amplitude of the mode strongly depends on the laser spot position (see insets). In the center of the disk (position (a)), no measurable motion signal is observed. In the positions (b) and (c), we detect 5 and 4 resonance modes, respectively. Measured resonance frequencies and spatial maps of the mode shapes (center row insets) agree very well with COMSOL simulation results (bottom row insets). We also observe interesting effects such as the off-center position of the pedestal lifting the frequency degeneracy between the first two modes and breaking the azimuthal symmetry in the mode shape of the third resonance mode, as well as electronically tuning the resonances, which we will report in detail in the full paper.

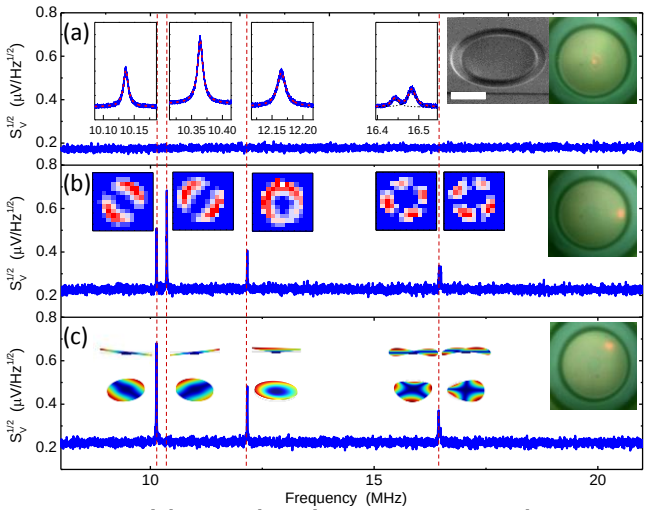

Fig. 1: Measured thermomechanical resonance spectra. Right insets: optical images showing the exact actual positions of the laser spot. Top insets: plots of resonances with fit (same *y* axis and scale as in main plots). Middle insets: spatial intensity map for each mode. Bottom insets: COMSOL simulation of the mode shapes. Top right: SEM image (scale bar: 10μm).

[205] W. K. Hiebert, D. Vick, V. Sauer, M. R. Freeman, *J. Micromech. Microeng.* **20**, 115038 (2010).
[206] J. Lee, P. X.-L. Feng, *Proc. IEEE Inter. Freq. Contr. Symp. (IFCS2012)*, DOI: 10.1109/FCS.2012.6243742.

Design of Ultra-Low-Power (2.5μW) 1GHz Low Phase Noise Pierce Oscillator with Nanowire NEMS Resonator

Hamidreza Zamani[1], Philip X.-L. Feng[1]

[1]Electrical Engineering, Case Western Reserve University, Cleveland, OH 44016, USA
Email: hamidreza.zamani@case.edu.edu, philip.feng@case.edu

Laterally-vibrating nanowire (NW) resonators with high resonance frequencies f_{res} and electrostatic transduction method are interesting for CMOS timing circuits. However, their motional resistance R_m is often very high, much larger than their rivals FBARs with R_m of several ohms. Since R_m is also proportional to the resonance frequency f_{res}, design of high frequency oscillators are even more difficult. In Pierce oscillators, the minimum MOS transconductance which makes oscillation feasible is[207] $g_{m,min} \propto \omega_{osc}^2 R_m C_1 C_2$ (parameters are identified in Fig. 1a). In this work, we propose and develop a modified architecture using two small (bondwire) inductors (also connecting the nodes to DC bias voltages) which reduce the effective motional resistance seen by the CMOS circuit. The analysis includes novel analytical formulas for design of these modified Pierce-family oscillators working with resonators of initially high-motional resistance. As a proof of concept, we have provided Spectre simulation results for a 1GHz oscillator with *very low power consumption* while having high voltage amplitude at the output (drain of transistor M in Fig. 1a). The mechanical resonator assumed for this simulation is a doubly-clamped Si NW with length, width, thickness and quality factor of respectively 419nm, 20nm, 80nm and 2000. Phase noise and spectral purity performance results are also provided. The specifications in this work are compared to several recent related works. The specifications reported in the Table for other works are measurement results.

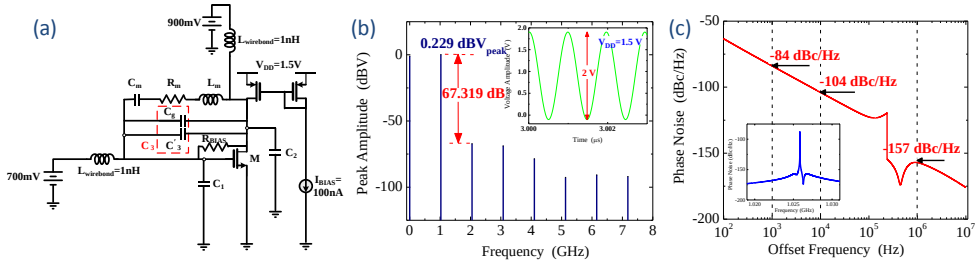

Fig. 65: (a) Schematic of a 1GHz modified Pierce oscillator. (b) Spectral response of the oscillator harmonics compared to the fundamental one. *Inset*: Oscillator output voltage in time domain (not connected to 50Ω load). (c) Phase noise simulation results for offset frequencies around the major oscillation frequency (f_{osc}=1.0256 GHz). *Inset*: Phase noise in a linear (absolute) frequency scale. The frequency resolution of sampling in the inset is lower, which causes difference in the phase noise for frequencies very close to f_{osc}.

	R_m	f_{osc} [GHz]	P_{con}	*Phase Noise* [dBc/Hz]
This work	**13.1MΩ**	1.026	**2.5μW**	-84 (@1kHz), -104 (@10kHz), -157 (@1MHz)
[Zuo-*CICC*][208]	22Ω	1.5	6.9mW	-85 (10kHz), -151 (@1MHz)
[Zuo-*TUFFC*][209]	25Ω	1.05	3.5mW	-81 (@1kHz)
[Lavasani-*ISSCC*][210]	750Ω	1.006	1.9mW	-94 (@1kHz)

[207] E. Vittoz, *Low-Power Crystal and MEMS Oscillators: The Experience of Watch Developments*, Springer 2010.
[208] C. Zuo, J. Van der Spiegel, G. Piazza, "1.5-GHz CMOS…", *CICC2010*, San Jose, CA, 2010.
[209] C. Zuo, J. Van der Spiegel, G. Piazza, "1.05-GHz CMOS…", *IEEE Trans. UFFC*, vol. 57, no. 1, p. 82-87, 2010.
[210] H. H. M. Lavasani, W. Pan, B. Harrington, R. Abdolvand, and F. Ayazi, "A 76dBOhm, 1.7 GHz, 0.18um CMOS tunable transimpedance amplifier…", *ISSCC 2010*, San Francisco, CA, Jan. 2010, p. 318-320.

IFCS-EFTF-SPC-6

High spectral purity microwave and terahertz oscillator

Gwennaël Danion[1], Goulc'hen Loas[1], Ludovic Frein[1], Cyril Hamel[1], Anthony Carré[1], Steve Bouhier[1], Marc Vallet[1], Marc Brunel[1], Antoine Rolland[1], Mehdi Alouini[1], François Bondu[1], Alain Brillet[2], Jean-Pierre Coulon[2], Frédéric Cleva[2], Mourad Merzougui[2], Alexandre Beck[3], Guillaume Ducournau[3], Jean-François Lampin[3], Mohamed Zaknoune[3], Christophe Coinon[3], Xavier Wallart[3], Emilien Peytavit[3], Tahsin Akalin[3], Grégoire Pillet[4], Loïc Morvan[4], Ghaya Baili[4] and Jérôme Bourderionnet[4]

[1]Departement Optique et Photonique, IPR, Université Rennes1 CNRS, Rennes, France

[2]ARTEMIS, Observatoire de la côte d'Azur, Nice, France

[3]Groupe Photonique/THz, IEMN, Université de Lille CNRS,Villeuneuve d'Ascq, France

[4]Thales Research and Technology, Palaiseau, France

Email: gwennael.danion@univ-rennes1.fr

We present a microwave/THz oscillator project (2012-2014) excepted to show below -150 dB rad^2/Hz phase noise at an offset frequency of 10 kHz for a 30 GHz carrier frequency as well as 18 GHz, 100 GHz, 400 GHz, 1 THz. The microwave/THz signal is obtained by mixing two optical frequencies with a photomixer.

A dual-axis two frequency cross polarization laser will be stabilized onto two resonances of one Fabry-Perot cavity. The two frequencies sense the same cavity length fluctuations so that the best possible relative stability of the beat note is limited by the relative dimensional stability of the cavity. This cavity spacer is made with an ultra low expansion ceramic (ULE) placed in vacuum. A 75% fraction of the beam transmitted by the cavity is used to stabilize the amplitude of the laser, and a 25% fraction is sent on a polarizer and a photomixer for optical to millimetre wave conversion. The AM/PM conversion, especially the opto-thermal conversion in the cavity i.e. the absorbed power fluctuations, is negligible at a 1 Hz frequency offset by stabilization of the optical carrier at the 8.10^{-9}/Hz$^{1/2}$ level.

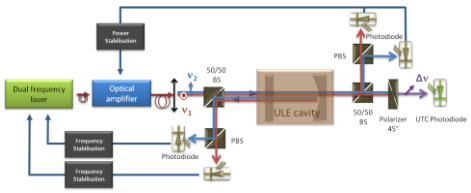

Fig. 66: One microwave/THz oscillator

This oscillator is based on a dual frequency laser system whose beat note frequency is continuously tunable from DC to 600 GHz. An Erbium/Ytterbium solid-state two-axis dual-frequency laser system followed by amplifier stage has been developed. Each polarization frequencies is independently tunable by 1.7 GHz steps by tilting its etalon and continuously with an electro-optic crystal. We have chosen two lithium tantalate (LiTaO3) crystals; thermo-optic (600MHz/°C) and electro-optic (1.1MHz/V) effects enable to lock each frequency on the resonance of a 1.5 GHz free spectral range Fabry Perot cavity. Each polarization light beam is amplified by a fiber system. Our system amplifier is composed of an erbium doped fiber amplifier (EDFA) and a semiconductor optical amplifier (SOA) per polarization axis. This amplifier system permits to deliver 18 dBm power, to stabilize the power fluctuations and to reduce the relative intensity noise by 20 dB, especially the relaxation oscillation.

IFCS-EFTF-SPC-7

Inverse Relationship between OEO *Q*-factor and *g*-sensitivity

James P. Cahill[1,2], Justin Pritchett[1], Ryan Sorensen[1], Morris Berman[1], Olukayode Okusaga[1], Weimin Zhou[1], Gary M. Carter[2], Curtis R. Menyuk[2]

[1]U.S. Army Research Laboratory, Adelphi, MD
[2]University of Maryland: Baltimore County, Baltimore, MD

Email: james.p.cahill.ctr@us.army.mil

We present evidence that the vibration (*g*-) sensitivity of a fiber-based OEO decreases as the fiber length wound to a single spool increases. This is the result of two effects. First, the magnitude of the vibration-induced perturbation remains constant with increasing fiber length because of diminishing mechanical coupling between the outer layers of fiber and the spool. Second, the power spectral density (PSD) of the phase noise induced by a constant magnitude perturbation decreases as the *Q* factor (i.e. fiber length) of the cavity increases. This is an oscillator filtering effect. We can exploit these effects to construct fiber-based OEOs with lower *g*-sensitivity.

A sinusoidal vibration induces a peak in the OEO phase noise at the vibration frequency with PSD proportional to $(\Delta l/l)^2$, where Δl is the vibration-induced change in length of the fiber delay, and l is the length of the total fiber delay.[xiv] We use t^{his} sideband to characterize both the filter effect and the mechanical coupling between fiber and spool. In order to maintain consistency we use identical spools in all tests.

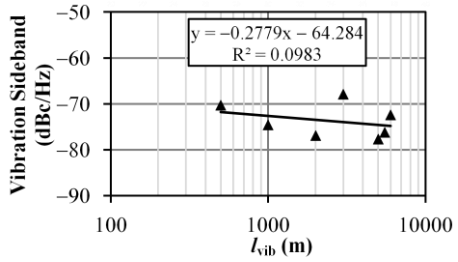

Figure 1. PSD of the vibration-induced phase noise peak as a function of the length of fiber exposed to vibration. Total OEO delay is fixed.

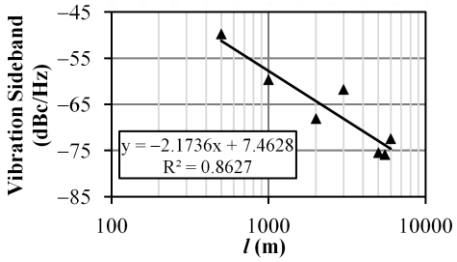

Figure 2. PSD of the vibration-induced phase noise peak as a function of total OEO fiber delay length. The entire delay is exposed to vibration.

To demonstrate the diminished coupling between fiber and spool, we keep the total fiber delay of the OEO at a constant length while exposing only a portion, l_{vib}, of the fiber delay to a sinusoidal vibration. Fig. 1 plots the PSD of the vibrational sideband as a function of l_{vib}. Because we hold all relevant parameters constant, the PSD of the vibrational sideband will be proportional to Δl^2. Yet fig. 1 shows that the PSD is independent of l_{vib}. Thus, the mechanical coupling between the fiber and spool has effectively saturated, and Δl is independent of the fiber length.

To demonstrate the oscillator filtering effect, we expose the entire fiber delay of the OEO to a sinusoidal vibration. Fig. 2 plots the PSD of the vibration-induced sideband as a function of the total delay length, l. The PSD of the sideband decreases approximately quadratically as fiber length increases. Thus, as the OEO Q increases, the vibrational noise is effectively filtered out.

IFCS-EFTF-SPC-8

Resonantly enhanced Fe^{3+} spin-spin interaction in cryogenic sapphire

Jeremy Bourhill[1], Karim Benmessai[1], Maxim Goryachev[1], Daniel Creedon[1], Warrick Farr[1] and Michael Tobar[1]

[1]EQuS Frequency and Quantum Control Metrology Laboratory, University of Western Australia, Perth, Western Australia

Email: jeremy.bourhill@uwa.edu.au

We report the observation of a new behaviour observed in sapphire crystal using paramagnetic Fe^{3+} ions at cryogenic temperatures. When the crystal is pumped at 12.04 GHz, exciting an extremely high Q-factor whispering gallery mode (WG mode) at the central frequency of a Fe^{3+} spin transition, an additional signal is generated around 11.8 GHz, at the location of another WG mode. We show that this signal is excited due to the broadened Fe^{3+} spin bath interacting with the 11.8 GHz mode; forming an effective three level system through population inversion. We also observe complex interaction between the pump at 12.04 GHz and the signal at 11.8 GHz when pumping is close to the former's bandwidth, resulting in Van der Pol oscillations of the output power.

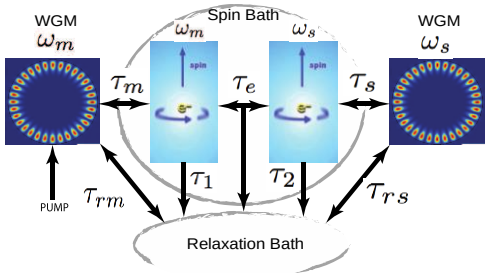

Figure 67: Model representing coupling between the two WG mode resonances, ω_m corresponding to the master or pumped WG mode at 12.04 GHz and ω_s corresponding to the slave WG mode at 11.8 GHz, via the Fe3+ spin bath.

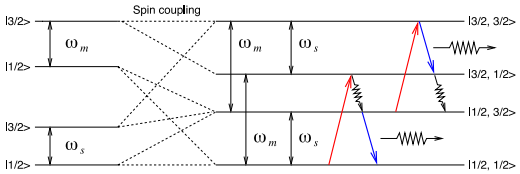

Figure 68: Energy level diagram of uncoupled spins (left) and coupled spins (right). Spin coupling is due to their simultaneous occupation, in frequency, of the Fe^{3+} spin bath, and close proximity in space. The resulting three level system is made possible by the dissipation of energy equivalent to the difference between the two signal

Fe^{3+} ions are unintentionally substituted into the crystal lattice during the manufacture process, and due to the crystal under investigation's over annealing, they exist in populations much larger than normally observed. The spins excited by the pump can couple to other spins located nearby in the crystal with different frequency transitions (see Figure 1). The different energy transitions exist as a result of the inhomogenously broadened spin resonance. The pump can decay through lower energy transitions, and two in particular, the 11.8 GHz transitions, are enhanced by the fact that they are located at the nearest lower neighbour high-Q WG modes, and hence these signals are observable, and an effective three level system is established (see Figure 2).

As pump detuning from ω_m decreases, we first reach the masing threshold and hence we see the ω_s signal switch on. As we tune more and approach our resonant frequency, more photons enter the system at ω_m until we reach a point where there is sufficient power at this frequency that the transitions of the coupled spins becomes significant enough to cause oscillations in power of the two photonic modes. We observe forced Van der Pol oscillations of the output power, as predicted by the model we derive from Figure 1. The characteristics of these oscillations are controllable by varying the detuning.

IFCS-EFTF-SPC-9

Short term noise investigation on a compact CPT clock

Danet Jean-Marie, Yun Peter, Guerandel Stephane, de Clercq Emeric

LNE SYRTE, Observatoire de Paris, Paris, France

Email: jean-marie.danet@obspm.fr

Towards the development of on-board atomic clock, alkali vapor cells clocks have shown that besides their robustness and relative simplicity, cell technology clocks are competitive with the cold atoms compact setups in term of stability[211] [212]. Among the different vapor cell clock technologies, the coherent population trapping (CPT) prototype developed at SYRTE offer an alternative where no microwave cavity is needed. The microwave is optically carried by the frequency difference between two lasers. Using crossed linear polarized beams and Ramsey temporal interrogation, signals with 15 % contrast and 125 Hz linewidth have been observed. Such a signal, combined with a noise at the shot noise limit would lead to sub $10^{-13}\ \tau^{-1/2}$ stability clocks. In this paper we report investigations on the noise processes currently limiting the short term stability of the clock at the level of $5.5\ 10^{-13}$ at 1s.

Five main noise sources are investigated: magnetic field, beam polarization, laser frequency, laser intensity and finally microwave phase. A contribution to the clock stability below 10^{-14} at 1s is shown for the two first ones. The effect of the optical frequency detuning has been measured and its conversion on the clock stability is under investigation. The influence of the laser intensity noise has been carefully studied, it is not negligible in the 10^{-13} range. A stabilization system has been implemented lowering the RIN of 15 dB down to -137 dB/Hz$^{-1/2}$ at 160 Hz. Finally the local oscillator noise contribution to the clock stability has been studied using the Dick formalism[213]. This aliasing effect, well understood for a two level system, had never been investigated for a three level one as the CPT. The numerical calculation, in good agreement with measurements, allowed us to deduce a phenomenological equation for the Dick effect in CPT, usable for others CPT clocks. The application of those calculations to our prototype pointed out the local oscillator as main noise source contributor, followed by the intensity noise. Solutions have been designed and will be implemented on our set-up. The latest results will be shown at the conference.

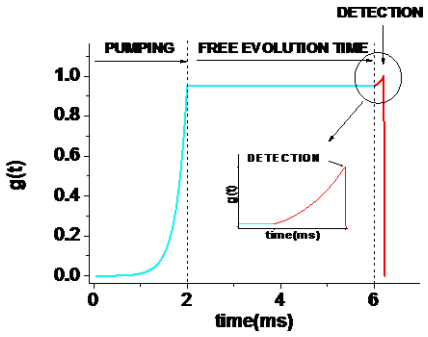

Fig. 69: Sensitivity function of a pulsed CPT clock. Pumping 2ms, Free evolution time 4ms, Detection: 25 µs, 200 µs after switching lasers on.

[211] S. Micalizio et al., Metrologia, vol 49, 425, 2012.

[2] F. X. Esnault et al., Phys. Rev. A, 82, 033436, 2010.

[3] G. J. Dick et al, in Proc. 19th Annu. Precise Time Time Interval conf., pp. 133–147, 1987.

IFCS-EFTF-SPC-10

MiniAtom: realization of a compact atomic gravimeter

Jean Lautier[1], Baptiste Battelier[2], Arnaud Landragin[1], Philippe Bouyer[2]

[1]LNE-SYRTE, Observatoire de Paris, CNRS, UPMC, 61 boulevard de l'Observatoire, 75014 Paris, France

[2] LP2N, CNRS, IOGS, Universite Bordeaux 1, Batiment A30, 351 cours de la Liberation, 33405 Talence CEDEX, France

Email: jean.lautier@obspm.fr

We present here the realization of a highly compact absolute atomic gravimeter. The main purpose is to demonstrate that atomic interferometers can overtake the current limitations of inertial sensors based on "classical" technologies for field and on-board applications. We show that the complexity and the volume of cold-atom experimental set-ups can be drastically reduced while keeping the performances close to the state-of-the-art, enabling such atomic sensors to perform precision measurements outside of the laboratory.

The measurement of the acceleration of gravity (g) is made with a $\pi/2$ - π - $\pi/2$ interferometer using stimulated Raman transitions to couple |F=1, mf=0> and |F=2, mf=0> hyperfine states of free-falling ^{87}Rb atoms[214]. The use of an innovative hollow pyramid as the usual retro-reflecting mirror of quantum inertial sensors enables to perform all the steps of the atomic measurement (trapping and cooling the atoms, performing the interferometer and reading out its outputs) with one single laser beam instead of 6 normally[215]. The laser system is based on a single telecom laser diode, which is phase modulated and frequency doubled[216]. This leads to a drastic reduction of the complexity and the size of the apparatus: the overall physical package is of a few tens of litters in volume only: the sensor head (that includes the vacuum chamber) fits in a cylinder 40 cm high and 20 cm in diameter; the entire laser bench, the electronics and the power supplies fit in a cube of 70 cm of side.

We target a relative sensitivity to acceleration of gravity below 10^{-7} at one shot, which will allow to monitor time variation of g due to tides and to detect significant mass anomalies and mass displacements. We have shown promising long-term stability with a flicker floor on the 10^{-9} range and up to two day long measurements have been recorded with such architecture[2].

Particular efforts have been made to push on the integration of the micro-wave frequency standards used to drive the clock frequency of ^{87}Rb atoms at 6.835 Ghz and to deliver quantum state selective pulses. Although an output power of 25 dBm and a 500 MHz agility are required, our chain features a phase noise that will only limit our relative sensitivity to acceleration at the 10^{-8} level. We thus show an attractive trade-off between the integration in a two-litter package and a satisfactory phase noise level that other field or on-board quantum sensors could benefit from.

The final assembly of the gravimeter is currently under way and the loading of few 10^8 atoms in a 3D MOT has already been obtained. The first atomic signals are expected soon.

---

[214] M. Kasevich "Atomic interferometry using stimulated Raman transition", PRL, vol. 67, p. 181 - 184, 1991.

[215] Q. Bodard, "A cold atom pyramidal gravimeter with a single laser beam", APL, vol. 96, 134101, 2010.

[216] G. Stern, "Light-pulse atom interferometry in microgravity", Eur. Phys. J. D, vol. 53, p. 353 - 357, 2009.

IFCS-EFTF-SPC-11

Spatially Resolved Measurement of Relaxation Times in a Microfabricated Vapor Cell

Andrew Horsley[1], Guan-Xiang Du[1], Matthieu Pellaton[2], Christoph Affolderbach[2], Gaetano Mileti[2], and Philipp Treutlein[1]

[1]Departement Physik, Universität Basel, Switzerland
[2]Laboratoire Temps-Fréquence, Institut de Physique, Université de Neuchâtel, Switzerland

Email: andrew.horsley@unibas.ch

Microfabricated vapor cells are an important tool for atomic physics applications, showing particular success in miniaturised atomic clocks[217] and DC electromagnetic field sensing[218]. As a new application, imaging of microwave magnetic fields using a vapor cell has recently been demonstrated by our group[219]. A thorough knowledge of the properties of a cell is prerequisite to precision measurements. For microfabricated cells and imaging applications, the spatial dependence of relaxation times and excitation fields are of particular importance. We present the spatially resolved characterisation, performed using time-domain Ramsey and Rabi measurements, of a 5 mm diameter, 2 mm thick microfabricated cell, filled with ^{nat}Rb and 80 mbar of N_2 buffer gas[220].

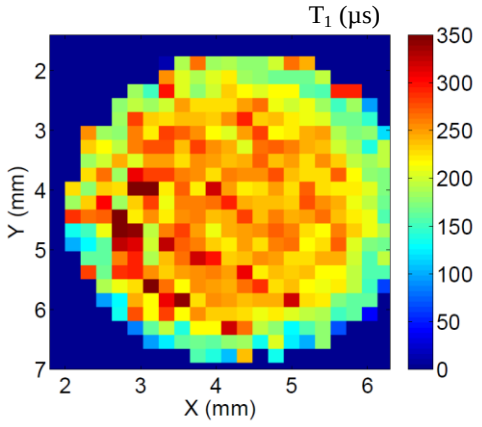

Fig. 70: T_1 times across the cell, obtained using relaxation in the dark, at a cell temperature of 90°C. Lifetimes are longer in the centre of the cell, where the effects of destructive Rb-wall collisions are minimised.

Atomic relaxation is described by the T_1 and T_2 times, representing the population and coherence lifetimes, respectively. The dominant relaxation mechanisms in a vapor cell are Rb-wall, Rb-buffer gas and Rb-Rb collisions. The coherence lifetime is also limited by inhomogeneities in applied static and microwave magnetic fields. Both lifetimes can be obtained in a single time-domain Ramsey measurement.

We characterise T_1 and T_2 relaxation in the cell as a function of position, performing Ramsey measurements as we scan a narrow laser beam across the cell. We also probe the homogeneity of our applied static and microwave fields using Rabi sequences. In addition we have implemented an imaging technique, whereby a CCD chip is used to perform measurements over the entire cell simultaneously. As an example, figure 1 shows an image of T_1 times across our cell.

This work was supported by SNSF and ESA. We thank Y. Pétremand for filling the cell.

[217] Svenja Knappe et al "A microfabricated atomic clock" Appl. Phys. Lett. 85, 1460 (2004)

[218] D. Budker and M. Romalis, "Optical magnetometry" Nat. Phys. 3, 227 (2007)

[219] Pascal Böhi and Philipp Treutlein "Simple microwave field imaging technique using hot atomic vapor cells" Appl. Phys. Lett. 101, 181107 (2012)

[220] M Pellaton, C Affolderbach, Y Pétremand, N de Rooij and G Mileti, "Study of laser-pumped double-resonance clock signals using a microfabricated cell" Phys. Scr. T149 (2012)

IFCS-EFTF-SPC-12

Towards a Large-Scale, Optical Timing Distribution System with Sub-Femtosecond Residual Timing Jitter

Michael Y. Peng[1], Patrick T. Callahan[1], Amir H. Nejadmalayeri[1], Stefano Valente[2,3], Kemal Ahmed[2], Ming Xin[2], Eric Monberg[4], Man Yan[4], Lars Grüner-Nielsen[4], John M. Fini[4], Tony D. Roberts[5], Philip Battle[5] and Franz X. Kärtner[1,2]

[1]Department of EECS and Research Laboratory for Electronics, Massachusetts Institute of Technology, Cambridge, MA, USA
[2]Center for Free-Electron Laser Science, Deutsches Elektronen-Synchrotron, Hamburg, Germany
[3]Department of Electrical Engineering and Computer Science, University of L'Aquila, L'Aquila, Italy
[4]OFS Laboratories, Somerset, NJ, USA and [5]AdvR, Inc., Bozeman, MT, USA

Email: mypeng@mit.edu

Over the past 10 years, we have developed a pulsed optical timing distribution system[221] for large-scale, long-term synchronization of radio-frequency and optical sources in X-ray laser facilities, which may extend over several kilometers. The system consists of a femtosecond laser tightly locked to a microwave reference and fiber links stabilized via compact, single-crystal balanced optical cross-correlators (BOCs). Sub-10-fs performance over days of operation has been achieved[222] but is limited mainly by polarization mode dispersion in standard single-mode fiber. In the near future, it is necessary to improve timing distribution down to sub-femtosecond precision; current facilities, such as LCLS at Stanford, can already produce X-ray pulses shorter than 10 fs and concepts for sub-fs X-ray pulse generation are already in place. In the past two years, we have developed key components and characterized commercial femtosecond lasers suitable for realizing the next-generation, sub-femtosecond, fiber-based timing distribution system.

As demonstrated by Kim et al.[223], BOCs can be used to characterize the timing jitter of mode locked lasers with attosecond precision. We used this technique to characterize the jitter of two identical, commercially-available femtosecond lasers (OneFive-ORIGAMI) and confirmed that their high-frequency jitter for frequencies higher than 1 kHz is less than 70 as (Fig.1a). These lasers therefore have sufficiently low noise to serve as master oscillators for sub-fs timing distribution. Second, to eliminate slow drifts induced by polarization mode dispersion, we implemented a 1.2-km polarization-maintaining fiber link using 1 km of standard PM fiber and 0.2 km of novel dispersion-compensating PM fiber from OFS. Link operation for 16 days showed only 0.9 fs RMS timing drift and during a 3-day interval only 0.2 fs drift (Fig.1b). Lastly, we present a hybrid integrated BOC fabricated by AdvR using PPKTP waveguides[224] (Fig.1c). We seek to solve long-term drift issues by eliminating alignment drifts in free-space BOCs and to reduce the required optical power by a factor of 10-100 while achieving similar signal-to-noise levels as those from bulk-crystal BOCs. With further development, these components can soon be interfaced to realize a completely fiber-coupled, sub-femtosecond optical timing distribution system.

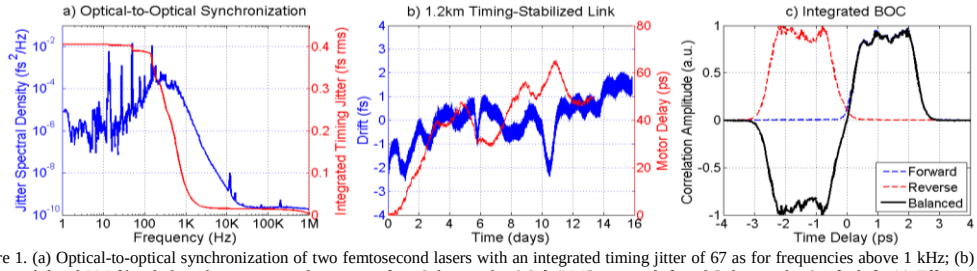

Figure 1. (a) Optical-to-optical synchronization of two femtosecond lasers with an integrated timing jitter of 67 as for frequencies above 1 kHz; (b) 1.2-km timing-stabilized PM fiber link with uninterrupted operation for 16 days with ~0.9 fs RMS timing drift and 3 days with ~0.2 fs drift; (c) Effective timing sensitivity curve for an integrated PPKTP waveguide operated as a double-pass, balanced optical correlator.

[221] J. Kim et al., "Drift-free femtosecond timing synchronization of remote optical and microwave sources," Nature Photon., 2: 12, 733–736, 2008.
[222] M. Ferianis et al., "All-optical Femtosecond Timing System for the Fermi@ Elettra FEL," Proc. FEL., Vol 11, 2011.
[223] J. Kim et al., "Attosecond-resolution timing jitter characterization of free-running mode-locked lasers," Opt. Lett., 32: 24, 3519–3521, 2007.
[224] A. Nejadmalayeri et al., "Guided wave optics in periodically poled KTP," Opt. Lett., 34, 2522-2524, 2009.

IFCS-EFTF-SPC-13

Optical Frequency Transfer over a single-span 1840 km Fiber Link

S. Droste,[1] F. Ozimek,[2,3] S. M. F. Raupach,[2] H. Schnatz,[2] G. Grosche,[2]
T. W. Hänsch,[1] Th. Udem,[1] and R. Holzwarth[1]

[1]Max-Planck-Institut für Quantenoptik, Hans-Kopfermann-Str. 1, 85748 Garching, Germany
[2]Physikalisch-Technische Bundesanstalt, Bundesallee 100, 38116 Braunschweig, Germany
[3]University of Warsaw, Faculty of Physics, ul. Hoza 69, 00-681 Warszawa, Poland

Email: stefan.droste@mpq.mpg.de

The development of optical frequency standards[225] raises a demand for transferring highly stable optical signals over continental distances. Such transfer would enable new experiments[226], and will be mandatory for a future redefinition of the SI-second based on optical frequency standards. We investigate optical frequency transfer via a 1840 km fiber link connecting Physikalisch-Technische Bundesanstalt (PTB) and Max-Planck-Institute of Quantum Optics (MPQ). The link consists of a pair of dark fibers[227], and is set up in a loop configuration with sender and receiver located at MPQ. It thus involves a single-span 1840 km stabilization. We use 20 Erbium-doped fiber amplifiers, and a fiber Brillouin amplifier at each institute, compensating for 420 dB loss.

Fig. 1 shows the instability of the transferred frequency after 1840 km of fiber for the stabilized fiber link, expressed as the Allan deviation (ADEV) and the modified ADEV. The servo bandwidth for the suppression of fiber-induced noise is limited to about 27 Hz due to the propagation delay of the light of around 18 ms. However, the low intrinsic noise of the fiber link together with active noise cancellation allow us to reach instabilities (modified ADEV) of 2.7×10^{-15} at 1 s, and about 4×10^{-19} after 100 s of integration time. The noise of the link peaks around 15 Hz and is lower at smaller frequencies which leads to a τ^{-2} dependency in the modified ADEV as shown in Fig. 1.

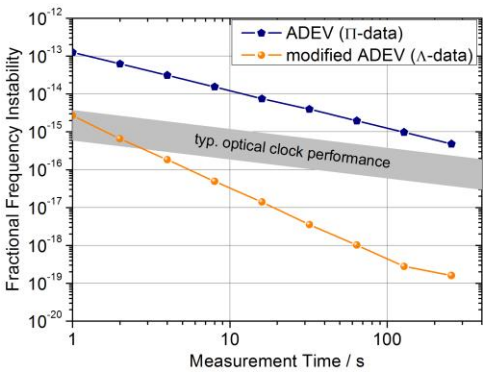

Fig. 71: Fractional frequency instability of the 1840 km stabilized link (squares) expressed as the ADEV. To distinguish between white phase, flicker phase and other noise types the modified ADEV (solid circles) is also shown.

To assess potential systematic frequency shifts, we analyzed the mean deviation of the transferred frequency from the input frequency, and found agreement within the statistical uncertainty of 2.6×10^{-19}. The results illustrate that for a remote comparison of state-of-the-art optical clocks, the short-term instability contribution of the stabilized ~2000 km link is negligible within one minute of integration time.

This work was supported by the European Metrological Research Programme EMRP under SIB-02 NEAT-FT. The EMRP is jointly funded by the EMRP participating countries within EURAMET and the European Union.

[225] N. Huntemann, et al., Phys. Rev. Lett. 108, 090801 (2012).

[226] C. W. Chou, et al., Science 329, 1630 (2010).

[227] K. Predehl, et al., Science 336, 441 (2012).

IFCS-EFTF-SPC-14

A Fiber Optic Gyroscope on multiplexed telecommunication network with a large enclosed area

C. Clivati[1,2], D. Calonico[1], G. A. Costanzo[1,2], A. Mura[1], M. Pizzocaro[1,2], F. Levi[1]

[1]Istituto Nazionale di Ricerca Metrologica, Torino, Italy
[2]Politecnico di Torino, Torino, Italy

Email: c.clivati@inrim.it

Optical gyroscopes exploiting the Sagnac effect are currently used as optical rotation sensors. Two kinds of devices exist: Fiber Optic Gyroscopes (FOGs) are used in several commercial applications, being very reliable and robust. They are limited by shot noise and typically achieve resolutions of ~10^{-6} rad/s[1]. On the converse, Ring Laser Gyroscopes achieve higher resolution, being able to detect rotation signals well below 10^{-9} (rad/s)/√Hz. They are thus attractive for a detailed study of rotational ground motion induced by teleseismic waves[2,3]. However, they are complex experiments using sophisticated optics.

To combine a simple and robust setup with high-resolution, we realized a FOG enclosing a 20 km^2 area[4] on a 47 km fiber. The fiber is used for the internet data traffic and has a Dense Wavelength Division Multiplexed architecture. The setup is the same as for passive FOGs (see Fig. 1). A laser beam is split into two beams that travel over the loop in opposite directions, acquiring a phase shift that depends on the Earth rotation. After a round trip, the two beams are recombined to detect the Sagnac phase. A well-known technique of non-reciprocal phase modulation is used to this purpose. We developed a closed loop system in which the nonreciprocal phase is compensated inserting a small frequency offset between the two beams. Thanks to its large area, this system could be suitable to detect variations in the Earth rotation rate with a sensitivity of 10^{-8} (rad/s)/√Hz, limited by the non-reciprocal mechanical noise of the fiber.

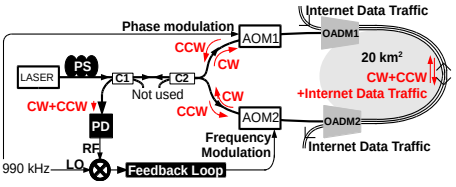

Fig. 72: Setup of the FOG. PS polarization scrambler, C couplers, AOM acousto optic modulators, OADM Optical Add&Drop Multiplexers, CW(CCW) clockwise (counter-clockwise) propagating beams.

At the conference we will present a description of our system, the results we obtained, and an analysis of the present limitations and of possible perspectives of this technique, also in consideration of the present widespread of phase-coherent optical links across large geographical areas.

1. A. Velikoseltsev, K. U. Schreiber, A. Yankovsky, J.-P. R. Wells, A. Boronachin, A. Tkachenko, "On the application of fiber optic gyroscopes for detection of seismic rotations" J. Seismol. 16 , 623 (2012).

2. H. Igel, K. U. Schreiber, A. Flaws, B. Schuberth, A. Velikoseltsev, A. Cochard, "Rotational motions induced by the M 8.1 Tokachi-oki earthquake, September 25, 2003", Geophis. Res. Lett. 32 , L08309 (2005).

3. J. Belfi, N. Beverini, G. Carelli, A. Di Virgilio, E. Maccioni, G. Saccorotti, F. Stefani, A. Velikoseltsev, "Horizontal rotation signals detected by "G-Pisa" ring laser for the M=9.0, March 2011, Japan earthquake", J. Seismol. 16, 767 (2012).

4 C. Clivati, D. Calonico, G. A. Costanzo, A. Mura, M. Pizzocaro, F. Levi "A Large Area Fiber Optic Gyroscope on multiplexed fiber network", accepted for pubblication in Opt. Lett.

IFCS-EFTF-SPC-15

Towards large scale metrological fibre network

Anthony Bercy[1], Fabio Stefani[1], Olivier Lopez[1], Paul-Eric Pottie[2], Christian Chardonnet[1], Anne Amy-Klein[1] and Giorgio Santarelli[2,3]

[1]Laboratoire de Physique des Lasers, Université Paris 13, Sorbonne Paris Cité, CNRS, Villetaneuse, France

[2]LNE-SYRTE, Observatoire de Paris, CNRS, UPMC, Paris, France

[3]Laboratoire Photonique, Numérique et Nanosciences, Université de Bordeaux 1, Institut d'Optique and CNRS, Talence, France

Email: paul-eric.pottie@obspm.fr

In the frame of the REFIMEVE+ project, aiming at disseminating an optical frequency standard to more than 20 laboratories in France, we present the progress made towards a metrological fibre wide-area network.

As a master piece for building long-haul links in a dark channel approach, we introduced previously Remote Laser Stations, which act as repeater stations for the metrological signal[228]. The supervision of the equipment, and the ability to remotely operate the station, plays a major role for an operational large scale network. We will first report on the progress for the realization of a remotely operated Remote Laser Station.

Second we address the question of multiple users distribution. In that case, a point-to point network needs a lot of fibers and is not the optimum solution. In-line extraction, as first proposed 3 years ago by G. Grosche[229], enables a more flexible distribution : the signal is extracted from the main link and either directly distributed to a lab or fed to another secondary link. Figure 2 displays the frequency stability at the extraction together with the end-to-end stability of the main link. The frequency stability at the extraction end is below 5×10^{-18} at 500 s integration time thus providing the stability performance at the same level than with a simple link.

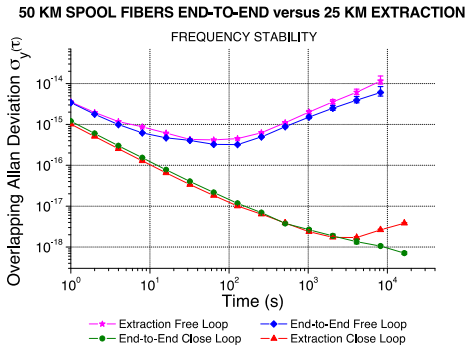

Fig. 73: Frequency Allan deviation for the end-to-end and extracted-to-end signals, in close and open loop

[228] Lopez O., Haboucha A., Chanteau B., Chardonnet C., Amy-Klein A., Santarelli G., "Ultra-stable long distance optical frequency distribution using the Internet fiber network," Optics Express **20**, p 23518-23526, 2012.

[2] G. Grosche, "Dissemination of Frequency References to Many Locations Along an Optical Telecommunication Fiber", EFTF'2010

IFCS-EFTF-SPC-16

Microwaves generation from mode-locked Er-fiber lasers with sub-fs-level absolute timing jitter

Kwangyun Jung, Junho Shin, and Jungwon Kim*

Korea Advanced Institute of Science and Technology (KAIST), Daejeon 305-701, Korea

*Email: jungwon.kim@kaist.ac.kr

Ultralow phase noise RF/microwave signal sources are important for various science and engineering applications, ranging from precision time-frequency metrology to future electronic clocks, radar and measurement systems. Recently, photonic generation of ultralow phase noise microwave signals using ultrastable cavity-stabilized CW lasers and optical frequency combs has attracted great interest.[230] Also, we have recently demonstrated that the timing jitter (>1 kHz offset frequency) from free-running mode-locked fiber lasers can be engineered well below 1 fs level.[231] Therefore, for applications that require ultralow short-term (<1 ms time scale) timing jitter/phase noise microwave signals, one can directly use a simple free-running mode-locked fiber laser without state-of-the-art ultrastable cavity references.

In this paper, we show the generation of 10-GHz microwave signals from 78-MHz free-running mode-locked Er-fiber lasers with 0.49 fs absolute rms timing jitter integrated from 10 kHz to 10 MHz offset frequency, with a single-sideband phase noise of -142 dBc/Hz at 10 kHz offset frequency. In order to mitigate the shot-noise-limited high-frequency phase noise in the optical-to-electronic conversion process (typically limited around -140 dBc/Hz level when standard 100-MHz fiber lasers and photodetectors are used), we synchronize a low-noise voltage-controlled oscillator (VCO, 10-GHz dielectric resonator oscillator) to the mode-locked fiber laser using our recently demonstrated Fiber Loop Optical-Microwave Phase Detector (FLOM-PD)[232] with -157 dBc/Hz background noise. Figure 1 shows the experimental setup and the phase noise measurement results. In addition, 600-m remote generation[233] of a microwave signal from a mode-locked Er-fiber laser with 2.7 fs rms relative timing drift for 7 hours is demonstrated.

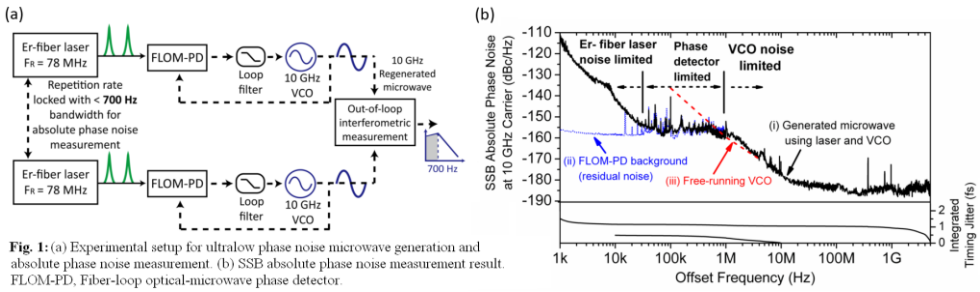

Fig. 1: (a) Experimental setup for ultralow phase noise microwave generation and absolute phase noise measurement. (b) SSB absolute phase noise measurement result. FLOM-PD, Fiber-loop optical-microwave phase detector.

[230] T. M. Fortier et al. "Sub-femtosecond absolute timing jitter with a 10 GHz hybrid photonic-microwave oscillator," Appl. Phys. Lett. **100**, 231111 (2012).

[231] T. K. Kim et al. "Sub-100-as timing jitter optical pulse trains from mode-locked Er-fiber lasers," Opt. Lett. **36**, 4443 (2011).

[3] K. Jung and J. Kim, "Subfemtosecond synchronization of microwave oscillators with mode-locked Er-fiber lasers," Opt. Lett. **37**, 2958 (2012).

[4] J. Kim et al. "Drift-free femtosecond timing synchronization of remote optical and microwave sources," Nature Photon. **2**, 733 (2008).

IFCS-EFTF-SPC-17

Optical lattice clocks with ^{87}Sr in a cryogenic environment

Ichiro Ushijima[1,2,3], Takuya Ohkubo[1,2,3], Manoj Das[2,3], Masao Takamoto[2,3], and Hidetoshi Katori[1,2,3]

[1]Department of Applied Physics, Graduate School of Engineering, The University of Tokyo, 7-3-1 Hongo, Bunkyo-ku, Tokyo 113-8656, Japan

[2]Quantum Metrology Laboratory, Advanced Science Institute, RIKEN, 2-1 Hirosawa, Wako, Saitama 351-0198, Japan

[3]Innovative Space-Time Project, ERATO, JST, 7-3-1 Hongo, Bunkyo-ku, Tokyo 113-8656, Japan

Email: ushijima@amo.t.u-tokyo.ac.jp

A relative frequency stability of 10^{-17} has been reached by comparing two Sr optical lattice clocks[1]. At this level of stability, the frequency shift due to blackbody radiation (BBR) from the room temperature environment becomes a major limitation for Sr lattice clocks[1,2]. In order to reduce the uncertainties of BBR shift, we have developed Sr optical lattice clocks that operate in a cryogenic environment. The BBR shift for Sr atoms is theoretically calculated to be about 2.4 Hz at 300 K. To reach the uncertainties of 10^{-18}, the fluctuation and inhomogeneity of the ambient room temperature T has to be controlled to within ΔT = 0.01 K at 300 K. As the sensitivity of BBR shift varies as T^3, the uncertainties can be decreased by cooling down the environmental temperature. At the temperature of T = 70 K, the BBR shift reduces to 10 mHz and even with a temperature fluctuation of ΔT = 1 K, clock uncertainties of 10^{-18} can be reached. We can evaluate the BBR shift directly as a frequency difference of two clocks by comparing two clocks operating at different environmental temperature.

We realize the cryogenic environment by surrounding the region for clock spectroscopy with a cryogenic chamber of few cm^3 in volume. In order to introduce atoms and lasers, the chamber has two apertures with diameters of 0.5 and 1 mm. The uncertainty due to BBR shift caused by the radiation that irradiates the atoms through these apertures can be reduced to 1×10^{-18} by moving the atoms 5 mm inside the chamber and thereby reducing the solid angle from atoms to the environment to 0.5 msr. The cryogenic chamber is cooled down to 70 K by a Stirling refrigerator and the temperature fluctuation can be maintained to within ΔT = 10 mK.

In this poster presentation we will discuss our cryogenic setup for two Sr lattice clocks and the latest experimental results. By using synchronous interrogation[1] and comparing two clocks, one in a cryogenic and the other in a room temperature environment, the BBR shift can be observed as the frequency difference of the two clocks with high stability. Comparing two clocks synchronously in a reduced BBR environment will allow us to evaluate other systematic errors such as atomic interactions and lattice light shifts with high precision.

---

[1] M. Takamoto, T. Takano, and H. Katori, "Frequency comparison of optical lattice clocks beyond the Dick limit", Nat. Photon. vol. 5, p. 288-292. 2011.

[2] T. Middelmann, Ch. Lisdat, St. Falke, J. S. R. Vellore Winfred, F. Riehle and U. Sterr, "Tackling the blackbody shift in a strontium optical lattice clock", IEEE Trans. Instrum. Meas.. vol. 60, p. 2550-2557. 2011.

IFCS-EFTF-SPC-18

First spectroscopy of the $^1S_0$ – $^3P_0$ transition in Lamb-Dicke confined magnesium atoms

André Kulosa, Steffen Rühmann, Dominika Fim, Klaus Zipfel, Wolfgang Ertmer, Ernst M. Rasel

Institut für Quantenoptik, Leibniz Universität Hannover, Hannover, Germany

Email: kulosa@iqo.uni-hannover.de

We report on the status of the magnesium optical clock experiment in Hannover. Recently, we demonstrated the first spectroscopy of the spin-forbidden $^1S_0$ – $^3P_0$ clock transition in µK cold magnesium atoms that were trapped in an optical lattice at the predicted magic wavelength of 469 nm.

Due to the lack of sub-Doppler cooling techniques, we prepare our atoms using a continuous loading scheme for an optical dipole trap at 1064 nm[234]: Atoms with milli-Kelvin temperature are continuously transferred to the dipole trap by creating a loss channel for $^3P_0$ atoms. The coldest among them can be captured by the optical potential for subsequent transfer into the optical lattice.

Applying an external homogeneous magnetic field creates a mixture of the $^3P_0$ and $^3P_1$ states weakly allowing the $^1S_0$ – $^3P_0$ transition[235]. Performing such a magnetic field-induced spectroscopy, we have been able to de-excite 25% of $^3P_0$ atoms on the 458 nm intercombination transition to the $^1S_0$ ground state.

The interrogation laser for the ultra-narrow clock transition is a frequency doubled diode laser at 916 nm stabilized to a vibration insensitive optical cavity. The laser system shows a fractional frequency instability of $\sigma_y(\tau = 1\ \mathrm{s}) = 5 \times 10^{-16}$.

As a next step, we will experimentally investigate the magic wavelength for magnesium.

[234] M. Riedmann, et al., Phys. Rev. A **86**, 043416 (2012)

[235] A. V. Taichenachev, et al., Phys. Rev. Lett. **96**, 083001 (2006)

IFCS-EFTF-SPC-19

Optical lattice clocks near the QPN limit: A tenfold improvement in optical clock stability

Travis L Nicholson[1], Michael J Martin[1], Jason R Williams[1], Benjamin J Bloom[1], Michael Bishof[1], Matthew D Swallows[2], Sara L Campbell[1], and Jun Ye[1]

[1]JILA, University of Colorado, Boulder, CO USA
[2]AOSense, Sunnyvale, CA USA

Email: nicholtl@jilau1.colorado.edu

Two classes of optical atomic clocks have surpassed microwave frequency standards: single-ion clocks and optical lattice clocks. Single-ion clocks hold the record for the lowest systematic uncertainty[236]; however, many-atom lattice clocks[237] have the potential to outperform single-ion clocks because the standard quantum limit to atomic clock instability (known as quantum projection noise or QPN) scales as $(1/N_{atoms})^{1/2}$. For realistic atom numbers and coherence times, QPN-limited lattice clocks could average down to a given stability hundreds of times faster than the best ion clocks.

Up to now lattice clocks with ~1000 atoms have not shown improvement over the stability of single-ion clocks. Lattice clock stability has been limited by laser noise (via the optical Dick effect). To address this problem, we constructed a new clock laser with a thermal noise floor of 1×10^{-16}—an order of magnitude improvement over our previous clock laser. With this laser, we compare two lattice clocks, reaching instability of 1×10^{-17} in 2000 s for a single clock. This instability is within a factor of 2 of the theoretical QPN limit for ~1000 atoms, representing the lowest reported instability for an independent clock[238].

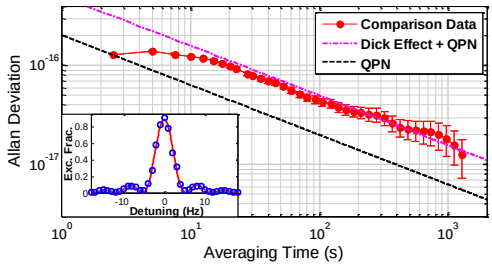

Fig. 74: A comparison between two independent Sr optical lattice clocks. The stability is $4.4\times10^{-16}/\tau^{1/2}$. The inset depicts typical scans of the clock transition (open circles), and the red line is a fit to the data using the Rabi model.

The high stability of many-particle clocks can come at the price of larger systematic uncertainty due to a frequency shift from atomic interactions. To minimize this shift, we use a cavity-enhanced lattice[239] for our second clock. The high circulating power inside the cavity allows for a large trap volume, yielding a density at 2000 atoms that is 27 times smaller (than in our first clock) and permitting us to trap as many as 5×10^4 atoms. For 2000 atoms in our lattice, we measure a value for this shift (which is linear in density) of -3.11×10^{-17} with an uncertainty of 8.2×10^{-19}.

[236] Chou, et al., PRL **104**, 070802 (2010)

[237] Ludlow, et al., Science **319** 1805 (2008)

[238] Nicholson, et al., PRL **109**, 230801 (2012)

[239] Westergaard, et al., PRL **106**, 210801 (2011)

A 120-μW GSM Phase Noise-Compliant Pierce Oscillator Referenced to a 61-MHz Wine-Glass Disk Resonator

Thura Lin Naing, Tristan O. Rocheleau, Elad Alon, and Clark T.-C. Nguyen

University of California at Berkeley, Berkeley, California, USA

Email: thura@eecs.berkeley.edu

A 61-MHz Pierce oscillator referenced to a single polysilicon surface-micromachined wine-glass disk resonator has achieved phase noise marks of -120dBc/Hz at a 1-kHz offset and -139dBc/Hz at far-from-carrier offsets. When divided down to GSM's 13MHz, this corresponds to -133 dBc/Hz at 1-kHz and -152dBc/Hz at far-from-carrier offsets, both of which satisfy GSM reference oscillator phase noise requirements. This Pierce oscillator not only provides improvements of 10dB at 1kHz and 7dB at far-from carrier offsets versus a transimpedance amplifier (TIA) topology[240] using a similar single disk, it also reduces power consumption down to only 120μW, which is ~3 times smaller. Such low phase noise and power achieved by a tiny MEMS device might soon be key enablers for low power "set and forget" autonomous sensor networks with substantial communication capability.

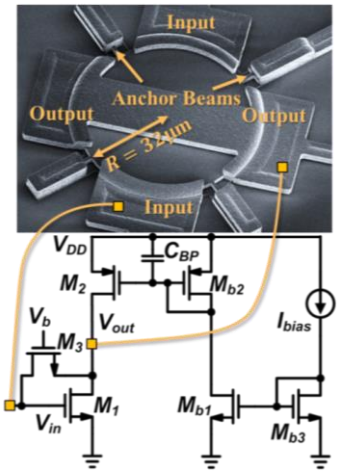

Fig. 75: The 61-MHz Pierce oscillator.

Previous TIA-based oscillators[1] attained GSM specs by arraying MEMS devices to boost oscillator loop power to reduce far-from-carrier phase noise. In contrast, the work presented here achieves the same GSM spec using only a single MEMS resonator with significant area savings versus the previous large array. It does this via the remarkably simple Pierce configuration of Fig.1 that yields better performance in two ways: 1) by reducing noise-figure by using only two active transistors; and 2) by increasing voltage swing, thereby raising oscillator loop power.

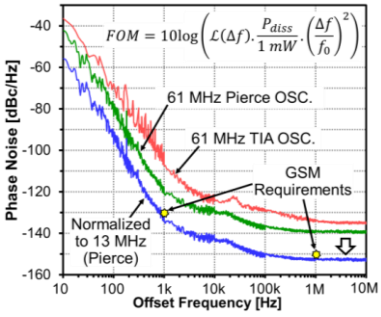

Fig. 76: Measured phase noise of 61-MHz oscillators and normalized to 13 MHz (Pierce) for comparison to GSM spec.

Fig. 2 compares measured phase noise data for a 61-MHz TIA-based oscillator with that of the Pierce oscillator at 61MHz (and divided down to 13MHz), clearly showing the performance difference, and from the 13MHz curve, clearly meeting GSM specs. When power consumption is taken into account using the popular Figure of Merit (*FOM*) (given in the plot inset), this performance marks the best *FOM* at 1 kHz among published on-chip oscillators to date, as illustrated in the table below.

Device Type	**This work**	Wine-glass array[1]	FBAR[241]	Quartz[242]
FOM@ 1 kHz (dB)	**-225**	-223	-220	-211

[240] Y.-W. Lin, et al., "Low phase noise array-composite micromechanical ..," *Tech. Dig. IEDM 2005*, pp. 287-290.
[241] A. Nelson, et al., "A 22μW, 2.0GHz FBAR oscillator," *RFIC 2011*, pp. 1-4.
[242] J. T. M. van Beek, et al., "A review of MEMS …," *J. Micromech. Microeng*, vol 22, no.1, 2011.

IFCS-EFTF-SPC-21

A 2.8 GHz Combined Mode of Vibration Aluminum Nitride MEMS Resonator with High Figure of Merit Exceeding 45

Yu Hui, Zhenyun Qian and Matteo Rinaldi

Department of Electrical and Computer Engineering, Northeastern University, Boston, MA/USA

Email: hui.y@husky.neu.edu, rinaldi@ece.neu.edu

This paper presents the first demonstration of a high frequency (2.8 GHz), lateral field excited (simple two masks fabrication process), combined lateral-thickness extensional mode of vibration aluminum nitride (AlN) micro-electro-mechanical (MEMS) resonator with unprecedentedly high figure of merit ($k_t^2 \cdot Q > 45$). For the first time, a single interdigital electrode was employed to excite a high frequency mode of vibration in an AlN plate (1.5 µm thick) by making use of both the d_{33} and d_{31} AlN piezoelectric coefficients[243]. The resulting MEMS resonator showed high quality factor, Q~2000, (thanks to the high quality AlN film directly deposit on top of the Silicon substrate) and the highest electromechanical coupling coefficient ever reported for AlN MEMS resonators employing a single electrode, k_t^2~*2.5%* (thanks to the coherent combination of d_{33} and d_{31} coefficients to transduce one single mechanical mode of vibration).

The use of a single interdigital electrode to excite (lateral field excitation, *LFE*) a high frequency contour-extensional mode of vibration in AlN microstructures has been previously demonstrated[244]. However, due to the relatively low d_{31} coefficient of AlN, the maximum predicted electromechanical coupling coefficient[245] for such class of devices is only 1.5%. In this work, by properly optimizing the ratio between the thickness of the AlN film (t) and the pitch of the interdigital top electrode (W_p) the d_{33} and d_{31} coefficients have been coherently combined and harnessed to transduce one single mechanical vibration mode. The combined lateral-thickness mode of vibration was simulated using COMSOL showing a maximum value of electromechanical coupling coefficient, k_t^2 = 2.82%, for $t/W_p \approx 0.94$. A device with such optimum t/W_p was fabricated (Fig. 1), showing high quality factor (Q = 1855) and a value of electromechanical coupling coefficient (k_t^2 = 2.48%) ~2 times higher than what is typically achieved with conventional LFE AlN contour-extensional mode resonators[2] (Fig. 2).

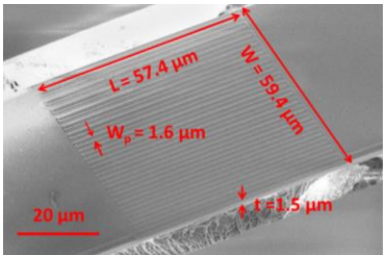

Fig. 1: SEM image of the fabricated AlN combined mode of vibration MEMS resonator. t/W_p was set to be *~0.94*, resulting in a resonance frequency of the 2.8 GHz. It is worth noting that the fabricated device is fully

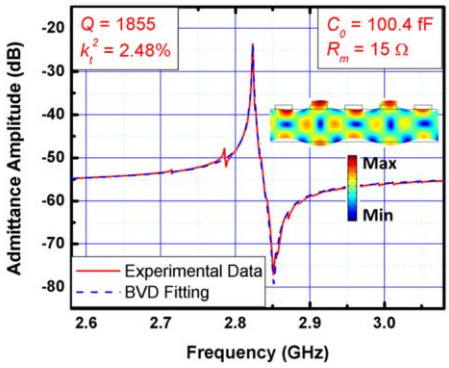

Fig. 2: Measured admittance curve and BVD model fitting of the fabricated AlN resonator. High device figure of merit ($FOM = k_t^2 \cdot Q$ = 46) and low motional resistance (R_m = 15 Ω) were achieved at 2.8 GHz. The inset shows the 2D FEM simulation

[243]C. J. Zuo, et al. IEEE IFCS 2012, pp. 1-4.
[244]C. J. Zuo, et al. IEEE IFCS 2009, pp. 381-384.
[245]J. H. Kuypers, et al. IEEE IFCS 2008, pp. 240-249.

IFCS-EFTF-SPC-22

Close-in Phase Noise Reduction in an Oscillator based on 222 MHz Non-Linear Contour Mode AlN Resonators

J. Segovia-Fernandez, C. Cassella, G. Piazza

Electrical and Computer Engineering, Carnegie Mellon University, Pittsburgh, PA, USA

Email: jsegovia@andrew.cmu.edu

Phase Noise (PN) reduction in oscillators has been traditionally accomplished by using low noise amplifiers or high quality factor (Q) resonators, in accordance with Lesson theory[246]. However, previous work on nonlinearly driven resonators has suggested that locking the device into a particular nonlinear state (so-called bifurcation) can help evading the amplifier noise[247]. AlN Contour Mode Resonators (CMRs) are an emerging class of piezoelectric MEMS devices exhibiting high Q and low motional resistance at high frequencies (f_{res}). Because of their micron-scale size the AlN CMRs have revealed a nonlinear behavior induced by self-heating when driven with relatively high power[248]. In this work, we show a substantial improvement of the PN close-in (-20dBc/Hz @ 100Hz) of a 222 MHz oscillator that incorporates a nonlinearly driven AlN CMR.

The oscillator circuit presented here was built using coaxial electronic components (Fig. 1). The experiments were carried out by setting the DC bias of the amplifier to 6V, therefore ensuring enough gain to both sustain oscillations and drive the resonator nonlinearly. The phase shifter was manually tuned in steps of 5° to increase the circuit delay and, hence, lock the oscillator at different frequencies (f_{osc}) on the non-linear resonance curve of the 222 MHz AlN CMR device. Fig. 2 depicts PN (dBc/Hz) versus offset frequency (f_{off}) for different phase delays. A dramatic change of slope in the PN close-in (f_{off}<1kHz) is observed when $f_{osc}<f_{res}$ (f_{res} is indicated on the plot). This frequency corresponds to the device operating past bifurcation, as we can infer by measuring the resonator admittance in open loop for the same output power. The data highlight that for particular phase shifts >15°, the PN curve experiences a significant reduction in slope (from $1/f^4$ to $1/f^2$). Furthermore, the experimental results show that the AlN CMR thermal time constant $(\tau_{TH})^3$ limits the maximum f_{off} for which a PN improvement can be recorded.

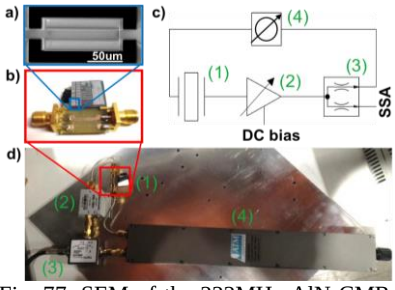

Fig. 77: SEM of the 222MHz AlN CMR; b) wirebonded AlN CMR on a PCB; and both c) schematics and d) actual oscillator setup including (1) AlN CMR, (2) amplifier, (3) power splitter, and (4) phase shifter.

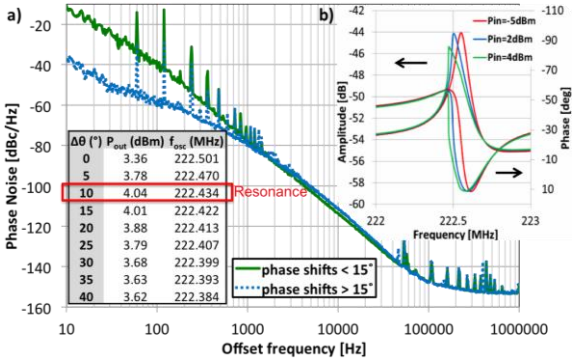

Fig. 78: a) *PN* vs f_{off} at DC bias=6V and different phase shifts ($\Delta\theta$). b) Open loop amplitude and phase of AlN CMR admittance for various input powers.

[246] D. B. Leeson, "A simple model of feedback oscillator noises spectrum," Proc. IEEE, vol. 54, pp. 329–330, 1966.

[247] B. Yurke, D.S. Greywall, A.N. Pargellis, and P.A Busch, "Theory of amplifier-noise evasion in an oscillator employing a nonlinear resonator," Phys. Rev. A, vol. 51, pp. 4211-4229, 1995.

[248] J. Segovia-Fernandez, A. Tazzoli, M. Rinaldi, G. Piazza, "Nonlinear lumped electrical model for contour mode AlN resonators," *IEEE Int. Ultrasonics Symp.*, pp.1846-1849, 2011

IFCS-EFTF-SPC-23
Lisha Shi[1], Gianluca Piazza2
[1]Electrical and Computer Engineering, Carnegie Mellon University, Pittsburgh, Pennsylvania, USA, [2]Department of Electrical and Computer Engineering, Carnegie Mellon University, Pittsburgh, PA, USA

Ion-Sliced Lithium Niobate on Silicon Dioxide for Engineering the Temperature Coefficient of Frequency of Laterally Vibrating Resonators

Lisha Shi, Gianluca Piazza
Department of Electrical and Computer Engineering, Carnegie Mellon University, Pittsburgh, PA, USA

Email: lishashi@andrew.cmu.edu, piazza@ece.cmu.edu

This paper reports, for the first time, on the demonstration of Laterally Vibrating Resonators (LVRs) based on Y-cut Ion-Sliced Lithium Niobate (LN) thin films on silicon dioxide (SiO_2) (Fig.1a-b). By adding a thermally grown layer of SiO_2 to the resonator stack, it is possible to engineer the temperature coefficient of the resonator and therefore ensure the use of these devices for applications where tight temperature specifications are required.

Prior demonstrations of LN LVRs[249, 2] have shown the capability of attaining a high K_t^2 *(> 20%)* and Qs of about 1,000, but exhibited a rather large and negative temperature coefficient of frequency (TCF) of about - 80 ppm/°C. Furthermore, they were built on a LN substrate with either BCB or SiO_2 as sacrificial layers, which required a wet etch step for the release of the resonator. In this work, the LN LVR is built on top of a SiO_2 layer and released from the underlying silicon wafer by dry etching in XeF_2. With the h_{LN} set at 420nm and h_{SiO2} at 1600nm, this first demonstration (Fig.1b) yielded TCF of + 11ppm/°C, + 18ppm/°C and + 20.4ppm/°C for devices respectively oriented at 80˚, 50˚, and 20˚ to the x-axis. The positive TCF clearly indicates the effect of the SiO_2, matches with FEM simulations, and offers evidence that TCF engineering is possible. Most importantly, these LN LVRs still exhibited high values of the electromechanical coupling, K_t^2, around 6.2% (see Fig.1c) and Qs in excess of 1,300 in air at 419.3 MHz (Fig.1d). By optimizing the relative values of h_{LN} and h_{SiO2} it is ultimately possible to attain devices with zero first order TCF.

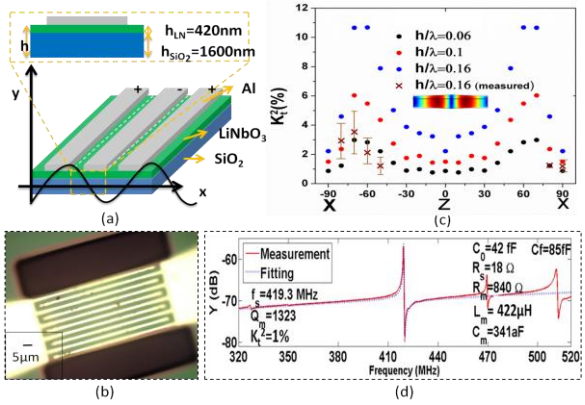

Fig.1 (a) Mock-up view of $LiNbO_3$-on SiO_2 MEMS micro-resonator (b) Optical image of a 511.8MHz LN LVR. The period of the interdigitated finger was set to be 6 μm with each metal line having a width of 2μm (c) The comparison of the averaged measured and simulated K_t^2 for LN on SiO_2 LVRs for various orientations. (d)The measured and fitted admittance response of LN on SiO_2 LVRs with Qs in

[1]R.Wang, S. Bhave, and K. Bhattacharjee "High K_t^2×Q, Multi-frequency Lithium Niobate Resonators" MEMS 2013(2013)

[2] S. Gong, L. Shi, G. Piazza, "High electromechanical coupling MEMS resonators at 530 MHz using ion sliced x-cut $LiNbO_3$ thin film", International Microwave Symposium (2012).

Micromechanical Disk Array-Composite for Enhanced Frequency Stability Against Bias Voltage Fluctuations

Lingqi Wu[1], Mehmet Akgul[1], Zeying Ren[1], Clark T.-C. Nguyen[1]

[1]Dept. of EECS, University of California at Berkeley, Berkeley, CA, USA

Email: wulingqi@berkeley.edu

A 215-MHz polysilicon capacitive-gap transduced micromechanical resonator array employing 50 mechanically coupled contour mode disks (*cf.* Fig. 1)—the largest such array yet fabricated and measured—has achieved 3.5× better frequency stability than single stand-alone disk counterparts against fluctuations in the dc voltage (V_P) normally dropped across the electrode-to-resonator gaps during device operation. Here, connection of numerous resonators via half-wavelength ($\lambda/2$)-dimensioned coupling beams produces a single array-composite resonator that selectively resonates at a single mode frequency with all resonators moving in phase. The key to enhanced frequency stability against bias voltage variation is the electrode-to-resonator capacitance (C_o) generated by the parallel combination of input/output electrodes overlapping each resonator in the array. C_o dominates among elements loading the resonator and effectively raises its stiffness (beyond the stiffness increase resulting from mechanical coupling), much like a varactor does in crystal circuits. This in turn reduces the efficacy of the bias voltage-controlled electrical stiffness[250]. The more resonators in the array, the smaller the frequency shift imposed by a given bias voltage change. This result suggests that the most stable MEMS-based oscillators (e.g., against supply noise and acceleration[251]) are ones that utilize mechanically-coupled arrays of resonators.

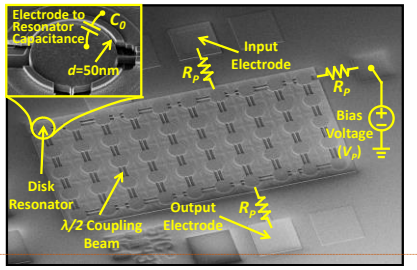

Fig. 79: SEM of a 215-MHz 50nm capacitive-gap transduced contour mode disk array employing 50 mechanically coupled resonators.

Fig. 2 presents measured curves of frequency versus bias voltage for the array-composite resonator of Fig. 1, all alongside theoretical curves predicted by an equivalent circuit modeling the above phenomena for arrays with different numbers of resonators. Here, theory and measurement match quite well. The 50-element 215-MHz array experiences a 20ppm frequency change when V_P varies by 9V, which represents a 3.5× improvement over the 70ppm of a single resonator and could potentially improve the acceleration sensitivity of a MEMS based oscillator by 11dB.

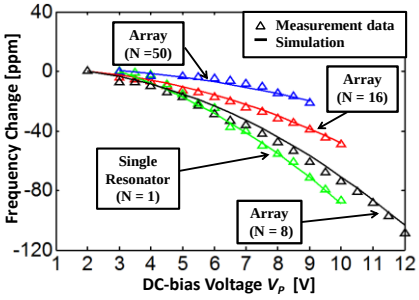

Fig. 2: Measured curves of resonance frequency versus dc-bias voltage V_P plotted against simulation using equivalent circuit models for resonator arrays with N=1, N=8,

[250] Frank D. Bannon III, J. R. Clark, and C. T.-C. Nguyen, "High-*Q* HF Microelectromechanical Filters", *IEEE J. Solid-State Circuits*, vol. 35, no. 4, pp. 512-526, April 2000.

[251] T.L. Naing, T. O. Rocheleau, Z. Ren, E. Alon, and C. T.-C. Nguyen, "Vibration-Insensitive 61-MHz Micromechanical Disk Reference Oscillator", *IEEE Int. Frequency Control Symposium*, Baltimore, Maryland, pp. 276-281, May 2012.

Comment [ctn3]: Somewhere in the figure, you need to show the dc bias.

Comment [ctn4]: reference Frank Bannon's JSSC filter paper.

Compact High-Performance Clocks and Sensors

CLUB H

Tuesday, July 23 2013, 10:30 am - 12:00 pm

Chair: **John Kitching**
NIST

IFCS-EFTF3-D1-1

Miniature trapped-ion frequency standard with $^{171}Yb^{+}$

Peter D. D. Schwindt[1], Yuan-Yu Jau[1], Heather Partner[1], Darwin Serkland[1], Adrian Casias[1], Ronald Manginell[1], Matthew Moorman[1], Robert Boye[1], John Prestage[2], James Kellogg[2], Nan Yu[2], Taye Gebrewold[3], Sheng Chang[3], Igor Kosvin[3], Dan Boschen[3]

[1]Sandia National Laboratories, Albuquerque, NM/USA
[2]Jet Propulsion Laboratory, Pasadena, CA/USA
[3]Symmetricom, Beverly, MA/USA

Email: pschwin@sandia.gov

We are developing a highly miniaturized trapped ion clock by probing the 12.6 GHz hyperfine transition in the $^{171}Yb^{+}$ ion. The clock development is being funded by the Integrated Micro Primary Atomic Clock Technology (IMPACT) program from DARPA where the stated goals are to develop a clock that consumes 50 mW of power, has a size of 5 cm^3, and has a long-term fractional frequency instability of 10^{-14} at one month. Trapped ion systems are an excellent candidate for such extreme miniaturization because ions are well isolated from the environment independent of the size of the trap. A large degree of miniaturization has already been demonstrated with the $^{199}Hg^{+}$ trapped ion clock developed at the Jet Propulsion Laboratory.[252]

We will discuss the development of the ion trap physics package and its integration with other key elements of the frequency standard, including miniaturized laser sources at 369 and 935 nm, a local oscillator, control electronics, and a microfabricated Yb source for trap loading. We have demonstrated a compact, portable clock system that utilizes a 3 cm^3 metal ion trap vacuum package integrated with a magnetic shield, C-field coils, and ion loading and detection systems.[253] We have demonstrated continuous operation of the ion clock for 31 days, and with 49 days of data from several clock runs combined, the long-term fractional frequency instability of the clock is shown to be in the 10^{-14} range. Current work is focused on integrating the optics, laser sources, ion trap drive, and 12.6 GHz microwave synthesizer with the vacuum package.

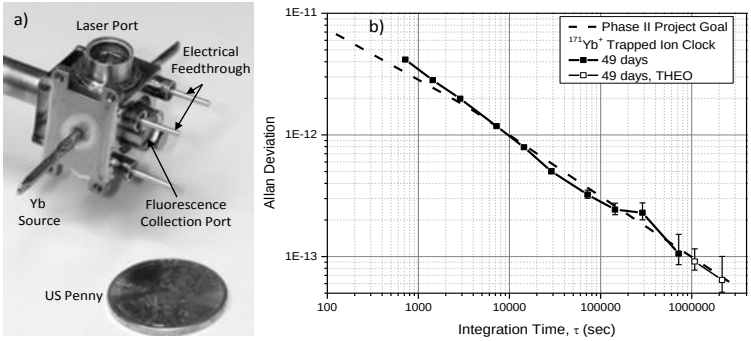

Fig. 1.(a) Picture of the 3 cm^3 vacuum package. (b) Performance of the clock prototype.

[252] J.D. Prestage, G L. Weaver, 2007, "Atomic clocks and oscillators for deep-space navigation and radio science," Proceedings of the IEEE, Vol. 95 No. 11, pp. 2235-2247.

[253] Y.-Y. Jau, H. Partner, P. D. D. Schwindt, J. D. Prestage, J. R. Kellogg, N. Yu, 2012, "Low-power, miniature ^{171}Yb ion clock using an ultra-small vacuum package," Appl. Phys. Lett., Vol. 101, pp. 253518.

IFCS-EFTF3-D1-2

Absolute frequency of a trapped atom clock

C. Deutsch[+], W. Maineult, V. Dugrain[+], R. Szmuk, J. Reichel[+], P. Rosenbusch
LNE-SYRTE, Observatoire de Paris, CNRS, UPMC, Paris, France
[+]LKB, Ecole Normale Supérieure, CNRS, UPMC, Paris, France

Trapped atoms have become wide-spread for the development of atomic clocks: In optical clocks the trap absorbs the photon momentum; embarquable clocks benefit from the reduced volume. However, when interrogating an ensemble of many atoms, as wanted for high stability, the confinement enhances atom-atom interactions and thereby possible frequency shifts.

Operating a microwave clock with ^{87}Rb atoms trapped on a chip [1], we study the effects of interactions. At ultra-low temperatures, we have observed the opening of an energy gap between the symmetric and anti-symmetric 2-body-wavefunction, which causes spin-locking and gives access to very long coherence times [2]. Spectroscopy with deliberately inhomogeneous Rabi excitation has provided a direct measurement of the energy gap [3] and has confirmed the prediction [4], that trapped fermion clocks, too, may suffer a collisional shift if the excitation is inhomogeneous.

Here we present measurement of the absolute frequency of our trapped atom clock for standard operation (i.e. homogeneous excitation). We observe an intriguing evolution of the clock frequency with the Ramsey time. We relate this evolution to the dynamics of spin-locking and develop a model based on the identical spin rotation effect [5]. We identify a range of parameters presenting particular advantages to the clock operation. Our findings apply to any trapped boson (fermion) clock, where s(p)-wave scattering is dominant.

[1] C. Lacroute et al., IEEE Trans. Ultrason. Ferroelectr. Freq. Control **57**, 106 (2010).
[2] C. Deutsch et al., Phys. Rev. Lett, **105**, 020401 (2010); G. Kleine Büning et al Phys. Rev. Lett. **106**, 240801 (2011)
[3] W. Maineult et al, Phys. Rev. Lett. **109**, 020407 (2012)
[4] K. Gibble Phys. Rev. Lett. **103**, 113202 (2009)
[5] C. Lhuillier and F. Laloë, J. Phys. (Paris) **43**, 197 (1982).

IFCS-EFTF3-D1-3

Cancellation of Doppler Shifts in a Cold-Atom CPT Clock

E. A. Donley, F.-X. Esnault, E. Blanshan, and J. Kitching

NIST, Boulder, CO, USA

Email: elizabeth.donley@nist.gov

A compact cold-atom clock based on coherent population trapping (CPT) is being developed that aims to achieve a timing uncertainty of a few nanoseconds per day. The clock is based on laser-cooled atoms, which eliminates the buffer-gas shift but in general can introduce a 1st-order Doppler shift since the atom cloud expands and falls during interrogation. The atoms are interrogated with Ramsey absorption spectroscopy in the lin || lin CPT[254] configuration. This talk will give an overview of the clock design and function, and will present a systematic evaluation of the 1st-order Doppler shift.

When the atoms are probed with travelling-wave CPT beams along the direction of gravity, the Doppler shift is 3×10^{-10} for a 10 ms Ramsey time. To substantially reduce this shift, the atoms are probed with standing waves by applying CPT beams symmetrically from above and below.

To evaluate the shift, an extra period of free fall is inserted before the first Ramsey pulse and atoms are probed from a single direction, which enlarges the shift so that it can be easily compared to a basic model. Measurements of frequency shift versus free-fall period, Ramsey period, and probe direction show very good agreement with a simple kinematic model for the atoms' average position and velocity.

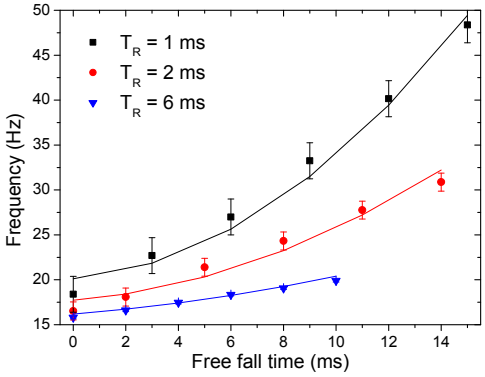

Clock frequency versus extra free-fall time for different Ramsey periods compared to a basic kinematic model for the Doppler shift. The offset frequency is the only fit parameter. Only the signal from the downward beam was used to calculate the clock frequency, which maximizes the shift. The full scale (35 Hz) corresponds to a fractional frequency shift of 5×10^{-9}.

When the atoms are probed symmetrically along the direction of gravity, the total shift for the clock's typical Ramsey period of 6 ms is consistent with zero and has a current uncertainty of 1×10^{-11}. The shift magnitude should be more than an order of magnitude smaller when the probe direction is perpendicular to gravity.

The clock stability in our unshielded system is presently limited by the Zeeman shift to 2×10^{-12} at 1000 seconds of averaging time. A next-generation physics package that includes magnetic shielding is under development. The new system will be based on an antireflection-coated cell, which should improve the laser-cooling performance and allow for symmetric standing-wave interrogation with a simple retro-reflected CPT beam.

[254] A.V. Taichenachev et al., *JETP Lett.* **82**, 398, 2005.

IFCS-EFTF3-D1-4

Rubiclock: towards the first industry-ready cold-atom clock

Luigi De Sarlo[1], Baptiste Battelier[2], Natascia Castagna[1], Michel Lours[1], David Holleville[1], and Noël Dimarcq[1]

[1]LNE-SYRTE, Observatoire de Paris, CNRS and UPMC, 61 avenue de l'Observatoire, 75014 Paris, France

[2]LP2N, Université Bordeaux 1, IOGS and CNRS, 351 cours de la Libération, 33405 Talence, France

Email: luigi.de-sarlo@obspm.fr

We will present the Rubiclock project, an activity started at LNE-SYRTE – Observatoire de Paris two years ago, funded by ANR and CNES. The project develops a prototype of a vapour-cell clock based on cold atoms which can deliver a short term stability better than that of passive hydrogen maser (relative instability below 5×10^{-13} at 1s), while at the same time bringing an accuracy specification at the level of a few 10^{-15} which is inherently superior to the GPS+H-MASER systems currently in use. We aim at obtaining these performances while keeping the concept interesting from an industrial perspective.

The operation of the clock is based on the Ramsey interrogation of a sample of ultracold (microkelvin temperature) Rubidium atoms in free fall inside a microwave cavity. Taking advantage of the so-called isotropic laser cooling[255], the atoms are cooled from a vapour directly inside the microwave cavity thereby eliminating the need of a separate cooling chamber. The use of ultracold atoms allows one to benefit from interrogation times of several tens of milliseconds at the same time decreasing the effect of systematic shifts. Rubiclock represents the evolution of the Cs-based HORACE concept which has recently demonstrated a short-term stability in the range of 10^{-13} and long term stability in the range of 10^{-15} arguably limited by atomic collisions[256].

We will present all the subsystems of the clock including a compact laser system at λ=780 nm based on frequency doubling of a telecom qualified source[257], a new microwave synthesis chain and a new physical package for optimal thermal management, together with the first scientific results and the perspectives for the industrialisation and an eventual space application of the concept.

[255] E. Guillot *et al.*, "Three-dimensional cooling of cesium atoms in a reflecting copper cylinder", Opt. Lett. **26**, p. 1639 (2001)

[256] F.-X. Esnault *et al.*, "High-stability compact atomic clock based on isotropic laser cooling", Phys. Rev. A **82**, 033436 (2010)

[257] F. Lienhart *et al.*, "Compact and robust laser system for rubidium laser cooling based on the frequency doubling of a fiber bench at 1560 nm", Appl. Phys. B **89**, p. 177 (2007).

IFCS-EFTF3-D1-5

MiniAtom: realization of a compact atomic gravimeter

Jean Lautier[1], Baptiste Battelier[2], Arnaud Landragin[1], Philippe Bouyer[2]

[1]LNE-SYRTE, Observatoire de Paris, CNRS, UPMC, 61 boulevard de l'Observatoire, 75014 Paris, France

[2] LP2N, CNRS, IOGS, Universite Bordeaux 1, Batiment A30, 351 cours de la Liberation, 33405 Talence CEDEX, France

Email: jean.lautier@obspm.fr

We present here the realization of a highly compact absolute atomic gravimeter. The main purpose is to demonstrate that atomic interferometers can overtake the current limitations of inertial sensors based on "classical" technologies for field and on-board applications. We show that the complexity and the volume of cold-atom experimental set-ups can be drastically reduced while keeping the performances close to the state-of-the-art, enabling such atomic sensors to perform precision measurements outside of the laboratory.

The measurement of the acceleration of gravity (g) is made with a $\pi/2$ - π - $\pi/2$ interferometer using stimulated Raman transitions to couple |F=1, mf=0> and |F=2, mf=0> hyperfine states of free-falling ^{87}Rb atoms[258]. The use of an innovative hollow pyramid as the usual retro-reflecting mirror of quantum inertial sensors enables to perform all the steps of the atomic measurement (trapping and cooling the atoms, performing the interferometer and reading out its outputs) with one single laser beam instead of 6 normally[259]. The laser system is based on a single telecom laser diode, which is phase modulated and frequency doubled[260]. This leads to a drastic reduction of the complexity and the size of the apparatus: the overall physical package is of a few tens of litters in volume only: the sensor head (that includes the vacuum chamber) fits in a cylinder 40 cm high and 20 cm in diameter; the entire laser bench, the electronics and the power supplies fit in a cube of 70 cm of side.

We target a relative sensitivity to acceleration of gravity below 10^{-7} at one shot, which will allow to monitor time variation of g due to tides and to detect significant mass anomalies and mass displacements. We have shown promising long-term stability with a flicker floor on the 10^{-9} range and up to two day long measurements have been recorded with such architecture[2].

Particular efforts have been made to push on the integration of the micro-wave frequency standards used to drive the clock frequency of ^{87}Rb atoms at 6.835 Ghz and to deliver quantum state selective pulses. Although an output power of 25 dBm and a 500 MHz agility are required, our chain features a phase noise that will only limit our relative sensitivity to acceleration at the 10^{-8} level. We thus show an attractive trade-off between the integration in a two-litter package and a satisfactory phase noise level that other field or on-board quantum sensors could benefit from.

The final assembly of the gravimeter is currently under way and the loading of few 10^8 atoms in a 3D MOT has already been obtained. The first atomic signals are expected soon.

---

[258] M. Kasevich "Atomic interferometry using stimulated Raman transition", PRL, vol. 67, p. 181 - 184, 1991.

[259] Q. Bodard, "A cold atom pyramidal gravimeter with a single laser beam", APL, vol. 96, 134101, 2010.

[260] G. Stern, "Light-pulse atom interferometry in microgravity", Eur. Phys. J. D, vol. 53, p. 353 - 357, 2009.

Optical Fiber T+F Transfer II

CLUB E

Tuesday, July 23 2013, 10:30 am - 12:00 pm

Chair: **Helen Margolis**
National Physical Laboratory

Controlling distant pulsed laser timing via interferometry

Russell Wilcox[1], Ronald Holzwarth[2], Giuseppe Rizzelli Martella[1], Klaus Hartinger[2]

[1]Lawrence Berkeley National Laboratory, Berkeley, CA/USA
[2]Menlo Systems, Martinsried, Germany

Email: rbwilcox@lbl.gov

Ultrafast pump/probe experiments in large laser facilities require femtosecond laser synchronization over distances of hundreds of meters. Some ways to achieve this use an amplitude modulated carrier or short optical pulses over fiber. This new scheme[1] uses an unmodulated optical wave, synchronizing to the optical phase. This is an application of frequency metrology techniques in the time domain, utilizing the full optical bandwidth. Optical nonlinearities (e.g. dispersion and self phase modulation) are avoided. Timing information is carried by optical phase, which provides for sub-femtosecond timing resolution due to the ~200THz optical frequency.

Our scheme controls envelope timing of CEP (carrier/envelope phase) stabilized comb lasers by locking the carrier to a transmitted single frequency. Since the CEP stabilization synchronizes the carrier and envelope, the pulse envelopes are temporally controlled. A clock comb laser provides stable optical frequencies, one of which is transmitted via interferometer as a reference.

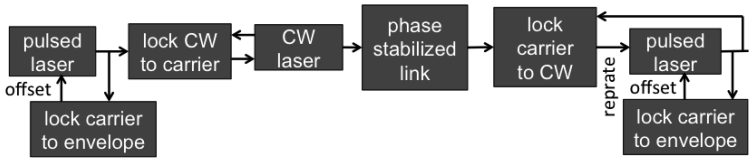

Fig. 80: Optical timing control scheme. Each subsystem transfers optical phase information to the next subsystem.

We have recently demonstrated low jitter performance of each subsystem in the timing signal path, including single frequency selection from the clock (320as), transmission via fiber interferometer (410as), phase locking a fiber modelocked laser to a single frequency (280as), and controlling two comb lasers via a single frequency (5.6fs). Our current experiment improves the bandwidth of laser control to 1MHz by adding an intracavity EO modulator. Based on optical phase stability results with similar lasers, we expect sub-femtosecond timing jitter.

[1] R. B. Wilcox et al, "Towards attosecond synchronization of remote mode-locked lasers using stabilized transmission of optical comb frequencies", J. Mod. Opt., vol. 58, p. 1460-1469, 2011.

Simultaneous remote transfer of accurate timing and optical frequency over a public fiber network

Olivier Lopez[1], Amale Kanj[2], Paul-Eric Pottie[2], Daniele Rovera[2], Joseph Achkar[2], Christian Chardonnet[1], Anne Amy-Klein[1] and Giorgio Santarelli[2,3]

[1]Laboratoire de Physique des Lasers, Université Paris 13, Sorbonne Paris Cité, CNRS, Villetaneuse, France

[2]LNE-SYRTE, Observatoire de Paris, CNRS, UPMC, Paris, France

[3]Laboratoire Photonique, Numérique et Nanosciences, Université de Bordeaux 1, Institut d'Optique and CNRS, Talence, France

Email: paul-eric.pottie@obspm.fr

We present a novel method to simultaneously disseminate an ultra-stable optical frequency and accurate timing over a public telecommunication network on a 540-km optical link simultaneously carrying Internet data traffic[261]. An ultra-stable laser is carrying both the frequency and timing signals through the fiber (see Fig. 1). The frequency information is the laser optical carrier frequency. Timestamps signals are consisting in spread spectrum pseudorandom modulation codes (20 Mchip/s) and are provided by a pair of two-way satellite time transfer modems, one for each direction. They are encoded on the optical carrier by electro-optic phase modulators. The optical frequency stability results are substantially equivalent to the ones reported previously[262]. The timing stability is below 20 ps for integration time up to 10^5 s. The time delay variation remains below 50 ps when the fiber length is scaled from 10 m up to 540 km. This method is very robust, with an overall conservative timing error of about 250 ps determined by the measured time delay over several weeks of measurement. These results outperform the satellite techniques. They are easily scalable to a wide area network and open the way to a novel approach of precise remote synchronization with the potential to realize even better accuracy.

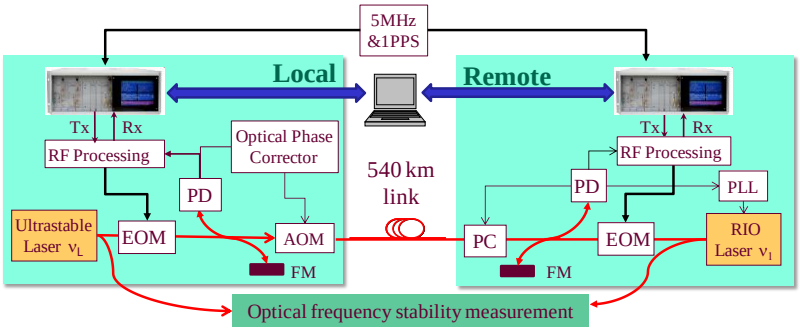

Fig. 81: Principle of simultaneous two-way time transfer and frequency transfer

[261] Lopez O., Kanj A., Pottie P.E., Rovera D., Achkar J., Chardonnet C., Amy-Klein A., Santarelli G., "Simultaneous remote transfer of accurate timing and optical frequency over a public fiber network," Appl. Phys. B **110**, p 3-6, 2013.

[262] Lopez O., Haboucha A., Chanteau B., Chardonnet C., Amy-Klein A., Santarelli G., "Ultra-stable long distance optical frequency distribution using the Internet fiber network," Optics Express **20**, p 23518-23526, 2012.

Remote synchronization via phase-stabilized chirped continuous-wave frequency transfer

Sebastian M. F. Raupach, Gesine Grosche

Physikalisch-Technische Bundesanstalt (PTB), Bundesallee 100, 38116 Braunschweig, Germany

Email: sebastian.raupach@ptb.de

Both optical as well as radio or microwave frequency transfer have been demonstrated at relative instabilities below 10^{-18} using optical fibres[263]. For true clock operation and comparison not only a continuous timescale has to be established, but also means for transferring time information. Local timescales can then be synchronized to each other (or to TAI). Applications include e.g. very large baseline interferometry. Recently, several groups[1,264,265,4] have demonstrated time transfer, and time and frequency transfer[1,3,4], using glass fibre links. The equipment employed was adopted from satellite two-way time and frequency transfer[1,2] or was developed for achieving a stable delay along a fibre link[3,266].

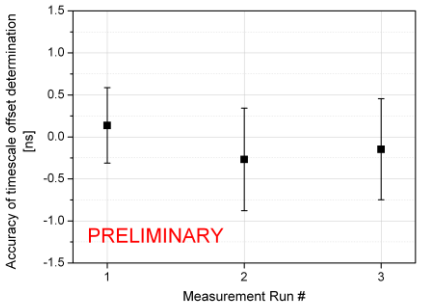

[263] O. Lopez et al., "Simultaneous remote transfer of accurate timing and optical frequency over a public fiber network", Appl. Phys. B, DOI 10.1007/s00340-012-5241-0, 2012, and refs. therein

[264] M. Rost et al., "Time transfer through optical fibres over a distance of 73 km with an uncertainty below 100 ps", Metrologia, vol. 49, p. 772-778, 2012.

[265] Ł Śliwczyński, P. Krehlik, A. Czubla, Ł. Buczek and M. Lipiński, "Dissemination of time and RF frequency via a stabilized fibre optic link over a distance of 420 km", Metrologia, vol. 50, doi:10.1088/0026-1394/50/2/133, 2013.

[266] B. Wang et al., "Precise and continuous time and frequency synchronization at the $5x10^{-19}$ accuracy level", Sci. Rep., vol. 2, p. 1-5, 2012.

Here we present results from a proof-of-principle experiment, demonstrating a different technique for remote synchronisation. It is based on the phase-stabilized transfer of a continuous-wave, chirped optical frequency, and it is demonstrated via a 150 km underground fibre link in a loop configuration. Using standard equipment from frequency metrology, it allows for simultaneous optical frequency transfer with instabilities of the order of 10^{-19}.

Here, we achieve high-fidelity transfer of an optical frequency chirped by more than 100 kHz/s and demonstrate the suppression of delay related effects. Hence we measure the true offset between two timescales remotely via the optical link. We find good agreement with results from independent, direct side-by-side measurements as shown in fig. 1, which indicates a capability of the technique of around 300 ps. Finally we will discuss how this technique can be extended further to yield statistical uncertainties below 1 ps.

Figure 82. Accuracy of the timescale offset measurement via a phase-stabilized optical link. The error bars indicate the combined statistical and systematic uncertainties.

This work was supported by the European Metrology Research Programme EMRP under SIB-02 NEAT-FT. The EMRP is jointly funded by the EMRP participating countries within EURAMET and the European Union.

LIFT: The Italian Fiber Network For Frequency and Time Distribution

R. Ambrosini[3], D. Calonico[1], C. E.Calosso[1], C. Clivati[1,2], G.A.Costanzo[2], P.Denatale[4], G. Galzerano[5], F. Levi[1], D. Mazzotti[4], A. Mura[1], N. Poli[6], G.M. Tino[6], M. Zucco[1].

[1] INRIM, Istituto Nazionale di Ricerca Metrologica, Torino, Italy
[2] Politecnico di Torino, Torino, Italy
[3]INAF, Istituto Nazionale di Astrofisica, Bologna, Italy
[4]CNR INO, Istituto Nazionale di Ottica, Firenze, Italy
[5]CNR IFN, Istituto di Fotonica e Nanotecnologie, Milano, Italy
[6]INFN, Istituto Nazionale di Fisica Nucleare, Firenze, Italy

Email: f.levi@inrim.it

LIFT is an Italian national project aimed to realize a backbone structure to distribute along optical fibers, to a variety of scientific users, high accuracy frequency and time signals, directly derived by INRIM primary frequency reference.

The project is funded by the Italian Ministry of Research, and allows for a long term rental of the fiber[267]. In the first stage four cities and five research institutions will be connected together, Torino (National Institute of Metrological Research), Milano (Institute of Photonics and Nanotechnology belonging to National Research Council, CNR), Bologna (National Astrophysics Institute, VLBI Radiotelescope in Medicina) and Firenze (National Institute of Nuclear Physics and National Optic Institute belonging to CNR); we target to connect others scientific and industrial users to the present backbone. The reference frequency signal will be delivered by INRIM through a dedicated dark fiber for a total length of 650 km, provided by Italian NREN GARR.

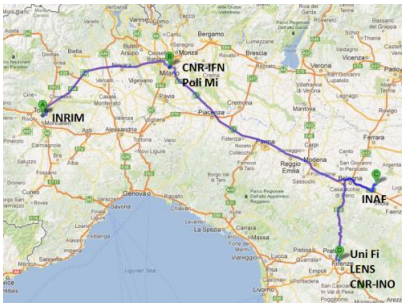

Path of the LIFT fiber link connecting Torino, Milano Bologna and Firenze.

Given the variety of scientific users involved in this project and their different needs, both frequency and time (currently under study) dissemination will be implemented. The four main locations will be equipped with fiber optic combs to refer all the frequency measurements to INRIM H-Maser referenced to IT CSF2 and to UTC(IT), or to an Yb lattice clock. LIFT in perspective will link INRIM to other European NMIs and will constitute an important section of a wider European fiber network connecting NMIs and other scientific and industrial users.

We have already defined a long-standing rental agreement with GARR, to provide us the dark fibers, and we are now installing our bidirectional amplifiers along the path, expecting to be able to measure the Sr clock located in Firenze against INRIM fountain by the end of the year.

[267] The connection Torino-Firenze was initially funded by PRIN2009 (2009ZJJBLX), the realization of a wider network is funded by "Progetti Premiali 2012". Both research grants are provided by Italian Research Ministry.

IFCS-EFTF5-D2-5

Time and Frequency Optical Transfer Infrastructure

Vladimir Smotlacha[1], Alexander Kuna[2], Josef Vojtěch[3]

[1,3]CESNET, Prague, Czech Republic
[2]Institute of Photonics and Electronics AS CR, v.v.i.,
Prague, Czech Republic

Email: vs@cesnet.cz

CESNET operates national research network using DWDM (Dense Wavelength Division Multiplexing) technology. Based on our previous experience with time transfer between Czech and Austrian national time and frequency laboratories, which regular operation started in August 2011, and having access to own DWDM optical network, we designed and started to build national infrastructure for time and frequency transfer – TF-infrastructure.

Time and frequency transfer can't be operated at higher network layers, as they require non-standard, asynchronous signal modulation with extremely low jitter, and therefore we designed own data coding at physical layer. We use heterogeneous infrastructure based on both bidirectional and unidirectional dedicated channels in our productive DWDM network. We proved that there is no interference with any standard traffic, including data channels 10 and 100 Gbps .

TF-infrastructure goals include:

- time transfer from existing Cesium primary standards to Laboratory of the National Time and Frequency Standard in UFE – Institute of Photonics and Electronics,
- comparison of national approximation of UTC with that one in neighboring countries,
- time and frequency distribution from Cesium clocks and Hydrogen masers.

Links between CESNET and involved organizations utilize available technology, in most cases it is a combination of commercial and open DWDM transmission systems:

- pair of channels (with the same wavelength in both directions) in a production DWDM optical network,
- pair of DWDM channels with different wavelengths in single fiber bidirectional transmission system,
- pair of DWDM channels (both uni- and bi-directional) in experimental links,
- dark fiber – usually last mile in the urban area.

Despite this heterogeneous physical layer, the transport layer provides parameters required for accurate time (resp. frequency) transfer. Depending on the optical path lengths (20 to 550 km), we reach stability better than 30 ps in terms of TDEV and 10^{-15} in terms of ADEV. Utilized wavelengths are amplified by productive unidirectional Erbium Doped Fiber Amplifiers (EDFA) or dedicated bidirectional amplifiers depending on the particular link.

The TF-infrastructure currently connects 6 organizations in the Czech Republic and also Austrian national T&F laboratory BEV in Vienna. We also operate cross-border link to Polish network Pioneer, however there are administrative problems to set up time transfer channel to laboratories GUM (Warsaw) or AOS (Borowiec).

Phase Noise & Performances

CLUB D

Tuesday, July 23 2013, 10:30 am - 12:00 pm

Chair: **Jeremy Everard**
University of York

IFCS-EFTF2-D3-1

Generalized phase measurement and processing with application in the time-frequency measurement control and link

Wei Zhou, Zhiqi Li, Huimin Song, Qiaoyan Fan

Department of measurement and instrument, Xidian University, Xi'an, China

Abstract

Traditional phase measurement is limited by identical frequency nominal values of two comparing signals. In a lot of applications, there are higher requirements on not only measurement accuracy, but also the frequency range of comparing signals. In the area of precise frequency source synchronization and link, phase processing, measurement between completely different frequency signals are required in the accuracy and stability transmission of frequency signals with complex relationship. Through the past 20 years' study that we found some concepts and features which can reflect the phase relationship between the different frequency signals, such as the Least Common Multiple Period, Quantitative Phase Difference Step, Equivalent Phase Comparison Frequency, and the continuous phase difference group characteristics with an interval of the least common multiple period and quantized phase step according to specific frequencies between the two different nominal frequency signals. Phase processing can be used between not only the same nominal frequencies but also the different nominal frequencies. The breakthrough in the phase comparison can lead to realize the frequency &phase measurement instruments with higher resolution and the new high performance Phase-locked loop device. At the same time the complex frequency link with high precision and the reform of different quantum frequency standard can be realize. it also improve the performance. As phase processing generalized in concepts and technical realization, it will not only advance the time &frequency measurement, control and frequency source technology, but also can take advantage in wider application fields.

IFCS-EFTF2-D3-2

Source Impedance Influence on Cross-Correlation Phase Noise Measurements

Jason Breitbarth

Holzworth Instrumentation, Boulder, CO USA

Email: jason@holzworth.com

The phase noise floor of a source has been shown both theoretically and experimentally to be the ratio of source power divided by the phase component of the noise power. In a 50Ω system this is determined by P_{OUT} – 177dBm in dBc/Hz. Recent measurements have shown what appears to be better than theoretical noise floors in some oscillators, assuming a 50Ω environment. However, oscillators rarely exhibit an output impedance of exactly 50Ω and vary significantly farther from the carrier. While the input impedance of a modern cross correlation analyzer may be 50Ω, the assumption this load noise is common between both channels is incomplete. This leads to the possibility that the extremely low phase noise measured is real and not in violation of theoretical limits. This paper presents theoretical arguments and measurements demonstrating the assumptions for these limits are merely incomplete.

The impedance outside the 3dB point of the resonator within an oscillator becomes relevant in low noise systems. Depending on the architecture of the resonator and how the power is delivered out of oscillator, the output impedance far from the carrier may be either a good match or nearing an open or short circuit. This paper deals with the latter. In the short circuit scenario, the output impedance will be very low far from the carrier and the equivalent noise impedance is also reduced proportionally. Far from the carrier source impedance therefore may not be considered to be the same as the center frequency of the source power and the signal to noise ratio of the oscillator may have a different theoretical limits based on offset frequency relative to the carrier power.

The cross correlation phase noise engine, if designed appropriately, can be viewed as two independent loads in terms of noise. With noise incoherent loads for each channel, the cross correlation phase noise engine has the ability to analyze source impedance other with other than 50Ω. The received source power is still measured as a voltage in a 50Ω environment and is consistent to a power meter.

In consideration of the cross correlation phase noise engine with a frequency dependent source impedance, measurements exceeding the theoretical limit of a 50Ω system is both theoretically and practically possible. The abnormally low measurements do not violate theoretical limits once both the proper source impedance and measurement methods are taken into account.

This paper presents the signal to noise analysis both theoretically and experimentally in terms of source impedance utilizing cross correlation analysis. The experimental data is shown both at base band and at microwave frequencies. The experimental setup uses an additive phase noise measurement with the introduction of variable source impedance to demonstrate the theoretical limits.

Phase Noise Measurement Techniques, Associated Uncertainty and Limitations

Ulrich L. Rohde, Ajay K. Poddar
Synergy Microwave Corp., Paterson, NJ 07504, USA (Email: akpoddar@synergymwave.com)

One of the important parameters of oscillators is phase noise and there are several methods explaining how to do this and the right one must be chosen when performing measurements. It is necessary to know the weakness and strength of different measurement systems, because none of these methods is perfect for every situation. In general, measuring phase noise is more difficult than measuring amplitude or frequency and phase related properties. The major challenge is the requirement of huge dynamic range in the phase noise measurement process [1]-[2].

The new generation of Crystal Oscillators and SAW oscillator exhibits superior phase noise performance: Close-in phase noise: -149dBc/Hz @ 100 Hz offset and noise floor ~ -195dBc @ 100 kHz offset from the carrier of 100 MHz OCXO. SAW resonator based oscillator exhibits -165dBc/Hz @ 10 kHz offset from the carrier frequency of 1GHz and noise floor is better than 180dBc. The phase noise performance of ultra low noise Crystal oscillator has been driving the specifications of phase noise analyzers and it is time consuming exercise to measure the noise floor below the KT of -177dBm for SSB and 0 dBm output powers.

Once adequate for advanced designs, a noise floor dictated by SSB thermal noise (Johnson Noise) KT of -177dBm for zero dBm output power is not enough anymore for some special requirement and also marketing of these reference frequency sources. The noise correlation technique allows us to look below KT level (< -177dBm). But the usefulness of the noise contribution below KT is debatable in the perspective of following: reliability, accuracy, speed of test, range, repeatability, data retrieval, and cost. Despite all these hazards, automatic phase noise measurement systems have been developed successfully [2]-[3].

For validation, we build the ultra low noise 100 MHz Crystal oscillator and noise measurement is conducted using different equipments (Agilent E5052B, R&S FSUP, Holzworth, Noise XT, and Anapico APPH6000-IS) available on the market. Figures (1), (2), and (3) show the block diagram of ultra low noise 100 MHz crystal oscillator, theoretical phase noise plot and noise floor of PN equipment using delay line, PLL and cross-correlation techniques. Table 1 describes the theoretical calculated and measured phase noise on different test equipment for comparative analysis of phase noise data under similar test condition.

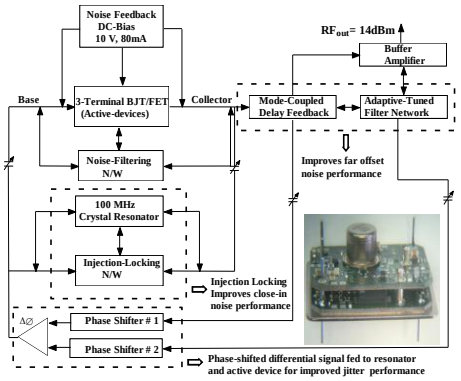

Fig 1: Block diagram and prototype of low phase noise 100 MHz Crystal oscillator for evaluation on different PN Equipments

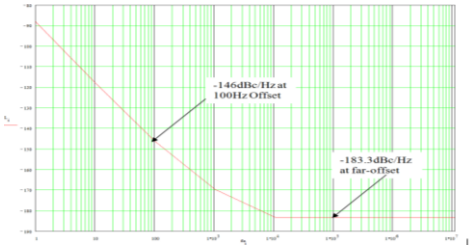

Fig 2: Theoretically calculated Phase Noise Plot for 100MHz Crystal Oscillator circuit (LNXO 100) as shown in Figure (1)

Table 1 describes the theoretical and measured phase noise on different test equipments available in market

100 MHz OCXO O/P=14dBm, NF=7dB	Theoretical Model [1]	Agilent E5052B	R & S FSUP 26	Anapico APPH6000-IS	Holzworth HA7402-A	Noise XT DCNTS
@ 100 Hz offset	-146 dBc/Hz	-143 dBc/Hz	-143 dBc/Hz	-141 dBc/Hz	-149 dBc/Hz	-140 dBc/Hz
@ 1 kHz offset	-170 dBc/Hz	-167 dBc/Hz	-163 dBc/Hz	-170 dBc/Hz	-170 dBc/Hz	-170 dBc/Hz
@ 10kHz offset	-182 dBc/Hz	-173 dBc/Hz	-174 dBc/Hz	-172 dBc/Hz	-178 dBc/Hz	-181 dBc/Hz
@ 100KHz offset	-183 dBc/Hz	-174 dBc/Hz	-183 dBc/Hz	-181 dBc/Hz	-179 dBc/Hz	-183 dBc/Hz
@ 1 MHz offset	-184 dBc/Hz	-174 dBc/Hz	-184 dBc/Hz	-182 dBc/Hz	-179 dBc/Hz	-186 dBc/Hz
@ 10MHz offset	-184 dBc/Hz	-174 dBc/Hz	-185 dBc/Hz	-188 dBc/Hz	-178 dBc/Hz	-196 dBc/Hz

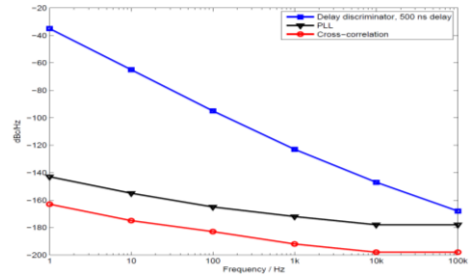

Fig.3 Typical predicted phase noise plots for 100MHz OCXO and noise floor for 3-techniques (PLL, Delay-line, and cross-correlation)

The theoretical analysis, experimental outcome and observation conclude that there is uncertainty and limitation of phase noise measurement equipments. For example, if the equipment in use, after many correlations gives out a better number, it violates the laws of physics and if it gives a worse number, then either the correlations settings needs to corrected or the dynamic range of the equipment is insufficient. This measurement is exhaustive, but it was necessary to explain how things fall in place. At 20dBm output, the output amplifier certainly has a higher noise figure, as it is driven with more power and there is no improvement possible. There is an optimum condition and some of the measurements showing -200dBc/Hz @ 100 kHz offset for 100 MHz OCXO advertized are dubious for exactly these reasons. In addition to this uncertainty in phase noise measurement due to: harmonics, output load mismatch, output phase match, cable length, sweet-spot, dynamic range can lead to error of 10-20dB, which is scary. The theoretical treatment and PN measurement related problems with possible cure will be discussed in full length paper.

[1] D. Calbaza, C. Gupta, U. L. Rohde, A. K. Poddar, "Harmonics Induced Uncertainty in Phase Noise Measurements", MTT-S Digest, pp. 1-3, June 2012
[2] Rubiola and F. Vernotte. (2010, Feb 27). *The cross-spectrum experimental method* [http://arxiv.org/, document arXiv:1003.0113v1]
[3] W. F. Walls, "Cross-Correlation Phase Noise Measurements", 1992 IEEE FCS, pp. 257-261

IFCS-EFTF2-D3-4

Phase noise of optomechanical oscillators

King Yan Fong, Menno Poot, Xu Han, and Hong X. Tang

Department of Electrical Engineering, Yale University, New Haven, CT 06520, USA

Email: kingyan.fong@yale.edu

Cavity optomechanics describes a system consists of an optical cavity coupled to a mechanical resonator through the optical force. When the optical cavity is blue-detuned, the optical force provides a positive feedback that can drive the mechanical resonator into self-sustained oscillation. Such oscillations have been demonstrated in various structures such as micro-toroids[268], flexural beams[269], photonic crystals[270], micro-rings[271], and micro-disks[272] resonators, with an oscillating frequency ranging from MHz to GHz, an oscillating mass from ng down to tens of fg, and threshold powers as low as a few μW. This technology promises to build oscillators that are on-chip integrated, scalable, CMOS-compatible, with low phase noise and low operating power. However, so far there is still lack of theoretical understanding that can deterministically predict the oscillator phase noise spectrum. In this talk, we will present our work in this aspect.

Fig. (a) shows an example of an optomechanical oscillator made in our lab, which has an optical whispering-gallery mode coupled to a mechanical radial breathing mode. We analyze the system by treating it as a feedback loop, as illustrated in Fig. (b), with the thermomechanical force noise and the laser light as the inputs. We linearize the equations of motion at a limit-cycle solution[273] and derive the noise transfer functions for each of the loop components. The amplitude noise and the phase noise can be treated in a unified approach by using the complex number notation and the noise transfers between phase-phase, amplitude-amplitude, and phase-amplitude are fully quantified. As a result, the phase noise spectral density of the closed-loop system can be computed once the input noises are known. We consider the oscillator phase noise contributions for three kinds of noise sources: thermomechanical force noise, laser shot noise, and a $1/f$ technical laser phase noise. As an example we calculated the individual and combined phase noise spectra for the systems demonstrated in Ref. 2 and 5 shown in Fig. (c).

[268] H. Rokhsari, T. J. Kippenberg, T. Carmon, and K. J. Vahala, Opt. Express, vol. 13, p. 5293, 2005.

[269] G. Anetsberger, *et al.*, Nature Physics, vol. 5, p. 909, 2009.

[270] M. Eichenfield, J. Chan, R. M. Camacho, K. J. Vahala, and O. Painter, Nature, vol. 462, p. 78, 2009.

[271] S. Tallur, S. Sridaran, and S. A. Bhave, Opt. Express, vol. 19, p. 24522, 2011.

[272] W. C. Jiang, X. Lu, J. Zhang, and Q. Lin, Opt. Express, vol. 20, p. 15991, 2012.

[273] M. Poot, K. Y. Fong, M. Bagheri, W. H. P. Pernice, H. X. Tang, Phys. Rev. A, vol. 86, p. 053826, 2012.

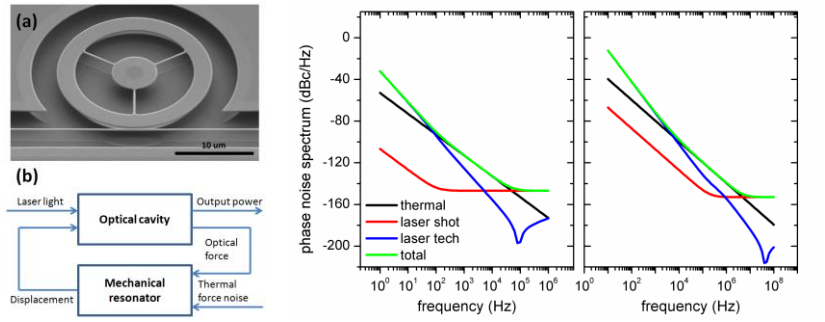
(a)
10 um
(b)
Laser light
Optical cavity
Output power
Optical force
Mechanical resonator
Thermal force noise
Displacement
phase noise spectrum (dBc/Hz)
0
-40
-80
-120
-160
-200
thermal
laser shot
laser tech
total
frequency (Hz)
frequency (Hz)

ULISS project : 2013 progress report

Vincent Giordano[1], Serge Grop[2], Benoît Dubois[2,], Jean-Louis Masson[1],

Gregory Haye[1], Enrico Rubiola[1]

[1]Time and Frequency Dpt., FEMTO-ST Institute, Besançon, France
[2] ULISS-ST, SAIC UNiv. Franche-Comté, Besançon, France

Email: giordano@femto-st.fr

The ULISS Cryogenic Sapphire Oscillator (CSO) offers unprecedented short-term frequency performances. It was specially designed to be transportable by car in order to test this new technology in different European sites. During the last 18 months, it was used to qualify with success few high stability frequency sources [1,2,3]. In February 2013, a new measurement campaign was lead at CNES, Toulouse (France) to qualify the flight model of the frequency synthesis of the PHARAO clock.

During the same period we built a second CSO unit based on the same design and conducted new characterisations of frequency stability and environmental sensitivity. Optimisation of the system has led to an improved frequency stability reaching currently $1x10^{-15}$ at 10,000 s integration times. Newly developed digital electronic controls were also implemented that makes the system more reliable and versatile/upgradable. Eventually we developed a new low phase noise and high-resolution frequency synthesis delivering 10 GHz, 100 MHz and 9.192 GHz ultra stable signals.

Fig. 83: The CSO ULISS

In this paper we draw a progress report on the ULISS project, updating performances and describing the latest experiments conducted with our CSO in different sites in Europe.

[1] *ULISS: A Mobile Cryogenic Ultra-Stable Oscillator.* S. Grop et al. Proc. of the 2011 EFTF/IFCS Joint Meeting, San Francisco (CA), US, May 2-5, 2011.

[2] *Direct comparison of two Cryocooled Sapphire Oscillators presenting relative frequency instability at the* 10^{-15} *level* . S. Grop et al. Proc. of the 2012 EFTF, Gothenburg, Sweden, 24-26 April 2012.

[3] *New Generation of Cryogenic Sapphire Microwave Oscillator for Space, Metrology and Scientific Applications.* V. Giordano et al. Rev. of Scientific Instruments, **83,** (2012)

Ultra-stable lasers and resonators

CLUB H

Tuesday, July 23 2013, 02:00 pm - 03:30 pm

Chair: **Longsheng Ma**
East China Normal University

IFCS-EFTF6-E1-1

Tenfold reduction in Brownian noise with crystalline coatings

Garrett D. Cole[1,2], Wei Zhang[3], Michael J. Martin[3], Jun Ye[3], and Markus Aspelmeyer[1]

[1]Vienna Center for Quantum Science and Technology (VCQ),
Faculty of Physics, University of Vienna, A-1090 Vienna, Austria
[2]Crystalline Mirror Solutions GmbH, A-1090 Vienna, Austria
[3]JILA, National Institute of Standards and Technology, and University of Colorado,
Boulder, Colorado 80309-0440, USA

Email: garrett.cole@univie.ac.at

Coating Brownian noise,[274] driven by excess mechanical dissipation in high reflectivity ion-beam sputtered (IBS) films imposes a severe limit on the performance of state-of-the-art precision measurement systems, such as stabilized lasers for optical atomic clocks and interferometric gravitational wave detectors. As a consequence, a concerted effort has been focused on the identification of multilayer materials capable of simultaneously achieving high reflectivity and minimal mechanical dissipation. Recently, AlGaAs resonators have displayed an exceptional mechanical quality factor, Q, up to 4×10^4 at room temperature.[275] This stands in stark contrast with the Q of SiO_2/Ta_2O_5, which is typically a few thousand.

Building upon advances in semiconductor microfabrication, we have successfully implemented low-loss epitaxial multilayers in a standard optical reference cavity design. Our novel coating technology entails the selective removal of crystalline films from the original growth wafer, followed by direct bonding to an arbitrary (curved or planar) optical component. Here, we present the optomechanical performance of cavity end mirrors based on a 40.5-period (6.83 μm thick) GaAs/AlGaAs Bragg reflector directly-bonded to fused silica.

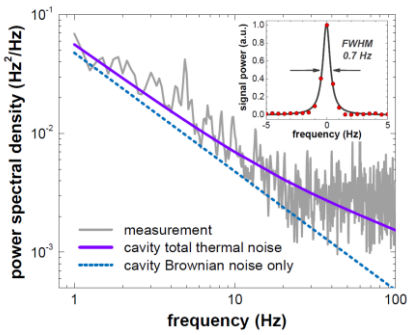

Fig. 84: Thermal-noise-limited NPSD of the cavity-stabilized 1064-nm laser, with a 0.7 Hz linewidth (0.5 Hz resolution bandwidth) shown in the inset.

Using a pair of bonded mirrors contacted to a 35-mm zerodur spacer, we confirm that our "crystalline coatings" exhibit both high reflectivity and an intrinsically low mechanical loss. Optical ringdown at 1064 nm yields a finesse of $1.5(1)\times10^5$, in excellent agreement with the theoretical estimate of 1.53×10^5. We next probe the coating loss angle through a direct measurement of the cavity thermal noise (Fig. 1). This is realized by locking a solid-state 1064 nm Nd:YAG laser to the crystalline coating cavity. A 698 nm Sr lattice clock laser[276] acts as a reference, while an Yb fiber comb[277] is used to transfer the frequency stability between the sources. We extract a loss angle ($1/Q$) of $0(4)\times10^{-5}$ for the bonded AlGaAs mirrors, a tenfold reduction when compared with the best dielectric multilayers. These results pave the way for a significant advancement in the sensitivity of optical interferometers, as well as a new level of performance for cavity-stabilized laser systems.

[274] G. Harry *et al.*, *Optical Coatings and Thermal Noise in Precision Measurement*. Cambridge University Press, 2012.
[275] G. D. Cole, *Proc. SPIE Optical Trapping and Optical Micromanipulation IX*, vol. 8458, 8458-07, 2012.
[276] T. L. Nicholson *et al.*, *Phys. Rev. Lett.* vol. 109, 230801, 2012.
[277] C. Benko *et al.*, *Opt. Lett.* vol. 37, pp. 2196-2198, 2012.

IFCS-EFTF6-E1-2

Ultra-stable laser with fractional long-term drift below 10^{-20}/s

C. Hagemann[1], T. Legero[1], T. Kessler[1], C. Grebing[1], U. Sterr[1], F. Riehle[1],
M. J. Martin[2], L. Chen[2], and J. Ye[2]

[1]Physikalisch-Technische Bundesanstalt (PTB), 38116 Braunschweig, Germany
[2]JILA/NIST, University of Colorado, 440 UCB, Boulder, CO 80309-0440

Email: christian.hagemann@ptb.de

Recently, we have set up a cavity-stabilized laser system that has demonstrated so far unreached short-term stabilities of $mod\ \sigma_y(\tau) \leq 1 \times 10^{-16}$ for averaging times of $\tau = 1 \ldots 10$ s [1]. This performance below the thermal noise limit of state-of-the-art glass resonators[2] has been enabled by the use of a cryogenic single-crystal silicon cavity.

Material creep is absent in single-crystal cavities[3] and thermal expansion is suppressed by operating the cavity close to a temperature of 124.2 K, where its coefficient of thermal expansion is zero. Thus, the silicon cavity can in principle provide an excellent long-term length-stability.

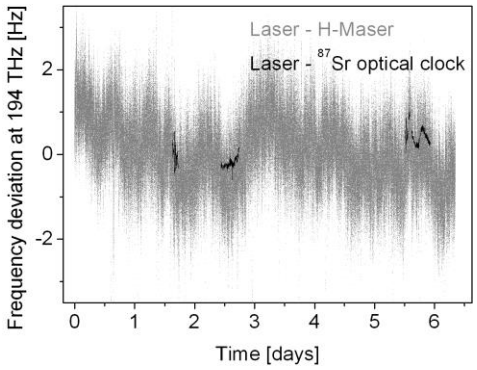

Fig.85: Frequency record of the laser stabilized to the silicon cavity relative to a hydrogen maser and a ^{87}Sr optical lattice clock at PTB (moving average, window: 100 s). An average drift of -2.2 μHz/s of the maser with respect to the Cs fountain clock has been removed.

Utilizing a frequency comb, the frequency instability of the laser operating at 194 THz and locked to the silicon cavity has been evaluated in comparison to a hydrogen maser referenced to a primary caesium fountain standard and to a ^{87}Sr optical lattice clock[4,5] at PTB. The observed average drift against the Cs fountain was 1.7 μHz/s in a time interval of about one week, which is in good agreement with the average frequency drift of the laser to the strontium clock of 1.8 μHz/s. These values correspond to a fractional frequency drift of less than 10^{-20}/s. The fractional frequency instability of the laser was below $\sigma_y(\tau) = 3 \times 10^{-16}$ for averaging times of $\tau = 10 \ldots 1000$ s and reached a minimum of $\sigma_y(500\ \mathrm{s}) = 8 \times 10^{-17}$. For longer averaging times up to 10^4 s, the frequency instability increases, but remains below the frequency instability of the hydrogen maser of $\sigma_y = 1 \times 10^{-15}$. Only at much longer time-scales the instability of the laser is visible with respect to the hydrogen maser.

---

[1]T. Kessler et al., *Nature Photonics*, **6**, 687-692 (2012).

[2]T. L. Nicholson et al., *Phys. Rev. Lett.*, **109**, 230801 (2012).

[3]R. Storz et al., *Opt. Lett.*, **23**, 1031-1033 (1998); J. G. Hartnett et al., *Appl. Phys. Lett.*, **100**, 183501 (2012).

[4]St. Falke et al., *Metrologia*, **48**, 399 (2011).

[5]C. Hagemann et al., *IEEE Trans. Instrum. Meas*, DOI: 10.1109/TIM.2013.2242597 (2013).

IFCS-EFTF6-E1-3

Ultra-Stable Cryogenic Optical Resonators – Towards a Thermal Noise Limited Frequency Stability < $3 \cdot 10^{-17}$

Moritz Nagel, Katharina Möhle, Klaus Döringshoff, Sylvia Schikora,
Evgeny V. Kovalchuk, and Achim Peters

Institut für Physik, Humboldt-Universität zu Berlin, Berlin, Germany

Email: moritz.nagel@physik.hu-berlin.de

Many experimental and technical applications, e.g. optical atomic clocks, demand ultra-stable optical resonators for laser frequency stabilization. Nowadays, the frequency stability of all optimized room-temperature optical reference cavities is limited by the displacement noise within the resonator substrates and mirror coatings due to thermal noise. The rather straightforward method to simply reduce the influence of thermal noise by cooling down the resonators to cryogenic temperatures is not well applicable for most room-temperature cavities.

Therefore, we worked out a special design for an ultra-stable sapphire optical cavity system operating at 4 Kelvin, with a prospective thermal noise limited frequency stability better than $3 \cdot 10^{-17}$ (see Fig. 1). We will present details on the design of this ultra-stable system as well as first frequency stability measurements conducted by direct comparison of two such new sapphire optical cavities.

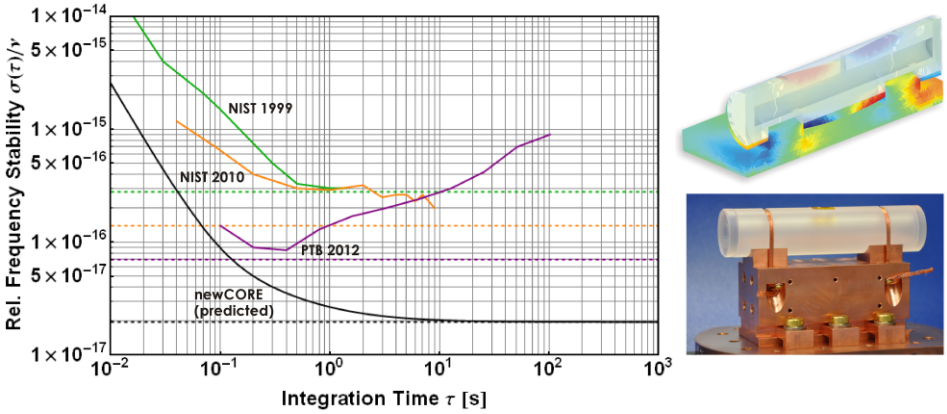

Fig. 1: *Left* Comparison of the predicted rel. freq. stability of our newly designed cryogenic optical resonators (newCORE operated at 4K, black line) with the measured stabilities of the best room temperature cavities (ultra-low-expansion glass, Young et. al [NIST 1999] green line and Jiang et. al [NIST 2010] orange line) as well as measured stability of the best optical reference cavity (silicon cavity operated at 124K, Kessler et. al [PTB 2012] purple line). The dashed lines indicate the theoretical thermal noise limits at the operating temperatures. *Upper Right* Illustration of the optimized design of our new COREs superimposed with a FEM simulation of vertical vibration (gravitational) induced bending (deformation scaled up by a factor of 10^{10}). *Lower Right* Picture of one of the new sapphire cavities mounted on a copper support.

IFCS-EFTF6-E1-4

Laser Frequency Stabilization Using Micro Resonators

Lukas Baumgartel[1,2] and Nan Yu[1]
[1]Jet Propulsion Laboratory, California Institute of Technology, Pasadena, CA, USA
[2]Department of Physics, University of Southern California, Los Angeles, CA, USA

Email: nan.yu@jpl.nasa.gov

Optical frequency standards and clocks with impressive precision have been demonstrated. Efforts are being made for more portability and compactness of these high performance devices. To that end, we have been investigating the possibility of using optical micro resonators as frequency reference cavities in place of conventional Fabry-Perot cavities. The micro resonators used are high-Q crystalline whispering gallery mode (WGM) resonators with linewidths on the order of kilohertz -- comparable to high-finesse Fabry Perot cavities -- yet of just millimeters in diameter and inherently robust to acceleration.

A primary challenge of using WGM resonators as reference cavities is stabilizing the eigenmode frequency itself due to thermal effects. The common thermally stable materials such as ULE are not suitable for WGM resonators due to poor optical transparency. Small WGM mode volumes inside dielectric bulk also increase fundamental noise level. Nevertheless, when properly implemented, micro resonators can potentially provide high frequency stability suitable for optical frequency standards[1].

We are investigating the feasibility of the micro resonator reference through both passive and active stabilization approaches. In the active approach, a dual-mode temperature stabilization method has been demonstrated[2], which suppresses the overall temperature coefficient of the cavity to 1.7×10^{-7} K^{-1} – just 6 times higher than that of commercial ultra-low expansion glasses. This actively temperature-stabilized resonator has already reached a fractional frequency stability of $1x10^{-12}$ at one second.

In the passive stabilization scheme, we investigate a number of thermal compensation schemes employing a hetero-structure to reduce the WGM resonator's temperature sensitivity. In one approach, we showed through modeling that a surface coating of compensating material can create a resonator with a temperature-coefficient turning point near room temperature[3]. However, the technique is limited by material choices and fabrication precision. Currently, we are investigating a compound structure where the resonator is made of two or more materials of different thermal and mechanical properties. Significantly, our simulations show that existing low thermal expansion materials can be utilized to suppress the temperature coefficient of the resonator. Experimental efforts are under way, and we will present our latest results.

[1] "Whispering-gallery-mode resonators as frequency references. II. Stabilization," A. A. Savchenkov, A. B. Matsko, V. S. Ilchenko, N. Yu, and L. Maleki, Journal of The Optical Society Of America B-Optical Physics, Vol.24, pp2988-2997 (2007).
[2] "Frequency stability of a dual-mode whispering gallery mode optical reference cavity," L. M. Baumgartel, R. J. Thompson, and N. Yu, OPTICS EXPRESS Vol. 20, p29798 (2012).
[3] L. Baumgartel, R. Thompson, D. Strekalov, I. Grudinin, and N. Yu "Whispering Gallery Mode Resonators as Optical Reference Cavities," Proceeding of FCS-EFTF, 2011.

IFCS-EFTF6-E1-5

Laser local oscillators for optical atomic clocks

David R. Leibrandt, Shon M. Cook, Michael J. Thorpe*, Chin-Wen Chou**, Tara M. Fortier, Scott A. Diddams, James C. Bergquist, and Till Rosenband

National Institute of Standards and Technology, Boulder, CO, USA
*Present address: Bridger Photonics, Bozeman, MT, USA
**Present address: Sandia National Laboratories, Albuquerque, NM, USA

Email: david.leibrandt@nist.gov

We stabilize the frequency of lasers by use of spectral holes in cryogenically cooled $Eu^{3+}:Y_2SiO_5$, or alternatively by use of acceleration insensitive Fabry-Pérot cavities.

Laser frequency stabilization via spectral-hole burning has the potential to extend laser coherence beyond what is possible with Fabry-Pérot cavities[278]. Several properties of $Eu^{3+}:Y_2SiO_5$ spectral holes are measured[279], including an upper bound of the thermomechanical noise floor at 3.4×10^{-17} (50 % confidence). The absolute frequency has an Allan deviation of $0.8^{+1.1}_{-0.2}\times10^{-16}$ (1000 s averaging time) and a typical drift rate of 3×10^{-17}/s (see Fig. 1). This instability is attributed to technical noise sources.

For field applications, robust and compact spherical Fabry-Pérot cavities exhibit an Allan deviation of 2×10^{-15} and a passive acceleration sensitivity of $2(1)\times10^{-11}$/g that is reduced to below 10^{-12}/g by use of feed-forward techniques[280]. The entire laser system fits inside a $46\times46\times29$ cm^3 enclosure and its mass is 29 kg, a form-factor that is suitable for applications[281] like geodesy and low-phase-noise microwave synthesis.

The latest results from both experiments will be presented. This work is supported by ONR, AFOSR, and DARPA.

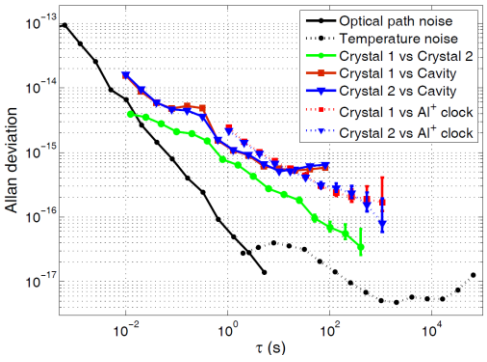

Fig. 86: Optical frequency comparisons of a laser locked to 1.0 at. % $Eu^{3+}:Y_2SiO_5$ site 1 spectral hole patterns at 3.65 K with a Fabry-Pérot cavity, an Al^+ optical atomic clock, and a second spectral hole burning optical frequency reference. Linear frequency drift is removed. The predicted frequency noise due to laser path length fluctuations and cryostat temperature fluctuations are shown in black.

[278] M. J. Thorpe, L. Rippe, T. M. Fortier, M. S. Kirchner, and T. Rosenband, "Frequency stabilization to 6×10^{-16} via spectral-hole burning," Nature Photonics **5**, 688–693 (2011).

[279] M. J. Thorpe, D. R. Leibrandt, T. Rosenband, "Shifts of optical frequency references based on spectral-hole burning in $Eu^{3+}:Y_2SiO_5$," arXiv:1210.4458 (2013).

[280] D. R. Leibrandt, J. C. Bergquist, and T. Rosenband, "Cavity-stabilized laser with acceleration sensitivity below 10^{-12} g^{-1}," Phys. Rev. A **87**, 023829 (2013).

[281] D. R. Leibrandt, M. J. Thorpe, J. C. Bergquist, and T. Rosenband, "Field-test of a robust, portable, frequency-stable laser," Opt. Express **19**, 10278 (2011).

Two-Way Satellite Time and Frequency Transfer

CLUB E

Tuesday, July 23 2013, 02:00 pm - 03:30 pm

Chair: **Victor Zhang**
NIST

Development of Carrier Phase Two-Way Satellite Frequency Transfer at NICT

Miho Fujieda[1], Tadahiro Gotoh[1], Masanori Aida[1], Jun Amagai[1], Fumimaru Nakagawa[1],

Hideo Maeno[1], Ryo Tabuchi[1], Yuko Hanado[1]

[1]Space-Time Standards Laboratory, National Institute of Information and Communications Technology, Koganei, Tokyo, 184-8795, Japan

Email: miho@nict.go.jp

Optical frequency standards require precise frequency transfer techniques to confirm the reproducibility. Optical fiber transfers already demonstrated the high performance. However, the establishment of an intercontinental link remains an issue. The National Institute of Information and Communications Technology has contributed to the development of advanced two-way satellite time and frequency (TWSTFT) techniques. In general, the measurement precision of TWSTFT is determined by the group delay precision of the pseudorandom noise signal. With a usually used chip rate of 2.5 MHz, the nominal precision of a conventional TWSTFT equals to 0.5 ns. The usage of DPN (dual pseudorandom noise) signals is equivalent to increase the chip rate. In this method two separated narrow band signals work like a signal with a chip rate which is equal to the band separation. We used two 127.75-kHz signals with a frequency separation of 20 MHz and achieved a measurement precision of 30 ps[1]. Additionally, narrower band signals allowed us to decrease the rental fee on the satellite transponder.

For further precision improvement, we started the development of carrier phase two-way satellite frequency transfer. This concept was first demonstrated by Fonville et al[2]. We succeeded to establish an operational link for the first time. The phase jitter from the onboard oscillator and Doppler effects due to the satellite motion are removed by using four phase measurements performed between two ground stations. In a common clock measurement on a zero baseline we obtained a precision of 0.2 ps. As a next step, a hydrogen maser comparison was performed on a 100-km baseline[3]. The result was compared with that of GPS carrier phase measurement and agreed on the 10^{-16} level. At present, measurements on a 1000-km baseline are ongoing. As shown in Fig. 1, a baseline length dependency for both short and long term stabilities could not be seen. However, more detailed study will be required, especially on the effects caused by the ionosphere. Our presentation will discuss recent results.

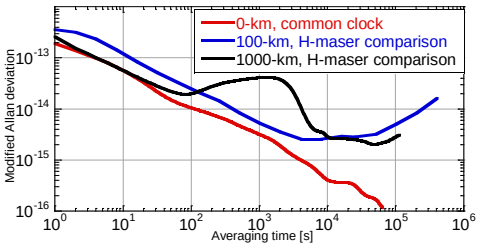

Fig. 87: Transfer stability for different baseline lengths. The bump in the black curve is caused by indoor temperature variation.

IFCS-EFTF5-E2-2

TWSTFT Calibration Involving Four Sites Using a Mobile Station on a Trailer

Thorsten Feldmann[1], Arvind Balu[1], Shuo Liu[1], Wolfgang Schäfer[1], Andreas Bauch[2], Jürgen Becker[2], Dirk Piester[2], Joseph Achkar[3], Amale Kanj[3,*], Christian Schlunegger[4]

[1]TimeTech GmbH, Stuttgart, Germany
[2]Physikalisch-Technische Bundesanstalt (PTB), Bundesallee 100, 38116 Braunschweig, Germany
[3]Observatoire de Paris (OP/LNE-SYRTE), Paris, France
[4]Federal Institute of Metrology (METAS), Bern-Wabern, Switzerland

Email: info@timetech.de

Calibrated time transfer between two remote locations using the Two-Way Satellite Time and Frequency Transfer (TWSTFT) technique with telecommunication satellites requires the accurate knowledge of the internal delays of the equipment involved, the asymmetry between signal paths, and the delays of the connections of the equipment to local time scales. In case of a single satellite transponder used for both signal paths, these delays depend only on the ground equipment, because free space and atmospheric induced delays cancel out in the two-way combination. A single transponder also enables time transfer between two stations located at the same site. The traveling station is operated together with the fixed equipment at each site in a common-clock setup for some days. For each pair of ground sites the differences between the common-clock data reflect the delays of the fixed stations, while ideally the delays associated with the traveling equipment cancel out.

In November 2012 the time transfer links between Physikalisch-Technische Bundesanstalt (PTB), Observatoire de Paris (OP/LNE-SYRTE), Swiss Federal Institute of Metrology (METAS), and TimeTech GmbH were calibrated using TimeTech's mobile TWSTFT calibration station assembled on a trailer.

The calibration trailer was firstly introduced at EFTF 2012[282]. Its stability during the initial calibration campaign was verified by taking common-clock data at TimeTech before and after the trip to the metrology laboratories, and by triangle closures, which are based on the principle that the sum of calibrated links between three sites should be zero within the combined uncertainty.

We report on the current status of the calibration station and present the results of the calibration campaign, the uncertainty estimation, and comparisons to previous calibrations. Since the mobile station allows for a standardized and easily executable procedure at each laboratory, the systematic uncertainties are significantly below one nanosecond.

[*] Present address: Bureau International des Poids et Mesures (BIPM), Pavillon de Breteuil, F-92312 Sèvres Cedex, France.

[282] T. Feldmann, A. Balu, C. Molard, W. Schäfer, D. Piester, "State-of-the-Art Time Link Calibration with a mobile TWSTFT Station", Proc. EFTF, Gothenburg, Sweden, April 24-26, 2012.

IFCS-EFTF5-E2-3

Simulation Study for Commercial Time Transfer Service over Geostationary Satellite

Jacqueline Walker[1], Marco Genova[2]

[1]Department of Electronic and Computer Engineering, University of Limerick, Limerick, Ireland
[2]Mixed Processing Ltd, Office 301, Shannon Airport House, Shannon, Ireland

Email: jacqueline.walker@ul.ie

Over the last twenty years, many technologies and services have come to rely on the GPS for precise timing. However, concern is increasing about the wisdom of being reliant on a single timing solution[283] provided by a single country and because of the susceptibility of the GPS signal to unintentional interference, jamming and spoofing. There are several projects underway to develop similar systems, e.g. Galileo, or upgrade existing ones, e.g. GLONASS. There are also other approaches to timing transfer available: over optical media, using high power LF signals and over commercial satellite links. Timing transfer over optical media shows promising performance but requires the installation of a dedicated network infrastructure. High power, low frequency radio signals are an established solution but cannot easily cover such a wide geographical area as a satellite solution. Timing transfer over geostationary satellite has been pursued since the start of the satellite era[284], but a commercial timing service product of this kind is not yet available.

In the paper, we report on further development of our system for timing signal transfer from a precision reference clock using commercial satellite links[285]. The system will use the projected ephemeris information provided by the satellite operator and, with a set of master stations tracking the satellite position and using TWTFT measurements to synchronize their clocks, data transmitted with the reference timing signal will allow slave stations to adjust the timing signal, compensating for the satellite motion and other uncertainties in the path delay. Using projected ephemeris data and comparing that data in real time with measurements which themselves are affected by other sources of delay is a challenging task when the goal is timing signal transfer with no more than 100 ns of jitter peak-to-peak at the receiving stations. Analysis has focused on quantifying the impact of errors in satellite ranging on the satellite position calculation. Numerical evaluation of the error expressions suggests that range errors would have to be less than 50 m to achieve the desired performance.

We will report on a simulation of the full system implementation with three master stations, including models for the master station clocks and TWTT measurements, using a Kalman filter to track the satellite position. The Kalman filter has been developed in the ECEF co-ordinate frame and uses real world archived satellite ephemeris data as the ground truth for the simulation incorporating models for extraneous delays such as atmospheric effects. Preliminary results from the simulation suggest that the range error goal could be met and results will be presented of a simulation study of the relationship between range measurement error and timing signal transfer performance.

---

[283] M. A. Lombardi, "Microsecond accuracy at multiple sites: is it possible without GPS?" IEEE. Instrum. Meas. Mag., vol. 15, no. 5, p. 14-21, 2012.

[284] D. W. Hanson and W. F. Hamilton, "One-way time synchronization via geostationary satellites at UHF," IEEE T. Instrum., vol. 20, no. 3, pp. 147-153, 1971.

[285] J. Walker and M. Genova, "Experimental and Simulation Study for Commercial Time Transfer Service over Geostationary Satellite", Proc. 44th PTTI Meeting, pp. 221-237, 2012.

IFCS-EFTF5-E2-4

Time Service through BD GEO Satellites

YUAN Haibo[1,3], YANG Fan[1,2,3], GUANG Wei[1,3]

[1]Natioanl Time Service center,CAS, Xi'an China
[2]University of Chinese Academy of Sciences, Beijing, China
[3]Key Laboratory of Time & Frequency Primary Standard, CAS, Xi'an China

Email: yuanhb@ntsc.ac.cn

The Space segment of BeiDou(Compass) global navigation satellite system consists of the 5 Group On Earth Observations (GEO) satellites and 30 Non-GEO satellites(Medium Earth Orbit (MEO) satellites and Inclined Geo Stationary Earth Orbit (IGSO) satellites). At present the Beidou system has begun to regional services based on the GEO satellites and the IGSO satellites. The range of services is covering China and neighboring countries and area. There are 5 GEO satellites on orbit. Users can receive the BeiDou system time which is steered to the UTC through the UTC(NTSC) by GNSS CV and TWSTFT. The time service performance of the BeiDou system is concerned by the time users. In this paper, the BeiDou system is introduced firstly, then the satellite time service and the data processing methods are analyzed, based on the analysis, the time service performance of the 5 GEO satellites is discussed, and the results show that Eliminating the ionospheric delay and reducing the impact of the troposphere and relativistic effects, the time service performance of the 5 GEO satellites are all stable and their accuracy is quite close to 10ns which can meet the needs of the vast majority of high-precision time users. Fig 1 is the result of the BDT-UTC(NTSC) by GEO5 between MJD 56293 and 56323.

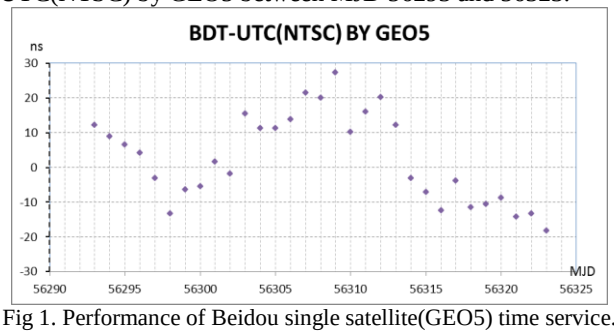

Fig 1. Performance of Beidou single satellite(GEO5) time service. The reference of BDT is UTC(NTSC) which is kept by Naional Time Service Center, Chinese Academy of Sciences.

IFCS-EFTF5-E2-5

Review of Two-way Satellite Time and Frequency Transfer for UTC and TAI generation

Z. Jiang, H. Konaté and W. Lewandowski

Time Department, Bureau International des Poids et Mesures (BIPM)
Pavillon de Breteuil F-92312, SÈVRES CEDEX, France

zjiang@bipm.org

The initial studies of time transfer through geostationary communication satellites started in the 1962 using the Telstar satellite. Earlier experiments continued with a number of other carriers. The technique of Two-Way Satellite Time and Frequency Transfer (TWSTFT)[286] started its experimental steps earlier than GNSS as a promising tool for accurate time and frequency transfer.

The Consultative Committee for the Definition of the Second (CCDS, at present Consultative Committee for Time and Frequency, CCTF) made a declaration in 1989 to encourage the use of TWSTFT and suggested the International Bureau of Weights and Measures (BIPM) to create a working group on TWSTFT. In 1992, several commercial satellite systems were available, and modems adapted for the technique were commercialized. Some ten UTC laboratories were equipped with different types of modems and other facilities for the clock comparisons with TWSTFT. On the other hand the International Telecommunication Union (ITU) approved in 1995 a recommendation fixing the standard data format for the TWSTFT operations.

The first TWSTFT link introduced in the UTC computation was between TUG in Austria and the PTB, and was published in the BIPM *Circular T* for July 1999. ınter-continental TWSTFT links between Europe, America and Asia were then established, as well as the continental links. TWSTFT become complementary to the already in use GPS time transfer. It presented the advantage of being independent from GPS, thus enhancing the robustness of the system of time links for UTC/TAI. The accuracy of TWSTFT rapidly proved to be better than that of GPS time transfer and this is still the case today. Meanwhile, since recent years the noise of GPS time transfer, represented by the type A uncertainty u_A, dramatically decreased with the use of GPSPPP for the UTC/TAI routine computations. From 2011 the combination of TWSTFT and GPSPPP is used for computing time links for UTC/TAI to take the advantages of both techniques.

In addition to its contribution to the computation of UTC/TAI, TWSTFT has also served to the validation of the GNSS techniques and methods incorporated in the past 10 years; examples are the GPS all in view, the GPSP3, the GPSPPP and the implementation of clock comparisons using GLONASS. This paper reviews fourteen years of contribution of TWSTFT to the maintenance of UTC and discusses its future developments, such as the use of the TWSTFT carrier phase and DPN. It also intends to render tribute to the pioneers of the TWSTFT.

Key words: UTC and TAI, Time and frequency transfers, TWSTFT

[286] In the earlier documents, the term TWSTT (Two-Way Satellite Time Transfer) was used.

Temperature Stabilization for MEMS

CLUB D

Tuesday, July 23 2013, 02:00 pm - 03:30 pm

Chair: **Jan Kuypers**
Sands 9, Inc.

IFCS-EFTF1-E3-1

We Know That MEMS is Replacing Quartz. But Why? And Why Now?

Aaron Partridge

SiTime Corp., Sunnyvale, CA/USA

Email: ap@sitime.com

MEMS-based oscillators were first produced commercially six years ago. Now MEMS is making significant incursions into what was once the exclusive territory of quartz. By the time this paper is delivered in July 2013, over 200M MEMS oscillators will have been shipped, with over 100M units expected to ship in 2013, at a growth rate of about 70% per year.

There are five fundamental drivers for the transition from quartz to MEMS: (1) Basic MEMS oscillators are maturing with decreasing phase-noise and decreasing power consumption in smaller packages, and with these improvements they are reaching further into common quartz applications. (2) Specialized MEMS oscillators are transitioning new markets, for example in applications requiring ultra-low power, sub-ppm precision, high frequency differential signaling, sub-picosecond integrated jitter, voltage control, digital control, spread, and output edge-rate control. (3) MEMS oscillators have shown higher reliability and lower failure rates than quartz oscillators. (4) MEMS oscillators have demonstrated lower electromagnetic, vibration, and acceleration sensitivity than quartz oscillators. (5) MEMS oscillators sell at lower price points than the quartz parts they replace.

Why is this transition happening now, rather than ten years ago or ten years from now? One answer is that the transition has been paced by the MEMS community developing the necessary high stability, high frequency, high Q, and high output resonators. A second answer is that MEMS oscillators rely on advanced circuit architectures, particularly leveraging fractional-PLLs and precision temperature sensors. And these specialized circuits have only recently become sufficiently small, low noise, power efficient, and accurate.

Looking forward, the depth and breadth of the applications served by MEMS oscillators will continue to expand, while the drivers favoring MEMS oscillators will further accelerate their adoption.

IFCS-EFTF1-E3-2
Lisha Shi[1], Gianluca Piazza2
[1]Electrical and Computer Engineering, Carnegie Mellon University, Pittsburgh, Pennsylvania, USA, [2]Department of Electrical and Computer Engineering, Carnegie Mellon University, Pittsburgh, PA, USA

Ion-Sliced Lithium Niobate on Silicon Dioxide for Engineering the Temperature Coefficient of Frequency of Laterally Vibrating Resonators

Lisha Shi, Gianluca Piazza
Department of Electrical and Computer Engineering, Carnegie Mellon University, Pittsburgh, PA, USA

Email: lishashi@andrew.cmu.edu, piazza@ece.cmu.edu

This paper reports, for the first time, on the demonstration of Laterally Vibrating Resonators (LVRs) based on Y-cut Ion-Sliced Lithium Niobate (LN) thin films on silicon dioxide (SiO_2) (Fig.1a-b). By adding a thermally grown layer of SiO_2 to the resonator stack, it is possible to engineer the temperature coefficient of the resonator and therefore ensure the use of these devices for applications where tight temperature specifications are required.

Prior demonstrations of LN LVRs[287, 2] have shown the capability of attaining a high K_t^2 *(> 20%)* and Qs of about 1,000, but exhibited a rather large and negative temperature coefficient of frequency (TCF) of about - 80 ppm/°C. Furthermore, they were built on a LN substrate with either BCB or SiO_2 as sacrificial layers, which required a wet etch step for the release of the resonator. In this work, the LN LVR is built on top of a SiO_2 layer and released from the underlying silicon wafer by dry etching in XeF_2. With the h_{LN} set at 420nm and h_{SiO2} at 1600nm, this first demonstration (Fig.1b) yielded TCF of + 11ppm/°C, + 18ppm/°C and + 20.4ppm/°C for devices respectively oriented at 80˚, 50˚, and 20˚ to the x-axis. The positive TCF clearly indicates the effect of the SiO_2, matches with FEM simulations, and offers evidence that TCF engineering is possible. Most importantly, these LN LVRs still exhibited high values of the electromechanical coupling, K_t^2, around 6.2% (see Fig.1c) and Qs in excess of 1,300 in air at 419.3 MHz (Fig.1d). By optimizing the relative values of h_{LN} and h_{SiO2} it is ultimately possible to attain devices with zero first order TCF.

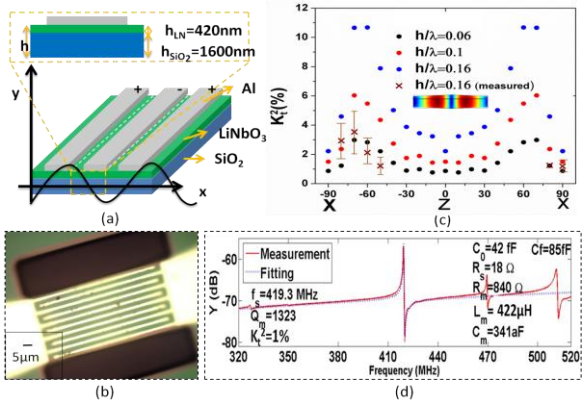

Fig.1 (a) Mock-up view of $LiNbO_3$-on SiO_2 MEMS micro-resonator (b) Optical image of a 511.8MHz LN LVR. The period of the interdigitated finger was set to be 6 μm with each metal line having a width of 2μm (c) The comparison of the averaged measured and simulated K_t^2 for LN on SiO_2 LVRs for various orientations. (d)The measured and fitted admittance response of LN on SiO_2 LVRs with Qs in

[1]R.Wang, S. Bhave, and K. Bhattacharjee "High K_t^2×Q, Multi-frequency Lithium Niobate Resonators" MEMS 2013(2013)

[2] S. Gong, L. Shi, G. Piazza, "High electromechanical coupling MEMS resonators at 530 MHz using ion sliced x-cut $LiNbO_3$ thin film", International Microwave Symposium (2012).

IFCS-EFTF1-E3-3

Experimental determination of the temperature dependency of elastic constants of degenerately n-doped silicon

Antti Jaakkola, Mika Prunnila, Tuomas Pensala, Panu Pekko, James Dekker

VTT Technical Research Centre of Finland, Espoo, Finland

Email: antti.jaakkola@vtt.fi

Degenerate doping of silicon has recently been found as an attractive method of passive temperature compensation in MEMS resonators, and it has been shown that with n-type doping one can change the typical silicon resonator TCF of about -30 ppm/K to zero, or even to positive values [1]. To optimize the temperature stability of a resonator, a designer needs to know the thermal dependencies of the elastic parameters c_{11}, c_{12} and c_{44}. However, published experimental material data has been scarce and limited to a maximum dopant concentration of $n=2\times10^{19}\text{cm}^{-3}$ [2]. In this work we determine silicon elastic parameters for five different n-dopant concentrations in the range of n = 1.7 … $7.0\times10^{19}\text{cm}^{-3}$.

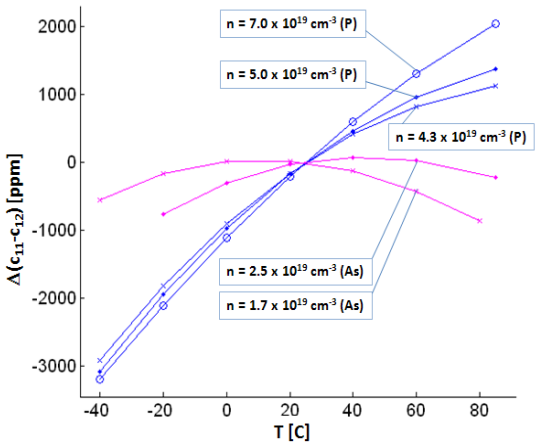

Fig. 88: Temperature dependence of the shear constant c_{11}-c_{12} for different dopant concentrations. Data with lowest two dopant concentrations is from arsenic doped wafers; phosphorus is the dopant for the remaining cases.

Extraction of the elastic parameters is based on the measurement of the resonance frequencies of electrostatically coupled bulk mode MEMS resonators as a function of temperature. The devices were fabricated on (100) SOI wafers. The set of resonators consists of two Lamé mode resonators aligned with 100 and 110 crystal directions, and five length extensional beam resonators spanning directions from 100 to 110. Since the functional dependency of the modal frequencies on the elastic parameters varies among the resonators, one can extract the elastic parameters from the frequency data.

We present the method of elastic parameter extraction, and show full experimental results for elastic parameters c_{11}, c_{12} and c_{44}. The temperature behavior of the shear constant c_{11}-c_{12} is shown in Fig. 1 for different dopant concentrations as an exemplary illustration of the data set. Reliability of the obtained results is discussed.

[1] T. Pensala, A. Jaakkola, M. Prunnila, J. Dekker, “Temperature compensation of silicon MEMS resonators by heavy p and n type doping”, IEEE International Ultrasonics Symposium, Orlando, FL, Oct. 2011, pp. 1952-1955.

[2] J.J. Hall, “Electronic Effects in the Elastic Constants of n-Type Silicon”, Physical Review, vol. 161, no. 3, 1967, pp. 756-761.

IFCS-EFTF1-E3-4

Temperature Dependence of the Elastic Constants of Degenerately Doped Single Crystal Silicon

Eldwin J. Ng[1], Chae Hyuck Ahn[1], Yushi Yang[1], Vu A. Hong[1], Thomas W. Kenny[1]

[1]Department of Mechanical Engineering, Stanford University, Stanford, California, USA

Email: eldwin@stanford.edu

Degenerate doping in silicon has been recently demonstrated to reduce the frequency-temperature dependence of MEMS resonators[288]. Doping induces a strain in the silicon crystal and causes a shift in the electronic band structure, which in turn affects the elastic properties of the material[2]. For monocrystalline silicon (an orthotropic material), the elastic properties[3] are characterized by c11, c12, c44. Empirical temperature dependences of the elastic constants (Tc11, Tc12, Tc44) can be extracted using at least three different resonators, as performed by Bourgeois for lightly doped silicon[4]: firstly, finite element analysis (FEA) is used to model the frequency dependence on the elastic constants for each resonator; next, frequency-temperature dependences are measured for fabricated resonators; putting these two pieces together, the temperature dependence of elastic constants can be extracted (Fig. 1). Double-ended tuning forks (DETF), breathe-mode double rings, and wineglass (second mode) disk resonator gyroscopes (DRG) were fabricated and encapsulated with epitaxial polysilicon in an ultra-clean environment free of contamination and native oxide. Frequency-temperature curves were measured for these resonators (Fig. 2), and the extracted temperature dependences of the elastic constants are listed in Table 1.

With the extracted material constants and FEA, the method can be reversed to predict the frequency-temperature dependence of any acoustic silicon resonator with the given doping. For validation, predicted and experimental values of the frequency-temperature dependence of the third resonant mode of the DRG (not used in the extraction) are compared (Fig. 3).

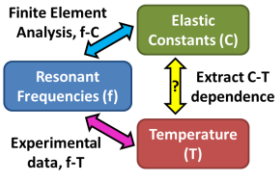

Fig. 89: Method used to extract the temperature dependence of the elastic constants.

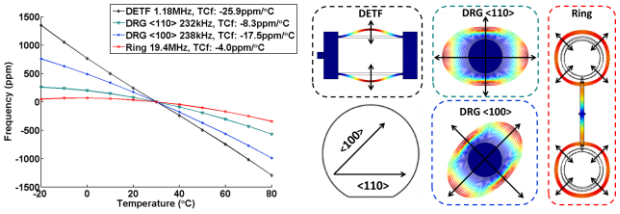

Fig. 2: Frequency-temperature dependences of various resonators fabricated with 8e19 cm^{-3} phospho

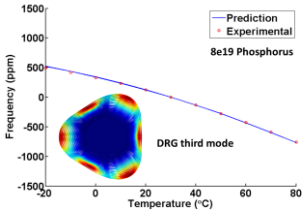

Fig. 3: f-T prediction compared against experimental data for the DRG's third resonant mode using the extracted values.

Table 1. First-order dependence of the elastic constants on temperature, extracted from experimental data and FEA models.

Dopant, Concentration	Tc11 (ppm/°C)	Tc12 (ppm/°C)	Tc44 (ppm/°C)
Boron, 1e20 cm^{-3}	-70.1	-140.1	+14.9
Phosphorus, 8e19 cm^{-3}	-45.1	-181.4	-65.1

This work was supported by the DARPA PNT program, managed by Dr. Andrei Shkel, contract #N66001-12-1-4260.

[1] A.K. Samarao, Trans. Elect. Dev. 59 (1), 2012.
[2] R.W. Keyes, Solid State Physics 20, pp. 37-90, 1968.
[3] M. Hopcroft, J. MEMS 19 (2), pp. 229-238, 2010.
[4] C. Bourgeois, Freq. Ctrl. Symp., pp. 791-799, 1997.

IFCS-EFTF1-E3-5

A Piezoresistive CMOS-MEMS Resonator with High *Q* and Low TC_f

Cheng-Syun Li[1], M.-H. Li[1], C.-H. Chin[1], C.-Y. Chen[1], Philip X.-L. Feng[2], and S.-S. Li[1]

[1]Nat. Tsing Hua Univ., Hsinchu, Taiwan, and [2]Case Western Reserve Univ., OH, USA

Email: s9835815@m98.nthu.edu.tw

Combining merits of quality (*Q*) factor greater than 15,000, temperature coefficient of frequency (TC_f) around -12.5ppm/°C, and operating power lower than 400μW all in a ***single*** device, a high frequency CMOS-MEMS bulk-mode resonator is demonstrated here via differential piezoresistive transduction[289]. This makes an excellent candidate for timing reference and frequency control applications. To attain ***the highest Q*** among reported CMOS-MEMS resonators, a dog-bone design (Fig.1a) has been adopted via two bulk-mode longitudinal vibrating beams which consist of only low-loss materials (*i.e.*, poly-Si and SiO_2) from a standard 0.35μm 2P4M CMOS technology. To achieve ***the better temperature stability*** as compared with those of other CMOS-MEMS resonators, a constant-resistance control approach[290] was implemented to enable an ovenized resonant element where the poly-Si heater and thermometer were both embedded inside the resonator structure, hence providing excellent thermal isolation, localized heating capability, and on-site/real-time temperature measurement. With much higher gauge factor and resistivity than that in our previous design[1], a poly-Si layer originally used for CMOS resistors was purposely chosen to serve as a piezoresistor for motion detection, thus exhibiting decent performance under ***sub-mW operation***. This technology is expected to pave the way for future single-chip oscillators with low power, high performance, and excellent thermal stability.

Fig.1a presents an optical micrograph of the fabricated resonator, showing its dog-bone structure with embedded electrodes (yellow) and piezoresistors (blue and pink) since the high-*Q* structural material (SiO_2) is transparent to visible light. With the differential piezoresistive transduction[1] to reduce the feedthrough, Fig.1b presents the measured frequency characteristics with clear resonance behavior under poly1 (original gate poly-Si) and poly2 (original resistor poly-Si) detections, both of which show *Q* > 15,000 and more than 20dB stopband rejection. It is worth noting that the poly2 sensing scheme indicates a low-power operation (only 363μW) and high electromechanical coupling coefficient due to its larger gauge factor than that of the poly1 scheme. Fig.1c presents the measured thermal stability using constant-current (CC), constant-voltage (CV), and constant-resistance (CR) controls of the piezoresistor (poly1), demonstrating the lowest TC_f to date in CMOS-MEMS resonators under the CR approach[2].

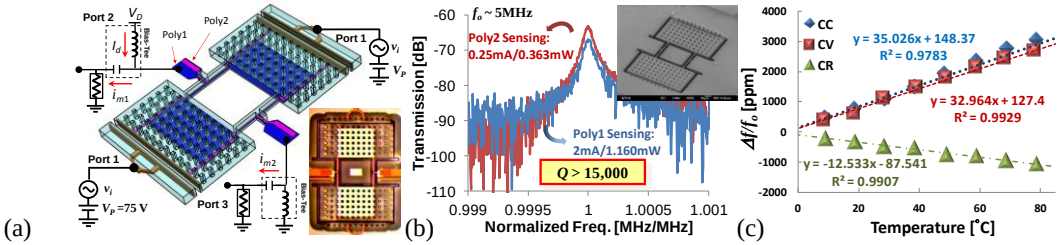

Fig. 1: (a) Schematic and OM views, (b) measured frequency response, and (c) measured thermal stability of the CMOS-MEMS bulk-mode resonator under differential piezoresistive transduction.

---

[289] C,-S. Li, *et al.*, "Capacitively-driven and piezoresistively-sensed ….," MEMS'12, Paris, France, pp.539-542, 2012.

[290] C.-C. Chen, *et al.*, "Enhancement of temperature stability via …," MEMS'13, Taipei, Taiwan, pp.765-768 , 2013.

Ion Clocks

CLUB H

Tuesday, July 23 2013, 04:30 pm - 06:00 pm

Chair: **Scott Diddams**
NIST

Yb^+ Single-Ion Optical Frequency Standard with Systematic Uncertainty at the 10^{-17} Level

N. Huntemann, B. Lipphardt, Chr. Sanner, M. V. Okhapkin, Chr. Tamm, E. Peik

Physikalisch-Technische Bundesanstalt, Bundesallee 100, 38116 Braunschweig, Germany

Email: ekkehard.peik@ptb.de

The electric octupole transition $^2S_{1/2}(F = 0) \rightarrow {}^2F_{7/2}(F = 3, m_F = 0)$ of the $^{171}Yb^+$ ion at 467 nm with a natural linewidth in the nHz range possesses a low sensitivity to frequency shifts induced by static electric or magnetic fields[291]. Because of the extremely small oscillator strength of the transition, its excitation requires high spectral power density. The required intensity introduces a significant light shift of the transition frequency. With a real-time extrapolation scheme that eliminates this shift, the unperturbed transition frequency has been realized with a fractional uncertainty of 7.1×10^{-17} and the frequency was measured as 642 121 496 772 645.15(52) Hz[1], where the uncertainty was dominated by the systematic uncertainty of the caesium fountain clock. Recently, we have implemented the Hyper-Ramsey excitation scheme (HRS)[292] with a pulse sequence that is tailored to produce a resonance signal that is immune to the light shift induced by the probe laser. In the HRS scheme, the effect of the light shift on the spectrum is compensated by introducing a frequency step of the probe light during the interrogation pulses. The experiments demonstrate a suppression of the light shift by four orders of magnitude and an immunity against its fluctuations[293].

For the operation as a frequency standard, a servo scheme using HRS is combined with an interleaved servo using Rabi excitation with the same probe light intensity. The frequency offset between the Rabi and HRS interrogations is taken to control the light shift compensating frequency step in the HRS. This ensures that slow variations of the light shift will not degrade its suppression. This method was applied in frequency comparisons between the $^{171}Yb^+$ single-ion clock and the Sr lattice clock of PTB. It has allowed us to perform a more precise measurement of the static quadratic Stark shift of the $^2S_{1/2} \rightarrow {}^2F_{7/2}$ transition. Together with improved knowledge of the thermal radiation emitted by the ion trap and its mounting structure, this will reduce the systematic uncertainty contribution of the Stark shift induced by blackbody radiation, which presently dominates the uncertainty budget.

This work is partly funded by the EMRP project SIB04 Ion Clock. The EMRP is jointly funded by the EMRP participating countries within EURAMET and the European Union.

---

[291] N. Huntemann, M. Okhapkin, B. Lipphardt, S. Weyers, Chr. Tamm, and E. Peik, "High-Accuracy Optical Clock Based on the Octupole Transition in $^{171}Yb^+$", Phys. Rev. Lett. **108**, 090801 (2012).

[292] V. I. Yudin, A. V. Taichenachev, C. W. Oates, Z. W. Barber, N. D. Lemke, A. D. Ludlow, U. Sterr, Ch. Lisdat, and F. Riehle, „Hyper-Ramsey spectroscopy of optical clock transitions", Phys. Rev. A **82**, 011804(R) (2010).

[293] N. Huntemann, B. Lipphardt, M. Okhapkin, Chr. Tamm, E. Peik A.V. Taichenachev and V. I. Yudin, "Generalized Ramsey Excitation Scheme with Suppressed Light Shift", Phys. Rev. Lett. **109**, 213002 (2012).

Control of the systematic shifts of the $^{88}Sr^{+}$ single-ion optical frequency standard at 2 parts in 10^{17}

Pierre Dubé, Alan A. Madej, and John E. Bernard

National Research Council of Canada, Ottawa, ON, Canada K1A 0R6

Email: pierre.dube@nrc-cnrc.gc.ca

Recently, our group has reported an evaluation of the systematic shifts on the $^{88}Sr^{+}$ ion clock transition frequency at the 2.3×10^{-17} level,[294] an order of magnitude lower than that of state-of-the-art cesium fountain atomic clocks.[295] This low uncertainty was achieved using a number of methods employed to measure, reduce, and even cancel the most important shifts that are known to affect the 5s $^{2}S_{1/2}$-4d $^{2}D_{5/2}$ clock transition frequency of the $^{88}Sr^{+}$ ion.

In our experiments, the center frequency of the *S-D* transition is determined by taking the average frequency of three pairs of symmetric Zeeman components specially chosen to connect to all the upper state sublevels. This effectively averages over the energies of the $^{2}D_{5/2}$ sublevels with the important benefit of a very high cancellation level of the electric quadrupole shift (EQS).[296] The uncertainty on the canceled EQS is estimated at $< 3\times10^{-19}$ in our system.[297] In addition, this method cancels the tensor part of the Stark shift caused by micromotion and other sources.

The ion micromotion at the trap frequency causes second-order Doppler and Stark shifts. These shifts are reduced to a level of 2.2×10^{-17} after minimization of micromotion along three mutually orthogonal directions. An additional suppression of these shifts is obtained by observing that the scalar Stark and second-order Doppler shifts have opposite signs for the $^{88}Sr^{+}$ ion and that they cancel each other when the trap is operated at a frequency of 14.39(25) MHz.[297] The suppression factor obtained is 28, determined by the uncertainty on the differential scalar polarizability of the *S-D* transition.[298] After minimization and with the trap operated at the special frequency, the uncertainty on the micromotion shifts is $\approx1\times10^{-18}$.

The blackbody radiation (BBR) shift uncertainty was estimated using measurements of the endcap trap electrode temperatures and a model to determine the field at the ion. The estimated uncertainty is 2.2×10^{-17}, primarily from that of the differential scalar polarizability.[297] The BBR shift is currently the largest source of uncertainty for the $^{88}Sr^{+}$ ion optical frequency standard. A detailed analysis of the systematic shifts affecting the $^{88}Sr^{+}$ *S-D* frequency[297] indicates that the total uncertainty is 2.3×10^{-17}.

We have also reported recently a measurement of the $^{88}Sr^{+}$ *S-D* frequency made over a 2-month period by comparison with a maser referenced to the SI second.[294] The frequency measured is 444 779 044 095 485.5 (9) Hz, with an uncertainty determined by the evaluation of the maser which had a fractional frequency uncertainty of 2×10^{-15}. The measured value was recommended by the Consultative Committee for Time and Frequency (CCTF) for an update of the 5s $^{2}S_{1/2}$-4d $^{2}D_{5/2}$ transition frequency of $^{88}Sr^{+}$ which is used as a secondary representation of the second.

---

294 A. A. Madej, P. Dubé, Z. Zhou, J. E. Bernard, and M. Gertsvolf, Phys. Rev. Lett. **109**, 203002, 2012.
295 J. Guéna *et al.*, IEEE Trans. Ultrason. Ferroelectr. Freq. Control **59**, 391, 2012.
296 P. Dubé, A.A. Madej, J.E. Bernard, L. Marmet, J.S. Boulanger, and S. Cundy, Phys. Rev. Lett. **95**, 033001, 2005.
297 P. Dubé, A.A. Madej, Z. Zhou, and J.E. Bernard, Phys. Rev. A **87**, 023806, 2013.
298 D. Jiang, B. Arora, M.S. Safronova, and C.W. Clark, J. Phys. B **42**, 154020, 2009.

IFCS-EFTF6-F1-3

Measurement of the optical frequency ratio between two clock transitions in a single ion of $^{171}Yb^{+}$

Steven King, Rachel Godun, Peter Nisbet-Jones, Helen Margolis, Luke Johnson and Patrick Gill

National Physical Laboratory, Hampton Road, Teddington, TW11 0LW, UK

Email: steven.king@npl.co.uk

Singly-ionised ytterbium-171 has two clock transitions that are currently under investigation as candidates for the redefinition of the SI second. In particular, the $^2S_{1/2} - {}^2F_{7/2}$ electric octupole transition has shown great promise. Two recent absolute frequency measurements of this transition at NPL[299] and PTB[300] are in good agreement, which demonstrates that this transition has potential to realise a reproducible optical frequency standard despite the previously limiting ac Stark shift that arises from the relatively high probe laser intensities required to drive a transition with a natural linewidth on the order of nanohertz.

In addition to its use as an optical frequency standard, this system also offers the intriguing possibility of measuring any present-day time-variation of the fine structure constant, α. By repeatedly measuring an optical frequency ratio between the electric octupole transition at 642 THz and the $^2S_{1/2} - {}^2D_{3/2}$ electric quadrupole transition at 688 THz, any variation in α is amplified[301] by nearly a factor of 7.

We will present our results from our first measurements of this optical frequency ratio. Two probe lasers are stabilized to high-finesse optical cavities with resulting fractional short-term instabilities near 1×10^{-15}, and are then further stabilized to their respective atomic transitions in a single ion in an interleaved manner. An optical frequency comb is then able to measure the ratio between the optical frequencies of these two stabilized lasers in real-time. We will discuss the various challenges that arise from a measurement performed in this manner, and in particular we will discuss the compromises that have to be made between various systematic shifts. Recent experimental upgrades will also be presented including a new, more reliable probe laser to drive the electric quadrupole transition, a distributed feedback diode (DFB) repumper laser to clear out the extremely long-lived $^2F_{7/2}$ level, and the successful implementation of automatic re-locking of many of the lasers in the experiment. We will also present the results of ongoing improvements that will reduce the systematic uncertainties associated with future measurements.

---

[299] S. A. King *et al*., "Absolute frequency measurement of the $^2S_{1/2} - {}^2F_{7/2}$ electric octupole transition in a single ion of $^{171}Yb^{+}$ with 10^{-15} fractional uncertainty", New J. Phys., vol. 14, 013045, 2012

[300] N. Huntemann *et al*., "High-accuracy optical clock based on the octupole transition in $^{171}Yb^{+}$", Phys. Rev. Lett., vol. 108, 090801, 2012

[301] S. N. Lea, "Limits to time variation of fundamental constants from comparisons of atomic frequency standards", Rep. Prog. Phys., vol. 70, p1473, 2007

IFCS-EFTF6-F1-4

The Optical Frequency Standard of Trapped and Cold $^{40}Ca^{+}$

H. Guan, [1, 2] Y. Huang, [1, .2] J. Cao, [1, 2] P. Liu, [1, 2] X. Huang, [1, 2] and K. Gao[1, 2, *]

[1]State Key Laboratory of Magnetic Resonance and Atomic and Molecular Physics

[2]Key Laboratory of Atomic Frequency Standards,Wuhan Institute of Physics and Mathematics, Chinese Academy of Sciences, Wuhan 430071, China

*Email: klgao@wipm.ac.cn[xv]

Progress on the development of the optical frequency standard based on single-trapped $^{40}Ca^{+}$ with a "clock" transition at 729 nm is described. A single Ca ion was trapped and laser cooled in a miniature Paul trap. The commercial Ti:sapphire laser systems at 729 nm were referenced respectively to the super cavities to meet the requirements of probing $4s\ ^2S_{1/2}$-$3d\ ^2D_{5/2}$ clock transition with ultra narrow linewidth. The 729 nm laser was locked to the clock transition by four points locking scheme. The overall systematic uncertainty of the $4s\ ^2S_{1/2}$-$3d\ ^2D_{5/2}$ clock resonance has been characterized to be at 10^{-16} level [1-2]. The absolute frequency of the clock transition is measured based on the GPS system. In our measurement, an optical frequency comb is referenced to a Hydrogen maser, which is calibrated to the SI second through the Global Positioning System (GPS). Using the GPS satellites as a link, we can measure the frequency difference of the two Hydrogen masers with a long distance, one in WIPM (Wuhan) and another in NIM (Beijing). The frequency difference of the Hydrogen maser in NIM (Beijing) and the SI second calculated by BIPM is published on the BIPM website every 1 month, with a time interval of every 5 days. By analyzing the experimental data obtained with a total averaging time of $> 2\times10^6$ s within 32 days, the absolute frequency of the $^{40}Ca^{+}$ $4s\ ^2S_{1/2}$–$3d\ ^2D_{5/2}$ clock transition is measured as 411 042 129 776 393.0 (1.6) Hz with a fractional uncertainty of 3.9×10^{-15}[2], which is adopted by the Consultative Committee for Time and Frequency conference (CCTF 19) in 2012.

IFCS-EFTF6-F1-5

Direct frequency comparison between a single Ca^+ clock and a Sr lattice clock

Kensuke Matsubara[1], Hidekazu Hachisu[1], Shigeo Nagano[1], Ying Li[1], Asahiko Nogami[1], Clayton Locke[1], Kazuhiro Hayasaka[1], Mizuhiko Hosokawa[1], Tetsuya Ido[1,2]

[1]Space-time standards laboratory, NICT, Tokyo, Japan, [2]JST-CREST, Tokyo, Japan

Email: ido@nict.go.jp

Comparison between independent frequency standards is the most reliable means to evaluate their reproducibility and stability. Optical frequency standards have a strong advantage in the speed of this comparison process, requiring less than 1,000 seconds to evaluate a fractional frequency difference at the 10^{-16} level of uncertainty. In contrast, state-of-the-art Cs fountain clocks operating in the microwave regime require more than six hours of integration time[302]. Optical frequency combs can be used to measure a frequency ratio as well as relative instability of optical clocks. Such a frequency ratio is equivalent to a measurement based on not the SI second but an optical frequency standard. Hence, precision measurements of frequency ratios are lately encouraged to support and confirm the validity of the metrology based on optical frequency standards. Frequency ratios can be also used in searches for temporal variation of fundamental constants[303].

We report frequency comparison of a $^{40}Ca^+$ $^2S_{1/2}$-$^2D_{5/2}$ with an ^{87}Sr $^1S_0$-$^3P_0$ lattice clock transition. The accuracy and the instability of the ^{87}Sr clock at NICT have been previously confirmed to be at the 10^{-16} level[304] and the absolute frequency of the Sr clock is consistent with those of other laboratories[305]. We therefore characterized the Ca^+ clock by comparison with the Sr clock. The frequency ratio measurement has shown that the fractional instability of the Ca^+ clock reaches parts in 10^{-16} in less than 1,000 s (see Fig. 1), with long term stability characterized as $\sigma(\tau) = 2.4 \times 10^{-14} / \tau^{1/2}$, consistent with the quantum projection noise limit derived from the Fourier limited spectral width of 26 Hz of the Ca^+ clock. Taking systematic uncertainties into consideration, the frequency ratio $f(Ca^+) / f(Sr)$ is determined with uncertainty of 2.3×10^{-15}, in agreement with independent absolute frequency measurements[306] of $^{40}Ca^+$ based on TAI link.

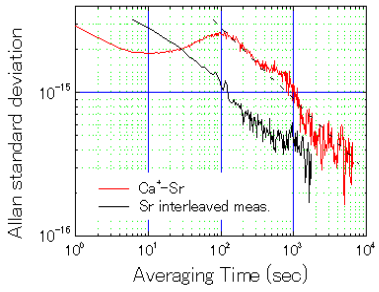

Fig. 90: Instability of the frequency ratio (red), limited by the instability of the Ca^+ clock. An interleaved measurement of the Sr clock indicates the instability shown by a black line.

[302] J. Guena, et al., "Progress in atomic fountains at LNE-SYRTE" IEEE Transactions on Ultrasonics, Ferroelectrics and Frequency Control, vol. 59, p. 391-420, 2012.

[303] J.-P. Uzan, "The fundamental constants and their variation: observational and theoretical status", Rev. Mod. Phys. vol. 75 p. 403-455, 2003.

[304] A. Yamaguchi, et al., "Direct comparison of distant optical lattice clocks at the 10^{-16} uncertainty", Appl. Phys. Express vol. 4 082203, 2011.

[305] A. Yamaguchi, et al., "Stability transfer between two clock lasers operating at different wavelengths for absolute frequency measurement of clock transition in ^{87}Sr", Appl. Phys. Express vol. 5 022701, 2012.

[306] K. Matsubara, et al., "Direct comparison of a Ca^+ single-ion clock against a Sr lattice clock to verify the absolute frequency measurement", Optics Express, vol. 20, p. 22034-22041, 2012.

Global Navigation Satellite Systems

CLUB E

Tuesday, July 23 2013, 04:30 pm - 06:00 pm

Chair: **Patrizia Tavella**
INRIM

IFCS-EFTF5-F2-1

Exploring the performance of GNSS frequency transfer

Petit G.[1], Kanj A.[1,2], Harmegnies A.[1], Delporte J.[2], Mercier F.[2], Perosanz F.[2]

[1] Time Department, BIPM, 92312 Sèvres, France
[2] CNES, 31401 Toulouse, France

Email: gpetit@bipm.org

Since many years, the time and frequency community has been using GNSS phase and code observations to compute time links. The BIPM has adopted the Precise Point Positioning (PPP) technique because it is relatively simple to operate while delivering state of the art results, thanks to the precise satellite orbits and clock products generated by the International GNSS Service.

In this paper, we investigate the time stability of PPP links for an averaging duration between a few hours up to tens of days, which directly provides the performance of such links for frequency transfer. Besides instabilities intrinsic to the receiving systems, the main limitations at these averaging times come from uncertainties in the phase ambiguity resolution and from the marginal effect of the simultaneous resolution of other parameters such as troposphere delay and station position.

We study several approaches aiming at improving the PPP results over long durations by ensuring a continuous processing over the whole interval under study rather than concatenating results obtained over short intervals. One approach is the use the Integer-PPP (IPPP) technique implemented by the CNES. IPPP is based on the resolution of the phase data integer ambiguities at the un-differenced level and needs precise GPS satellite orbit and clock products with a priori knowledge of individual satellite fractional-cycle biases as derived by the CNES-CLS IGS Analysis Center.

We compare the different GNSS phase and code solutions with one another and with independent Two-way time transfer results. In order to best assess their achieved performances, we then use the different methods to compute links between laboratories operating atomic fountains and study how the different results succeed in attaining the known frequency stability of the fountains. This test may be limited at short averaging time due to the sampling of the fountain data but is most efficient for averaging time above one day.

IFCS-EFTF5-F2-2

Dual-Frequency Time Transfer Unit for Comparisons of the Remote Clocks Using GLONASS and GPS Signals

P.P.Bogdanov, A.S.Bandura, M.G.German, K.S.Kol'chenko, O.E.Nechaeva

"Russian Institute of Radionavigation and Time" JSC, St.Petersburg, Russia

E-mail: niiss@rirt.ru

The method of using GLONASS and GPS signals is still being used for accurate comparison of the remote clocks.

Time Transfer Unit (TTU) using GLONASS and GPS signals developed at Russian Institute of Radionavigation and Time (RIRT) in 2002 was the first Russian device to realize this method. However, its abilities were considerably limited as it was designed on the base of 16-channel single-frequency GLONASS/GPS receiver.

In this connection, the new Time Transfer Unit (TTU-1) based on 36-channel dual-frequency GLONASS/GPS receiver was developed in 2011. TTU-1 is intended for determining the offset between local clock and GLONASS-time and GPS-time with the purpose of subsequent determining the mutual time and frequency offset between remote clocks, as well as for generating time scale signals synchronized to Russian National Universal Time Coordinated UTC(SU) or to GLONASS-time.

TTU-1 provides the following output data:

- time measurement results in the standard international format "cggtts_format_v2" including:
  L1C - L1 code measurements;
  L2C - L2 measurements;
  L3C - ionosphere-free combination of dual-frequency code measurements;
  CL3 - ionosphere-free combination of dual-frequency code and carrier phase measurements;
- measurements of the radionavigation parameters and digital information included into navigation message from SV in the standard international format RINEX.

Antenna box and receiver are calibrated during their manufacturing process. The calculated signal delays for GLONASS and GPS are accounted for then during the measurements processing. The special testing equipment including GPS/GLONASS signals simulator are used to calibrate the devices. The total error of the determined absolute signal delays is about 5 ns. Besides, the delay corrections are measured for each GLONASS frequency with the error no more than 1 ns.

Test results show that the accuracy parameters of the new TTU-1 are higher than the same characteristics of TTU equipment and TTS-3 и TTS-4 receivers, mostly when operating by GLONASS signals.

The improvement of time comparison accuracy is possible in post-processing mode with using a *posteriori* ephemeris and other data from GNSS information centers including Information/Analytical Center of "TSNIIMASH" Federal State Unitary Enterprise.

IFCS-EFTF5-F2-3

Advances in multi-GNSS time transfer

Defraigne P.°, Harmegnies A.*, Petit G. *

°Royal Observatory of Belgium, Brussels, Belgium
*BIPM, France

Email: p.defraigne@oma.be

Measurements from Global Navigation Satellite Systems (GNSS) are used since the eighties to perform precise and accurate Time and Frequency Transfer (TFT). Only the GPS constellation was used during the last 25 years, with some experiments based on GLONASS measurements. The GLONASS constellation is presently completed, the first four Galileo satellites are already operational, and the COMPASS system also provides signals that can be additionally used for time transfer. Increasing the number of satellites, and hence the number of observations, will reduce the noise level of the solution. However, such a combination requires the knowledge of some inter-system biases in the receivers and the existence of satellite clock products which can be expressed with respect to a common reference. This paper will propose recent advances in these combinations, focusing on GPS, GLONASS and Galileo.

IFCS-EFTF5-F2-4

Stability of GPS PPP link on the baseline of 270 km compared to glass fiber measurements

J. Nawrocki[*], P. Dunst[*], D. Lemański[*], P. Nogaś[*], P. Lejba[*], A. Czubla[**], R. Osmyk[**], P. Szterk[**]

[*]Polish Academy of Sciences, Space Research Centre, Borowiec Astrogeodynamical Observatory, Borowiec, Poland

[**]Time and Frequency Laboratory, Electricity Department, Central Office of Measures, Warsaw, Poland

Email: nawrocki@cbk.poznan.pl

Central Office of Measure (GUM) in Warsaw and Borowiec Astrogeodynamical Obserwatory (AOS) in Borowiec near Poznan are equipped with TTS-4 time transfer systems, GPS/GLONASS dual frequency receivers, lately calibrated for GPS C/A code during BIPM calibration campaign in 2010. Both laboratories, GUM and AOS, distant from each other by 270 km geographically, are, since February 2012, also connected by the optical fiber time transfer link[307] with stabilization of propagation delay at the level of about a few-dozen of picoseconds. This optical fiber link is fully calibrated for time transfer with total expanded uncertainty of about 0.6 ns, and its calibration can be easy updated in the case of the change in the optical path, or in configuration of transmitted signals. Glass fiber measurements, currently performed every 5 s, are not limited by satellites observation schedule, and are not disturbed by the changing conditions in the ionosphere as in satellite methods.

After the first stage of verification of operation of the optical fiber link between GUM and AOS, we have started to monitor stability and precision of GPS PPP time transfer link between our laboratories, using as a reference the results obtained from glass fiber measurements. This allows us not only to compare the stability of measurement results obtained with the usage of the both methods, but also to reduce the common bias and noise of the compared clocks by differential analysis. It is a very good method for improvement of the GPS PPP time transfer calculations and further development of the glass fibre method.

In this presentation, we plan to show and discuss the latest results of our measurements and analysis performed over the last year for UTC(PL)-UTC(AOS) glass fibre link and GPS PPP method.

[307] Ł Śliwczyński, P. Krehlik, A. Czubla, Ł. Buczek and M. Lipiński, "Dissemination of time and RF frequency via a stabilized fibre optic link over a distance of 420 km", Metrologia vol. 50, pp. 133-145, 2013.

IFCS-EFTF5-F2-5

Time and Frequency Transfer Using Satellite Based Augmentation System GAGAN

Petr Panek, Alexander Kuna

Institute of Photonics and Electronics, AS CR, Chaberska 57, 182 51 Prague, Czech Republic

Email: panek@ufe.cz

GAGAN (GPS - Aided Geo Augmented Navigation) is an Indian satellite navigation system which augments GPS and makes it suitable for safety critical applications. It is one of the Satellite Based Augmentation Systems (SBAS). GAGAN uses a geostationary satellite transmitting signals almost identical to the GPS signals thus it can be used for time and frequency transfer in similar way. In contrast to the European EGNOS, this system already supports the navigation function and it transmits signals both in L1 and L5 frequency channels. The signals are available in good quality in the central Europe area.

We used the GAGAN signals for an experimental common-view time transfer between IPE Prague and PTB Braunschweig which is a distance of 370 km. The stability of the measured time difference was limited by stability of the clock in IPE and could be considered TDEV(1 min) < 30 ps and TDEV < 250 ps for averaging intervals up to 1 hour. GTR51 time and frequency transfer GNSS receivers were employed at both sites.

We analyzed one-minute measurement data from a continuous one-day measurement. The L1 code measurement has markedly lower accuracy compared to a GPS common-view. This is caused by the rather narrow bandwidth of the SBAS signals in this frequency channel. The observed fluctuations can be described as white noise with standard deviation of 7 ns. The L5 code measurement provides much better precision. In this case we assessed the stability TDEV < 1.3 ns for averaging intervals from 1 min to several hours. Since the geostationary satellite moves just slightly towards the receivers, the observed variations caused by the multipath effect are very slow compared to GPS.

The results obtained from the carrier phase measurements are promising. The stability of the ionosphere free combination is TDEV(1 min) < 40 ps and for longer averaging intervals it follows the expected stability of the measured time difference. Interesting results followed from our comparison of the single frequency measurements and the ionosphere free combination where relatively fast fluctuations induced by ionosphere are obvious in the single frequency measurements. During the daytime, the amplitude of these fluctuations reaches 5 ns in the L1 frequency channel. This behavior is quite far from classical ionospheric delay models.

We believe that using GAGAN and other SBAS for permanent carrier phase frequency transfer could be ideal solution for continuous comparisons of precise frequency sources.

IFCS-EFTF5-F2-6

Preliminary Implementation of Time and Frequency Transfer by BDS

LIANG Kun[1], JIN Zhaofeng[2]

[1]Division of Time and Frequency Metrology, National Institute of Metrology, Beijing, China
[2]Beijing Hoyateq Science&Technology Co., Ltd, Beijing, China

Email: liangk@nim.ac.cn

Abstract: Since 27th Dec 2012, BeiDou Navigation Satellite System(BDS) Signal in Space Interface Control Document-Open Service Signal B1I (Version 1.0)[1] has been released. It mainly includes the system introduction, signal standards and navigation message, which defines the related contents of open service signal B1I between BDS and users terminals. Error correction and clock bias solution for BDS have been studied, and time and frequency transfer method by BDS has been developed by NIM(National Institute of Metrology, Beijing, China). Based on BDS OEM model, the original BDS observation has been acquired and the BDS C1 and P2 code time and frequency transfer has been implemented preliminarily after the difference between BDT(BDS system time) and GPST(GPS system time) is taken into account. To verify its performance and feasibility, the remote time and frequency transfer experiments and the CCD(Common Clock Difference) experiments have been implemented, using the two BDS receivers and the other GPS receivers including IMEU, IMEN and IMEW sites(NIMTFGNSS-1[2] receivers), IMPR and BJNM sites(Septentrio PolaRx2eTR and PolaRx3eTR receivers respectively) and IMEJ site(Dicom GTR50 receiver) of NIM located at NIM. The stability and accuracy of BDS time and frequency transfer have been evaluated. The long baseline results characterize that the remote transfer performance of BDS time and frequency transfer is comparable with GPS(Global Positioning System). The standard deviation of the BDS C1 code CCD results using AV(All-in View) method could be about 3 ns with one day measurement. In the near future, using BDS post, near real-time or real-time precise ephemeris products, BDS carrier phase time and frequency transfer will be studied and applied at NIM.

References:

2. China Satellite Navigation Office, “BeiDou Navigation Satellite System Signal In Space Interface Control Document Open Service Signal B1I (Version 1.0),” 2012
3. LIANG Kun, ZHANG Aimin, GAO Xiaoxun,WANG Weibo, NING Dayu， ZHANG Side, “Study and Development of a New GNSS Receiver for Time and Frequency Transfer,” Proc. of EFTF 2012, pp. 529-536, 2012.

Wireless Sensors

CLUB D

Tuesday, July 23 2013, 04:30 pm - 06:00 pm

Chair: **Leonhard Reindl**
University of Freiburg

An Integrated SAW Sensor with Direct Write Antenna

Mark W. Gallagher[1], William Smith[2], Donald C. Malocha[1]

[1]Deparment of Electrical Engineering and Computer Science,
University of Central Florida, Orlando, FL 32816
[2]MesoScribe Technologies Inc., St. James, New York 11780

Email: MGallagher@knights.ucf.edu

This paper presents a wafer-level integrated SAW sensor using conventional thin-film fabrication for the SAW, and the direct write of a thicker dissimilar metal for the antenna. Previous proof-of-concept results using thin antenna films demonstrated the feasibility of planar device integration, but had limited interrogation range.[308] For the first time, a direct write process is utilized to deposit the antenna conductor onto the SAW substrate, providing ease of fabrication, optimal film thickness, and superior adhesion. Shown in Figure 64, the automated thermal spray process selectively deposits conductive or dielectric films onto a CAD defined area for rapid, conformal fabrication, allowing sensor integration on a range of surfaces. Results presented will show an increase in range, compared to previous work, through an improved low loss design.

Using the direct write process, shown in Figure 64, 15 μm thick copper is 'written' onto lithium niobate without a mask. Thick antenna traces lower antenna resistive losses, because of increases in conductivity and decreased skin depth effects. The traces adhere well to the 80 nm aluminum SAW transducer pads that are patterned previously by a traditional photolithographic process. The process allows multiple metal levels, trenching, and trimming, for optimum design and fabrication of research or a commercial product. The updated design yields three devices on a 76 mm wafer and requires no mechanical bonds; bond free devices are ideal for demanding environmental sensors.

Antenna gain and bandwidth trade-offs must be made to the integrated design to meet device size and system performance requirements. The design of a 915 MHz meandered dipole antenna with low mismatch loss and maximized radiation efficiency over an 8% SAW fractional bandwidth is demonstrated. Experimental performance results of antennas fabricated on standard FR4 and on-wafer by electroplating or direct write process will be contrasted. Temperature sensors are fabricated on YZ-$LiNbO_3$ and simultaneous operation, over temperature, in a multi-sensor system will be demonstrated wirelessly at several meters. The integration of SAW and direct write technology offers a multitude of opportunities for new sensor and communication system embodiments.

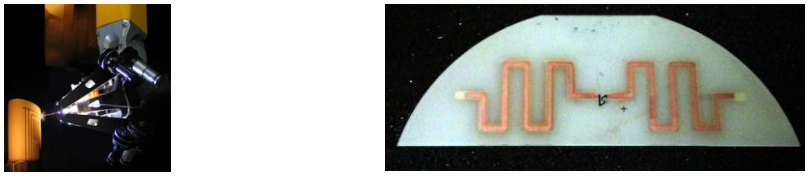

(a) (b)

Figure 91: (a) The automated direct write robot printing to a part. (b) An example of a 915 MHz SAW sensor and direct write dipole antenna integrated onto a 76 mm Y-cut lithium niobate wafer.

[308] M. W. Gallagher, B. C. Santos and D. C. Malocha, "Wireless wideband SAW sensor - antenna design," in *IEEE Int. Frequency Control Symp.*, Newport Beach, CA, 2010, pp.291-296.

IFCS-EFTF4-F3-2

Ultra-Wide-Band SAW sensors and tags

Lamothe Marc[1], Plessky Victor[2], Ostertag Thomas[3], Friedt Jean-Michel[1]

[1]Temps-fréquence, Femto-st institute, Besancon, France
[2]GVR Trade SA, Gorgier, Switzerland
[3]RSSI GmbH, Geretsried, Germany

Email: marc.lamothe@femto-st.fr

SAW tags and sensors often operate in 2.45 GHz ISM band with relatively narrow Band=82.5 MHz available there. The characteristics of SAW tags and sensors can be radically improved due to the possibility to use ultra wide band (UWB) frequency range [1]. Wide band means large bit capacity ***B*T*** with even decreased size of the device. In this work we develop prototype devices operating in 2000MHz- 2500MHz UWB frequency range. First measurement results with new UWB reader will be reported.

A few different SAW sensor devices for operation in the UWB were designed, manufactured and tested. The test devices included chirp LFM IDT, wide band reflectors. For simulation of devices FEM/BEM software "FEMSAW" (homemade software) was used. The UWB reader operating in continuous wave radar regime was developed and manufactured. The current reading distance is about 1 meter but this distance should be increased.

The first remote measurements has shown that we get compressed RF pulses of about 2 ns duration (Fig.1), including unique RF pulse of a few sinusoids with amplitude modulation. Due to this many advantages can be obtained:

- the precise measurement of the pulse position is possible by correlation methods, avoiding the phase ambiguity problem. The precision of the temperature definition of 1 °C can be obtained. Only 2 reflectors are necessary for such a sensor.
- The correlation method works even in multi-path environment with strong reflections form metal objects
- The short compressed pulses allow measuring a number of sensors simultaneously just separating them in time (TDMA). Figure 1 shows 2 sensors measured simultaneously, each device including 3 reflectors.
- For the tag application in theory at least 100 tags can be identified simultaneously in a limited temperature range $\Delta T < 100°C$. For such limited number of tags there is no "collision" problem.

The measurements are currently under way. The radiated power level will be estimated and the reading distance for the signals satisfying the US UWB standatds will be determined.

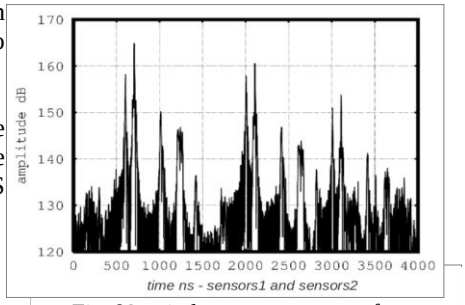

Fig. 92: wireless measurement of two sensors.

IFCS-EFTF4-F3-3

A Wireless Langasite Resonant Electrical Field/Voltage Sensor

Haifeng Zhang[a] and Tinghui Fan[b]
[a]Department of Engineering Technology, University of North Texas, Denton, TX, 76207
[b]Department of Electrical Engineering, University of North Texas, Denton, TX, 76207
Email: haifeng.zhang@unt.edu

Abstract

Langasite ($La_3Ga_5SiO_{14}$), a promising new piezoelectric crystal, has attracted interest from piezoelectric communities around the world for its superior behavior such as having a high Q, stable frequency-temperature behavior, high electrical-mechanical coupling coefficient and no phase transition to a high temperature form. Langasite resonators are generally more sensitive to electrical fields than quartz resonators as they have higher piezoelectric coefficient [1], which is ideal for high accuracy electrical field sensor applications in harsh environments. This article presents a system for a wireless langasite resonator electrical field sensor. The system uses frequency conversion techniques to convert the sensor's ultrasonic signal to a microwave signal in order to transmit the signal wirelessly without digitization. The sensor is able to transmit the ultrasound signal by using passive components that modulate and transmit the full waveform. A special circuit is designed to apply the high voltage on the langasite resonator without causing damage to other instruments. The wireless transmission system was tested using a doubly rotated plano-plano langasite resonator (YXlw)θ/Φ 45°/85° operating on its third overtone (6.304844 MHz) as its sensor. Wireless system data obtained using a network analyzer was compared with similar wired system data. The electric field-frequency effect was measured for both wired and wireless configurations. The result shows a good agreement between the wired and wireless signals (Fig.1). The demonstrated system has a potential for high voltage/electrical field sensing applications in harsh environments.

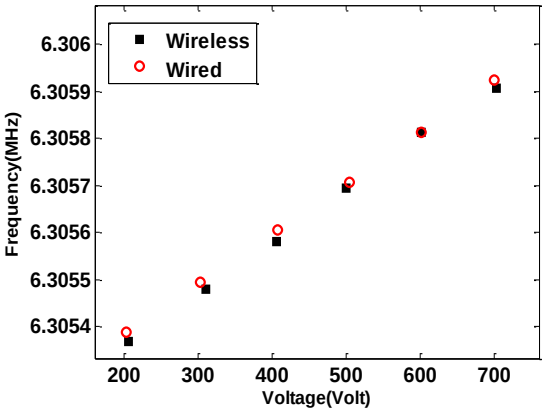

Fig. 1. The measured frequency-voltage relation for the doubly rotated langasite resonator (YXlw θ/Φ 45°/85°).

[1] H. Zhang, J. A. Turner, J. S. Yang, and J. A. Kosinski, "Electroelastic effect of thickness mode langasite resonators," *IEEE Trans. Ultrason. Ferroelectr. Freq. Control.*, vol. 54, no. 10, pp. 2120-2128, 2007.

IFCS-EFTF4-F3-4

Resonant SAW Torque Sensor for Wind Turbines

Victor Kalinin[1], Arthur Leigh[1], Alexander Stopps[1], Estefania Artigao[2]

[1]Transense Technologies plc, Bicester, Oxon., UK
[2]Brunel Innovation Centre, Brunel University, Cambridge, UK

Email: victor.kalinin@transense.co.uk

Wind farms are at the moment one of the fastest growing sources of renewable energy. However, the cost of electricity generated by offshore wind turbines is still noticeably higher than that for fossil fuel power plants, and maintenance cost is an important contribution to it. Up to 80% of this cost is associated with unexpected failures of rotating components that could be prevented by predictive and corrective maintenance based on adequate condition monitoring systems. Currently they mainly include vibration, temperature and oil debris sensors but there is also a clear demand for sensing torque. That would allow a more accurate estimation of load on rotating parts, correlation of this load with the data obtained from other sensors and overload protection.

At the moment torque sensors used on wind turbines are mostly realized with strain gauges but the latter are difficult to apply, require telemetry system for signal transmission and non-contact power supply, they are expensive and used mainly at the development stage rather than for continuous load monitoring. The aim of this paper is to present a batteryless non-contact SAW torque sensor suitable for easy after-market installation on the high-speed shafts of wind turbine gearboxes.

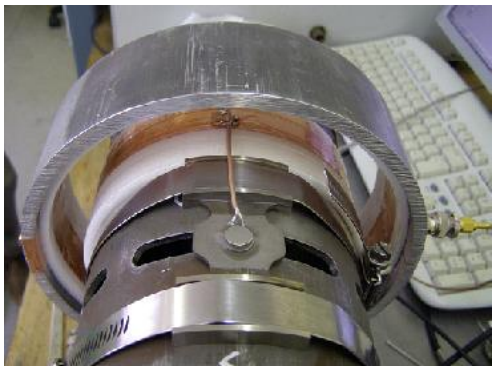

Fig. 93: Torque plate transducer with the SAW resonant sensing element installed on test shaft and connected to a large diameter RF coupler.

Resonant SAW torque sensors have been developed for automotive industry[309] but in this case the SAW die is attached by an adhesive directly to the surface of a relatively small part that can be cured in an oven. Dimensions of the wind turbine gearbox high-speed shafts are too large for curing them in ovens. A novel design of a torque plate transducer with the SAW sensing element is proposed that allows easy clamping of it on the surface of a large shaft. The main design issue is repeatability of the sensor readings and minimization of the hysteresis associated with a state of the interface between the shaft and the transducer. Another issue is a design of the RF rotary coupler with a large 20 mm gap between the rotor and the stator that would tolerate vibrations of the shaft and provide wireless resonant frequency measurements insensitive to the angular position of the shaft and its radial and axial movement. The use of a specially designed test shaft for calibration of the sensor within the temperature range from +20°C to +85°C is discussed in the paper. The achieved accuracy of the sensor tested after calibration is approximately 1% of the full range that is ±5 kNm. Installation of the sensor on the 750 kW NEG MICON 48 wind turbine is also discussed.

[309] V. Kalinin. "Wireless physical SAW sensors for automotive applications", Proc. IEEE Int. Ultrason. Symp., pp. 212 – 221, 2011.

IFCS-EFTF4-F3-5

High-overtone Bulk Acoustic Resonator as passive sensor acting a buried cooperative target interrogated by Ground Penetrating RADAR.

J.-M Friedt[1], A. Saintenoy[2], T. Baron[3], E. Lebrasseur[3], T. Laroche[3], S. Ballandras[3], M. Griselin[4]

[1] SENSeOR, Besançon, France
[2] IDES, UMR CNRS 8148, Université Paris Sud, France
[3] FEMTO-ST Time & Frequency department, UMR CNRS 6174, Besançon, France
[4] ThéMA, UMR CNRS 6049, Université de Franche Comté, Besançon, France

Email: jmfriedt@femto-st.fr

Acoustic transducers have demonstrated superior capabilities when used as passive sensors interrogated through a wireless radiofrequency (RF) link. However, exploiting these devices has been associated with dedicated hardware.

In this presentation, we consider acoustic sensors as passive cooperative targets to Ground Penetrating RADAR (GPR), one particular type of impulse mode ultrawideband characterization instrument widely used for geophysical purposes. Because acoustic resonators and delay lines only operate in a single frequency band defined by the spatial periodicity of the interdigitated transducer, one particular transducer can be probed by only one associated GPR operating in the same frequency bands.

Various RADAR frequencies are used for various applications as a trade off between penetration depth of the electromagnetic wave and spatial resolution: the higher the operating frequency as defined by antenna dimensions, the shallower the penetration depth but the better the spatial resolution. Our objective here is to demonstrate the use of High-overtone Bulk Acoustic Resonators (HBAR) as GPR cooperative targets compatible with multiple frequency bands.

HBAR is a bulk acoustic wave transducer in which a stack of piezoelectric substrate acting as the active layer (conversion from electromagnetic to mechanical wave) and a thick substrate (low acoustic loss medium) are combined to generate a comb of modes in the frequency domain. Since the Fourier transform of a frequency comb is a comb of reflections in the time domain, the impulse response of such a transducer is a series of echoes whose delay is representative of the acoustic velocity. If substrate orientations are selected to exhibit strong dependency with a given physical property, measuring the delay between echoes allows for the measurement of this quantity.

A same HBAR transducer has been interrogated using a commercial, off the shelf Malå RAMAC CUII GPR unit operating at 100 and 200 MHz ranges (the hardware remains the same and the operating frequency is selected by changing the length of the dipole antenna fitted to the emitter and receiver units). The temperature of the transducer is extracted from a cross-correlation between adjacent echo signals, yielding a measurement insensitive to environmental conditions other than the quantity under investigation (e.g distance between RADAR and sensor). We thus demonstrate the compatibility of acoustic transducers – either for identification or measurement purposes – as buried sensors with virtually infinite life expectancy once installed in environments unsuitable for battery replacement (civil engineering structures, concrete curing and stress, soil temperature measurement or stress measurement in the case of moving environments such as glacier or landslides).

IFCS-EFTF4-F3-6

Passive Wireless Surface Acoustic Wave CO_2 Sensor for Geological Sequestration Sites Monitoring

Yizhong Wang, Minking K. Chyu, Qing-Ming Wang*,

Department of Mechanical Engineering and Materials Sciences, University of Pittsburgh, Pittsburgh, PA, USA

Email: qiw4@pitt.edu

Geological sequestration, where the CO_2 was collected and dumped into the mines and oil fields deep under ground, has attracted lots of attention. There is urgent need for developing a sophisticated system that can monitor the ground leakage in those remote sequestration sites. Surface acoustic wave sensor equipped with on-chip sensitive layer is the best choice[310] for low cost wireless monitoring of sequestration sites leakage monitoring with minimum power consumption.

Surface acoustic wave sensor with delay line structure was adopted. The sensitive layer was initially composed of carbon nanotube (CNT) and polyimide (PI). CNT was chosen due to its high surface volume aspect ratio and chemical stability. PI was used to promote sensor performance in harsh environment.

Test of PI based nanocomposite showed less than 0.4% resistance increase over pure CO_2. Based on sensor frequency dependence on film conductivity, this will cause about 10ppm frequency change. Polyethyleneimine (PEI) was then used for its better chemical reaction between CO_2 gas molecule and CNT. The gas response for the new nanocomposite was about 10% resistance increase under pure CO_2, which gave an estimated 1000ppm frequency change. The fabricated sensor frequency change was around 300ppm for pure CO_2. The lowest detection limit of the sensor is 1% gas concentration, with 36ppm frequency change.

With paralyne packaging, the sensor frequency change on humidity reduced to less than 100ppm from over 1000ppm for unprotected sensor while maintaining the same gas sensing performance. Wireless module was tested and showed over one foot transmission distance at preferred parallel orientation.

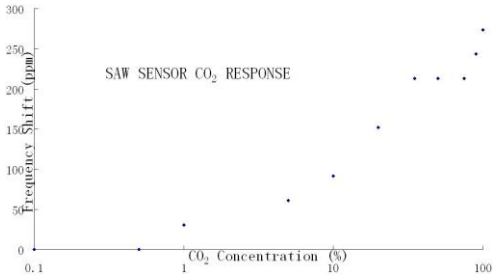

Fig. 94: Sensor response to CO_2 with various concentrations.

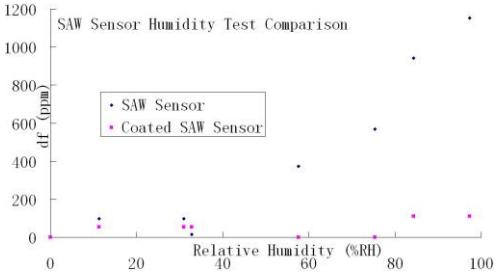

Fig. 95: Sensor response to different relative humidity levels for sensors with and without parylene packaging.

[310] Wen Wang, et al, Wireless surface acoustic wave chemical sensor for simultaneous measurement of CO_2 and humidity. J. Micro/Nanolith. MEMS MOEMS. Vol.8(3),pp.031306.1-6. Jul–Sep 2009.

IFCS-EFTF Awards and Plenary Talk

CH

Wednesday, July 24 2013, 08:30 am - 10:00 am

Chair: **Gaetano Mileti**
Université de Neuchâtel

Plenary III-1

Chip-scale atomic clocks

CLUB E

Wednesday, July 24 2013, 10:30 am - 12:00 pm

Chair: **Miao Zhu**
Agilent Technologies

Spatially Resolved Measurement of Relaxation Times in a Microfabricated Vapor Cell

Andrew Horsley[1], Guan-Xiang Du[1], Matthieu Pellaton[2], Christoph Affolderbach[2], Gaetano Mileti[2], and Philipp Treutlein[1]

[1]Departement Physik, Universität Basel, Switzerland
[2]Laboratoire Temps-Fréquence, Institut de Physique, Université de Neuchâtel, Switzerland

Email: andrew.horsley@unibas.ch

Microfabricated vapor cells are an important tool for atomic physics applications, showing particular success in miniaturised atomic clocks[311] and DC electromagnetic field sensing[312]. As a new application, imaging of microwave magnetic fields using a vapor cell has recently been demonstrated by our group[313]. A thorough knowledge of the properties of a cell is prerequisite to precision measurements. For microfabricated cells and imaging applications, the spatial dependence of relaxation times and excitation fields are of particular importance. We present the spatially resolved characterisation, performed using time-domain Ramsey and Rabi measurements, of a 5 mm diameter, 2 mm thick microfabricated cell, filled with ^{nat}Rb and 80 mbar of N_2 buffer gas[314].

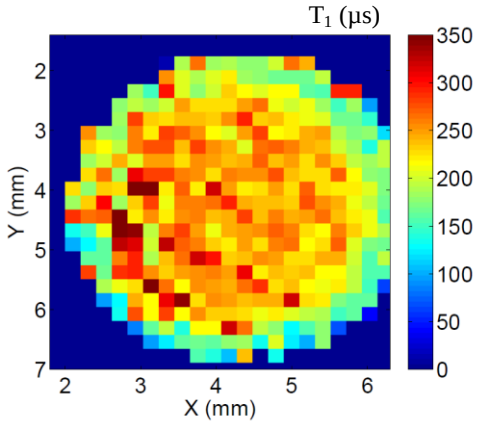

Fig. 96: T_1 times across the cell, obtained using relaxation in the dark, at a cell temperature of 90°C. Lifetimes are longer in the centre of the cell, where the effects of destructive Rb-wall collisions are minimised.

Atomic relaxation is described by the T_1 and T_2 times, representing the population and coherence lifetimes, respectively. The dominant relaxation mechanisms in a vapor cell are Rb-wall, Rb-buffer gas and Rb-Rb collisions. The coherence lifetime is also limited by inhomogeneities in applied static and microwave magnetic fields. Both lifetimes can be obtained in a single time-domain Ramsey measurement.

We characterise T_1 and T_2 relaxation in the cell as a function of position, performing Ramsey measurements as we scan a narrow laser beam across the cell. We also probe the homogeneity of our applied static and microwave fields using Rabi sequences. In addition we have implemented an imaging technique, whereby a CCD chip is used to perform measurements over the entire cell simultaneously. As an example, figure 1 shows an image of T_1 times across our cell.

This work was supported by SNSF and ESA. We thank Y. Pétremand for filling the cell.

[311] Svenja Knappe et al "A microfabricated atomic clock" Appl. Phys. Lett. 85, 1460 (2004)

[312] D. Budker and M. Romalis, "Optical magnetometry" Nat. Phys. 3, 227 (2007)

[313] Pascal Böhi and Philipp Treutlein "Simple microwave field imaging technique using hot atomic vapor cells" Appl. Phys. Lett. 101, 181107 (2012)

[314] M Pellaton, C Affolderbach, Y Pétremand, N de Rooij and G Mileti, "Study of laser-pumped double-resonance clock signals using a microfabricated cell" Phys. Scr. T149 (2012)

The Integrated Swiss Miniature Atomic Clock

Jacques Haesler, Laurent Balet, Thomas Overstolz, Jörg Pierer, Rony Jose James, David Ruffieux, Steve Lecomte

CSEM SA, Jaquet-Droz 1, CH-2002 Neuchâtel, Switzerland

Email: jacques.haesler@csem.ch

The detailed design of the Swiss Miniature Atomic Clock (Swiss-MAC) was presented by CSEM at the 2012 EFTF[315]. This paper describes the progress made since then towards the realization of the integrated Swiss-MAC, by presenting a first prototype showing preliminary but very promising performances.

Miniature atomic clocks (MACs), typically based on the coherent population trapping scheme (CPT), show the promise of having miniature (< 1 cm^3) and low-power (< 100 mW) portable microwave frequency standards. The Swiss-MAC was designed to target such state of the art specifications. The current prototype integrates most of the desired functionalities, except the vacuum encapsulation of the physics package and its integrated temperature regulation. The prototype is powered by a separate PCB equipped with a battery pack and different monitoring and debugging inputs/outputs. The main PCB has dimensions of 50 x 100 mm^2 with 1/3rd of its surface populated by test jumpers and connectors.

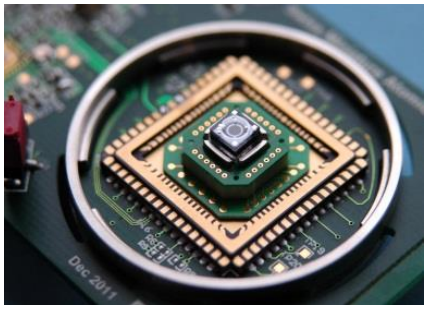

Fig. 97: Picture of the physics package developed for the Swiss Miniature Atomic Clock

The core physics package is realized by a stacking of PCB layers (Fig. 1). It has dimensions down to 11 x 11 x 8.5 mm^3 (1 cm^3), including the functionalized atomic vapor cell with dimensions downsized to 4 x 4 x 1.6 mm^3 (26 mm^3). The core physics package is mounted in a commercial ceramic package for vacuum encapsulation. The resulting assembly is surrounded by an external Ø 42 mm magnetic shielding, the overall volume of the physics package reaching 22 cm^3. The Swiss-MAC prototype is controlled by means of a LabVIEW® interface communicating with an MSP430 microcontroller. The latter drives the 3rd generation of a dedicated proprietary ASIC, with built-in RF lock loop and laser lock loop, and with integrated laser bias current source, three temperature sensors, and four heating current sources.

The Swiss-MAC prototype is currently in its integration and test phase. The main lock loops could already be closed and preliminary frequency stability measurements were successfully be realized using an external miniature glass atomic vapor cell (100 mm^3). The results, reaching $\sigma_y = 3 \cdot 10^{-11}$ at one day integration time and an impressive $\sigma_y = 6 \cdot 10^{-11}$ at 1 s are very close to telecom specifications. Moreover, they confirm that our integrated electronics supports good short term frequency stability. Improvements and further tests are ongoing. The complete prototype will be fully characterized in 2013 and more results are expected for the conference.

[315] J. Haesler et al., "Swiss Miniature Atomic Clock: first prototype and preliminary results", European Time and Frequency Forum (EFTF), Gothenburg, April 2012.

Double resonance spectroscopic studies using a new generation of microfabricated microwave cavity

M. Pellaton[1], M. Violetti[2], C. Affolderbach[1], J.-F. Zürcher[2], A. Skrivervik[2], G. Mileti[1]

[1]Laboratoire Temps Fréquence (LTF), Université de Neuchâtel, Neuchâtel, Switzerland
[2]Laboratory of Electromagnetics and Acoustics (LEMA), EPFL, Lausanne, Switzerland

Email: matthieu.pellaton@unine.ch

Our research concerns a miniature vapor-cell atomic clock based on double-resonance instead of CPT[316], using a newly designed microwave resonator, the μ-LGR[317], and its dedicated micro-fabricated cell[318] (see Fig. 1). In this communication we present an improved version of the atomic resonator package using an ^{87}Rb cell and more detailed spectroscopic studies, including analysis of the main sources of medium and long term frequency instability.

Preliminary measurements show promising results. The Zeeman spectrum (see Fig. 2) demonstrates a clean and well controlled microwave field sustained by the resonator that is composed of a stack of planar electrodes. The determination of its field orientation factor[319] (FOF) gives an excellent value of 0.7.

After a first optimization step, a nearly 13% contrast signal with a FWHM of 3.8 kHz is obtained; this allows a shot-noise limit prediction of $2.8 \times 10^{-12}\ \tau^{-1/2}$. Fig. 3 shows the stability obtained using this signal, which is in good agreement with the predicted signal-to-noise limit of $7 \times 10^{-12}\ \tau^{-1/2}$. Long term stabilities issues such as light shift and temperature shift will also be discussed.

Acknowledgement: This work was supported by the Swiss National Science Foundation and the European Space Agency (ESA). We thank Y. Pétremand (EPFL, SAMLAB) for the cell fabrication, and F. Gruet, P. Scherler, and M. Dürrenberger (all from LTF) for their contributions to the realization of the hardware.

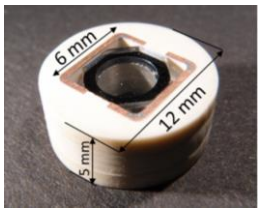

Fig. 98: Atomic resonator used for this study; internal cell dimensions are 4 mm diameter and 4.05 mm height.

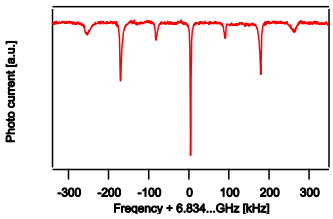

Fig. 2: Zeeman's spectrum at low RF power showing excellent field geometry.

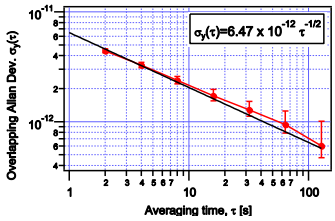

Fig. 3: Overlapping Allan deviation.

[316] T. Bandi et al., "*Double Resonance in Alkali Vapor Cells for High Performance and Miniature Atomic Clocks*", Invited talk of G. Mileti and Proc. IEEE IFCS 2012, pp. 1-6 (2012)

[317] M. Violetti et al., "*New Miniaturized Microwave Cavity for Rubidium Atomic Clocks*", Proc. IEEE Sensors 2012, pp. 315-318 (2012).

[318] Y. Pétremand et al., "*Microfabricated rubidium vapour-cell with a thick glass core for small scale atomic clock applications*", J. Micromech. Microeng. 22, 025013 (2012).

[319] C. Stefanucci et al., "*Compact Microwave Cavity for High Performance Rubidium Frequency Standards*", Rev. Sci. Instrum.83, 104706 (2012).

IFCS-EFTF3-G1-4

Short term noise investigation on a compact CPT clock

Danet Jean-Marie, Yun Peter, Guerandel Stephane, de Clercq Emeric

LNE SYRTE, Observatoire de Paris, Paris, France

Email: jean-marie.danet@obspm.fr

Towards the development of on-board atomic clock, alkali vapor cells clocks have shown that besides their robustness and relative simplicity, cell technology clocks are competitive with the cold atoms compact setups in term of stability[320] [321]. Among the different vapor cell clock technologies, the coherent population trapping (CPT) prototype developed at SYRTE offer an alternative where no microwave cavity is needed. The microwave is optically carried by the frequency difference between two lasers. Using crossed linear polarized beams and Ramsey temporal interrogation, signals with 15 % contrast and 125 Hz linewidth have been observed. Such a signal, combined with a noise at the shot noise limit would lead to sub $10^{-13}\ \tau^{-1/2}$ stability clocks. In this paper we report investigations on the noise processes currently limiting the short term stability of the clock at the level of $5.5\ 10^{-13}$ at 1s.

Five main noise sources are investigated: magnetic field, beam polarization, laser frequency, laser intensity and finally microwave phase. A contribution to the clock stability below 10^{-14} at 1s is shown for the two first ones. The effect of the optical frequency detuning has been measured and its conversion on the clock stability is under investigation. The influence of the laser intensity noise has been carefully studied, it is not negligible in the 10^{-13} range. A stabilization system has been implemented lowering the RIN of 15 dB down to -137 dB/Hz$^{-1/2}$ at 160 Hz. Finally the local oscillator noise contribution to the clock stability has been studied using the Dick formalism[322]. This aliasing effect, well understood for a two level system, had never been investigated for a three level one as the CPT. The numerical calculation, in good agreement with measurements, allowed us to deduce a phenomenological equation for the Dick effect in CPT, usable for others CPT clocks. The application of those calculations to our prototype pointed out the local oscillator as main noise source contributor, followed by the intensity noise. Solutions have been designed and will be implemented on our set-up. The latest results will be shown at the conference.

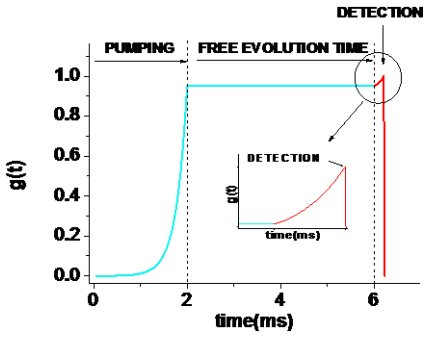

Fig. 99: Sensitivity function of a pulsed CPT clock. Pumping 2ms, Free evolution time 4ms, Detection: 25 µs, 200 µs after switching lasers on.

[320] S. Micalizio et al., Metrologia, vol 49, 425, 2012.

[2] F. X. Esnault et al., Phys. Rev. A, 82, 033436, 2010.

[3] G. J. Dick et al, in Proc. 19th Annu. Precise Time Time Interval conf., pp. 133–147, 1987.

IFCS-EFTF3-G1-5

Continuous and Ramsey spectroscopy of CPT resonances in Cs vapor cells with push-pull optical pumping

X. Liu[1], J-M. Merolla[1], S. Guérandel[2], C. Gorecki[1], E. de Clercq[2], R. Boudot[1]

[1] FEMTO-ST, CNRS, 32 avenue de l'observatoire 25044 Besançon cedex, France.
[2] LNE-SYRTE, Observatoire de Paris, CNRS, UPMC, 77 avenue Denfert-Rochereau 75014 Paris, France.

Email: rodolphe.boudot@femto-st.fr

We studied theoretically and developed an experimental set-up to detect high-contrast CPT resonances in buffer-gas-filled Cs vapor cells using push-pull optical pumping (PPOP) [1]. The laser source of the system is a distributed-feedback (DFB) diode laser tuned on the Cs D_1 line at 894.6 nm. A Mach-Zehnder electro-optic modulator (MZ EOM) is driven by a 4.596 GHz local oscillator to generate two first-order optical sidebands frequency-separated by 9.192 GHz. The dc electrode bias voltage of the MZ EOM is actively controlled using an original microwave synchronous detector technique to stabilize optical carrier rejection (~28dB) at the output of the EOM. A Michelson-like interferometer allows to generate the so-called push-pull interaction scheme [1]. The laser light is transmitted through a buffer-gas-filled Cs vapor cell. The laser power at the output of the cell is detected by a photodiode.

Using a continuous (CW) interaction regime, the effect of the laser intensity onto the clock resonance parameters (linewidth, contrast, ratio linewidth-contrast) was studied for 3 different cells, including a microfabricated Cs-Ne cell. The PPOP technique was found to be less efficient in microfabricated cells to obtain high-contrast resonances. For the 0-0 clock transition, CPT resonance contrasts as high as 78% were measured in a 5-cm-long cell with high operating laser intensities [2], i.e at the expense of a relevant CPT line power broadening.

To circumvent this issue, with minor changes of the setup, we demonstrated the detection of high-contrast and narrow CPT Ramsey fringes by combining PPOP and a temporal Ramsey-like interrogation. The major originality of the experiment is the use of the single MZ EOM both for optical sidebands generation and light intensity modulation for pulsed interaction. As in [3], atoms interact with an optical pulse train sequence where each pulse is used both CPT state pumping and atomic signal detection. Figure 1 shows typically obtained 166 Hz-linewidth Ramsey fringes with a contrast of 33% in a cm-scale cell. The impact of different experimental parameters (laser power, Ramsey time, CPT pumping time,..) on the CPT fringe will be reported. First frequency stability results of the system, operating as an atomic clock, in the CW regime and-or pulsed regime, will be reported at the conference.

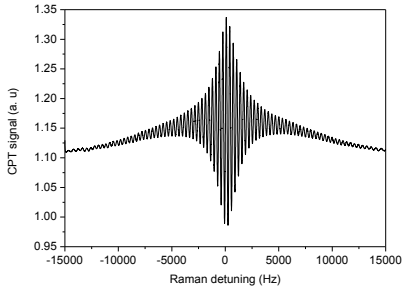

Figure 1: Ramsey fringes detected with PPOP.

[1] Y. Y. Jau et al., Phys. Rev. Lett. 93, 160802 (2004).
[2] X. Liu et al., Phys. Rev. A 87, 013416 (2013)
3 T. Zanon et al., Phys. Rev. Lett. 94, 193002 (2005).

IFCS-EFTF3-G1-6

A Digitized Atomic Clock Based on Transient Oscillation of Detuned Coherent Population Trapping

Zhong Wang*, Jianye Zhao, Dong Hou, Shuangyou Zhang, Mingyu Wan, Yeqing Li and Daiting Shi
School of Electronics Engineering & Computer Science, Peking University,
Beijing, 100871, P. R. China
*Email: zw@pku.edu.cn

We have implemented and experimentally verified a digitized atomic clock based on transient oscillation of detuned coherent population trapping (DCPT). In this design, the output standard frequency can be achieved by directly adding/subtracting the transient oscillation frequency of DCPT to/from the RF frequency, which is used for the pump laser modulation. We modulate the RF frequency with a 100 Hz square wave, and the RF frequency is set to alternate between the ground state hyperfine splitting frequency and the detuned frequency (a few kHz higher/lower). After the laser beam passes through the rubidium atom cell, a series of laser intensity oscillation will be detected when the RF frequency is detuned. This is the DCPT transient oscillation signal, and the frequency is theoretically equal to the detuning frequency.

In our DCPT atomic clock, the oscillation signal is detected, reshaped, and amplified, in order to facilitate the digital processing. Since the detuning frequency is 10^3 Hz, using typical digital processing with instability better than 10^{-6}, we can extract the oscillation frequency with 10^{-3} Hz accuracy, which allows us to acquire the detuning frequency of the RF oscillator accurate up to 0.1 Hz. When we use the RF oscillator signal as the reference frequency, and use the detected oscillation frequency to compensate for the RF frequency detuning as well as its shift with time, we will be able to obtain the DCPT atomic clock's standard frequency, which equals the two ground states hyperfine splitting frequency. In our preliminary experiments, the frequency instability of $1X10^{-11}/\tau^{1/2}$ (τ=1000s) has been achieved.

Comparing with traditional atomic clocks, This DCPT atomic clock does not require a circuit to lock the microwave frequency. This eliminates the instability and loose locking probability brought on by the phase locking loop, which makes the DCPT atomic clock more stable and more reliable, especially when used in harsh environments. In addition, the transient signal as the amplitude 3 to 4 times that of the CPT signal, which further benefits observation and analysis. This data processing section can be easily digitized and integrated. As a result, this scheme has great potential in the design and manufacture of miniature atomic clocks.

Space Missions and Clocks I

CLUB H

Wednesday, July 24 2013, 10:30 am - 12:00 pm

Chair: **Pierre Waller**
ESA

T2L2 : Five Years in Space

P. Exertier[1], E. Samain[1], Ph. Guillemot[2], S. Léon[2]
N. Martin[1], C. Foussard[1], C. Courde[1], J.M. Torre[1], M. Laas-Bourez[1]
[1]*OCA – Observatoire de la Côte d'Azur, Caussol, France*
[2]*CNES –French Space Agency, Toulouse, France*

pierre.exertier@oca.eu

Abstract

The Time Transfer by Laser Link (T2L2) experiment, developed by both the Observatoire de la Côte d'Azur (OCA) and the Centre National d'Etudes Spatiales (CNES), performs optical ground to space time transfer. Its principle is derived from laser telemetry technology with dedicated space equipment designed to record arrival time of laser pulses at the satellite. According to the capabilities of ground laser stations (laser operations are weather dependent) T2L2 permits to realize some links between distant clocks with expected time stability of a few picoseconds and accuracy better than 100 ps.

The T2L2 space experiment has been launch in July 2008 on-board the oceanography satellite Jason2. The International Laser Ranging network has been applied to track the satellite permanently, the Satellite Laser Ranging (SLR) technique being primarily used to support the precise orbit determination of the satellite. Thanks to T2L2, this tracking permitted to link SLR observatories (most of them equipped with GPS and some of them ultra stable clocks) and to promote time synchronization within intercontinental distances, as a service to the space geodesy community. In addition, several dedicated campaigns have been conducted from 2009 to 2013 to analyze carefully the T2L2 performances in terms of time stability and time accuracy, to realize some synchronization between remote ultra stable clocks and to perform microwave time transfer comparison such as with GPS. A detailed analysis of all the sensitive elements used in the measurement chain of the ground segment was recently done in some SLR stations in order to improve time stability and to reach the performance that was primary specified.

Through 5 years of activity supported by both CNES and OCA, this work highlights the performances of T2L2 and tries to enlighten the community on the advantages and disadvantages of space optical technique. It summarizes the results as qualitative and quantitative.

IFCS-EFTF5-G2-2

ACES MicroWave Link and Ground Segment

Hess MP, Helm A, Kehrer J, Schäfer W[+], Cacciapuoti L*, Much R*, de Parolis L*

Astrium Space Transportation, Friedrichshafen, Germany
[+] TimeTech, Stuttgart, Germany
* European Space Agency, ESTEC, Noordwijk, The Netherlands

Email: Marc-Peter.Hess@astrium.eads.net

Atomic Clock Ensemble in Space (ACES) is a mission using high-performance clocks and links to test fundamental laws of physics in space. The ACES payload is accommodated externally on the ISS Columbus laboratory. The ACES microwave link (MWL) will make the ACES clock signal available to ground laboratories equipped with atomic clocks and outfitted with dedicated MWL Ground Terminals.

The ACES Ground Segment will perform all monitoring and control tasks of the payload as well as of the word-wide distributed set of MWL Ground Terminals. The ACES Ground Segment collects all housekeeping and science data generated by the payload and ground terminals. The science raw data is processed into higher level data products that can be retrieved by a large science community.

We will give a brief status overview on the development of the ACES payload, where the integration of the flight model has started. The latest results obtained with the MWL will be discussed. Further we will detail the Ground Segment and MWL Ground Terminal design, which is presently undergoing acceptance testing with a focus on the description of the ACES science data products and underlying algorithms.

IFCS-EFTF5-G2-3

Towards a free space satellite to ground coherent optical link

P. Wolf[1], N. Chiodo[1], K. Djerroud[1], O. Acef[1], G. Santarelli[1]

E. Samain[2], J. Paris[2], B. Fleury[3], J. Montri[3], C. Petit[3]

[1]LNE-SYRTE, Observatoire de Paris, CNRS, UPMC, Paris, France
[2] Géo-Azur, Observatoire de la Côte d'Azur, CNRS, Grasse, France
[3]DOTA, ONERA, Chatillon, France

Email: peter.wolf@obspm.fr

Coherent links are based on the direct measurement of the optical phase rather than an amplitude modulation (pulses) as in conventional laser ranging. A limiting factor in this kind of links is the time variation of the refractive index of the terrestrial atmosphere due to the turbulence phenomenon that adds phase noise and intensity fluctuations both decreasing the performance of the link. Based on first results of a ground-ground coherent link[323] with 5 km propagation through the turbulent atmosphere we estimate the potential performance of such links for ground to space frequency comparison of clocks, showing that significant improvement with respect to existing methods can be expected, potentially down to 10^{-17} in relative frequency in less than 1000 s integration time.

Our next step towards this goal is the experimental realization of a link from a ground telescope to a low Earth orbit (LEO) satellite equipped with corner cube reflectors. We describe the requirements on the laser system for such a link (stability at the 10^{-13} level or below, whilst being tunable over 20 GHz) and present our solution for that challenge showing the performance of our laser system.

We describe first (unsuccessful) experiments that took place in November 2012 and January 2013 at the 1.5 m lunar ranging telescope of the Observatoire de la Côte d'Azur in collaboration with ONERA (French aerospace lab) who provides the adaptive optics bench. We discuss the encountered challenges and difficulties, and the implemented or planned solutions. Additional experiments will take place in 2013 before the conference, and depending on their outcome we might show first signals received from the satellite.

[323] K. Djerroud, et al., "Coherent Optical Link Through The Turbulent Atmosphere", Opt. Lett.., vol. 35, p. 1479-1481, 2010.

IFCS-EFTF5-G2-4

Design of the F&T Subsystem for ESA's Deep Space Antenna 3

Solana, A.[1], Schaefer, W.[1], Schwall, T.[1] , Ramos, M.[2] , de Vicente, J.[2], Froidevaux, S.[3] , Giordano, V.[4] , Grop, S.[5] , Dubois, B.[5]

[1] TimeTech GmbH, Stuttgart, Germany
[2] ESA-ESOC, Darmstadt, Germany
[3] T4Science, Neuchâtel, Switzerland
[4] Femto-ST, Besançon, France
[5] ULISS-ST, SAIC Université de Franche-Comté, Besançon, France

Email: Ainhoa.Solana@timetech.de

New concepts and techniques to try to improve the overall performance of Frequency and Timing subsystems were developed and applied to ESA's third Deep Space Antenna (DSA3), near Malargüe in Argentina.

Independent and well-controlled clocks room, together with an improved short term stability and phase noise lead the way into the introduction of a 100 MHz distribution system, maintaining the same level of performance at both ends of the cross-site link. Lower frequencies, such as 5 MHz and 10 MHz, were locally generated in each building from the 100 MHz source.

The introduction of a cryogenic cooled sapphire oscillator (in addition to the two redundant active hydrogen masers), accomplished to combine its good short term stability while remaining locked to one of the masers profiting of the maser's long-term performance.

The performance achieved after adaptation and optimization of the key elements of the F&T subsystem and the reduction of the thermal sensitivity, allowed distribution to the antenna site, at a distance of approximately 100m.

The system design and the results of final on-site acceptance tests are presented.

Fig. 100: CSO (Cryogenic Sapphire Oscillator)

IFCS-EFTF5-G2-5

Clock Composition by Wiener Filtering Illustrated on Two Atomic Clocks

Marek Peca[1,2], Vojtěch Michálek[1,2], Michael Vacek[1,2]

[1]Serenum, a. s., Beranových 130, Praha – Letňany, Czech Republic
[2]České vysoké učení technické v Praze, Břehová 7, 115 19 Praha 1, Czech Republic

e-mail: peca@serenum.cz

Clock ensembling, i.e. calculation of best time estimate given readings from multiple clocks, is a must for state-of-art timekeeping. Clock drift and jitter are usually modelled as colored noise, therefore a linear estimation is naturally the tool of choice. The crux of the matter is that unlike traditional estimation problems, the clock ensemble is both marginally stable (drifting) and partially unobservable (only time differences are measurable). Modifications of Kalman filter estimator to handle these conditions were made using special covariance matrix treatment[324,325].

As an alternative to Kalman filter approach, a Wiener filter has been elaborated on the simplest yet useful example of two distinct atomic clocks, motivated by ACES project[326]. The resulting estimator is structurally and computationally simpler than Kalman filter, and in case of time invariant models it is equally optimal. Design procedure is described covering clock noise modelling (including flicker approximation), and polynomial estimator calculation, concentrated on numerical pitfalls, and common marginally stable factors. Both non-causal (infinite lag) and causal (real-time) estimators are discussed.

Performance of the resulting estimator is simulated based on published ACES project models[3]. Results are plotted by means of power spectral density (PSD) and Allan deviation (Fig. 1), and compared to current solution based on feedback loops. It is shown that Wiener estimator performs better than the ACES feedback loops; generally, better than any possible feedback system so far. Most importantly, the system integrated with Wiener estimator is substantially simpler, inherently stable, contains less noise sources, and it is optimal up to an arbitrary roundoff error floor.

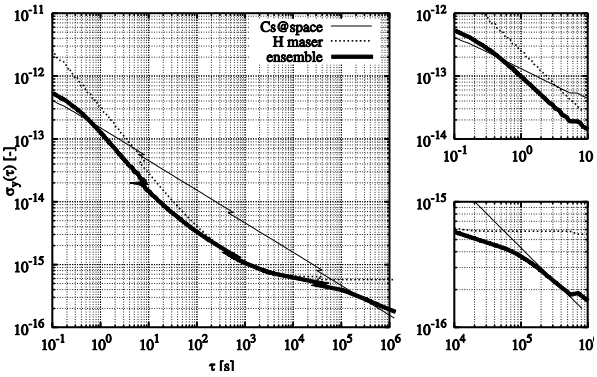

Fig. 101: Allan deviation of PHARAO-Cs and SHM clocks[3] and Wiener filtered ensemble.

[324] K. R. Brown, "The Theory of the GPS Composite Clock", Proceedings of ION GPS-91, p. 223–241, 1991.

[325] C. A. Greenhall, "Forming stable timescales from the Jones-Tryon Kalman filter", Metrologia, vol. 40, no. 3, p. 335–341, 2003.

[326] J. K. Dam et al, "Simulation of Servo Loops in Atomic Clock Ensemble in Space (ACES)", 24th European Time and Frequency Forum, 2010.

IFCS-EFTF5-G2-6

Characterization of atomic clock anomalies in the dynamic Allan variance domain

Lorenzo Galleani[1], Patrizia Tavella[2]

[1]Politecnico di Torino, Torino, Italy
[2]INRIM, Torino, Italy

Email: galleani@polito.it

The stability of an atomic clock changes with time due to several factors, such as mechanical vibrations, temperature, and radiations. To represent this time variation, we introduced the dynamic Allan variance (DAVAR)[327,328,329]. The DAVAR is a surface function of time and the observation interval. This surface is stationary with time when the clock follows the specifications, whereas it changes with time when an anomaly occurs. We derive the analytic DAVAR for a series of common anomalies, namely, a phase jump, a frequency jump, and a short duration sinusoid, that is, a sinusoid with finite time support. These anomalies are of fundamental interest in space clocks. Our results establish a clear connection between the nature and properties of the anomalies and the corresponding shape of the DAVAR.

[327] L. Galleani, "The Dynamic Allan Variance III: Confidence and Detection Surfaces," *IEEE Trans. Ultrason. Ferroelectr. Freq. Control*, vol. 58, no. 8, pp. 1550-1558, 2011.

[328] L. Galleani, "The Dynamic Allan Variance II: A Fast Computational Algorithm," *IEEE Trans. Ultrason. Ferroelectr. Freq. Control*, vol. 57, no. 1, pp. 182-188, 2010.

[329] L. Galleani and P. Tavella, "The Dynamic Allan Variance," *IEEE Trans. Ultrason. Ferroelectr. Freq. Control*, vol. 56, no. 3, pp. 450-464, 2009.

MEMS Oscillators

CLUB D

Wednesday, July 24 2013, 10:30 am - 12:00 pm

Chair: **Wan-Thai Hsu**
Discera Inc

IFCS-EFTF2-G3-1

Exploiting Dynamics to Achieve Tiny High-Performance Frequency Sources

Jeffrey L. Rogers

Microsystems Technology Office, Defense Advanced Research Projects Agency (DARPA), Arlington, VA, USA

Email: jeffrey.rogers@darpa.mil

The traditional understanding that reductions in size and associated improvements of oscillator performance are ultimately limited by the deleterious effects of nonlinearity and noise explain MEMS based oscillators failing to realize their technological promise. The MEMS advantages in size, weight, power, and integrability with CMOS have been limited to those applications where performance can be sacrificed to realize these advantages. As a result, MEMS have not been useful in many important applications that depend on performance, e.g., acquiring and tracking GPS. In light of modern advances in dynamics and the broader breakdown of assumptions underlying these performance expectations, conventional limitations must be reassessed.

The premise of the Mesodynamic Architectures (Meso) program at DARPA is that nonlinearity and noise inherent to all small-scale oscillators can be exploited to surpass traditional performance limits. In particular, the Meso program seeks to achieve frequency sources with unprecedentedly low phase-noise-per-unit-device-volume. Phase noise is particularly difficult since it cannot be filtered without the overhead of active canceling or put through a limiter without also removing oscillation signal. Complicating the problem further is that oscillators are inherently noisy close to the characteristic frequency and in the phase of oscillation. At the same time, dynamics offer novel mechanisms that can be used to improve oscillator behavior. Examples include decoupling amplitude modulation from phase modulation and tuning background fluctuations to enhance oscillator phase purity.

This talk will summarize the Meso program and provide a context for the results to be reported in this session. The architectures being pursued include tiny beams of different materials, disks, and thin films. Advances in the key figures of merit of phase noise and device size will be discussed along with results in maintaining temperature stability and acceleration stability. Potential avenues for further study will also be discussed.

IFCS-EFTF2-G3-2

Dynamics of Microscale Thin Film AlN Piezoelectric Resonators Enables Low Phase Noise UHF Frequency Sources

Gianluca Piazza[1], Augusto Tazzoli[1], Nicholas Miller[1], Jeronimo Segovia[1], Cristian Cassella[1], Jabeom Koo[2], Brian Otis[2], Kamala McNaul[3], Brian Gibson[3], Kimberly Turner[3], Todd Palmer[4]

[1]Department of Electrical and Computer Engineering, Carnegie Mellon University, Pittsburgh, PA, USA
[2]Department of Electrical and Computer Engineering, University of Washington, Seattle, WA, USA
[3]Department of Mechanical Engineering, University of California, Santa Barbara, CA, USA
[4] Vectron International, Mount Holly, PA, USA

Email: piazza@ece.cmu.edu

Low phase noise (PN) frequency sources from 100 MHz to 1.5 GHz rely on single crystalline mechanical resonators such as quartz crystals and surface acoustic wave devices to form a stable reference. Despite the impressive performance, these components cannot be directly integrated with CMOS electronics, are relatively bulky and are far from attaining the ultimate size, weight and power consumption that would be desirable for high-end commercial, industrial, and especially military applications.

Thin film micro and nanoscale resonators have emerged as a promising class of devices for the synthesis of stable frequency sources. Thin film piezoelectrics have shown to be the only viable transduction mechanism to demonstrate Ultra High Frequency (UHF) references. AlN contour-mode resonators[1] can provide high Q and low motional impedance and are especially suited for the implementation of CMOS-integrable multi-frequency sources on a single chip.

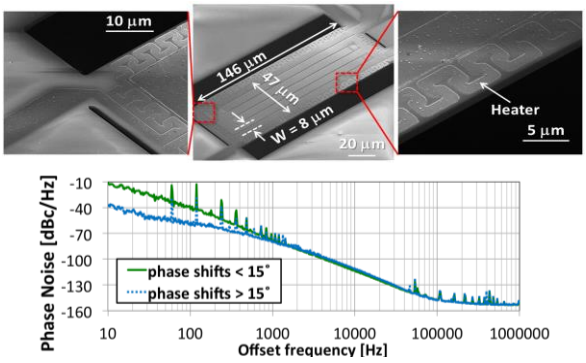

Fig. 102: (top) SEM figures of an ovenized thin film AlN resonator used as a frequency reference for temperature stable UHF oscillators. (bottom) Example of how the resonator dynamics can be exploited to evade amplifier noise for particular phase shifts in a close-loop oscillator (220 MHz carrier).

Nonetheless, the ultimate performance of these devices is hindered by their miniaturized dimensions, their complex dynamics and the unknown noise mechanisms associated with it. Here we analytically and experimentally explain how the non-linear dynamics of the AlN resonators are due to self-heating. Furthermore, we experimentally show how the dynamics of the resonator can be exploited to evade amplifier noise and reduce the close-in PN of the oscillator. We also measure, for the first time, the intrinsic noise of these resonators in an open-loop configuration, a particularly challenging task at frequencies above 500 MHz, but of paramount importance in order to fully understand the limiting mechanisms of phase noise.

With the aim of delivering temperature stable and acceleration insensitive oscillators, we introduce geometrical variations in the resonator layout to enable low power ovenization and reduce flexural deflections. Preliminary demonstration of UHF sources have yielded devices with PN < -94 dBc/Hz and – 160 dBc/Hz at 1kHz and 10 MHz offsets, temperature stability of 2 ppm from - 20 to + 85 ºC, and acceleration sensitivity < 30 ppb/G.

IFCS-EFTF2-G3-3

Single Transistor Oscillator Based on a Graphene-Aluminum Nitride Nano Plate Resonator

Zhenyun Qian[1], Yu Hui[1], Fangze Liu[2], Swastik Kar[2] and Matteo Rinaldi[1]

[1]Dept. of Electrical and Computer Engineering, Northeastern University, Boston, MA, USA
[2]Dept. of Physics, Northeastern University, Boston, MA, USA

Email: qian.z@husky.neu.edu, rinaldi@ece.neu.edu

This paper reports on the first demonstration of a high frequency (245 MHz) single transistor oscillator based on Graphene-Aluminum Nitride (G-AlN) nano-plate resonator (NPR). For the first time, a 2-dimensional (2D) electrically conductive graphene layer was integrated on top of an ultra-thin (500 nm) AlN nano-plate and excited into a high frequency contour-extensional mode of vibration by piezoelectric transduction (Fig.1). The resulting ultra-thin, low mass and high frequency G-AlN nanomechanical resonator showed high values of electromechanical coupling coefficient ($k_t^2 \approx 1.8\%$) and quality factor ($Q \approx 1000$) which enabled the implementation of a low phase noise (-87 dBc/Hz @ 1kHz offset and -125 dBc/Hz floor) single transistor oscillator.

The physical and electrical properties of the metal electrodes fundamentally limit volume and frequency scaling of conventional MEMS/NEMS piezoelectric resonators [1]. Furthermore, it has been recently shown that metal electrode damping and interface strain are responsible for the *Q* limits in conventional AlN Lamb wave resonators [2]. In this work a stepping stone towards the development of metal-free piezoelectric NEMS resonators is set by integrating a 2D graphene electrode on top of an AlN resonant nano-plate in lieu of a relatively thicker and heavier metal electrode. Despite a bottom metal interdigital electrode is still employed in this first prototype, the fabricated G-AlN resonator is characterized by reduced mass (~53%) and volume (~20%), increased sound velocity, hence resonant frequency (~36%), and improved device figure of merit ($k_t^2 \cdot Q \approx 18$) compared to a conventional AlN NPR device ($k_t^2 \cdot Q \approx 12$) based on the same core design but employing a 150 nm thick gold top electrode instead of the single atomic layer graphene. Both the G-AlN NPR prototype and the conventional AlN NPR were directly wire-bonded to Pierce oscillator circuits implemented with an ATF-551M4 E-pHEMT GaAs transistor. Despite the 150 fold smaller volume of the top electrode and the 36% higher operating frequency, improved phase noise performance was recorded for the G-AlN device (Fig.2) demonstrating the great potential of using graphene as 2D electrode in piezoelectric NEMS resonators.

[1] M. Rinaldi et al., IEEE T-UFFC, vol. 57, n. 1, pp. 38-45. [2] T. Yen et al., Proc. *IEEE MEMS 2013*, pp. 114-117.

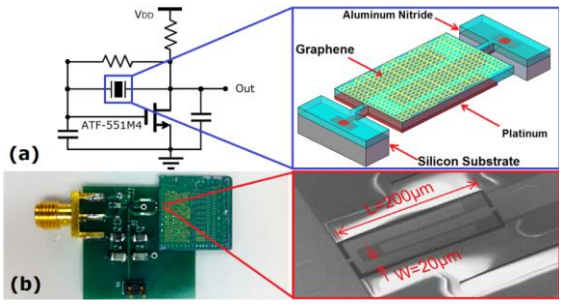

Fig. 103: (a) Schematic diagram of G-AlN NPR oscillator. (b) Picture of the G-AlN NEMS die wire-bonded to the oscillator printed circuit board and SEM image of G-AlN resonator.

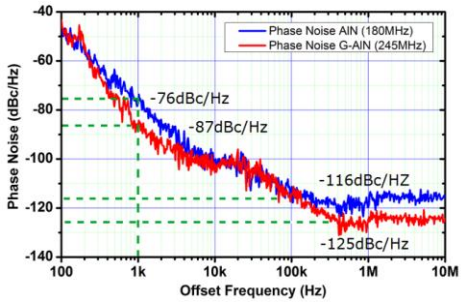

Fig. 2: Measured phase noise of the two oscillators for best bias conditions (using an Agilent N9010A EXA signal analyzer).

IFCS-EFTF2-G3-4

A 120-μW GSM Phase Noise-Compliant Pierce Oscillator Referenced to a 61-MHz Wine-Glass Disk Resonator

Thura Lin Naing, Tristan O. Rocheleau, Elad Alon, and Clark T.-C. Nguyen

University of California at Berkeley, Berkeley, California, USA

Email: thura@eecs.berkeley.edu

A 61-MHz Pierce oscillator referenced to a single polysilicon surface-micromachined wine-glass disk resonator has achieved phase noise marks of -120dBc/Hz at a 1-kHz offset and -139dBc/Hz at far-from-carrier offsets. When divided down to GSM's 13MHz, this corresponds to -133 dBc/Hz at 1-kHz and -152dBc/Hz at far-from-carrier offsets, both of which satisfy GSM reference oscillator phase noise requirements. This Pierce oscillator not only provides improvements of 10dB at 1kHz and 7dB at far-from carrier offsets versus a transimpedance amplifier (TIA) topology[330] using a similar single disk, it also reduces power consumption down to only 120μW, which is ~3 times smaller. Such low phase noise and power achieved by a tiny MEMS device might soon be key enablers for low power "set and forget" autonomous sensor networks with substantial communication capability.

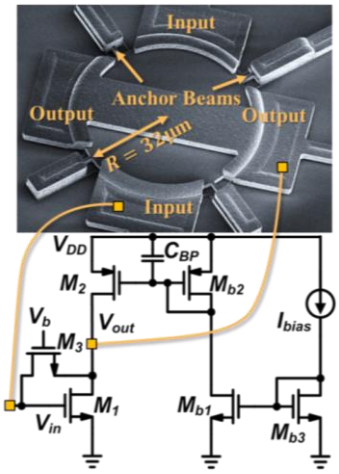

Fig. 104: The 61-MHz Pierce oscillator.

Previous TIA-based oscillators[1] attained GSM specs by arraying MEMS devices to boost oscillator loop power to reduce far-from-carrier phase noise. In contrast, the work presented here achieves the same GSM spec using only a single MEMS resonator with significant area savings versus the previous large array. It does this via the remarkably simple Pierce configuration of Fig.1 that yields better performance in two ways: 1) by reducing noise-figure by using only two active transistors; and 2) by increasing voltage swing, thereby raising oscillator loop power.

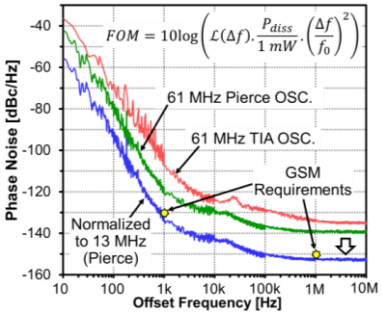

Fig. 105: Measured phase noise of 61-MHz oscillators and normalized to 13 MHz (Pierce) for comparison to GSM

Fig. 2 compares measured phase noise data for a 61-MHz TIA-based oscillator with that of the Pierce oscillator at 61MHz (and divided down to 13MHz), clearly showing the performance difference, and from the 13MHz curve, clearly meeting GSM specs. When power consumption is taken into account using the popular Figure of Merit (*FOM*) (given in the plot inset), this performance marks the best *FOM* at 1 kHz among published on-chip oscillators to date, as illustrated in the table below.

Device Type	**This work**	Wine-glass array[1]	FBAR[331]	Quartz[332]
FOM@ 1 kHz (dB)	**-225**	-223	-220	-211

[330] Y.-W. Lin, et al., "Low phase noise array-composite micromechanical ..," *Tech. Dig. IEDM 2005*, pp. 287-290.
[331] A. Nelson, et al., "A 22μW, 2.0GHz FBAR oscillator," *RFIC 2011*, pp. 1-4.
[332] J. T. M. van Beek, et al., "A review of MEMS …," *J. Micromech. Microeng*, vol 22, no.1, 2011.

IFCS-EFTF2-G3-5

A 995MHz Fundamental Nonlinear Quartz MEMS Oscillator

R.G. Nagele, H.P. Moyer, D. J. Kirby, Y. Yoon, R.L. Kubena, R.J. Joyce, P.D. Brewer
and D.T. Chang
HRL Laboratories, LLC, Malibu, CA, 90265 USA

Email: rgnagele@hrl.com

Recent work over the last few years has focused on developing methods to characterize resonator dynamics by measuring the impedance of the resonator under drive in a closed loop oscillating system[1][2]. Work at HRL Laboratories has enabled the capability to measure resonators in the 500-600MHz range and determine the magnitude of the admittance vs. frequency and the associated phase noise levels.

Our work focuses on using this technique to plot the phase noise vs. frequency at a fixed drive level. The device measured is a 995 MHz AT-cut quartz fundamental thickness-shear mode resonator. The rectangular quartz plate dimensions are 320 μm x 290 μm with 100 μm diameter, 0.08 μm thick circular aluminum electrodes on the top and bottom surfaces of the quartz. An unloaded Q of 13,390 and motional resistance of 67.8 ohms was measured in vacuum. This yields an fxQ product of $1.33e^{13}$ Hz, close to the expected limit for quartz devices. Fig. 1. shows the phase noise at a 1KHz offset for the resonator. The minimum phase noise achieved is ~ -106dBc/Hz which to our knowledge is the best reported for a quartz resonator operating in the fundamental mode at this frequency.

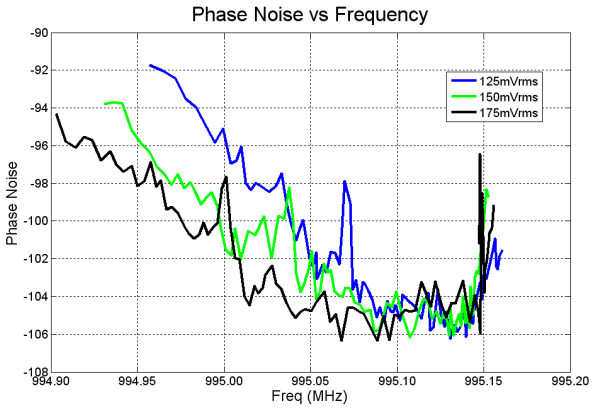

Fig.1. Plot of phase noise vs. frequency at a 1KHz offset for three different drive levels.

The loop oscillator consists of a Mini-Circuits amplifier, voltage controlled phase shifter, voltage controlled variable attenuator, power splitter and a resonator circuit with ZIF voltage probe connections that utilize Agilent low parasitic differential active probes used for measuring resonator admittance. Oscillator output goes to a frequency counter and phase noise analyzer. Upon establishing an oscillation condition, a computer program reads the voltage from the oscilloscope and adjusts the variable attenuator to achieve the desired voltage drive level. The phase shifter is adjusted in 5° increment and the process is repeated until the phase shifter reaches a state where the oscillation condition is not satisfied. Fig. 1. shows the resulting phase noise at a 1KHz vs. frequency for three different voltage drive levels. The nonlinear drive level, 175mVrms, shows the best phase noise performance over the range of oscillation frequencies.

---

[1] H.K. Lee et al., "Motional Impedance of Resonators in the Nonlinear Regime," in Proc. 2011 IEEE International Frequency Control Symposium, San Francisco, CA, USA, May 2-5, 2011, pp. 1-6.

[2] H.P. Moyer et al., "Nonlinear Behavior of an UHF Quartz Resonator in an Oscillating System," in Proc. 2012 IEEE International Frequency Control Symposium, Baltimore, MD, May 21-24, 2012, pp. 1-5.

Special Considerations for Specifying Oscillator Components with Resonators on the Micro/Nanoscale

Jon Lovseth[1], Ted Hoffmann[1], Sai Kalyanaraman[2], Vadim Olen[1], Jennet Volden[1], Paul Opsahl[1]

[1]Advanced Technology Center, Rockwell Collins, Cedar Rapids, Iowa/USA
[2]Government Systems Airborne Navigation, Rockwell Collins, Cedar Rapids, Iowa/USA

Email: jalovset@rockwellcollins.com

Some micro/nanoscale resonator oscillators' phase noise and temperature stability performance is inferior to traditional quartz crystal oscillators. But, does that matter? In other areas, micro/nanoscale resonator oscillators have demonstrated one or two orders of magnitude better performance. Measured devices have demonstrated frequency stability under vibration and a resiliency to shock not possible in traditional-sized quartz. Certain applications may have component specifications which can be derived differently by keeping in mind how a micro/nanoscale component will respond differently under these environmental conditions.

A comparison of most important requirements for oscillator components in communication, navigation, and radar radio applications is presented. Areas of specification relief are identified related to measured performance of micro/nanoscale oscillators. Rockwell Collins has measured developmental and COTS MEMS/NEMS resonator oscillators as part of the DARPA Mesodynamics program. This includes piezoelectric, piezoresistive, and electrostatic devices. Rockwell Collins has used these devices to demonstrate improved performance to existing radio hardware[334].

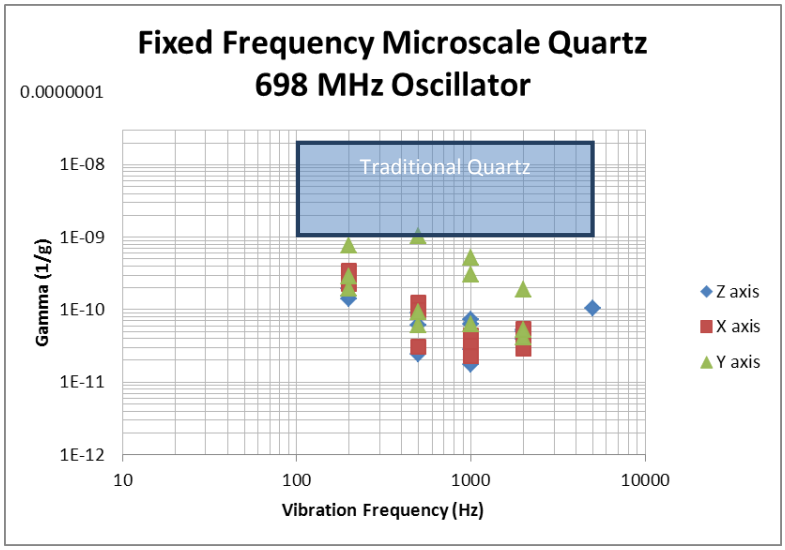

Fig. 106. Measured vibration sensitivity of a microscale resonator oscillator

[334] J. Lovseth, et. al. "Communication and navigation applications of nonlinear micro/nanoscale resonator oscillators," SPIE, Baltimore, MD, 2012

Frequency Combs II

CLUB H

Wednesday, July 24 2013, 02:00 pm - 03:30 pm

Chair: **Andre Luiten**
University of Adelaide

An Optical-Microwave Phase Detector for Generation of Low-Noise Microwave Signals from a Frequency Comb

Maurice Lessing[1, 2], Giuseppe Marra[1], Helen Margolis[1], Tom Brown[2], Patrick Gill[1]

[1]National Physical Laboratory, Hampton Road, Teddington, TW11 0LW, UK
[2]School of Physics and Astronomy, University of St Andrews, St Andrews, Fife, KY16 9SS, UK

Email: maurice.lessing@npl.co.uk

Ultra-stable microwave signals generated by transferring the stability of ultra-stable lasers to the microwave domain using femtosecond optical frequency combs could benefit applications such as radar systems, long baseline interferometry, precision spectroscopy and telecommunication systems[335]. Microwave signals at harmonics of the repetition-rate can be generated via photodetection of the pulse train of a frequency comb, but the performance is usually limited by saturation effects in the photodetectors. Significant improvements in phase noise have been achieved using a repetition-rate multiplication scheme[336] but long-term stable operation requires power stabilization of the laser source[337]. A simple technique that can provide both ultra-low residual phase noise and long term phase drift is the optical-microwave phase detector (OM-PD) [338].

We have investigated the performance of fibre-based[4] and free-space OM-PDs locked to the 80th harmonic of the repetition-rate of an Er-fibre comb. The free-space OM-PD has the advantage that it can be used at wavelengths for which no commercial PM fibre components exist. The residual phase noise of the extracted 8 GHz signal was measured by comparing two identical systems in each case. We present the best performance achieved with a free-space OM-PD to date, whilst the phase noise of our fibre OM-PD is only 10 dB higher than the best previously reported fibre OM-PD results[4]. The limitations to the current performance are being investigated, and we have already shown for the free-space OM-PD that the noise between 100 Hz and 1 kHz can be suppressed by using more stable mounts. Measurements of the amplitude-to-phase conversion coefficients and the long-term performance of the OM-PDs will also be presented.

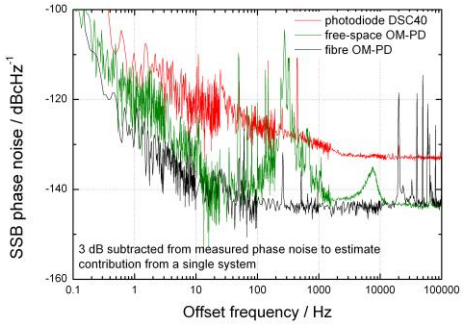

Fig. 107: Residual single sideband (SSB) phase noise of the generated 8 GHz signals from the OM-PDs. For comparison the results achieved using commercial photodiodes are also shown.

This work is supported by the UK National Measurement System and the European Metrology Research Programme (EMRP). The EMRP is jointly funded by the EMRP participating countries within EURAMET and the European Union.

[335] T. M. Fortier *et al.*, Nature Photonics, 5, 425–429, 2011.

[336] A. Haboucha *et al.*, Optics Letters, 36, 3654-3656, 2011.

[337] W. Zhang *et al.*, Applied Physics Letters, 96, 211105, 2010.

[338] K. Jung and J. Kim, Optics Letters, 37, 2958-2960, 2012.

IFCS-EFTF6-H1-2

Spectral purity transfer between optical wavelengths at the 10^{-18} level

Nicolodi Daniele, Argence Bérengère, Zhang Wei,
Le Targat Rodolphe, Santarelli Giorgio, Le Coq Yann

LNE-SYRTE, Observatoire de Paris, CNRS, UPMC, 61 avenue de l'Observatoire, Paris, France

Email: daniele.nicolodi@obspm.fr

Ultra-stable lasers are a basic building block for numerous high precision experiments. Such systems traditionally rely on stabilization by high-finesse optical cavities and typically reach their thermal-noise fundamental limit at 2×10^{-16} fractional frequency stability. Some applications require even better performance, most particularly optical lattice clocks, whose fundamental quantum projection noise limit could exceed 10^{-17} at one second, with interrogation lasers capable of sustaining such performance[339]. This has recently stimulated the emergence of new solutions for improved laser frequency stability[340]. Those approaches trade improved stability with increased complexity. Furthermore, most promising laser stabilization techniques are not based on ultra-stable optical cavities and are restricted to specific wavelengths by the physics of the exploited stabilization mechanism. To effectively take advantage of the potential of these new solutions, it is therefore of paramount importance to develop techniques for frequency stability transfer from a single laser frequency stabilization system to any optical wavelength.

We will present a scheme for optical phase locking through a commercial-core optical frequency comb based on a Erbium-doped fiber-based femtosecond laser capable of frequency stability transfer in the 1µm – 2µm spectral region. We demonstrate spectral purity transfer without frequency stability degradation from a 1062 nm master laser, stabilized by an high-finesse optical cavity, independently characterized at the 4×10^{-16} stability level, to a 1542 nm slave laser. Operating two independent quasi-identical setups measuring the phase difference between a common pair of master and slave lasers and comparing the phase difference signals from the two setups, we demonstrate that the optical frequency comb does not limit the frequency stability transfer at the 2×10^{-18} level at one second. This stability transfer capability exceeds by more than one order of magnitude the stability any optical oscillator demonstrated to date.

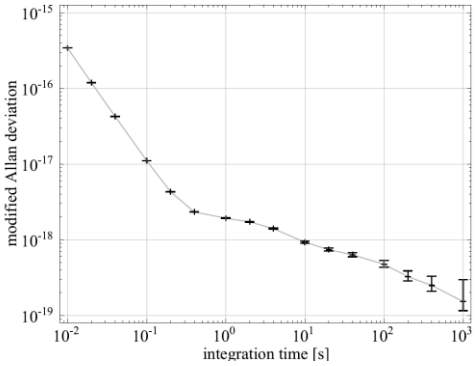

Fig. 108: Fractional frequency stability residual noise of the spectral purity transfer system accessed by comparing two independent quasi-identical setups.

[339] M. Takamoto et al. "An optical lattice clock", Nature, 435, 321, 2005.

[340] Y. Y. Jiang et al. "Making optical atomic clocks more stable with 10^{-16}-level laser stabilization", Nat. Phot., 5, 158, 2011. M. J. Thorpe,et al. "Frequency stabilization to 6×10^{-16} via spectral hole burning", Nat. Phot., 5, 688, 2011. T. Kessler, et al. "A sub-40-mHz-linewidth laser based on a silicon single-crystal optical cavity", Nat. Phot., 6, 687, 2012.

IFCS-EFTF6-H1-3

Optical frequency comb with an absolute linewidth of 1 Hz

S. Fang[1], H. Q. Chen[1], Y. Y. Jiang[1], T. Y. Wang[1], Z. Y. Bi[1], L. S. Ma[1]

[1]State Key Laboratory of Precision Spectroscopy, East China Normal University, 3663 N. Zhongshan Road, Shanghai 200062, China

Email: lsma@phy.ecnu.edu.cn

Narrow-linewidth lasers with ultra-low phase noise and spectral purity are widely used in precision measurement and metrology. By phase-locking an optical frequency comb to a subhertz-linewidth reference laser, each comb line inherits the phase coherence and frequency stability of the reference laser. In recent years, several groups have used their home made hertz or sub-hertz linewidth lasers to phase-lock optical frequency combs and investigated the linewidth of the comb teeth. Relative linewidth of sub-mHz to tens mHz and absolute linewidth of a few Hz have been demonstrated[1-4]. In this presentation, using the techniques of collinear self-referencing[5] and cross-phase modulation[6], a Ti:Sapphire femtosecond (fs) laser frequency comb with a repetition rate of 800 MHz is phase-locked to a sub-hertz linewidth Nd:YAG laser at 1064 nm. By comparing against a second similar Nd:YAG laser, the absolute linewidths of optical frequency comb teeth have been measured at 0.6~1.2 Hz over an octave spectrum. The diagram of the experimental setup and measurements is shown in Fig. 1.

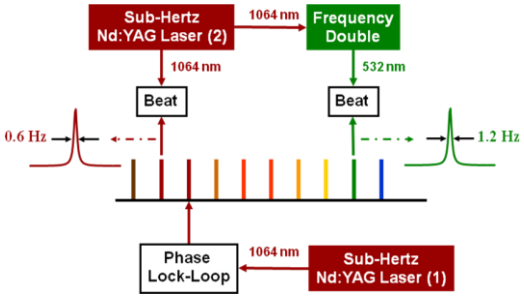

Fig. 109: The diagram of the experimental setup and measurements.

[1] A. Bartels, *et al.*, "Stabilization of femtosecond laser frequency combs with subhertz residual linewidths", Opt. Lett., vol. 29, p. 1081-1083, 2004.

[2] I. Coddington, *et al.*, "Coherent optical link over hundreds of metres and hundreds of terahertz with subfemtosecond timing jitter", Nature Photonics, vol. 1, p. 283-287, 2007.

[3] T. R. Schibli, *et al.*, "Optical frequency comb with submillihertz linewidth and more than 10 W average power", Nature Photonics, vol. 2, p. 355-359, 2008.

[4] K. Iwakuni, *et al.*, "Narrow linewidth comb realized with a mode-locked fiber laser using an intra-cavity waveguide electro-optic modulator for high-speed control", Opt. Express, vol. 20, p. 13769-13776, 2012.

[5] Y. Y. Jiang, *et al.*, "A collinear self-referencing set-up for control of the carrier-envelope offset frequency in Ti : sapphire femtosecond laser frequency combs", Metrologia, vol. 42, p. 304-307, 2005.

[6] D. J. Jones, *et al.*, "Frequency comb generation using femtosecond pulses and cross-phase modulation in optical fiber at arbitrary center frequencies", Opt. Lett., vol. 25, p. 308-310, 2000.

IFCS-EFTF6-H1-4

Microwaves generation from mode-locked Er-fiber lasers with sub-fs-level absolute timing jitter

Kwangyun Jung, Junho Shin, and Jungwon Kim*

Korea Advanced Institute of Science and Technology (KAIST), Daejeon 305-701, Korea

*Email: jungwon.kim@kaist.ac.kr

Ultralow phase noise RF/microwave signal sources are important for various science and engineering applications, ranging from precision time-frequency metrology to future electronic clocks, radar and measurement systems. Recently, photonic generation of ultralow phase noise microwave signals using ultrastable cavity-stabilized CW lasers and optical frequency combs has attracted great interest.[341] Also, we have recently demonstrated that the timing jitter (>1 kHz offset frequency) from free-running mode-locked fiber lasers can be engineered well below 1 fs level.[342] Therefore, for applications that require ultralow short-term (<1 ms time scale) timing jitter/phase noise microwave signals, one can directly use a simple free-running mode-locked fiber laser without state-of-the-art ultrastable cavity references.

In this paper, we show the generation of 10-GHz microwave signals from 78-MHz free-running mode-locked Er-fiber lasers with 0.49 fs absolute rms timing jitter integrated from 10 kHz to 10 MHz offset frequency, with a single-sideband phase noise of -142 dBc/Hz at 10 kHz offset frequency. In order to mitigate the shot-noise-limited high-frequency phase noise in the optical-to-electronic conversion process (typically limited around -140 dBc/Hz level when standard 100-MHz fiber lasers and photodetectors are used), we synchronize a low-noise voltage-controlled oscillator (VCO, 10-GHz dielectric resonator oscillator) to the mode-locked fiber laser using our recently demonstrated Fiber Loop Optical-Microwave Phase Detector (FLOM-PD)[343] with -157 dBc/Hz background noise. Figure 1 shows the experimental setup and the phase noise measurement results. In addition, 600-m remote generation[344] of a microwave signal from a mode-locked Er-fiber laser with 2.7 fs rms relative timing drift for 7 hours is demonstrated.

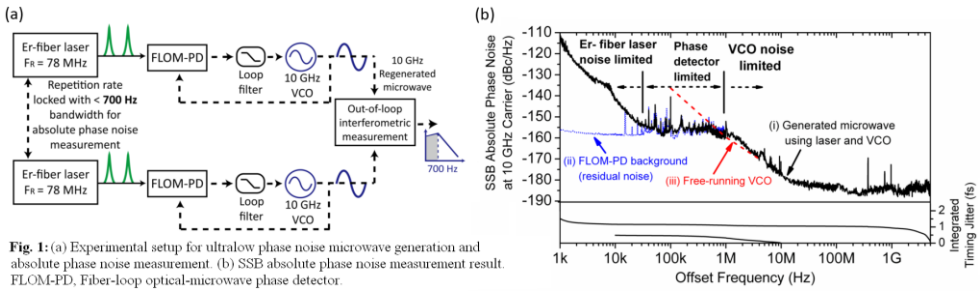

Fig. 1: (a) Experimental setup for ultralow phase noise microwave generation and absolute phase noise measurement. (b) SSB absolute phase noise measurement result. FLOM-PD, Fiber-loop optical-microwave phase detector.

[341] T. M. Fortier et al. "Sub-femtosecond absolute timing jitter with a 10 GHz hybrid photonic-microwave oscillator," Appl. Phys. Lett. **100**, 231111 (2012).

[342] T. K. Kim et al. "Sub-100-as timing jitter optical pulse trains from mode-locked Er-fiber lasers," Opt. Lett. **36**, 4443 (2011).

[3] K. Jung and J. Kim, "Subfemtosecond synchronization of microwave oscillators with mode-locked Er-fiber lasers," Opt. Lett. **37**, 2958 (2012).

[4] J. Kim et al. "Drift-free femtosecond timing synchronization of remote optical and microwave sources," Nature Photon. **2**, 733 (2008).

IFCS-EFTF6-H1-5

Broadband cavities for noise analysis and filtering in optical frequency combs relative to the quantum limit.

Roman Schmeissner[1], Valerian Thiel[1], Claude Fabre[1], Nicolas Treps[1]

[1]Laboratoire Kastler Brossel, Université Pierre et Marie Curie, CNRS, ENS, Paris, France

Email: nicolas.treps@upmc.fr

Balanced homodyne detection with a shaped local oscillator can extract timing information and any other parameter of femtosecond (fs) pulses with ultimate sensitivity[345]. To reach best sensitivities, a laser beam that is quantum-limited in amplitude and phase is required at lowest possible frequencies.
To filter classical noise of a 25fs, 156MHz Ti:Sa oscillator at the quantum limit, we study a passive optical cavity of Finesse 1200 that is a low-pass filter at 100kHz. A simultaneous resonance of over 100nm FWHM and >50% transmission of power is achieved. These are currently the best values for broadband high finesse cavities.

The effects of the cavity are studied by transfer function measurements and balanced (homodyne) detection, a new technique for this application. Figure 1. It compares any signal to the shot noise limit and thus allows for ultimate measurement precisions.

The cavity filters amplitude and phase noise. An amplitude quantum limited comb is retrieved at >500kHz. Phase noise filtering reduces the r.m.s. phase induced timing jitter at 1µs integration time by 20dB leading to scales of approx. 10 yoctoseconds (10^-23s).

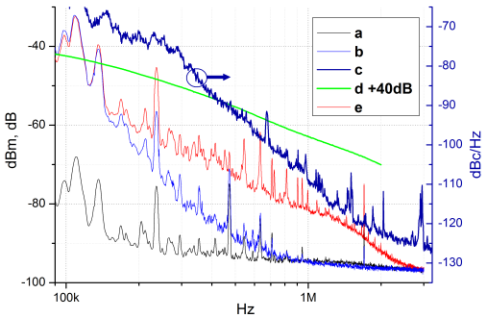

Fig. 110: amplitude noise of the mode-locked laser **a**, of the cavity output **b**; *right scale* carrier-envelope-phase noise **c**; amplitude transfer function of the cavity **d,** filtered phase noise accessible by balanced homodyne detection down to µrad sensitivities **e**

Noise quadrature interconversion leads to excess noise in amplitude of the transmitted beam. We theoretically model this effect and show that it can be exploited to detect (spectral) phase noise of any seed with highest sensitivity. The latter can be simultaneously measured over the entire optical spectrum covered by the cavity. A shot noise limited sensitivity is of approx. <10^-10 rad/Hz is found. This method is applied to reveal spectrally non-constant phase noise distributions of Ti:Sa and fiber-based comb sources.

[345]B.Lamine, C.Fabre and N.Treps, Quantum improvement of Time Transfer between remote clocks, Phys. Rev. Lett. 101, 2008, 123601

IFCS-EFTF6-H1-6

Optical lattice clocks with ^{87}Sr in a cryogenic environment

Ichiro Ushijima[1,2,3], Takuya Ohkubo[1,2,3], Manoj Das[2,3], Masao Takamoto[2,3], and Hidetoshi Katori[1,2,3]

[1]Department of Applied Physics, Graduate School of Engineering, The University of Tokyo, 7-3-1 Hongo, Bunkyo-ku, Tokyo 113-8656, Japan

[2]Quantum Metrology Laboratory, Advanced Science Institute, RIKEN, 2-1 Hirosawa, Wako, Saitama 351-0198, Japan

[3]Innovative Space-Time Project, ERATO, JST, 7-3-1 Hongo, Bunkyo-ku, Tokyo 113-8656, Japan

Email: ushijima@amo.t.u-tokyo.ac.jp

A relative frequency stability of 10^{-17} has been reached by comparing two Sr optical lattice clocks[1]. At this level of stability, the frequency shift due to blackbody radiation (BBR) from the room temperature environment becomes a major limitation for Sr lattice clocks[1,2]. In order to reduce the uncertainties of BBR shift, we have developed Sr optical lattice clocks that operate in a cryogenic environment. The BBR shift for Sr atoms is theoretically calculated to be about 2.4 Hz at 300 K. To reach the uncertainties of 10^{-18}, the fluctuation and inhomogeneity of the ambient room temperature T has to be controlled to within ΔT = 0.01 K at 300 K. As the sensitivity of BBR shift varies as T^3, the uncertainties can be decreased by cooling down the environmental temperature. At the temperature of T = 70 K, the BBR shift reduces to 10 mHz and even with a temperature fluctuation of ΔT = 1 K, clock uncertainties of 10^{-18} can be reached. We can evaluate the BBR shift directly as a frequency difference of two clocks by comparing two clocks operating at different environmental temperature.

We realize the cryogenic environment by surrounding the region for clock spectroscopy with a cryogenic chamber of few cm^3 in volume. In order to introduce atoms and lasers, the chamber has two apertures with diameters of 0.5 and 1 mm. The uncertainty due to BBR shift caused by the radiation that irradiates the atoms through these apertures can be reduced to 1×10^{-18} by moving the atoms 5 mm inside the chamber and thereby reducing the solid angle from atoms to the environment to 0.5 msr. The cryogenic chamber is cooled down to 70 K by a Stirling refrigerator and the temperature fluctuation can be maintained to within ΔT = 10 mK.

In this poster presentation we will discuss our cryogenic setup for two Sr lattice clocks and the latest experimental results. By using synchronous interrogation[1] and comparing two clocks, one in a cryogenic and the other in a room temperature environment, the BBR shift can be observed as the frequency difference of the two clocks with high stability. Comparing two clocks synchronously in a reduced BBR environment will allow us to evaluate other systematic errors such as atomic interactions and lattice light shifts with high precision.

---

[1] M. Takamoto, T. Takano, and H. Katori, "Frequency comparison of optical lattice clocks beyond the Dick limit", Nat. Photon. vol. 5, p. 288-292. 2011.

[2] T. Middelmann, Ch. Lisdat, St. Falke, J. S. R. Vellore Winfred, F. Riehle and U. Sterr, "Tackling the blackbody shift in a strontium optical lattice clock", IEEE Trans. Instrum. Meas.. vol. 60, p. 2550-2557. 2011.

Atom-based sensors and fundamental physics

CLUB E

Wednesday, July 24 2013, 02:00 pm - 03:30 pm

Chair: **Peter Wolf**
Observatoire de Paris, CNRS, UPMC

IFCS-EFTF3-H2-1

Precision gravity measurements with atom interferometry

Guglielmo M. Tino

Dipartimento di Fisica e Astronomia and LENS Laboratory
Università degli Studi di Firenze
Istituto Nazionale di Fisica Nucleare, Sezione di Firenze
via Sansone 1, Sesto Fiorentino (Firenze), Italy

Email: guglielmo.tino@fi.infn.it

I will discuss experiments we are conducting using cold atom interferometry for precision tests of gravitational physics. In particular, I will report on the experiment to measure the gravitational constant G with a Rb Raman interferometer, and the one based on Bloch oscillations of Sr atoms confined in an optical lattice for precision gravity measurements.

IFCS-EFTF3-H2-2

Atomic Magnetometry for Biomedical and Fundamental Research

Antoine Weis[1]

[1]Physics Department, University of Fribourg, Fribourg, Switzerland

Email: antoine.weis@unifr.ch

I will report on past and ongoing research in atomic magnetometry by our team. I will illustrate the principle of laser-driven magnetometers based on optically detected magnetic resonance (ODMR), and review our use of a multi-sensor array of ODMR magnetometers for recording the dynamics of human magneto-cardiographic field maps[346] and for detecting magnetic nano-particles. We also deploy an array of similar sensors (in vacuum and near a 100 kV electrode) for monitoring and controlling the spatio-temporal variations of a 1 μT field in an experimental search for a neutron electric dipole moment at the Paul Scherrer Institute[347].

Current work focuses on the development of vector magnetometers and the exploration of magnetically silent magnetometers based on amplitude-, frequency-, or polarization-modulated laser light. We have developed an algebraic model that describes the complex structure of the multiple resonances encountered in silent magnetometers[348], in which the magnetic resonance transitions between sublevels are driven by second-order electric dipole interactions with the (modulated) light field. Model predictions yield excellent agreement with specific experimental case studies using amplitude- and polarization-modulation, respectively. Our sensors (Fig. 1) are based on 30 mm diameter room temperature Cs bulbs with paraffin-coated walls and have a shot noise limited magnetic field sensitivity[349] of 10-20 fT/Hz$^{1/2}$. They are operated using a phase-locked feedback loop and their absolute accuracy is severely limited by the stability and control of the feedback phase. In order to circumvent systematic reading errors due to phase noise and/or drift, we currently explore feedback-free schemes, in which we record the free induction decay of the atomic orientation and/or alignment following pulsed excitation.

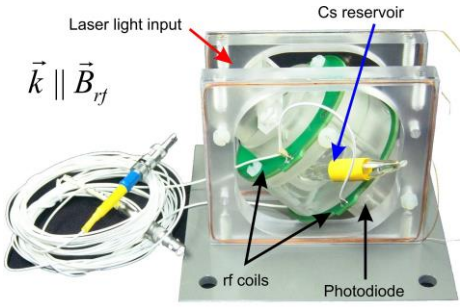

Fig. 111: Modular ODMR magnetometer sensor head comprising a fiber coupler, collimation and polarization optics, a photodetector, and rf coils.

[346] G. Bison, N. Castagna, A. Hofer, P. Knowles, J.-L. Schenker, M. Kasprzak, H. Saudan, and A. Weis, "A room temperature 19-channel magnetic field mapping device for cardiac signals", Appl. Phys. Lett., 95, 173701, 2009.
[347] P. Knowles, G. Bison, N. Castagna, A. Hofer, A. Mtchedlishvili, A. Pazgalev, and A. Weis, "Laser-driven Cs magnetometer arrays for magnetic field measurement and control", Nucl. Instrum. Meth., A611, 306-309, 2009.
[348] Z. Grujic and A. Weis, "Atomic magnetic resonance induced by amplitude-, frequency-, or polarization-modulated light", submitted to Phys. Rev. A, 2013.
[349] N. Castagna, G. Bison, G. di Domenico, A. Hofer, P. Knowles, C. Macchione, H. Saudan, and A. Weis, "A large sample study of spin relaxation and magnetometric sensitivity of paraffin-coated Cs vapor cells", Appl. Phys., B96, 763-772, 2009.

IFCS-EFTF3-H2-3

Testing Fundamental Physics with Microwave Cavities

Stephen R. Parker[1], Moritz Nagel[2], Paul L. Stanwix[1], Evgeny Kovalchuk[2], John G. Hartnett[1,3], Eugene N. Ivanov[1], Achim Peters[2], Michael E. Tobar[1],

[1]School of Physics, The University of Western Australia, Crawley, Australia
[2]Institut für Physik, Humboldt Universität zu Berlin, Berlin, Germany
[3]Institute of Photonics and Advanced Sensing, School of Chemistry and Physics, University of Adelaide, Adelaide, Australia

Email: stephen.parker@uwa.edu.au

We present an overview and status update of recent experiments at The University of Western Australia and collaborating institutions that utilize microwave frequency resonant cavities to test aspects of fundamental physics.

Microwave cavities loaded with sapphire exhibit quality factors on the order of 10^9 at cryogenic temperatures and when used as a frequency discriminating element enable the creation of loop oscillators with fractional frequency stabilities below 2×10^{-16} for integration time of 100 seconds[350]. We describe a modern Michelson-Morley experiment that uses the beat frequency of two actively rotated orthogonally aligned cryogenic sapphire oscillators to search for orientation dependent deviations in the speed of light. The sensitivity of the experiment is dictated by the stability of the beat frequency. Potential variations are expressed as bounds on coefficients in the Standard Model Extension framework[351] and describe possible violations of local Lorentz invariance. Preliminary bounds from our most recent experiment demonstrate at least an order of magnitude improvement over previous work.

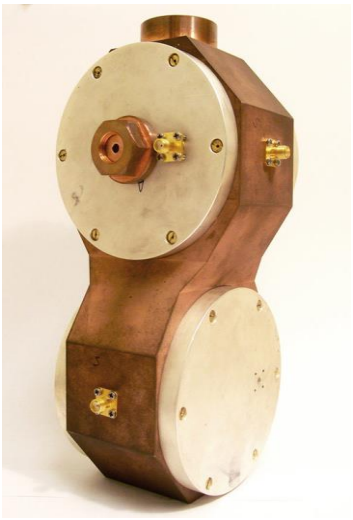

Fig. 112: A dual sapphire loaded cavity mount for testing Lorentz invariance.

We also discuss our most recent "light shining through a wall" experiment that searches for the hidden sector photon, a hypothetical particle that weakly interacts with the photon via kinetic mixing. An empty room temperature copper cavity and an empty cryogenic niobium cavity are separated by a barrier impenetrable to standard photons. By actively driving the copper cavity at resonance there is a possibility that photons will mix in to paraphotons, cross the barrier and then mix back in to photons in the cryogenic niobium cavity. By measuring the power transmitted between the two cavities a bound can be placed on the probability of kinetic mixing between photons and paraphotons.

[350] J.G. Hartnett, N.R. Nand and C. Lu, "Ultra-low-phase-noise cryocooled microwave dielectric-sapphire-resonator oscillators," Appl. Phys. Lett., vol. 100, no. 18, 2012.

[351] V.A. Kostelecky and M. Mewes, "Signals for Lorentz Violation in Electrodynamics", Phys. Rev. D 66, 056005, 2002.

IFCS-EFTF3-H2-4

Cold Atom Test Masses and Their Applications In Space

Nan Yu, James R. Kellogg, James M. Kohel and Robert J. Thompson
Jet Propulsion Laboratory, California Institute of Technology, Pasadena, CA, USA

Email: nan.yu@jpl.nasa.gov

Laser-cooled cold atoms in free fall provide ideal test masses for inertial and gravity measurements. Cold atom-based inertial sensors have demonstrated the state-of-the-art sensitivity and stability in laboratories. Operation of this type of sensors in space offers new ways for improved gravity measurements. Examples of potential application in space using cold atoms as test masses include quantum test of universality of free fall, Earth and planetary gravity measurements, and gravitational wave detection.

In this paper, we will describe some of our exploration of using free-fall cold atoms and atom interferometry in space. Two major activities are being carried out. First, we are developing a transportable gravity gradiometer based on a dual atom interferometer accelerometer system. We have recently modified and upgraded the laser and optics system for improvement robustness and portability. At the same time, we have significantly improved the atom interferometer contrast and signal to noise over our previous reports [1]. The system is designed to achieve the differential gravity measurement sensitivity below $1x10^{-9}$ g per measurement. We will describe the latest results and discuss their significance.

In parallel, JPL is developing an ISS ultra-cold atom research facility, CAL (Cold Atom Laboratory) [2]. The facility is foremost designed to be a multi-user facility for ultra-cold atom and quantum degenerate gas research in micro gravity environment. The development of the facility and experiments to be done in the facility will also serve as a technology pathfinder for cold atom experiments in space in general and cold atom-based matter-wave interferometers in particular. We will briefly introduce the CAL project, its science objectives, the facility design and configuration, as well as report of its development and progress.

[1] "Development of a Transportable Quantum Gravity Gradiometer for Gravity Field Mapping," James M. Kohel, Robert J. Thompson, James R. Kellogg, David C. Aveline, and Nan Yu, *The eighth annual NASA Earth Science Technology Conference (ESTC2008),* University of Maryland University, June 24-26. 2008; "Development of a Quantum Gravity Gradiometer for Gravity Measurement from Space," Nan Yu, James M. Kohel, James R. Kellogg, and Lute Maleki, J. Appl. Phys. B. **84**, 647 (2006).

[2] CAL – Cold Atom Laboratory website: http://coldatomlab.jpl.nasa.gov.

Time Scales

CLUB D

Wednesday, July 24 2013, 02:00 pm - 03:30 pm

Chair: **Dirk Piester**
PTB

IFCS-EFTF5-H3-1

Timekeeping Advances in Russian Federation and Time Reference Frame for GLONASS

S.Donchenko[1], S.Revnivykh[2], I. Blinov[1], N.Koshelyaevsky[1], V.Palchikov[1]

[1]The Main Metrology Center of the State Time and Frequency Service
FSUE "VNIIFTRI," Mendeleevo, Moscow region, Russia
email: nkoshelyaevsky@vniiftri.ru
[2]Information-Analytical Centre
FSUE "TSNIIMASH," Korolyov, Moscow region, Russia

The new national time and frequency standard (NTFS) of Russian Federation in pursuance of Decree No. 1226 28 December 2012 of Federal Agency on Technical Regulation and Metrology have been commissioned. Along with it new realization of atomic time scale TA(SU) based on new time algorithm [1] have been introduced on MJD 56289 – 28 December 2012 [2].

Composition of the new NTFS consists of:

- Primary CS standards for national realization of the SI time unit;
- Clocks comparison and time keeping instrumentations;
- Time and frequency transfer and dissemination instrumentations;
- Infrastructure

According to ICD GLONASS [3] national time scale of universal coordinated time UTC(SU) is the reference time frame for GLONASS.

The paper will deliver detailed information on above mention NTFS components, their performances including time links between NTFS and GLONASS synchronizer, results of investigations and time scale comparisons relative TAI and UTC.

References

1. *Koshelyaevskiy N., Maslennikova M., Sokolova O., The new time algorithm for national time scales of Russian Federation, Proceeding of the 6th International Symposium "Metrology of Time and Space", 17-19 September 2012, Morozovka Holiday Hotel, Mendeleevo.*
2. *On time unit changes in Atomic Time Scale TA(SU), Bulletin G-136, NOTIFICATION, ISSN 0135-2415, The Main Metrology Center of the State Time and Frequency Service, 3 November 2012, Mendeleevo.*
3. *Global navigation satellite system GLONASS, Interface Control Document, Navigational radiosignal in bands L1, L2, Edition 5.1, Moscow, 2008.*

IFCS-EFTF5-H3-2

The New UTC(OP) based on the LNE-SYRTE Atomic Fountains

G. D. Rovera, M. Abgrall, S. Bize, B. Chupin, J. Guéna, Ph. Laurent, P. Rosenbusch, P. Uhrich

LNE-SYRTE, Observatoire de Paris, UMR CNRS 8630, UPMC, Paris, France

Email: daniele.rovera@obspm.fr

The generation of a timescale by steering a H-maser signal to the average of all SYRTE commercial clocks has been tested for a few years[352]. After running this time scale in parallel with the official UTC(OP) which is based on one single commercial Cs clock, we concluded that the performances were not justifying the complexity of the system. Instead, we have developed a very simple new algorithm for the steering of a H-maser signal to the SYRTE atomic fountain ensemble (comprising 3 Cs primary frequency standard and one Rb fountain). Preliminary tests of the new algorithm started in December 2011. For these tests we used a new 100 MHz micro phase stepper developed by SKK Electronics in collaboration with the SYRTE[2]. The results were very promising so that in October 2012 we implemented the new algorithm to generate the official realization of UTC(OP).

At SYRTE all fountains share the same cryogenic oscillator which is phase locked to a H-maser. This way, all fountains measure the frequency of the same H-maser. Automatic fountain data processing provides preliminary data corrected of all systematic frequency shifts, hourly. At the present stage, the daily steering to this data-stream is sufficient to drive the new UTC(OP) with a stability in the low 10^{-16}.

Where previously a few tens of ns were observed, the difference between UTC(OP) and UTC has not exceeded 5 ns since the implementation of this new UTC(OP).

[352] M. Abgrall, P. Uhrich, and D. Valat, "Ongoing improvements of ...", Proc. of the 24th EFTF 2010

[2] D. Rovera, M. Abgrall, and M. Siccardi, "Characterization of an auxiliary ...", Proc. 26th EFTF 2012

IFCS-EFTF5-H3-3

A new weighting procedure for UTC

Gianna Panfilo, Aurélie Harmegnies

International Bureau of Weights and Measures (BIPM)
Pavillon de Breteuil, 92312, Sèvres, France

Email: aharmeg@bipm.org

Three main algorithms are used in the generation of UTC: the prediction and the weighting algorithms to calculate the free atomic time scale (EAL) and the steering algorithm to steer the EAL frequency on the SI frequency provided by the Primary Frequency Standards.

The clock frequency prediction method has been reviewed and changed in September 2011 [353] with significant effects in terms of improvement of the EAL stability. As aimed, the frequency drift affecting EAL has almost completely disappeared after the introduction of the new prediction algorithm. However the distribution between H-masers and caesium clocks on the total weight did not change because the frequency prediction does not influence the weighting procedure which considers the difference [EAL-clock] as the relevant weighting parameter. In particular in the current weighting algorithm the inverse of the variance of the frequency of [EAL – clock] over one year is used to estimate the performance of the atomic clocks and to assign a weight. The long term performance of the time scale is guaranteed by de-weighting those atomic clocks presenting a frequency drift (case of H-masers) or an aging. One consequence of this procedure was the low impact of the contribution of the H-masers in the time scale ensemble.

This paper presents a new version of the weighting algorithm, supported on the concept of weighting the clocks according to their predictabilities. In this case, only the difference between the reading of the clock and its prediction is used. The main idea is that a clock with strong signatures like frequency drift or aging can be correctly used in the timescale ensemble if well predicted.

In the new weighting algorithm the difference between the predicted and the real frequency of the atomic clocks is evaluated. A filter over one year of these data is applied to evaluate the weights and to guarantee the long term stability of the clock ensemble.

The effect of the new weighting model on the EAL stability is presented. A frequency stability improvement of the time scale at short and long term is observed, as well as a better clock weight distribution that allows the H-masers to play a very important role on the time scale.

[353] G. Panfilo , A. Harmegnies, L. Tisserand, “A new prediction algorithm for the generation of International Atomic Time”, Metrologia, vol. 49, n°1, pp. 49-56, 2012.

IFCS-EFTF5-H3-4

Reconstruction of UTC (NIM)

Aimin Zhang, Yuan Gao, Kun Liang, Weibo Wang, Zhiqiang Yang, Dayu Ning

Time and Frequency Division, National Institute of Metrology, Beijing, China

Email: zhangam@nim.ac.cn

Abstract

NIM has reconstructed UTC (NIM) since 2010 at new campus, and the official UTC (NIM) was switched to the new campus in October 2012. The new clock ensemble includes 6 Hydrogen masers and 7 Cesium clocks, with 1 Hydrogen maser and 2 Cesium clocks placed at the old campus. The master clock is a Hydrogen maser at new campus, and UTC (NIM) is generated from a microphase stepper steered by a new algorithm and UTC, the frequency of the Hydrogen maser is predicted and rapid UTC data is used to steer UTC (NIM). A dual mixer time difference measurement system is used to measure the time difference between the clocks and UTC (NIM) at new campus, the clocks at old campus are linked to UTC (NIM) by GPS. GPS and TWSTFT data are reported to BIPM everyday automatically. The GPS receivers at new campus are calibrated with reference to one GPS receiver calibrated by BIPM. The UTC (NIM) has been operated normally at new campus, the accuracy and stability are improved. In this paper the generation of new UTC (NIM) is described and the performance of UTC (NIM) is presented.

IFCS-EFTF5-H3-5

Methods for predicting corrections for polish time scale UTC(PL) using GMDH neural networks

Łukasz Sobolewski[1]

[1]Institute of Electrical Metrology, University of Zielona Góra, Zielona Góra, Poland

Email: sobolewski.l@gmail.com

The problem of maintaining the best compliance of the UTC(PL) with UTC is due to the complexity of calculating the UTC scale[354]. Consequently, this leads to a delay in issuing the BIPMs "Circular T" bulletin, which contain the corrections for the UTC(PL) relative to UTC. In order to ensure the best compatibility of the UTC(PL) with UTC the prediction of the corrections is required, which may be carried out based on analytical methods or neural networks (NN). Central Office of Measures (Główny Urząd Miar, GUM), which is responsible for the implementation of UTC(PL), carry out the prediction of the correction values using the linear regression method. However, this method is very labor intensive and requires a lot of experience of the person performing the analysis.

The Institute of Electrical Metrology of University of Zielona Góra, in collaboration with GUM, is working on predicting the corrections for UTC(PL) using neural networks (NN). The obtained results indicate the possibility of using MLP, RBF and GMDH neural networks[355]. The disadvantage of MLP and RBF networks is a need to select the number of neurons in the hidden layer in the training process, for the prediction in the given month in order to achieve the result of the prediction with a sufficient level of accuracy. A disadvantage of this type of NN was eliminated using GMDH neural networks (Group Method of Data Handling), belonging to the group of self-organizing networks. Preliminary studies for a period of 5 months showed that the GMDH networks are good in task of predicting the corrections for the UTC(PL). The results of these research was presented in the journal[356].

The article will present the extended results for the period of 28 months on predicting the corrections for the UTC(PL) using GMDH neural networks based on two methods: time series analysis and regression. A better method of predicting the corrections for the UTC(PL) has proven to be a method of time series analysis. The obtained results of prediction error does not exceed the value of ± 16 ns, and are much smaller than the results received in GUM.

Currently the BIPM is working on a "UTC Rapid" project. The main goal of the project is to publish more frequently corrections for UTC(k) relative to UTCr for national time scales. Corrections are designated for each day and published once a week. A few days delay in publishing the corrections was decisive in the initiation of research on predicting the corrections for the UTC(PL), using GMDH neural networks, based on previous known values of UTCr – UTC(PL) corrections. The results of preliminary studies indicate that it is possible to predict the corrections for the UTC(PL) based on Rapid UTC data. The application of GMDH neural networks makes it possible to obtain predicted correction value, which differs only to a few ns, to UTCr – UTC(PL) correction value read from BIPMs ftp server.

[354] BIPM Annual Report on Time Activities, Vol. 6, Sevres, BIPM 2011.

[355] Miczulski W., Sobolewski Ł., Application of the GMDH neural networks in prediction of corrections of the national time scale; Elektronika: Konstrukcje, Technologie, Zastosowania, nr 6, 2011, s. 45-47.

[356] Miczulski W., Sobolewski Ł., Influence of the GMDH neural network data preparation method on UTC(PL) correction prediction results, Metrology and Measurement Systems, Vol. XIX, No. 1, 2012, pp. 123-132.

Vapor Cell Clocks and Magnetometers

CLUB E

Wednesday, July 24 2013, 04:30 pm - 06:00 pm

Chair: **Christoph Affolderbach**
University of Neuchatel

IFCS-EFTF3-I1-1

Pulsed Optically Pumped Rb Standard: a high stability vapor cell clock.

Filippo Levi, Claudio Calosso, Aldo Godone, Salvatore Micalizio

Optic Division, INRIM, Torino Italy.

Email: f.levi@inrim.it

We have realized a prototype of a Rb vapor cell clock based on pulsed operation, where optical pumping, microwave excitation and optical detection of the transition signal are separated in time[1]. Besides suppressing the laser induced light shift, the pulsed operation allows a full optimization of the laser parameters both in the pumping and in the detection stages, where different power levels are required.

A short term frequency instability of $1.7\times10^{-13}\tau^{-1/2}$ was measured, together with a long term frequency drift below 10^{-14}/day. The drift is thought to be due to a residual sensitivity to environmental parameters like temperature, atmospheric pressure and humidity. In fact subsets of the recorded data achieve medium term stability of 2×10^{-15} at 10^4 s.

We conducted in depth analysis of the various noise sources affecting our prototype both on the long and on the short term, identifying possible avenue to improve the clock stability.

Among others, the Dick effect and the laser detection noise are the most important sources of frequency instability on the short term, while the shape of the cell is demonstrated to affect the temperature sensitivity of the system.

In the talk we will present the most recent experimental results and we will discuss the ultimate stability that can be achieved by this pulsed frequency standard.

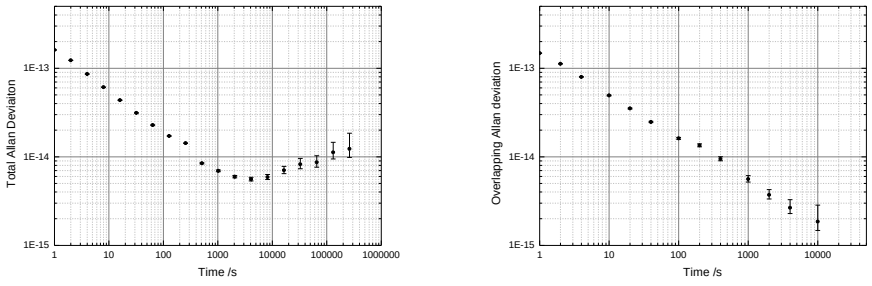

Fig. 1 - Allan deviation of the prototype: typical results (left) and a data subset (right)

[1]This work was funded by ESA, ESTEC contract 21504/08/NL/GLC

Study of an observation method based on Crossed Polarizers for High-contrast Coherent Population Trapping

Yuichiro Yano, Shigeyoshi Goka

Graduate School of Science and Engineering, Tokyo Metropolitan University,
Hachioji, Tokyo 1920397, Japan

Email: yano-yuichiro@ed.tmu.ac.jp

We proposed an observation method based on crossed polarizers for obtaining high-contrast coherent population trapping (CPT) resonance with parallel linearly polarized light (lin||lin field). Experiment result shows that high resonance contrast (88.4%) can be observed using a ^{133}Cs gas cell and the D_1-line vertical-cavity surface-emitting laser (VCSEL).

Figure 1 shows an optical system of the proposed observation method. A single-mode VCSEL was used to excite ^{133}Cs at the D_1-line. The VCSEL was driven by a dc injection current using a bias T and modulated at 4.6 GHz. The cylindrical gas cell was 20 mm long and contains a mixture of Cs atoms and 4 kPa of Ne buffer gas at a controlled temperature, and was placed at a static magnetic field of 93.0 μT. Two polarizers were placed on both sides of the gas cell, and these transmission axes were set nearly orthogonal to each other. A parallel linearly beam was incident on the gas cell by the first polarizer.

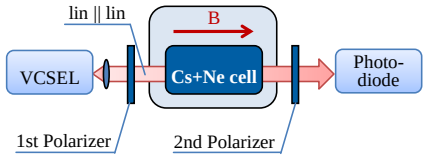

Fig. 113: Optical system for observing CPT resonance.

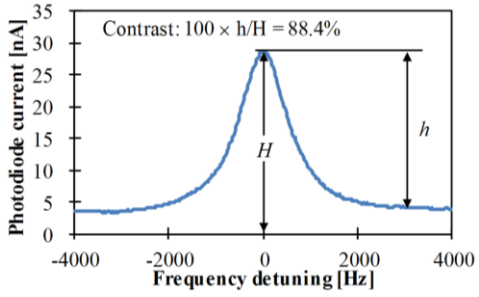

Fig. 114: Measured CPT resonance. Center frequency was 4.596 GHz.

The polarization of wavelength components which excite CPT is rotated by Faraday effect after passing through the cell[357]. On the other hand, the polarization of wavelength components which do not excite CPT is not rotated. Therefore, the second polarizer blocks the not-exciting CPT wavelength components incident on a photodiode. As a result, the photodiode DC current can be reduced because the unwanted wavelength components incident on the photodiode decreases, thus, high-contrast CPT resonance can be obtained.

The measured CPT resonance with our method is shown in Fig. 2. When the transmission axis of second polarizer was optimized, the contrast of 88.4% was achieved. As a contrast with a conventional lin||lin method was 3.3%, the contrast with our method was about 25 times better than that with the conventional method.

Since our optical system is very simple, this method has the potential to be powerful tool for enhancing frequency stability of CPT atomic clocks.

[357]P. M. Anisimov, R. A. Akhmedzhanov, I. V. Zelensky, and E. A. Kuznetsova, Journal of Experimental and Theoretical Physics, Vol. 97, No. 5, 2003, pp. 868-874.

IFCS-EFTF3-I1-3

Frequency Stability Performance of a Laser Pumped Rubidium Vapor Cell Atomic Frequency Standard

Miao Zhu

Agilent Laboratories, Agilent Technologies, Santa Clara, CA, USA

Email: miao_zhu@agilent.com

The AC Stark shift (the light shift) is very important in the performance of laser-pumped vapor cell atomic frequency standards, both in the population-altering-pumping (PAP) configuration and in the coherent-population-trapping (CPT) configuration. A continuous wave population-altering-pumping method with reduced light shift was proposed and implemented [1, 2]. Because there is no optical switch (such as an acousto-optical modulator) required, this method can be implemented in a compact vapor cell atomic frequency standard.

Here we report the frequency stability performance of a rubidium vapor cell atomic standard using this PAP method. In the setup a microwave cavity/oven assembly contained a ^{87}Rb cell (inner diameter ~ 8.5 mm, inner length ~ 13.5 mm). A diode laser with a wavelength of 795 nm was used for optical pumping. The laser frequency was stabilized to the ^{87}Rb transition ($F = 2 \rightarrow F' = 1$ & 2) using the injection current to the diode laser while the slow change of the laser power was corrected using the laser temperature. In addition, the transition frequency between the states $|F = 1, m_F = 1\rangle$ and $|F = 2, m_F = 1\rangle$ was used to adjust the bias magnetic field.

The device has been operating for more than 240 days continuously. The short term frequency stability data shows $\sigma_y(\tau) < 3\times10^{-12}\ s^{-1/2}$. Figure 1 shows that the absolute value of the relative frequency (averaging time = 1000 s) is smaller than 2.5×10^{-12}. The updated results will be reported at the conference.

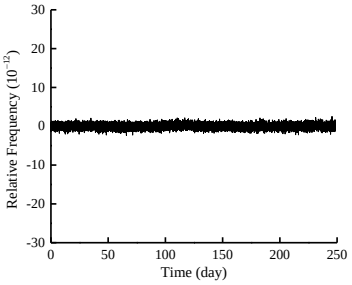

Fig. 1 Relative frequency (averaging time = 1000 s) vs. time. See the text.

References:

[1] Miao Zhu, 2007 Joint Meeting of IEEE Frequency Control Symposium and European Frequency and Time Forum, page 1334.

[2] Miao Zhu and Jeffrey F. DeNatale, 2009 Joint Meeting of IEEE Frequency Control Symposium and European Frequency and Time Forum, page 1183.

IFCS-EFTF3-I1-4

The Influence of Laser Polarization Noise on the Short-Term Stability of CPT Atomic Clocks

James Camparo, Michael Huang, and Travis Driskell
james.c.camparo@aero.org
Physical Sciences Laboratories
The Aerospace Corporation, 2310 E. El Segundo Blvd., El Segundo, CA, 90245, USA

The Coherent-Population-Trapping (CPT) vapor-cell atomic clock represents a clear break from previous vapor-cell clock technology. Beyond its already demonstrated utility for clock miniaturization, the underlying physics of CPT has advantages that may result in significant frequency stability improvements; for example, without a microwave cavity there is no sensitivity to microwave cavity-Q variations. However, along with the technology's benefits come new effects that may limit the CPT clock's capabilities, and one such effect is laser polarization noise. In the typical CPT clock, right-circularly polarized light (for example), σ_+, creates a superposition state composed of the two $m_F = 0$ ground state sublevels of an alkali atom via a common $m_F = +1$ excited state. If the polarization suddenly changes to left-circularly polarized light, σ_-, and back again, the common excited state will change from $m_F = +1$ to $m_F = -1$ and then back to $m_F = +1$. This will introduce a transient in the CPT signal, and thereby a degradation of the CPT clock's signal-to-noise ratio, S/N.

In previous work, we showed that when an atom interacts with a polarization modulated field, the CPT signal will first increase in amplitude as the polarization switching decreases the vapor's electronic spin-polarization (i.e., the atomic density in the "trapping state"), and then the CPT signal will split into a doublet as the rate of coherence modulation becomes larger than the natural CPT linewidth.

Here, we consider the problem of the CPT signal and noise when the laser polarization switches *randomly*. Specifically, in our experiments the laser polarization is characterized by a binomial process, as might be the case for VCSEL diode lasers, and we measure the CPT-signal amplitude, the CPT-signal linewidth, $\Delta\nu_{CPT}$, and the CPT-signal noise level at low Fourier frequencies (i.e., $\sim 10^2$ Hz): S/N and $Q = \nu_{hfs}/\Delta\nu_{CPT}$. Based on these measurements, we then infer the short-term stability of a CPT clock subject to a laser undergoing stochastic polarization variations: $(QS/N)^{-1}$.

For a CPT clock based on the traditional excitation scheme (i.e., use of right *or* left-circularly polarized light), the large transients in the transmitted light intensity following a polarization change (which result from a bulk motion of atomic population among Zeeman sublevels) yield a degradation in the CPT clock's short-term stability, even for relatively rare polarization switching events. Alternatively, for CPT clock's based on more novel excitation schemes (i.e., essentially the use of right *and* left-circularly polarized light) we anticipate only a modest change in short-term stability, which results from a small increase of the CPT-signal's linewidth. Thus, in addition to producing significantly larger CPT atomic clock signals, these more novel CPT signal excitation schemes may be less sensitive to laser-polarization noise.

IFCS-EFTF3-I1-5

A push-pull magnetometer

E. Breschi[1], Z. Grujic, P. Knowles, and A. Weis

[1]Physics Department, University of Fribourg, Switzerland

Email: evelina.breschi@unifr.ch

We report on an experimental study of a "push-pull magnetometer" based on polarization modulation. Although originally proposed to increase the resonance contrast in atomic clocks[358], the push-pull technique can be applied to a variety of interaction schemes. The fundamental concept behind push-pull is to drive a beat resonance between magnetic sublevels with modulated light, whose modulation is phase-coherent with the dynamic evolution of the atomic quantum state.

In the experiment, the laser polarization is modulated at a fixed frequency (ω_{mod} between 100 Hz and 10 kHz). The laser frequency is actively stabilized on the $F_g=4 \rightarrow F_e=3$ D1-transition in cesium via a Doppler-free DAVLL. The atoms are confined in an evacuated paraffin-coated cell maintained in a controlled magnetic field, of which one Cartesian component is scanned, while the two others are carefully compensated to zero. Light transmitted through the cell is collected by a photodiode whose signal is demodulated by a lock-in amplifier referenced to a harmonic q of ω_{mod}.

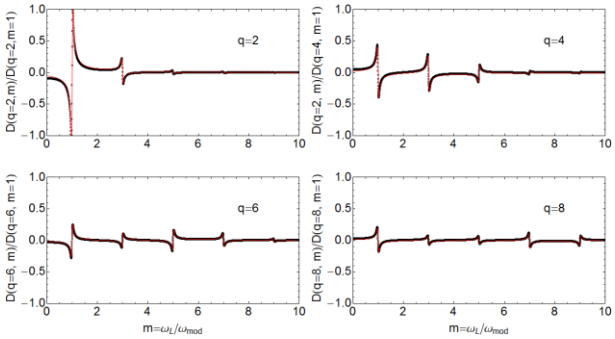

Fig. 1: Magnetic field dependence of dispersive lock-in signals for q=2,4,6, and 8, where q indicates the modulation frequency harmonic used for lock-in detection. Dots are measurements and the red-line shows model results. All spectra are normalized to the amplitude of the (q=2, m=1)-resonance.

We study spectra obtained by lock-in detection under different polarization modulation configurations. Figure 1 shows the results for a square-wave modulation between left- and right-circular polarizations, with the magnetic field component orthogonal to the laser propagation vector being scanned. Resonances are observed whenever $m \cdot \omega_{mod} = \omega_L$. An algebraic model[359] describing the dynamics of atomic spin orientation has been used for data interpretation. Experimental results and model predictions are in excellent agreement. The dispersive lock-in signal can be used as an error signal for magnetic field measurements. In order to evaluate the sensitivity of the push-pull magnetometer, we estimate the noise-equivalent-magnetic field[360] defined as the ratio between photocurrent's shot noise, and the reference resonance discriminator slope. Different harmonic signals can be considered and compared for magnetic sensitivity.

---

[358] Y.-Y. Jau, E. Miron, A. B. Post, N. N. Kuzma, and W. Happer "Push-pull Optical Pumping of pure superpositions states" Phys. Rev. Lett. vol. 93 p. 160802, 2004.

[359] Z. Grujic, and A. Weis, "Atomic magnetic resonance induced by amplitude-, frequency-, or polarization-modulated light", submitted to Phys. Rev. A, 2013.

[360] G. Di Domenico, H. Saudan, G. Bison, P. Knowles, and A. Weis, "Sensitivity of double-resonance alignment magnetometers"Phys. Rev. A. vol. 76 p. 023407, 2007.

Liquid Sensing

CLUB D

Wednesday, July 24 2013, 04:30 pm - 06:00 pm

Chair: **Sylvain Ballandras**
frec|n|sys SAS

IFCS-EFTF4-I2-1

Probing colloid-substratum contact stiffness by acoustic sensing in a liquid phase

Adam L.J. Olsson,[1] Henny C. van der Mei,[1] D. Johannsmann[2], Henk J. Busscher,[1] Prashant K. Sharma[1]

[1] Department of Biomedical Engineering, University Medical Center Groningen and University of Groningen, P.O. Box 196, 9700 AD Groningen, The Netherlands.

[2] Institute of Physical Chemistry, Clausthal University of Technology, D-38678 Clausthal-Zellerfeld, Germany

Email: johannsmann@pc.tu-clausthal.de

In QCM, particles adhering to a sensor crystal are perturbed around their equilibrium positions, via thickness-shear vibrations at the crystal's fundamental frequency and overtones.[xvi] The amount of adsorbed molecular mass is measured as a shift in resonance frequency. In inertial loading, frequency shifts are negative and proportional to the adsorbed mass, contrasting to "elastic loading" where particles adhere via small contact points. Elastic loading in air yields positive frequency shifts according to a coupled resonance model. We here explore the novel application of a coupled resonance model for colloidal particle adhesion in a liquid phase theoretically and demonstrate its applicability experimentally. Particles with different radii and in absence and presence of ligand-receptor binding showed evidence of coupled resonance. By plotting the frequency shifts *versus* the QCM-D overtone number, frequencies of zero-crossing could be inferred indicative for adhesive bond stiffness. As a novelty of the model, it points to a circular relation between bandwidth *versus* frequency shift, with radii indicative of bond stiffness. The model indicated that bond stiffness for bare silica particles adhering on a crystal surface is determined by attractive Lifshitz-Van der Waals and ionic-strength-dependent, repulsive electrostatic forces. In presence of ligand-receptor interactions, softer interfaces develop that yield stiffer bonds due to increased contact areas. In analogy with molecular vibrations, the radii of adhering particles strongly affect the resonance frequencies, while bond stiffness depends on environmental parameters to a larger degree than for molecular adsorption.

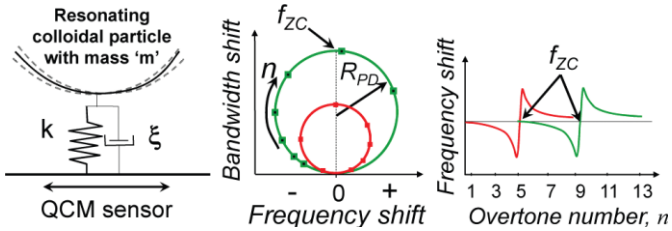

Fig. 115: Adsorbed particles give rise to a "coupled resonance". When Frequency and bandwidth are displayed in a polar diagram, the radius of this diagram is proportional to the stiffness of the link.

Sensor Design and Characterization Method for New Multimode Downhole Sonic Measurements

Hiroshi Hori[1], Yuichiro Wada[1], Hiroshi Nomura[1], Atsushi Oshima[1], Tadashi Tajima[1], Junko Fujikawa[1], Takeshi Fukushima[1]

[1]Sonic Product Line, Schlumberger K.K., Sagamihara, Kanagawa/Japan

Email: hori1@slb.com

Downhole sonic measurements provide compressional and shear wave propagation speeds of formation for hydrocarbon exploration purposes. Recorded data is combined with other logging data to fully characterize the formation and wellbore for safe and effective well placement. Such information is valuable when provided during the early stages of well placement, such as during drilling. The demand for logging while drilling (LWD) is increasing.

Conventional LWD sonic tools are equipped with monopole transmitters and array receivers as sensors. Receiver elements are distributed on the tool collar along the axial direction at a controlled distance. The transmitter excites acoustic pulses in borehole fluid. Acoustic waves are radiated into the formation, and a part of the energy propagates along the tool near the wellbore and is refracted back to the borehole. Refracted waves are recorded as the time-domain signals and processed downhole to provide formation velocities using semblance method. The problem in shear velocity measurements occurs when formation shear velocity is smaller than that of well fluid because refracted wave ceased to present. In such condition as the alternative method, we excite higher-order borehole modes, such as dipole and quadrupole, from which the shear velocity is obtained using model-based inversion techniques.

To realize new multimode measurements, we designed transmitters and receivers that consist of azimuthally segmented units. Azimuthal transmitter output and receiver sensitivity matching is critical to provide quality multimode measurements, especially in an acoustically challenging environment where unwanted mode rejection is necessary.

We characterized receivers mounted on sonic tools using our in-house test facility. To ensure measurements downhole, we recorded signals up to high pressure and temperature of 172MPa and 150°C and normalized them using azimuthal average. Normalized amplitude is representative of the sensitivity matching. Figure 1 shows the distribution of normalized signal amplitude of the receivers over 500 elements. We concluded the standard deviation of receiver sensitivity was 2%.

In summary, we designed the sensor for new multimode sonic measurements while drilling, established their characterization methods at high pressure and temperature, and demonstrated good sensor matching.

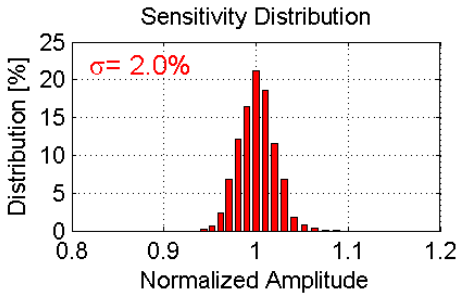

Fig. 116: Histogram of normalized signal amplitude of downhole sonic receivers under high pressure and temperature, representing sensitivity distribution. The standard deviation was 2%.

IFCS-EFTF4-I2-3

Analysis of the Detection of Organophosphate Pesticides in Aqueous Solutions Using Polymer-Coated SH-SAW Sensor Arrays

Tian Newman, Arnold Mensah-Brown, Florian Bender, Fabien Josse
Dept. of Electrical and Computer Eng., Marquette University, Milwaukee, WI 53201-1881

email: fabien.josse@mu.edu

The presence of hazardous contaminants, including pesticides, in the environment continues to be of great concern to public health. Among the class of pesticides, the agro-industry has increasingly relied on organophosphate and carbamate pesticides because of their high insecticidal activity and relatively low persistence in the environment. However, recent research shows that organophosphate pesticides (OPs) still persist in the environment for long enough to produce residues in ground water, soil, and agricultural products. The presence of OPs in surface and ground water is a major concern to public health. As a result, there is a need to monitor these environmental contaminants in water. The use of organophosphates indoors has been discontinued but monitoring the output in industrial and agricultural setting has continued. Current means of detection still require transportation to a laboratory for analysis, resulting in costly and time consuming procedures. Therefore, there is a need for a portable and low-cost sensor system for real-time detection, identification and quantification of organophosphates pesticides in groundwater. In this work, the coated shear horizontal surface acoustic wave (SH-SAW) device is investigated as a micro-chemical sensor for the direct, rapid and in-situ monitoring of chemical contaminants in groundwater and wastewater. The chemical contaminants being tested here are organophosphate-based compounds (parathion, parathion-methyl, and paraoxon). The polymers used as partially chemically selective coatings on the SH-SAW devices are 2,2'-diallylbisphenol A - 1,1,3,3,5,5-hexamethyltrisiloxane (BPA-HMTS), 2,2'-diallylbisphenol A - polydimethylsiloxane (BPA-PDMS), and polyepichlorohydrin (PECH).

An array of sensors consisting of devices with the different coatings and coating thicknesses (0.25μm and 0.50μm) is designed to increase frequency sensitivity and selectivity by providing a specific response pattern for each analyte. Analyte identification is performed using a visual pattern recognition technique based on radial plots for the analytes, parathion, paraoxon, and parathion-methyl, at concentrations from 0.5mg/L to 3.0mg/L. These specific radial plots are made using the steady-state frequency shifts and time responses of BPA-HMTS, BPA-PDMS, and PECH at a thickness of 0.5μm as the axes, providing a total of six parameters for analyte recognition. It is demonstrated that each analyte can be identified within the above concentration range using this approach. In addition, level-of-confidence calculations are presented to estimate the concentration of an unknown sample by quantifying the similarity between known response patterns and the response pattern of the unknown sample. It is shown that this method can successfully estimate the concentrations of measured test samples (e.g. 3.0mg/L of parathion, 2.0mg/L of paraoxon, 0.5mg/L of parathion-methyl) and extrapolate response patterns for sample concentrations that were not included in the pattern recognition design database (e.g. 1.49mg/L of parathion and 1.75mg/L of parathion). It was noted that the highest levels of confidence for the latter test sample were found for 1.5mg/L and 2.0mg/L, giving identical level-of-confidence values for these concentrations, thus indicating the algorithm correctly identifies the test sample as 1.75mg/L of parathion. In summary, using the absorption time constant, which is unique to a given analyte-coating pair, in conjunction with steady-state frequency shifts permits direct identification and quantification of organophosphate pesticides in liquid-phase at low-ppm and sub-ppm concentrations.

IFCS-EFTF4-I2-4

Resonant Characteristics of Rectangular Hammerhead Microcantilevers Vibrating Laterally in Viscous Liquid Media

Jinjin Zhang[1], Fabien Josse[1], Stephen M. Heinrich[2], Oliver Brand[3], Isabelle Dufour[4], Nicholas Nigro[2]

[1] Electrical and Computer Engineering, Marquette University, Milwaukee, WI/USA
[2] Civil, Construction and Environmental Engineering, Marquette University, Milwaukee, WI/USA
[3] School of Electrical and Computer Engineering, Georgia Institute of Technology, Atlanta, GA/USA
[4]Université de Bordeaux, IMS Laboratory, Talence, France
email: fabien.josse@marquette.edu

Dynamically driven prismatic microcantilevers excited in the in-plane direction have been investigated and used in liquid-phase sensing applications due to their relatively high frequency stability and mass sensitivity. However, in bio-chemical sensing applications, the performance of prismatic microcantilever-based sensors is restricted due to their limited surface sensing area. The higher stiffness in shorter and wider prismatic microcantilevers also makes them difficult to excite when electrothermally driving the sensor devices near the base. Thus, in order to increase the surface sensing area, further improve sensor characteristics (increase the adsorbed mass and the sensitivity of detection) and make microcantilevers easier to excite electrothermally, it has been proposed to investigate rectangular hammerhead microcantilevers driven in the in-plane flexural vibration mode in viscous liquid media. In this work, the resonant characteristics of rectangular hammerhead microcantilevers vibrating in the in-plane vibration mode in viscous liquid media are investigated. The rectangular hammerhead microcantilever consists of a stem and a head. The stem is modeled as an Euler-Bernoulli beam while the head is modeled as a rigid body. As the microcantilever vibrates, both translational and rotational motions of the head are taken into account. A semi-analytical expression for the hydrodynamic function in terms of the Reynolds number and aspect ratio, h/b (thickness over width) is first obtained. Using this expression, the resonance frequency and quality factor are investigated as functions of both the rectangular hammerhead microcantilever geometry and liquid media properties.

Analyses are performed and results are compared for the resonant characteristics of rectangular prismatic and hammerhead microcantilevers laterally vibrating in water. For appropriate comparison, the surface sensing area of the microcantilevers is considered. For example, for a rectangular prismatic microcantilever of dimensions (200×45×12) μm^3 and two hammerhead microcantilevers of dimensions [(200×45×12) +(50×200×12)] μm^3 and [(150×45×12) +(50×200×12)] μm^3, the results show that the resonance frequencies are 1.412 MHz, 0.512 MHz and 0.738 MHz, the percent changes of the resonance frequency from air to water are 8.8%, 3.8% and 3.0%, the quality factors are 36, 30 and 40 in water, and the normalized surface mass sensitivities (relative frequency shift/unit mass/unit area) are 14.9 μm^2/ng, 16.7 μm^2/ng and 16.8 μm^2/ng, respectively. For the hammerhead microcantilever with a shorter stem, the quality factor and normalized surface mass sensitivity are 11% and 13% higher than those of the prismatic microcantilever, respectively, although the resonance frequency is lower. For the range of dimensions considered, if only the length of the stem or head increases, the resulting resonance frequency, quality factor and mass sensitivity will decrease. In contrast, if only the width of the head increases, the resonance frequency and mass sensitivity will decrease and the quality factor will increase for the shorter heads. Such trends can be used to optimize sensor device geometry and frequency stability. The increase in the surface sensing area and quality factor are expected to yield higher sensitivity of detection and improved signal-to-noise ratios in liquid-phase chemical sensing applications.

IFCS-EFTF4-I2-5

Design of SH-Surface Acoustic Wave Sensors for Detection of ppb Concentrations of BTEX in Water

Florian Bender[1], Rachel Mohler[2], Antonio J. Ricco[3], Fabien Josse[1]

[1]Dept. of Electr. and Computer Eng., Marquette University, Milwaukee, WI 53201-1881
[2]Chevron Energy Technology Co., 100 Chevron Way, Richmond, CA 94801
[3]Dept. of Electr. Eng., Center for Integrated Systems, Stanford University, Stanford, CA 94305

email: fabien.josse@mu.edu

An SH-SAW (shear-horizontal surface acoustic wave) sensor system for speciation of BTEX (benzene, toluene, ethylbenzene, and xylenes) in water is under development. Due to the carcinogenicity of benzene, it is necessary to quantify benzene concentrations in the presence of the other aromatic compounds down to parts per billion (ppb) levels. This is not trivial as benzene has the highest solubility in water among the BTEX compounds. While the required selectivity can be achieved through the use of different polymer coatings in a sensor array and evaluation of transient response information, various strategies are currently under investigation to improve the detection limit for benzene, including new designs of the SH-SAW sensor platform.

Using suitable multi-electrode IDT (interdigital transducer) designs, a sensor array can be implemented utilizing identical devices with different coatings and operating at different frequencies, hence achieving different sensitivities and with different optimal sensing film thicknesses. Fig. 1 shows the spectrum of an SH-SAW sensor using an S_e = 20 transducer design (S_e is the number of fingers per electrical period): for each electrical period, two electrode fingers connected to the positive bus bar alternate with 18 fingers connected to the negative bus bar. A spectrum of well-separated SH-SAW harmonics can be seen, which is useful to obtain a maximum of information in sensor array measurements. It also permits a more comprehensive characterization of the viscoelastic behavior of polymer films (at various thicknesses) at different frequencies in a single measurement. Fig. 2 shows initial measurements on the detection of 5 ppm benzene in water, performed with this sensor design using a 0.55 µm thick poly(ethyl acrylate) coating. A ratio of the frequency shifts, Δf (164 MHz) / Δf (123 MHz), of 2.80 was found, higher than the ratio of 1.78 expected for pure mass loading where $\Delta f \propto f^2$. This finding indicates more efficient waveguiding and/or frequency-dependent viscoelastic effects at 164 MHz for this coating. In a separate experiment, detection of 200 ppb benzene in water was successfully demonstrated for the164-MHz harmonic. A detection limit of 20 ppb is also estimated for ethylbenzene.

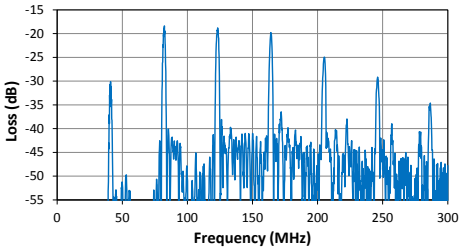

Fig. 117: Transmission spectrum of an SH-SAW sensor, coated with 0.3 µm poly(methyl methacrylate), in air, showing harmonics at multiples of 41 MHz.

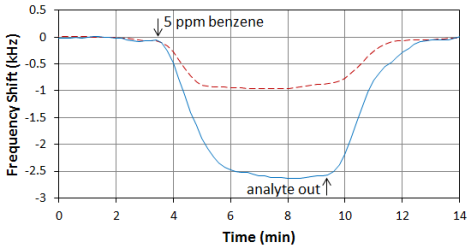

Fig. 2: Response of the SH-SAW sensor, coated with 0.55 µm poly(ethyl acrylate), to 5 ppm benzene (- - 123-MHz mode, — 164-MHz mode).

Integrated MEMS Circuits

CLUB H

Wednesday, July 24 2013, 04:30 pm - 06:00 pm

Chair: **Gianluca Piazza**
Carnegie Mellon University

IFCS-EFTF1-I3-1
Wentao Wang[1], Radhika Marathe[1], Bichoy Bahr[1], Laura C. Popa[1], **Dana Weinstein[1]**
[1]*MIT, USA*

RF Solid-State Vibrating Transistors

Wentao Wang, Radhika Marathe, Bichoy Bahr, Laura C. Popa, Dana Weinstein
MIT, Cambridge, MA, USA
Email: dana@mtl.mit.edu

Semiconductor micro-electromechanical (MEM) resonators, with quality factors (Q) often exceeding 10^4 can provide a high performance, low-power, compact IC-compatible alternative to electrical components in clocking, communication, and sensing applications. Key challenges to wide-spread implementation of these devices include complex fabrication, packaging, and frequency scaling. The work presented here focuses on new transduction mechanisms and new resonant structures that enable intimate integration with ICs at multi-GHz frequencies.

The majority of electromechanical devices require a release step to freely suspend moving structures. This necessitates costly complex encapsulation methods and back end-of-line processing of large-scale devices. Instead, we present the development of *unreleased* Si-based MEMS resonators in CMOS, allowing seamless integration into Front End of Line (FEOL) processing with no post-processing or packaging.

To address frequency scaling up to mm-wave frequencies, we introduce the Resonant Body Transistor (RBT) which can be integrated into a standard CMOS process. The unreleased, Si bulk acoustic resonators are driven capacitively using the thin gate dielectric, and actively sensed using a field-effect transistor (FET) incorporated into the resonant cavity. *FET sensing* with the high f_T, high performance transistors in CMOS amplifies the mechanical signal before the presence of parasitics. The resulting RF-MEMS resonators can provide low power, low cost, small footprint building blocks for on-chip signal generation and processing. For low loss and high power applications, this concept can be extended to III-V semiconductors commonly used for mm-wave ICs (MMICs). We present our latest results on multi-GHz MEMS-HEMT resonators in GaN and their implications for channel-select radio design.

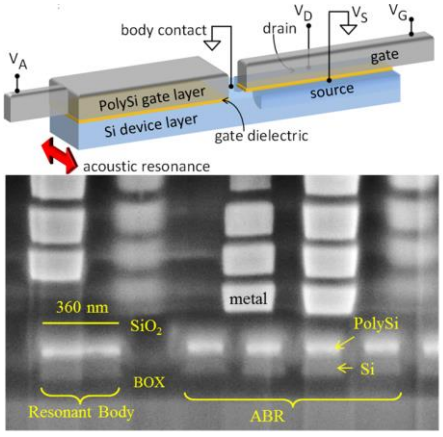

Fig. 1. Si Resonant Body Transistor demonstrated in IBM's 32nm SOI process. The unreleased resonator is acoustically confined with Acoustic Bragg Reflectors formed using the CMOS stack, and exhibits resonance at 11 GHz.

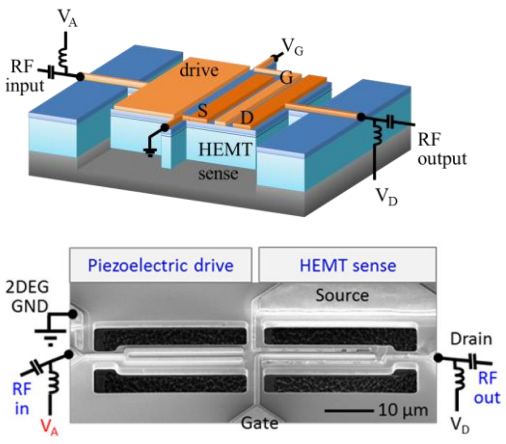

Fig. 2. AlGaN/GaN Resonant Body Transistor using HEMT sensing to achieve >3 GHz resonance with the highest $f.Q$ product in GaN to date. Furthermore, unique properties of AlGaN/GaN enable DC switching of piezoelectric transduction in the

IFCS-EFTF1-I3-2

Enhanced Temperature Sensitivity of a Single CMOS-MEMS Resonator via Resonant Modes in Orthogonal Axes

Ming-Huang Li, Chao-Yu Chen, Cheng-Syun Li, Chi-Hang Chin, and Sheng-Shian Li

Inst. of NanoEngineering and MicroSystems, National Tsing Hua University, Hsinchu, Taiwan

Email: s100035807@m100.nthu.edu.tw

A novel CMOS-MEMS composite ring resonator capable of a ***dual-mode*** operation has been proposed to enable self-temperature sensing in a ***single*** device. To maximize the temperature sensitivity between the dual modes, two resonant modes of a single resonator vibrating in orthogonal axes (i.e., in-plane and out-of-plane) are chosen due to the large difference of their temperature coefficients of frequency (TC_f). The different thermal-frequency behaviors were realized by the flexibility of the structural configuration from the CMOS back-end-of-line materials where metals (aluminum and tungsten) provide a negative TC_f while, in contrast, dielectrics (SiO_2) offer a positive TC_f. By adjusting the constituent ratio and the position of metals and dielectrics through CAD layouts, different TC_f's have been successfully demonstrated in a single CMOS-MEMS resonator. From the experimental results, the measured frequency and temperature response of the in-plane (INP) resonant mode yields a resonance frequency of 6.5 MHz, Q of 1100, and TC_f of -53 ppm/°C. In contrast, the out-of-plane (OOP) resonant mode yields a resonance frequency of 5 MHz, Q of 2300, and TC_f of -79 ppm/°C. As compared to the prior arts[361,362], ***a largest TC_f difference enabled by a single resonator*** (-26 ppm/°C between modes) to date is achieved.

A ring-shaped resonator with four nodal supports surrounded by its INP side electrodes and OOP bottom electrodes is depicted in Fig.1. This device was fabricated in a maskless metal wet-etching 0.35μm CMOS-MEMS platform[363]. A detailed cross-section view of the resonator is shown in Fig.2a where the dotted arrows indicate the vibrating directions. Since the resonator is a sandwiched metal-oxide composite, it allows us to design different TC_f's in different axes. To understand the temperature sensitivity of the dual-mode resonator, the measured thermal response is shown in Fig.2b. The beat frequency of the dual-mode resonator[2] is defined by $f_{beat} = (f_{INP}/N_1)-(f_{OOP}/N_2)$ where N_1 and N_2 are scaling factors. By properly choosing N_1=64 and N_2=50, an ***estimated maximum beat frequency sensitivity of 3760 ppm/°C is obtained*** by a liner curve fit (R^2=0.92), as shown in the right Y-axis of Fig.2b.

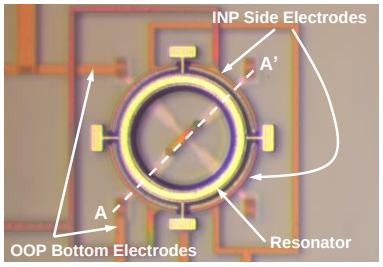

Fig. 118: Optical view of a CMOS-MEMS ring resonator, indicating its in-

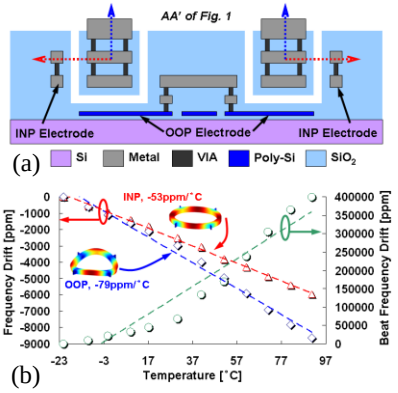

Fig. 119: (a) Cross-section view of the proposed resonator. (b) Measured temperature responses of the resonator. The estimated beat frequency drift is shown in the right Y-axis.

[361] M. Koskenvuori, *et al.*, "Temperature measurement …," *MEMS'08*, Tucson, USA, pp. 78-81, 2008.

[362] M. J. Dalal, *et al.*, "Simultaneous dual-mode ...," *MEMS'11*, Cancun, Maxico, pp. 489-492, 2011.

[363] W.-C. Chen, *et al.*, "A fully-differential …," *IEEE Electron Device Lett.*, vol. 33, no. 5, pp. 721-723, May 2012.

IFCS-EFTF1-I3-3

Stress-enhanced chemical vapor deposited graphene NEMS RF resonators

Michael Lekas[1], Sunwoo Lee[1], Changyao Chen[2], James Hone[2], Kenneth Shepard[1]

[1]Department of Electrical Engineering, Columbia University, New York, NY, USA
[2] Department of Mechanical Engineering, Columbia University, New York, NY, USA

Email: msl22@ee.columbia.edu

Graphene has received much attention owing to its exceptional electrical and mechanical properties[364,365]. For electronic applications, graphene has been explored as a channel material for RF field-effect transistors (FETs)[366]. In nano-mechanics research, RF mechanical resonators have been made using graphene to take advantage of its high strength and stiffness, and low mass[367].

By operating a graphene nanoelectromechanical resonator (GNER) as a mechanically resonant FET, both the electrical and mechanical advantages of the material can be combined to improve the transduction of mechanical resonance[368]. Vibrations are electrostatically actuated in a suspended graphene channel by applying an RF signal and DC bias between the channel and an underlying gate. Displacement of the graphene channel relative to the gate modulates the charge density in the graphene, which is then sensed as a drain current modulation. This transduction technique has opened the possibility of using GNERs in RF circuits such as filters and oscillators.

Current obstacles to application of GNERs include process scalability concerns, poor transduction at room temperature, and low resonance frequencies (f_o). In this work we present RF measurements of GNERs taken at room temperature with Q's of about 100 at frequencies above 190 MHz, which, to the best of our knowledge, are the highest values to date for non-cryogenic measurements of GNERs. Additionally, tuning of f_o over more than 5% bandwidth is demonstrated through application of a DC gate bias of 5V. Yield and f_o are improved by straining the suspended graphene using an SU-8 polymer clamp, and chemical vapor deposited (CVD) graphene is used to demonstrate the scalability of the process.

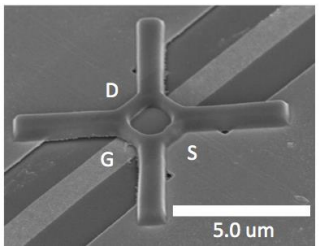

Fig. 120: SEM of GNR with SU-8 clamp.

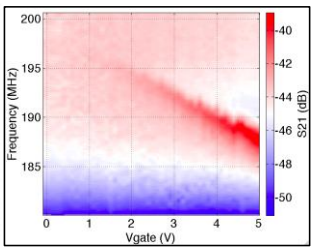

Fig. 121: Resonance signal (S21) as a function of gate voltage.

[364] Novoselov, K. *et al*, "Electric field effect in atomically thin carbon films," Science, vol. 306, p.666-669, 2004.

[365] Lee, C. *et al*, "Measurement of the Elastic Properties and Intrinsic Strength of Monolayer Graphene," Science, vol. 321, p. 385-388, 2008.

[366] Meric, I. *et al*, "Current saturation in zero-bandgap, top-gated graphene field-effect transistors," Nature Nanotech., 2008.

[367] Bunch, J.S. *et al*, "Electromechanical resonators from graphene sheets," Science, vol. 315, p. 490-493, 2007.

[368] Xu, Y. *et al*, "Radio frequency electrical transduction of graphene mechanical resonators," Appl. Phys. Lett., vol. 97, 2010.

Micromechanical Disk Array-Composite for Enhanced Frequency Stability Against Bias Voltage Fluctuations

Lingqi Wu[1], Mehmet Akgul[1], Zeying Ren[1], Clark T.-C. Nguyen[1]

[1]Dept. of EECS, University of California at Berkeley, Berkeley, CA, USA

Email: wulingqi@berkeley.edu

A 215-MHz polysilicon capacitive-gap transduced micromechanical resonator array employing 50 mechanically coupled contour mode disks (*cf.* Fig. 1)—the largest such array yet fabricated and measured—has achieved 3.5× better frequency stability than single stand-alone disk counterparts against fluctuations in the dc voltage (V_P) normally dropped across the electrode-to-resonator gaps during device operation. Here, connection of numerous resonators via half-wavelength ($\lambda/2$)-dimensioned coupling beams produces a single array-composite resonator that selectively resonates at a single mode frequency with all resonators moving in phase. The key to enhanced frequency stability against bias voltage variation is the electrode-to-resonator capacitance (C_o) generated by the parallel combination of input/output electrodes overlapping each resonator in the array. C_o dominates among elements loading the resonator and effectively raises its stiffness (beyond the stiffness increase resulting from mechanical coupling), much like a varactor does in crystal circuits. This in turn reduces the efficacy of the bias voltage-controlled electrical stiffness[369]. The more resonators in the array, the smaller the frequency shift imposed by a given bias voltage change. This result suggests that the most stable MEMS-based oscillators (e.g., against supply noise and acceleration[370]) are ones that utilize mechanically-coupled arrays of resonators.

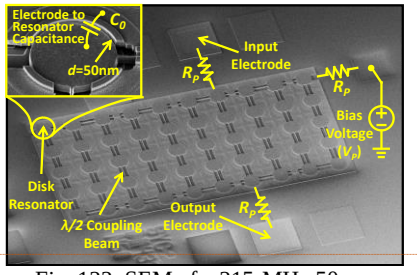

Fig. 122: SEM of a 215-MHz 50nm capacitive-gap transduced contour mode disk array employing 50 mechanically coupled resonators.

Fig. 2 presents measured curves of frequency versus bias voltage for the array-composite resonator of Fig. 1, all alongside theoretical curves predicted by an equivalent circuit modeling the above phenomena for arrays with different numbers of resonators. Here, theory and measurement match quite well. The 50-element 215-MHz array experiences a 20ppm frequency change when V_P varies by 9V, which represents a 3.5× improvement over the 70ppm of a single resonator and could potentially improve the acceleration sensitivity of a MEMS based oscillator by 11dB.

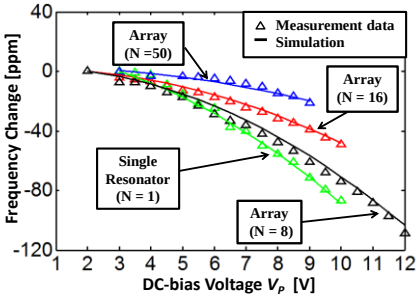

Fig. 2: Measured curves of resonance frequency versus dc-bias voltage V_P plotted against simulation using equivalent circuit models for resonator arrays with N=1, N=8,

[369] Frank D. Bannon III, J. R. Clark, and C. T.-C. Nguyen, "High-*Q* HF Microelectromechanical Filters", *IEEE J. Solid-State Circuits*, vol. 35, no. 4, pp. 512-526, April 2000.

[370] T.L. Naing, T. O. Rocheleau, Z. Ren, E. Alon, and C. T.-C. Nguyen, "Vibration-Insensitive 61-MHz Micromechanical Disk Reference Oscillator", *IEEE Int. Frequency Control Symposium*, Baltimore, Maryland, pp. 276-281, May 2012.

Comment [ctn5]: Somewhere in the figure, you need to show the dc bias.

Comment [ctn6]: reference Frank Bannon's JSSC filter paper.

IFCS-EFTF1-I3-5

Exploiting Structural Nonidealities in MoS_2 NEMS Resonators for Mode Shape Engineering and Frequency Control

Zenghui Wang[1*], Jaesung Lee[1], and Philip X.-L. Feng[1*]

[1]Electrical Engineering, Case Western Reserve University, Cleveland, OH 44106, USA

Email: zenghui.wang@case.edu, philip.feng@case.edu

Nanoelectromechanical systems (NEMS) made of atomically-thin crystalline nanostructures have demonstrated attractive potential for new actuators and sensors[xvii,xviii]. New types of 2D materials are often first obtained by mechanical exfoliation which usually leads to imperfect device geometries. In this work, we study ***ultrathin molybdenum disulfide (MoS_2) NEMS resonators***, with focus on ***investigating the effects of structural nonidealities and asymmetries on the device characteristics***. We observe that structural nonidealities such as irregularities in shapes, boundaries, thicknesses, and geometrical asymmetries do not compromise device performances. Instead, they provide an additional geometrical degree of freedom which allows novel engineering of the device's mechanical behavior, such as controlling the mode shape and mode index, as well as tuning the frequency ratio between different resonant modes. This capability is interesting for designing multimode and nonlinear resonant components in nanomechanical circuits.

We fabricate MoS_2 NEMS resonators using photolithography, wet etching, and mechanical exfoliation. For each device, we measure its room-temperature thermomechanical resonance with an ultrasensitive interferometric system, and characterize the device with optical microscope, SEM, and AFM (Fig. 1 top insets). We observe that devices with nonideal geometries can have high fundamental-mode resonance frequency f (in the VHF band) and good quality factor (Q>300), showing no degradation from normal devices.

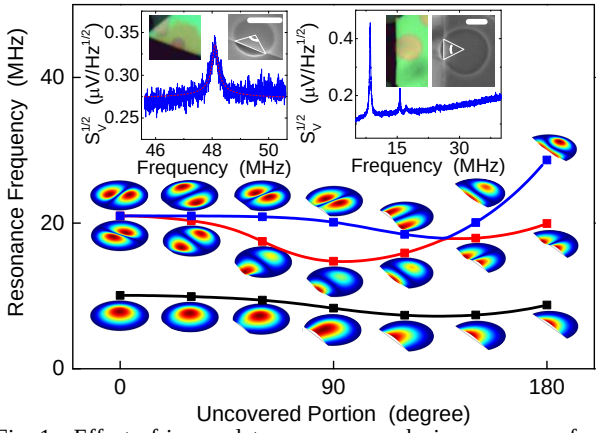

Fig. 1: Effect of incomplete coverage on device resonance for a MoS_2 diaphragm clamped above a circular microtrench. The three lowest modes are shown, with mode shapes illustrated for different degrees of partial coverage. *Top Insets*: measured mechanical resonances, optical images, and SEM images of two such MoS_2 nanomechanical devices. The uncovered portion is quantified by its radius angle (SEM images). Scale bars: 2μm.

Figure 1 shows results from COMSOL simulations of incompletely covered resonators. Data in this work reveal very interesting effects and rich insight into the mode shape and frequency scaling. These include: (i) mode splitting due to symmetry breaking; (ii) robust performance in spite of structural irregularities; (iii) non-monotonic dependence of frequency on the degree of geometric imperfection; (iv) mode crossing in multimode systems; (v) lifting of degeneracy from broken symmetry.

IFCS-EFTF Group 1 poster session 2

Forum Hall

Wednesday & Thursday, July 24-25, 2013, 1:00 pm - 2:00 pm and 3:30 pm - 4:30 pm

Chair: **Derek Puccio**
Quartzdyne

Experimental and theoretical results on SC-cut quartz resonators collectively realized on 4” wafers

A. Clairet[1], T. Laroche[2], L. Couteleau[1] and J-J. Boy[3]

[1]RAKON France, 2 rue Robert Keller, 10150 Pont-Sainte-Marie, FRANCE
[2]FEMTO-ST, Frequency & Time Dept, 26 chemin de l’Epitaphe, 25000 Besançon, FRANCE
[3]ENSMM, FEMTO-ST, 26 chemin de l’Epitaphe, 25000 Besançon, FRANCE

Email: alexandre.clairet@rakon.com

In the light of modern computer modeling, innovative processes and a multidisciplinary approach of research and industry, our project (for more details, see also 1) has been proposed to revisit designing low-cost miniaturized quartz resonators without compromising performance characteristics. The use of CAD tools has allowed the optimization of quartz resonators.

In order to produce collective SC-cut quartz resonators, we achieved 4” wafers (standard of microelectronics) in which our prototypes are cut. Each of these resonators are encapsulated under vacuum to not damage their performances and to insure the best of them, furthermore guaranteed by selected clamping. In order to ensure these two requirements, a procedure of wafer bonding (quartz on quartz with SC-cut wafers) is adopted (see Fig. 1). This process is well known in the silicon industry and has been adapted to quartz and intended products.

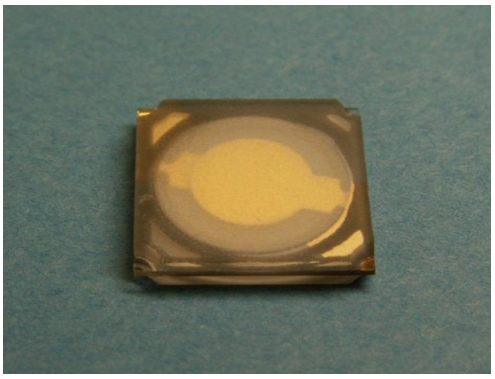

Fig. 123: Prototype

Considering the active part of the resonator and knowing that a structure with radius of curvature is hardly compatible with collective fabrication, we have realized plano-plano structure working at 14 MHz on the 3rd overtone of their slowest thickness shear mode, called C-mode (corresponding to the thickness of the wafer of about 380 µm). The main task of this project was to optimize the geometrical and the physical parameters of the prototypes. Thanks to Finite Elements Method (FEM), we were able to find optimal characteristics such as Motional parameters, Q-factor…

In this paper, first of all, we present the characterization of the wafers (in terms of orientation, roughness …) and then, we describe the manufacturing steps of the prototypes (collective process for micro-machining of the entire surface of the quartz …).

Next, the theoretical results are compared to measurements performed on prototypes. We have observed a good agreement between the experimental results and those obtained with FEM software (COMSOL Multiphysics®).

[1] A. Clairet et al., “Modeling of BVA resonators for collective fabrication”, Proceedings of the European Frequency and Time Forum, pp. 49-52, Gothenburg, Sweden, April 2012

IFCS-EFTF1-PCD1-2

Vector Network Analyzer Measurements of Frequency Fluctuations in Aluminum Nitride Contour-Mode Resonators

Nicholas Miller, Gianluca Piazza

Department of Electrical and Computer Engineering, Carnegie Mellon University, Pittsburgh, Pennsylvania, USA

Email: njmiller@andrew.cmu.edu

In order to engineer high precision compact MEMS enabled frequency sources it is of fundamental importance to identify the principle noise mechanisms in the oscillator circuit. These noise sources can be mainly partitioned into two groups: those originating in the amplifier and those originating in the resonator. In this work we investigate the latter, and, for the first time, we demonstrate the measurement of frequency fluctuations in a 586MHz one-port aluminum nitride contour-mode resonator using a vector network analyzer (VNA). We compare the resonator measurement with measurements of a closed-loop oscillator employing the same resonator and find good agreement, see figure 1.

The frequency fluctuations of a 1-port resonator create a phase noise in the reflected signal through the phase/frequency slope of the resonator at resonance, $\mathrm{Im}\left[\frac{1}{\Gamma}\frac{\partial\Gamma}{\partial\omega}\right]$, where Γ is the reflection coefficient. This factor depends on the resonator's motional inductance and impedance matching relative to the 50Ω VNA. For small high frequency resonators with a few Ohms of impedance mismatch, number can be very small and renders homodyne measurement particularly challenging. For our resonator, this factor is 8×10^{-6}. In order to uncover noise it is necessary to employ a sufficiently low noise homodyne setup remove the phase noise of the source. A bridge setup is also required if the source frequency noise is greater than of the resonator[1], though this was not needed in our case. In order to achieve sufficiently low measurement noise, the frequency bandwidth of the VNA must sufficiently low and sets the upper bound of the spectral offset frequency can be measured.

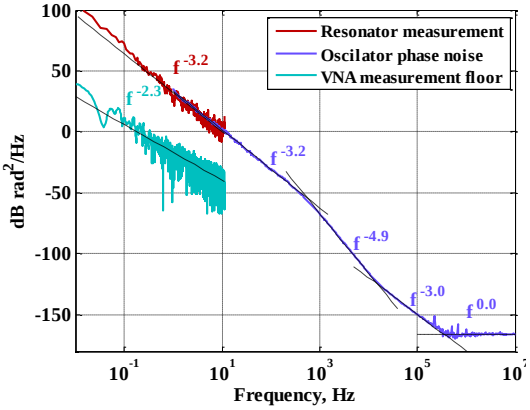

Figure 1: Open-loop measurement of resonator frequency fluctuations, referred to closed-loop phase noise by dividing by f^2, compared with the phase noise of a closed-loop oscillator employing the same resonator. The open-loop measurement is shown to be well above the VNA measurement floor. The noise exponents were fit with least

only this any this to that IF be that of

[1] E. Rubiola *et al.* "Flicker Noise Measurement HF Quartz Resonators", *IEEE Trans. on Ultrason., Ferroelectr., Freq. Control*, vol. 47, no. 2, 2000.

IFCS-EFTF1-PCD1-3

New Calibration Method for Experimental Study of the Nonlinear Behavior of a Bulk Acoustic Wave Resonator Subject to a High-Power Signal

Catherinot Lise[1], Bila Stéphane[2], Chatras Matthieu[2], Cros Dominique[2]

[1]Innovation Department, TRONICO, Nantes, France
[2]XLIM -UMR n°7252- Université de Limoges/CNRS, Limoges, France
Mail: lcatherinot@tronico-alcen.com

This paper deals with experimental studies of nonlinear behavior of Bulk Acoustic Wave (BAW) devices, in a Solidly Mounted Resonator (SMR) structure. The purpose is to extend the Modified Butterworth Van Dyke model to a complete non-linear model of a BAW resonator, which takes into account all nonlinear effects. Frequency shifts were studied when high Radio Frequency (RF) power (up to 5W) is applied to the resonators. We have focused on the W-CDMA frequency standards, for resonators of emission filters of a front-end module in mobile phones. To stabilize the input power, we have developed a new calibration method, which is able to match the data correction between a high and small signal at any frequency. With this method, we have access to the power waves, and we recalculate the S-parameters externally as a function of the frequency sweep.

A 4-port Vectorial Network Analyzer (VNA) is used both as a measuring device and an RF source. It delivers -20dBm power, swept around 2GHz. The signal is amplified by a Power Amplifier (PA) (40dB gain) previously characterized as sufficiently linear for the frequency range used. All used devices for the test bench, including attenuators and couplers, have been chosen to be functional in the frequency band. Finally, the test bench is connected to a probe station to overcome various effects such as landslides, claw arks on the wafer or apparatus damage. In addition, the set up has a power sensor connected to the resonator's input, in order to monitor the input power, which enables a power feedback loop. This is a particularly delicate step that requires the establishment of an original procedure of double calibration (frequency/power). This calibration method simplifies the equipment and locates the input power measurement very close to the resonator. Initially, a calibration is performed on the power level output of the coupler, so that the VNA corrects the power supplied simultaneously: the power is well known in the DUT plane and it is fixed, and we also take into account the losses in the probe cables. In a second step, a standard S-parameters calibration is carried out under the probes (Short Open Load Thru), so low power and high power are enabled. The choice of the maximum power value was studied taking into account return wave limits of the measuring devices and power densities permitted on the resonators that are being evaluated for future use as the input stage of mobile phones emission filters.

We performed measurements on small resonators ($100*100\mu m^2$ and $50*50\mu m^2$), with rectangular and apodized shape. The maximum input power value is 34 dBm, above which we observe device breakage (deterioration of the top electrode, undesirable resistive effects on the access pads). The power density varies between $36dB/mm^2$ and $60dB/mm^2$. In particular, a frequency shift is observed on the resonant frequency, which decreases by 5% from its initial value from 20 dBm to 34 dBm. Contrary to what was expected, the anti-resonant frequency, which is directly related to the electric C_0 capacitance value, does not vary. To conclude, the observation leads to consider the couple L_m/C_m, of the motional branch of the MBVD model, as nonlinear lumped components. Evolution of the test bench is being considered, specifically to further knowledge on mechanical and spectral aspects.

IFCS-EFTF1-PCD1-4

Numerical Study of the Impact of Process Variations on the Motional Resistance of Weakly Coupled MEMS Resonators

Andreja Erbes, Pradyumna Thiruvenkatanathan, Ashwin A. Seshia

Engineering Department, University of Cambridge, Cambridge, United Kingdom

Email: ae279@cam.ac.uk

Although one-dimensional mechanical coupling (1D-κ) has been suggested as a potential route to reduce the motional resistance (R_x) of electrostatically transduced MEMS resonators[371], variations induced by manufacturing tolerances in weakly coupled systems often result in non-uniform reductions in the R_x from the case of perfect symmetry[372]. In an attempt to obtain a better scalability and more predictable R_x reduction of such weakly coupled arrays, this paper presents a numerical study of the robustness of the achievable R_x to process induced variations for three classes of mechanical coupling topologies: 1D-κ (Fig. 1a), cyclic-coupling (C-κ, Fig. 1b) and cross-coupling (X-κ, Fig. 1c). The numerical study is based on a flexural mode Si MEMS double-ended-tuning fork (DETF) resonator operating at 270 kHz (Fig. 1a) where the normalized inter-resonator spring coupling is $\kappa = k_c/k = 5\text{x}10^{-3}$. Monte Carlo numerical simulations, which accounted for up to ± 1.35% random variations in resonator beam widths (nominal value of 6 μm), were initiated to produce R_x estimates of the three coupling schemes for N = 1, 2, 3, 4, 5 and 9 resonators. The R_x distribution for the special case of N = 4 and N = 9 is shown in Fig.2 where a clear decrease in the spread and mean value of R_x is seen as we switch towards the X-κ topology. The results for the other array lengths N are summarized in Table 1 where the mean (μ) and standard deviation (σ) of the R_x distribution for the different coupling schemes are reported. The numerical trends suggest an improvement in the mean and spread of R_x as N is increased for the X-κ scheme. These numerical results motivate in-depth studies of alternative coupling topologies, in the case of weakly coupled resonators, towards designing process tolerant, highly scalable resonator arrays.

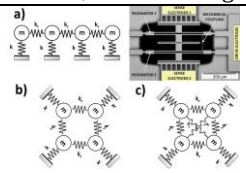

Fig. 1: Discrete element model N = 4 a) 1D-κ and optical micrograph of the equivalent coupled DETF MEMS device; b) C-κ; c) X-κ scheme.

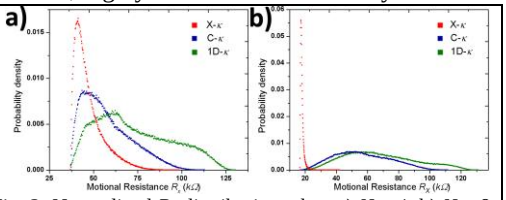

Fig. 2: Normalized R_x distribution when a) N = 4; b) N = 9 for 1D-κ, C-κ and X-κ schemes.

Table 1

N	1		2		3		4		5		9	
Scheme	μ ($k\Omega$)	σ ($k\Omega$)	μ ($k\Omega$)	σ ($k\Omega$)	μ ($k\Omega$)	σ ($k\Omega$)	μ ($k\Omega$)	σ ($k\Omega$)	μ ($k\Omega$)	σ ($k\Omega$)	μ ($k\Omega$)	σ ($k\Omega$)
1D-κ	**140**	*1.05*	**92.0**	*13.4*	**77.2**	*18.5*	**71.6**	*20.8*	**69.13**	*22.0*	**66.5**	*22.4*
C-κ					**63.1**	10.63	**56.1**	*13.1*	**53.9**	*14.8*	**54.7**	*17.1*
X-κ							**46.5**	*7.8*	**35.8**	*5.14*	**17.8**	*0.99*

[371] Demirci, M.U.; Abdelmoneum, M.A.; Nguyen, C.T.-C.; , "Mechanically corner-coupled square microresonator array for reduced series motional resistance," TRANSDUCERS, Solid-State Sensors, Actuators and Microsystems, 12th International Conference on, pp. 955- 958 vol.2, 2003.

[372] Erbes, A.; Thiruvenkatanathan, P.; Seshia, A.A.;, "Impact of mode localization on the motional resistance of coupled MEMS resonators," in Proc. 2012 IEEE Int. Freq. Control Symp., 2012, pp. 609-614.

IFCS-EFTF1-PCD1-5

Unwanted Transverse Modes in SAW Resonators Caused by Stitching Errors And Stripe Nonlinearities

Pierre Dufilie, Raymond Zeitler, Merle Yoder
Phonon Corporation, Simsbury, CT, USA

Email: pierred@phonon.com

High Q SAW and STW resonators utilize interdigital transducers with transverse weighting. This weighting is fit to the fundamental mode (S0) of the resonator cavity, so the transducer should not couple to the higher order transverse modes (S1, S2, ...). Errors in the actual resonator pattern caused by stitching errors in laser generated photomasks will introduce an asymmetry which can excite both higher order symmetric (S2, S4, ...) and antisymmetric (S1, S3, ...) transverse modes. Non-uniformities due to processing can also contribute to these higher order modes. Higher order modes in oscillators are undesirable because they degrade linearity or induce frequency popping.

The majority of high resolution (0.5um or better) 1X photomasks are fabricated using laser mask-making machines. This approach is adequate for most SAW devices; however SAW resonators are very sensitive to small variations in linewidths and line positions -- variations that cannot be detected by normal optical examination. A typical resonator pattern is too large to be exposed in a single laser stripe (2mm x 2mm active area).

The objective of this study is to determine the photomask fabrication method which can minimize the higher order transverse modes. A 695MHz STW resonator was designed and realized in an array of 26 rows and 16 columns on multiple 1x dark field quartz masks exposed with different photomask tools. The tools were Etec Alta 3500 and 3900 laser pattern generators, Micronic laser writer and an ASET 645 15" Image Repeater used with a 10x reticle.

Multiple wafers were contact-printed from each mask, and all dies on the wafers were RF-probed to acquire S11 over a span of 40MHz centered at 695MHz. The data was converted to admittance, and the main response was fitted to a lumped-element model, which was then removed. The residual data, which contained the extraneous modes, was then analyzed for correlation to: position in the array of dies; mask technology; wafer number.

Electrical measurements of SAW resonators fabricated with different photomask tools do exhibit differences in transverse mode levels, the newer pattern generators having the lower high order modes. Those fabricated with mask generated with the 10X stepper exhibited the best performances.

IFCS-EFTF1-PCD1-6

Imaging surface acoustic waves propagating on ST-quartz using stroboscopic synchrotron radiation X-ray topography.

B. Capelle, A. Soyer, Y. Epelboin, J. Detaint.

Institut de Minéralogie et de Physique des Milieux Condensés (IMPMC), UMR 7590 CNRS. Université Pierre et Marie Curie et CNRS. 4, place Jussieu 75005 Paris. France.

Email: Bernard.Capelle@impmc.upmc.fr

This method allows obtaining instantaneous images of the acoustic wave propagating on crystal if the frequency of the wave is an exact integer multiple of that of the very short x-ray pulses delivered by the synchrotron [1]. Depending on the diffraction set–up it is often possible to image separately the different components of the displacement (or more precisely of several of their spatial derivatives, proportional to them). Last year, we have shown that the observation technique using section images allows getting information about the distribution of the amplitude in the depth direction. This was done for the normal component of the Rayleigh waves propagating on YZ lithium niobate (LNB) with experiments using the Bragg setting and in comparing the experimental images with simulated ones. The properties of this material (X-ray absorption and crystal perfection [2]) do not allow good imaging conditions for the other component of the mechanical displacement (directed along the propagation direction).

The surface waves propagating on ST-quartz in the x direction present three components of displacement that can be observed practically separately due to the existence of lattice planes whose diffraction vectors are very nearly or exactly in the direction of these components. Experiments using ST quartz delay lines operating at 9.507, 11.361 12.781 and 22.722 MHZ were conducted, using different diffraction conditions, mostly with the BM05 beam line of the ESRF. Translation and section stroboscopic topographs in Laue or Bragg geometry were obtained using principally the $(\bar{2}1.0)$, (01.1) and $(0\bar{1}.1)$ reflections. As expected from the much lower coupling coefficient, the contrasts given by the progressive SAW are weaker for ST quartz than for YZ LNB, at equal excitation voltage, but they are fully discernable. As expected, also, the in-plane component perpendicular to the propagation direction is the smallest one. In the reflection topographs, the static strains due to the metallic films used in the transducer, produce noticeable contrasts so that the observations of SAW have to be made outside of it. The section topographs (reflection setting), contain intense contrasts, that are different of those obtained for lithium niobate. These contrasts contain also information about the decrease of the normal displacement in the depth direction (their positions in the image indicate that they were generated at various depths in the substrate). The translation and section topographs obtained in the Laue geometry with practically or exactly in plane diffraction vectors display periodic contrasts. The translation topographs contain mostly information about the in-plane distribution of the SAW amplitude close to the surface. The section images contain a particular distribution of contrast in the depth direction; they give so, in an indirect manner, information about the variations of the amplitude of a component with the depth. To better understand these features and the information contained in the various kinds of topographs, simulated images are being computed in solving numerically the Takagi-Taupin partial derivative equations governing the diffraction process in the crystal deformed by the theoretical surface waves (or by waves with different spatial variations). They will be compared between them and with the experimental ones. It is suspected that in few experimental cases, using not very thick substrates and long wave length (9,507 MHz), another kind of wave not decreasing as the theoretical SAW may be propagating in the plate.

IFCS-EFTF1-PCD1-7

X-ray imaging of the surface acoustic wave propagation in $La_3Ga_5SiO_{14}$ crystal

Dmitrii Roshchupkin[1], Luc Ortega[2], Anatolii Snigirev[3], Iraida Snigireva[3]

[1]Institute of Microelectronics Technology and High-Purity Materials Russian Academy of Sciences, Chernogolovka, Russia
[2]Laboratoire de Physique des Solides, Univ. Paris-Sud, CNRS, Orsay, France
[3]ESRF, Grenoble, France

Email: rochtch@iptm.ru

Progress in modern telecommunication systems and sensors based on SAW-devices urges the development of methods to study the SAW propagation in solids. Most interesting and promising methods for the analyses of acoustic wave field in solids are scanning electron microscopy and X-ray diffraction and topography. Scanning electron microscopy in the mode of the low-energy secondary electron registration permits the visualization of surface and bulk, traveling and standing acoustic waves and makes it possible to study diffraction phenomena in acoustic beams and interaction of acoustic waves with crystal structure defects[373]. X-ray diffraction and topography are the methods of quantitative analysis and permit studying the acoustic wave fields both in piezoelectric and non-piezoelectric materials[2].

The aim of this work is to study the SAW propagation in the $La_3Ga_5SiO_{14}$ crystal by X-ray topography on a synchrotron radiation source.

The possibility of direct imaging of an acoustic wave filed on the crystal surface was demonstrated on an acoustically modulated LGS crystal in the saggital geometry of X-ray diffraction (fig. 1). It is shown that the formation of an acoustic wave field image is connected with the Talbot effect that can be realized on a synchrotron radiation source under the conditions of a partially coherent X-ray radiation and strongly periodic modulation of the crystal lattice with a surface acoustic wave. It was shown that Talbot effect is an ideal instrument for direct imaging of acoustic wave fields and investigation of acoustic wave interaction with the crystal structure defects.

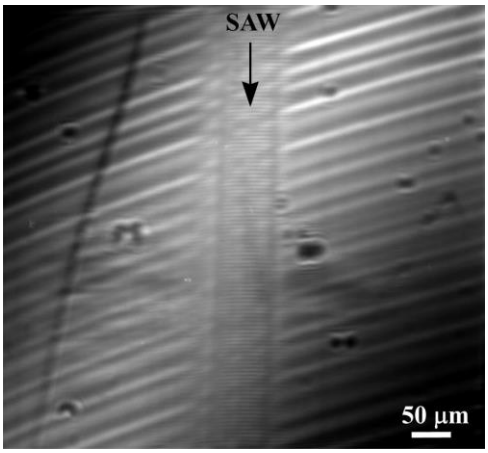

Fig. 124: X-ray topograph of the $Y-$cut of an LGS crystal excited by SAW. $\lambda = 1$ Å; $\Lambda = 10$ μm; $f_0 = 234$ MHz; reflection (100); $\Theta_B = 4.175°$.

[373] D.V. Roshchupkin, M. Brunel, "Scanning electron microscopy observation of surface acoustic wave propagation in the $LiNbO_3$ crystals with regular domain structures". IEEE Transaction on Ultrasonics, Ferroelectrics, and Frequency Control, vol. 41, pp. 512-517, 1994.

[2] V. Roshchupkin, E. D. Roshchupkina, D. V. Irzhak, "X-Ray topography analysis of acoustic wave fields in the SAW-resonators structures", IEEE Transaction on Ultrasonics, Ferroelectrics, and Frequency Control, vol. 52, pp. 2081-2087, 2005.

IFCS-EFTF1-PCD1-8

Investigation of surface and pseudo-surface acoustic waves excitation and propagation in $La_3Ga_5SiO_{14}$, $La_3Ga_{5.5}Ta_{0.5}O_{14}$, and $Ca_3TaGa_3Si_2O_{14}$ crystals

Dmitrii Roshchupkin[1], Dmitrii Irzhak[1], Olga Ploticyna[1], Evgeny Emelin[1], Luc Ortega[2], Sergey Sakharov[3], Oleg Buzanov[3]

[1]Institute of Microelectronics Technology and High-Purity Materials Russian Academy of Sciences, Chernogolovka, Russia
[2]Laboratoire de Physique des Solides, Univ. Paris-Sud, CNRS, Orsay, France
[3]FOMOS Materials, Mosscow, Russia

Email: rochtch@iptm.ru

X-ray diffraction on acoustically modulated ordering ($Ca_3TaGa_3Si_2O_{14}$: CTGS) and non-ordering ($La_3Ga_5SiO_{14}$: LGS; $La_3Ga_{5.5}Ta_{0.5}O_{14}$: LGT) crystals of langasite family was used to study the process of surface (SAW) and pseudo-surface acoustic waves (PSAW) excitation and propagation[374]. The process of the SAW and PSAW propagation in CTGS, LGS, and LGT crystals can be characterized by the difference in the directions of the acoustic energy propagation (PFV) and acoustic wave-vectors.

SAW and PSAW are excited by the same interdigital transducer (IDT) but at different resonance excitation frequencies. Propagation of SAW and PSAW causes the sinusoidal modulation of a crystal lattice and appearance of diffraction satellites on the rocking curve, with their number, angular positions, and intensities depending on acoustic wavelength and amplitude. The distribution of the diffracted X-ray intensity on the crystal surface was used for mapping of SAW and PSAW propagation in CTGS, LGS, and LGT crystals.

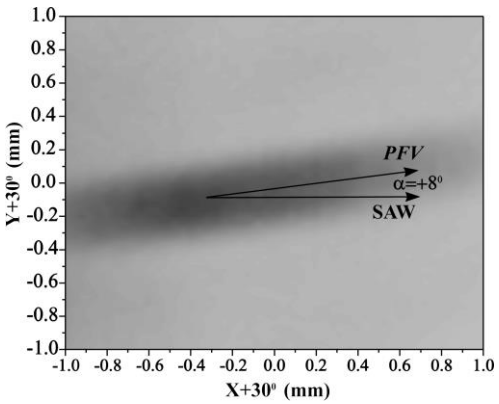

Fig. 125: Map of acoustic wave field distribution of SAW on the $Z-$cut surface of LGT. $E=11$ keV; reflection (001); $\Theta_B=6.595°$; $\Lambda=8$ μm. Dark contrast corresponds to the SAW propagation.

It was shown that SAW and PSAW are excited by the same IDT with the same wavelength, but at different frequencies with different velocities. Also it was measured that SAW and PSAW have the different power flow angles. Fig. 1 shows the difference between the PFV and SAW wave-vector in $Z-$cut of LGT crystal ($\alpha=+8°$) at the SAW propagation along $(Y+30°)$-direction. Furthermore it was shown that PSAW is a flow wave, which propagates inside the crystal and can be observed only near IDT.

[374] D. V. Roshchupkin, A. I. Erko, L. Ortega, D. V. Irzhak, "X-ray diffraction analysis of the surface acoustic wave propagation in langatate crystal", Applied Physics A, vol. 94, pp. 477-484, 2009.

IFCS-EFTF1-PCD1-9

Investigation of optimal electrode structure of SC-cut resonators

Lepetaev Alexandr, Kosykh Anatoly

Omsk state technical university, Omsk, Russian Federation

Email: LAN@inbox.ru

High-Q SC – cut resonators widely used in precision OCXOs. They have many advantages: higher compared with the AT-cut value of the frequency factor, high Q, small temperature – dynamic frequency coefficient. However, these resonators have one disadvantage: the high activity of B – mode (thermosensitive mode), comparable with the activity of the main C – mode, making it difficult to use in some cases. This is due to the fact that the traditional design of electrodes for double rotated cut resonators is not optimal. In this paper we consider the optimal design of the electrode SC – cut resonators. It reduces the resistance of the mode C (Rc) and increases resistance to mode B (Rb), allowing you to get the ratio of Rb / Rc > 5.

Earlier[375] we consider the formulas to determine the surface density of the polarization charges at resonator plate surface of arbitrary cut (including SC - cut). This allows you to correctly determine the resistance of a given excitation mode in case of an off-center location of the electrodes, using information on the distribution of the vibration amplitude by the technique described at article[2].

In this paper the results of calculations of the surface charge density carried out for SC – cut resonators for different values of the design parameters (contour radius, thickness, harmonic number). The electrodes on each side were dividing on two segments, which are connected to different ports of the resonator. The shapes of the electrode segments were changed to obtain high ratio of resistances Rb/Rc.
All calculations were performed using the finite element analysis software FlexPDE and Comsol Multiphysics.
These constructions are more complex than traditional, but provide the best parameters and stable excitation of the fundamental mode.

[375]Lepetaev A.N., Kosykh A.V. New method of multy-mode oscillations control in crystal resonators. 2012 IEEE International Frequency Control Symposium Proceedings. Baltimore, MD, USA. May 21-24, 2012, P. 146 – 149.
[2]Lepetaev A., Kosykh A., Khomenko I. Numerically-analytical calculation method for vibration amplitude distributions of inharmonic modes of double rotated cuts thickness-shear resonators. / Proc. of 2007 IEEE Ultrasonics Symposium: New York, USA, 2007. P. 1393 -1396.

IFCS-EFTF1-PCD1-10

Correction Factors for the Mindlin Plate Equations for Thickness Vibrations of Crystal Plates with Thicker Electrodes

Dejin Huang, Guijia Chen, Wenjun Wang, Tingfeng Ma, Jianke Du, Ji Wang

Piezoelectric Device Laboratory, School of Mechanical Engineering and Mechanics,
Ningbo University, 818 Fenghua Road, Ningbo, Zhejiang 315211, CHINA

E-mail: wangji@nbu.edu.cn

The Mindlin plate theory has been widely used for the study of high frequency vibrations of quartz crystal plates for resonator design and analysis. To improve the accuracy, the plate equations have to be corrected for the exact thickness-shear frequencies which in turn ensure the accurate results for other coupled modes. The correction procedure was suggested by Mindlin and the correction factors for the first-order equations have been available. Lately, a systematic procedure for the correction factors up to the fifth-order has been established and two correction schemes with different correction factors have been adopted for the higher-order vibrations[376]. These results have expanded applications of the Mindlin plate equations to the overtone vibration analysis which is required for the overtone resonators. One critical issue concerning the applications of the Mindlin plate with correction factors are the effect of electrodes, which are essential part of resonators and complications are resulted. Furthermore, crystal blanks in resonators are shrinking in the thickness while the electrodes remaining constant, showing the relative increasing of influence of electrodes on the performance of resonators. As a result, further studies with the consideration of electrodes have been performed for effects on the vibration equations and solutions[377]. With this objective in mind, we start from the Mindlin plate equations with a full set of vibration modes for the consideration of electrode mass and stiffness effects as a continuation of our earlier studies which only considered the mass effect in terms of mass ratios. The analysis regarding to the AT-cut of quartz crystal plates show that the consideration of electrode stiffness and mass will change the correction factors, thus making the equations more accurate in the calculation of frequency spectra and mode shapes. For very thin electrodes, the correction factors should be the same as suggested by earlier studies. The same procedure is implemented to the SC-cut quartz crystal plates which have more enhanced couplings of vibration modes due to the material anisotropy. Correction factors for both AT- and SC-cut quartz crystal plates with consideration of electrode stiffness are given in polynomials of mass ratios for different metals. We expect the relatively adequate consideration of electrodes will provide more effective basis for vibrations of quartz crystal resonators with the truncated equations for analytical solutions based on the straight-crested wave assumptions and the finite element implementation of the higher-order equations with a full set of variables.

---

[376] J. Wang, J.-D. Yu, and Y.-K. Yong, "On the correction of the higher-order Mindlin plate theory," *Intl. J. of Applied Electromagnetics and Mechanics*, 22, 83-96, 2005.

[377] Jianke Du, Guijia Chen, Wenjun Wang, Rongxing Wu, Tingfeng Ma, and Ji Wang, "Correction Factors of the Mindlin Plate Equations with the Consideration of Electrodes," *IEEE TUFFC*, 59(10):2352-2358, 2012.

IFCS-EFTF1-PCD1-11

Optimizing UHF Quartz MEMs Resonators for High Thermal Stability

D.J. Kirby, Y.K. Yong*, R.L. Kubena, R. Perahia, D.T. Chang, H. Nguyen, F.P. Stratton, R.J. Joyce, H.P. Moyer R.G. Nagele & P.D. Brewer

HRL Laboratories, Malibu California, USA, *Rutgers University, Piscataway, New Jersey, USA

Email: djkirby@hrl.com

Frequency stability of oscillators used in timing applications is of paramount importance. It is well known that one dominant source of frequency instability in quartz oscillators relates to the mounting stresses incurred during wafer bonding[1]. A resonator bonded to a substrate at elevated temperature and subsequently cooled can experience significant residual stress in the device active region. As the operating temperature of the device varies, so does the magnitude of the residual stress. This stress acts to perturb the device resonant frequency thereby compromising frequency stability. As the need for higher frequency and smaller devices has developed for many new commercial applications, these effects are exacerbated in smaller packages. This paper discusses how ~ 1 GHz ultra-high-frequency (UHF) MEMs thickness-shear quartz resonator designs[2] can be optimized for improving thermal frequency stability via reduced residual stresses.

A newly developed 3-D FEA simulation technique which includes mounting stresses[3] is applied to optimize UHF device designs for high thermal stability. One of the effects of stress is to produce a rotation of the frequency-temperature (*f-T*) characteristic. Very small stresses can produce significant frequency shifts, especially for fundamental mode UHF devices. This rotation can often mask the true quartz *f-T* characteristic and results in resonator thermal instability. As an example, Figure 1 shows a simulation of frequency perturbation versus stress in the active region for a 770 MHz 2-µm-thick AT-cut quartz resonator. The insert of Figure 1 shows a simulation of the thermally induced stress for a ΔT = +75°C of a single-thickness quartz resonator rigidly bonded to a silicon substrate with zero stress at 25° C. A mounting stress of 130 MPa near the mounts produces a stress of 1 MPa in the active region and a resulting resonator frequency shift of 21 ppm.

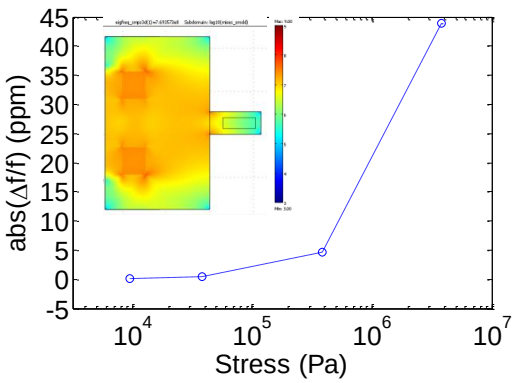

Figure 1. Frequency perturbation of a 2-µm-thick 770-MHz AT-cut resonator versus stress in the active region.

We determine a sensitivity of 1 ppm/50 kPa stress in the active region which represents a significantly higher frequency sensitivity than for larger and thicker designs. In this paper, simulation results will be compared with experimental data and new UHF resonator designs will be explored for mitigating this effect in sub-mm-size UHF quartz resonators.

[1] John R.Vig, "Quartz Crystal Resonators and Oscillators for Frequency Control and Timing Applications - A Tutorial", Rev.8.5.4.4, April 2012.

[2] "D. Chang et al, "Nonlinear UHF Quartz MEMs Oscillator with Phase Noise Reduction", Proceedings of IEEE MEMS 2013, Taipei, Taiwan, January 20 – 24, pp. 781, 2013.

[3] Yook-Kong Yong et al, "Modeling Approach to Analyze Bonding Stress in UHF Quartz Resonators"., IEEE FCS 2013, Prague, Czech Republic, submitted abstract.

IFCS-EFTF1-PCD1-12

Modeling Approach to Analyze Bonding Stress in UHF Quartz Resonators

Yook-Kong Yong[1], Randall Kubena[2], Deborah Kirby[2], Raviv Perahia[2], and David Chang[2]
[1]Rutgers University, Piscataway, New Jersey, USA, [2]HRL Laboratories, Malibu California, USA

Bonding and mounting stress in quartz resonators is known to produce frequency shifts which can also modify the frequency-versus-temperature (f-T) profiles.[1] This stress/strain is produced by two events. First, when the quartz plate is initially bonded into the final package, the bonding process may require high temperature annealing or processing. When the package is cooled, the difference in thermal expansion coefficients between the quartz and the package produces stress that can partially relax to yield an initial stress condition at room temperature. Second, when the package is then varied over temperature during use, this initial stress is modified by the same thermal expansion coefficient differences. Depending on the thermal history of the device, the mounting stress can be minimized or reduced to zero at a particular temperature (T_{ref2}) as evidenced by a very low relaxation or aging rate. Previous numerical models for quartz f-T profiles[2] have not included this zero stress condition nor the variations in the stress and strain in the quartz due to the mounts in calculating the f-T profiles. In this paper, we describe a method within a COMSOL finite element analysis to include these effects for the first time.

Figure 1. below shows the four states of the resonator and its respective material displacement vectors $\underline{\mathbf{U}}^{(a)}$, $\underline{\mathbf{U}}^{(b)}$, $\underline{\mathbf{U}}^{(c)}$, and $\underline{\mathbf{U}}^{(d)}$. The small piezoelectric vibrations of the resonator are superposed upon the material displacement $\underline{\mathbf{U}}^{(c)}$. We derived the governing equations for small piezoelectric vibrations superposed on displacement $\underline{\mathbf{U}}^{(c)}$ and employed the derived equations in a COMSOL finite element model. The displacement $\underline{\mathbf{U}}^{(c)}$ includes both thermal stress and thermal strain but our governing equations neglect the thermal stress as they are second order effects compared to the thermal strains. The f-T effect is calculated by the change in eigenfrequency of the thickness shear mode as a function of the temperature. Compared to soft mounts such as rubber or epoxy, hard mounts can create larger rotations of the f-T profiles. Our general analysis can be applied to any resonator geometry and mounting design to optimize the predictability of the f-T profiles and minimize hysteresis and aging. This is particularly important for UHF shear-mode device designs where micron-thick quartz plates are utilized. Examples of this effect will be described and presented.

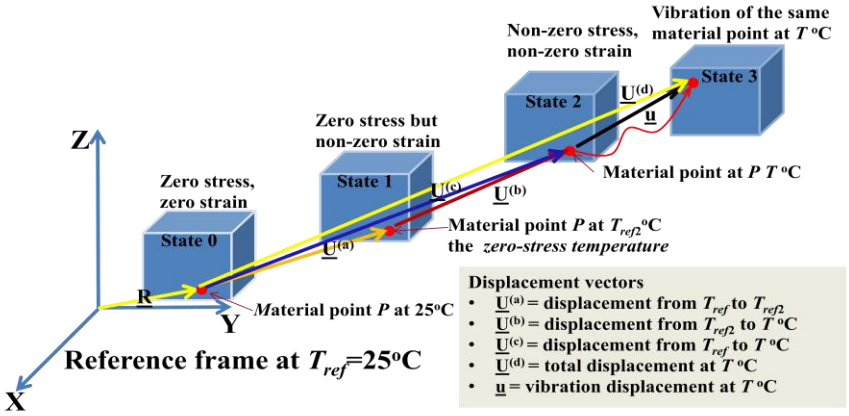

Figure 1: Four states of the resonator and its displacement of material points $\underline{\mathbf{U}}^{(a)}$, $\underline{\mathbf{U}}^{(b)}$, $\underline{\mathbf{U}}^{(c)}$, and $\underline{\mathbf{U}}^{(d)}$, respectively.

[1]"Quartz Crystal Resonators and Oscillators For Frequency Control and Timing Applications - A Tutorial", April 2012, John R.Vig.

[2]**"Effects of Thermal Stresses on the Frequency-Temperature Behavior of Piezoelectric Resonators", Y-K Yong, M. Patel, M. Tanaka, Journal of Thermal Stresses, Vol. 30, No. 6, June 2007, pp. 639 -661.**

IFCS-EFTF Group 2 poster session 2

Forum Hall

Wednesday & Thursday, July 24-25, 2013, 1:00 pm - 2:00 pm and 3:30 pm - 4:30 pm

Chair: **Fabrice STHAL**
FEMTO-ST

Dynamic Range Vs Spectral Clarity Trade-off in All-Digital Frequency Synthesis via Single-Bit Sinewave Quantization

Paul P. Sotiriadis[1], Natalia Miliou[1]

[1]Department of ECE, National Technical University of Athens, Greece

Email: miliou@ieee.org

Single-bit Nyquist-rate dithered quantization has been proposed for all-digital frequency synthesis and RF signal generation[378]. This work demonstrates how we can improve the Dynamic Range (DR) beyond that achieved using independent and uniformly distributed dithering sequences by selectively allowing some of the harmonics to be present in the spectrum; here DR is the ratio of the carrier's power to noise's power spectral density. For a dithered single-bit quantized sinewave, $\mathbf{x}_k = \mathrm{sgn}\left(\cos(\Omega k) - \mathbf{u}_k\right)$, where $\mathbf{u}_k$ is the dithering, we express the Cumulative Distribution Function (CDF) of $\mathbf{u}_k$ using Chebyshev polynomials, i.e. $G(u) = \frac{1}{2} + \frac{1}{2}\sum_{j=0}^{\infty} \alpha_j T_j(u)$, where a_j are appropriately chosen. Allowing the 3rd harmonic $(3\Omega \bmod 2\pi)/(2\pi T_S)$ to be present is equivalent to having $\alpha_1, \alpha_3 \neq 0$ and all other coefficients $\alpha_k = 0$. In this case the feasible set of a_1, a_3 is $a_1 = (6+3\rho)/8$ and $a_3 = (2-3\rho)/8$ with $\rho \in [0,1]$. It is $DR = 10\log_{10}\left(a_1^2/\left(2-a_1^2-a_3^2\right)\right) + 10\log_{10}(f_S) - 3.01$, when $q > 4$, and DR is maximized for $a_1 = 9/8$ and $a_3 = -1/8$ as shown in Fig. 1 (89.5 dB for $f_S = 1\,GHz$). Allowing both the 3rd harmonic and the 5th one, $(5\Omega \bmod 2\pi)/(2\pi T_S)$, means that $\alpha_1, \alpha_3, \alpha_5 \neq 0$ and all other coefficients α_k are zero. The feasible set of a_1, a_3, a_5 is the union of a triangle and an ellipse, including their interior points, in the plane of α_3, α_5. It is $DR = 10\log_{10}\left(a_1^2/\left(2-a_1^2-a_3^2-a_5^2\right)\right) + 10\log_{10}(f_S) - 3.0$, when $q > 6$, and DR is maximized for $a_1 = 1.1906$, $a_3 = -0.2375$, $a_5 = 0.0469$ as shown in Fig. 2 (91.3 dB for $f_S = 1\,GHz$) giving a 4.3 dB improvement with respect to uniformly distributed dither. In some sense part of noise's power is absorbed by the harmonics improving DR. The paper provides a methodology for optimizing the DR along with guidelines for selecting those harmonics located away of the carrier.

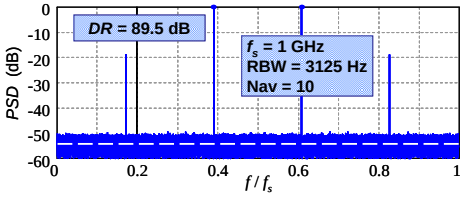

Fig 126: Normalized PSD when $a_1 = 9/8$, $a_3 = -1/8$ and all other coefficients $\alpha_k = 0$; $w = 25$, $q = 64$

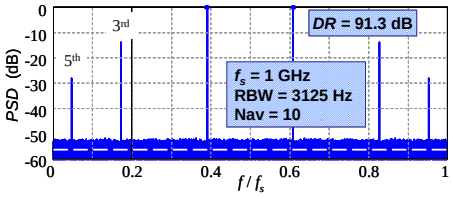

Fig 127: Normalized PSD for $a_1 = 1.191$, $a_3 = -0.237$, $a_5 = 0.047$ and all other coefficients zero.

[378] P.P. Sotiriadis, N. Miliou, "All-Digital Frequency Synthesis based on Single-Bit Nyquist-Rate Sinewave Quantization with IID Random Dithering", subm. to IFCS 2013.

Measuring an optical frequency difference of semiconductor lasers based on coherent detection and frequency dividers

Ł. Buczek[1]

[1] AGH University of Science and Technology, Mickiewicza 30, 30-057 Krakow, Poland

Email: lbuczek@agh.edu.pl

Currently a number of electronic components capable of processing multi-GHz electrical signals is available on the market. This allows building a system for measuring the difference of optical carrier frequencies of two semiconductor lasers, exploiting high-speed frequency prescalers and based on coherent detection.

The idea of proposed method is presented in Fig. 1. Two optical signals from distributed feedback (DFB) semiconductor lasers are supplied to a high-speed photodiode and resulting beatnote with the frequency equal to the difference of the laser carriers is further processed by a set of high-speed prescalers. They divide the high-speed signal to the value low enough for counting by the system based on a field programmable gate array (FPGA) and microcontroller. The prototype system was designed to operate with the frequencies up to 18 GHz that corresponds to the wavelength difference of the lasers up to 0.14 nm. Using currently available technology this difference may be easily extended to 26 GHz (i.e. 0.2 nm).

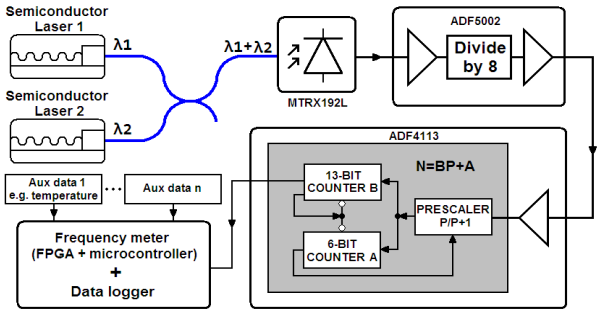

Fig. 1: An idea of measuring the difference of semiconductor lasers carrier frequencies using high-speed prescalers.

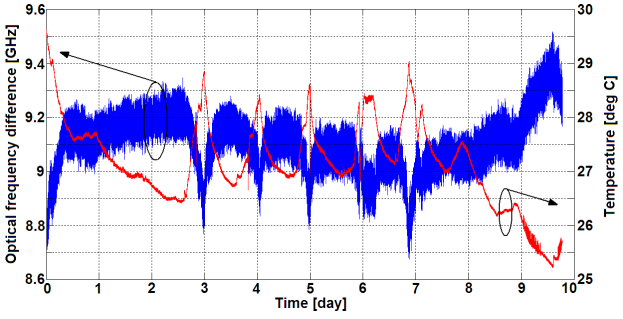

Fig. 2 The record of 10-days measurement of frequency difference of two DFB lasers stabilized using Fabry-Perot etalons.

An example of 10-day record showing the relative stability of two telecommunication-grade DFB lasers stabilized using Fabry-Perot etalons is presented in Fig. 2. Presented method may be used for calibration of time transfer in fiber optic system exploiting two closely spaced lasers[379] or for characterizing ultra-dense WDM laser sources.

[379] P. Krehlik, Ł. Śliwczyński, Ł. Buczek and M. Lipiński, "Fiber optic joint time and frequency transfer with active stabilization of the propagation delay", IEEE Trans. Instrum. Meas. **61**, 2844–2851, 2012.

IFCS-EFTF2-PCD2-3

A 15 mW, 4.6 GHz frequency synthesizer ASIC with -84 dBc/Hz at 2 kHz for miniature CPT clocks

Yazhou Zhao[1], Steve Tanner[1], Luc Schneller[2], Florian Gruet[2], Christoph Affolderbach[2], Gaetano Mileti[2], Pierre-André Farine[1]

[1]ESPLAB, Ecole Polytechnique Fédérale de Lausanne (EPFL), Lausanne, Switzerland
[2]Laboratoire Temps-Fréquence (LTF), University of Neuchâtel, Neuchâtel, Switzerland

Email: yazhou.zhao@epfl.ch, pierre-andre.farine@epfl.ch

We report on the development and evaluation of a 4.6 GHz frequency synthesizer CMOS ASIC for miniature atomic clocks based on Coherent Population Trapping (CPT) in micro-fabricated Cs vapor cells. The circuit consumes 15 mW and features a frequency resolution below 10^{-13}.

For guaranteeing the lowest power consumption and the smallest form factor for miniature atomic clocks, an application specific integrated circuit (ASIC) is the best choice compared to commercially available synthesizers. Here we report on an improved circuit compared to a previous design[380]. It includes an LC Voltage-Controlled Oscillator (VCO) and a fractional PLL with a reference frequency of 20 MHz and a bandwidth of 200 kHz. The 40-bit fractional divider allows sub-mHz frequency resolution at the 4.6 GHz output. The VCO controls a high-efficiency Power Amplifier (PA) with programmable differential output power from -10 to 0 dBm in 64 steps. The circuit is fabricated into a 130 nm CMOS process, is powered at 1.2 Volt.

The circuit was characterized with a 20 MHz reference OCXO featuring a phase noise of –87 dBc/Hz at 1 kHz from carrier (referred to a 4.6 GHz carrier). The ASIC phase noise was measured at –82 dBc/Hz at 1kHz and ≤ –84 dBc/Hz between 2 kHz and 200 kHz offset (Fig. 1). This phase noise is only marginally above the one of the reference OCXO, and at frequency offsets between 1 kHz and 10 kHz (which is of highest relevance for the clock application) presents an improvement by up to 10 dB compared to a previous version of the ASIC[1]. From the measured phase noise, we calculate the limit to the clock stability arising from the Dick effect to be on the level of 2×10^{-11} at 1 second.

The previous ASIC version was used as microwave synthesizer in a CPT clock setup based on a DFB laser and a micro-fabricated Cs vapor cell. The measured clock stability is $< 4\times10^{-10}\ \tau^{-1/2}$ up to τ=10s, currently limited by the modulation scheme.

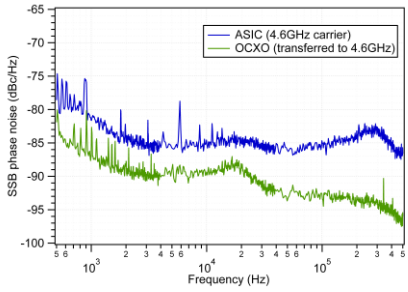

Fig. 128: Phase noise of the 4.6 GHz signal measured for the ASIC synthesizer.

Acknowledgments: this work was supported by the EU FP7 (MAC-TFC project www.mac-tfc.eu, grant no. 224132) and the Swiss National Science Foundation. We thank M. Haldimann for helpful discussions.

[380] Y. Zhao, S. Tanner, A. Casagrande and P.-A. Farine, "A 4.6-GHz, 15-mW frequency synthesizer CMOS ASIC with milli-Hertz frequency resolution for miniature atomic clocks", Conf. IEEE Int. Freq. Control Euro. Freq. Time Forum, pp. 1- 4, May, 2011.

Reducing the time transfer uncertainty in the fiber optic time and frequency dissemination system

Wojciech Słowik[1]

[1] Department of Electronics, AGH University of Science and Technology, Krakow, Poland

Email: wslowik@agh.edu.pl

In last years our group is developing the fiber optic system for accurate time and frequency (T&F) dissemination[381,382,383]. The main idea is to actively stabilize the propagation delay of the link by organizing a delay locked loop (DLL) system, using the feedback signal from remote side of the system. The core element of the hardware is a set of two precisely matched electronic delay lines, fabricated as an application-specific integrated circuit (ASIC). In the current realization mismatch of the tuning characteristics of the delay lines is about 30 ps, and it affect the overall T&F dissemination accuracy and stability[1,2].

In this work we present a newly designed compensating module, which reduces the delay mismatch (Fig. 1). In the poster we will show the measured results of the compensation efficiency, both in nominal temperature, and for ± 5°C temperature excursions. We find the remaining mismatch as no greater than 3 ps. After applying the compensation module, the problem of the delay lines mismatch go below other factors limiting the overall system performance.

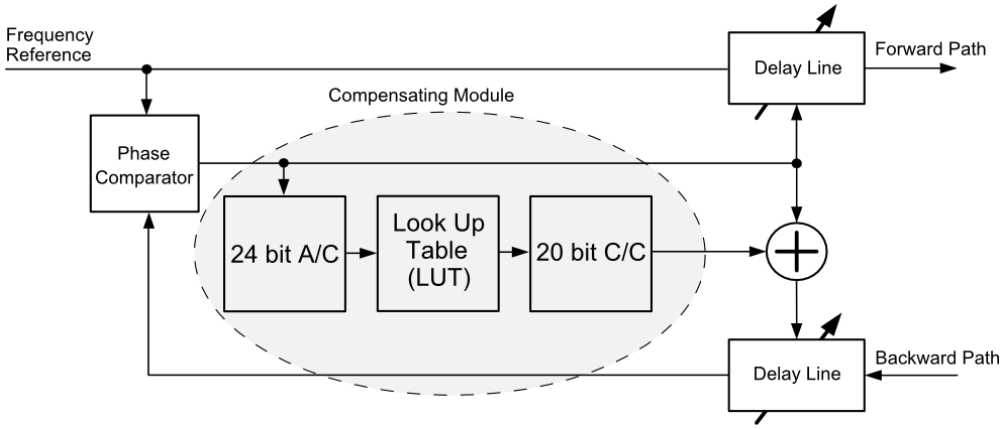

Fig. 129: General concept of compensating module for active stabilization of the delay

[381] Ł. Śliwczyński, P. Krehlik, Ł. Buczek, and M. Lipiński, "Active propagation delay stabilization for fiber optic frequency distribution using controlled electronic delay lines," IEEE Trans. Instrum. Meas., vol. 60, no. 4, pp. 1480–1488, Apr. 2011.

[382] P. Krehlik , Ł. Śliwczyński , Ł. Buczek , M. Lipiński,: Fiber-optic joint time and frequency transfer with active stabilization of the propagation delay; IEEE Transactions on Instrumentation and Measurement

[383] Ł. Śliwczyński, P. Krehlik, A. Czubla, Ł. Buczek and M. Lipiński, "Dissemination of time and RF frequency via a stabilized fibre optic link over a distance of 420 km", Metrologia 50, 133-145, 2013.

IFCS-EFTF2-PCD2-5

Research on Hybrid-compensation technology for reducing acceleration sensitivity of TCXO

Liangpeng Chen[1], Qingxiao Shan[1]

[1] National University of Defence Technology, Changsha,Hunan,China

Email: tsingxiao@163.com

Temperature compensated crystal oscillator (TCXO) is widely used in GPS receiver for its small size and low cost. But GPS receiver often used at mobile devices such as aircraft and missile which suffer from serious vibration. The g sensitivity of TCXO decrease the frequency stability and deteriorate the performance of GPS receiver. To reduce the g sensitivity, the way used prevalently is mechanic cushion but it is not efficient at low frequency vibration below 300Hz,as shown in fig.1. This paper proposed hybrid-compensation which is made up of electronic compensation and mechanic cushion. The electronic compensation aims at low frequency vibration while mechanic cushion aims at high frequency. The electronic compensation comprised of a MEMS sensor ,a digital controller and a D/A converter is with low cost and small size due to high integrate of digital device. The volume of mechanic cushion can be with small size for it only aims at high frequency.The method proposed can reduce the g sensitivity and improve reliability of TCXO by adding extra devices to the original TCXO.

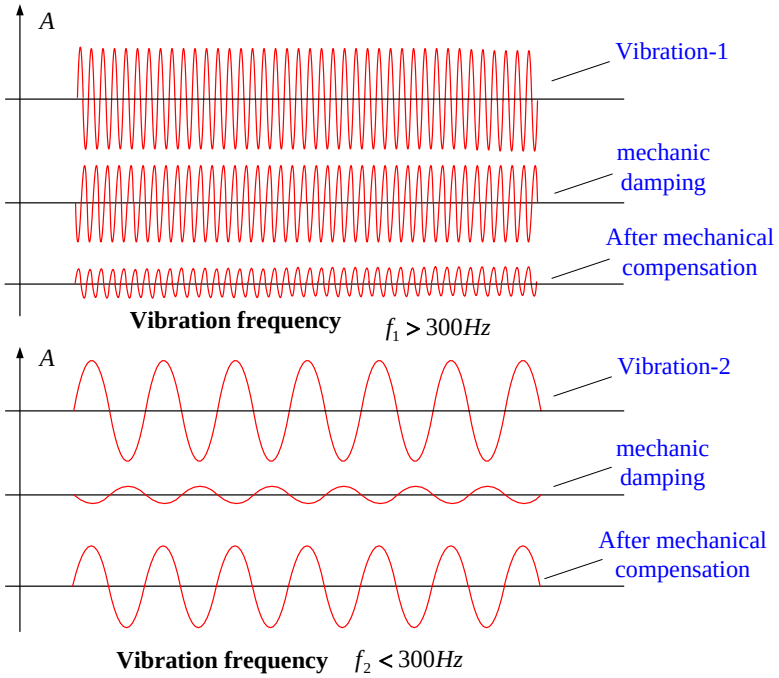

Fig.1: The effect of Mechanical compensation under different vibration frequency

IFCS-EFTF2-PCD2-6

Demonstration of doubly rotated X-cut quartz plate oscillators with a slot vibrating in length extensional mode

Tomiharu Yamaguchi, Kiyoto Katakura, Yusuke Todo, Hisashi Kanie

Department of Applied Electronics, Tokyo University of Science, Katsushika, Japan

Email: t-yama@te.noda.tus.ac.jp

We analyzed doubly rotated X-cut quartz plate oscillators with a slot in the resonator vibrating essentially in length extensional (LE) mode by FEM and fabricated oscillators monolithically by the wet etching process. To reduce the series resistance R_1 and increase the quality factor Q, two rotation angles of the doubly rotated X-cut plates (XY*lt*) with an aspect ratio w/l = 920/2000 were varied in the region from 0°/0° to −60°/−10°[384]. The rotation on the Y-axis of an X-cut plate allows to use a wet etching process to fabricate a complex shape oscillator consisting of a resonator, supports, and a mount (Fig. 1). The negative rotation angle around the X-axis increases the positive value of the first order temperature coefficient α caused by the mixture of flexure mode. The slot at the center of the resonator dampens the displacement at the long sides of the resonator by the vibration in both LE and flexure modes that prevent the resonator from being supported at the middle of the sides. The resonator was supported at the points 40 μm off-center where the total displacement becomes almost zero.

A fabricated doubly rotated X-cut quartz plate (XY*lt*) −35°/−1° oscillator showed the frequency-temperature characteristics with $\alpha = -0.6 \times 10^{-6}$ /°C, the second order temperature coefficient $\beta = -3.5 \times 10^{-8}$ /°C^2 (Reference temperature T_0 = 20°C) as shown in Fig. 2. The parameters of the electrical equivalent circuit of the oscillator measured in the air are the followings: R_1 =1080 Ω, the series inductance L_1 = 2.70 H, and the capacitance ratio r = 192 at Q =19000.

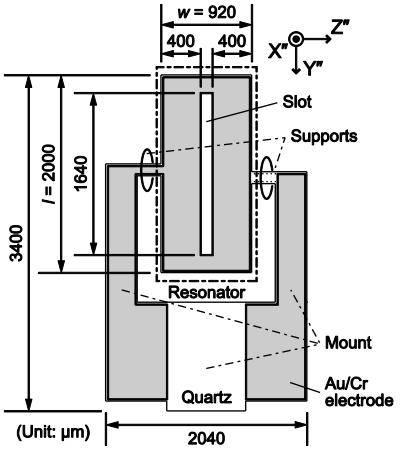

Fig. 130: Schematic diagram of the designed quartz resonator.

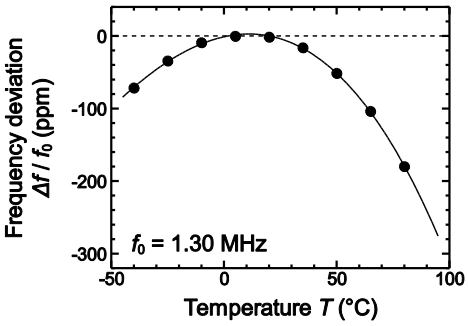

Fig. 131: Frequency-temperature characteristics of the fabricated quartz resonator ($\alpha = -0.6 \times 10^{-6}$ /°C, $\beta = -3.5 \times 10^{-8}$ /°C^2).

[384] IEEE Standard, "IEEE Standard on Piezoelectricity", 176-1987.

IFCS-EFTF2-PCD2-7

Investigation into Spectrum Shape Fluctuations of Oscillators and Signal Sources

Michael Underhill[1]

[1]Underhill Research Ltd, Lingfield, UK

Email: mike@underhill.co.uk

Spurious 'spikes' or 'spurs' can be observed in the spectra of oscillators and signal sources using both analogue and digital spectrum analyzers Some tentative explanations for the occurrence of these spurs and related phase and frequency jumps have been put forward[385],[386]. The fluctuations of these in time need further investigation so that some theory for them may be constructed.

Also the spectrum shape of an oscillator may vary with time both symmetrically, corresponding to pure amplitude, or pure phase, noise and fluctuations, or asymmetrically, corresponding to a mixture of amplitude and phase noise and fluctuations[387]. A software receiver, such as the RFSpace SDR-IQ, can act as a versatile digital spectrum analyzer and with suitable signal processing software, such as SpectraVue, can give a 'time-waterfall' display of the spectrum. For example the spectrum shape can be seen at the top of Fig. 1 with a 50s time (colored) waterfall below.

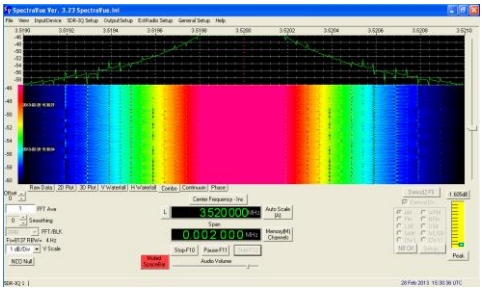

Fig. 132: A 2kHz Spectrum with 1dB amplitude scale steps at top, and 'time-waterfall below, of a 3520kHz DDS signal, showing fluctuating 'spurs' in the 50s time-waterfall using 'rectangle' windowing, and a 4Hz resolution bandwidth.

The Leeson Model[388] of an oscillator can be and is extended to investigate the factors that can cause fluctuations in spectrum shape with time. The amplitude limiting process always present in oscillators provides a total energy constraint on the oscillator but it does not exactly define the spectrum shape. Energy may be coupled and exchanged between one part of the spectrum with another. The (new) proposition that is incorporated in the investigation is that sideband components are lightly coupled by an amount that is also frequency spacing dependent.

Some further results to extract, define, validate and calibrate suitable proposed theory will be presented.

---

[385] M. J. Underhill, "Fundamental Phase Jumps in Oscillators?" Proc 20th EFTF, Braunschweig, Germany, 2006

[386] M. J. Underhill, "More fundamental instabilities in oscillators?", 15th EFTF'09: IEEE-IFCS'09, Besancon, France, 20-24 April 2009, pp 334-337.

[387] M. J. Underhill., "Time jitter and phase noise — Now and in the future?" IEEE International Frequency Control Symposium (FCS), p1-8, 2012.

[388] D. B. Leeson, "A simple model of feedback oscillator noise spectrum," Proc. IEEE, 54, No. 2, 1966, pp. 329-330.,

IFCS-EFTF2-PCD2-8

All-Digital Video RF Transmitter with Embedded Direct Digital Frequency Synthesizer

Konstantinos Vasiliou[1] , Kostas Galanopoulos[1] , Paul P. Sotiriadis[1]

[1]Department of ECE, National Technical University of Athens, Greece

Email: costas290a@gmail.com

This work presents an all-digital PAL video RF transmitter with embedded all-digital frequency synthesizer for the generation of the carrier. Converting traditionally analog to equivalent digital circuits and systems has been a major trend the past few years due to the automation and fabrication advantages of digital integrated circuits vs. analog ones, especially in deep-sub-micron integrated circuits technologies. The proposed topology can be easily implemented in FPGAs or ASICs providing an alternative to popular analog-RF ones and offering extremely fast concept-to-market time, versatility, low cost, minimal chip-area and power requirements.

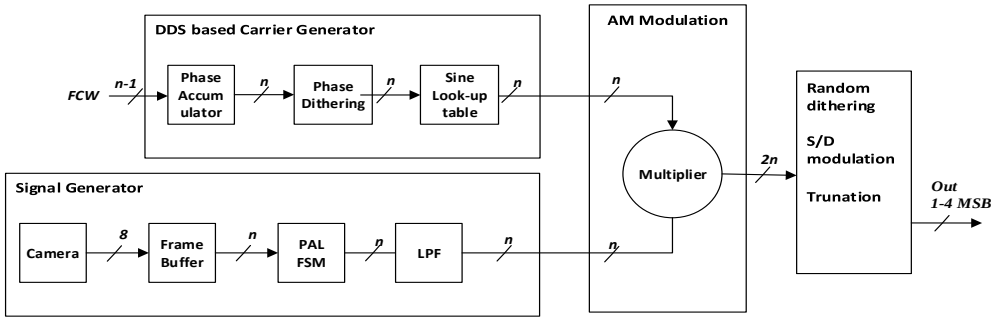

Fig.1 DDS-based all-digital PAL video RF transmitter architecture using a 1 to 4 bit Sigma-Delta DAC

The architecture used is illustrated in Fig. 1. An 8-bit image signal is captured by a digital Video camera and is temporarily stored in a RAM frame buffer. It is then accessed and encoded to a composite PAL signal. Using a digital multi-bit-output phase-dithered DDS we generate an *n*-bit carrier signal where phase-dithering is mainly used to reduce the size of the *sin* look-up table. AM modulation is then implemented by multiplying the carrier with the DC-shifted composite data stream. Using digital amplitude dithering[389] the modulated RF signal is converted to 1 to 4 bits (programmable) via a sigma-delta DAC.

The presentation of the paper will be accompanied by a live demo (Fig.2) of the proposed architecture. For this purpose an all-digital television transmitter has been implemented on an FPGA board (Papilio One / Xilinx Spartan 3E). This entry level FPGA (Xilinx 3E XC3S250E) has an equivalent of 250K gates and only 216K of Block RAM bits. For video capturing we use the Omnivission OV7670 VGA camera and the PAL video signal is transmitted at VHF television channel 2 (48.25 MHz).

Fig. 2: Footage from the FPGA-based PAL Video RF transmitter

[389] K. Galanopoulos, P. Sotiriadis, "Optimal Dithering Sequences for Spurs Suppression in Pulse Direct Digital Synthesizers", IEEE International Frequency Control Symposium 2012.

IFCS-EFTF2-PCD2-9

Theoretical and experimental investigations on 1/f noise of quartz crystal resonators

Ghosh Santunu[1], Sthal Fabrice[1], Imbaud Joel[1], Devel Michel[1], Bourquin Roger[1], Vuillemin Cedric[1], Bakir Ahmed[1], Cholley Nathalie[1], Abbe Philippe[1], Vernier David[1], and Cibiel Gilles[2]

[1]FEMTO-ST Institute, UFC, CNRS, ENSMM, UTBM, Besançon, France
[2]Microwave and Time-Frequency, CNES, Toulouse, France

Email: fsthal@ens2m.fr

The Centre National d'Etudes Spatiales (CNES), Toulouse, France and the FEMTO-ST Institute, Besancon, France, have initiated investigations on the origins of noise in bulk acoustic wave resonators together with several European manufacturers[390]. Theoretical and experimental works are reported in this paper.

We first improve on our previous study using fluctuation dissipation theorem by adding a term for internal damping[391] to the classical wave equation already studied[392]. This allows us to recover a 1/*f* noise spectral density at low frequency. The level of this 1/*f* noise is governed by a single fitting parameter that can be connected to the onset frequency of this 1/*f* regime. It constitutes the fundamental intrinsic limit of quartz crystal. Some preliminary considerations on the physical origin of this parameter in terms of microscopic processes in the crystal are given.

Experimentally, quartz crystal resonators have been cut from a quartz crystal block supplied specifically for this study on 1/*f* noise. The reader is reminded of the description of the blank realization and the topology of the resonator prototype is exposed. The resulting resonators are SC-cut with a 5 MHz resonant frequency. Then, we report noise measurements made on these quartz crystal resonators using a passive phase noise measurement system. The short-term stabilities of several resonators have been measured to be lower than $8 \cdot 10^{-14}$. A comparison of these resonators is given and the results are discussed according to the position of the resonators inside the crystal block.

[390] F. Sthal, S. Galliou, J. Imbaud, X. Vacheret, P. Salzenstein, E. Rubiola, G. Cibiel, "About Quartz Crystal Resonator Noise: Recent Study", Proc. ICNF, Pisa, Italie, 15-19 June, pp. 607-610, (2009).

[391] G. I. Gonzalez and P. R. Saulson, "Brownian motion of torsion pendulum with internal friction," Phys. Lett. A, vol. 201, pp. 12-18, May 1995.

[392] M. Devel, R. Bourquin, S. Ghosh, J. Imbaud, G. Cibiel, F. Sthal, "Quartz crystal resonator noise and fluctuation-dissipation theorem considerations", Proc. IEEE Int. Freq. Cont. Symp., Baltimore, Maryland, 22-24 May, pp. 425-429, (2012).

IFCS-EFTF2-PCD2-10

Switching Down-Converting RF Mixer with Embedded Single-Bit-Output All-Digital Frequency Synthesizer

Nikos Stamatopoulos[1], Kostas Galanopoulos[1], Paul P. Sotiriadis[1]

[1]Department of ECE, National Technical University of Athens, Greece

Email: nstam@ieee.org

This work proposes a switching down-converting RF mixer with an embedded single-bit-output all-digital frequency synthesizer, an architecture having the advantages of digital circuit design (portability, reconfigurability, automated checking and verification), compared to traditional analog solutions, in both ASIC and FPGA implementations.

Although switching mixers are popular in discrete-component designs[393] and have been implemented in RFICs[394], they are typically driven by classical PLLs or complex mixed-signal frequency synthesizers. The proposed mixer is based on digital transmission gates which are driven directly by the single-bit output stream of the embedded all-digital frequency synthesizer. Dithering techniques are used to make the synthesizer's spectrum sinewave-like and convert spurs to continuous noise floor[395]. The paper elaborates on the mathematical estimation and measurements of the mixer's spectrum.

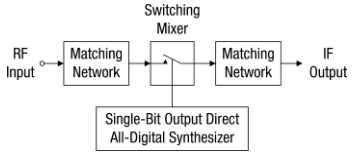

Fig 133: Switching mixer with embedded all-digital frequency synthesizer

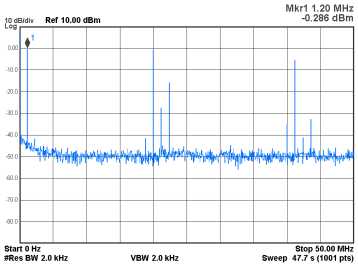

Fig 2: Switching mixer's output

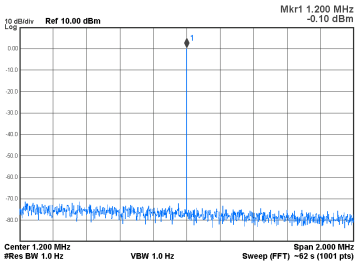

Fig 3: Spectrum centered at $f_{LO} - f_{RF}$

Our test setup, serving as a proof of principle, consists of the mixer whose transmission gate is controlled by the all-digital frequency synthesizer implemented in a mini FPGA board (XuLA-50 / Xilinx Spartan 3A). Both the low-cost o*ff-the-shelf* transmission gate (with on/off switching time ~ 5ns) and the low-cost FPGA limit the frequency of operation of the mixer to a few tens of MHz. The RF signal at $f_{RF} = 20$ MHz is provided by the signal generator while the synthesizer's output frequency (LO) is $f_{LO} = 21.2$ MHz. The mixer's output spectrum 0-50MHz is shown in Fig. 1 as well as in Fig. 2 which is centered at the desirable output component at $f_{LO} - f_{RF}$. The conversion loss, LO/RF isolation, RF/IF isolation and input IP3 are estimated analytically and measured experimentally. Further measurements at higher frequencies are also presented in the paper.

[393] U.L. Rohde, *Microwave and Wireless Synthesizers: Theory and Design*, Singapore: Wiley-Interscience, 1997.

[394] Robert B. Staszewski et al, "All-Digital PLL and Transmitter for Mobile Phones", IEEE Journal of Solid-State Circuits, Vol. 40, No. 12, December 2005.

[395] Kostas Galanopoulos, Paul P. Sotiriadis, "Optimal Dithering Sequences for Spurs Suppression in Pulse Direct Digital Synthesizers", IEEE International Frequency Control Symposium, 2012.

IFCS-EFTF2-PCD2-11

433 MHz Wide-tunable High Q SAW Oscillator

Tsubasa Yasuda[+], Shasika Shaminda Senanayaka[++],

Shyoji Izumiya, and Takehiko Adachi [*]

Division of Electrical and Computer Engineering
Yokohama National University
Yokohama, Japan
* Email: ada@ynu.ac.jp

A piezoelectric resonator, as a quartz crystal resonator and a SAW resonator, is widely used in a voltage control piezoelectric oscillator. Recently, demand for wide tunability and low phase noise of a piezoelectric voltage controlled oscillator has been increasing. But the frequency tunable range is limited by the capacitance ration of a piezoelectric resonator within a few hundred ppm. And, the phase noise of a piezoelectric oscillator is mainly determined by the effective quality factor of a piezoelectric oscillator, degraded from the piezoelectric resonator's unloaded quality factor. The dual-T quartz crystal resonator circuit was developed as the wide-tunable resonator circuit having quality factor comparable with the component piezoelectric resonator. We showed wide-tunability and quality factor enhancement method of a dual-T circuit, using 10 MHz crystal resonators.

In this paper, we have developed a 433 MHz dual-T SAW oscillator. Figure 1 shows the schematic diagram of the oscillator. The oscillator is made of an amplifier, variable gain amplifiers, phase shifters and dual-T SAW resonator circuit. Oscillation frequency can be changed by controlling the gains of variable gain amplifiers. The effective quality factor of the oscillator is enhanced by adjusting phase shifts. Figure 2 shows the measured frequency tunability. Measured frequency tunable range is about 1,700 ppm, exceeding the limit restricted by used SAW resonators. The effective quality factor of the oscillator was obtained by measured open-loop voltage transmission function. The obtained effective quality factor of the oscillator is about 30,000, about three times of the unloaded Q of SAW resonators. Figure 3 shows the measured spectrum at the center frequency of the frequency tunable range. Phase noise of the oscillator is estimated from the measured spectrum. Above 6 dB improvement of phase noise is obtained at 1kHz offset frequency compared to that of a colpitts oscillator.

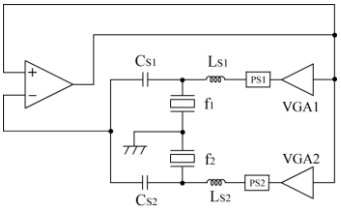

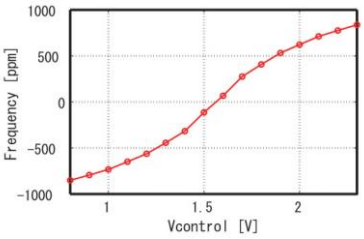

Fig. 2:Measured frequency

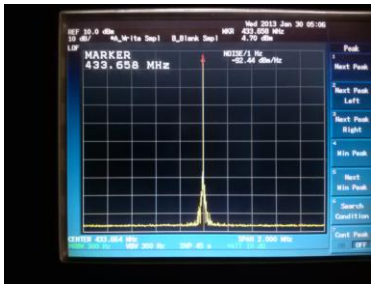

Fig. 3: Measured spectrum at the center frequency of tunable range.

[+] He will join AISIN COMCRUISE Co., Ltd. on 1 April, 2013.

[++] He is working for NIHON DEMPA KOGYO Co. Ltd., now.

IFCS-EFTF2-PCD2-12

Tracking DDS in Time and Frequency Metrology

C. E. Calosso[1]

[1]Optics Division, INRIM, Torino, Italy.

Email: c.calosso@inrim.it

The Phase-Locked Loop (PLL) in electronics was introduced in early 1930s to surpass the superheterodyne technique in radio receiver[396]. Since then, its diffusion has been very wide: in telecommunication, in digital electronics, in motor controls… and also in time and frequency: indirect frequency synthesis, clean-up and tracking oscillators, phase noise measurement, but also comb stabilizations, laser locks or even fiber link compensation.

In time and frequency applications, the interest is mainly directed to the output of the locked oscillator, considered as a filtered or frequency multiplied replica of the reference signal. This is inherently due to the poor performance of the controlled oscillator that, for long measurement time, is worse than the input one that is considered, for this reason, the PLL reference (fig. a).

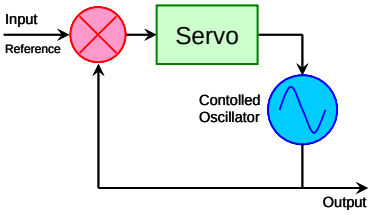

Fig. a: Typical PLL.

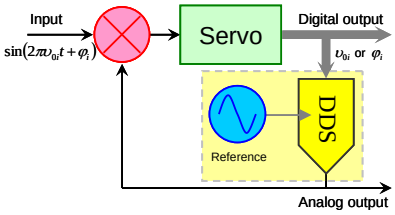

Fig. b: Tracking DDS.

By replacing the controlled oscillator with a Direct Digital Synthesizer (DDS) (fig. b), it is possible to reverse this point of view: now the local oscillator, the DDS referred to a stable and accurate clock, can be better than the PLL input that now takes on the meaning of measurand instead of reference. In this manner, the PLL can be used not only as generator, but also as frequency and phase meter, simply considering the corrections applied to the DDS to track the input. The inversion of the usual approach to PLLs, joined with DDS qualities[397], opens new possibilities in the time and frequency field because leads to a compact, low noise, cheap, wide input range, real time, digital phase/frequency meter that can be used in a wide range of applications.

At the conference I will expose the key points to correctly implement this scheme and reach the ultimate limit, represented by the DDS residual phase noise. On the opposite, I will discuss how to deal with high noise input signals as those encountered frequently in the growing field of optical frequency metrology.

[396]de Bellescize, Henri (June 1932), "La réception Synchrone", *L'Onde Electrique* 11: 230–240.

[397] C. E. Calosso, Y. Gruson, E. Rubiola, "Phase noise in DDS," Proc. 2012 IFCS p. 777–782.

IFCS-EFTF2-PCD2-13

A miniature timing microsystem using two silicon resonators

David Ruffieux[1], Jacek Baborowski[1], Nicola Scolari[1], Thanh C. Le[1], Antti Jaakkola [2], Tuomas Pensala[2], James Dekker [2], Charles A. Manier[3] , Kai Zoschke[3], Hermann Oppermann[3]

[1]CSEM, Neuchâtel, Switzerland
[2]VTT, Espoo, Finland
[3]Fraunhofer IZM, Berlin, Germany

Email: dru@csem.ch

This paper presents a miniature timing microsystem based on a pair of co-integrated low and high frequency silicon resonators -430kHz and 26MHz respectively- so as to implement an accurate, low power, temperature-compensated real time clock (RTC) and to generate reprogrammable clocks between 1-50MHz in a reconfigurable way.

Legacy quartz crystals have recently continuously been challenged by the announcement of new products relying on silicon MEMS resonators for either programmable HF clocks generation[398] or to implement RTCs[399]. The novelty of this work resides in the compact implementation of both functions using a pair of co-integrated piezo-electrically driven silicon resonators. A temperature compensated 32,768Hz clock further driving the RTC sub-circuit is generated by frequency interpolation and fractional division of the signal of a 430kHz electro-mechanical oscillator. The temperature information is obtained periodically by turning on a mostly linear temperature sensitive 10MHz RC oscillator whose periods are counted over a time window defined by the low frequency MEMS oscillator. An on-chip state machine using calibration data stored in a non-volatile one-time programmable memory then calculates and updates the compensation parameters using a 4th order polynomial fit. Any of the above clocks can be made available externally on demand or when an IRQ is generated in the RTC via its timer, alarm or time stamping request.

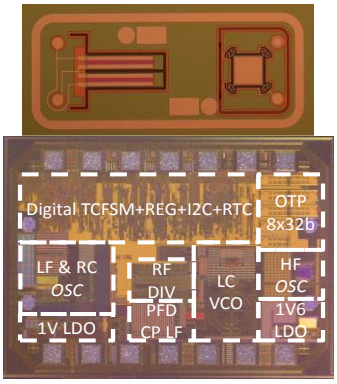

Fig. 135: Photos of ASIC and dual resonator

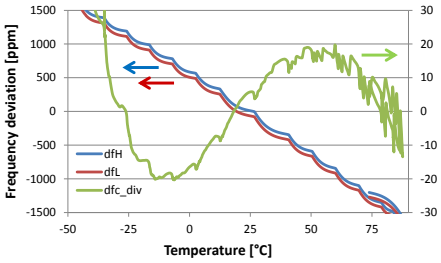

Fig. 2: LF oscillator temperature stability

The 26MHz high frequency silicon resonator temperature compensation is implemented indirectly via the same state machine by adjusting the fractional-N divider ratio of a 2GHz PLL whose RF output is further divided by an integer and/or fractional divider(s) to produce up to two programmable clocks of unrelated frequencies. Fig.2. shows a measurement of the temperature stability of the low frequency MEMS-based oscillator with and without compensation. The system draws 2µA in RTC mode and 4mA when HF clocks are generated. It achieves ±20ppm stability with a 3-points trim.

[398] http://www.sitime.com/products/low-power-oscillators/sit8008

[399] http://www.maximintets/low-powegrated.com/datasheet/index.mvp/id/6861

Background, Motivation and Objective:

One of the issues facing many types of oscillators is the transference of stress from the external world through the die to the resonator. Typically, resonators are clamped at more than one location. Integrated FBAR oscillators (referred to as FMOS[1,2]), uses a resonator that is clamped on all sides and integrated into an all-silicon, chip-scale package with integrated circuits. Mounting FBAR oscillators (epoxy die attach, over-molding and soldering) onto a customer board exposes the FBAR oscillator to stresses that occur during the assembly, plus additional stresses that occur during use. Although applied stress will change frequency of the resonator, it is hard to quantify. This paper does a first cut model of the stresses and then matches that to the changes in the measured frequency. Next, we discuss several designs that help mitigate the effect of external stresses on the resonator.

Statement of Contribution and Methods:

We use a 'Plan of Record' (POR) FBAR resonator that follows the design rules used in high volume FBAR manufacturing and then study the effects of stress on the resonator/oscillator frequency when thousands of die on a wafer are subjected to an external stress. This stress is modeled and from that, we match the modeled in-plane stress (and spatial wave form across wafer) to measured frequency shifts as measured over thousands of die across wafer. We then compare the mean and standard deviation and maximum stress for 3 types of resonator designs; the POR and two kinds of stress relieved resonators (SRR).

Results/Discussion:

The experiment consisted of measuring the frequency of thousands of oscillators on a 6" wafer (mounted on a vacuum chuck) and then re-measuring of the same die, where the wafer was removed and then placed on top of a thin Mylar substrate 57 mm in diameter – all on the same vacuum chuck. The resulting plot of the change in frequency (using false colors) highlights clearly the shape of the underlying piece of Mylar and the resulting stress created by the bending of the wafer due to the wafer being held by the vacuum around the edges. From this and with modeling, we conclude that we are getting about 0.8 ppm/MPa shift in frequency due to in-plane stresses. The figure shows the plots of δf frequency for 3 types of resonators, a POR resonator, and two designs of stress relieved resonators.

1) R. Ruby et al., "Positioning FBAR Technology in the Frequency and Timing Domain", Trans. Ultrasonics. Ferroelectrics, and Freq. Control (TUFFC), v. 59 #3, March 2012, pp. 334-345
2) R. Ruby M. Small, "Packaged Device with Acoustic Resonator and Electronic Circuitry and Method of making the same", Pub. # US 2012/0075026 A1, Pub. Date: March 29 2012

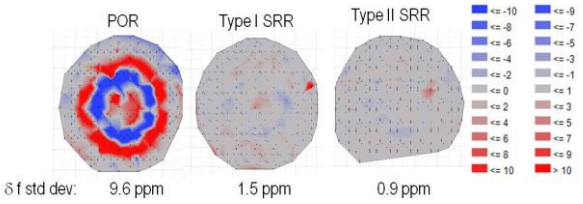

IFCS-EFTF2-PCD2-15

New thermal design to develop excellent stability and ultra low power compact OCXO.

Kamalkumar S[#], Mariyappa Chandrashekar[*], M Brahmananda Reddy,

Varaprasad Rayudu, Nalini C V

[#]*R and D Deportment Centumrakon India pvt ltd. Bangalore*

kamalk@centumrakon.com

Abstract— **Due to the cost, power and size constraints, improvements are made by introducing new thermal design, which has been developed to achieve compactness, low power and excellent stability OCXO.**

Power consumption and stability are both closely related to the size of the entire OCXO package. During last year's, making the oven smaller in order to affect a quicker warm up and will reduce frequency stability, as the smaller mass is more responsive to ambient temperature fluctuations. However, making the oven larger for better frequency stability will raise the amount of power required to maintain oven temperature. In order to achieve high frequency stability verses temperature, low power consumption and compact package with low cost, new thermal design and a radical new oven's design is worked out.

This paper demonstrates a new thermal layout design to achieve excellent frequency stability verses temperature by ensuring thermal conduction and convention paths are small and thermal gradient between the crystal, sensor and critical components are very less, the component selection has done in such a way that the thermal exchange between the critical components induced is linear and the temperature set point is compared with the actual value measured by the sensor and error signal is amplified and converted into a current controlling the heating elements. With reference to series of trails conducted by varying the crystal drive level, stability over the temperature has still improved by optimising the drive level. The details illustrations are clearly explained in this paper.

In this design the new heating mechanism has introduced and the PCB area is reduced to inducing low power dissipation in the circuit of less than 0.8W. Cost has been reduced by using HC43 crystal and single oven structure with smaller package. This paper presents development of single oven for excellent frequency stability, low power and compact package OCXO.

The achieved main parameters of new thermal design OCXO model are: Frequency 10MHz, frequency stability less than ±1.5ppb at -40 to 80°C. A SC-cut HC43 crystal with optimized drive level strengthens our aspect of low power consumption less than 0.8W and package style is 36×25×10mm3.

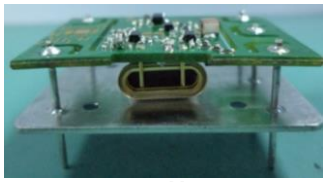

Fig1. OCXO assembly.

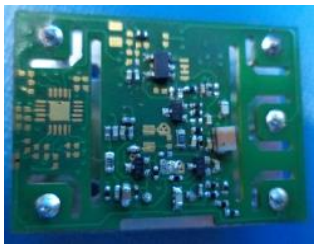

Fig2. PCB structure.

IFCS-EFTF2-PCD2-16

Electronic Signal Transduction in Collectively-Sensed Arrays of Parallel Piezoresistive NEMS Resonators

Hamidreza Zamani[1], Philip X.-L. Feng[1]

[1]Electrical Engineering, Case Western Reserve University, Cleveland, OH 44106, USA

Email: hamidreza.zamani@case.edu.edu, philip.feng@case.edu

NEMS resonators based on piezoresistive (PZR) nanowires and nanocantilevers are among the most interesting high-speed nanosensors. While it is desirable to use NEMS arrays[400,401], today's works have been very limited, and very little has been studied in analyzing and modeling the fundamental limits in signal transduction for integration of PZR NEMS arrays with CMOS. In this work, we focus on parallel arrays of PZR NEMS with single CMOS readout circuit.

We first investigate electromechanical modeling of a prototype PZR NEMS with both series and parallel PZR resistors (Fig. 1a). We have developed a comprehensive and precise equivalent circuit (Fig. 1b) for such systems. Then, using analytical formulas, we discuss that the noise voltage power (due to CMOS, NEMS resonator and PZR noise sources) is approximately $4k_BT(\frac{R_{PZR,parallel}^2 BW_{NEMS}}{R_m} + R_{tot,PZR}\Delta f + \gamma g_m R_{tot,PZR}^2 \Delta f)$ for the case of NEMS-CMOS co-integration and $\frac{KT}{C_{g'}}(\frac{R_{tot,PZR}}{R_m} + 1 + \gamma g_m R_{tot,PZR})$ for the case of off-chip integration with $R_{tot,PZR} = R_{PZR,parallel} + R_{PZR,series}$, $C_{g'}$ the total shunt capacitance at MOS gate, BW_{NEMS} the bandwidth of the NEMS, and Δf the frequency range over which noise and signal power are calculated. The above equations show that SNR will increase by a factor of either N or N^2 based on g_m value of the readout circuit. The analytical results verified by Cadence simulations (Fig. 1c) give designers a means to better co-design PZR NEMS arrays and CMOS readout circuits.

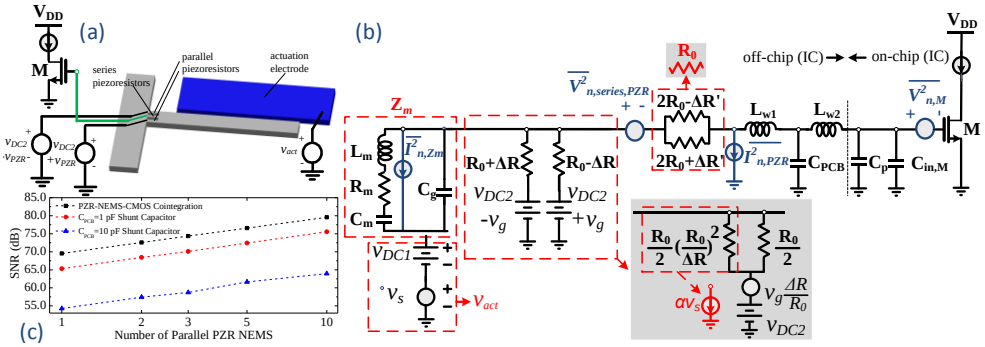

Fig. 136: (a) Illustration of piezoresistive (PZR) NEMS unit used for electromechanical modeling. (b) Equivalent circuit of (a) connected to the CMOS circuit. Both on-chip and off-chip parasitic capacitances as well as bonding wires (in case of PCB integration) are also shown. (c) Cadence simulation results for SNR of PZR NEMS arrays with CMOS integration.

---

[400] M.U. Demirci, C.T.-C. Nguyen, "Mechanically corner-coupled square microresonator array for reduced series motional resistance", in *Digest Tech. Papers, Transducers'2003,* 955-958, Boston, June 8-12 (2003).

[401] I. Bargatin, E.B. Myers, J.S. Aldridge, C. Marcoux, P. Brianceau, L. Duraffourg, E. Colinet, S. Hentz, P. Andreucci, M.L. Roukes, "Large-scale integration of nanoelectromechanical systems for gas sensing applications", *Nano Letters*, **12**, 1269-1274 (2012).

IFCS-EFTF Group 3 poster session 2

Forum Hall

Wednesday & Thursday, July 24-25, 2013, 1:00 pm - 2:00 pm and 3:30 pm - 4:30 pm

Chair: **John Kitching**
NIST

IFCS-EFTF3-PCD3-1

Estimates Of Achievable Frequency Stability Values In Atomic Gas Cell Frequency Standards With Coherent Population Trapping

V.S.Zholnerov[1], K.A.Barantsev[2], I.M. Sokolov[2], A.N.Litvinov[2]
[1]Russian Institute of Radionavigation and Time, St.-Petersburg, Russia
[2] St.-Petersburg State Polytechnical University, St.-Petersburg, Russia
Email: zholnerov@mail.ru

Use of coherent population rapping effect in atomic gas-cell frequency standards enables one, on one hand, to drastically reduce standard's dimensions due to the refusal from using a microwave cavity and, on the other hand, to improve a frequency stability of such standards.

The frequency stability values achieved in chip-scale atomic frequency standards developed by various companies are well known. It seems to be necessary, however, to estimate potentially achievable values of frequency stability, taking into account actual fluctuation performances of frequency standard's physical package assemblies and electronic circuitry when a selection of the physical package mode is optimal.

The frequency stability values achieved in rubidium gas-cell frequency standards of a traditional type used aboard GPS/Galileo satellite are also well known. The further improvement of these devices can be realized through using a coherent population trapping effect with double-frequency laser emission[xix].

The paper is dedicated to the investigation of frequency stability values achievable in atomic gas-cell frequency standards when using Rb^{87} D-1 line with buffer gases in coherent population trapping[xx,xxi,xxii]. Estimates of frequency stability are performed using a computer program for multi-parametric optimization as regards parameters of the physical package and frequency-lock loop of the controlled crystal oscillator. Estimates produced for a gas cell of standard dimensions show a possibility to achieve daily frequency stability at level of $(2\div3)\cdot10^{-15}$. For a chip-scale atomic frequency standard, frequency stability over 1-hour measurement interval could achieve a value of $(2\div3)\cdot10^{-12}$ with the appropriate selection of parameters as regards physical package and electronic components.

IFCS-EFTF3-PCD3-2

Outlook of Developing the Absorption Cells with Double Anti-Relaxation Components (Coating + Buffer gas) for Improving a Long-Time Stability of Atomic Frequency Standards and Quantum Magnetometers

E. Pestov

[1] The Fed. State Scient./Prod. Ent. "Geologorazvedka", 19/1 Knipovich str., St.-Petersburg 192019 [2] The Russian Institute of Radionavigation and Time, RIRT, 2 Rastrelli sq., St.-Petersburg 191124, Russia
E-mail: infra-balt@peterlink.ru

Use of absorption cells with anti-relaxation wall (ARW) coating by high-molecular paraffins was extremely fruitful for creating the quantum magnetometers of various purpose in the USSR - from mass application in geophysics when exploring mineral resources up to space units installed on 'Cosmos-321' and 'Cosmos-355' satellites (1969 and 1971). In these magnetometers the quantum sensors were moved to a distance of 8 m from the satellites using a rod and operated under open space conditions.

During the same years, extensive studies were performed with respect to Zeeman's resonance frequency shifts in cells with ARW-coating and dependencies were established between systematic errors for all used alkali atoms - ^{133}Cs, ^{85}Rb, ^{87}Rb, ^{39}K, ^{41}K - and various parameters of optical pumping (A. Kozlov, E. Pestov - IZMIRAN, Troitsk, Moscow). In particular, it was established that, when increasing a cell temperature from 35 to 55°C, Zeeman's resonance frequency, ω_0, decreased.

Application of cells with ARW-coating for atomic frequency standards was retarded due to an opinion on the insufficient stability of coating properties over time, which could result in non-reproducibility of a standard's frequency from one switch-on to another. The result of recent works [1], including also this work, can, however, significantly change this situation. The authors of work [1] have demonstrated a technique for relaxation processes' stabilization on coating surface which resulted in ^{87}Rb standard's frequency stability improvement.

The proposal of Dr. G. Mileti to the author of this work seems to be interesting: the case in point is the advisability to add a buffer gas of low pressure into the cell with ARW-coating which could improve the parameters of a quantum device. This work is just dedicated to this problem.

Following processes are investigated in this work:

1. Dynamics of synchronous relaxation of magnetization M_z- and M_x- components at Zeeman's resonance frequency, ω_0 [2] in ^{87}Rb-cell (ARW-coating + buffer gas, Ar) when changing a cell temperature, t°C.
2. Dynamics of a frequency shift, $\delta\nu$ (t°C) of the hyperfine 0-0 resonance at frequency, $\nu_{0\text{-}0} \sim 6{,}834$ GHz.

As a result, following is fixed.

In the vicinity of some temperature, t*(°C), a break in the relaxation dependence between coherence Zeeman's M_x- component (τ_2) and cell temperature occurs.

The growth of a negative '0-0'resonance frequency shift, ($-\delta\nu$), from relaxation action on the coating surface is slowing down with temperature growing, and in the vicinity of the same temperature value, t*(°C), a temperature -frequency coefficient becomes equal to zero due to the compensating action of the volume ^{87}Rb-atoms' relaxation within a buffer gas.

In such a way, addition of a buffer gas with a positive value of the frequency shift, ($+\delta\nu$), into a cell with ARW-coating enables one to realize a zero temperature -frequency coefficient in the vicinity of some temperature, t*(°C), and improve standard's long-term frequency stability.

---

[1] M. Pellaton, C. Affolderbach, G. Mileti, et. al. Proc. Joint Conf. of the IFGS-EFTF, Gothenburg, Sweden, pp. 87-90, 2012. [2] E. Pestov. Proc. Joint Conf. of the IFGS-EFTF, San. Fransisco, California, USA, pp. 623-627, 2011.

IFCS-EFTF3-PCD3-3

Measurements of optical frequency shift in sealed Cs vapor cells filled with He, Xe buffer gases

E. Kroemer, V. Giordano, R. Boudot

FEMTO-ST, CNRS, 26 chemin de l'épitaphe 25044 Besançon cedex, France.

Email: rodolphe.boudot@femto-st.fr

FEMTO-ST developed an original technology for filling and fabrication of Cs vapor microfabricated cells filled with buffer gas [1]. A great originality of this method is that Cs vapor is generated after the complete sealing of the cell by laser activation of a Cs dispenser developed by SAES Getters. Additionally, we pointed out the possibility to cancel the temperature-dependence of the Cs clock frequency at a temperature inversion of about 80°C using a single Ne buffer gas [2]. In this single gas configuration, the main advantage is that the so-called inversion temperature where the Cs clock will typically operate does not depend on the buffer gas pressure. At the opposite, this single-gas cell configuration prevents the clock to operate at high ambient temperature (typically above 100°C) without the use of a power-consuming Peltier element to cool down the cell. This can be an issue for the development for low-power consumption chip scale atomic clocks devoted to be used in applications with stringent and severe environmental conditions. Moreover, we observed that N_2 buffer gas can not be used with our cell technology because this gas reacts and is absorbed by zirconium compound of the Cs dispenser. This prevents the use of a N2-Ar buffer gas mixture.

In this sense, we started a study to measure the Cs buffer gas collisional clock frequency shift in presence of several buffer gas, mainly including Xe and He. Towards our objective, we decided in a first step to measure the actual buffer gas pressure in sealed cells through optical red shift measurements. The procedure is similar to the one described in [3].

We bought cm-scale commercially-available Cs cells filled with buffer gas. A physics package was developed to receive the cells. It includes a copper cell support inside a copper oven warmed by a thin heating foil around it. These elements are surrounded by a solenoid used to generate a static magnetic field to split Zeeman transitions. The ensemble is inserted into a double-layer mu-metal magnetic shield.

The laser source is a 1 MHz-linewidth distributed-feedback (DFB) diode laser tuned on the Cs D_1 line at 894.6 nm. The laser output is split in two directions. In the first one, the laser beam is sent through a Cs reference cell without buffer gas. In the second direction, the laser beam is sent through the buffer gas-filled Cs cell to be tested. Low laser intensities (< 10 uW/cm^2) are used. Optical absorption spectra from both cells are recorded with a photodiode and fitted by a sum of four Voigt profiles. After correct calibration of the frequency axis, the optical frequency shift between both cells is extracted to estimate the actual buffer gas pressure in the buffer-gas-cell using coefficients reported in [4,5].

Preliminary measurements will be reported at the conference for several cells filled with Xe or He.

[1] M. Hasegawa et al., Sensors Actuators: Phys. A 167, 594-601 (2011).
[2] D. Miletic et al., Elec. Lett. 46, 15 (2010).
[3] O. Kozlova, S. Guérandel, and E. de Clercq, Phys. Rev. A **83**, 062714 (2011).
[4] A. H. Couture et al., Journ. Appl. Phys., 104, 094912 (2009).
[5] E. Bernabeu and J. M. Alvarez, Phys. Rev. A 22, 6, 2690 (1980).

IFCS-EFTF3-PCD3-4

An Accurate Measuring Method for the Transient Oscillation Frequency of Detuned Coherent Population Trapping Atomic Clock

Daiting Shi , Yeqing Li and Zhong Wang*
School of Electronics Engineering & Computer Science, Peking University,
Beijing, 100871, P. R. China
*Email: zw@pku.edu.cn

We proposes a method for measuring the transient oscillation frequency observed when Coherent Population Trapping is excited by means of optical pumping radiation fields whose frequency difference is detuned slightly from the ground state hyperfine frequency of the atom used. In the technique, the pumping radiation fields are created by modulating the frequency of a laser. We call this technique Detuned Coherent Population Trapping (DCPT). Using narrow-band simulation filter and phase matching techniques this measuring method can provide a measurement precision of about 0.5Hz. Based on this reading accuracy the DCPT atomic clocks frequency instability can be better than $5\times10^{-11}/\tau^{1/2}$ (τ=100s) and tend to be more stable at longer integration time. According to our experimental results, we demonstrate that a DCPT atomic frequency standard could give good short and long term frequency stability.
An atomic frequency standard based on the concept could be implemented by directly reading the transient oscillation caused by the detuning of the applied optical field difference from the hyperfine states transition frequency and summing it to the microwave frequency used to modulate the laser frequency. It would eliminate the use of a frequency-lock-loop.

IFCS-EFTF3-PCD3-5

Microwave Cavity Design for an Optically-pumped Rubidium Atomic Beam Clock

Chang Liu, Yanhui Wang

School of Electronics Engineering and Computer Science, Institute of Quantum Electronics, Peking University, Beijing, China

Email: wangyanhui@pku.edu.cn

Previously, most commercial clocks are based on magnetic selection, the main shortcoming of which is short-term stability. We are developing a compact rubidium beam clock with lamp-pumping and fluorescence-detection[402]. Pumping and detecting lights are provided by ^{87}Rb lamps and ^{85}Rb filter cells. This scheme is simple in structure and stable for long-term working. A short-term stability better than $\sigma(\tau) = 2\times10^{-12} \times\tau^{-1/2}$ is expected. For interaction of rubidium atoms and microwave signal, a compact, stable cavity is needed. Identically with most commercial beam frequency standards, we use a U-shape cavity with apertures at both ends. On account of size constraints, distance between the ends is about 0.2m in our scheme.

A method of constructing microwave cavity for manufactured beam clocks is discussed in this paper. The cavity is designed in three parts, including a U-shape cavity, a vacuum window and a coaxial-to-waveguide adapter. These parts are machined separately and connected with flanges. We create models of each part and calculate detailed dimensions with the help of *ANSYS HFSS*, commercial software for high frequency electromagnetic stimulation based on finite element method.

Several frequency offsets are related to the interrogation method, which is mainly determined by the cavity. The main causes of uncertainty related to the cavity are end-to-end phase difference, distributed phase difference and cavity pulling effect. As a result, resonant frequency and phase difference are priorities in the design. In addition, a tunable resonant frequency and a low loaded quality factor helps to keep cavity pulling effect negligible.

We choose WR137 waveguide as the U-shape cavity's arms, lengths of which are 5 halves of guide wavelength respectively. Actually, instead of bend in waveguide, two symmetrical halves of machined copper blocks are soldered to form a whole cavity in order to get a good reproducibility. The resonant frequency is 6.835GHz, with a tunable range of tens of MHz. The drift length is 0.205m, leading to a Ramsey line-width of about 600Hz. The end-to-end phase difference is below 5×10^{-6}rad for an asymmetry less than 0.05mm, which can be guaranteed in manufacturing. We give an estimate of the cavity's influence on accuracy and stability in the discussion.

[402] Y. H. Wang, J. Q. Huang, Y. Gu, S. Q. Liu, T. Q. Dong, Z. H. Lu, Rubidium atomic beam clock based on lamp-pumping and fluorescence-detection scheme, J. Eur. Opt. Soc. Rapid Pub., vol. 6, 11005, 2011.

IFCS-EFTF3-PCD3-6

Extreme Resolution of the Laser Optical Pumped Alkaline Vapor Quantum Generator

S.V. Ermak, R.V.Smolin, V.V.Semenov, P.V.Zimnitsky

Department of Quantum electronics, Saint-Petersburg State Polytechnic University, Saint-Petersburg, Russia

Email: smolin_roman@inbox.ru

We present the results of analytic research of characteristics of self-oscillating magnetometer with laser pumping. The mechanism of amplitude limiting is based on alkaline atom saturation effect. This mode provides the best short-term stability of the quantum generator for average time about 100 seconds. Exceeding of this limit causes Allan deviation of the generator operating frequency increasing due to technical noise in feedback loop which spectral density is $S_{\delta n} = A_f/2\pi\omega^n$, where A_f – noise intensity constant, index n varies in range from 0.6 to 3.

Our research is based on analysis of stochastic differential equations for amplitude and frequency fluctuations. We obtained the equations for technical linewidth of the quantum generator for different values of n and evaluated dynamic range of relative rate of pump Γ and gain of feedback k variation within a range where generation signal has amplitude R_0 (Fig.1)

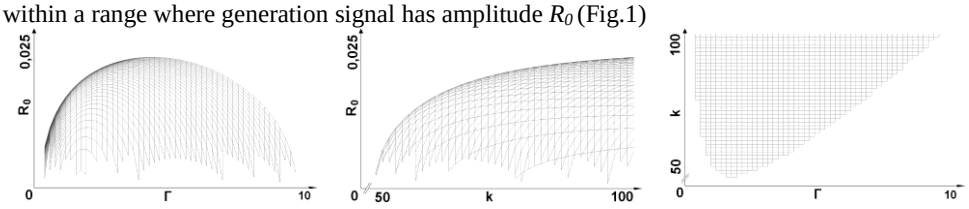

Fig.1. Dependence R_0 of relative parameters Γ and k for one of rubidium optical transitions (represented at three axonometric projections).

The experimental value of A_f for Si photodetector has magnitude of ~10^{-13} Hz. After substitution of A_f and $n \approx 2$ into equation for technical linewidth we get a value similar to the flicker floor estimations for hundreds of seconds (rubidium self-generating magnetometer operating frequency is 10^4 Hz)[403].

[403] E.B.Aleksandrov, M.V.Balabas, A.K.Vershovskiy, A.S.Pazgalev. Experimental demonstration of optical pumped quantum magnetometer resolution, JTF, 74, VOL.6, 118-122, (2004)

IFCS-EFTF3-PCD3-7

Wafer-level integration of getters in cesium-neon cells for miniature atomic clocks

M. Hasegawa[1], R. K. Chutani[1], R. Boudot[1], V. Maurice[1], L. Mauri[2], C. Gorecki[1], N. Passilly[1]

[1]FEMTO-ST Institute, 25044 Besançon cedex, France
[2]SAES Getters, Viale Italia 77, 20020 Lainate, Milan, Italy

Email: vincent.maurice@femto-st.fr

This paper reports on the integration of wafer-level gettering solution PageWafer® from SAES Getters into hermetically-sealed miniature cells for MEMS atomic clocks. Its ability to sorb the gaseous residues produced by the anodic bonding process used for sealing the cells, while preserving the required cesium and neon atmosphere, is demonstrated.

Miniature cells are obtained by sandwiching a silicon wafer between two glass wafers bonded by anodic bonding. First, the silicon wafer is etched-through to pattern the cavities necessary for the optical interrogation and the containment of a cesium dispenser. The second anodic bonding is performed under neon atmosphere (buffer gas), following the two-step process described in [404]. Once the cells sealed, the cesium is finally released from the dispenser by local heating with a high power laser. The PageWafer® consists in a getter film which is selectively deposited inside 10-µm deep cavities etched on a glass wafer. For this study, the latter was used as one of the capping wafers of our cell assembly (Fig. 1).

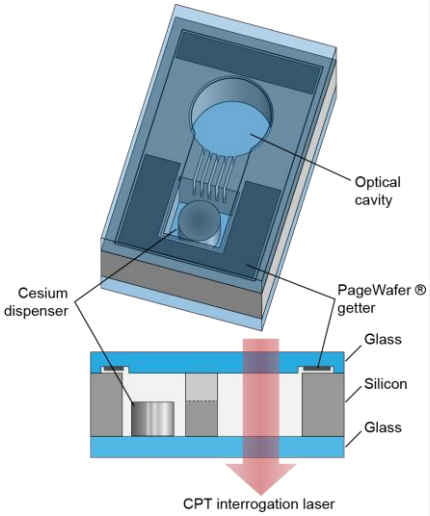

Fig. 1: Schematic of a miniature Cs-vapor cell

In order to assess the getter's effects, a residual gas analysis was performed on cells featuring getters and cells without getter. The inner atmosphere of the cells was analyzed with a high sensitivity quadrupole mass spectrometer. The comparison of the results exhibits the getter's strong ability to reduce the residual pressure of the main impurities generated during the anodic bonding process, e.g. H_2, N_2, O_2 and CO_2 [405]. In particular, the average pressure of the total impurities in getter-integrated cells was found to be $4 \cdot 10^{-2}$ mbar while it was 2 mbar in getter-free cells, which represents a 50-fold improvement. In addition, the pressure errors among the cells were drastically reduced for the getter-integrated cells. The difference in the pressure of neon was within the pressure error range typically obtained with our neon filling technique, indicating that neon was not absorbed by the getter.

Since this residual gas analysis was only performed on cesium-free cells, further investigations were carried out by coherent population trapping spectroscopy on cells embedding a dispenser and cesium vapor. The uniformity in neon pressures was verified, along with the quality of the cesium-neon atmosphere.

---

[404] M. Hasegawa et al., "Microfabrication of cesium vapor cells with buffer gas for MEMS atomic clocks", Sensors and Actuators A: Physical 167.2, p 594-601, 2011.

[405] S. Mack, et al. "Analysis of Bonding-Related Gas Enclosure in Micromachined Cavities Sealed by Silicon Wafer Bonding", Journal of the Electrochemical Society 144.3, p 1106-1111, 1997.

IFCS-EFTF3-PCD3-8

Improved frequency instability of PTB's fountain clocks

V. Gerginov, B. Lipphardt, M. Kazda, N. Nemitz, S. Weyers

Time and Frequency Department, Physikalisch-Technische Bundesanstalt, Braunschweig, Germany

Email: Stefan.Weyers@ptb.de

Since a couple of years the PTB fountain clocks CSF1[406] and CSF2[407] regularly contribute to the steering of International Atomic Time TAI[408]. At the same time they are used for the realization of the time scale UTC(PTB)[409], which is the basis for legal time in Germany. Work and investigations towards further improvements of the fountains' systematic uncertainties and their frequency instabilities are continued. This is particularly important in view of the demands of optical frequency standards, which nowadays surpass the performance of fountain clocks in terms of frequency instability and uncertainty.

The frequency instabilities of CSF1 and CSF2 contribute both to the statistical and to the systematic uncertainties of frequency measurements. An example for the latter contribution is the collisional shift uncertainty, which is dominated by the statistical uncertainty of its evaluation. To reduce the contribution to the fountain frequency instability, which is caused by the Dick effect[410], we set up an optically stabilized microwave source as described in previous work[411]. In the new setup a dielectric resonator oscillator (DRO) is stabilized to a cavity stabilized laser which in turn is referenced either to one of the optical clock transitions of a single Yb^+ ion[412] or to a hydrogen maser. The DRO signal can be used by both fountains for the generation of the required clock transition signal. Recently we measured the electric quadrupole transition frequency in a single trapped $^{171}Yb^+$ ion with the fountain CSF2. During this measurement campaign the DRO stabilized to the same optical transition was utilized, resulting in a frequency instability improvement by a factor of 2.

The second contribution to the fountain frequency instability, which is caused by quantum projection noise, can be reduced by increased atom numbers. For this purpose, we recently employed a cold atom beam source for loading the optical molasses of CSF2. As a result, another factor of 2 improvement of the frequency instability reaching $<5\times10^{-14}$(1s) was achieved when the optically stabilized DRO was utilized at the same time.

---

[406] S. Weyers *et al*., Metrologia 38, 343 (2001); S. Weyers *et al*., Proc. 6th SFSM, St. Andrews 2001, 64–71

[407] V. Gerginov *et al*., Metrologia 47, 65 (2010); S. Weyers *et al*., Metrologia 49**,** 82 (2012)

[408] BIPM CircularT, monthly, available at: http://www.bipm.org/jsp/en/TimeFtp.jsp

[409] A. Bauch *et al*., Metrologia 49, 180 (2012)

[410] G. J. Dick, Proc. 19th Precise Time and Time Interval (PTTI) Meeting, Redondo Beach, California, 133-147, 1988

[411] B. Lipphardt *et al*., IEEE Transactions on Instrumentation and Measurement 58, 1258 (2009); S. Weyers *et al*., Phys. Rev. A 79, 031803(R) (2009)

[412] Chr. Tamm *et al*., Phys. Rev. A 80, 043403 (2009); N. Huntemann *et al*., Phys. Rev. Lett. 108, 090801 (2012)

IFCS-EFTF3-PCD3-9

NPL Rb fountain: upgrade and new frequency measurements

Yuri B. Ovchinnikov[1, 2], Krzysztof Szymaniec[1], Soliman Edris[2]

[1]National Physical Laboratory, Teddington, UK
[2]University College London, London, UK

Email: yuri.ovchinnikov@npl.co.uk

The NPL Rb fountain frequency standard[413] was characterized in 2010 with a total Type B uncertainty of 3.7×10^{-16}. The first measurement of the absolute frequency of the ground Rb hyperfine transition in 2010 gave the value of 6834682610.904308(5.2), which agreed well with the SYRTE measurement of 2009[414]. In 2012 the minimization and characterization of the distributed cavity phase shifts reduced the total Type B uncertainty of the NPL Rb fountain down to 2.4×10^{-16}.

Recently we have found that, after 8 years of operation of the Rb fountain, the background pressure of the Rb thermal vapors in the MOT chamber and the detection section has increased to 5×10^{-10} mbar. To eliminate problems related to the presence of thermal Rb atoms, the fountain was opened and its detection section upgraded. An additional detection chamber with optical viewports has been introduced at the bottom of the fountain to increase the optical access to the atoms, which should essentially increase the efficiency of the detection and thus the frequency stability of the fountain. In addition, the orientation of the probe detection beams in the new setup is rotated by 45° with respect to the feeds of the Ramsey microwave cavity. This will essentially suppress the m=2 term of the distributed cavity phase shift[415].

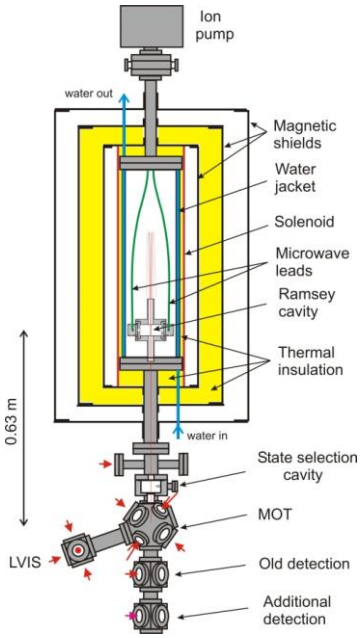

Fig. 137: Upgraded NPL Rb fountain.

The results of new measurements of the ground Rb hyperfine splitting in the clean and upgraded NPL Rb fountain will be reported.

[413] Y. Ovchinnikov and G. Marra, "Accurate rubidium atomic fountain frequency standard", Metrologia, vol. 48, p. 87-100, 2011.

[414] J. Guena et al, "Demonstration of a dual alkali Rb/Cs atomic fountain clock", IEEE Trans. Ultras. Ferr. Freq. Cont., vol. 57, p. 647-53, 2010.

[415] R. Li and K. Gibble, "Evaluating and minimizing distributed cavity phase errors in atomic clocks", Metrologia, vol. 47, p. 534-51, 2010.

IFCS-EFTF3-PCD3-10

Current status of NICT atomic fountains

Motohiro Kumagai[1], Clayton R. Locke[1], Hiroyuki Ito[1], Kohta Kido[2], Nobuyasu Shiga[1,2], Masatoshi Kajita[1], Yuko Hanado[1] and Mizuhiko Hosokawa[1]

[1]Space-time Standards Laboratory, National Institute of Information and Communications Technology (NICT), Tokyo, Japan
[2]PRESTO, Japan Science and Technology Agency (JST), Japan

Email: mkumagai@nict.go.jp

Atomic fountain frequency standards have been developed at NICT for contributions to the determination of TAI, frequency calibration of Japan standard time, and accuracy evaluation of optical frequency standards. The first fountain (NICT-CsF1 [1]) has been in operation since 2006 and has a typical frequency uncertainty of 1.4×10^{-15}. A recent vacuum system overhaul and resulting improvement in residual gas pressure now means it is possible to capture more atoms, leading to an improved short-term stability of $6 \times 10^{-14} / \tau^{1/2}$. As before, a cryogenic sapphire oscillator is used as a reference. However, this high atomic density is associated with a large collisional shift. To reduce the uncertainty of the collisional shift, we have installed rapid adiabatic passage method for state-selection [2]. This method allows the number of the atoms contributing to the signal to be changed by a precise factor of 2. Installation of rapid adiabatic passage enables both high frequency stability and accuracy. Additionally, following the new approach proposed in [3], we are currently re-evaluating the distributed cavity phase (DCP) shift in CsF1.

A recently constructed second fountain (NICT-CsF2) has now attained the goal of operation at the 10^{-16} level. This second fountain is vital for inter-comparison evaluation of frequency shifts and their associated uncertainties with the first fountain, and also provides redundancy necessary for guaranteed contribution to TAI. In contrast to CsF1 which uses a (0,0,1) laser cooling geometry with quadruple magnetic field, CsF2 adopts (1,1,1) geometry enabling many atoms to be captured without a magnetic gradient in large diameter laser beams, resulting in a reduction in the atomic density and thus a smaller collisional shift. Moreover, large initial size of the molasses makes it insensitive to phase distribution inside the Ramsey cavity. Currently CsF2 has a frequency stability of $3 \times 10^{-13} / \tau^{1/2}$ and averages down to a statistic uncertainty at the 10^{-16} level. We have completed evaluations of most systematic frequency shifts and their uncertainties for CsF2 at a level below 5×10^{-16}, and the remaining measurements for microwave related shifts are currently underway.

[1] M. Kumagai et al; "Evaluation of caesium atomic fountain NICT-CsF1" Metrologia 45, 139-148, 2009
[2] Dos Santos et al; "Controlling the cold collision shift in high precision atomic interferometry" Phys. Rev. Lett. 89, 23, 2002
[3] J. Guena et al; "Evaluation of Doppler Shifts to Improve the Accuracy of Primary Atomic Fountain Clocks" 106 130801, 2011

IFCS-EFTF3-PCD3-11

Distributed cavity phase calculation for a rectangular Ramsey cavity in NRC-FCs1

Louis Marmet[1], Nicolás A. Shtin[2], Pierre Dubé[1], J. Mauricio López R.[3]

[1]Measurement Science and Standards, NRC, Ottawa, Canada
[2]SMK Electronica S.A. de C.V., Tijuana, México
[3]Time and Frequency Division, CENAM, Queretaro, México

Email: louis.marmet@nrc-cnrc.gc.ca

We describe a numerical calculation of the contributions to the frequency shifts from the distributed cavity phase used in the fountain clock FCs1. The Ramsey cavity is rectangular as opposed to the cylindrical cavities used in most fountain clocks. It operates on the TM_{210} mode with a transversal C-field (X-axis). The microwave signal is coupled into the Ramsey cavity via two low-coupling magnetic antennas (rectangular loops 2.6mm × 0.5mm) through slits located on the sides of the cavity (Fig. 1). The cavity has a loaded Q=4600. It is made of two identical halves held together symmetrically about the YZ-plane. The cutoff waveguides have cylindrical symmetry, with a conical shape near the cavity center in order to keep the atoms away from the high fields at the edges and minimize phase shifts[416].

The numerical evaluation of the field in the cavity is made using of a full-wave finite element EM solver. Only the TM_{210} mode is coupled to perfectly symmetrical antennas. A mode expansion[417] is also used to evaluate the contributions from other modes to the phase variations.

The frequency shift of the cavity is evaluated by simulating the path of the atoms along the free-fall trajectories through the cavity while solving numerically for the Bloch vector with the TM_{210} mode. Contributions from phase gradients and other modes are added as a perturbation to the Bloch vector solution.

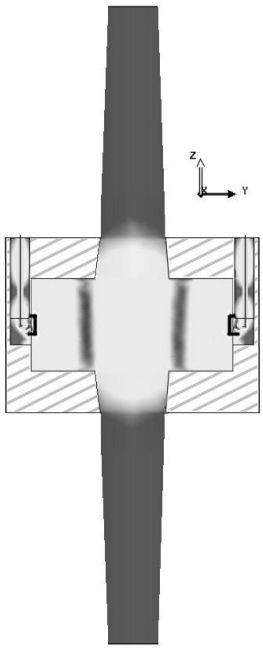

Fig. 138: Magnetic field amplitude of the TM210 mode (white: large, black: weak) in the YZ-plane through the center of the cavity. The field is in the X-direction (into the page).

[416] L. Marmet, B. Hoger, P. Dubé, A.A. Madej, J.E. Bernard, "Detailed description of FCs1: NRC's cesium fountain primary standard", Proceedings of the IEEE IFCS, pp. 386-391, 2008 and references within.

[417] N. Ashby, S. Römisch, S.R. Jefferts, "Endcaps for TE01 cavities in fountain frequency standards", Proc. Frequency Control Symposium, pp. 1076–83, 2003.

IFCS-EFTF3-PCD3-12

An atomic gravimeter at KRISS: Current status

Sang-Bum Lee[1], Sang Eon Park[1], Myoung-Sun Heo[1], Shin Hyuk Yim[2], Dai-Hyuk Yu[1], Chang Yong Park[1], Won-Kyu Lee[1], and Taeg Yong Kwon[1]

[1]Korea Research Institute of Standard and Science, Daejeon 305-340, Korea
[2]Agency for Defense Development, Daejeon 305-154,Korea

Email: lsbum@kriss.re.kr

Figure 1 shows a physics package for atomic gravimeter which consists of a Magnetic Optical Trap (MOT) chamber followed by Raman interferometer and detection zone below. The MOT chamber has 1,1,1 geometric configuration with three fold symmetry cooling beams (three upward beams, three downward beams) about vertical axis. The vacuum components were made of nonmagnetic titanium in order to reduce the distortion of a magnetic field. Distance from the center of the MOT chamber to detection zone is about 30cm corresponding to duration time 100 ms between the pulses in the Mach-Zehnder-type interferometer using $\pi/2 - \pi - \pi/2$ sequence of Raman pulses. The zone is composed of two parts whose upper part and lower part are used to measure atoms of an excited state and atoms of a ground state for normalizing population rate by measuring the number of total atom, respectively. We use rubidium-87 (Alvatec, Alvasource), which can be controlled by the heating current, as an atomic source.

We use a three home-made external cavity diode lasers (ECDL) as laser system for atomic gravimeter[418]. ECDL1 is stabilized to D2 line (F=2 to F'3) using modulation transfer spectroscopy (MTS) and is used for detecting populated atom and pushing for state selection. ECDL 2 is frequency-locked to ECDL1 and is alternatively used as a repumper and a mater Raman laser by controlling the frequency difference between the two lasers. ECDL3 is frequency or phase-locked to ECDL2 and is alternatively used as a cooling laser and a slave Raman laser. We have achieved the residual phase noise below-120 dBrad^2/Hz between two phase-locked lasers in the frequency range from 100 Hz to 350 kHz, which will give a limit to the sensitivity at a level of 1×10^{-10}g/Hz$^{-1/2}$.

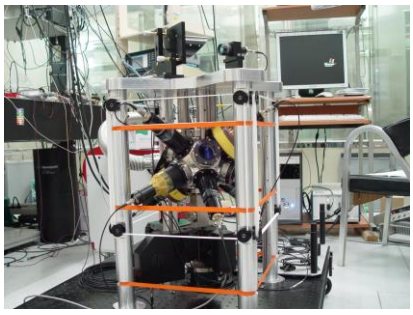

Fig. 139: Photograph of an atomic gravimeter developing at KRISS.

[418] P. Cheinet, F. Pereira Dos Santos, T. Petelski, J. Le Gouet, J. kim, K. T. Therkildsen, A. Clairon, A. Landragin, "Compact laser system for atom interferometry", *Appl. Phys*. B, vol. 384, p. 643-646, 2006.

IFCS-EFTF3-PCD3-13

A trapped atom interferometer for the measurement of short range forces

Minkang Zhou, Bruno Pelle, Adèle Hilico, Peter Wolf and Franck Pereira dos Santos

LNE-SYRTE, Observatoire de Paris, CNRS, UPMC, LNE, Paris, France

Email: minkang.zhou@obspm.fr

I will present the status of an experiment, which aims at performing precise measurements of the interaction forces between atoms and a macroscopic surface, for surface separations from 0.2 μm to 10 μm, where QED effects are predominant[419]. In our experimental apparatus, we have demonstrated laser controlled tunneling of ^{87}Rb atoms in a vertical optical lattice using two- photon Raman transitions[420], allowing performing high resolution laser spectroscopy of Wannier Stark (WS) states. With this shallow optical lattice, three different kinds of trapped atom interferometers are realized by using a state-labeling technique with WS states: a Ramsey-type interferometer sensitive both to clock frequency and external forces[421]; a symmetric accordion-type interferometer, sensitive to external forces only[422]; and a multiwave interferometer, insensitive to Raman and lattice light shifts. The Bloch frequency $\nu_B=mg\lambda/2h$ has been measured with a relative sensitivity of 9.1×10^{-6} at 1 s by the accordion-type interferometer. The limits in terms of sensitivity of those schemes are analyzed.

[419] P. Wolf, P. Lemonde, A. Lambrecht, S. Bize, A. Landragin and A. Clairon, Physical Review A **75**, 063608, 2007.

[420] Q. Beaufils, G. Tackmann, X. Wang, B. Pelle, S. Pelisson, P. Wolf and F. Pereira dos Santos, Physical Review Letters **106**, 213002, 2011.

[421] G. Tackmann, B. Pelle, A. Hilico, Q. Beaufils and F. Pereira dos Santos, Physical Review A **84**, 063422, 2011.

[422] B. Pelle, A. Hilico, G. Tackmann, Q. Beaufils and F. Pereira dos Santos, Physical Review A **87**, 023601,2013.

IFCS-EFTF3-PCD3-14

Large Area Cold Atom Gyroscope

M. Meunier, I. Dutta, C. Guerlin, C. Garrido Alzar, A. Landragin

LNE-SYRTE, Observatoire de Paris, CNRS, UPMC, 61 avenue de l'Observatoire, 75014 Paris, France

Email: arnaud.landragin@obspm.fr

After demonstrating a new butterfly geometry based on a 4 pulses sequence using one Raman beam[423], we developed a new ultra large area cold atom gyroscope, allowing a 300-fold increased area, up to 11 cm^2 and aiming to achieve a sensitivity in the range of 10^{-10} rad/s @ 1000 s. Wave-front distortions were identified as the main limitations to the accuracy and the long term stability on the previous experiment[424], and have been addressed. The use of one single source of atoms and a vertical trajectory as in atomic fountains lead also to a more robust configuration. This new experiment will enable us to explore the fundamental limits of these interferometers, demonstrating continuous rotation measurements (at 2 Hz) for inertial sensing, or participating in new improvements in geophysics, for the study of tilt fluctuations of the Earth rotation axis.

This new large area gyroscope is made of a 1 m high titanium vacuum chamber, surrounded by two layers of mu-metal, protecting from the ambient magnetic field fluctuations. Cesium atoms are loaded from a 2D MOT with a loading rate of 10^9 atoms/s into the 3D MOT, where the atoms are cooled down to a temperature of about 1.2 μ K. The atoms are launched vertically at a velocity up to 5 $m.s^{-1}$ thanks to a moving molasses technique. After the launch, the atoms in the level $|F = 3, m_F = 0\rangle$ are selected in order to reduce the sensitivity of the interferometer to parasitic magnetic fields. The number of atoms entering the interferometer is about $2 .10^7$.

Atomic wave packets are manipulated by Raman lasers, enabling the transition between the two fundamental states of the Cesium atom. The Raman lasers are horizontal and applied 4 times, in a π/2-π-π_π/2 pulse sequence, to realize a folded 8 shape interferometer[1], insensitive to DC acceleration. The atoms in free fall are then sensitive to the Sagnac phase shift, which can be written as $\Delta\varphi = 2\vec{\Omega}.\vec{A}\frac{E}{hc^2}$ where A is the area of the interferometer and E the particle Energy.

The total interaction time can be adjusted by using either one pair of Raman laser for short interaction times (below 125 ms) or two pairs of Raman laser for long interaction time (up to 800 ms). We got first atomic fringes using two pairs of stimulated Raman lasers in the two bottom windows (480 ms), doing a interferometer of 2.5 cm^2. We achieve a sensitivity of 7.10^{-7} rad/s @ 1s limited by spurious vibrations.

We are now optimizing the filtering of the parasitic vibrations in order to improve the signal to noise and to benefit from the maximum interrogation time of 800 ms reachable, leading to the macroscopic area of 11 cm^2.

[423] B. Canuel, F. Leduc, D. Holleville, A. Gauguet, J. Fils, A. Virdis, A. Clairon, N. Dimarcq, Ch. J. Bordé, A. Landragin et P. Bouyer, "Six-axis inertial sensor using cold-atom interferometry", Phys. Rev. Lett. 97, 010402, (2006).

[424] A. Gauguet, B. Canuel, T. Lévèque, W. Chaibi, and A. Landragin, "Characterization and limits of a cold atom Sagnac interferometer", Physical Review A 80, 063604, (2009).

IFCS-EFTF3-PCD3-15

Figure of merit and limit of short-term stability in passive hydrogen maser

Kozlov S.A., Vasilyev V.I.

Institute of Electronic Measurements KVARZ, Nizhny Novgorod, Russia

Email: nnipi_kvarz@sinn.ru

We present an investigation of frequency short-term stability of a passive hydrogen maser (PHM) by single frequency modulation[425].

Frequency stability of any passive frequency standard is associated with the figure of merit of a quantum discriminator (physics package), characterized by the ratio of signal/noise to the width of the atomic transition spectral line during indicating the atomic resonance. The larger this parameter, the higher is short-term frequency stability of the maser.

Calculations of the figure of merit of the discriminator in the PHM are carried out. The relationship between the figure of merit and frequency stability of PHM is shown. The method of the discriminator figure of merit measuring is presented. The lowest achievable short-term frequency stability is evaluated. The experimental results of measuring the figure of merit and short-term stability of the passive hydrogen maser are given.

For investigation of a limit of stability we studied change of the slope of discriminator curve S_d (therefore, figure of merit) at change of a excitation signal power[426]. The theoretical prediction of the maximum S_d is based on the solution of the passive hydrogen maser equations in a «steady-state» approximation.

Amplitude characteristics of the quantum hydrogen discriminator were experimentally investigated for verification of theoretical model. The result of investigation presented in Figure 1, shows that the spectral line shape corresponds to Lorentz line shape only at small ($-90...-100$ dBm) excitation signal power. With increase in a excitation signal power it is observed not only broadening, but also strong distortion of the spectral line. The line shape can be considered as the sum of several spectral lines. We explain the spectral line splitting by Stark – Zeeman dynamic effect that appears in strong alternating electromagnetic fields.

The discovered effect limits short-term stability of PHM.

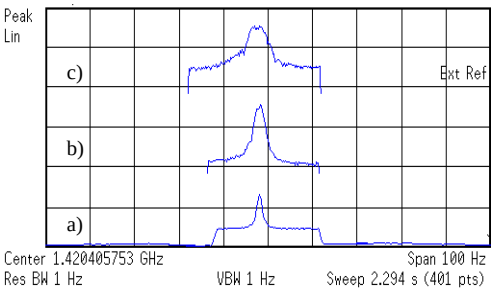

Fig. 140. The PHM spectral line shape at a different excitation signal power:

a) – 94 dBm; b) – 74 dBm; c) – 67 dBm.

425 Demidov N.A., Pastukhov A.V., Uljanov A.A. Progress in the development of IEM Kvarz passive hydrogen masers// Proc. of the 31 Annual Precise Time and Time Interval Applications and Planning Meeting, – USA, California, Dana Point. – 1999, pp. 579-588.

426 Kozlov S.A., Logachev V.A. Influence of the various factors on the passive hydrogen maser frequency instability// Proc. of the 51 Annual Frequency Control Symposium. – USA, Orlando. – 1997, pp. 286-294.

IFCS-EFTF3-PCD3-16

A new laser frequency locking method based on the normal and abnormal saturated absorption spectroscopy of ^{87}Rb

Jian Guo[1,2], Jianhong Wan[1], Yanhui Wang[1,2]

[1]School of Electronics Engineering and Computer Science, Institute of Quantum Electronics, Peking University, Beijing, China

[2]Department of Applied Electronic Engineering, School of Software and Microelectronics, Peking University, Beijing, China

Email: wangyanhui@pku.edu.cn

The normal saturated absorption spectroscopy has been widely used to probe closely spaced fine and hyperfine structures of atoms and molecules with a high resolution, and also is used to lock the laser frequency. This kind of locking method is already accepted and used by many groups to do some research work in the application of high precision measurements, cold atoms experiments and atomic frequency standards. However, due to the "many peaks" of the saturated absorption spectrums, wrong locking position phenomenon can happen sometimes. And the system is fragile for some kind of vibrations. These restrict the further applications of the traditional locking method.

The abnormal saturated absorption spectrum was found more than 30 years ago. By changing the polarization and the optical power, reversed peak of saturated absorption spectra can be observed.

In our experiment, we first obtained the normal and abnormal saturated absorption spectrums of ^{87}Rb simultaneously. With the help of the electronic circuits, these two signals are subtracted and only "one main peak" spectrum is left, which is shown in fig.1. This new spectrum is the reference for one diode laser frequency locking. After more than one month measurement, we find that the new system is quite insensitive for the sudden vibrations and also can avoid the wrong locking. The long-term locking performance of the diode laser is improved.

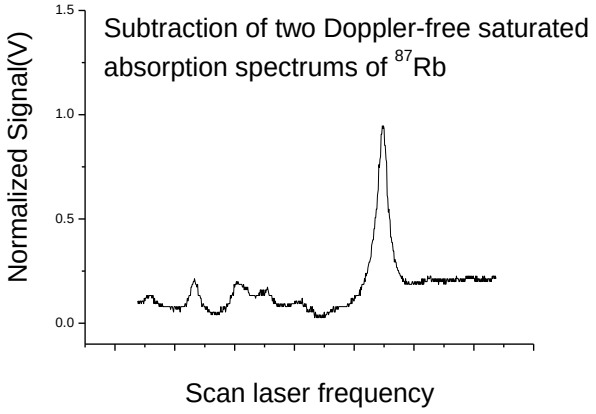

Fig.1. The subtraction of two Doppler free saturated absorption spectrum of ^{87}Rb

Electron Spin Resonance Spectroscopy of Macroscopic Crystals

Warrick Farr,[1] Karim Benmessai,[1] Daniel L. Creedon,[1] Yarema Reshitnyk,[2] Nitin Nand,[1] Maxim Goryachev,[1] Jean-Michel Le Floch,[1] Timothy Duty,[3] and Michael E. Tobar[1]

[1]ARC Centre of Excellence for Engineered Quantum Systems, University of Western Australia, Crawley WA 6009, Australia
[2]ARC Centre of Excellence for Engineered Quantum Systems, University of Queensland, St Lucia QLD 4067, Australia
[3]ARC Centre of Excellence for Engineered Quantum Systems, University of New South Wales, Sydney NSW 2052 , Australia

Email: farrw01@student.uwa.edu.au

The development of a new era of quantum devices requires an understanding of how paramagnetic dopants or impurity spins behave in crystal hosts. In the most recent experiment HEMEX grade sapphire used as a Classical Cryogenic Sapphire or a maser oscillator in the range 10-40 GHz, specific ions, such as the Fe^{3+} ion are at the heart of poorly understood, phenomena [1]. The ion parameters, the active ions concentrations, their spin-spin and, spin-lattice relaxation times are not well known in our crystals and need to be characterized.

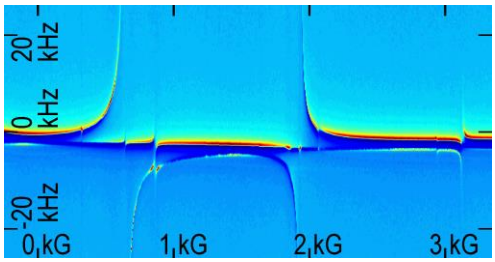

Fig. 141: The transmission of a Whispering Gallery (WG) mode doublet at 13.868 GHz, interacting with Electron Spin Resonance (ESR) packets of ion impurities under the influence of a DC magnetic field.

We present a new spectroscopic technique which uses traditional Electron Spin Resonance (ESR) combined with the measurement of a large population of high Q factor electromagnetic Whispering Gallery (WG) modes.

Measurements of high purity sapphire and rutile crystals cooled close to 20 mK in temperature, are used to identify and determine the concentration of trace paramagnetic ions, their sensitivity to a DC magnetic field, and the width of such ions. Our measurement is different to ESR in that it is possible to track the resonant frequency of the ions over a wide range of negative and positive magnetic fields up to ± 10 kG, allowing excellent measurement of the AC magnetic susceptibility. This high precision reveals anisotropic behavior of the Zeeman splitting. In our sapphire crystals, we observe a different g-factor for the two Zeeman components of the $|\pm 3/2\rangle$ to $|\pm 1/2\rangle$ transition in the Fe^{3+} ion.

[1] Creedon, D.L.; Benmessai, K.; Tobar, M.E.; Hartnett, J.G.; Bourgeois, P.-Y.; Kersale, Y.; le Floch, J.-M.; Giordano, V.; , "High-power solid-state sapphire whispering gallery mode maser," *Ultrasonics, Ferroelectrics and Frequency Control, IEEE Transactions on* , vol.57, no.3, pp.641-646, March 2010, doi: 10.1109/TUFFC.2010.1460

IFCS-EFTF Group 4 poster session 2

Forum Hall

Wednesday & Thursday, July 24-25, 2013, 1:00 pm - 2:00 pm and 3:30 pm - 4:30 pm

Chair: **Fabien Josse**
Marquette University

A stroboscopic approach to surface acoustic wave delay lines interrogation

Chrétien N.[1], Friedt J.-M.[1], Ballandras S.[1,2], Martin G.[2]

[1]SENSeOR, Besançon, France
[2]Time & Frequency, Femto-ST, Besançon, France

Email: nicolas.chretien@femto-st.fr

Acoustic delay lines are well known transducers used as passive sensors interrogated through a wireless link. Multiple electronic reader units have been presented in the literature, most of which are based on the FMCW RADAR approach whose control of the spectrum use and radiofrequency synthesis circuit is most basic, although requiring significant computational power (periodic audio-frequency rate sampling and Fourier transform) to extract the electrical properties of the acoustic delay line acting as cooperative target. Furthermore, FMCW requires a well linearized voltage controlled oscillator or linear digital synthesis for the Fourier transform components to coherently sum throughout the frequency excursion over the transfer function of the transducer.

Here, we assess the use of a pulsed RADAR approach in which the instantaneous power reaching the target is greatly increased, even though the average power consumption (depending on pulse repetition rate) is of the same order of magnitude than those found in FMCW. A carrier frequency generated by various sources (868 or 2450 MHz center frequency, 30 to 80 MHz bandwidth) with different phase noise stabilities is chopped by a fast (< 30 ns rise time) switch to load energy in an acoustic delay line. In order to comply with the requirements of compact, low power receiver electronics, a stroboscopic equivalent time sampling approach is demonstrated. The two values representative of the physical quantity detection by the transducer are the returned power magnitude and phase, as provided by an I/Q demodulator.

This demodulator provides an output signal of 20 MHz to 100 MHz bandwidth which involves digitizing a signal at 200-1000 MSamples/s to obtain a sufficient number of points to extract magnitude and phase with the targeted resolution aimed at only being limited by the local oscillator phase noise. The equivalent-time sampling approach provides a trade-off between reducing the demand for fast electronics components and increasing the acquisition time.

A strategy for generating high resolution time delays ($\Delta\tau$ =250 ps for an equivalent sampling rate of 4 GS/s) while allowing for long interrogation durations (up to 5 microseconds) is implemented by combining an FPGA-based delay generator with commercially available delay lines. The measurement sequence of generating interleaved combs is due to the long delay line reconfiguration duration (SPI communication) with respect to the coarse comb (FPGA based counter). I and Q components are recorded and processed to acquire the coarse acoustic velocity information through magnitude measurement, and an accurate physical quantity estimate is computed thanks to the phase information. Using this strategy, the optimum recording duration of 100 ms for sampling 20000 points (20000 points x 5 µs/point = 100 ms) is achieved with a sufficient resolution for identifying an 8-bit code.

SAW sensor exploiting palladium layer properties for selective detection of hydrogen

Vanotti Meddy[1], Rauch Jean-Yves[2], Ballandras Sylvain[3], Blondeau-Patissier Virginie[1]

[1]Time and Frequency Department, Femto-st Institut, Besançon, France
[2]Department of Optics, Femto-st Institut, Besançon, France
[3]Freq'N'sys, Besançon, France

Email: meddy.vanotti@femto-st.fr

For an increasing number of applications, hydrogen represents a solution for the future. However, due to its unstable properties, a particular care must be dedicated to control any leakage. In previous works, it has been shown that surface acoustic wave (SAW) sensors functionalized with a thin PVD palladium layer allow for detecting gaseous hydrogen[427]. Here we propose a study of different sensitive layer (thickness and composition) for these detections. It has been shown[428] that the two main parameters that influence the phase velocity change of elastic waves are mass- and elastic-loading.

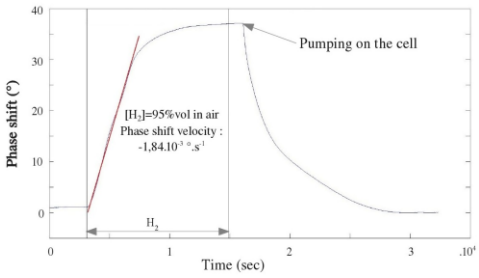

Fig. 1: Phase shift due to hydrogen absorption in a palladium layer which thickness is 300nm (performed at atmospheric pressure in air).

First it can be seen in Fig. 1 that our device functionalized with a 300nm palladium overlay enables for the detection of hydrogen in standard conditions. Such a detection is made by exploiting elastic-loading. Indeed, changes of elastics properties of the palladium layer consecutive to the hydrogenation[2] induce an increase of the phase velocity.

Secondly, as shown in Fig. 2, hydrogen absorption in a thin palladium layer (15nm) deposited onto the same type of delay line induces totally different observations. Indeed for such an overlay, the main phenomenon that is observed is no more elastic-loading but mass-loading.

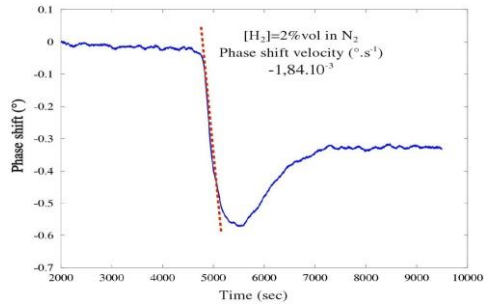

Fig. 2: Phase shift due to hydrogen absorption in a palladium sensitive layer which thickness is 15nm (performed at atmospheric pressure in nitrogen).

Finally, as an Yttrium doping of the palladium layer is expected to provide improvement on the detection[429], part of this study is also dedicated to its benefits.

[427] M. Vanotti and al, "Selective Detection of Hydrogen with Surface Acoustic Wave Devices Using Palladium Layer Properties", Sensors and Transducers, vol. 14-1 special, pp. 197 – 211, 2012.

[428] V. Anisimkin and al, "Elastic properties of thin-film palladium for surface acoustic wave (SAW) sensors", Sensors and Actuators B: Chemical, vol. 23, no. 23, pp. 203 – 208, 1995.

[429] L. Yia and al, "Hydrogen gas sensor based on palladium and yttrium alloy ultrathin film", Review of scientific instruments, vol. 83, 2012.

IFCS-EFTF4-PCD4-3

Large capacity SAW tag

Xin Huang[1], Zhijun Chen[1], Hailin Xu[2], Mengyang Wang[1], Ruan Peng[1], Peidi Chen[2]
[1]College of Automation Engineering, Nanjing University of Aeronautics and Astronautics, Nanjing, China,
[2]China Electronics Technology Group Corporation No.55 Research Institute, Nanjing, China
Email: huangxin931@126.com

The research on SAW tag has lasted many years. However, the application and promotion are unsatisfactory due to the inherent defects of the manufacturing technology of large capacity SAW tag. In order to ensure the consistent amplitude of reflector echoes and time domain resolution sensitivity, tags with different codes need to be designed and manufactured separately, leading to high manufacturing cost. This paper proposes a new method using anti-collision tag units to form a combined tag so as to expand the capacity of SAW tag and reduce the cost.

The key of an anti-collision SAW tag unit is the coding IDT. By using barker code sequence or Orthogonal Frequency Coding (OFC) method etc., the coding IDT obtains coding and anti-collision characteristics. The output of coding IDT achieves the maximum peak value, which is defined as autocorrelation, only if the code of the input pulse is the same as the code of IDT. For example, Fig.1 shows the simulation result of the coding IDT output when 7-bit barker code sequence [1110010] is used, wherein Fig. 1(a) shows the autocorrelation. Fig. 1(b) is the output when input sequence is [1011000], which is the minimum cross-correlation peak value between 7-bit barker codes.

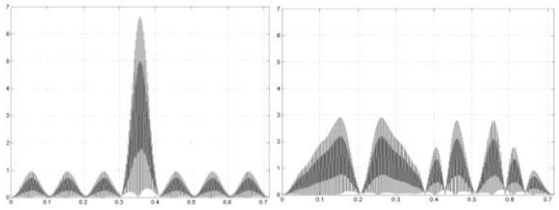

(a)7-bit barker code autocorrelation (b)[1011000] with [1110010] cross-

The structure of the tag unit is shown in Fig.2, including a coding IDT and a number of reflectors. With the anti-collision characteristic of coding IDT, each tag unit responds to a specific code modulation carrier pulse. When reader sends a sequence of different inquiry code modulation carrier pulses, the tag units with corresponding codes respond one by one according to the order of the inquire pulses. The consistency degree N, determined by the method used in the coding IDT, is the number of tag units in a combined tag. Thus, a high consistency degree of non-periodic polar code group is necessary in large capacity applications. Our group recently has found a 13-bit encoding group based on the communications coding theory, the consistency degree of which reaches 8. If the number of reflectors in each unit is 10, the capacity of this tag is 1.2*10^24 (1024^8=1.2*10^24), which is enough for most applications. While under the same circumstance, the capacity of a traditional SAW tag is only 1024*8.

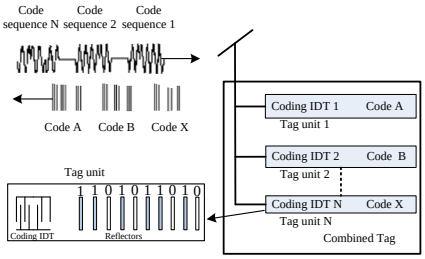

Fig. 2: The structure of tag unit and combined tag

This paper proposes a novel SAW tag consisting of several anti-collision tag units and combining code division and time division. By means of such novel SAW tag, a new low-cost and universal RFID system can be formed, which facilitates the implementation of large capacity SAW tags and multifunctional SAW wireless sensors.

IFCS-EFTF4-PCD4-4

A micro-machined Tonpilz hydrophone for audible frequency sounds

Min Sung[1], Hak Sue Lee[2], Won Kyu Moon[1]

[1]Dept. of Mechanical Engineering, Pohang Univ. of Science and Technology(POSTECH), Pohang, Kyungbuk/Republic of Korea

[2]Agency for Defense Development, Changwon, Kyungnam/ Republic of Korea

Email: wkmoon@postech.ac.kr

Micro-machined underwater acoustic sensors have been studied because of their many advantages including small size and low-cost by batch-fabrication[430-431]. But the sensitivity is not good enough at the low audible frequency such at 100 Hz for use in SONAR. In this study, a micro-machined Tonpilz hydrophone based on the piezoelectric thickness mode was designed for the audible frequency range 20 Hz ~ 20 kHz. The basic structure of the sensor was motivated by the structure of conventional Tonpilz transducers, but two different design approaches were adopted to enhance sensitivity and to endure the high underwater hydrostatic pressure. For improved sensitivity, the area ratio of the head-mass and the piezoelectric body was designed to be several hundreds to one, which amplifies the input of the transduction body due to acoustic pressure. Since this approach is adopted in order to develop a miniaturized hydrophone manufactured by batch processing, the size of the piezoelectric transduction body becomes too small to generate a sufficient amount of charge for using the conventional pre-amplifier for signal detection at low frequencies below 500 Hz. For endurance to the hydrostatic pressure in deep-water, the proposed structure needs oil backing for balancing the hydrostatic pressure from the environment on the front surface of sensing membrane as can be seen in Fig. 1.[432]

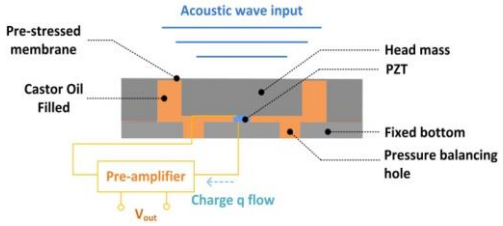

Fig. 143: Concept of the proposed micro-machined Tonpilz hydrophone (circular shape in top view)

We have developed a lumped parameter model to identify the requirements for the pre-amplifier circuits and the available sensitivity at low frequencies and to search for the appropriate design for miniaturized hydrophones. The designed hydrophone was then fabricated by micromachining. The eutectic bonding technique was used to combine the pressure amplification structure and the patterned PZT. The fabricated device was packaged with the custom-made pre-amplifier inside the castor oil-filled rubber housing. The constructed hydrophone was tested using the commercial hydrophone in a small anechoic bath to confirm the feasibility to be used as an effective micro-size underwater sound receiver.

[430] J. Bernstein, "A micromachined condenser hydrophone," in Digest IEEE Solid-State Sensor and Actuator Workshop, pp. 161–165, 1992

[431] J. Bernstein et al., "Micro-machined high frequency ferroelectric sonar transducers," IEEE Trans. Ultrason. Ferroelectr. Freq. Control 44, pp. 960–969, 1997

[432] T. D. Sullivan and J. M. Powers, "Piezoelectric polymer flexural disk hydrophone," J. Acoust. Soc. Am. 63, 1396–1401, 1978

IFCS-EFTF4-PCD4-5

Characterization of Parylene-C Using Quartz Thickness Shear Mode (TSM) Resonators

Huiyan Wu, Hongfei Zu, Qing-Ming Wang

Department of Mechanical Engineering & Materials Science, University of Pittsburgh, Pittsburgh, Pennsylvania, USA

Email: qiw4@pitt.edu

Shear-Horizontal Surface Acoustic Wave Devices (SH-SAW, Love Mode) are promising in fundamental biology as well as biomedical engineering, detecting behaviors of cells on their surface in a non-invasive, simple and quantitative manner[1]. Parylene-C, deposited on SH-SAW devices' surface, plays an important role as both an effective wave-guiding layer and biocompatible interfacial layer. In order to establish reliable theoretical analysis for SH-SAW device, however, complex shear modulus of Parylene-C is required first. As a result, due to its high sensitivity, repeatability and easy connection with electrical measurement systems[1], quartz thickness-shear-mode (TSM) resonator is adopted to characterize the mechanical properties of Parylene-C coating. Nevertheless, some problems of coating property extraction in TSM resonator applications have not been solved completely, including approximately-theoretical measurement and calculation error control. It has been found that viscous coatings of various thicknesses could induce other resonance modes[2], leading to incompatible with calculation model. Therefore, in this study, Parylene-C films of different thicknesses were deposited on the surface of AT-cut quartz TSM resonators with Au electrodes on both sides. Admittance spectra of these uncoated and coated resonators were measured by an impedance analyzer. Correspondingly, electrical admittance of coated TSM resonators was derived based on Transmission-Line-Matrix Model (TLM), which is also widely used in SH-SAW devices. Resonance frequency shift Δf and quality factor Q for TSM resonators with different-thickness Parylene-C coatings were obtained from admittance spectra as shown in Fig. 1. Results indicated that the ideal thickness range for TLM model is from 1.3 μm to 2.5 μm, and the extracted complex shear modulus of Parylene-C appeared to be uniform in this range through curve-fitting analysis. The storage modulus and loss modulus of Parylene-C are 798 MPa and 54 MPa, respectively.

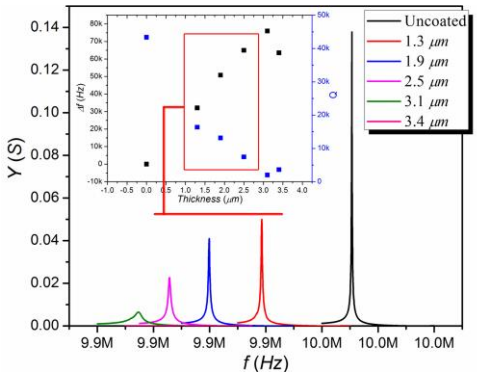

Fig. 144: Admittance Magnitude Y near fundamental resonance of the TSM resonator with Parylene-C coatings of different thicknesses. Inset is Resonance Frequency Shift and Quality Factor of Y curve for different Parylene-C coatings.

[1] D. S. Ballantine, R. M. White, S. I. Martin, A. J. Ricco, E. T. Zellers, G. C. Frye, and H. Wohltjen, "Acoustic Wave Sensor: Theory, Design, and Physico-Chemical Applications", Academic Press.

[2] S. J. Martin, H. L. Bandey, R. W. Cernosek, A. R. Hillman, and M. J. Brown,"Equivalent-circuit model for the thickness-shear mode resonator with a viscoelastic film near film resonance", Anal. Chem., vol.72, p.141-149, 2000.

IFCS-EFTF4-PCD4-6

A SH-APM liquid viscosity sensor based on PZT-5H

Zhijun Chen[1], Mengyang Wang[1], Jingyong Liu[2], Peng Ruan[1], Xin Huang[1]

College of Automation Engineering, Nanjing University of Aeronautics and Astronautics, Nanjing, China
No.55 Research Institute, China Electronics Technology Group Corporation, Nanjing, China

Email: zjchen76@sina.com

Compared with SAW (surface acoustic wave) device, the APM (acoustic plate mode wave) device has two interfaces. When one interface is deposited with IDTs as acoustic excitation, the other interface can be loaded with liquid sample. Furthermore, when the APM has only SH (shear-horizontal) particle displacement normal to the propagation direction and parallel to the plate surface, the attenuation because of the liquid sample is very small. So the SH-APM device is applicable for liquid sensing. Because of the variety of liquid's characteristic parameters and the complexity of APM's propagation characteristics, the researches on APM liquid sensing mainly focus on non-viscous liquid. In fact, the measurement of liquid viscosity is required and important in many applications.

In this paper, according to the material symmetry character, the excitation mechanism of SH-APM on the basis of material constants is derived. The liquid viscosity is introduced by adding the imaginary part in liquid elastic tensor, and the theoretical model of SH-APM device loaded with viscous liquid is built using the propagation characteristics of acoustic wave in layered mediums. The liquid volume elastic modulus doesn't affect the propagation velocity and attenuation of SH-APM because of its SH particle displacement. When the electrical boundary condition is free at the plate interface deposited with IDTs and metalized at the other interface loaded with liquid, only the liquid's density and viscosity influence SH-APM's propagation characteristics.

The influences of liquid density ρ_L and viscosity η_L on propagation velocity v and attenuation γ of SH-APM are numerically analyzed. v and γ of SH-APM have linear relation with the square root of ρ_L and η_L. The velocity v decreases with the increases of ρ_L and η_L. On the contrary, the attenuation γ increases with the increases of ρ_L and η_L. The changes of v and γ because of η_L are much larger than those because of ρ_L. It could be approximated that the changes of v and γ result mainly from liquid viscosity η_L, and the SH-APM device could be utilized as liquid viscosity sensor. The changes of SH-APM sensitivity to liquid viscosity with the ratio of the plate thickness to the acoustic wavelength are numerically analyzed, and the optimization design of the SH-APM device is implemented.

Using PZT-5H piezoelectric ceramic as substrate material, the SH-APM device is fabricated. The encapsulation and photo of the SH-APM device are shown in Fig. 1. Using different ratios of pure water and glycerol as the liquid samples, the experimental results are in agreement with the theoretical analyses. When the device is used as liquid viscosity sensing, not more than one milliliter liquid samples are needed, satisfying the requirement of minim liquid measurement. The superiority of the ceramic material PZT-5H used as SH-APM liquid sensing is testified.

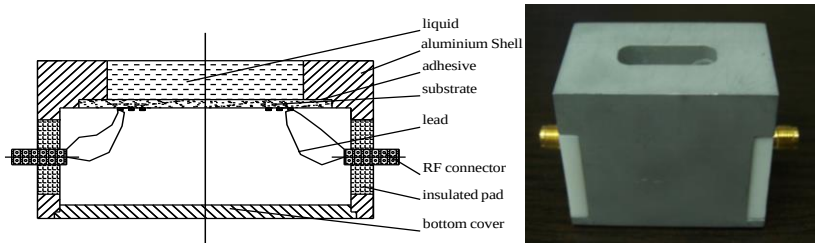

Fig. 1 The encapsulation and photo of the SH-APM device

IFCS-EFTF4-PCD4-7

Absolute control of the scale factor in the GP2 laser gyroscope: toward a ground based detector of the Lense-Thirring effect

J. Belfi[1], N. Beverini[1,2], M. Calamai[1], G. Carelli[1,2], D. Cuccato[3,4], A. Di Virgilio[2], E. Maccioni[1,2], A. Ortolan[3] and R. Santagata[2,5]

[1]Dept. of Physics, University of Pisa, Largo Bruno Pontecorvo 3, Pisa, Italy
[2]INFN Section of Pisa, Largo Bruno Pontecorvo 3, Pisa, Italy
[3]Dept. of Information Engineering, University of Padova, Via Gradenigo 6/B, Padova, Italy
[4]INFN National Laboratories of Legnaro, Viale dell'Università 2, Legnaro, Padova, Italy
[5]Dept. of Physics, University of Siena, Via Roma 56, Siena, Italy

Email: beverini@df.unipi.it

Laser gyroscopes measure the angular velocity of a ring cavity with respect to an inertial frame by reading the beat frequency between the counter-propagating laser beams (Sagnac effect). GP2 is a new ring laser gyroscope with the side length of 1.65 m, engineered to be the building block of a larger triaxial detector of the frame-dragging (Lense-Thirring effect) induced by the Earth rotation on ground based laboratory. To reach this goal, an accuracy better than 10^{-9} on the Earth angular velocity is required. The Sagnac frequency is related to the rotational speed of the gyroscope reference frame through a geometrical scale factor $S = \frac{A \times \cos q}{P}$, where P is the cavity optical length, A the area enclosed by the beam path, and q is the angle between the Earth rotation axis and the area vector. In a cavity where 4 identical spherical mirrors are placed in "perfect square" geometry, the sensitivity of S to the geometrical inaccuracy can be minimized, by stabilizing to an identical value the absolute length of the two Fabry-Pérot linear resonators along the square diagonal (Fig. 1). This control scheme will be tested in GP2 experimental setup, equipped with tridimensional PZT control system of the mirrors positions. We will present a simulation of the control automated system, and the experimental results on the stabilization of the absolute length of two identical linear cavities to a He-Ne I_2 frequency standard.

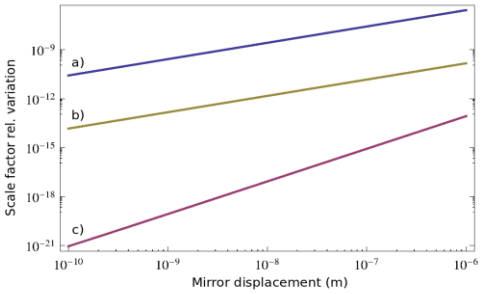

Fig. 1: Calculated scale-factor relative variation due to cavity misalignment. The displacement of one cavity mirror from the ideal position is considered: a) diagonal shift; b) shift out of the plane; c) tangential shift.

IFCS-EFTF4-PCD4-8

A heterodyne frequency-stabilization method for large ring laser gyroscopes with sub-nW output power

Fabio Stefani[1], Jacopo Belfi[2], Enrico Maccioni[2]

[1]Laboratoire de Physique des Lasers (LPL), Paris 13 University, Villetaneuse, France
[2]Physics Department, University of Pisa, Pisa, Italy

Email: fabio.stefani@univ-paris13.fr

He-Ne ring lasers with cavity dimensions larger than 1 m can operate as ultra stable rotation rate sensors. For such systems, the two opposite beams generated inside the cavity are frequency split because of the Sagnac effect. The information about the rotation rate of the cavity is encoded in the optical beat between the counter propagating beams. In order to reduce the mutual coupling between the two opposite beams, a high Q-factor of the optical resonator is required and no intracavity elements can be used to select single mode operation. This implies, in general, a very low output power down to the level of some hundreeds pW. Such a low power and the large acoustic phase jitter make the extraction of a clean measurement of the optical frequency of the gyroscope a not trivial operation.

We will present the characteristics and the performances of a heterodyne detection scheme (see the block scheme in the figure) allowing a robust frequency lock of the G-Pisa[433] ring laser to a He-Ne-I_2 reference laser. The system demonstrated a continuous unattended control of the laser frequency for several days of operation of the gyroscope with a single mode output power of about 500 pW.

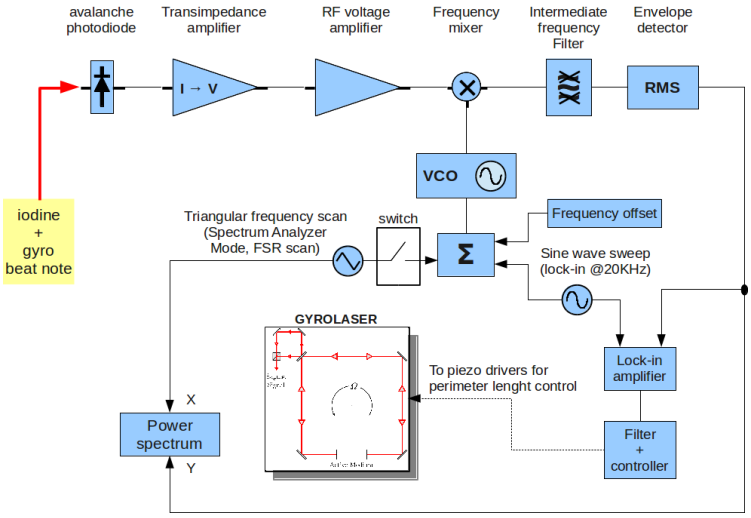

[433] J. Belfi, N. Beverini, F. Bosi, G. Carelli, A. Di Virgilio, E. Maccioni, A. Ortolan, F. Stefani, "A 1.82 m2 ring laser gyroscope for nano-rotational motion sensing", Appl. Phys. B, 106, 271–281 (2012).

IFCS-EFTF4-PCD4-9

Finite Element Simulation of Piezoelectric Ultrasonic Devices with Elements from Porous Piezoceramics

Andrey Nasedkin[1], Maria Shevtsova [2]

[1]Department of Mathematical Modeling, Southern Federal University, Rostov on Don, Russia
[2] Department of Mech., Phys. & Nanotechn., Southern Center of RAS, Rostov-on-Don, Russia

Email: nasedkin@math.sfedu.ru

Porous piezoceramic materials have received considerable attention due to their application in ultrasonic transducers, hydrophones and other piezoelectric devices. Porous piezoceramics has ultra high volume piezosensitivity, expanded passband of frequencies and lower impedance than the dense ceramics, giving a better acoustic agreement between piezoelectric and acoustic media. On the other hand its thickness piezoelectric module remains almost the same as for the dense ceramics.

In this work the methodology of the computer modeling for piezoelectric ultrasonic devices drom porous piezoceramics consists in the following steps. For determination of effective moduli of 3-0 and 3-3 porous piezocomposites we use an approach based on the effective moduli methods, and by the finite element (FE) modelling of representative volumes for porous piezoceramics. FE models of high-porous ceramics assuming the heterogeneity of the polarization vector for a variety of piezoelectric finite elements were developed.

For determination of the effective moduli the sets of the static piezoelectric problems were determined for representative volumes with boundary conditions, which guarantee the constant values of electric displacements, strains, stresses and electric fields for homogeneous material. The finite element computations were implemented using ANSYS. At that, the generation of the range of the structures for representative volumes were carried out using separate programs in C++ developed by Remizov V. and subsequent transfer to ANSYS. To take into account the heterogeneity of polarization field the electrostatic problem for a dielectric composite was firstly solved, and the electric field that identifies the polarization field was determined. As a result we had a representative volume of piezocomposite with inhomogeneous properties of piezoelectric matrix (generally near the pores).
Finally the effective moduli for different types of porous piezoceramics were defined. A comparison of the calculated basic characteristics for porous piezocomposites with the experimental data obtained at the Research Institute of Physics, (Southern Federal University), was carried out.
We investigate 1-3 piezocomposite (piezoelectric generator), hydro-acoustic emitters made of solid ceramics with intermediate interjacent non-piezoelectric layers and piezoelectric emitter from porous piezoceramics without such layers. From the FE solutions of static and dynamic problems we can conclude that high porous piezoceramics is very effective material for quasistatic and low-frequency applications in piezogenerators, since its piezo-sensitivity rapidly increases on the porosity growth. We also note that porous ceramics is preferred for different hydro acoustic ultrasonic applications.

IFCS-EFTF Group 5 poster session 2

Forum Hall

Wednesday & Thursday, July 24-25, 2013, 1:00 pm - 2:00 pm and 3:30 pm - 4:30 pm

Chair: **Wolfgang Schaefer**
TimeTech GmbH

IFCS-EFTF5-PCD5-1

High stability composite clock performances

Vernotte François[1], Plantard Cedric[2], Mbaye Papa Mamadou[3]

[1]UTINAM, THETA Observatory/University of Franche-Comté & CNRS, Besançon, France
[2]ESTEC, ESA, Noordwijk, Netherlands
[3]ATOS, Paris, France

Email: francois.vernotte@obs-besancon.fr

The composite clock architecture we explored is composed of a VCO controlled by both a hydrogen maser and a cesium standard. We realized two composite clock prototypes: an industrial one (passive maser + commercial cesium) and another one suitable for metrological laboratories (active maser + high stability cesium).

This paper will describe the performances of both systems, from 0.01 s to 10 days. It will focus on the optimizations of the system parameters for achieving the ultimate performances of this type of device, i.e. the stability of the best reference for a given integration time.

As a conclusion, we will give the development potential of this type of composite clock and some applications.

IFCS-EFTF5-PCD5-2

Research on timescale algorithms in Database for TA(PL)

Michał Marszalec[1], Albin Czubla[2], Włodzimierz Lewandowski[3], Marzenna Lusawa[4]

[1]Central Chamber for Telecommunications Measurements, National Institute of Telecommunications, Warsaw/Poland

[2]Electricity Department, Central Office of Measures, Warsaw/ Poland

[3] Time Department, International Bureau of Weights and Measures, Sevres

[4]Central Chamber for Telecommunications Measurements, National Institute of Telecommunications, Warsaw/Poland

Email: M.Marszalec@itl.waw.pl

The group of Polish Time Laboratories has been cooperating closely from at least 15 years. From very beginning also Lithuania was participating in this group. The first common initiative was organizing independent Polish Atomic Timescale TA(PL)[434]. In 2004 has started a project to develop Database for Polish Atomic Timescale TA(PL)[435] to automate the process of time-standards comparison and calculate implemented group timescale ensembles algorithms (weighted average algorithm for a group of time-standards).

Ensemble algorithms are supposed to be more stable than any of the standard within the group. This very useful feature makes an ensemble a very good stable reference to control and supervise behavior of every standard. In the future it could be also used to steer Polish official realization of international Universal Coordinated Time (UTC) the UTC(PL) maintained by Central Office of Measurement (GUM). The set of ensemble algorithms was primary implemented in Database: original algorithm of TA(PL) based on ALGOS (algorithm developed by International Bureau of Measurements –BIPM[436]), one day-shifted ALGOS version and AT1(algorithm developed by National Institute of Standard and Technology -NIST).

During last years the Time-team of Institute of Telecommunications has implemented in Database a realization of AT2 algorithm developed on the basis of theorem published by NIST. Preliminary results shows that AT2 is more stable than others.

The last part of article shows analysis of results of new implemented algorithms and comparison to former implementations.

---

434 J. Azoubib, J. Nawrocki, and W. Lewandowski, "Independent atomic time scale in Poland –organization and results", Metrologia, vol. 40, p.245-248, 2003.

435 M. Marszalec, A. Czubla and D. Nerkowski, "DataBase for TA(PL) and UTC(PL),", Proceedings of the 40th Annual Precise Time and Time Interval (PTTI) Systems and Applications Meeting, p. 680-690, 2008.

436 W. Lewandowski, "International Atomic Time Scales and Related Time Transfer", special issue of MAPAN-JMSI, 2006.

IFCS-EFTF5-PCD5-3

Iterative Method for Signal Path Delay Difference Estimation of Two-way Satellite Time and Frequency Transfer

Wenke Yang[1], Jianwei Zhan[1], Hang Gong[1], Xiangwei Zhu[1], Guangfu Sun[1],

[1] School of Electronic Science and Engineering, National University of Defense Technology, Changsha, Hunan 410073, China

Email: ywk@nudt.edu.cn

There are several causes of non-reciprocity in Two-way Satellite Time and Frequency Transfer (TWSTFT), including Sagnac correction, ionospheric correction, tropospheric correction, earth station delay difference and signal path delay difference due to satellite motion in an earth-fixed frame. In previous studies, the ranging data between the ground station and geostationary satellite should be used to estimate signal path delay difference. In BeiDou Navigation System, TWSTFT via navigation geostationary satellite is implemented. The broadcast ephemeris is available for Geostationary Earth Orbit (GEO) satellite in BeiDou Navigation System, which gives a chance for a new method called iterative method to estimate signal path delay difference.

The positions of GEO satellite when it transmits signals for two-way links are important for signal path difference estimation. The iterative method is a way to estimate these GEO satellite positions when the receiving epoch is known and the broadcast ephemeris is available. The proposed iterative method works as follows. Step 1: to estimate an initial signal transfer delay from GEO satellite to the receiving ground station. Step 2: to estimate the epoch when GEO satellite transmits signal with the receiving epoch subtracted by the initial signal path delay. Step 3: to estimate the GEO satellite position at the transmitting epoch with the broadcast ephemeris. Step 4: to estimate the signal transfer delay between the estimated GEO satellite position and the position of ground station receiving signal. Step 5: to repeat from Step 1 to Step 4 using the updated estimated signal transfer delay as the initial signal transfer delay in Step 1, until the error between the adjacent estimated signal path delays is below the defined threshold. Then, the GEO satellite position at the transmitting epoch for two-way links can be estimated. Finally, signal path delay difference between two ground stations via GEO satellite can be obtained by the difference of geometry distances of two-way links after Sagnac correction.

The TWSTFT experiment data for one day with BeiDou GEO satellite at 140°E experiment between Beijing and Sanya has been analyzed. The signal path delay difference is estimated using ranging data and the iterative method respectively. The experiment results show that the signal path delay difference is about 0.115ns and the difference of the results using these two methods is less than 0.2ps. This implies that there is no need to conduct ranging when the broadcast ephemeris is available for the estimation signal path delay difference.

IFCS-EFTF5-PCD5-4

Study and Application of Real-Time Frequency Deviation Adjustment Algorithm in Establishing a Time Scale

Yiwei Wu[1], Lei Chen[1], Xiangwei Zhu[1], Gang Ou[1]

[1] Satellite Navigation R&D Center, School of Electronic Science and Engineering, National University of Defense Technology, Changsha, China

Email: Yiwei_Wu_sh@126.com

Satellite navigation system is essentially a time synchronization system. It is necessary to establish a stable time scale of satellite navigation system. The time scale algorithm is the key of the establishment of a time scale. Since satellite navigation system needs real-time forecasting the state of onboard atomic clocks, the time scale should be real-time and predictive. For high-precision positioning and timing, the requirement for the short-term stability of the time scale is relatively high.

There are a large number of papers focusing on time scale algorithms. Based on these studies and analyses, this paper proposes a real-time frequency deviation adjustment algorithm. The main steps of this algorithm are follows. Firstly, use a Kalman filter to estimate the time deviation, the frequency deviation and the frequency drift between the master clock and another clock. Secondly, adjust the frequency deviation and predict the next time deviation between these two clocks and thus reconstruct the time deviation sequence.

This paper proves that the Kalman filter can effectively filters out amounts of the white phase noise as well as the measurement noise, the white frequency noise and the walk random frequency noise from the time deviation, the frequency deviation and the frequency drift respectively. The simulate results indicate that the amount of the white frequency noise of this time deviation sequence is decreased and the stability of this time deviation sequence is improved effectively. Since the time deviation sequence is the adjusted clock difference between the master clock and the other clock, conclusion can be got that the stability of the master clock's time scale is also improved effectively.

This paper gives the propositional implementation. The algorithm is real-time, and its implementation is with low cost and easy to realize and control, so the algorithm is of high engineering and application values.

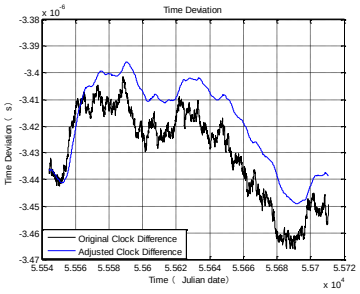

Fig. 145: The original clock difference and the adjusted clock difference.

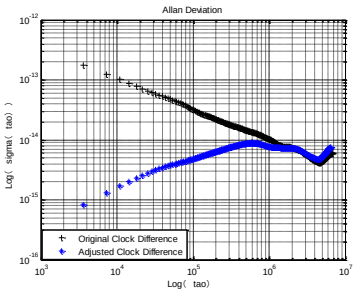

Fig. 2: The Allan Deviations of the original clock difference and the adjusted clock difference.

IFCS-EFTF5-PCD5-5

An Adaptive Filtering Algorithm With Packet Delay Variation For IEEE 1588 Servo System

ChenLei[1], ZhuTianlin[2]

[1]9th Lab, BITTT, BEIJING, CHINA
[2]Science and Technology Section, BITTT, BEIJING, CHINA

Email: chenlei0831@126.com

IEEE 1588 is a protocol for precision timing via packet networks. In the protocol, servo system in the slave will output an adjustment signal according to the calculated offset between master and slave, to achieve the goal of synchronization. Traditional IEEE 1588 servo system will be inactive after it entries the stability state, which is caused by packet delay filtering. And unfortunately most now networks do not support PTP(IEEE 1588, Precision Time Protocol), so the delay will be changed when routing or waiting. For these networks in which packet delay maybe variable, traditional filtering in servo system cannot follow packet delay variation for its inertia, and this limits the application of protocol.

To make a contribution for solving the problem that how to apply the protocol in existing networks without mass alteration, this paper puts forward an adaptive filtering algorithm based on IEEE 1588 servo system, which can make system both filter out high-frequency noise, impulse noise and continuous impulse noise, and adjust the cut-off frequency and output function adaptively according to packet delay listening results to realize the fast and accurate tracking to packet delay variation. Verified by simulations on MATLAB, just as Fig 1 shows, the adaptive algorithm mentioned in this paper is much better than traditional filtering in tracking character, and meanwhile has almost the same filtering character.

To sum up, the adaptive filtering algorithm putted forward by this paper, can make servo systems have both good tracking and filtering characters. Partly this paper provides a reference idea for applying the protocol large-scale with low cost.

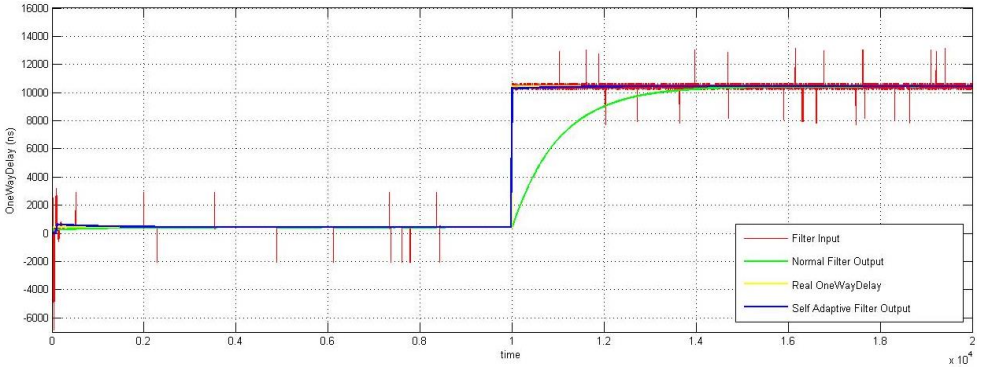

Fig 1: Output comparison of filtering and tracking between adaptive and traditional filtering

IFCS-EFTF5-PCD5-6

Precise Point Positioning technique for short and long baselines time transfer

P. Lejba[1)], J. Nawrocki[1)], D. Lemanski[1)], A. Foks-Ryznar[1)], P. Nogas[1)], P. Dunst[1)]

[1)] Space Research Centre, Polish Academy of Sciences,

Astrogeodynamic Observatory, Borowiec, plejba@cbk.poznan.pl

In this work the clock parameters determination of several timing receivers TTS-4 (AOS), ASHTECH Z-XII3T (OP, ORB, PTB, USNO) and SEPTENTRIO POLARX4TR (ORB, since February 11, 2012) by use of the Precise Point Positioning (PPP) technique were presented. The clock parameters were determined for several time links based on the data delivered by time and frequency laboratories mentioned above. The computations cover the period from June 1 to May 31, 2012 and were performed in two modes with 7-day and one-month solution for all links. All RINEX data files which include phase and code GPS data were recorded in 30-second intervals. All calculations were performed by means of Natural Resource Canada's GPS Precise Point Positioning (GPS-PPP) software based on high-quality precise satellite coordinates and satellite clock delivered by IGS as the final products. The received results were compared with the results obtained by GPS CV, TWSTFT and optical fibre with stabilization of propagation delay.

The used independent PPP technique is a very powerful and simple method which allows for better control of antenna positions in AOS and a verification of other time transfer techniques like GPS CV, GLONASS CV and TWSTFT. The PPP technique is also a very good alternative for calibration of a glass fiber link PL-AOS realized at present by AOS. Currently PPP technique is one of the main time transfer methods used at AOS what considerably improve and strengthen the quality of the Polish time scales UTC(AOS), UTC(PL), and TA(PL).

KEY-WORDS: Precise Point Positioning, GPS CV, TWSTFT, optical fibre, time transfer, IGS products, GNSS, time scales.

IFCS-EFTF5-PCD5-7

The study of GPS Time Transfer Based on Extended Kalman Filter

Wu Jian-feng[1,2,3], Jing Wen-fang[1,2,4],Hu Yong-hui[1,2,3], He Zai-min[1,2,3], Zhang fan[1,2,3,4], Lv Hong-chun[1,2,3,4]

1.National Time Service Center, CAS, Xi'an 710600,China

2.Key Laboratory of Precision Navigation and Timing Technology, National Time Service Center, CAS, Xi'an 710600,China

3.Key Laboratory of Time and Frequency Primary Standards, National Time Service Center, CAS, Xi'an 710600,China

4.University of Chinese Academy of Sciences, Beijing 100039,China

Abstract： The Global Positioning system (GPS) is global satellite navigation system that provides three major functions of positioning, velocity measurement, and time transfer. The key of the precise time transfer is three types of time synchronization which are the time synchronization between Universal Time Coordinated (UTC), GPS Time (GPST), satellite clock and user clock. GPS Time Transfer is a perfect combination of the advantages of GPS atomic clock group and the receiver crystal oscillator. GPS atomic clock group can provide the time and frequency of high accuracy and good long-term stability, and the receiver crystal oscillator can provide good short-term stability. In other words, the long-term stability of GPS timing receiver depends on GPS atomic clock group mostly. The short-term stability of GPS timing receiver is determined by the receiver crystal oscillator. But is now mostly just used code pseudorange observation equation solving user clock offset in GPS timing receiver, while ignoring the impact of the receiver clock drift. In order to improve the GPS receiver Timing precision, the single satellite timing method is discussed, and the extended Kalman filter algorithm is used to estimate and predict the clock offset and clock drift. GPS antenna position is fixed and known , and a receiver can determine precise time by tracking a single satellite. The receiver clock model is constructed by the clock offset and clock drift. The clock offset and clock drift have integral relationship, and often used as Kalman filter state variables. The white noise spectral amplitudes of clock offset noise and clock drift noise can be related to the classical Allan variance parameters Based on relationship between Allan Variances and Power spectral density Parameters. Process-noise covariance matrix is deduced. The pseudorange-rate equation is derived according to pseudorange observation equation. The pseudorange-rate is represented by the carrier phase difference of the adjacent sampling time, and this method can improve the measurement accuracy of the Clock drift. The error source is analyzed and quantified with respect to the pseudorange and the pseudorange-rate, and the measurement noise covariance matrix is presented. The EKF method is tested and verified based on IGS data, and the timing precision of the GPS single satellite can be improved through this method.

Keywords: kalman filter；the single satellite timing；clock offset；clock drift

IFCS-EFTF5-PCD5-8

A method of High precision time transfer based on DVB-S

Xiang Yu[1,2,3], Hua Yu[1,2],Xu Linshen[1,2],Dong Daopeng[1,2,3],Huang Changjiang[1,2,3]
[1] National Time Service Center, Chinese Academy of Sciences, Xi'an China
[2] Key Laboratory of Precision Navigation and Timing Technology, NTSC,CAS, Xi'an , China
[3] University of Chinese Academy of Sciences, Beijing China

This paper puts forward a method of high precise time transfer based on satellite digital TV broadcasting system (DVB-S), with technology of television broadcasting, communication and time-frequency. Through intensive analyzing the digital satellite TV signals characteristic, and solving many key problem such as insertion and broadcasting of timing signal in DVB-S, coding method of timing signal, predict method of broadcasting delay of timing signal and capture-tracking method of timing signal in receiver, the timing transfer method of high precision is proved practicable.

In this paper the high precise timing is achieved through such steps as fellow:

(1) Program clock reference(PCR) in the TS of DVB-S is proposed as the flag bit;

(2) Each PCR is given a high precise timing stamp in transmitter and receiver;

(3) The accurate position of the broadcasting satellite in the orbit is provided by NTSC's the real-time observation, then sended with timing stamp to receiver via the satellite after coding;

(4) The coding is received and decoded by user, then the PCR is also given another time stamp in the local time system. The cute synchronization is achieved with the information both the accurate position of satellite and the two timing stamps;

(5) The local time system is synchronized accurately with the transmitter time system after the calculation with the signal delay, satellite accurate position and user position.

The formula is shown :

$$T_{u\_pcr} = t_{s\_pcr} + (t_{r\_pcr} - t_{s\_pcr})/2 + \rho/c + \tau_{ion} + \tau_{tro} + \tau_{oth} \quad \text{.....(1)}$$

Which:

T_{u_pcr} user time;

t_{s_pcr} time of transacting PCR in transaction end;

t_{r_pcr} time of receiving PCR in transaction end;

ρ distance of satellite to user;

τ_{ion}, τ_{tro} delays of ionosphere and troposphere effects;

At the end of 2011, the result of tests in five cities in China (Nanjing, Xi 'an, Urumqi, Changchun, Haikou) proves synchronization accuracy < 100 ns (1σ).

IFCS-EFTF5-PCD5-9

A simple computation technique for improving the short term stability and the robustness of GPS TAIP3 Common-Views

G. D. Rovera, B. Chupin, M. Abgrall and P. Uhrich

LNE-SYRTE, CNRS, UPMC, Observatoire de Paris, 61 avenue de l'Observatoire, 75014 Paris, France

Email: Daniele.Rovera@obspm.fr

The Observatoire de Paris (LNE-SYRTE) is the institute designated by the French National Metrology Institute (NMI) Laboratoire National de Métrologie et d'Essais (LNE) in the field of Time and Frequency Metrology. In this frame, the laboratory has a long history in developing remote clock comparisons by using the well-known Common-View (CV) technique on signals from the Global Positioning System (GPS)[1]. In order to improve the short term stability of GPS CV by using data in the CGGTTS TAIP3[2] format, we propose here a new averaging technique.

From CGGTTS GPS TAIP3 CV daily files between two remote stations, we compute a linear fit, and we average out all 3 sigma outliers in an iterative process without any limitation. This allows to suppress either "bad" CV due to some problems in the reception of a given satellite signal, or CV exhibiting abnormal high noise, or any unusual outliers. A mean value between the remaining CV is then computed for each common CGGTTS epoch, leading to the time transfer results for the remote time scales.

We have applied this new technique on two typical links: a short baseline between OP and PTB (Braunschweig, Germany), and a long baseline between OP and USNO (Washington, USA). As expected, the short term noise over a short baseline is only marginally improved compared to the results from the former processing[1], but the average number of remaining CV between remote stations after filtering of the outliers is twice as large for a given epoch, increasing that way the time transfer robustness. Over a long baseline, as can be seen on Fig. 1, we obtain a short term noise in terms of Allan Time Deviation (TDEV) twice smaller for averaging periods from about 10 000 s to 1 d, the TDEV reaching about 300 ps at 1 d, together with an average increase of 20 % on the remaining CV after filtering of the outliers.

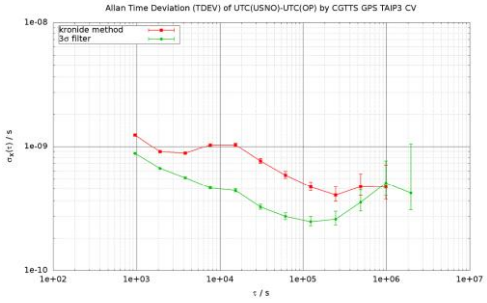

Fig. 146: TDEV comparison of CGGTTS GPS TAIP3 CV between UTC(USNO) and UTC(OP) over 100 d when applying either the Kronide software developed years ago[1] or the new 3 sigma filtering technique over daily files.

Hence in all cases, this new simple technique improves the short term noise of time transfer and increases robustness simultaneously, the improvement depending on the baseline. This technique might also be useful for any upcoming new GNSS time transfer based on code data.

---

[1] J. Achkar, P. Uhrich, Ph. Merck and D. Valat, "Recent Time and Frequency Transfer Activities at the Observatoire de Paris", Proc. of the 2005 IEEE Frequency Control Symposium and Annual Precise Time and Time Interval Meeting, Vancouver, 2005.

[2] P. Defraigne and G. Petit, "Time transfer to TAI using geodetic receivers", *Metrologia* 40 (2003) 184-188.

IFCS-EFTF5-PCD5-10

Design and Implementation of Dual One-way Precise Ranging and Time Synchronization System

Hong-Jiao Ma[1, 2, 3], HuaBing Wu[1, 2, 3, 4], Meng Li[1, 2, 3, 4], ZaiMing He[1, 2, 3], JianFeng Wu[1, 2, 3], Kang Wang[1, 2, 3, 4]
[1]National Time Center, Chinese Academy of Sciences, Xi'an, Shaanxi, China
[2]Key Laboratory of Precise Navigation and Timing Technology, CAS, Xi'an, Shaanxi, China
[3]Key Laboratory of Time and Frequency Primary Standards, CAS, Xi'an, Shaanxi, China
[4]University of Chinese Academy of Sciences, Beijing, China
Email: mahj@ntsc.ac.cn

Abstract: With the development of science technique in aeronautic and astronautic testing navigation, communication, as well as electric power, etc, time synchronization has been needed in more and more engineers and sciences fields. Dual one-way ranging can get more veracity of measure precision than one-way due to eliminating the common measure error between two points. This article describes the use of dual one-way pseudo-code and carrier phase precise measurement for realizing time synchronization technique. The results from experiment show that ranging and time synchronization resolution of system reach 0.15cm and 5ps in 1s time interval, its precision reach 3.46ns or 9.43ps using different or same frequency reference of the order of e-11/d respectively. Dual one-way ranging and time synchronization can be applied in aeronautic and astronautic measurement and control system, and in achieving high precision time platform in message transfer field. It also can provide time service between satellite and satellite, satellite and ground station, aircrafts, stations and other patterns.

Key words: Precise Ranging; Time Synchronization; Dual One-way Ranging Measurement.

IFCS-EFTF5-PCD5-11

Analysis on GNSS space clocks performances

A.Cernigliaro[3], S. Valloreia[1], L. Galleani[1], P. Tavella[2]

[1]Politecnico di Torino, Torino, Italy
[2]INRIM, Torino, Italy
[3]Aizoon, Torino, Italy

Email: a.cernigliaro@inrim.it

In Global Navigation Satellite Systems (GNSS) the role of atomic clocks is essential for the determination of the user position. Nowadays, several satellite navigation systems are operating and different clock technologies have been employed on board satellites, taking benefit of the improvements reached during the last decades. The analysis of GNSS clock performance is thus crucial for ensuring the GNSS positioning and timing capabilities.

We performed an analysis on the clock estimates generated by the Information-Analytical Centre [437](IAC) of the Russian Federal Space Agency, which provides a service similar to the one of the International GNSS Service (IGS). Therefore, we collected and processed the RINEX for clock files containing satellite clock estimates for GPS and GLONASS constellations, from 2010 to 2012: with our statistical tools[438] we made a comparative analysis on the performances of the different clock technologies employed on board (RAFS, Cesium clocks), and of the different navigation systems. In particular, we focused the attention on the clock frequency behaviour and the frequency stability, evaluating also the stationarity of these characteristics. Besides, an assessment of experimental on board clock data with respect to the theoretical deterministic and stochastic behaviour of the atomic clock, as obtained from clock specifications, is reported.

Our results show that some aspects are common to the different clock types and navigation systems, while some differences can be observed in the different families.

[437] http://www.glonass-ianc.rsa.ru/en/

[438] A.Cernigliaro, I.Sesia, "Satellite Clocks Characterization and Monitoring for Global Navigation Satellite Systems", in Proc of the XXX URSI General Assembly and Scientific Symposium of International Union of Radio Science, August 13th-20th 2011, Istanbul, Turkey

IFCS-EFTF5-PCD5-12

A Method of GNSS System Time Offset Monitoring

Huijun Zhang[1,2], Lin Zhu[1,2,3], Xue Zhang[1,2,3], Xiaohui Li[1,2]

[1]National Time Service Center, Chinese Academy of Sciences, Xi'an, China
[2]Key Laboratory of Precision Navigation and Timing Technology, National Time Service Center, Chinese Academy of Sciences, Xi'an, China
[3]University of Chinese Academy of Sciences, Beijing, China

Email: zhj@ntsc.ac.cn

With the progress of Global Navigation Satellite System(GNSS),which mainly include GPS,GLONASS,GALILEO as well as BeiDou, multi-system joint working mode has become research focus and application trend. But, Each satellite navigation system has its own independent system time, such as GPST,GLONASST,GST and BDT. The System time offset between the two satellite navigation systems is one of the most important aspects of their interoperability. It will cause combined navigation position solution bias. Therefore, it is necessary and significant to monitor and research system time offset.

A method of GNSS System Time Offset monitoring which is called signal- in-space receiving method is put forward and its principle is described. In this method, UTC(NTSC) time scale is regarded as reference time scale on account of its status of standard time and frequency resources. Then, The time offset between each satellite navigation system time and UTC(NTSC) which include UTC(NTSC)-GPST,UTC(NTSC)-GLONASST,UTC(NTSC)-BDT,UTC(NTSC)-GST can be acquired. Thus, system time offset among satellite navigation systems, such as GPST-GLONASST, can be acquired with the 5ns (1 σ) precision.

On the basis of above described method, GNSS System time offset monitoring system has been set up since 2011 and it is gradually improved and perfected. A great deal of monitoring data has been collected. Addition to common error sources, some special error sources related to GNSS timing receiver such as receiver delay, inter-system hard delay bias, inter-frequency biases and so on are analyzed, as they can effectively affect monitoring results and precision. The monitoring data and IGS precision orbit and clock bias data as well as corresponding data published by BIPM Circular T Bulletin are combined together to determine above error values. The results of the error items and GNSS system time offset monitoring results are to be showed.

IFCS-EFTF5-PCD5-13

Implementation of the Real-Time Multi-Channel ADEV, TDEV, and HDEV Computation Methods

Michal Kasznia

Poznan University of Technology, Poznan, Poland

Email: mkasznia@et.put.poznan.pl

Proper quality of timing (synchronization) signals in the telecommunication network is a necessary condition of the effective data transmission throughout the network. In order to examine this quality several parameters are computed using the sequences of time error samples measured at some network interface. Allan deviation ADEV and time deviation TDEV allow the variations of time interval provided by the synchronization signal to be assessed and the type of phase noise affecting the signal to be recognized. Hadamard deviation HDEV is insensitive for the presence of frequency drift and can be used for recognition of higher types of phase noises. The application of real-time computation of these parameters performed during time error measurement process allows to simplify the evaluation procedure.

One may occur, that more than one timing signal has to be analyzed in the same time. Such situation can be considered in the node of the telecommunication network, where the signals arrive from several directions, or when we want to perform the three cornered hat procedure. A multi-channel time error meter with computation algorithms applied could be suitable for this analysis.

The computation methods enabling assessment of the parameters in the real time were proposed and tested[439,440]. The experimental tests have proved the ability of the computation of these parameters in the real time for a single data series as well as for multi-channel time error measurement.

In the paper the results of the implementation of the algorithms enabling real-time ADEV, TDEV, and HDEV assessment during multi-channel time error measurement are presented. To test these methods in a real measurement process, a special measuring system SP-4000 was used[441]. This system, designed and developed in the laboratories of Poznan University of Technology, enables multi-channel time error measurement. Several conditions were considered during the implementation: number of measurement channels, values and ranges of observation intervals considered, data structures and its organization. Some hardware and software solutions enabling to join the time error measurement and parameters' computation in one effective process are discussed and suggested.

[439] A. Dobrogowski, M. Kasznia, "Joint real-time computation of Allan deviation, time deviation, and Hadamard deviation", Proc. of 24th European Frequency and Time Forum, 13-16 April 2000, Noordwijk, Netherlands.

[440] M. Kasznia, "Multi-channel real-time computation of ADEV and TDEV", Proc. of 24th European Frequency and Time Forum, 13-16 April 2000, Noordwijk, Netherlands.

[441] A. Dobrogowski, M. Kasznia, M. Jessa, K. Lange, M. Jaworski, „Hardware and software realization of time terror measurements with real-time assessment of ADEV, TDEV, and MTIE", Proc. of 24th European Frequency and Time Forum, 13-16 April 2000, Noordwijk, Netherlands.

IFCS-EFTF5-PCD5-14

Experimental Tests of the Real-Time MTIE Assessment Methods for Multi-Channel Time Error Measurement

Andrzej Dobrogowski, Michal Kasznia

Poznan University of Technology, Poznan, Poland

Email: mkasznia@et.put.poznan.pl

Maximum Time Interval Error (MTIE) is one of the parameters describing the quality of the telecommunication network timing signals. MTIE identifies maximal phase differences within considered observation intervals and therefore it is well suited for dimensioning of buffers (elastic stores) at the boundaries of the time scales. This parameter can be computed off-line, following the time error measurement process as well as in the real time, during the time error measurement[442,443].

The maintenance of the telecommunication network often requires the analysis of several timing signals in the telecommunication network node performed in the same time. A multi-channel time error meter with computation algorithms applied could be suitable for this analysis.

Authors of this paper have proposed and described[444] two methods enabling MTIE assessment performed in the real time for multi-channel time error measurement. First solution is based on the time effective MTIE computation method with binary decomposition[445]. This method offers regularly and data-independent running data reduction which can be effectively applied for the real-time multi-channel computation. Second solution exploits the time effective extreme fix (EF) method successfully applied earlier for single-channel real-time MTIE assessment[2]. According to this method, the computation for some observation intervals may be suspended in order to reduce the number of operations carried out within the duration of one sampling interval. The analysis of suspended intervals is performed when the measurement is finished.

In order to compute the MTIE estimate simultaneously for several observation intervals and several data series (obtained from the measurement channels) in the real time, all necessary operations have to be done in the time interval between two successive time error samples, i.e. during the sampling interval τ_0. The ability of real-time assessment depends on the several conditions: number and length of the observation intervals considered, number of measurement channels, data structures and organization, computation ability of the equipment, and time error data behavior.

In the paper the results of experimental tests of these methods are presented. The calculations were performed for several data sequences representing different behavior of time error taken with sampling interval τ_0=1/30 s, which is often used in the telecommunication applications. The results of calculation for different conditions using both methods are presented and discussed.

---

[442] A. Dobrogowski, M. Kasznia, "On-line computation of MTIE using binary decomposition and direct search with sequential data reducing," Proc. of the 2007 IEEE IFCS and EFTF, pp. 877-882, 29 May – 01 June 2007, Geneva.

[443] A. Dobrogowski, M. Kasznia, "Implementation of Real-Time MTIE Assessment Method", Proc. of 2011 Joint Conference of the IEEE FCS and EFTF, pp. 304-309, May 2-5, 2011, San Francisco, California, USA

[444] A. Dobrogowski, M. Kasznia, "Some Concepts of the Real-Time MTIE Assessment for Multi-Channel Time Error Measurement," Proc. of 2012 IEEE IFCS, pp. 493-498, May 22-24, 2012, Baltimore, USA,

[445] S. Bregni, S. Maccabruni, "Fast computation of Maximum Time Interval Error by binary decomposition," IEEE Trans. Instrum. Meas., vol. 49, No. 6, pp. 1240-1244, Dec. 2000.

IFCS-EFTF5-PCD5-15

Application of three-cornered-hat method for estimation uncertainties type u_A and u_B of time measurement instruments

S.Bolginova, N.Koshelyaevsky, S.Pesterev, N.Pol'nikov, E.Popkova

The Main Metrology Center of the State Time and Frequency Service
FGUP "VNIIFTRI," Mendeleevo, Moscow region, Russia
email: nkoshelyaevsky@vniiftri.ru

The accurate estimations uncertainties type u_A and u_B in time measurement instruments is very important because of at next step these transform in performances of time and frequency standards.

The usual methods [1, 2, 3] based on feeding device under test by frequency/time signals from the same source as a matter of fact produce very rough approximation, and typically overestimated, to actual values of uncertainties type u_A and u_B.

On other hand quite often laboratories posses several T&F measuring instruments of the same type with similar performances, but do not have more perfect and accurate instruments to calibrate these ones.

The three-cornered-hat method does require neither high accurate reference instrument, nor a priori knowledge of time/frequency relations of signals used in measurements.

The paper will deliver several examples of estimations uncertainties type u_A and u_B for different types of phase comparators and time interval meters. For the best instruments obtained uncertainties type u_A and u_B are in conformity with claimed performances.

References

4. Time interval meter I4-10, Manuals, E32.817.040, chapter 15.5.8 and 15.5.9
5. Unit of phase comparators, Manual, E32.721.701, chapter 15.5.6
6. Multichannel phase comparators, Manual, ЯКУР 411146.018, chapter 5.8.3.1

IFCS-EFTF5-PCD5-16

A Novel Timing-Delay Measuring Method Based On PN Code in Telephone Time Service

Dong Dao-peng[1,2] , Zeng Ting[1,2] , Xiang Yu[1,2] , Huang Chang-Jiang[1,2]

(1. National Time Service Center, Chinese Academy of Sciences, xi'an 710600 China;

2. Graduate University of Chinese Academy of Sciences, Beijing 100039 China)

The key problem of telephone time service by PSTN is how to synchronize user time with standard time, in other words, measuring time delay of transmission is the important problem. Now, there are two methods of measuring time delay, the first way is by transmitting character signal; the second way is through phase-detecting. The precision of measuring time delay will have a directly influence on system synchronization time precision, also, The traditional analog modulation/demodulation will highly effect the precision, but the phase error is inevitably because of the effect caused by the noise and channel characteristic when using phase-detecting.

The new method, using correlation of PN code will be presented in this paper. The delay time can be got by detecting the peak of the correlate function. The server will transmit PN code to the user, the user end will generate the local code with some time difference, which is same as transmit code .Then compared local code with received PN code bit by bit, the correlation value will be got. It can be seen second signal have synchronized when the correlation value reach to the maximum, which only include one transmit delay Δt. At this time the user will send generated PN code to the server again, operated correlatively with PN code generated by server, the time difference between server and user can be confirmed through measuring the position of correlative peak. Suppose the delay of transmit and receive is consistent, the gotten time difference divided by two is transmission delay.

The correlation of PN code is depended on the type and length of code. It was analyzed that the correlation of PN code and local code will close to 1/p of maximum output when received PN code and native code is a gap of one code element, and the output is maximal when time discrepancy is equal to zero. Moreover, the correlation value will change according to the time discrepancy when time discrepancy is in a positive code or a negative code. Also in a sequence period, the correlation value varies evidently in a code, but no change in other time.

The synchronization of PN code is divided into coarse synchronizing and accurate synchronizing, which means the capture and track of PN code. It is the capture of PN code that make local pseudocode synchronize with received code, which can attain the precision of 1/2 width in one code. However, according to the need of measuring time delay, the received signal must be farther tracked so as to improve the precision. The track of PN code can control the synchronized precision to more small code period range, so the precise time delay will be gotten.

Measuring time delay based on PN code in telephone time service has many advantages, high accuracy of detection; good resist noise interference capability; simple to implement. It can solve many disadvantages on existing measure transmission delay effectively, and enhance precision of time synchronization.

IFCS-EFTF5-PCD5-17

VLBI receiver chain monitoring

Vojtěch Michálek[1], Jan Kodet[2], Ulrich Schreiber[2], Christian Plötz[3], Ivan Procházka[1], Petr Pánek[4]

[1]Czech Technical University in Prague, Břehová 7, 115 19 Prague 1, Czech Republic
[2]Technische Universität München, Wettzell Observatory, 93444 Bad Koetzting, Germany
[3]Bundesamt für Kartographie und Geodäsie, Geodätisches Observatorium Wettzell, Germany
[4]Institute of Photonics and Electronics, Chaberská 57, 182 51, Prague, Czech Republic

Email: kodet@fs.wettzell.de

The most demanding goal of the Global Geodetic Observing System initiative is the definition of station positions to an accuracy of 1 mm and the corresponding velocities to 0.1 mm/year. The main remaining sources of error are caused by systematics, leading to intra- and inter- technique biases. In this work, we have focused on Very Long Base Interferometry (VLBI) and phase calibration generator currently in operation. This unit is injecting calibration tones into the detection chain through an input coupler located near the input of the antenna. The tones propagate further through entire detection chain and are recorded with the observed signal. Then they are extracted in post processing. These tones are generated out of an atomic frequency standard. The supplied frequency is significantly influenced by temperature and mechanical changes since usually a long cable is employed to bring the frequency to the calibration unit. To monitor the electrical length of the cable, calibration with a picosecond precision is essential.
We have redesigned a phase calibration unit so that it enables the implementation of the Two Way Time Transfer (TWTT) method on single coaxial cable using two event timers to monitor the electrical length of the critical cable. Such a system has been installed in parallel to the unit currently in operation. Preliminary experiments suggest, that such a technique can be used for monitoring of the electrical cable length with precision of one picosecond of rms. The comparison of the TWTT method with previous measurement method is presented.

IFCS-EFTF5-PCD5-18

An Algorithm with Periodic Item for Steering UTC(NTSC) to UTC

REN Ye[1,2] , LI Xiao-hui[1,2],XUE Yan-rong[1,2,3] ,LI Yu-wei[1,2]

[1]National Time Service Centre, Chinese academy of Sciences, Xi'an, China

[2]Key Laboratory of Precision Navigation and Timing , National Time Service Centre, Chinese academy of Sciences, Xi'an,China

[3]Graduate University of Chinese Academy of Sciences, Beijing, China

Email: renye@ntsc.ac.cn,

In order to steer master clock in timekeeping laboratory, it is necessary to identify a suitable algorithm for steering UTC(NTSC) to UTC for a period of 45 days. By representing residual term as a series of periodic item in a quadratic polynomial model, a modified model is established and it is used to predict UTC-UTC(NTSC) time offest. In this case, two considerations, rank of periodic item and data size, are considered. Moreover, two kinds of spectrum analysis, peiodogram and correlogram, is discussed to identify a proper rank of periodic item and a . The analysis illustrate that the modified model based on correlogram with 12 months data shows plausible results in terms of both stability and accuracy.

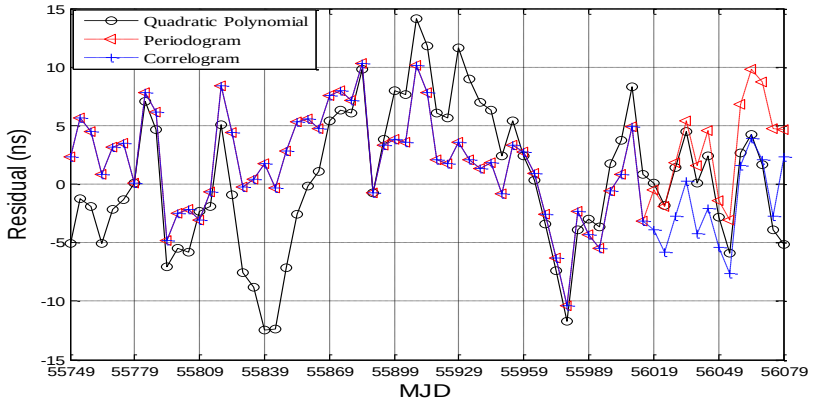

Fig. 147: The predicted residual based on three fitting steering algorithm (quadratic polynomial model, modified model with pariodogram, modified model with correlogram) from July 2011 to June 2012

IFCS-EFTF5-PCD5-19

Progress in the link calibration for UTC time transfer

Z Jiang[1], G Petit[1], L Tisserant[1], P Uhrich[2], G D Rovera[2] and S Y Lin[3]

1 Time Department, Bureau International des Poids et Mesures (BIPM), Pavillon de Breteuil F-92312, SÈVRES CEDEX, France
2 Laboratoire National de Métrologie et d'Essais-Systèmes de Référence Temps-Espace (LNE-SYRTE), CNRS, UPMC, Observatoire de Paris, France
3 National Standard Time and Frequency Laboratory, Telcommunication Laboratories (TL), Chunghwa Telecom

zjiang@bipm.org

The dominant part of the total uncertainty budget in the [UTC-UTC(*k*)] is from the time transfer calibration. In 2011, the International Bureau of Weights and Measures (BIPM) launched a pilot experiment aiming at improving the calibrations using the link calibration method, in particular for the Asia-Europe very long baselines. The goal is to reach the expected type B uncertainty to be less than 2 ns. In this frame, the BIPM developed a standard calibration scheme in which an integrated and pre-cabled portable calibration station is used. It is composed of a 10 MHz distributor, a PPS distributor and two GNSS geodetic setups each include a set of independent receiver, antenna and cables. Other receivers are stationary at the BIPM for start and closure checks. Using this system, we performed some tests on zero and short baselines at the BIPM between the present time laboratory and the new one, and between the BIPM and the LNE-SYRTE in Observatoire de Paris. Another experiment using the same scheme is carried out by TL (National Standard Time and Frequency Lab. Telecommunication Laboratories). In this paper, we present the results of these studies. We analyze the uncertainties of this link calibration and compare them to the traditional differential receiver calibration methods.

Key Words: UTC, Time transfer, Calibration

IFCS-EFTF5-PCD5-20

Research on precision measurement of phase difference between different frequency signals

Miao Miao[1], Wei Zhou[1], Xueping Zhang[1], Zhiqi Li[1], Changsheng Liu[1]

[1] Department of Measurement and Instrument, Xidian University, Xi'an, P.R. China

Email: mmiao@mail.xidian.edu.cn

Traditional phase comparison must be carried out between the two frequency sources with the same values. However, recent researches have found that phase comparison also can be implemented between frequency sources with different values and obtain higher resolution.

The paper analyzes the phase difference regularity of arbitrary period signals' comparison. Discuss in detail that fine quantized phase step phenomenon and how the step value to reflect the higher resolution. When two signals with different frequencies are compared, their phase differences are in special order according to the frequency ratio, and, because of small frequency deviation existing, corresponding phase differences in every least common multiple period are different. As for the equivalent phase-discrimination frequency, $\frac{1}{ABf_{maxc}}$ *, has very high resolution, under the condition of proper reference frequency, the technology in the paper can reach higher measuring resolution. As for the development of present base standard sources and the research on fine quantified phase step phenomenon between period signals, the signal comparison in RF band could reach ps resolution and even fs. Because the hardware used in detecting coincidence information will bring some trigger error and compared signals' own noise will bring some phase uncertainty, the software in connection with algorithm can be used in the technology. On account of instruments' own drift, pulse average method and pulse filling method can be used, and moreover, self-calibration.

*: When the frequency values of compared signals are respectively f_1 and f_2 and their greatest common factor frequency is f_{maxc}, $f_1=Af_{maxc}$, $f_2=Bf_{maxc}$.

IFCS-EFTF5-PCD5-21

NTP Accuracy in Practice

Demetrios Matsakis[1]

[1]United States Naval Observatory, Washington, DC, USA

Email: dnm@usno.navy.mil

Over three years of Network Timing Protocol (NTP) timing data will be presented and analyzed for accuracy. Data are presented from UNIX, LINUX, and MAC clients, and from the USNO facilities in Washington DC, the Alternate Master Clock (AMC) in Colorado Springs, Colorado, as well as two private locations in the DC area. These clients are used to extract time from servers maintained by USNO, NIST, and other timing centers in the USA, Europe, and Asia under the assumption that the servers are synchronized to the accuracy far better than observable via NTP.

IFCS-EFTF5-PCD5-22

Time and frequency distribution improving in Calern/Geoazur laboratory for T2L2 campaign

Myrtille Laas-Bourez[1], Daniele Rovera[2], Michel Abgrall[2], Etienne Samain[1], Jean-Louis Oneto[1,] Philippe Guillemot[3]

[1]Géoazur, Université de Nice Sophia-Antipolis, Observatoire de la Côte d'Azur, Centre National de la Recherche Scientifique (UMR 7329), 250 av. Einstein 06560 Valbonne, France

[2]LNE-SYRTE, Observatoire de Paris, UPMC, UMR CNRS 8630, 61 av. de l'Observatoire, 75014 Paris, France

[3]CNES, French Space Agency, Toulouse, France

Email: Myrtille.Laas-Bourez@oca.eu

The Time Transfer by Laser Link (T2L2)[446] experiment aim to synchronise remote ultra stable clocks over large-scaled distances using two laser ranging stations. T2L2 ultimate time transfer capability can only be demonstrate with a picosecond range ground mastering. We focus this year in knowledge and equipment improvement to perform a T2L2 time transfer with accuracy and stability of a few picoseconds.

A deep analysis of signals stability has been carried out this year in the time and frequency laboratory in *Plateau de Calern*. The aim was to better understand the limits and hardware configuration and to enhance time and frequency distribution for T2L2 experiment. We showed phase noise and stability problem on our H-maser distribution. Final measures were conducted in October in collaboration with SYRTE. Then a complete equipment reorganisation was done.

This paper focus on the time and frequency laboratory characterization before and after the reorganisation. We introduce our new equipments and present our new H-maser time scale and discuss the performances obtained.

[446] E. Samain, "T2L2: ground to ground Time Transfer", EFTF 2012, Goteborg, Sweden, 23-37 may 2012.

IFCS-EFTF5-PCD5-23

Synchronization of Ultrafast Lasers

Huan Zhao, Jun Ge, Nuan-rang Wang

Science and Technology on Metrology and Calibration Laboratory, Beijing Institute of Radio Metrology & Measurement, Beijing 100854, China

Email: huanzhao@sina.com

Timing synchronization between femtosecond lasers is indispensable in various scientific researches. This Letter reports our work on highly precise active synchronization between two independent femtosecond Ti:sapphire lasers based on a combination scheme of three phase locked loops(PLLs). The lasers are firstly synchronized by two PLLs at relative large timing-jitter, then the sum frequency generation(SFG) signal of the two lasers is fed back to the above PLLs, which acts as the third PLL and improves the precision of the synchronization significantly.

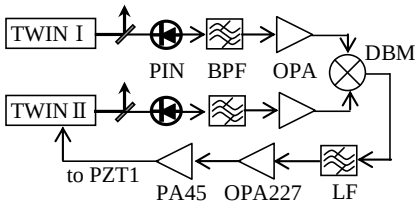

Fig.1 master

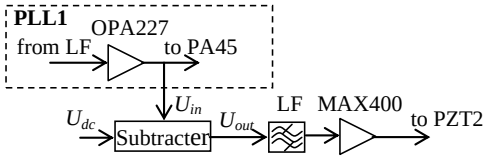

Fig.2 slave PLL(PLL2)

In the experiment, we made two self-mode-locked Ti:sapphire lasers named as TWIN Ⅰ and TWIN Ⅱ with similar scheme[xxiii]. There are two piezoelectric actuators(PZT) with different maximum displacement and response velocity, either of which is attached with a cavity mirror inside the laser separately. Since the repetition rate depends on the cavity length of the laser, the PLL can compensate the relative variation of the cavity length and then synchronize the two trains of femtosecond laser pulses precisely by controlling the displacement of the PZT. The master PLL(PLL1, shown in fig.1) works for primary synchronization and the slave PLL(PLL2, shown in fig.2) maintains long-term stability, the PLL2 can work together with PLL1 by controlling the loop gain. Once these two PLLs activate normally, TWIN Ⅰ and TWIN Ⅱ could output synchronized laser pulses trains stably. However, the timing jitter is about hundreds of femtoseconds, which is obviously too large compared to the 100fs laser pulse width, thus we should improve the precision of synchronization further for the practical application.

When TWIN Ⅰ and TWIN Ⅱ are synchronized by the two PLLs mentioned above, we focus two laser beams into a nonlinear crystal to generate sum frequency laser. The SFG Laser signal intensity is very sensitive to the temporal position of the laser pulses, much more sensitive than the output of DBM in PLL1. If feeding this SFG signal back to the above PLLs, which acts as an optical PLL(PLL3, shown in fig.3), it could improve the precision of active synchronization significantly. Once PLL3 activates normally together with PLL1 and PLL2, the timing jitter of TWIN Ⅰ and TWIN Ⅱ could reduce to tens of femtoseconds. We have measured the precision of synchronization with correlation method[xxiv], and the calculated rms timing jitter is about 30fs within 10s measurement time, which means the precision of the synchronization is improved significantly up one order of magnitude.

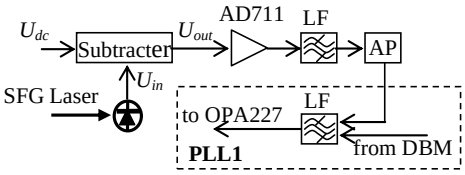

Fig.3 optical

IFCS-EFTF5-PCD5-24

Multipoint dissemination of RF frequency in delay-stabilized fiber optic link in a side-branch configuration

Śliwczyński Ł, Krehlik P, Buczek Ł, Lipiński M

Department of Electrical Engineering, AGH University of Science and Technology, Kraków, Poland

Email: krehlik@agh.edu.pl

Recently our group proposed a method of tapping an RF frequency signal[447] from a fiber optic dissemination link with the stabilization of the propagation delay[448]. In its basic configuration this gives an access to just the points located along the trunk fiber that connects the Local and the Remote Modules. We tested this approach at our lab obtaining the residual instability of the frequency transfer at both the main and tapped outputs around 2×10^{-17} at 10^5 s averaging.

The idea of tapping the frequency signal from the delay-stabilized link is flexible and may be further expanded into a tree-like structure including so-called side-branches, allowing disseminating the frequency signal to the points that do not lie on the route of the trunk fiber. The side-branch fiber may be tapped as well and even equipped with subsequent side-branches. The network built with such a technology may cover large areas, giving the access to the same, high quality clock to many distributed users.

In this paper we present for the first time the experimental data concerning the stability of the frequency

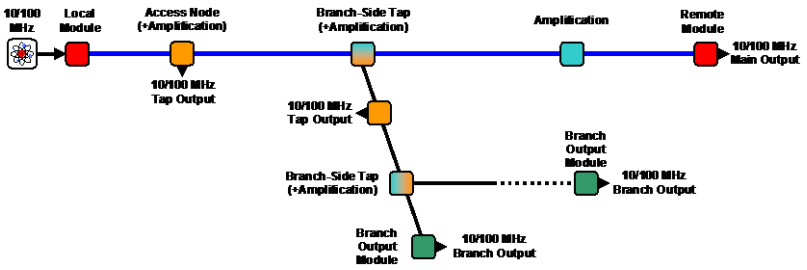

Fig. 148: An example of the delay-stabilized fiber optic network for multipoint frequency dissemination exploiting simple taps as well as side-branches. In entire network the propagation delay from the input to each output is stabilized.

signal at the output of the branch, measured on both a field-deployed and spooled fibers. The measurements are performed having all the Local, Remote and Branch Output Modules at the same laboratory, because this is the only way to examine the stability of the dissemination without using any additional transfer system that will incur the obtained results. We are also discussing the problem of degradation of the signal at the Branch Output depending on the length of the side-branch and location of the Branch-Side Tap.

Acknowledgment

This work was supported by Polish National Science Centre under the decision DEC-2011/03/B/ST7/01833.

[447] P. Krehlik, Ł. Śliwczyński, Ł. Buczek, M. Lipiński, "Multipoint dissemination of RF frequency in fiber optic link with stabilized propagation delay", paper submitted to IEEE Trans. UFFC, 2013

[448] Ł. Śliwczyński, P. Krehlik, Ł. Buczek, M. Lipiński, "Active propagation delay stabilization for fiber optic frequency distribution using controlled electronic delay lines", IEEE Trans. Instr. Meas., vol. 60, pp. 1480-1488, 2011

IFCS-EFTF5-PCD5-25

Evaluation of the AGH-designed Time and Frequency transfer system on a 149 km PTB-Hannover-PTB fiber link

P. Krehlik[1], G. Grosche[2], S. Raupach[2], D. Piester[2], H. Schnatz[2], Ł. Śliwczyński[1]

[1] AGH University of Science and Technology, Mickiewicza 30, 30-057 Krakow, Poland
[2] Physikalisch-Technische Bundesanstalt, Bundesallee 100, 38116 Braunschweig, Germany

Email: sliwczyn@agh.edu.pl

We describe experiments with the AGH-designed fiber optic system for time and frequency dissemination, based on active stabilization of the fiber delay[449,450]. The measurements were performed at the Physikalisch-Technische Bundesanstalt (PTB), Braunschweig, over a field-deployed optical fiber loop going from PTB to the Magnesium clock laboratory in the Leibniz Universität Hannover (LUH)[451] and back (149 km, 45 dB attenuation). Both the transmitting and receiving modules of the system were located in the same laboratory, allowing accurate measurements of the system performance.

We detected strong optical reflections (> -20 dB) within the last-mile fiber hops at LUH, at both sides of our bi-directional optical amplifier installed at LUH. The multiple reflections in the vicinity of the amplifier caused severe degradation of the intensity-modulated optical signals, or even lasing of the amplifier, making accurate time dissemination impossible. However, inserting a wavelength selective optical isolation module at one side of the amplifier proved to be very effective, breaking the resonant structure and eliminating signal distortions. Thus, for the first time, we undertook measurements in the presence of strong reflections in the optical path.

To assess the fiber link stabilization, we simultaneously used different measurement methods. We measured the instability of a10 MHz frequency signal with a dual mixer and harmonic tracker system developed at PTB. Simultaneously, we measured 100 PPS time signals with either a standard time interval counter, or a high-speed digital oscilloscope controlled by dedicated software. The modified Allan deviation (MADEV) for 10 MHz frequency signal was approaching 10^{-17} at one-day averaging and the time deviation (TDEV) of 100 PPS remained below 1 ps over the measurement duration. The outstanding results obtained for the time transfer are partly due to using 100 PPS instead of 1 PPS, thus averaging short-term noise of both the measurement setup and the transmission system.

We also performed a check of absolute calibration of the time transfer, and found only 18 ps difference between 100 PPS input-to-output delay measured directly, and obtained from a calibration procedure, which uses only the data available at the transmitting side of the system[1].

Acknowledgement:
This work was supported by the European Metrological Research Programme EMRP under SIB-02 NEAT-FT. The EMRP is jointly funded by the EMRP participating countries within EURAMET and the European Union. We thank Steffen Rühmann from LUH for his invaluable technical help.

[449] P. Krehlik, Ł. Śliwczyński, Ł. Buczek and M. Lipiński, "Fiber optic joint time and frequency transfer with active stabilization of the propagation delay", IEEE Trans. Instrum. Meas. **61**, 2844–2851, 2012.

[450] Ł Śliwczyński, P. Krehlik, A. Czubla, Ł. Buczek and M. Lipiński, "Dissemination of time and RF frequency via a stabilized fibre optic link over a distance of 420 km", Metrologia **50**, 133-145, 2013.

[451] A. Pape, O. Terra, J. Friebe, M. Riedmann, T. Wübbena, E. M. Rasel, K. Predehl, T. Legero, B. Lipphardt, H. Schnatz, and G. Grosche, "Long-distance remote comparison of ultrastable optical frequencies with 10^{-15} instability in fractions of a second", Optics Express **20**, 21477-21483, 2010

IFCS-EFTF5-PCD5-26

Bi-directional optical amplifiers for long-distance fibre links

Sebastian M. F. Raupach[1], Andreas Koczwara[1], Gesine Grosche[1], Fabio Stefani[2], Olivier Lopez[2], Anne Amy-Klein[2], Christian Chardonnet[2], Paul-Eric Pottie[3], and Giorgio Santarelli[3,4]

[1]Physikalisch-Technische Bundesanstalt (PTB), Bundesallee 100, 38116 Braunschweig, Germany

[2]LPL, Université Paris 13, Sorbonne Paris Cité, CNRS, Villetaneuse, France

[3]LNE-SYRTE, Observatoire de Paris, CNRS, UPMC, Paris, France

[4]LP2N, Université de Bordeaux 1, Institut d'Optique and CNRS, Talence, France

Email: sebastian.raupach@ptb.de,

Within the European Metrology Research Programme (EMRP), project "NEAT-FT" aims at developing instrumentation for ultra-stable long-distance frequency transfer via optical fibre networks, such as special amplifiers adapted to bi-directional optical frequency transfer[452,453].

Two approaches are followed, one based on Erbium-Doped Fibre Amplifiers (EDFA), the second on Fibre Brillouin Amplifiers (FBA). Both systems are intended for deployment along a fibre link that will connect PTB/Germany and SYRTE/France.

EDFA are widely used amplifiers for telecommunication. Due to their sensitivity to backscattering and back reflections, EDFA are commonly equipped with optical isolators making them uni-directional devices. Here we report on fully bi-directional EDFA with a maximum gain of 20 dB and improved optical filtering to limit ASE and conditions of self-oscillations. Additionally, remote control was implemented for these special amplifiers, so that the maximum gain below oscillation can be used in a large-scale network

Fibre Brillouin amplifiers are of particular interest for very long distance fibre links. These distributed amplifiers are based on Brillouin scattering, i.e. the coherent build-up of a phonon wave, that by scattering light from an optical pump coherently amplifies an incoming optical signal. Such fibre Brillouin amplifiers feature narrow gain bandwidths of ~10 MHz [454]. This allows for an efficient distinction between the two directions of the signal in a bi-directional fibre link, which typically are coded by frequency shifts of several tens of Megahertz. Compared to bi-directional EDFAs, such narrow-band amplifiers can operate at a much higher gain. For fibre Brillouin amplifiers located in a laboratory, a small-signal gain in excess of 50 dB has been demonstrated[455]. As this allows for larger distances between the amplifiers, the deployment of fibre Brillouin amplifiers is expected to substantially decrease the complexity of long-distance fibre links. We now report on progress in developing autonomous fibre Brillouin tracking amplifiers (FBTA). In a first field test, a FBTA module was placed in a remote container located at a distance of around 160 km (length of fibre) from the signal source. We achieved automated locking of the FBTA to an incoming signal of less than 100 nW, and observed an amplification of around 40 dB.

This work was supported by the European Metrology Research Programme EMRP under SIB-02 NEAT-FT. The EMRP is jointly funded by the EMRP participating countries within EURAMET and the European Union.

[452] O. Lopez *et al.*, Appl. Phys. B, DOI 10.1007/s00340-012-5241-0, 2012, and refs. therein

[453] K. Predehl *et al.*, Science, vol. 336, p. 441-444, 2012.

[454] F. Rohde, E. Benkler, and H. R. Telle, Opt. Lett., vol. 38, p. 103-105, 2013, and refs. therein

[455] O. Terra, G. Grosche, and H. Schnatz, Opt. Expr., vol. 18, p. 16102-16111, 2010.

IFCS-EFTF5-PCD5-27

Tracking DDS for Coherent Optical Links

C. E. Calosso[1], E. K. Bertacco[1], D. Calonico[1], C. Clivati[1,2], G. A. Costanzo[1,2], F. Levi[1], S. Micalizio[1], A. Mura[1]

[1]Optic Division, INRIM, Torino, Italy.
[2]Politecnico di Torino, Torino, Italy

Email: c.calosso@inrim.it

Frequency transfer via optical fiber is a mature technology that allows coherent frequency dissemination over hundreds of kilometers with a residual uncertainty in the 10^{-19} range[456,457]. The electronics involved is well established and is based on a frequency mixer as phase comparator, joined with a frequency divider to extend its phase input range and a tracking oscillator or a quartz filter to clean up the beat note of the local laser with the round trip one. In addition two frequencymeters or phasemeters are needed to measure the correction applied to the fiber and to monitor the link performance.

Here we propose an alternative digital solution that integrates the whole electronics: compensation and monitoring of the fiber link, comprehensive of phasemeters, into a single board based on three Direct Digital Synthesizers (DDS) driven by one Field Programmable Gate Array (FPGA).

Two DDSs are used to track the phase of the two beat notes (the one that measures the fiber delay and the one that monitors the link) while the third one is used to compensate for the fiber fluctuations by acting on a Acousto Optic Modulator (AOM). The FPGA drives the three DDSs, calculates the correction and interfaces a PC to set the working parameters and to monitor the internal signals, in particular the correction to the fiber and the link performance.

This system is compact, flexible and cost effective and, at the same time, it allows a complete characterization of the link.

At the conference we will present the electronics in details, comparing the present architecture with the one commonly used.
Furthermore, we will show the experimental tests performed in laboratory environment (up to 100 km dark fiber link) and on a real coherent optical link (47 km, DWDM architecture with coexisting data traffic).

---

[456]K. Predehl, G. Grosche, S. M. F. Raupach, S. Droste, O. Terra, J. Alnis, Th. Legero,T. W. Hansch, Th. Udem, R. Holzwarth, H. Schnatz, "A 920-Kilometer Optical Fiber Link for Frequency Metrology at the 19th decimal place," Science 336, 441-444 (2012).

[457] O. Lopez, A. Haboucha, F. Kefelian, H. Jiang, B. Chanteau, V. Roncin, C. Chardonnet, A. Amy-Klein, G. Santarelli,"Cascaded multiplexed optical link on a telecommunication network for frequency dissemination," Opt. Expr. 18, 16849-16857 (2010).

IFCS-EFTF5-PCD5-28

Simultaneous Transmission of Time and Frequency Signals over Optical Fibers

Yang Fei, Gui Youzhen, Cai Haiwen, Han Chunhao, Cai Zhiwu

Shanghai Key Laboratory of All Solid-State Laser and Applied Techniques,
Shanghai Institute of Optics and Fine Mechanics, Chinese Academy of Sciences, Shanghai, China

Email: yzgui@siom.ac.cn

In this report, we realized the simultaneous transmission of time and frequency signals over optical fibers based on wavelength division multiplexer (WDM) and two way optical compensation techniques. Firstly the fiber link was stabilized by frequency signal propagation errors. Once the fiber link is stabilized, any signal transfer in the link would be stabilized. Then the fluctuations of the frequency and time signal are compensated simultaneously. On the other hand, for being not affected by each other, the time and frequency signals would be modulated independently on different wavelength lasers, then access the stabilized fiber link making use of WDM.

We transfer the 1 pps time signal and the 100 MHz frequency signal over 80 km optical fiber spool in laboratory. And the spool is composed of 6 fiber spools with length of 1 km, 2 km, 2 km, 25 km, 25km and 25 km. They are joined with FC/UPC connector in order to simulate the loss and reflection of the commercial optical fiber network. The schematic of the system is shown in Fig.1.

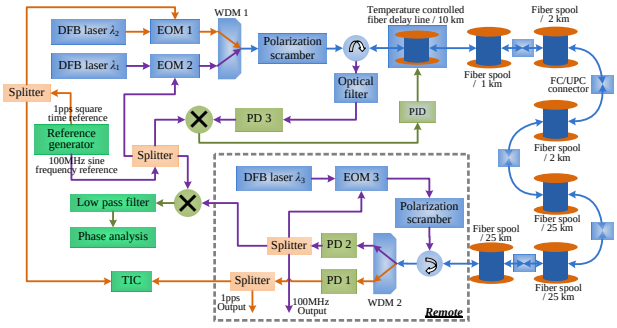

Fig. 149: Schematic of the time and frequency transfer system based on WDM and two way optical compensation.

In the un-compensated case, the Allan deviation of the fractional frequency stabilities of the 100 MHz in the whole 80 km link, the root mean square (RMS) and peak-peak fluctuated values of the propagation delay of the 1 pps signal between the local and remote end are 8.3×10^{-14} @ 10^4 s, 2529 ps @ 11 hour, and 12400 ps @ 11 hour respectively. And they are 2×10^{-17} @ 10^4 s, 59 ps @ 13 hour, 398 ps @ 13 hour in the compensated case.

Meantime, we found the fluctuation of pps signal induced by the electro-optical modulation may be a little high. But the fluctuation could be reduced by increasing frequency and averaging. We made the 1 pps signal to trigger a function generator. And it generated an output pulse signal with a rate of 100 Hz. The time interval counter (TIC) gave the propagation delay time of the pulse signal between the local and remote end averaged over every 100 measurement samples. In the condition, the RMS and peak-peak values of the output data are 11 ps @ 12 hour and 59 ps @ 12 hour respectively.

IFCS-EFTF5-PCD5-29

Distributed Time Transfer Using Optical Fiber Links

Liang Hu, Guiling Wu, Jianguo Shen, Huang Huang, Jianping Chen

State Key Laboratory of Advanced Optical Communication Systems and Networks, Shanghai Jiao Tong University, Shanghai 200240, China

Email: wuguiling@sjtu.edu.cn

Time transfer over optical fiber links[458] has attracted extensively interests due to its advantages of broad bandwidth, low loss and so on. In this paper, we propose a one point to multi-points distributed time transfer scheme using optical fiber links. A 1 to 8 experimental system over 20km single-mode fiber with stabilities less than 50ps is demonstrated.

The experimental setup of the proposed scheme is shown in Fig.1. The system consists of a master node, a 1 to 8 optical splitter and 8 slave nodes. The length of the optical fiber between the master and each slave is 20 km. The slaves are accessed to the master by using the time division multiple access mechanism. The bidirectional fiber path between the master and each slave is built under the control of the master by designating time slot for each slave in a certain sequence. Time at master is transferred to each slave over the corresponding bidirectional fiber path by the two-way time transfer method during assigned time slots.

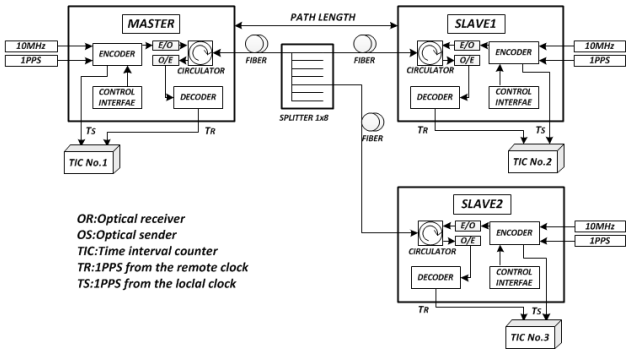

Fig. 1: the setup of the propose distributed time transfer

Fig.2 shows the measured time differences between the master and two slaves and their RMS in each time slot of 1 hour within 21 hours measurement. We can see that the system can implement distributed time transfer successfully and reach stabilities less than 50ps in each time slot.

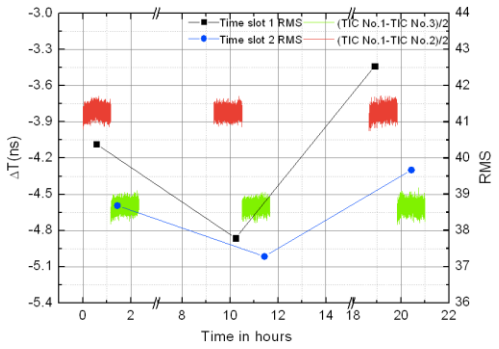

Fig. 2: the measured time difference and RMS

[458] A. Imaoka and M. Kihara, "Accurate time/frequency transfer method using bidirectional WDM transmission," IEEE trans. On Instrumentation and Measurement, Vol.47,No.2, pp.537-542, 1998.

IFCS-EFTF5-PCD5-30

Compass Receiver Positioning Algorithm under Bad conditions Based on Unequal Interval Clock Prediction

Jianwei Zhan[1], Peng Wu[1], Hang Gong[1], Guozhu Zhang[1], Gang Ou[1]

[1] School of Electronic Science and Engineering, National University of Defense Technology, Changsha, Hunan 410073, China

Email: sophy_zjw@nudt.edu.cn

It is widely known that at least four code pseudorange measurements are required before a position can be determined. However, positioning service is untermittent in the area where the satellite visibility is limited or the satellite signal is weak due to the blockage or signal jamming, such as in the underground traffic rountes, the tunnels, and park garages.

To solve this problem, a positioning method based on the unequal interval series of receiver clock bias is utilized to augment COMPASS receiver. The current researches do not refer the prediction model based on the unequal interval data. The conventional grey model in previous studies is based on the equal interval data. In this paper, an improved prediction grey model is proposed, which adopts a time interval coeffident and the TDOP coeffident to generate the difference clock series. And then a predicted clock value from the proposed model is introduced to aid positioning.

Actual test data were used to verify the methods which are under unequal and equal conditions respectively. Experimental test results with COMPASS data demonstrate that the prediction model in this paper is more suitable for predicting receiver clock bias，and the proposed positioning method can implement a good estimation of three-dimensional position when only three satellites are available.

IFCS-EFTF Group 6 poster session 2

Forum Hall

Wednesday & Thursday, July 24-25, 2013, 1:00 pm - 2:00 pm and 3:30 pm - 4:30 pm

Chair: **Sébastien Bize**
SYRTE-Observatoire de Paris

IFCS-EFTF6-PCD6-1

Development of Optical Frequency Standard based on ^{87}Sr

Sergey Slyusarev[1], Ksenia Khabarova[1], Alexey Kostin[1],
Sergey Strelkin[1], Gleb Belotelov[1], Vitaliy Pal'chikov[1], Nikolay Kolachevsky[2]

[1]FSUE "VNIIFTRI", Mendeleevo, Russia
[2]LPI RAS, Moscow, Russia

Email: vitpal@mail.ru

In the present work we discuss the experiment on creating frequency standard based on the clock transition $^1S_0 - {}^3P_0$ at $\lambda_0 = 698$ nm in ^{87}Sr atoms, trapped in a 1D vertical optical lattice.

The first stage of atoms cooling and trapping was realized using the Zeeman slower and a "blue" magneto-optical trap on $^1S_0 — {}^1P_1$ transition ($\lambda = 461$ nm), with 496 nm and 679 nm repumping lasers. For the second stage, a laser system with a narrow generation line has been developed and investigated. A 689-nm semiconductor laser has been stabilised using an external reference ultrastable cavity with vibrational and temperature compensation near the critical point. The lasing spectral width was 80 Hz (averaging time 40 ms), and the frequency drift was at a level of 0.3 Hz s^{-1}. Comparison of two independent laser systems yielded a minimum Allan deviation: 2×10^{-14} for 300-s averaging. It is shown that this system satisfies all requirements necessary for secondary cooling of ^{87}Sr atoms using the spectrally narrow $^1S_0 — {}^3P_1$ transition ($\lambda = 689$ nm).

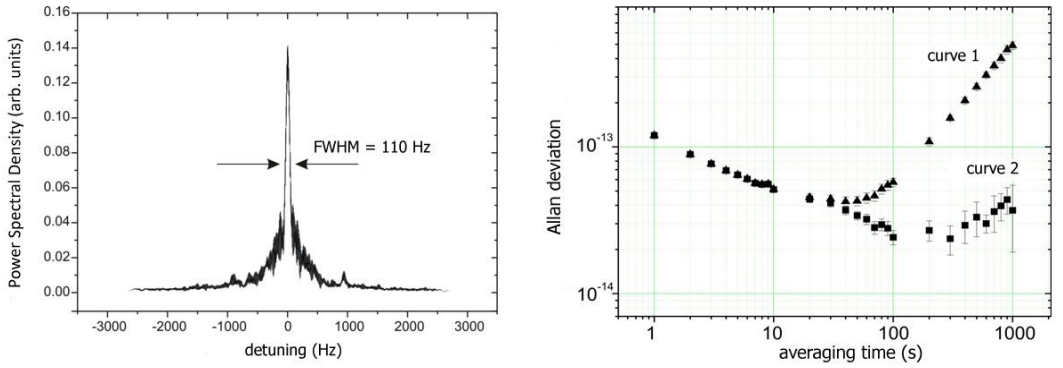

(a) (b)

Fig. 150: (a) The beating spectrum of two identical lasers, locked to ULE1 and ULE2 resonators (14 data sets were taken each with the resolution 47 Hz in 40-μs time, and then averaged). (b) Allan deviation of the beating signal, while subtracting linear drift (curve 1) and without subtracting it (curve 2).

IFCS-EFTF6-PCD6-2

Development of a Moving system for cavity-build-up Lattice

Chang Yong Park, Dai-Hyuk Yu, Won-Kyu Lee, Sangkyung Lee, Sang Eon Park,
Sang-Bum Lee, Jongchul Mun, Myoung-Sun Heo, and Taeg Yong Kwon

Division of Physical Metrology, Korea Research Institute of Standards and Science,
Daejeon 305-340, Korea

Email: cypark@kriss.re.kr

A moving system of cavity build-up lattice will be developed for an Yb optical lattice clock at Korea Research Institute of Standards and Science (KRISS). As the accuracy of optical clock has been improved, the black body radiation (BBR) shift becomes a major part of total uncertainty. The static and dynamic polarizability of Yb atoms was measured with 10^{-5} accuracy recently by the research group of NIST. To exploit the accuracy of the polarizability fully, a well-prepared black body condition is needed for the spectroscopy chamber like a cavity wherein trapped atoms are transferred by a moving lattice. Usually such a moving lattice can be formed by interference between counter-propagating two lasers with frequency offset to each other. However, in this way only the half of the potential depth is obtained, compared with the one obtained by normal way of using a reflection mirror for a counter propagating laser. Considering the temperature (10~20 μK) of cooled Yb atoms by inter-combination transition, obtaining a laser source for lattice with enough power is problematic. Our solution is to use cavity-build-up lattice and to move the whole build- up cavity system. We will design an optical cavity with enhancement factor of ~50 traveling vertically between magneto-optical trap region and the spectroscopy chamber. The advantage of this way is that atoms are always located in the beam waist of the lattice laser beam as is pointed out by other group[459] of PTB who already has built the lattice on moving stage. In our system, because of the cavity resonant condition the two cavity mirrors are mounted on one body moving stage, so that the separation of two mirrors preserves constant with less effort. By using fast PZT mounting a cavity mirror, the residual vibration will be compensated.

Optionally depending on the performance of the feedback control on the PZT, we expect to increase the enhancement factor of the cavity, from which we can obtain the higher leverage effect in evaluation of hyper-polarizability shift or larger volume of an each site of optical lattice to reduce the collisional shift. In this presentation we will describe details of our moving lattice system and experimental results.

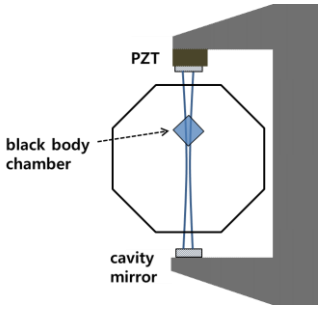

Fig.1 The proposed moving system of cavity-build-up lattice. Two curvature mirrors will be aligned vertically on a moving stage. Black body chamber is located 2 cm above the center of the magneto optical trap. A vacuum chamber with 18 viewports will be designed compactly to reduce the mass of moving stage.

[459] Thomas Middelmann, et al., "Long-range transport of ultracold atoms in a far-detuned one-dimensional optical lattice", New J. Phys. **14**, 073020 (2012)

IFCS-EFTF6-PCD6-3

Project of photoassociation measurments for determination of the density shift of $^1S_0$-$^3P_0$ clock transition in neutral strontium

Marcin Bober[1], Piotr Morzyński[1], Michał Zawada[1], Piotr Wcisło[1], Agata Cygan[1], Daniel Lisak[1], Roman Ciuryło[1], Jerzy Zachorowski[2], and Wojciech Gawlik[2]

[1]Institute of Physics, Nicolaus Copernicus University, Torun, Poland
[2]M. Smoluchowski Institute of Physics, Jagiellonian University, Cracow, Poland

Email: bober@fizyka.umk.pl

Recent progress in optical atomic clocks with neutral strontium atoms in an optical lattice allows to reduce uncertainty to 10^{-16} level[460]. Important contribution to accuracy budget came from cold atoms collisions in the lattice. In this work we report apparatus for determination of scattering properties of $^3P_0$ state in strontium.

We plan to make direct measurement with the clock transition (698 nm) or to use a three photons photoassociation using 689, 679 and 707 nm lasers. This measurement will be performed with the magneto-optical trap setup[461] designed for experiments with both ^{88}Sr and ^{87}Sr isotopes. At the same time we are preparing the second setup, exclusively designed as the optical lattice atomic clock with strontium atoms. With those two strontium systems we plan to study the density shift of $^1S_0$-$^3P_0$ clock transition in strontium.

460 R. Le Targat et al. "Experimenting an optical second with strontium lattice clocks", arXiv:1301.6046

461 M. Bober et al. "Precision spectroscopy of cold strontium atoms, towards optical atomic clock", Bull. Pol. Ac.: Tech., **60**(4), 707, 2012

IFCS-EFTF6-PCD6-4

Strontium Optical Lattice Clock Research at NIM

Yige Lin[1], Qiang Wang[1,2], Ye li[1,2], Shaokai Wang[1], Fei Meng[1], Baike Lin[1], Yang Zhao[1,2], Shiying Cao[1], Minming Wang[1], Jianping Cao[1], Erjun Zang[1], Tianchu Li[1], Zhanjun Fang[1]

[1]Division of Time and Frequency Metrology, National Institute of Metrology, Beijing, China
[2]Department of Precision Instruments and Mechanology, Tsinghua University, Beijing, China

Email: linyige@nim.ac.cn

A strontium lattice clock is being built at NIM. Our experiments started with laser cooling and trapping of ^{88}Sr. The atoms are cooled by two-stage laser cooling. After the first stage laser cooling on $^1S_0$-$^1P_1$ transition with a commercial 461 nm laser, about 10^8 ^{88}Sr atoms are cooled to 3 mK. The second stage cooling laser system has a master-slave configuration. The master laser is an external cavity diode laser (ECDL) which is lock to a reference cavity (finesse is ~ 10000). The linewidth of the master laser is reduced to 150 Hz by locking to the reference cavity with Pound-Drever-Hall technique. The slave laser is injection locked to the master laser. With this narrow 689 nm laser system, the ^{88}Sr atoms could be cooled to as low as 3 μK via $^1S_0$-$^3P_1$ transition. The horizontally oriented optical lattice is formed by an 813 nm Tapered-Amplifier laser with trap depth of 32 μK.

The 698 nm clock laser is an ECDL locked to a high finesse cavity (finesse is ~ 200,000). The support points of the cavity are optimized by finite element analysis. The beat of two similar systems show a linewidth of ~5 Hz, and the Allan deviation is ~ 3e-15 @ 1 s.

Magnetic field induced spectroscopy is introduced to make the single photon $^1S_0$-$^3P_0$ transition possible in ^{88}Sr.[462] The sideband resolved spectrum is obtained by logging the transition probabilities when scanning the probe laser frequency, and is shown in fig.1(a). The trapping sidebands are ~ 100 kHz away from the carrier. The fit to the blue detuned sideband shows that the temperature of the atom in the lattice is ~ 7 μK. The Narrowest transition we got is ~ 100 Hz.

The experiment was then transferred to ^{87}Sr. The ^{87}Sr atoms have been loaded into the optical lattice and the sideband resolved spectrum is obtained as shown in fig.1(b). We are now trying to compensate the earth magnetic field to narrow down the transition linewidth and make a preliminary lock to the atomic transition.

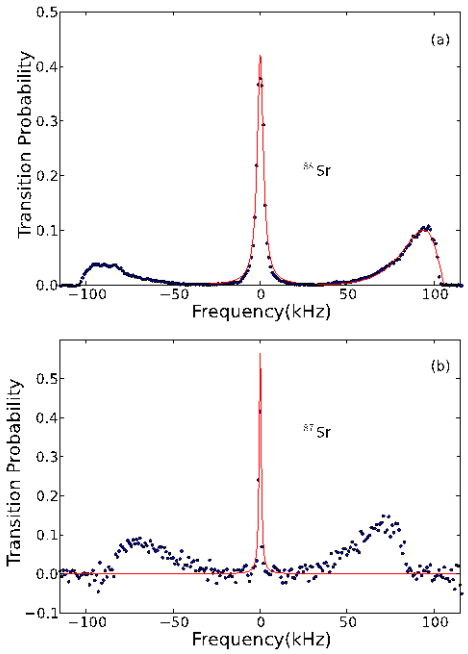

Fig. 151: sideband resolved spectroscopy of Strontium

[462] Y.G. Lin, Q. Wang, Y. Li et al. "Magnetic Field Induced Spectroscopy of ^{88}Sr Atoms Probed with a 10 Hz Linewidth Laser," Chin. Phys. Lett., vol. 30, no. 1, p. 014206, 2013.

IFCS-EFTF6-PCD6-5

Compact Atomics Package for a Transportable Strontium Lattice Clock

Yeshpal Singh, Lyndsie Smith, Ole Kock, Wei He, Huadong Cheng, Kai Bongs *and the SOC2 team*[2]

[1]Department of Physics and Astronomy, University of Birmingham, Edgbaston Park Road, Birmingham B15 2TT, UK
[2]Heinrich- Heine-Universität Düsseldorf, Germany
Physikalisch-Technische-Bundesanstalt,Germany
Leibniz Universität Hannover, Germany
Observatoire de Paris, France; Universita' di Firenze,
National Physical Laboratory Teddington, the United Kingdom
TOPTICA Photonics AG, Germany; EADS Astrium Friedrichshafen, Germany
Menlo Systems GmbH, Germany; Kayser-Threde GmbH, Germany; Kayser Italia S.r.l.,Italy
Centre Suisse d'Electronique et de Microtechnique SA, Switzerland ; Université de Neuchâtel, Switzerland ; Ecoles Polytechniques Fédérales Lausanne, Switzerland
Istituto Nazionale di Ricerca Metrologica, Italy

Email: y.singh.1@bham.ac.uk

With the rapidly improving performance of optical clocks, in the future, most applications requiring the highest accuracy will require these systems. The unprecedented accuracy in time promises new applications like relativistic geodesy which might benefit the exploration of oil and minerals, fundamental tests of general relativity and synchronization for long base line astronomical interferometry, deep space navigation. In the framework of the research project SOC2:"Towards Neutral-atom Space Optical Clocks" funded by the EU 7th framework programme (FP7/2007-2013) under grant agreement n. 263500, with the main aim of developing demonstrators of transportable lattice clocks with $5x10^{-17}$ relative frequency accuracy [1], we are reporting on the concept of a very compact, light and energy efficient atomics package for a Sr clock prototype. At the heart of the atomics package is a 3D MOT chamber (Fig.1) which can be loaded either with a permanent magnet Zeeman slower or with a 2D MOT facility. The total budget of the system will be <10 l, $<10^{-10}$ mbar, < 20 kg [2].

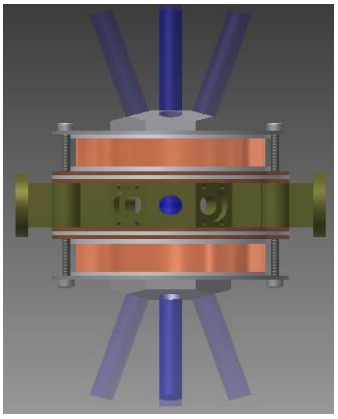

Fig. 152: Design of the 3D MOT chamber.

References:

[1] S. Schiller et al. "Towards Neutral-atom Space Optical Clocks (SOC2): Development of high-performance transportable and breadboard optical clocks and advanced subsystems" on "*Let's embrace space, volume II*" **45**, 452-463 (2012). ISBN 978-92-79-22207-8.

[2] www.soc2.eu

IFCS-EFTF6-PCD6-6

A ground based Yb lattice clock to participate in future space-clock missions: commencement

J.J, McFerran[1], N. Kostylev[1], E. Ivanov[1], J.G. Hartnett[2], A.N. Luiten[2] and M. Tobar[1]

[1]School of Physics, University of Western Australia, Australia
[2]IPAS, University of Adelaide

Email: john.mcferran@uwa.edu.au

Recent measurements in various laboratories have shown astonishingly high accuracy for a number of different clock transition frequencies and ratios [1-7]. However, these clocks are isolated in separate laboratories around the globe, which limits the degree of confirmation. With future space-clock missions such as the Atomic Clock Ensemble in Space (ACES) mission and possible future missions, such as Space Optical Clock (SOC) and STE-QUEST, a much greater opportunity will be granted for frequency comparisons between clocks distributed around the earth.

While optical fibre links can permit ultra-stable clock comparisons over many hundreds of kilometers [8], they cannot be used for clocks as isolated as; for example, Perth Western Australia. At UWA we are developing a Yb based 1-dimensional optical lattice clock with the aim of participating in future space-clock missions. Similar ^{171}Yb, $(6s^2)\ ^1S_0$ -- $(6s6p)\ ^3P_0$, based clocks have been developed before [2,9,10] and the transition is included in the CIPM's list of secondary representations of the second. In this poster presentation we outline the details of the clock design. To maximize the number of atoms available for probing we will use a Zeeman slower and two stages of cooling in a magneto-optical trap, before loading into a lattice trap. The main chamber is to be compact for easier current control and to minimize thermal gradients. Having a compact chamber and multiple stages of laser cooling presents a challenge. We will illustrate a scheme that addresses this issue and present some preliminary results in relation to the Yb oven and laser systems.

[1] N. Huntemann, M. Okhapkin, B. Lipphardt, S. Weyers, C. Tamm, and E. Peik , Phys. Rev. Lett. 108, 090801 (2012).
[2] C.W. Chou, D. B. Hume, J. C. J. Koelemeij, D. J. Wineland, and T. Rosenband, Phys. Rev. Lett. 104, 070802 (2010).
[3] N. D. Lemke, A. D.Ludlow,Z.W.Barber,T. M.Fortier, S. A. Diddams, Y. Jiang, S.R. Jefferts, T. P. Heavner, T. E. Parker, and C.W. Oates, Phys. Rev. Lett. 103, 063001 (2009).
[4] T. Rosenband, D. Hume, P. Schmidt, et al., Science 319, 1808 (2008).
[5] A. Ludlow, T. Zelevinsky, G. Campbell, et al., Science 319, 1805 (2008).
[6] J.J. McFerran, L. Yi, S. Mejri, S. Di Manno, W Zhang, J. Guéna, Y. L. Coq, and S. Bize, Phys. Rev. Lett. 108, 1830041 (2012).
[7] A.A. Madej, P. Dubé, Z. Zhou, J.E. Bernard, and M. Gertsvolf, Phys. Rev. Lett. 109, 203002 (2012).
[8] K. Predehl, G. Grosche, S. M. F. Raupach, S. Droste, O. Terra, J. Alnis, Th. Legero, T. W. Haensch, Th. Udem, R. Holzwarth, and H. Schnatz.. Science, 336, 441 (2012).
[9] T. Kohno, M. Yasuda, K. Hosaka, H. Inaba, Y. Nakajima, F-L Hong, Appl. Phys. Exp. 2, 072501 (2009)
[10] C.Y. Park, D.-H. Yu, W.-K. Lee, S.E. Park, E.B. Kim, S.K. Lee, J.W. Cho, T.H. Yoon, J. Mun, S.J. Park, T.Y. Kwon, S.-B. Lee, Metrologia, 50, 119 (2013).

IFCS-EFTF6-PCD6-7

Ion trap heating – measurement and model

Petr Balling[1], Miroslav Doležal[1], Hugh Klein[2], Steven King[2], Patrick Gill[2], Thomas Lindvall[3], Anders Wallin[3], Mikko Merimaa[3], Christian Tamm[4], Piet O. Schmidt[4], Tanja E. Mehlstäubler[4], Ekkehard Peik[4]

[1]Czech Metrology Institute, Prague, Czech Republic
[2]National Physical Laboratory, Teddington, United Kingdom
[3]Centre for Metrology and Accreditation (MIKES), Espoo, Finland
[4]Physikalisch-Technische Bundesanstalt (PTB), Braunschweig, Germany

Email: pballing@cmi.cz

Blackbody radiation-induced shifts make a significant contribution to the uncertainty budget of trapped ion optical clocks[463]. One of the tasks of EMRP project SIB04 Ion Clock is the development of a quantitative model of the thermal environment seen by the ion. FEM models, including skin effect and RF losses in dielectrics, were created using ANSYS/HFSS software for ion traps used by project partners. The models are being refined and verified using the temperature measurements of "dummy" traps; critical parts and parameters will be identified for optimization of the future trap designs.

Thermal imaging measurements of the traps involve calibration of both an infrared camera (FLIR A615) working in the 7 to 14 μm range and the transmission of an AR coated ZnS window. The emissivity of materials used (tantalum, molybdenum, titanium, macor, alumina, sapphire etc.) was estimated by comparison with a near-perfect black emitter at several known temperatures in vacuum. The results were used to correct the raw thermal image data. However they cannot be directly used to estimate the total emitted radiation in the case of spectrally dependent samples like sapphire. Preliminary measurements and simulations of an NPL end-cap trap are shown below. More details and other examples will be presented at the joint symposium.

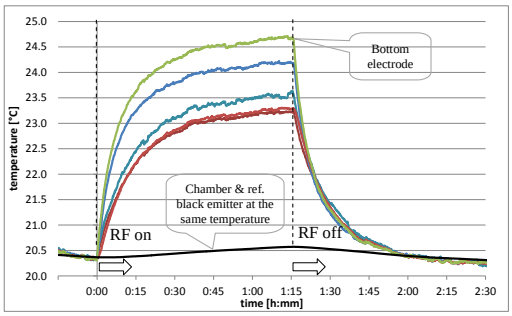

Radiometric measurement of various locations on the NPL end-cap dummy trap parts corrected for reflected radiation, window transmission and emissivity.

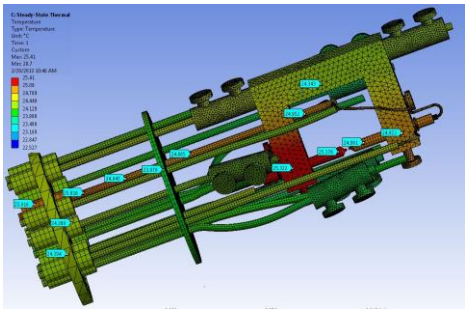

FEM results - steady state surface temperature

Discussion with consortium members is gratefully acknowledged. The EMRP is jointly funded by the EMRP participating countries within EURAMET and the European Union.

[463] Mitroy, J, et al. "Theory and applications of atomic and ionic polarizabilities." *J. Phys. B: At. Mol. Opt. Phys.* 43 (2010) 202001.

IFCS-EFTF6-PCD6-8

Design and construction of helical resonators for ion traps

Ke Deng, Yunlong Sun, Jie Zhang, Zehuang Lu, and Jun Luo

MOE Key Laboratory of Fundamental Quantities Measurement, School of Physics,
Huazhong University of Science and Technology, Wuhan, P.R. China

Email: zehuanglu@mail.hust.edu.cn

Single trapped ions are recognized as important candidates for realizing optical frequency standards. To drive the ion trap, a high-Q resonator is needed, and a predictable high driving frequency is generally preferred. Usually the high-Q resonator is realized through a helical resonator. The resonant frequency of a helical resonator without load can achieve rather large resonant frequency (50~60 MHz), which can be calculated by empirical formula. However, when the resonator is connected to the ion trap, the resonant frequency will be reduced substantially[464] due to the parallel capacitive impedance of the trap and feed-through. Less effort has been made on how to predict the resonant frequency when the resonator is attached to the trap electrodes.

In this paper we will model the resonator with a lumped element electrical equivalent model and predict the resonant frequency under the realistic condition when the helical resonator is connected to an ion trap. Based on our model, we construct a resonator and Fig. 1 shows a picture of the constructed helical resonator. Inside diameter of the shield of the resonator is 100 mm. The turn and direction of the antenna coil is adjusted to make it match 50 Ohm impedance. In order to maintain the winding pitch and the diameter of the main coil to be constant, we use a lathe and a tube to wind the coil instead of by hand. The unloaded Q-factor of the resonator is about 300. We measure the resonant frequencies under different loads. The experimental results concur with our prediction.

To test the practical performance of the resonator, we use it to drive a linear Paul trap. After optimization, the Q-factor of the resonator is still about 300 after the trap is connected. The trap electrodes are driven at 25 MHz. We trap $^{24}Mg^{+}$ by this resonator. Pictures of $^{24}Mg^{+}$ are recorded by an EMCCD camera. The result is shown in Fig. 2.

Fig. 1: Picture of the helical coil resonator

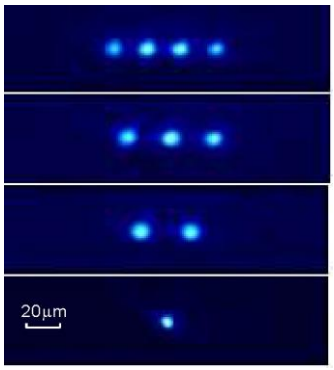

Fig. 2: Pictures of crystallized $^{24}Mg^{+}$

[464] J. D. Siverns, L. R. Simkins, S. Weidt, and W. K. Hensinger, "On the application of radio frequency voltages to ion traps via helical resonators", Appl. Phys. B, vol. 106, p. 327-338, 2012.

IFCS-EFTF6-PCD6-9

Incoherent Repumper and Clearout Light Sources for Sr^+ Ion Traps

Thomas Fordell, Thomas Lindvall, Tuomas Hieta, Mikko Merimaa

Centre for Metrology and Accreditation (MIKES), Espoo, Finland
Email: thomas.fordell@mikes.fi

In addition to the extremely stable clock laser, an optical clock requires several other light sources that must resonate with electronic transitions in the reference ion or atoms. If lasers are used, wavelength stabilization is required, which is usually a delicate process that calls for continuous operation of the lasers. If the requirement of frequency stabilization can be relaxed, a simplification of the light source ensemble results, which is a highly desirable feature particularly in transportable clocks and space clocks.

In a recent paper[465], the use of incoherent, unpolarized repumper and clearout light sources based on amplified spontaneous emission (ASE) was proposed. An unpolarized ASE source is broadband and as such requires no frequency stabilization. Moreover, in the case of the repumper, such a source requires no external polarization modulation to prevent dark states even in a zero magnetic field. It can also drive multiple hyperfine transitions simultaneously. In a Sr^+ single-ion clock, efficient cooling and detection requires a power spectral density (PSD) on the order of 1 mW/nm for an ASE repumper. Rapid emptying of the metastable clock state requires a PSD about an order of magnitude less for the clearout light source.

In this contribution we present prototype fibre optic light sources that meet these requirements. Both repumper and clearout sources are based on Yb-doped fibre, a 980 nm semiconductor pump laser and standard fibre optic components, such as fibre Bragg gratings, fused splitters, wavelength division multiplexers and isolators. The all fibre approach ensures adjustment free operation. Moreover, since no frequency stabilization is needed, the sources can be switched on and off electronically during the clock cycle simply by modulating the pump laser current. For the repumper the turn-on time is a few milliseconds, the turn-off time somewhat longer: about 10 ms to reach the 10^{-7} level that is needed for the light shift of the clock transition to be less than 10^{-17} at the start of the clock interrogation cycle.

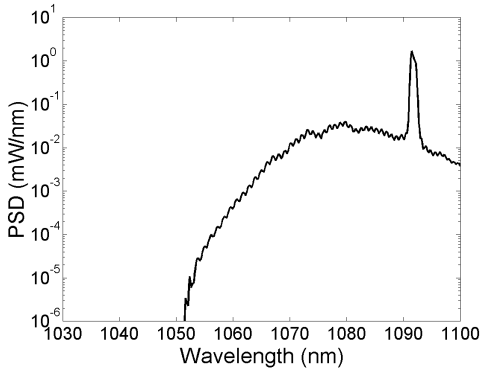

Fig. 153: PSD of the prototype ASE repumper. The spectrum has been engineered to be very low at 1033 nm in order for the repumper not to prevent the detection of clock transitions.

[465] Lindvall et al., "Unpolarized, incoherent repumping light for prevention of dark states in a trapped and laser-cooled single ion", Phys. Rev. A, vol. 87, 013439, 2013

IFCS-EFTF6-PCD6-10

Dark-State Suppression in a Trapped and Laser-Cooled Alkaline-Earth-Metal Single Ion

Thomas Lindvall[1], Thomas Fordell[1], Alan A. Madej[2], Ilkka Tittonen[3], Mikko Merimaa[1]

[1]Centre for Metrology and Accreditation (MIKES), Espoo, Finland
[2]Frequency and Time Group, National Research Council of Canada, Ottawa, Canada
[3]Department of Micro- and Nanosciences, Aalto University, Espoo, Finland

Email: thomas.lindvall@mikes.fi

We study dark states in a single laser-cooled alkaline-earth-metal ion in a radiofrequency trap. Both Doppler cooling and fluorescence detection of the ion rely on obtaining a high scattering rate on the $^2S_{1/2}$-$^2P_{1/2}$ transition. However, many commonly used ion species have a low-lying metastable $^2D_{3/2}$ state that can become populated due to spontaneous emission from the $^2P_{1/2}$ excited state. This requires a repumper laser to maintain the ion in the cooling cycle. The $^2D_{3/2}$-$^2P_{1/2}$ repumper transition has dark states for any laser polarization. These can be destabilized by an external magnetic field or by modulating the polarization, for example, using an electro-optic modulator[466]. Using $^{88}Sr^+$ as an example, we study the different types of dark states that can occur and how to prevent them in order to optimize the laser cooling and the scattering rate. The calculations are compared to experimental results obtained at the National Research Council of Canada and are found to be in good agreement (see Fig. 1).

Recently we proposed using unpolarized, incoherent amplified spontaneous emission (ASE) to drive the repumping transition[467]. The ASE repumper offers several advantages compared to a laser repumper. It prevents dark states without polarization modulation using a single beam even in the near-zero magnetic field required for an ion clock. Due to its broad bandwidth, it requires no frequency stabilization. In addition, the source can be switched on and off electronically simply by modulating the pump laser current. These features, and the fact that the ASE source is fiber based, make it very compact and robust, which is essential for the development of practical, transportable optical clocks.

This work was funded by the Academy of Finland (project 138894). TF acknowledges financial support from the European Commission (Marie Curie Integration Grant PCIG10-GA-2011-304084).

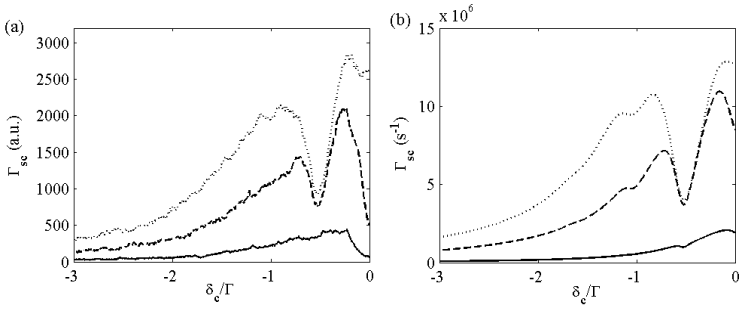

Fig. 154: (a) Measured and (b) calculated single-ion fluorescence spectra as a function of cooling laser detuning for increasing Rabi frequencies (bottom to top). The repumper was red-detuned to make the coherence dips visible.

[466] T. Lindvall, M. Merimaa, I. Tittonen, and A. A. Madej, "Dark-state suppression and optimization of laser cooling and fluorescence in a trapped alkaline-earth-metal single ion", Phys. Rev. A **86**, 033403 (2012).

[467] T. Lindvall, T. Fordell, I. Tittonen, and M. Merimaa, "Unpolarized, incoherent repumping light for prevention of dark states in a trapped and laser-cooled single ion", Phys. Rev. A **87**, 013439 (2013).

IFCS-EFTF6-PCD6-11

On the Interpolation Between Optical Frequency Standards and Primary Clocks by Use of Ultrastable Resonators

Fritz Riehle, Uwe Sterr, Christian Hagemann, Christian Grebing

Physikalisch-Technische Bundesanstalt (PTB), 38116 Braunschweig, Germany

Email: Uwe.Sterr@ptb.de

The frequency instability of state-of-the art primary caesium fountain clocks is ultimately limited to the quantum projection noise determined by the line quality factor of the caesium transition and the number of the atoms in the fountain to $4 \times 10^{-14}\ (\tau/s)^{-1/2}$ at best[468]. For typical operation of the best clocks the instability is higher by up to almost an order of magnitude as a result of limitations due to a reduced number of atoms usually employed to reduce systematic shifts or the Dick effect[469] of the interrogating oscillator.

On the other hand, optical frequency standards have already shown fractional instabilities as low as $5 \times 10^{-16}\ (\tau/s)^{-1/2}$ with the prospects to come down to the 10^{-17} regime[470]. So even with the very best caesium clocks the measurement of an optical frequency with a fractional uncertainty of 10^{-16} will range from several days to more than a month. Not many optical clocks have proven such a long operation time.

To bridge this gap of instability and allow for regular comparisons of cesium clocks to optical clocks at their best performance we propose the use of an ultrastable optical resonator like a silicon resonator at cryogenic temperature[471] to interpolate between relatively short averaging intervals with respect to optical clocks and the long intervals required to reach the accuracy of the primary standards. A laser stabilized to such a resonator has shown a fractional instability near or below 1×10^{-16} for interrogation times near 1 s with very small drifts on longer time scales. However, even these small varying drifts might limit the practical interpolation time.

We have investigated strategies to mitigate these limitations by measuring the resonator drift against the optical frequency standards to determine suitable intervals and to correct the frequency comparison between both clocks accordingly. We present a mathematical treatment of the interpolation method and compare it to available data from the systems at PTB. Applications of this concept as well as extrapolations to future standards and resonators will be discussed.

This work was supported by Deutsche Forschungsgemeinschaft DFG in the Centre of Quantum Engineering and Space-Time Research (QUEST) of the Leibniz Universität Hannover and the EMRP IND14. The EMRP is jointly funded by the EMRP participating countries within EURAMET and the European Union.

---

[468] G. Santarelli, P. Laurent, P. Lemonde, A. Clairon, A. G. Mann, S. Chang, A. N. Luiten, and C. Salomon, Phys. Rev. Lett. **82**, 4619 (1999).

[469] C. A. Greenhall and G. J. Dick, IEEE Trans. Ultrason. Ferroelec. Freq. Contr. **47**, 1593 (2000).

[470] Y. Y. Jiang, A. D. Ludlow, N. D. Lemke, R. W. Fox, J. A. Sherman, L.-S. Ma, and C. W. Oates, Nature Photonics **5**, 158 (2011).

[471] T. Kessler, C. Hagemann, C. Grebing, T. Legero, U. Sterr, F. Riehle, M. J. Martin, L. Chen, and J. Ye, Nature Photonics **6**, 687 (2012).

IFCS-EFTF6-PCD6-12

Nd:YAG lasers with a most probable linewidth of 0.6 Hz

H. Q. Chen[1], Y. Y. Jiang[1], S. Fang[1], Z. Y. Bi[1], L. S. Ma[1]

[1]State Key Laboratory of Precision Spectroscopy, East China Normal University,
3663 N. Zhongshan Road, Shanghai 200062, China

Email: zybi@phy.ecnu.edu.cn

Lasers with ultra-low phase noise and high frequency stability are pursued in many applications, such as optical atomic clocks, tests of fundamental physics, low-phase-noise microwave generation and gravitational wave detection. Lasers with sub-Hz linewidth can be realized by using the Pound-Drever-Hall (PDH) technique to stabilize the laser frequency to an external ultra-stable Fabry-Perot reference cavity[1-4]. In this work, two independent similar cavity-stabilized Nd:YAG lasers at 1064 nm are constructed, which can run continuously over three weeks. In each laser system, the reference cavity is 7.75-cm long and is vertically mounted[5-8]. The cavity has a finesse measured to be ~200,000, corresponding to a cavity linewidth of <10 kHz. Each cavity is located in a gold-coated copper cylinder thermal shield, which is enclosed in a vacuum chamber. Both of the vacuum assembles for the reference cavity and the optic components for the PDH technique are on a passive vibration isolation platform (VIP) for vibration reduction. The VIP resides in a home-made box for acoustic isolation with an attenuation of more than 20 dB. The temperature inside the box is stabilized. Both of the cavity spacer and mirror substrates are made of ultra-low-expansion (ULE) glass. Zero-expansion temperatures of the composite cavities are measured to be ~22.87 ^{o}C and ~10.58 ^{o}C, respectively. Since the vacuum chambers for the cavities are temperature-controlled by heating, one is maintained at near 22.87 ^{o}C with sub-mK instability and the other is stabilized at ~22.9 ^{o}C with mK instability. Light is transferred to the VIP by a single-mode fiber with fiber noise cancellation. Frequency stabilization is accomplished by controlling a piezoelectric transducer (PZT) bonded on the monolithic Nd:YAG crystal of the laser to keep the laser frequency on resonance with the reference cavity. 700 measurements of the beat note between two laser systems taken in four different days over 79 days show that each laser has achieved a most probable linewidth of 0.6 Hz and a fractional frequency instability of 1.3×10^{-15} at an averaging time of 1 to 40s. Systematic evaluation shows the performance of each laser system is close to the cavity thermal noise limit.

---

[1] R. W. P. Drever *et al.*, "Laser phase and frequency stabilization using an optical resonator", Appl. Phys. B, vol. 31, p. 97-105, 1983.

[2] B. C. Young *et al.*, "Visible lasers with subhertz linewidths", Phys. Rev. Lett., vol. 82, p. 3799-3802, 1999.

[3] Y. Y. Jiang et al., "Making optical atomic clocks more stable with 10^{-16}-level laser stabilization", Nature Photonics, vol. 5, p. 158-161, 2011.

[4] T. L. Nicholson et al., "Comparison of two independent Sr optical clocks with 1×10^{-17} stability at 10^{3} s", Phys. Rev. Lett., vol. 109, p. 230801, 2012.

[5] M. Notcutt *et al*., "Simple and compact 1-Hz laser system via an improved mounting configuration of a reference cavity", Opt. Lett., vol. 30, p. 1815-1817, 2005.

[6] A. D. Ludlow *et al*., "Compact, thermal-noise-limited optical cavity for diode laser stabilization at 1×10^{-15}", Opt. Lett., vol. 32, p. 641-643, 2007.

[7] J. Alnis *et al*., "Subhertz linewidth diode lasers by stabilization to vibrationally and thermally compensated ultralow-expansion glass Fabry-Pérot cavities", Phys. Rev. A, vol. 77, p. 053809, 2008.

[8] T. Kessler *et al.*, "A sub-40 mHz-linewidth laser based on a silicon single-crystal optical cavity", Nature Photonics, vol. 6, p. 687-692, 2012.

IFCS-EFTF6-PCD6-13

Clock Laser Systems for Yb Optical Lattice Clock at KRISS

Won-Kyu Lee, Chang Yong Park, Dai-Hyuk Yu, Sang Eon Park, Sangkyung Lee, Sang-Bum Lee, Jongchul Mun, Myoung-Sun Heo, and Taeg Yong Kwon

Division of Physical Metrology, Korea Research Institute of Standards and Science, Daejeon 305-340, Korea

Email: oneqlee@kriss.re.kr

Two types of yellow lasers at 578 nm were developed for a probe laser of an Yb optical lattice clock at Korea Research Institute of Standards and Science (KRISS) [472] by using sum-frequency generation (SFG) or second harmonic generation (SHG). In the SFG scheme, the output of an Nd:YAG laser at 1319 nm and that of an Yb-doped fiber laser at 1030 nm were passed through a periodically-poled lithium niobate (PPLN) waveguide for SFG at 578 nm with an output power of more than 20 mW. In the SHG scheme, the output of a high-power external-cavity diode laser at 1156 nm was sent through another PPLN waveguide for SHG with an output power of more than 10 mW.

The linewidth of the produced yellow light was narrowed by stabilizing the frequency to a super-cavity made of ULE glass. The cavity was horizontally mounted at the optimal support points to reduce vibration sensitivity. Also the cavity was installed in a vacuum chamber, and the temperature of the cavity was stabilized at the value for the zero thermal expansion within 10-mK-level accuracy. This vacuum chamber was placed on an active vibration-isolation table. This system was installed in an acoustic enclosure with a 20-dB isolation to block the acoustic noise.

Fig. 1 shows typical FFT spectrum of the beat note between the two independent clock laser systems. Since the full width at half maximum (FWHM) of the beat note was about 5 Hz (resolution bandwidth; 2 Hz), the linewidth of one clock laser was estimated to be about 3.5 Hz, assuming similar performance of both lasers. This FWHM linewidth varied between 2 ~ 10 Hz due to frequency jitters. The frequency jitter was measured to be about 25 Hz in 10 s. Although currently there is much room for improvement of the stability of our clock laser compared with the state-of-the-art technology, we expect it is stable enough for the frequency lock to the clock transition of the Yb lattice clock.

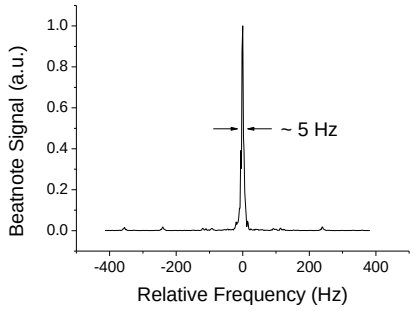

Fig. 1: Typical FFT spectrum of the beat note between two independent clock laser systems with the resolution bandwidth of 2 Hz, and the acquisition time of 1 s. The FWHM linewidth was estimated to be about 3.5 Hz assuming similar performance of both lasers.

[472] C. Y. Park, *et al*., "Absolute frequency measurement of $^{1}S_{0}(F = 1/2)$–$^{3}P_{0}(F = 1/2)$ transition of ^{171}Yb atoms in a one-dimensional optical lattice at KRISS", Metrologia, vol. 50, p. 119-128, 2013.

IFCS-EFTF6-PCD6-14

Determination of Mode Number Using Two Laser Combs with Large Difference in Repetition Rate

Jin-Long Peng, Tze-An Liu, and Ren-Huei Shu

Center for Measurement Standards, Industrial Technology Research Institute, Hsinchu, Taiwan

Email: jlpeng@itri.org.tw

To measure the frequency of a laser under measurement (LUM) using a mode-locked laser comb, the mode number of the beating comb line must be determined. Peng *et al.* developed methods based on two combs with repetition rate difference of kHz to measure the mode number, which can be independent of the frequency fluctuations of the LUM[473, 2]. Inaba *et al.* demonstrated the comb mode determination using two combs with large difference in repetition rate[3]. However, they need long measurement time (1000 s) to average down the uncertainty of the beat frequency difference. In this paper, we report method based on two-comb technique that can determine the mode number in short average time (1 s) for any different repetition rate.

This method relies on measuring the beat frequencies at two different repetition rates of comb1 while keeping the repetition rate of comb2 unchanged. Furthermore, a monochromator is used to measure the wavelength of the LUM to offer an approximate frequency to help determining the mode number shift of comb1 when its repetition reate is changed. For simplicity, assume that the offset frequencies are zero and the signs of the beat frequencies are determined to be positive. Thus, the frequency of the LUM can be expressed as:

$$f_L = n \cdot f_{r11} + f_{b11} = k \cdot f_{r21} + f_{b21} \quad (1)$$

$$f_L = (n+m) \cdot f_{r12} + f_{b12} = k \cdot f_{r21} + f_{b22} \quad (2)$$

where fb_{1x} and fb_{2x}, x=1 and 2, are the beat frequencies measured at two different repetition rates f_{r1x} of comb1 and single repetition rate f_{r21} of comb2; n and k are the mode number of comb1 and comb2, respectively; m is the mode number shift of comb1 when the repetition rate is changed from f_{r11} to f_{r12}. From Eqs. (1) and (2), the mode number n can be derived as

$$n = \frac{m \cdot f_{r12} + (f_{b21} - f_{b11}) - (f_{b22} - f_{b12})}{f_{r11} - f_{r12}} \quad (3)$$

The mode number shift m can be first determined from Eq. (3) by using an approximate n calculated from the approximate frequency of the LUM similar to that published by Liu *et al.*[2]. After m is determined, its value is substituted back to Eq. (3) to calculate the exact mode number n. Experimental results are presented in the conference.

---

[473] J.-L. Peng, T.-A Liu, and R.-H. Shu, "Optical frequency counter based on two mode-locked fiber laser combs," Appl. Phys. B, vol. 92, p. 513-518, 2008.

[2] T.-A. Liu, R.-H. Shu, and J.-L. Peng, " Semi-automatic octave-spanning optical frequency counter," Opt. Express, vol. 16, p. 10728-10735, 2008.

[3] H. Inaba, Y. Nakajima, F.-L. Hong, K. Minoshima, J. Ishikawa, A. Onae, H. Matsumoto, M. Wouters, B. Warrington, and N. Brown, "Frequency measurement capability of a fiber-based frequency comb at 633 nm," IEEE Trans. Instru. Meas. vol. 58, p.1234-1240, 2009.

IFCS-EFTF6-PCD6-15

Long-term Miniaturized Stabilization of Ultrafast Laser based on Rubidium Coherent Population Trapping Atomic Resonator

Jiutao Wu, Dong Hou, Zhong Wang and Jianye Zhao*

Department of Electronics, Peking University, Beijing, China

*Email: zhaojianye@pku.edu.cn

Many locking approaches have been exploited to stabilize the mode-locked laser (MLL), helping to generate high-stable microwave sources. In conventional locking approaches, the MLLs are usually phase-locked to very high-stable external frequency references, including atomic microwave, optical clocks, and narrow optical-linewidth continuous wave (CW) lasers. These approaches can improve the stability and phase noise of the MLL significantly. However, the large physical size and system complexity of these approaches is a problem in practical application. In this paper, we demonstrate a novel miniaturized MLL stabilization system (length of 5 cm, width of 5 cm and height of 2.2 cm) for directly frequency-locking the repetition rate of MLL to a ^{85}Rb coherent population trapping (CPT) atomic resonator, generating a stable microwave with a long-term stability of ~3×10^{-12}.

The setup of this MLL stabilization system based on CPT in ^{85}Rb is illustrated in Fig. 1. It contains a ^{85}Rb CPT resonator with the length of 33 mm, width of 13 mm and height of 18 mm, a passive Er-doped MLL with fundamental repetition rate of 144.5 MHz, and a servo-loop circuit. The objective of the stabilization system is to directly frequency-lock the 21st harmonic repetition rate of the MLL to the ^{85}Rb CPT resonance at a hyperfine frequency of 3.035 GHz.

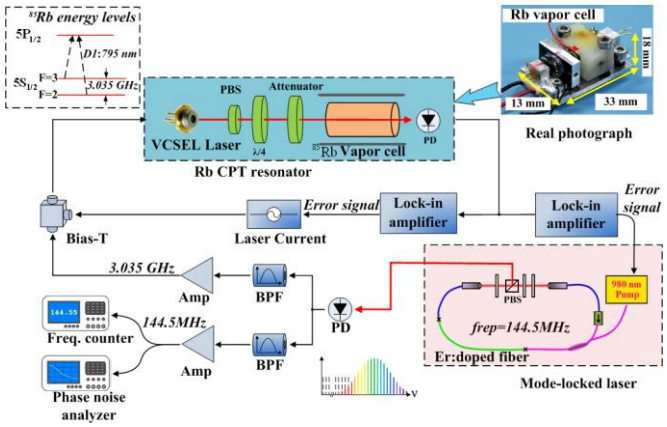

Fig. 155: Direct frequency stabilization scheme of MLL with a ^{85}Rb CPT atomic resonator. The stabilization system directly stabilizes the repetition rate of the MLL to the Rb CPT resonance.

By directly transferring the frequency stability of the atomic hyperfine frequency to the MLL, this approach can improve the frequency stability of the MLL significantly, and it can also simplify the system complexity and dramatically reduce the physical size because of the removal of the PLL servo circuit. Although some PLL stabilization schemes using high-stable Rb or Cs atomic clocks with big physical size have a better instability performance, the miniaturized stabilization scheme with a decent long-term stability is just the advantage of our approach. We believe that the proposed approach have a superior stability to other stabilization technique with the same small physical size.

IFCS-EFTF6-PCD6-16

Assessing the accuracy of the NPL femtosecond combs for a frequency ratio measurement with $^{171}Yb^{+}$

Luke Johnson, Helen Margolis, Steven King, Peter Nisbet-Jones, Rachel Godun, Patrick Gill

National Physical Laboratory, Teddington, Middlesex, UK

Email: luke.johnson@npl.co.uk

Optical clocks are of great interest for the study of fundamental physics. For example, the dimensionless optical frequency ratio $R = f_{E3}/f_{E2}$ between the $^{171}Yb^{+}$ octupole and quadrupole optical clock transition frequencies has a high sensitivity to variations in the fine structure constant α, scaling approximately as $\Delta R/R = -6.83\ \Delta\alpha/\alpha$ [1]. Also, without the need to measure relative to the SI second, a ratio measurement can benefit from the superior stability of the optical standards themselves, significantly reducing averaging times. Frequency ratio measurements separated by several years will allow a sensitive study of $\partial\alpha/\partial t$.

To support such measurements at NPL, we present details and results from a recent accuracy evaluation of two independent femtosecond frequency comb systems, based on Ti:Sapphire and Er-fibre mode-locked lasers. The optical frequency ratio between cavity-stabilised lasers at 934 nm and 871 nm has been measured synchronously using the two comb systems. The two combs act as transfer oscillators with the repetition and carrier envelope offset frequencies only loosely locked on both systems[2]. Our results show no detectable systematic offset between the two systems at the 2 x 10^{-19} level, which is limited by the averaging time of the comparison (see Fig. 1). The level of agreement is comparable to previous comb comparisons between Ti:Sapphire systems[3]. This performance demonstrates that $^{171}Yb^{+}$ frequency ratio measurements at NPL will be limited by the ion standards rather than the femtosecond combs.

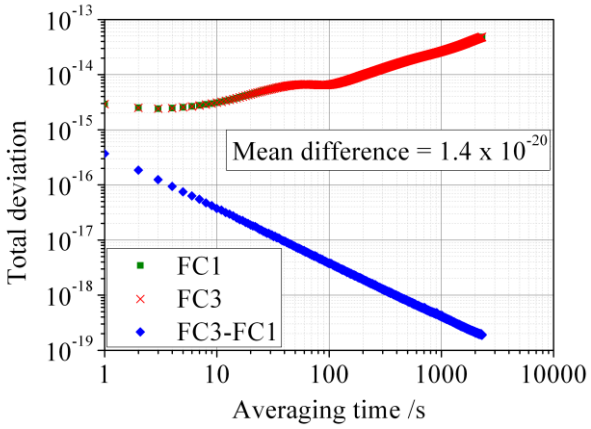

Fig. 156: Two-comb-comparison stability results between NPL-FC1 and NPL-FC3 from a continuous data set of 4600 s. The green squares and red crosses overlap and show the stability of the frequency ratio measured using each comb, displaying the associated cavity drift of the two lasers. The blue diamonds show the residual stability of the frequency ratio difference between the two systems, which averages down as $1/\tau$, reaching 2 x 10^{-19} after

[1] S. N. Lea, Rep. Prog. Phys. **70** 1473 (2007)

[2] H. R. Telle et al, Appl. Phys. B 74, 1 (2002)

[3] Long-Sheng Ma et al, Science 303, 1843 (2004)

IFCS-EFTF6-PCD6-17

International Timescales with Optical Clocks

H. S. Margolis[1], D. Calonico[2], P. Delva[3], H. Denker[4], S. Falke[5], R. M. Godun[1], D. Piester[5], S. Bize[3], J. Gersl[6], P. Gill[1], T. Lindvall[7], C. Lisdat[5], L. Lorini[2], M. Merimaa[7], M. Pizzocaro[2], S. L. Shemar[1], U. Sterr[5], L. Timmen[4], S. Weyers[5], P. B. Whibberley[1]

[1]National Physical Laboratory (NPL), Teddington, UK
[2]Istituto Nazionale di Ricerca Metrologica (INRIM), Torino, Italy
[3]LNE-SYRTE, Observatoire de Paris / UPMC, Paris, France
[4]Institut für Erdmessung (IfE), Gottfried Wilhelm Leibniz Universität, Hannover, Germany
[5]Physikalisch-Technische Bundesanstalt (PTB), Braunschweig, Germany
[6]Cesky Metrologicky Institut (CMI), Brno, Czech Republic
[7]Mittatekniikan Keskus (MIKES), Espoo, Finland

Email: helen.margolis@npl.co.uk

The most advanced optical atomic clocks have now reached levels of stability and accuracy that significantly surpass the performance of the best caesium primary frequency standards. As a result, the possibility of a future redefinition of the second in terms of an optical transition frequency is being actively considered by the international metrology community[474].

A new project funded within the European Metrology Research Programme (EMRP) aims to tackle the key challenges that must be addressed before an optical redefinition of the second can be implemented. A coordinated programme of European clock comparisons will be carried out at a level limited only by the accuracies of the clocks themselves, using transportable optical clocks, broad bandwidth satellite links and optical fibre links. Such a comparison programme is required to validate the performance levels of the optical clocks, to anchor their frequencies to the present definition of the second with the lowest possible uncertainty, and to establish the leading contenders for a new definition of the second.

To support the comparison programme, a complete evaluation will be made of all relativistic effects influencing time and frequency comparisons at the 10^{-18} level of accuracy, including the gravitational redshifts of the clock transition frequencies. Significant effort will be devoted to the design of setups to determine the static gravity potential at each clock location and the development of a refined geoid model incorporating gravity observations around each clock site.

The overall objective of the project is to develop a framework and procedures whereby the new generation of optical clocks can be integrated into international timescales, providing input to the Consultative Committee for Time and Frequency (CCTF) to prepare for a future redefinition of the second. The potential impact that high accuracy optical clocks could have on the field of geodesy will also be demonstrated, by carrying out a proof-of-principle experiment using optical clocks to measure with high temporal resolution the gravity potential difference between two well-defined locations separated by a long baseline (≈90 km) and a height difference of 1000 m.

The EMRP is jointly funded by the EMRP participating countries within EURAMET and the European Union.

[474] P. Gill, "When should we change the definition of the second?" Phil. Trans. Roy. Soc. A 369, 4109–4130 (2011).

IFCS-EFTF6-PCD6-18

JRP-EXL01: A Joint Research Project of the European Metrology Research Program to investigate Quantum Engineered States for Optical Clocks and Atomic Sensors

S. Bize[1], J. Lodewyck[1], R. Le Targat[1,2], G. Wilpers[3], U. Sterr[4], Chr. Lisdat[4], S. Falke[4], F. Levi[5], D. Calonico[5], A. Bertoldi[6], M. Chwalla[7], C. Klempt[8] and the JRP-EXL01 collaboration

[1]LNE-SYRTE, Observatoire de Paris, LNE, CNRS, UPMC, Paris, France
[2]Laboratoire National de Métrologie et d'Essais (LNE), Paris, France
[3]National Physical Laboratory (NPL), Teddington, United Kingdom
[4]Physikalisch-Technische Bundesanstalt (PTB), Braunschweig, Germany
[5]Istituto Nazionale di Ricerca Metrologica (INRIM), Torino, Italy
[6] LP2N, Institut d'Optique Graduate School, Bordeaux, France
[7]Institute for Quantum Optics and Quantum Information (IQOQI), Innsbruck, Austria
[8]Leibniz Universität Hannover, Hannover, Germany

Email: sebastien.bize@obspm.fr

The best optical clocks today have accuracies around 1 part in 10^{17}. Accuracies of 10^{-18} will be possible in the near future. However, investigating the physical phenomena, understanding the associated shifts of the clock frequency and using clocks at the 10^{-18} level is currently hindered by the prohibitively long averaging time needed to measure at this level. In current state-of-the-art systems, the stability is limited by two main causes, depending on the type of system. One limitation arises from the limited number of particles used for the clock, via the standard quantum projection noise, which is inversely proportional to the square root of the number of particles. The second limitation (called Dick effect) is due to the large amount of dead time of the sequence used to probe the clock transition combined with the probe laser frequency noise. This dead time is associated with the need to gather, to cool and to prepare atoms before the probe period and to detect the atomic state after probe period.

The use of quantum-entangled states can provide a mean to overcome these limitations. In this poster, we will give an overview of the recently started JRP-EXL01 project of the European Metrology Research Program (EMRP) aimed at exploring these possibilities. Limitations faced by optical clocks are reminiscent of limitations in other atom-based sensors, such as accelerometers, gravimeters, gyrometers or magnetometers. The research undertaken within JRP-EXL01 will benefit all these sensors. JRP-EXL01 is designed to account for the need of these sensors and more generally, to maximize exchanges and cross-fertilization between optical clocks and several other fields: atom interferometry, quantum gases, quantum information processing.

The EMRP is jointly funded by the EMRP participating countries within EURAMET and the European Union.

IFCS-EFTF6-PCD6-19

A Space-Based Optical Kennedy-Thorndike Experiment Testing Special Relativity

Thilo Schuldt[1,2], Sven Herrmann[2], Deborah Aguilera[1,2], Klaus Döringshoff[3], Ruven Spannagel[1,2], Claus Lämmerzahl[2], Achim Peters[3], Bernd Biering[1], Hansjörg Dittus[1], Claus Braxmaier[1,2]

[1]DLR Institute for Space Systems, Bremen, Germany
[2]Center for Applied Space Technology and Microgravity (ZARM), University Bremen, Germany
[3]Institute for Physics, Humboldt-University Berlin, Germany

Email: claus.braxmaier@dlr.de

We propose a small satellite mission that aims for testing the foundations of special relativity by performing a Kennedy-Thorndike (KT) experiment. A potential boost anisotropy of the velocity of light is measured by comparing a length reference (i.e. a highly stable optical resonator) with a molecular frequency reference. By employing clocks with $1*10^{-16}$ frequency stabilities at orbit time (~90 min) and by integration over 5000 orbits (corresponding to a 2 year mission lifetime with 50% duty cycle) a 1000-fold improvement in measuring the Kennedy-Thorndike coefficient is targeted, compared to the current best terrestrial test.

The experiment uses state-of-the-art laser technology. For realizing a small satellite compatible payload, the use of diode-laser technology is favorable and currently already under investigation with respect to other space experiments. A laser wavelength of 1016nm is foreseen as its second harmonics accesses narrow linewidth transitions in molecular iodine. For the KT experiment, one laser is stabilized to a high finesse cavity and a second laser is frequency doubled to a wavelength of 508nm and stabilized to a hyperfine transition in molecular iodine. Both lasers are directly compared in a beat measurement and analyzed with respect to a possible boost dependency of the speed of light.

In the last years, we realized an iodine-based frequency reference at a wavelength of 532nm on elegant breadboard (EBB) level where a frequency stability of $3*10^{-15}$ at 1000s integration time was demonstrated in a beat measurement with a laboratory-type cavity setup. In a current activity the iodine frequency reference is further developed with respect to compactness and thermal and mechanical stability. A compact iodine setup on engineering model (EM) level is currently developed using a fused silica baseplate with dimensions of 18cm x 35cm x 4cm, where the optical components are directly glued to, and a 10cm x 10cm iodine cell in nine-path configuration. The EM setup will be subjected to environmental tests such as vibration and thermal cycling. Using a corresponding laser system, the EM design can easily be adjusted to a wavelength near 508nm, where molecular iodine offers hyperfine transitions with more narrow linewidths than at 532nm, leading to a further increase in frequency stability by up to one order of magnitude.

In a parallel activity, the development of a space compatible optical resonator setup with a resonator finesse of 10^5 and a controlled temperature stabilization at the ~1µK level is planned.

Techniques for laser frequency stabilization are key technologies not only for the proposed KT experiment mission but also for a variety of other future space missions such as LISA/NGO, GRACE-FO, and missions using aperture-synthesis such as Darwin/TPF.

IFCS-EFTF6-PCD6-20

AOM-RN: an acousto-optic modulator extending the tools employed in laser spectroscopy as optical phase modulators

V.N. Baryshev

FGUP "VNIIFTRI", Mendeleevo, Moscow Region, Russian Federation

Email: baryshev@vniiftri.ru

This report completes the series of studies [1 and references therein] devoted to the experimental demonstration and justification for applying AOM-RN as a phase modulator in frequency modulation (FM) heterodyne spectroscopy of optical resonances. Fabricated at VNIIFTRI AOM-RN design is significantly simplified and its dimensions are minimized due to a decrease (by almost an order of magnitude in comparisons with existing AOMs) in the acousto-optic interaction length and the absence of impedance matching circuit (fig. 1).

The AOM-RN has the following advantages over electro-optic phase modulators (EOM): compactness, low energy consumption, wide range of modulation frequencies, and the absence of necessity to control the input and output polarizations.

The report is mainly devoted to the experimental confirmation of the last statement. Since the existing EOMs do not produce a pure FM spectrum due to the residual amplitude modulation (RAM) arising from étalon effects and birefringence properties of the electro-optic crystals [2], one has to control the polarization of the input and output beams and to angling the laser beam incidence onto the EOM in order to remove the residual amplitude noise. An investigation of the RAM, étalon and birefringence effects in particular case of AOM-RN based on the TeO_2 monocrystal with shortened to 2 mm acousto-optic interaction length will be presented.

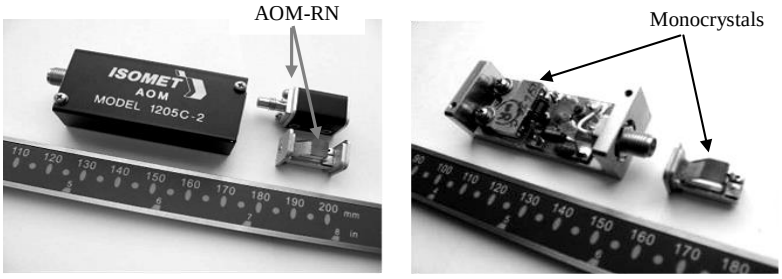

Fig. 1. The photographs of commercial AOM of "ISOMET" model 1205C-2 and AOM-RN without impedance matching circuit.

[1] V. Baryshev, V. Epikhin, S. Sliusarev, "Use of AOM-RN as a Phase Modulator in FM Sideband Heterodyne Technique in the Atomic Frequency Standards", *In Proc. of 2011 Joint Conference of the IEEE IFCS & EFTF*, San-Fransisco, California, USA, pp. 709-712, 2011.

[2] E. Whittaker, M. Gehrtz, and G. Bjorklund, "Residual amplitude modulation in laser electro-optic phase modulation", *J. Opt. Soc. Am. B*, vol. 2, No. 8, 1320-1326, 1985.

IFCS-EFTF6-PCD6-21

High performance laser stabilization using a Ramsey-Borde spectrometer

A. D. Ludlow[1], R. W. Fox[1], J. A. Sherman[1], J. B. Olson[1,2], E. de Carlos-Lopez[1,3], W. Douglas[1], C. W. Oates[1]

[1]Time & Frequency Division, National Institute of Standards and Technology, Boulder, Colorado USA
[2]Department of Physics, University of Colorado, Boulder, Colorado USA
[3]Centro Nacional de Metrologia, Queretaro, Mexico

Email: ludlow@boulder.nist.gov

Optical atomic clocks, coherent optical transfer and communication, and low-phase noise optical signal generation and division require highly-phase-stable optical sources. Commonly, these sources are derived from lasers that are phase or frequency stabilized to high finesse optical cavities. Such stabilized lasers have achieved fractional frequency instability approaching the $1x10^{-16}$ level. These state-of-the-art stabilized-lasers are sensitive to a fundamental limitation caused by Brownian thermal-mechanical noise of the optical cavity components, which complicates the continued improvement in the performance of these systems.

Here, we explore an alternative approach to high performance laser stabilization by implementing a high resolution atomic-beam spectrometer. The spectrometer employs 4-zone Ramsey-Borde spectroscopy of the $^1S_0$-$^3P_1$ transition in a thermal beam of calcium. We observe Doppler-free lineshapes with < 5 kHz resolution, comparable to the mode linewidth of high finesse optical cavities. Furthermore, the system is designed to achieve very high signal to noise ratio (S/N). By collecting fluorescence decay from the $^3P_1$ state at 657 nm after the Ramsey-Borde interrogation, we have observed a S/N approaching 1000 at 1 s. Under such conditions, the atom-stabilized laser exhibits an instability as good as $5x10^{-15}$ at 1 second. Such a system could serve as a simple, one-laser high stability frequency reference for a variety of precision timing applications. Furthermore, we have constructed a laser system at 431 nm as part of an improved detection scheme using the $^3P_1$-$^3P_0$ cycling transition, capable of enhancing the S/N by more than an order of magnitude. Together with additional efforts to enhance detection efficiency and reduce the observed Ramsey linewidth to less than 2 kHz, this system has the potential for stability competitive with the best cavity-stabilized lasers.

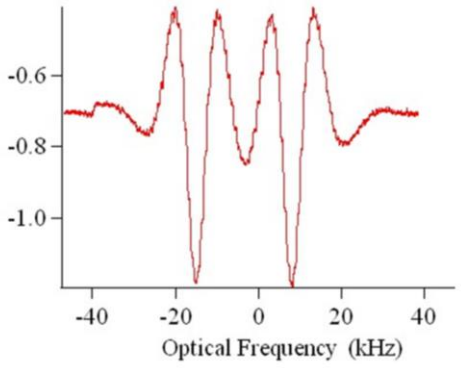

Fig. 157: Ramsey-Borde fringes from the calcium spectrometer used for laser stabilization. The fringe resolution of 4.5 kHz gives clear visibility of the recoil doublet.

Space missions and clocks II

CLUB H

Thursday, July 25 2013, 08:30 am - 10:00 am

Chair: **Kurt Gibble**
Penn State

IFCS-EFTF3-K1-1

Status of the flight model of the cold atoms space clock PHARAO

Igor MORIC [1], Philippe LAURENT [1], Michel ABGRALL[1], Pierre LEMONDE[1], Giorgio SANTARELLI[1], André CLAIRON[1], Sébastien BIZE[1], Daniele ROVERA[1], Jocelyne GUÉNA[1], Christophe SALOMON[2], Frédéric PICARD[3], Olivier GROSJEAN[3], Christophe DELAROCHE[3], Jean-François VÉGA[3], Benoît LÉGER[3], Muriel SACCOCCIO[3], Isabelle ZENONE[3], Benoît FAURE[3], Christian SIRMAIN[3], Didier MASSONNET[3], Sylvie LÉON[3], Serge BÉRAUD[3], Fabrice BUFFE[3], Philippe LARIVIÈRE[3], Claude ESCANDES[3], Nadine LADIETTE[3], Bernard VIVIAN[3], Didier BLONDE[3], Michel CHAUBET[3], Clément LUITOT[3], Philippe CHATARD[4],Charles Marie DE GRAEVE[4], Christian MACÉ[5], Stéphane THOMIN[5], Jean Pierre LELAY[5], Thierry POTIER[6], Yoann COSSART[6], Thierry NAULEAU[7], Arnaud GRANGET[8].

[1] LNE-SYRTE, 61 av. de l'Observatoire, 75014 PARIS, France.

[2] Laboratoire Kastler-Brossel, CNRS, 24 rue Lhomond, 75231 PARIS, France.

[3] CNES, 18 avenue Edouard Belin, 31401 TOULOUSE Cedex, France

[4] Sogeti, 24, rue du Gouverneur Général Eboué
92136 Issy-les-Moulineaux Cedex, France

[5] Sodern, 20 Avenue Descartes,B.P. 23, 94451 LIMEIL-BREVANNES Cedex, France.

[6] THALES, 2 avenue Gay-Lussac, 78851 ELANCOURT Cedex, France

[7] CS SI, ZAC de la Plaine – Rue Brindejonc des Moulinais, – BP 5872, 31506 TOULOUSE Cedex 5, France

[8] EREMS, Chemin de la Madeleine, ZI, 31130 FLOURENS, France.

PHARAO (Projet d'Horloge Atomique par Refroidissement d'Atomes en Orbite), which is being developed by the French space agency CNES, is the first Primary Frequency Standard (PFS) specially designed for operation in space. PHARAO is a main instrument of the ACES (Atomic Clock Ensemble in Space) mission. ACES is being developed by ESA and the payload will be installed on-board the International Space Station. The mission is based on comparisons with ground based clocks to perform fundamental physics experiments: gravitational redshift measurements, analysis of the stability of the fundamental constants and anisotropy of light. Planned duration of the mission is 18 months with a possible extension to 36 months. The frequency accuracy requirement for PHARAO is less than 3×10^{-16} and the expected frequency stability is $10^{-13}\tau^{-1/2}$.

An engineering model of PHARAO has been constructed and fully tested to validate the clock architecture. Two sub-systems for the flight model(FM) have been delivered: the cesium tube where the atoms are manipulated and the microwave source which generates the 9.2 GHz signals. The other sub-systems, the laser source and the computer, will be delivered this year. In this talk we will present the preliminary tests performed on the FM cesium tube and on the FM microwave source. To operate the cesium tube with cold atoms, it has been connected to the engineering model of the laser source. The goal is to measure the magnetic and thermal properties of the cesium tube in the orbit-like magnetic and thermal environments and deduce the blackbody radiation and the second order Zeeman correction uncertainties. Other effects will be evaluated when the whole FM clock is assembled.

IFCS-EFTF3-K1-2

Lifetime of Space Passive Hydrogen Maser

Qinghua Wang, Pierre Mosset, Fabien Droz, Pascal Rochat

Orolia Switzerland Inc, Neuchatel, Switzerland

Email: qinghua@spectratime.com

Accurate and ultra-stable space qualified atomic clocks represent critical equipment for the precision global navigation satellite systems. The Passive Hydrogen Maser (PHM), with its excellent frequency stability performance, is the master clock for European Galileo navigation payload, and is the first one of its type ever to fly. The PHM technology has flight heritage of several years through Galileo satellites (GIOVE-B and four IOV satellites) since Apr. 2008. More than thirty PHM flight physics packages have been manufactured and characterized by SpectraTime (under the industrial consortium led by Selex ES S.p.A).

Besides radiation effects on electronic components, lifetime in PHM depends on the lifetime of the physics package. In the frame of the "Lifetime Qualification of the PHM", two Qualification Model (QM) units had been subjected to test under vacuum since 2008. After the first 1.5-year test period as reported in previously published papers[475,476], one QM has been extended for another 2-year lifetime test. This paper provides test results of the overall period, and gives further comparison and analysis of key parameters of the physics package for 3.5 years of operation or 4 years including stay-alive period. The extended test provides additional statistical element, and obtains valuable results and better confidence to PHM lifetime evaluation, showing the compliance with Galileo requirements.

475 F. Droz, P. Mosset, Q. Wang, P. Rochat, M. Belloni, M. Gioia, A. Resti, and P. Waller, "Space Passive Hydrogen Maser – Performances and lifetime data", Proceedings of the Joint 2009 European Frequency and Time Forum & 2009 IEEE Frequency Control Symposium, 20-24 April, 2009, Besançon (France), pp 393-398.

476 M. Belloni, M. Gioia, S. Beretta, F. Droz, P. Mosset, Q. Wang, P. Rochat, A. Resti, P. Waller, and A. Ostillio, "Space Passive Hydrogen Maser - Performances, Lifetime Data and Giove-B Related Telemetries", 41st Precise Time and Time Interval (PTTI) Systems and Applications Meeting, 16-19 Nov. 2009, Santa Ana Pueblo (USA).

IFCS-EFTF3-K1-3

STE-QUEST: Atomic sensors in space for fundamental physics, time and frequency metrology and other applications

P. Tuckey[1] for the STE-QUEST collaboration[477]

[1]LNE-SYRTE, Observatoire de Paris, CNRS, LNE, UPMC, Paris, France

Email: philip.tuckey@obspm.fr

STE-QUEST – Space-Time Explorer and Quantum Equivalence Principle Space Test – is a candidate mission for the M3 flight opportunity of the European Space Agency's Cosmic Vision 2012-2025 programme (see http://sci.esa.int/ste-quest). STE-QUEST is currently undergoing a phase A study, in view of a possible launch in 2022-2024. This mission is designed to test different aspects of the Einstein Equivalence Principle: the gravitational time dilation effect and the universality of free fall in the case of matter waves, and to carry out studies on a variety of other subjects: atomic time scales, high-precision long-distance ground clock comparisons, long-distance relative geopotential measurements, microwave and optical ranging, cold-atom physics, etc. To achieve these objectives, the payload includes an atomic frequency standard, microwave and optical time and frequency links and an atom interferometer. This paper proposed here will discuss the mission objectives and present the results obtained thus far in the ongoing study.

The STE-QUEST clock is a modified version of the PHARAO clock, presently being developed in the frame of the ACES mission. In order to maximize the benefit of the PHARAO heritage, it has been decided to also use a Caesium clock for STE-QUEST, meaning that the physics and laser packages will be very similar to those of PHARAO. The local oscillator will however be significantly improved, using a femtosecond comb to down-convert the optical frequency from a laser stabilized on a high finesse cavity. The on-board clock aims to achieve an instability of $8\times10^{-14}\ t^{-1/2}$ at long times, where t is the integration time, and an inaccuracy of the order of $1\text{-}2\times10^{-16}$. High performance links, both in the microwave and optical domains, will compare the space clock with clocks on the ground. A highly elliptical orbit has been chosen in order to provide access to a strong gravitational time dilation effect at the apogee, as well as a significant modulation of this effect at the perigee, with the aim of measuring the effect due the field of the Earth to an inaccuracy of 2×10^{-7}. A consequence of this strategy is a quite harsh radiation environment for the payload instruments. STE-QUEST will also perform common-view comparisons of terrestrial clocks located on different continents and it will measure the periodic effect of the gravitational frequency shifts induced by the Sun and the Moon.

Concurrently to the clock measurements, a two-isotope matter-wave interferometer will measure the differential acceleration between two Bose-Einstein condensates composed respectively of ^{85}Rb and ^{87}Rb atoms. The atom interferometry measurement will be particularly important around perigee, where the signal-to-noise ratio of a possible violation of the Weak Equivalence Principle can be maximized. This instrument will test the universality of the free propagation of matter waves to an uncertainty in the Eötvös parameter of the order of 2×10^{-15}.

[477] The STE-QUEST collaboration is rather large compared with the format of the abstract; a full author list will be provided with the paper.

IFCS-EFTF3-K1-4

ACES data simulation and data analysis: an update

P. Wolf[1], P. Delva[1], C. Le Poncin Lafitte[1], F. Meynadier[1]

[1]LNE-SYRTE, Observatoire de Paris, CNRS, UPMC, Paris, France

Email: peter.wolf@obspm.fr

The Atomic Clocks Ensemble in Space (ACES/PHARAO mission), which will be installed on board the International Space Station (ISS), uses a dedicated two-way MicroWave Link (MWL) in order to compare the timescale generated on board with those provided by many ground stations disseminated on the Earth. The phase stability of this long range link is specified to reach 0.3 ps after 300 s integration time, with long term stability better than 7 ps over 10 days. This link will play a key role in the success of the ACES/PHARAO experiment.

The SYRTE laboratory is heavily involved in the design and development of the data processing software : from theoretical modeling and numerical simulations at the required precision to the development of the SYRTE data analysis software. Our team is working on a wide range of problems that need to be solved in order to achieve the required stability in (almost) real time.

We present some key aspects of the measurement, as well as current status of the software's development, including the results of tests with simulated data. We put particular emphasis on the scientific products that will be provided to the users and discuss how those products can be used for the purposes of time/frequency metrology.

IFCS-EFTF3-K1-5

Next Generation JPL Ultra-Stable Trapped Ion Atomic Clocks

Eric Burt, Blake Tucker, Kameron Larsen, Robert Hamell, John Prestage, and Robert Tjoelker

Jet Propulsion Laboratory, California Institute of Technology, Pasadena, CA

Email: eric.a.burt@jpl.nasa.gov

Over the past decade, trapped ion atomic clock development at the Jet Propulsion Laboratory (JPL) has proceeded in two parallel directions: 1) new atomic clock technology for space flight applications that require strict adherence to size, weight, and power requirements, and 2) ultra-stable atomic clocks, usually for terrestrial applications focusing on ultimate performance. In this paper we will present first results from two new ultra-stable trapped ion clocks in the second category currently under development.

The new identical clocks, designated L10 and L11, build on the successful demonstration of exceptionally low drift at the 3×10^{-17}/day level[478] by their predecessor, LITS-9, with changes in design intended to improve ultimate long-term performance. The first will be delivered to the Naval Research Lab, while the second, and eventually a third and fourth designated L12 and L13, will be retained as in-house standards at JPL.

The excellent long-term stability of LITS-9, and the anticipated equivalent or better performance of L10 and L11, has both engineering and scientific applications. It will be invaluable for characterizing the performance of flight clocks both at JPL and at NRL, as well as that of clocks being delivered to, and operated in NASA's Deep Space Network. In addition, L11 will also be used as a reference for an ACES ground station[479] at JPL when the ACES laser-cooled atomic clock becomes operational on the International Space Station in the 2016 time frame.

L10 with inner magnetic shield installed.

As with LITS-9, L10 and L11 use a quadrupole trap for loading ions and a separate 12-pole[480] trap for sensitive microwave clock interrogation that greatly reduces one of the largest systematic effects in this type of clock, the second order Doppler (SOD) shift. A key additional enhancement to LITS-9 was the use of magnetic compensation to reduce the SOD by a further order of magnitude[1]. The newer clocks use an improved version of magnetic compensation fully integrated into the design. Other enhancements include a sealed vacuum system bakeable to 450 C for improved stability of background gases, improved magnetic field uniformity, enhanced microwave coupling, improved optical efficiency, and a dedicated FPGA-based controller for better reliability.

The new standards are being assembled and tested in parallel. At present, we have observed a narrow clock transition in the L11 multi-pole trap and have observed trapped ions in the quadrupole trap of L10. In this paper we will describe the improvements to L10 and L11 that focus on better long-term performance and show the first results obtained from operating the new standards.

---

[478] E.A. Burt, W.A. Diener, and R. L. Tjoelker, IEEE Trans. UFFC **55**, 2586 (2008)

[479] E. Daganzo, et al., Proceedings of the 2009 joint IFCS-EFTF, 1146 (2009)

[480] J.D. Prestage, R.L. Tjoelker, and L. Maleki, Proceedings of the 1999 joint IFCS-EFTF, 121 (1999)

Optical fiber T+F Transfer III

CLUB E

Thursday, July 25 2013, 08:30 am - 10:00 am

Chair: **Anne Amy-Klein**
LPL

A 30-km-long optical fiber link for frequency comparison between distant strontium optical lattice clocks

Tomoya Akatsuka[1,2], Hitomi Ono[1,3], Keitaro Hayashida[1,3], Kuniya Araki[1,3], Masao Takamoto[1,2], Tetsushi Takano[1,3], and Hidetoshi Katori[1,2,3]

[1]Innovative Space-Time Project, ERATO, JST,
7-3-1 Hongo, Bunkyo-ku, Tokyo 113-8656, Japan
[2]Quantum Metrology Laboratory, Advanced Science Institute, RIKEN,
2-1 Hirosawa, Wako, Saitama 351-0198, Japan
[3]Department of Applied Physics, Graduate School of Engineering, The University of Tokyo,
7-3-1 Hongo, Bunkyo-ku, Tokyo 113-8656, Japan

Email: akatsuka@riken.jp

Recently, frequency comparison between two Sr optical lattice clocks demonstrated the quantum projection noise (QPN) limited stability of a few times $10^{-16}\tau^{-1/2}$ by synchronously operating the two clocks[481]. Further improvement by more than one order of magnitude is promising in the near future. Such a clock stability enables to probe the relativistically-curved space-time in real time. Because of its sensitivity to the gravitational potential, frequency comparison between two clocks operating at distant sites allows monitoring temporal fluctuation of the gravitational potential difference, which can lead to new applications in relativistic geodesy[482]. Coherent optical frequency transfer via optical fiber networks serves as an essential technique for frequency link between distant sites, though the link stability deteriorates as the fiber length increases because of the uncompensated fiber noise due to time delay[483]. In order to demonstrate frequency comparison between distant clocks at the stability of $10^{-17}\tau^{-1/2}$, we have developed a 30-km-long optical fiber link between Riken and the University of Tokyo located 15 km apart from each other.

Since we focus on frequency comparison between two Sr optical lattice clocks operating with 698 nm clock lasers, we implemented a novel scheme utilizing a 1397 nm transfer light which directly links to the clock frequency by the second harmonic generation (SHG). This scheme avoids the need of operating optical frequency combs where associated phase noises have to be analyzed carefully. Although conventional single-mode fibers have water-peak attenuation due to OH radical around 1383 nm, it is not a serious problem for the 30-km-long fiber, which causes additional transmission loss of 7 dB compared with 1550 nm light. In the future, OH-free fiber will be more popular for coarse wavelength division multiplexing (CWDM) application, which allows the frequency transfer in longer distance at this wavelength. Our scheme provides a simple platform for networking Sr optical lattice clock which has already become the most widespread optical clock.

We demonstrate an optical beat measurement between two clock lasers operating at the distant sites via the fiber link. The link stability was evaluated to be a few times of 10^{-17} for an averaging time of 1 s, which encourages the frequency comparison between distant clocks.

---

[481] M. Takamoto, T. Takano, and Hidetoshi Katori, "Frequency comparison of optical lattice clocks beyond the Dick limit", Nat. Photon., vol. 5, p. 288-292, 2011.

[482] H. Katori, "Optical lattice clocks and quantum metrology", Nat. Photon., vol. 5, p. 203-210, 2011.

[483] N. R. Newbury, P. A. Williams, and W. C. Swann, "Coherent transfer of an optical carrier over 251 km", Opt. Lett., vol. 32, p. 3056-3058, 2007.

IFCS-EFTF5-K2-2

Optical Frequency Transfer over a single-span 1840 km Fiber Link

S. Droste,[1] F. Ozimek,[2,3] S. M. F. Raupach,[2] H. Schnatz,[2] G. Grosche,[2]
T. W. Hänsch,[1] Th. Udem,[1] and R. Holzwarth[1]

[1]Max-Planck-Institut für Quantenoptik, Hans-Kopfermann-Str. 1, 85748 Garching, Germany
[2]Physikalisch-Technische Bundesanstalt, Bundesallee 100, 38116 Braunschweig, Germany
[3]University of Warsaw, Faculty of Physics, ul. Hoza 69, 00-681 Warszawa, Poland

Email: stefan.droste@mpq.mpg.de

The development of optical frequency standards[484] raises a demand for transferring highly stable optical signals over continental distances. Such transfer would enable new experiments[485], and will be mandatory for a future redefinition of the SI-second based on optical frequency standards. We investigate optical frequency transfer via a 1840 km fiber link connecting Physikalisch-Technische Bundesanstalt (PTB) and Max-Planck-Institute of Quantum Optics (MPQ). The link consists of a pair of dark fibers[486], and is set up in a loop configuration with sender and receiver located at MPQ. It thus involves a single-span 1840 km stabilization. We use 20 Erbium-doped fiber amplifiers, and a fiber Brillouin amplifier at each institute, compensating for 420 dB loss.

Fig. 1 shows the instability of the transferred frequency after 1840 km of fiber for the stabilized fiber link, expressed as the Allan deviation (ADEV) and the modified ADEV. The servo bandwidth for the suppression of fiber-induced noise is limited to about 27 Hz due to the propagation delay of the light of around 18 ms. However, the low intrinsic noise of the fiber link together with active noise cancellation allow us to reach instabilities (modified ADEV) of 2.7×10^{-15} at 1 s, and about 4×10^{-19} after 100 s of integration time. The noise of the link peaks around 15 Hz and is lower at smaller frequencies which leads to a τ^{-2} dependency in the modified ADEV as shown in Fig. 1.

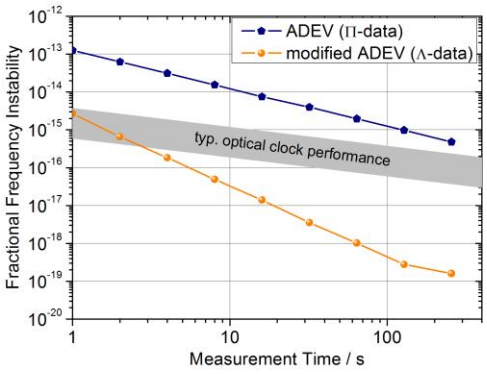

Fig. 158: Fractional frequency instability of the 1840 km stabilized link (squares) expressed as the ADEV. To distinguish between white phase, flicker phase and other noise types the modified ADEV (solid circles) is also shown.

To assess potential systematic frequency shifts, we analyzed the mean deviation of the transferred frequency from the input frequency, and found agreement within the statistical uncertainty of 2.6×10^{-19}. The results illustrate that for a remote comparison of state-of-the-art optical clocks, the short-term instability contribution of the stabilized ~2000 km link is negligible within one minute of integration time.

This work was supported by the European Metrological Research Programme EMRP under SIB-02 NEAT-FT. The EMRP is jointly funded by the EMRP participating countries within EURAMET and the European Union.

[484] N. Huntemann, et al., Phys. Rev. Lett. 108, 090801 (2012).

[485] C. W. Chou, et al., Science 329, 1630 (2010).

[486] K. Predehl, et al., Science 336, 441 (2012).

IFCS-EFTF5-K2-3

Distributed Raman Amplification for long-haul optical frequency dissemination

C. Clivati[1,2], G. Bolognini[3], D. Calonico[1], G. A. Costanzo[1,2], S. Faralli[4], F. Levi[1], A. Mura[1], N. Poli[5]

[1]Istituto Nazionale di Ricerca Metrologica, Torino, Italy
[2]Politecnico di Torino, Torino, Italy
[3] Consiglio Nazionale delle Ricerche, IMM Institute, Bologna, Italy;
[4] Scuola Superiore S. Anna, Istituto TeCIP, Pisa, Italy;
[5] Dip. di Fisica e Astronomia and LENS, Università di Firenze, INFN, sezione di Firenze, Italy

Email: c.clivati@inrim.it

Phase-compensated optical links are the most performing technique to disseminate optical frequencies on a continental scale[1,2]. Most National Metrology Institutes are thus cooperating to realize a pan-European fiber network, that will enable optical clocks comparisons at unprecedented levels of accuracy and stability. Dedicated amplification systems are thus needed, that have to be fully bidirectional to allow the compensation of the fiber phase noise. Bidirectional Erbium Doped Fiber Amplifiers are used, but their gain is limited by the back-reflections along the path, that may lead the amplifier to oscillate. Distributed Brillouin Amplifiers are much promising from this point of view[3]. We demonstrate that Distributed Raman Amplification (DRA) is a reliable technique as well, not degrading the transfer of the optical carrier at the 10^{-19} level of stability (see Fig. 1), and allowing to bridge hauls of 60 dB losses (i.e. more than 250 km) without intermediate amplification stations[4].

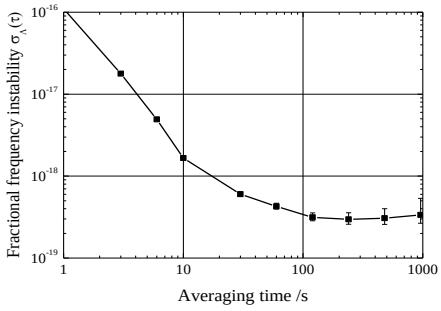

Fig. 159: Fractional frequency stability of the 200 km optical link using DRA.

We implemented DRAs on a 200 km optical link in the laboratory, evaluating gain, signal-to-noise ratio and phase noise added to the carrier. Nonlinear effects have been observed with a not optimized amplifier placement, resulting in degraded amplifier performance. At the conference, we will present the set-up, the results and the perspectives for application on the Italian Optical Fiber Link for Frequency and Time (LIFT).

1. K. Predehl, G. Grosche, S. M. F. Raupach, S. Droste, O. Terra, J. Alnis, Th. Legero,T. W. Hansch, Th. Udem, R. Holzwarth, H. Schnatz, "A 920-Kilometer Optical Fiber Link for Frequency Metrology at the 19th decimal place," Science 336, 441-444 (2012).

2. O. Lopez, A. Haboucha, F. Kefelian, H. Jiang, B. Chanteau, V. Roncin, C. Chardonnet, A. Amy-Klein, G. Santarelli,"Cascaded multiplexed optical link on a telecommunication network for frequency dissemination," Opt. Expr. 18, 16849-16857 (2010).

3 O. Terra, G. Grosche, and H. Schnatz, "Brillouin amplification in phase coherent transfer of optical frequencies over 480 km fiber," Opt. Expr. 18, 16102-16110 (2010).

4. C. Clivati, G. Bolognini, D. Calonico, S. Faralli, F. Levi, A. Mura, N. Poli, arXiv:1211.3910.

IFCS-EFTF5-K2-4

Two Color One-Way Frequency Transfer in an Urban Optical Fiber Network

Sven-Christian Ebenhag* and Per Olof Hedekvist*

SP Technical Research Institute of Sweden, Boras, Sweden

*also with Department of Microelectronics, Photonics Lab

Chalmers University of Technology

Göteborg, Sweden

Email: sven-christian.ebenhag@sp.se

SP Technical Research Institute of Sweden has previously presented results with a two color one- way method. This method is an alternative method to two-way time and frequency transfer that is useful if there are unknown asymmetries in the connection. The method is possible to use in existing infrastructure and is able to coexist with data channels for example in WDM systems, which make it possible to broadcast to multiple users and enables the user to be anonymous to the time or frequency transfer.

This paper will present the results from implementing the technique in an urban commercial optical fiber data communication WDM network between two clock labs in Sweden connecting two cesium clocks to each other for frequency transfer. The evaluation is performed with two wavelengths 8nm apart on 6 km of installed fiber in an urban city network. The transmitter and the receiver are installed in an electromagnetically shielded room several meters below ground, and the fiber runs to a building at a distance of 3 km, and then back again. The comparison will be within the laboratory, eliminating any errors from a reference system. Results and conclusion from this evaluation reveals the propagation delay variations in the propagation distance and will display the need of compensation for these variations.

IFCS-EFTF5-K2-5

Optical Frequency Transfer on Branching Fibre Networks

Sascha W. Schediwy[1], David Gozzard[1], Guido Aben[2], Kenneth G. H. Baldwin[3],Brian J. Orr[4], R. Bruce Warrington[5], Andre Luiten[1,6]

[1]School of Physics, University of Western Australia, Perth, Australia
[2]Australia's Academic and Research Network (AARNet), Perth, Australia
[3]Research School of Physics and Engineering, The Australian National University, Canberra, Australia
[4]Department of Physics and Astronomy, Macquarie University, Sydney, Australia
[5]National Measurement Institute, Sydney, Australia
[6]School of Chemistry & Physics, The University of Adelaide, Adelaide, Australia

Email: sascha.schediwy@uwa.edu.au

Ultra-precise time and frequency transfer via optical-fibre has developed rapidly over the last decade. Most progress has focused on the stabilisation of links between two fixed nodes. Recently a technique that provides stabilised signals at intermediate nodes along a fibre link was proposed for optical-frequency transfer[487] and demonstrated for microwave frequency transfer[488]. Nonetheless, this technique is mainly aimed at fibre networks with a linear topology.

We present a technique that can be used to distribute optical-frequency signals to multiple nodes on a branching optical-fibre network. Optical-fibre fluctuations are corrected at the output of the link rather than at the input. As the transmitted optical signal remains unaltered until it reaches the remote location it can be transmitted to multiple nodes simultaneously. Other techniques can only recreate such a branching network by 'daisy-chaining' stabilised links, thereby requiring that every stabilised link in the chain must be working correctly at all times.

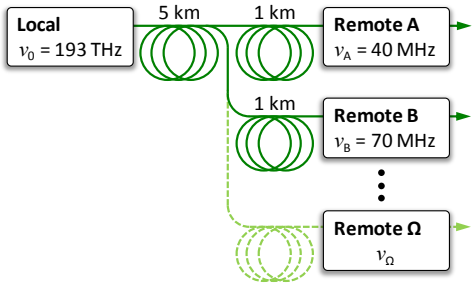

Fig. 160: Experimental implementation of the multibranch optical-fibre stabilisation technique implemented on a two node network (solid green lines); **Remote A** and **Remote B**. The dashed light green lines show an example of further branching.

We investigated this technique experimentally using the simplest configuration that demonstrates all the essential features of a branching network (see Figure 1). For **Remote A**, the out-of-loop fractional frequency stability of the free-running transfer was measured to be $(3.1\pm0.4)\times10^{-14}$ at 1 s of integration. With the **Remote A** stabilisation control engaged, the transfer stability was $(1.1\pm0.1)\times10^{-17}$ at 1 s while **Remote B** was disconnected from the network, and $(1.2\pm0.1)\times10^{-17}$ at 1 s when **Remote B** was included in the network. The equivalent measurement for **Remote B** produced corresponding results. We concluded that the inclusion of the extra node has negligible impact on the transfer stability, and thus the technique lends itself to applications such as the Square Kilometre Array, research campuses, or metropolitan areas where branching fibre networks are the most efficient configuration to transfer signals from a master site to many subsidiary remote nodes.

[487] G. Grosche, "Verfahren zum Bereitstellen einer Referenz-Frequenz," DPMA Patent application DE 10 2008 062,139 (2010).

[488] C. Gao, et al., "Fiber-based multiple-access ultrastable frequency dissemination," Opt. Lett. **37**, 4690-4692 (2012).

IFCS-EFTF5-K2-6

Fiber-based multiple-access ultrastable optical and radio frequency dissemination

Y. Bai[1,3], B. Wang[1,2], C. Gao[1,3], W. L. Chen[4], J. Miao[1,3], X. Zhu[1,3], and L. J. Wang[1,2,3,4]

[1]Joint Institute for Measurement Science, Tsinghua University, Beijing 100084, China
[2]The State Key Laboratory of Precision Measurement Technology and Instrument, Department of Precision Instruments, Tsinghua University, Beijing 100084, China
[3]Department of Physics, Tsinghua University, Beijing 100084, China
[4]National Institute of Metrology, Beijing 100013, China

Email: bo.wang@tsinghua.edu.cn

The multiple-access frequency dissemination is one of key technologies for a time and frequency network. We propose fiber-based multiple-access ultrastable frequency dissemination schemes for radio frequency (RF) and optical frequency, separately.

For the RF dissemination, we build up a time and frequency dissemination system via the 80 km urban telecommunication fiber link between Tsinghua University (THU) and the National Institute of Metrology (NIM) of China[1]. Using the proposed multiple-access RF dissemination scheme, the 9.1GHz disseminated RF signal with relative frequency stability of 7×10^{-14}/s and 5×10^{-18}/day can be reproduced at arbitrary nodes along the entire fiber pathway (as shown in Fig.1). For the optical frequency dissemination, G. Grosche proposed a technique for multiple access optical frequency dissemination in 2010[3]. However, in the scheme, a highly stable laser source whose wavelength is same with the disseminated optical signal is needed at an arbitrary accessing node to reproduce the highly-stable disseminated signal. It makes the system costly and technically complex. In this paper, we propose a more convenient and efficient scheme to solve this problem and the results will be presented in detail during the conference. Optical frequency transfer can provide better stability while the RF dissemination is relatively simple for practical applications. Using this method, we can regenerate the highly synchronized RF signal or the optical signal along the entire fiber link, which is crucial for a time and frequency network.

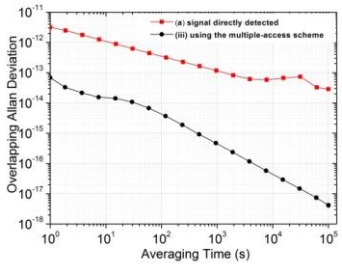

Fig. 161: Measured relative frequency stability of the reproduced 9.1GHz signal at an arbitrary accessing node of the fiber link. (a) signal directly detected, (b) signal obtained using the multiple-access RF dissemination method.

References:

1. B. Wang, C. Gao, W. L. Chen, J. Miao, X. Zhu, Y. Bai, J. W. Zhang, Y. Y. Feng, T. C. Li, and L. J. Wang, Sci. Rep. 2, 556 (2012).
2. C. Gao, B. Wang, W. L. Chen, Y. Bai, J. Miao, X. Zhu, T. C. Li, and L. J. Wang, Opt. Lett. 37, 4690-4692 (2012).
3. G. Grosche, "Verfahren zum Bereitstellen einer Referenz-Frequenz", DPMA Patent application DE 10 2008 062,139 (June 24, 2010).

Novel Frequency Sources

CLUB D

Thursday, July 25 2013, 08:30 am - 10:00 am

Chair: **Michael Tobar**
The University of Western Australia

IFCS-EFTF2-K3-1

Spintronics rf nano-oscillators based on spin transfer induced dynamics of vortex magnetization

E. Grimaldi[1], V. Cros[1], P. Bortolotti[1], A. Dussaux[1], J. Grollier[1], A. Fukushima[2], H. Kubota[2], K. Yakushji[2], S. Yuasa[2], A. Fert[1]

[1]Unité Mixte de Physique CNRS/Thales, Palaiseau, and Université Paris-Sud, Orsay/France
[2]National Institute of Advanced Industrial Science and Technology (AIST), Tsukuba/Japan

Email: vincent.cros@thalesgroup.com

A decade after the first observation of spin transfer (STT) induced magnetization dynamics, tremendous improvements have been achieved for the rf characteristics of spin transfer nano-oscillators (STNOs). Depending on the magnetic configuration and device shape, the emitted frequency goes from 100 MHz up to 50GHz, thus making them promising for integrated telecommunication devices[489]. The key advantages of these spintronics devices are their large frequency tunability, their nanoscale size and their CMOS compatibility, and finally their insensitivity to radiations. STNOs are by nature highly nonlinear oscillators. The understanding of the large coupling between phase and amplitude is thus crucial[490] either to increase the role of nonlinearities to improve the tunability[491] or to cancel the coupling when a stable reference signal with large spectral purity is targeted[492].

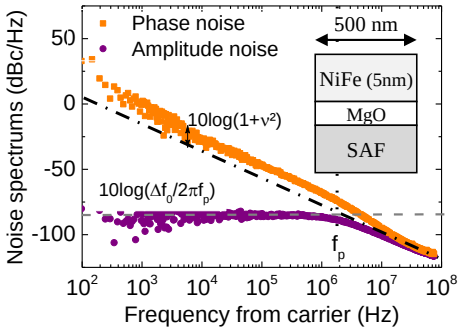

Fig. 1 Phase (grey dots) and amplitude (black dots) noise PDS in dBc/Hz for an external magnetic field of 4.8 kOe and a current of 3.3 mA. Inset: schema of the

Here we focus on STNOs based on vortex magnetization motion in a magnetic tunnel junction made of NiFe (5nm) / MgO (1nm) / Ferromagnetic polarizer (SAF) to investigate this coupling from phase and amplitude noise PDS measurements (Fig.1). In parallel, we derive nonlinear equations of the vortex dynamics[493] in the general framework for nonlinear oscillators[494]. We find that the phase noise is due to both intrinsic phase noise and conversion of amplitude noise into phase noise proportional to the coupling. By the extraction of the parameters and of their dependencies with current and magnetic field, we show that the intrinsic linewidth of the vortex based oscillator is of tenth of kHz which is promising for future applications.

We acknowledge CANON ANELVA for preparing the MTJ films. This work was supported by the ANR through SPINNOVA P2N and EU grant MOSAIC FP7- N°317950. E.G. acknowledges financial support from CNES and DGA.

[489] J.A. Katine, E.E. Fullerton, *J. Magn Magn. Mat.* 320, 1217 (2010)
[490] M. Quinsat et al., *Appl. Phys. Lett.* 97, 182507 (2010), L. Bianchini et al., *Appl. Phys. Lett.* 97, 032502 (2010)
[491] A. Dussaux *et al.*, *Nat. Comm.* 1, 8 (2010)
[492] N. Locatelli et al., *Appl. Phys. Lett.* 98, 062501 (2011)
[493] A. Dussaux *et al.*, *Phys. Rev. B* 86, 014402 (2012)
[494] A.N. Slavin and V. Tiberkevich , *IEEE Trans. Magn.* 45, 1875 (2009)

IFCS-EFTF2-K3-2

Recent Progress and Perspectives of Extremely Low Loss Acoustic Cavities: From Frequency Sources to Artificial Atoms

Maxim Goryachev[1], Michael Tobar[1], Serge Galliou[2]

[1] ARC Center of Excellence for Engineered Quantum Systems, School of Physics, The University of Western Australia, 35 Stirling Highway, Crawley 6009, Australia
[2] FEMTO-ST (UMR CNRS 6174), Département Temps Fréquence
ENSMM 26, Chemin de l'Epitaphe, 25000 Besançon, France

Email: maxim.goryachev@uwa.edu.au

In record low loss regimes at low temperatures[495], Bulk Acoustic Wave quartz resonators could be regarded as acoustic version of famous optical Fabry-Pérot cavities. Indeed, confining phonons in a plate of piezoelectric material is analogous to confining photons between two mirrors. In acoustic resonators, the small volume confinement, high phonon density, and long phonon storage time induce a very strong wave-matter and wave-wave interactions. The current state of affairs suggests that high-quality cryogenic BAW resonators could be a new platform for many physical experiments and system simultaneously being a mechanical resonator and a phonon cavity.

The latest results demonstrate the ability of such devices to have quality factors of above one billion for frequencies up to 400 MHz, and a hundred of million up to 720 MHz. Such results are achieved for very-high overtones (up to 227th) of the longitudinal mode never observed previously.

We briefly discuss basic requirements to achieve extremely high quality factor regimes in acoustic devices discussing main sources of losses. This includes material (two-level system, thermoelastic, Landau-Ruomer losses), surface, design (effective phonon) requirements. Several types of BAW quartz resonators are compared.

Finally, we discuss a range of application of extremely low loss acoustic cavities varying from designing of cryogenic ultra-stable frequency sources to creation of artificial atoms. On one hand, very narrow bandwidths of the cavities (of orders of tens of miliHz) can be exploited to build frequency discriminators for ultra-stable clocks at frequencies close to the laboratory standard (10 MHz). On another hand, high overtones with frequencies above 300 MHz can be cooled down to the ground state with conventional methods (down to 10mK with dilution refrigerators). So, BAW devices have a considerable advantage over traditional mechanical resonators like micro-toroids and membranes which require additional cooling techniques (parametric, sideband cooling). By coupling acoustic cavities to nonlinear elements like Josephson Junctions, quantum bits with extremely high coherence times could be designed. In addition, piezoelectric nature of a cavity can be exploited to create strong photon-phonon coupling regimes of a hybrid systems.

[495] M. Goryachev et al, "Extremely low-loss acoustic phonons in a quartz bulk acoustic wave resonator at millikelvin temperature", Appl. Phys. Lett. vol. **100**, 243504, 2012.

IFCS-EFTF2-K3-3

A Novel Evanescent-Mode Mobius-Coupled Resonator Oscillators

*Ajay K. Poddar, Ulrich L. Rohde,

University of Cottbus, BTU Cottbus 03046, Germany

*Synergy Microwave Corp., Paterson, NJ 07504, USA

Email: akpoddar@synergymwave.com

A novel Mobius-coupled printed resonator oscillators reported in this paper for the application of synthesized signal sources in RADAR and modern microwave communication systems. The concept of the Mobius strips is based on the fact that a signal coupled to a strip shall not encounter any obstruction when travelling around the loop, enables compact high Q-factor resonators. A necessary and sufficient condition for a Mobius surface to be developable is that its Gaussian curvature should everywhere vanish. Given a curve with non-vanishing curvature there exists a unique flat ruled surface (the so-called rectifying developable) on which this curve is a geodesic curve (Figure 1) is described by [1]

$$\vec{x}(s,t) = \vec{r}(s) + t[\vec{b}(s) + \eta(s)\vec{t}(s)] \quad (1)$$

$$\tau(s) = \eta(s)k(s), \quad s = [0,L], t = [-w,w] \quad (2)$$

Where $\vec{r}$ is a parameterization of a strip with r as centerline and of length L and width 2w, where $\vec{t}$ is the unit tangent vector, $\vec{b}$ the unit binormal, k the curvature and τ the torsion of the centerline, the parameterized lines s = const. are the generators, which make an angle β = arc[Tan(1/η)] with the positive tangent direction. The unique properties of Mobius strips, the shape minimizes the deformation energy, which is entirely due to bending, can be described by

$$V = \frac{1}{2} D \int_0^L \int_{-w}^{w} k_1^2(s,t)\,dt\,ds \quad (3)$$

where $D = 2h^3E/[3(1-\nu^2)]$, with $2h$ the thickness of the strip, and E and ν Young's modulus and Poisson's ratio of the material. In this paper, a planar Mobius-coupled resonator oscillator is described, and the method for miniaturization can be applied to tunable filters, antenna and matching networks.

Mobius-Coupled Evanescent-Mode (MCEM) resonators are attractive due to several reasons: the Mobius effect makes them very compact and can support evanescent mode coupling for obtaining Q-multiplier effect at resonant condition, thus low phase noise signal source solutions. Figure1 shows the block diagram and layout of the VCO using MCEM resonators resonator fabricated on low loss RF dielectric substrate material with a dielectric constant of 3.38 and thickness of 22 mils printed structure. Figure (2) shows the measured plot of unloaded Q-factor of MCEM, acts like a Q-multiplier, peaking at 10GHz due to evanescent- mode-coupling. Figure (3) shows the measured phase noise plot: –110dBc/Hz @ 10 kHz offset) from the carrier frequency of 10.24 GHz, which is best phase noise performance reported to date for a given size (0.3x0.3 inches) in planar form.

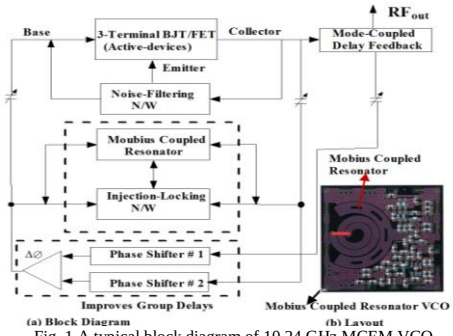

Fig. 1 A typical block diagram of 10.24 GHz MCEM VCO

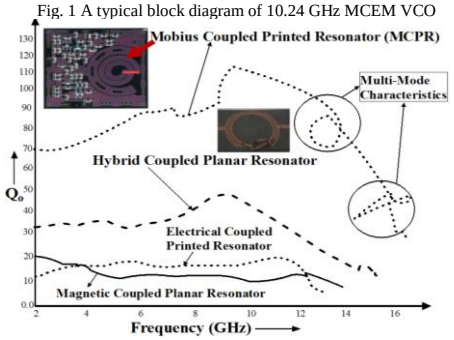

Fig.2 Measured quality factor (Q) of the Mobius coupled resonator

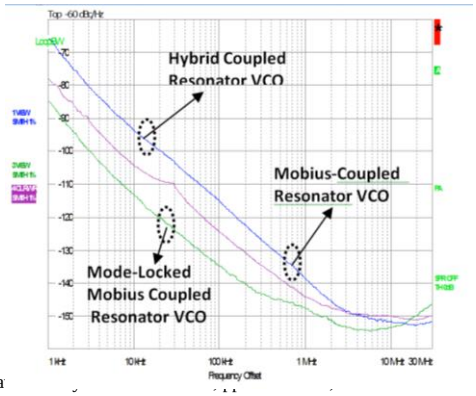

References:

[1] Starostin E.L., van der Heijden G.H.M. (2007). "The shape of a Möbius strip". Nature Materials 6 (8): 563–7. doi: 10.1038/nmat1929.PMID 17632519.

[2] J. M. Pond, "Mobius Dual Mode Resonators and Bandpass Filter", IEEE. Trans. of MTT Vol. 48, Dec 2000, pp 2465-2471.

[3] J.M.Pond, S.Liu, and N.Newman, "Bandpass Filters Using Dual-Mode and Quad-Mode Mobius Resonators," IEEE Trans. on Microwa

Design of Ultra-Low-Power (2.5μW) 1GHz Low Phase Noise Pierce Oscillator with Nanowire NEMS Resonator

Hamidreza Zamani[1], Philip X.-L. Feng[1]

[1]Electrical Engineering, Case Western Reserve University, Cleveland, OH 44016, USA
Email: hamidreza.zamani@case.edu.edu, philip.feng@case.edu

Laterally-vibrating nanowire (NW) resonators with high resonance frequencies f_{res} and electrostatic transduction method are interesting for CMOS timing circuits. However, their motional resistance R_m is often very high, much larger than their rivals FBARs with R_m of several ohms. Since R_m is also proportional to the resonance frequency f_{res}, design of high frequency oscillators are even more difficult. In Pierce oscillators, the minimum MOS transconductance which makes oscillation feasible is[496] $g_{m,min} \propto \omega_{osc}^2 R_m C_1 C_2$ (parameters are identified in Fig. 1a). In this work, we propose and develop a modified architecture using two small (bondwire) inductors (also connecting the nodes to DC bias voltages) which reduce the effective motional resistance seen by the CMOS circuit. The analysis includes novel analytical formulas for design of these modified Pierce-family oscillators working with resonators of initially high-motional resistance. As a proof of concept, we have provided Spectre simulation results for a 1GHz oscillator with *very low power consumption* while having high voltage amplitude at the output (drain of transistor M in Fig. 1a). The mechanical resonator assumed for this simulation is a doubly-clamped Si NW with length, width, thickness and quality factor of respectively 419nm, 20nm, 80nm and 2000. Phase noise and spectral purity performance results are also provided. The specifications in this work are compared to several recent related works. The specifications reported in the Table for other works are measurement results.

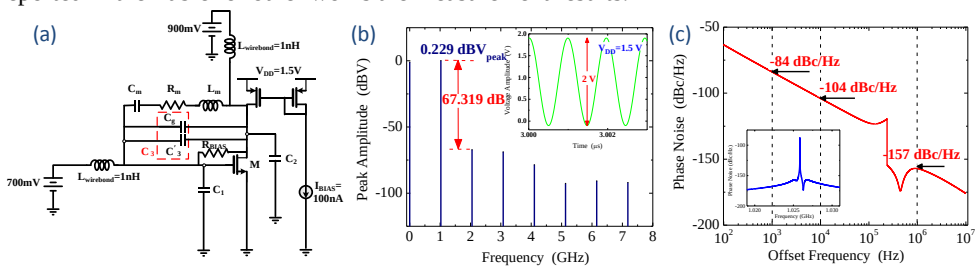

Fig. 162: (a) Schematic of a 1GHz modified Pierce oscillator. (b) Spectral response of the oscillator harmonics compared to the fundamental one. *Inset*: Oscillator output voltage in time domain (not connected to 50Ω load). (c) Phase noise simulation results for offset frequencies around the major oscillation frequency (f_{osc}=1.0256 GHz). *Inset*: Phase noise in a linear (absolute) frequency scale. The frequency resolution of sampling in the inset is lower, which causes difference in the phase noise for frequencies very close to f_{osc}.

	R_m	f_{osc} [GHz]	P_{con}	*Phase Noise* [dBc/Hz]
This work	**13.1MΩ**	1.026	**2.5μW**	-84 (@1kHz), -104 (@10kHz), -157 (@1MHz)
[Zuo-*CICC*][497]	22Ω	1.5	6.9mW	-85 (10kHz), -151 (@1MHz)
[Zuo-*TUFFC*][498]	25Ω	1.05	3.5mW	-81 (@1kHz)
[Lavasani-*ISSCC*][499]	750Ω	1.006	1.9mW	-94 (@1kHz)

[496] E. Vittoz, *Low-Power Crystal and MEMS Oscillators: The Experience of Watch Developments*, Springer 2010.
[497] C. Zuo, J. Van der Spiegel, G. Piazza, "1.5-GHz CMOS…", *CICC2010*, San Jose, CA, 2010.
[498] C. Zuo, J. Van der Spiegel, G. Piazza, "1.05-GHz CMOS…", *IEEE Trans. UFFC*, vol. 57, no. 1, p. 82-87, 2010.
[499] H. H. M. Lavasani, W. Pan, B. Harrington, R. Abdolvand, and F. Ayazi, "A 76dBOhm, 1.7 GHz, 0.18um CMOS tunable transimpedance amplifier…", *ISSCC 2010*, San Francisco, CA, Jan. 2010, p. 318-320.

Lattice Clocks II

CLUB H

Thursday, July 25 2013, 10:30 am - 12:00 pm

Chair: **Patrick Gill**
National Physical Laboratory

IFCS-EFTF6-L1-1

Optical lattice clocks near the QPN limit: A tenfold improvement in optical clock stability

Travis L Nicholson[1], Michael J Martin[1], Jason R Williams[1], Benjamin J Bloom[1], Michael Bishof[1], Matthew D Swallows[2], Sara L Campbell[1], and Jun Ye[1]

[1]JILA, University of Colorado, Boulder, CO USA
[2]AOSense, Sunnyvale, CA USA

Email: nicholtl@jilau1.colorado.edu

Two classes of optical atomic clocks have surpassed microwave frequency standards: single-ion clocks and optical lattice clocks. Single-ion clocks hold the record for the lowest systematic uncertainty[500]; however, many-atom lattice clocks[501] have the potential to outperform single-ion clocks because the standard quantum limit to atomic clock instability (known as quantum projection noise or QPN) scales as $(1/N_{atoms})^{1/2}$. For realistic atom numbers and coherence times, QPN-limited lattice clocks could average down to a given stability hundreds of times faster than the best ion clocks.

Up to now lattice clocks with ~1000 atoms have not shown improvement over the stability of single-ion clocks. Lattice clock stability has been limited by laser noise (via the optical Dick effect). To address this problem, we constructed a new clock laser with a thermal noise floor of 1×10^{-16}—an order of magnitude improvement over our previous clock laser. With this laser, we compare two lattice clocks, reaching instability of 1×10^{-17} in 2000 s for a single clock. This instability is within a factor of 2 of the theoretical QPN limit for ~1000 atoms, representing the lowest reported instability for an independent clock[502].

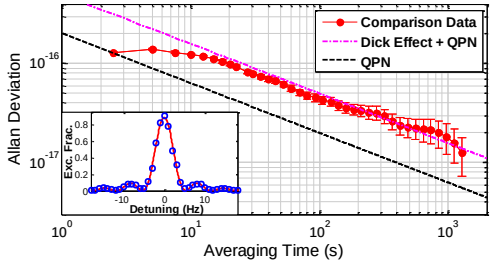

Fig. 163: A comparison between two independent Sr optical lattice clocks. The stability is $4.4\times10^{-16}/\tau^{1/2}$. The inset depicts typical scans of the clock transition (open circles), and the red line is a fit to the data using the Rabi model.

The high stability of many-particle clocks can come at the price of larger systematic uncertainty due to a frequency shift from atomic interactions. To minimize this shift, we use a cavity-enhanced lattice[503] for our second clock. The high circulating power inside the cavity allows for a large trap volume, yielding a density at 2000 atoms that is 27 times smaller (than in our first clock) and permitting us to trap as many as 5×10^4 atoms. For 2000 atoms in our lattice, we measure a value for this shift (which is linear in density) of -3.11×10^{-17} with an uncertainty of 8.2×10^{-19}.

[500] Chou, et al., PRL **104**, 070802 (2010)

[501] Ludlow, et al., Science **319** 1805 (2008)

[502] Nicholson, et al., PRL **109**, 230801 (2012)

[503] Westergaard, et al., PRL **106**, 210801 (2011)

IFCS-EFTF6-L1-2

Comparison of Sr optical lattice clocks at the 10^{-16} level

Jérôme Lodewyck, Chunayn Shi, Ulrich Eismann, M. Gurov, Rodolphe Le Targat

Y. Le Coq, J. Guéna, M. Abgrall, P. Rosenbusch, D. G. Rovera, S. Bize, P. Laurent.

LNE-SYRTE, Observatoire de Paris, CNRS, UPMC, Paris, France

Email: jerome.lodewyck@obspm.fr

In this paper, we present a comprehensive set of high resolution comparisons between optical lattice clocks using strontium atoms and three microwave cesium fountains. Two strontium optical lattice clocks are in agreement with a relative frequency difference of 1.1×10^{-16} between the two apparatuses, compatible with the combined accuracy budget of 1.6×10^{-16}, and a statistical resolution of 2×10^{-17}, reached after a few hours of measurement.

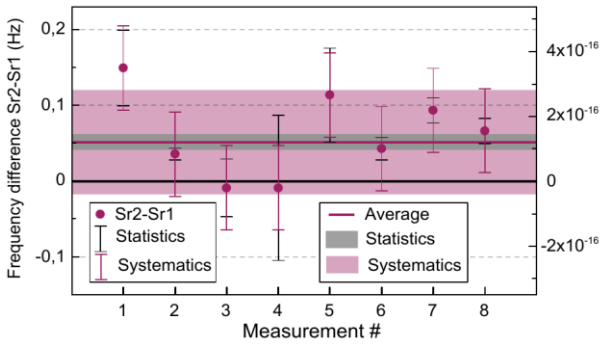

This is the first comparison between two optical lattice clocks at a level beyond what can be achieved by comparing optical clocks through microwave standards. It is a necessary step to confirm the established accuracy budget of these clocks.

The comparison of these clocks with three state-of the art microwave fountains gives a reproducible measurement of the absolute frequency of the Sr clock transition with respect to the SI second. It features record stability (limited by the Quantum Projection Noise of the microwave standards) and accuracy (3.1×10^{-16}).

The consistent set of optical-to-optical and microwave-to-optical clock comparisons presented here is a step towards a possible redefinition of the second with optical references.

Finally, we will discuss prospects for improving the accuracy and stability of strontium optical lattice clocks.

[1] R. Le Targat *et al.*, "Experimenting an optical second with strontium lattice clocks", arXiv:1301.6046 (2013)

IFCS-EFTF6-L1-3

s-Wave Collisional Frequency Shift of a Fermion Clock

Eric L. Hazlett[1], Yi Zhang[1], Ronald W. Stites[1], Kurt Gibble[1] and Kenneth M. O'Hara[1]

[1]Department of Physics, The Pennsylvania State University, University Park, PA, USA

Email: kgibble@psu.edu

We have observed the s-wave collisional frequency shift of an atomic clock based on fermions[504]. As $T \rightarrow 0$, only *s*-wave collisions are allowed. While *s*-wave collisions are allowed for bosons and are the most important limitation for the operation of Cs fountain clocks[505,506], they are forbidden for identical fermions. Even when dephasing made fermions distinguishable, collision shifts were absent[507]. Thus, fermions were thought to be immune to *s*-wave collisional frequency shifts (*s*CFS's), making them ideal for metrology. However, recent theoretical work predicted that fermions have *s*CFS's because excitation field inhomogeneities make particles distinguishable[508].

Here we experimentally observe *s*-wave collisional frequency shifts in a thermal gas of ultracold ^{6}Li fermions. Working near a Feshbach resonance, we tune the *s*-wave scattering length through 0 around 528G. Ramsey spectroscopy clearly distinguishes the novel behaviors of the *s*CFS, via unique dependences on the first and second Ramsey pulse areas, θ_1 and θ_2. We demonstrate that the shift is insensitive to θ_1 and thereby the difference of the spin populations[508], in stark contrast with the shifts for bosons and the often-used mean-field expression. Instead, the fermion *s*CFS depends strongly on θ_2, which reads out the interaction-induced phase shifts of each atom. The shift is canceled if the atoms' phases are detected, on average, with equal sensitivity at $\theta_2=\pi/2$.[508] Interestingly, we show that correlations in the sample perturb the null of the *s*CFS to θ_2 slightly greater than $\pi/2$. We explicitly see that the *s*CFS increases as expected with the independently characterized inhomogeneity of the clock field. The fermion *s*CFS we observe in the resolved sideband regime is analogous to those for optical lattice clocks. Recently, the fermion *s*CFS was simulated with an ^{87}Rb Bose gas[509]. They observed the predicted dependence on θ_2, but an unexpected dependence on θ_1. They elegantly showed a direct link between spin-waves and the fermion *s*CFS, which we observe in the resolved sideband regime.

---

[504] E. L. Hazlett, Y. Zhang, R. W. Stites, K. Gibble and K. M. O'Hara, "*s*-Wave Collisional Frequency Shift of a Fermion Clock," submitted to Phys. Rev. Lett. (arXiv:1212.4385).

[505] K. Gibble and S. Chu, "Laser-Cooled Cs Frequency Standard and a Measurement of the Frequency Shift due to Ultracold Collisions," Phys. Rev. Lett. vol. 70, p. 1771-1774, 1993.

[506] R. Li, K. Gibble and K. Szymaniec, "Improved accuracy of the NPL-CsF2 primary frequency standard: evaluation of distributed cavity phase and microwave lensing frequency shifts," Metrologia vol. 48, p. 283-289, 2011.

[507] M. W. Zwierlein, Z. Hadzibabic, S. Gupta, and W. Ketterle, "Spectroscopic insensitivity to cold collisions in a two-state mixture of fermions," Phys. Rev. Lett. vol. 91, p. 250404, 2003.

[508] K. Gibble, "Decoherence and Collisional Frequency Shifts of Trapped Bosons and Fermions," Phys. Rev. Lett. vol. 103, p. 113202, 2009.

[509] W. Maineult, C. Deutsch, K. Gibble, J. Reichel, and P. Rosenbusch, "Spin waves and Collisional Frequency Shifts of a Trapped-Atom Clock," Phys. Rev. Lett. vol. 109, p. 020407, 2012.

IFCS-EFTF6-L1-4

An Yb optical lattice clock: Current status at KRISS

Dai-Hyuk Yu, Chang Yong Park, Won-Kyu Lee, Sangkyung Lee, Sang Eon Park, Sang-Bum Lee, Jongchul Mun, Myoung-Sun Heo, and Taeg Yong Kwon

Korea Research Institute of Standards and Science, Daejeon, Rep. of Korea

Email: dhyu@kriss.re.kr

Current status of an Yb optical lattice clock at KRISS will be reported. The systematic uncertainty of the Yb clock in the first accuracy evaluation[510] was 5×10^{-14}. The uncertainty was dominated by the large uncertainties in the lattice ac Stark shift and collisional shift, which were mainly limited by the large linewidth and jitter of the clock laser. Recently, highly stable clock laser at 578 nm was developed with a short-term linewidth of 3.5 Hz and frequency jitter of about 25 Hz at 1 s, and 10 s measurement time, respectively. Long-term frequency drift showed only linear dependence on time confirming that the temperature of the super-cavity is maintained at the zero in the coefficient of thermal expansion of the cavity. The frequency of the lattice laser at 759 nm was phase locked to the optical frequency comb and it could be stabilized at the "magic wavelength" within 1 MHz uncertainty. With these and other improvements, new accuracy evaluation is underway and the results will be presented.

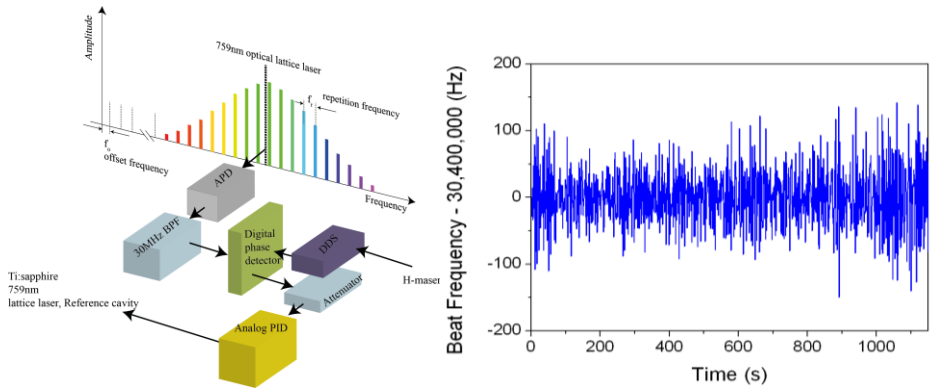

Fig. 164: Experimental setup for the frequency stabilization of the 759 nm laser by using the optical frequency comb and measured beat frequency after stabilization.

[510] C. Y. Park, et al., "Absolute frequency measurement of $^1S_0(F = 1/2)$–$^3P_0(F = 1/2)$ transition of ^{171}Yb atoms in a one-dimensional optical lattice at KRISS", Metrologia, vol. 50, p. 119-128, 2013.

IFCS-EFTF6-L1-5

Nonlinear and Anharmonic contributions to Uncertainties of Optical Clocks on Ultracold Alkaline-Earth-Like Atoms

Vitaly Ovsiannikov[1] and Vitaly Palchikov[2]

[1] Voronezh State University,394006 Voronezh, Russia

[2] FGUP "VNIIFTRI", 141570 Mendeleevo, Moscow Region,Russia

Email: vitpal@mail.ru

The progress in designing optical frequency standards with unprecedented fractional frequency uncertainty at a level 10^{-17} – 10^{-18} requires unprecedented accuracy in estimating the role of different uncertainties of optical clocks[5][11]. In this paper, we systematically evaluate various sources of uncertainty for the alkaline-earth-like-based optical lattice clocks either on odd isotopes or on even isotopes.

The method of determining "magic wavelength"[1], based on measuring the shift of the clock frequency in a weak field of a travelling wave[2] accounts for the Stark shift of energy levels, but only linear in the laser intensity, with inclusion of all multipole-interaction terms. However, the spatial distributions of multipole components in a lattice-atom interaction is not uniform, therefore higher multipole ac Stark shifts are a quarter wavelength out of phase with the electric dipole shift . In a 1D red-shifted MWL lattice, the first-order in the laser-wave intensity I (second order in the electric-field amplitude $\mathrm{E}_0 = 1.68862 \cdot 10^{-7}\sqrt{I}$, where E_0 is measured in *atomic units* and I is in *kW/cm*^{2}) clock frequency shift has a spatial distribution, as follows:

$$\Delta\nu_{cl}^{(2)} = -\Delta\alpha^{E1}\mathrm{E}_0^2\cos^2(k_m X) - \Delta\alpha^{qm}\mathrm{E}_0^2\sin^2(k_m X), \quad (1)$$

where $k_m = 2\pi/\lambda_m$ is the wave number and $\Delta\alpha = \alpha_e(\omega_m) - \alpha_g(\omega_m)$, X is the coordinate along the lattice axis, with the origin in the minimum of the lattice well.

High intensity of the lattice wave makes considerable the contribution of quadratic in I terms, determined by the atomic hyperpolarizabilities $\gamma_{e(g)}(\omega_m)$:

$$E_{e(g)}^{(4)} = -1/4 \cdot \gamma_{e(g)}(\omega_m)\mathrm{E}_0^4\cos^4(k_m X). \quad (2)$$

This term gives quadratic in I contribution to the atomic position-independent shift of the standard frequency. After averaging over the atomic oscillatory motion, the position-dependent part of the standard-frequency shift transforms into a term proportional to $I^{3/2}$, while anharmonic-interaction term transforms into linear in I shift. A significant advance of a lattice with a blue-shifted "magic wavelength" consists in elimination of a position-independent quadratic shift and transformation of hyperpolarizability effects into linear in I, which may be compensated by a slight redefinition of the lattice-laser frequency.

[1] **M. Takamoto, et al.,, "An optical lattice clocks," Nature, vol. 435**, p. 321-328, 2005.

[2] G.Takamoto et al., "Prospects for optical clocks with a blue-detuned lattice," Phys.Rev.Lett., vol. 102, p. 063002, 2009.

Geodesy and Radio Astronomy

CLUB E

Thursday, July 25 2013, 10:30 am - 12:00 pm

Chair: **Demetrios Matsakis**
US Naval Observatory

IFCS-EFTF5-L2-1

On the Importance of Time and Frequency in Geodesy

Ulrich Schreiber[1]

[1]Forschungseinrichtung Satellitengeodaesie,
Technische Universitaet Muenchen,
Muenchen, Germany

Email: schreiber@fs.wettzell.de

According to Friedrich Robert Helmert geodesy is the science of the measurement and mapping of the figure of the Earth. With the advent of the space age it was possible to establish a global reference frame, which can relate different locations across the entire Earth with an accuracy of currently about 1 cm with respect to each other. A rapid development of highly precise and stable frequency standards took place at the same time and is an important prerequisite for the actual quality of this global terrestrial reference frame. Therefore all measurement techniques in modern space geodesy are based on precise time and frequency. Growing demands for the monitoring of global change as one of several examples of the importance of a highly resolved reference frame require more than one order of magnitude improvement over the existing level of quality. Optical clocks, optical frequency combs and near lossless time and frequency transfer have the potential to provide significant improvements of the individual techniques of space geodesy. This talk reviews how time and frequency impacts space geodesy and how the observation techniques may benefit from the recent progress in this field.

IFCS-EFTF5-L2-2

A Fiber Optic Gyroscope on multiplexed telecommunication network with a large enclosed area

C. Clivati[1,2], D. Calonico[1], G. A. Costanzo[1,2], A. Mura[1], M. Pizzocaro[1,2], F. Levi[1]

[1]Istituto Nazionale di Ricerca Metrologica, Torino, Italy
[2]Politecnico di Torino, Torino, Italy

Email: c.clivati@inrim.it

Optical gyroscopes exploiting the Sagnac effect are currently used as optical rotation sensors. Two kinds of devices exist: Fiber Optic Gyroscopes (FOGs) are used in several commercial applications, being very reliable and robust. They are limited by shot noise and typically achieve resolutions of ~10^{-6} rad/s[1]. On the converse, Ring Laser Gyroscopes achieve higher resolution, being able to detect rotation signals well below 10^{-9} (rad/s)/√Hz. They are thus attractive for a detailed study of rotational ground motion induced by teleseismic waves[2,3]. However, they are complex experiments using sophisticated optics.

To combine a simple and robust setup with high-resolution, we realized a FOG enclosing a 20 km^2 area[4] on a 47 km fiber. The fiber is used for the internet data traffic and has a Dense Wavelength Division Multiplexed architecture. The setup is the same as for passive FOGs (see Fig. 1). A laser beam is split into two beams that travel over the loop in opposite directions, acquiring a phase shift that depends on the Earth rotation. After a round trip, the two beams are recombined to detect the Sagnac phase. A well-known technique of non-reciprocal phase modulation is used to this purpose. We developed a closed loop system in which the nonreciprocal phase is compensated inserting a small frequency offset between the two beams. Thanks to its large area, this system could be suitable to detect variations in the Earth rotation rate with a sensitivity of 10^{-8} (rad/s)/√Hz, limited by the non-reciprocal mechanical noise of the fiber.

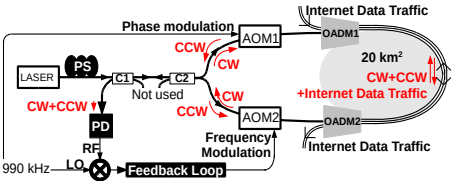

Fig. 165: Setup of the FOG. PS polarization scrambler, C couplers, AOM acousto optic modulators, OADM Optical Add&Drop Multiplexers, CW(CCW) clockwise (counter-clockwise) propagating beams.

At the conference we will present a description of our system, the results we obtained, and an analysis of the present limitations and of possible perspectives of this technique, also in consideration of the present widespread of phase-coherent optical links across large geographical areas.

1. A. Velikoseltsev, K. U. Schreiber, A. Yankovsky, J.-P. R. Wells, A. Boronachin, A. Tkachenko, “On the application of fiber optic gyroscopes for detection of seismic rotations“ J. Seismol. 16 , 623 (2012).

2. H. Igel, K. U. Schreiber, A. Flaws, B. Schuberth, A. Velikoseltsev, A. Cochard, “Rotational motions induced by the M 8.1 Tokachi-oki earthquake, September 25, 2003”, Geophis. Res. Lett. 32 , L08309 (2005).

3. J. Belfi, N. Beverini, G. Carelli, A. Di Virgilio, E. Maccioni, G. Saccorotti, F. Stefani, A. Velikoseltsev, “Horizontal rotation signals detected by “G-Pisa” ring laser for the M=9.0, March 2011, Japan earthquake”, J. Seismol. 16, 767 (2012).

4 C. Clivati, D. Calonico, G. A. Costanzo, A. Mura, M. Pizzocaro, F. Levi “A Large Area Fiber Optic Gyroscope on multiplexed fiber network”, accepted for pubblication in Opt. Lett.

IFCS-EFTF5-L2-3

Optical fiber-based radio frequency signal transfer and radio-astronomy applications

Yabai He,[1,2] Magnus T.L. Hsu,[1] Malcolm B. Gray,[1] R. Bruce Warrington,[1] Michael J. Wouters,[1] Brian J. Orr,[2] Andre N. Luiten,[3,4] Sascha Schediwy,[4] Kenneth G.H. Baldwin,[5] Tasso Tzioumis,[6] Chris Phillips,[6] Guido Aben[7] and Tim Rayner[8]

[1]National Measurement Institute, Sydney, Australia
[2]MQ Photonics Research Centre, Macquarie University, Sydney, Australia
[3]Institute of Photonics and Advanced Sensors, University of Adelaide, Australia
[4]University of Western Australia, Perth, Australia
[5]Research School of Physics and Engineering, The Australian National University, Australia
[6]CSIRO Astronomy and Space Science, Sydney, Australia
[7]AARNet, Perth, Australia
[8]AARNet, Canberra, Australia

Email: Magnus.Hsu@measurement.gov.au

A collaboration between the National Measurement Institute (NMI) and a number of Australian universities and research institutions has been working for several years to promote the construction of a continental-scale optical-fiber network in Australia for the distribution of optical and microwave reference frequencies. This network would connect a number of radio-astronomy sites and research laboratories with the NMI, allowing long-range comparison of frequency standards and dissemination of high precision reference signals for a wide range of applications.

We have developed two systems for the distribution of microwave reference frequencies via optical fiber; these systems have particular application to radio astronomy:

(i) One system implements algebraic cancellation of phase-noise in the link using analog radio-frequency (RF) electronics[512]. Recent results show transfer stabilities of 3×10^{-13} at 1 s and 6×10^{-17} at 10^4 s over 175 km of optical fiber including two bidirectional optical amplifiers.

(ii) The other system uses an all-digital architecture based on Field-Programmable Gate Array hardware[513]. Our published results reported radio frequency signal transfer with stabilities of 4×10^{-13} at 1 s and 6×10^{-17} at one day over 70 km of optical fiber, with more than two orders of magnitude in fiber phase noise suppression.

We are now applying these methods to real-world optical fiber links. We report on the latest results on our frequency transfer systems at CSIRO's Australian Telescope Compact Array (ATCA) radio-telescope facility located at Narrabri, NSW. The ATCA consists of an array of six 22 m radio-antennas, and can be operated as one site within a much larger Very Long Baseline Interferometry (VLBI) array. Typically, each site in the VLBI array has a local hydrogen maser; our aim, therefore, is to replicate this level of stability by transferring RF signals over fiber.

Our latest results involving fiber-based distribution of a common RF signal through a practical fiber link between two radio-antennae sites will be reported at the conference.

---

[512] Y. He *et al.*, "Long-distance analog and digital dissemination of reference radio frequencies over optical fibers", 20th AIP Congress, Sydney, Australia (2012)

[513] M.T.L. Hsu *et al.*, "All-digital radio-frequency signal distribution via optical fibers", IEEE Photonics Technology Letters **24**, 1015 (2012).

IFCS-EFTF5-L2-4

Ultra-Stable Oscillator Reference Spacecraft-to-Spacecraft Links For Planetary Exploration

Sami Asmar[1], Kamal Oudrhiri[1], Gregory Weaver[2]

[1]Radio Science Systems Group, Jet Propulsion Laboratory, California Institute of Technology, Pasadena, CA, USA

[2]Space Department, Johns Hopkins University Applied Physics Laboratory, Laurel, MD, USA

Email: asmar@jpl.nasa.gov

Thermally controlled quartz crystal Ultra-Stable Oscillators (USO) have been utilized on deep space missions for Radio Science experiments. Starting with the Voyager mission to the outer planets, atmospheric science has benefited tremendously from the radio occultation technique enabled by USOs. Recently, the GRAIL mission to the Moon, which applied the GRACE mission concept, utilized USOs as part of the science payload to investigate the lunar interior structure. Identical USOs on twin spacecraft flying in precision formation around the moon generated signals at X,- S-, and Ka-bands with the latter two exchanged between the spacecraft and the former broadcast to Earth. With 2 parts in EE-13 stability in the range of 10 to 100 second integration times, the USOs were precise enough to measure change in the range between the spacecraft (varied between 65 and 225 km) to the size of a blood cell. The velocity variations were measured to a few microns. This precision enabled the mission to reach its scientific objectives with large margins reveling the lunar composition from the crust to the core. Due to the low altitude of the mission and its duration, a gravitational field of the Moon in excess of 880 degree and order (spherical harmonic coefficients) was produced with a surface resolution of a few kilometers.

This paper will describe the roles of USOs in scientific discoveries in deep space with a brief historical overview, recent technological advances and future trends. The scientific applications will be described ranging from atmospheric and ionospheric occultations, surface scattering, and precision Doppler for gravitational field measurements.

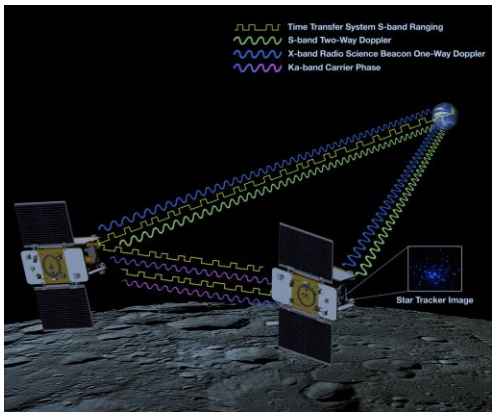

Fig. 166: Multiple radio links from the twin GRAIL spacecraft, Ebb and Flow, referenced to on-board Ultra-Stable Oscillators, utilized for precision gravity measurements.

IFCS-EFTF5-L2-5

GRACE Kinematic Orbit Determination: the Role of Clocks

Etienne Orliac[1], Adrian Jäggi[1], Heike Bock[1], and Rolf Dach[1]

[1]Astronomical Institute, University of Bern, Bern, Switzerland

Email: etienne.orliac@aiub.unibe.ch

The processing of a global network of ground Global Positioning System (GPS) tracking stations allows for the computation of orbits and clock corrections for the GPS satellites. This information provides the basis for precise kinematic orbit determination for Low Earth Orbiting (LEO) satellites based on the data collected with their onboard GPS receiver. One example are the twin satellites from the GRACE mission (Gravity Recovery And Climate Experiment), which carry highly stable onboard clocks.

The quality and consistency of the GPS satellite orbits and clock corrections is essential for the quality of the obtained kinematic LEO positions. The high-rate satellite clock corrections are typically computed using data from the International GNSS Service (IGS, GNSS standing for Global Navigation Satellite System) in the three-step scheme: first, based on code and phase data, a global solution containing all relevant parameters with a 5 minutes sampling is computed. For practical reasons the 5 minutes satellite clock corrections are interpolated down to 30 seconds using time differences of the carrier phase observations. A further densification to 5 seconds is done again with a phase measurement based interpolation but using a different set of stations (not all stations provide data with a sampling higher than 30 seconds). For GRACE kinematic orbit determination, 10 seconds clock corrections are needed.

We propose here to investigate the impact of the interpolation of the GPS satellite clock corrections on the determination of GRACE kinematic orbits and clock parameters, and to eventually assess the impact on subsequent gravity field recovery from the kinematic positions. We will vary the above described scheme for clock corrections computation and assess the impact on the obtained GRACE kinematic trajectories. Conventionally the receiver clock corrections are set up as epoch-wise independent parameters. However, the GRACE onboard clocks are highly-stable, which may allow it to model the clock over a few epochs with a sufficient accuracy. To assess the benefit on the derived kinematic positions, gravity fields are computed and compared with conventional solutions based on kinematic positions with receiver clock corrections estimated epoch-wise.

MEMS Resonators

CLUB D

Thursday, July 25 2013, 10:30 am - 12:00 pm

Chair: **Bernard Dulmet**
FEMTO-ST

IFCS-EFTF1-L3-1

CMOS-MEMS Resonators and Their Applications

Sheng-Shian Li

Inst. of NanoEngineering and MicroSystems, National Tsing Hua University, Hsinchu, Taiwan

Email: ssli@mx.nthu.edu.tw

In the past few years, the CMOS-MEMS technology has been thoroughly explored and implemented in vibrating MEMS applications. This paper reports the recent progress on CMOS-MEMS resonators and their implementations in our group, as shown in Fig. 1. These resonators (Fig. 1a) were fabricated using standard CMOS processes offered by foundry services, such as TSMC and UMC, to facilitate fast prototyping, quick turnaround time, batch production, low cost, and monolithic integration. Specifically, we take advantage of IC and semiconductor strength in Taiwan to develop several unique CMOS-MEMS resonator fabrication platforms[514][515] targeted for inherent integration of MEMS and circuitry, as a result towards single-chip implementation for timing reference and filter applications.

In this paper, resonator performance enhancement in terms of motional impedance, power handling capability (Fig. 1b), linearity, quality factor, frequency tunability (Fig. 1c), temperature compensation (Fig. 1d), and feedthrough reduction (Fig. 1e) addressed by the use of our proposed active gap reduction mechanism, mechanically-coupled array approach, bias-dependent electrical stiffness, oxide-type structural material, and fully differential scheme, respectively, would be presented. In addition, oscillator (Fig. 1f) and filter (Fig. 1g) implementations via these fabricated CMOS-MEMS resonators will also be illustrated, showing their device characterization and measured performance.

In sum, the main contribution of our group is on the development of CMOS-MEMS-based high-performance resonator circuits. This technology is expected to pave a way to realize fully-integrated CMOS-MEMS oscillators and filters which might benefit single-chip transceivers.

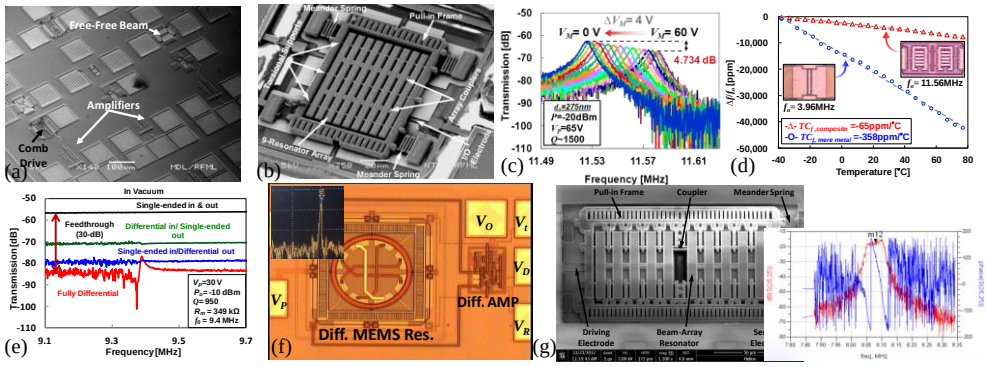

Fig. 167: (a) CMOS-MEMS integration. (b) Mechanically-coupled resonator array. (c) Frequency tuning. (d) Temperature compensation. (e) Feedthrough reduction. (f) Oscillator and (g) filter implementation.

[514] W.-C. Chen, W. Fang, and S.-S. Li, "A generalized CMOS-MEMS platform for micromechanical resonators monolithically integrated with circuits," *J. Micromech. Microeng.*, vol. 21, no. 6, pp. 065012, May 2011.

[515] W.-C. Chen, W. Fang, and S.-S. Li, "High-*Q* integrated CMOS-MEMS resonators with deep-submicron gaps and quasi-linear frequency tuning," *IEEE/ASME J. Microelectromech. Syst.*, vol. 21, no. 3, pp. 688-701, June 2012.

IFCS-EFTF1-L3-2

2DEG Electrodes for Piezoelectric Transduction of AlGaN/GaN MEMS Resonators

Laura Popa[1, 2], Dana Weinstein[2]
[1]Department of Physics, MIT, Cambridge, MA, USA
[2]Department of Electrical Engineering and Computer Science, MIT, Cambridge, MA, USA
Email: lpopa@mit.edu

This work presents the use of two-dimensional electron gas (2DEG) interdigitated transducers (IDT) for actuation of piezoelectric AlGaN/GaN MEMS resonators. Most piezoelectric resonators require patterned metal electrodes which can limit the performance through mass loading, increased damping and distortion of the mechanical mode. AlGaN/GaN heterostructures, increasingly used in millimeter-wave ICs, enable metal-free, high-*Q* resonators. Fig. 1 (a) illustrates the sharp conduction band potential well at the AlGaN/GaN interface which induces a high density, high mobility sheet of charge. This 2DEG can be patterned into IDTs by removing the AlGaN selectively (Fig. 1 b, c). 2DEG IDTs have been previously demonstrated in a SAW AlGaN/GaN filter[516] but this work is the first implementation in MEMS resonators.

Metal-free resonators can be used to directly interrogate GaN material properties in the absence of loss associated with metal electrodes. In Fig. 2, measured frequency response of 2DEG IDT bulk acoustic wave resonator shows a 1.225 GHz shear vertical mode, coupled with thickness shear. Measured Q_{load} is 1180 and $f.Q_{load}$ product 1.44×10^{12}, comparable to the highest in GaN[2]. Generally, *Q* factors are limited by dissipation mechanisms such as inelastic phonon scattering, thermoelastic damping, air damping, electrical and anchor losses. Here, testing is performed in vacuum, to minimize air damping, while quarter-wavelength matched suspension beams reduce anchor loss. By accounting for the parasitic series resistance of the 2DEG electrodes, the intrinsic mechanical Q_{mech} of the resonator is extracted to be 1290, giving an $f.Q_{mech}$ product of 1.58×10^{12}.

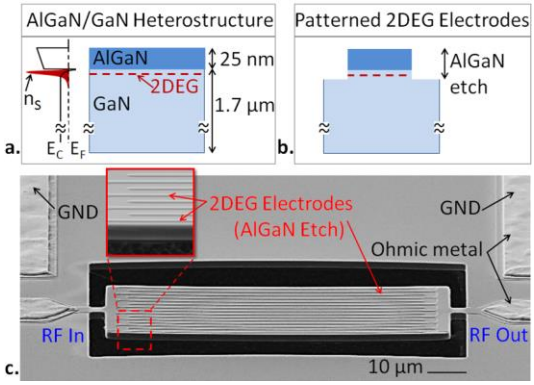

Fig. 1. (a) Conduction band potential well at AlGaN /GaN interface gives rise to conductive 2DEG. (b) 2DEG is removed in the regions where AlGaN is etched. (c) SEM shows resonator with 2DEG IDT. Ohmic metal makes contact to 2DEG off the resonator.

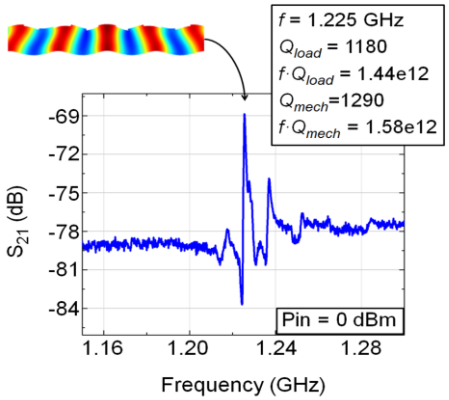

Fig. 2: Measured frequency response of metal-free IDT resonator with 2DEG electrodes after deembeding with an open structure. Inset shows out of plane displacement of 1.225 GHz resonant plate.

[516] K.-Y. Wong, K. Chen, *et. al.*, Applied *Physics Letters*, vol 90, 213506 (2007).

[2] A. Ansari, M. Rais-Zadeh, *et. al.*, *IEDM*, 485-88 (2011).

IFCS-EFTF1-L3-3

REDUCTION OF ANCHOR LOSSES BY ETCHED SLOTS IN ALUMINUM NITRIDE CONTOUR MODE RESONATORS

Cristian Cassella[1], Massimiliano Cremonesi[2], Jeronimo Segovia[1],Attilio Frangi[2],Gianluca Piazza[1]

[1]Carnegie Mellon University, Pittsburgh, PA, USA
[2]Politecnico of Milan, ITALY

The replacement of Quartz crystals and surface-acoustic wave devices by CMOS-integrable MEMS resonators requires simultaneously achieving high quality factors, Q, and high electromechanical coupling coefficients, k_t^2.AlN MEMS contour-mode resonators (CMR) have emerged as promising candidates, and exhibited k_t^2 in excess of 1% and Qs of ~ 2000 from 100 MHz to 1 GHz. It has been shown experimentally that the main dissipation mechanisms in AlN MEMS piezoelectric resonators are related to anchor and interfacial losses [1,2]. The former depends on acoustic energy escaping the resonator and being dissipated into the substrate; the latter arises from stress discontinuity at the interface between different materials and becomes dominant at frequencies in excess of 500 MHz [3].

In this paper, a new technique for reducing the anchor losses and correspondingly increasing the Q in 220 MHz AlN CMR devices is presented. The technique is based on the introduction of etched slots inside the body of the AlN resonant structure, in close proximity of the anchor location. The air slot acts as an acoustic reflector and reduces the energy lost into the substrate. Different dimensions of the etching slot have been investigated (see Fig. 1) and two sidewall angles for the AlN film were analyzed (30 and 60 degrees as defined in Fig. 1). A Q enhancement up to 50% was attained for an etching slot having a width equal to 0.35 times the acoustic wavelength. An analytical model that describes the expected improvement in Q varying the slot width was also developed. As shown in Fig. 2 the predicted trend follows the experimental results and is in line with the Finite Element Analysis code that was developed to predict anchor and surface dissipation in AlN MEMS resonators [3].

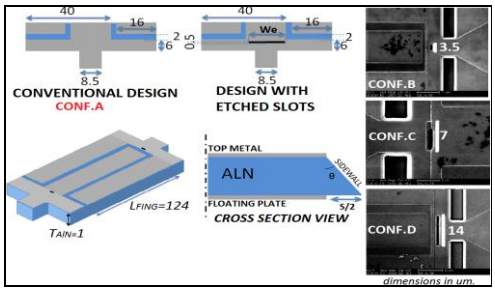

Figure 168: Geometry of 220 MHz resonators (λ≈ in 4 configurations (A, B, C, D) where the slot wi has been varied (0,3,7,14 um). Two different si angles have been investigated (30 degrees and 60 de SEM pictures of the etching slot for configuration B are also shown.

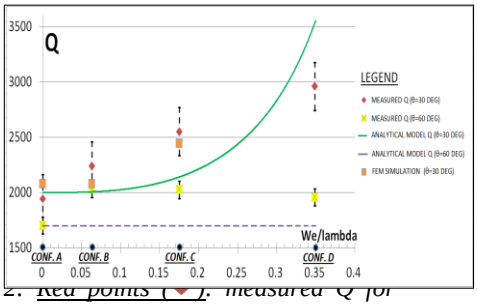

Figure 2: Red points (◆): measured Q for configurations A,B,C,D (θ=30 degrees). Yellow points(✕): measured Q for configurations A,B,C,D (θ=60 degrees). Green continuous line: analytical model for Q varying We (θ=30 degrees). Purple dotted line: analytical model for Q varying We

IFCS-EFTF1-L3-4

A 2.8 GHz Combined Mode of Vibration Aluminum Nitride MEMS Resonator with High Figure of Merit Exceeding 45

Yu Hui, Zhenyun Qian and Matteo Rinaldi

Department of Electrical and Computer Engineering, Northeastern University, Boston, MA/USA

Email: hui.y@husky.neu.edu, rinaldi@ece.neu.edu

This paper presents the first demonstration of a high frequency (2.8 GHz), lateral field excited (simple two masks fabrication process), combined lateral-thickness extensional mode of vibration aluminum nitride (AlN) micro-electro-mechanical (MEMS) resonator with unprecedentedly high figure of merit ($k_t^2 \cdot Q > 45$). For the first time, a single interdigital electrode was employed to excite a high frequency mode of vibration in an AlN plate (1.5 µm thick) by making use of both the d_{33} and d_{31} AlN piezoelectric coefficients[517]. The resulting MEMS resonator showed high quality factor, Q~2000, (thanks to the high quality AlN film directly deposit on top of the Silicon substrate) and the highest electromechanical coupling coefficient ever reported for AlN MEMS resonators employing a single electrode, k_t^2~*2.5%* (thanks to the coherent combination of d_{33} and d_{31} coefficients to transduce one single mechanical mode of vibration).

The use of a single interdigital electrode to excite (lateral field excitation, *LFE*) a high frequency contour-extensional mode of vibration in AlN microstructures has been previously demonstrated[518]. However, due to the relatively low d_{31} coefficient of AlN, the maximum predicted electromechanical coupling coefficient[519] for such class of devices is only 1.5%. In this work, by properly optimizing the ratio between the thickness of the AlN film (t) and the pitch of the interdigital top electrode (W_p) the d_{33} and d_{31} coefficients have been coherently combined and harnessed to transduce one single mechanical vibration mode. The combined lateral-thickness mode of vibration was simulated using COMSOL showing a maximum value of electromechanical coupling coefficient, k_t^2 = 2.82%, for $t/W_p \approx 0.94$. A device with such optimum t/W_p was fabricated (Fig. 1), showing high quality factor (Q = 1855) and a value of electromechanical coupling coefficient (k_t^2 = 2.48%) ~2 times higher than what is typically achieved with conventional LFE AlN contour-extensional mode resonators[2] (Fig. 2).

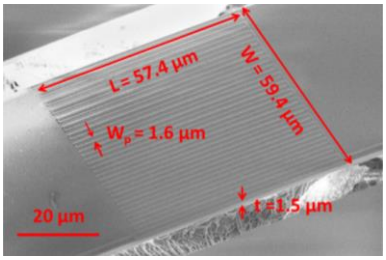

Fig. 1: SEM image of the fabricated AlN combined mode of vibration MEMS resonator. t/W_p was set to be *~0.94*, resulting in a resonance frequency of the 2.8 GHz. It is worth noting that the fabricated device is fully

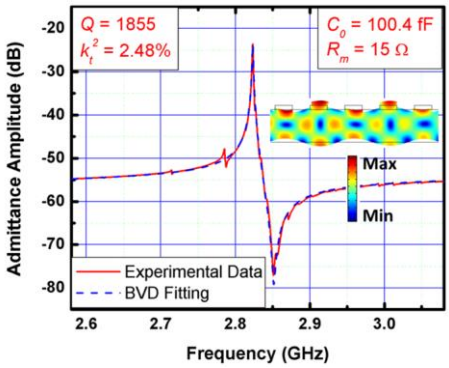

Fig. 2: Measured admittance curve and BVD model fitting of the fabricated AlN resonator. High device figure of merit ($FOM = k_t^2 \cdot Q$ = 46) and low motional resistance (R_m = 15 Ω) were achieved at 2.8 GHz. The inset shows the 2D FEM simulation

[517]C. J. Zuo, et al. IEEE IFCS 2012, pp. 1-4.
[518]C. J. Zuo, et al. IEEE IFCS 2009, pp. 381-384.
[519]J. H. Kuypers, et al. IEEE IFCS 2008, pp. 240-249.

IFCS-EFTF1-L3-5

Highly coupled resonator based on ridge-shaped periodically poled materials for radio-frequency applications

Fabien Henrot[1], Florent Bassignot[1], Clément Guyot[1], Jean-Yves Rauch[1], Blandine Guichardaz[1], Sylvain Ballandras[2]

[1]FEMTO-ST Institute, 32 avenue de l'Observatoire, 25000 Besançon, France
[2] FreC'N'Sys, 18 rue Alain Savary, 25000 Besançon, France

Email: fabien.henrot@femto-st.fr

Most resonator and filters are based on Surface Acoustic Wave (SAW) technology using inter-digitated transducer (IDT). This mature technology is particularly addressing radio-frequency filter demand, but it is limited by various factors. Recently, the interest of periodically poled transducer built on single crystal $LiNbO_3$ Z-cut plates was investigated as an interesting alternative to classical inter-digital transducers[520]. Performances of such a device were theoretically demonstrated showing many advantages such as electromechanical coupling and equivalent phase velocity. This paper shows the practical existence of high electromechanical coupling (k^2=15%) and high phase velocity (10000m.s^{-1}) for this kind of transducer.

This new device has been modeled with our finite and boundary elements simulation tool for both $LiTaO_3$ and $LiNbO_3$ to determine the most interesting design. $LiNbO_3$ is known as highly coupled material; $LiTaO_3$ is used for its similar properties and shows a better coefficient temperature of frequency. A high aspect ratio ridge-shaped transducer was made of $LiNbO_3$ to show the resonator capabilities. The manufacturing process is achieved by dicing a ridge in a poled plate with a diamond-tipped saw and plating the ridge walls to define the electrodes.

The dispersion properties analysis have shown one longitudinal mode (k^2_{max}=12%) and one shear mode (k^2_{max}=22%) for a "ridge width/poling period" ratio of 0.4 and 0.2 respectively. A 500µm-deep and about 120µm-wide ridge has been successfully fabricated on a periodically poled $LiNbO_3$ exhibiting a poling period of 600µm. The device characterization shows an electromechanical coupling about 15% and a difference between theoretical and experimental resonance frequencies under 1%. Parasitic effects shown on fig. 1 (b) are caused by a parallelism defect of the ridge sides, which is the main problem to fix for future improvement.

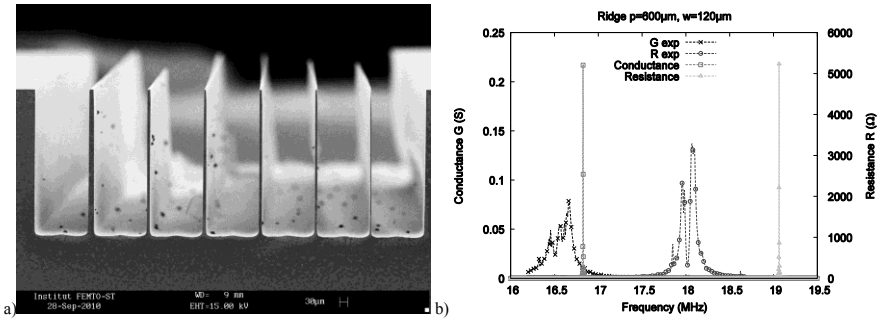

a) b)

Fig. 169: SEM view of ridge shaped transducer (a) and a comparison of theoretical (k^2=22%) and experimental (k^2=15%) results (b)

[520] E. Courjon et al., "Lamb wave transducers built on periodically poled Z-cut LiNbO3 wafers", vol. 102, 114107, 2007.

Optical Techniques

CLUB E

Thursday, July 25 2013, 02:00 pm - 03:30 pm

Chair: **Steve Lecomte**
CSEM

IFCS-EFTF6-M1-1

Optical absolute frequency reference for space applications

Klaus Döringshoff[1], Thilo Schuldt[2,3,4], Johannes Stühler[2,3], Evgeny V. Kovalchuk[1], Matthias Franz[2], Ulrich Johann[5], Claus Braxmaier[3,4], Achim Peters[1]

[1]Institut für Physik, Humboldt-Universität zu Berlin, Berlin, Germany
[2]Institute for Optical Systems, University of Applied Sciences Konstanz, Konstanz, Germany [3]Center for Applied Space Technology and Microgravity (ZARM), University Bremen, Germany
[4]DLR Institute for Space Systems, Bremen, Germany
[5]Astrium GmbH – Satellites, Friedrichshafen, Germany

Email: Klaus.Doeringshoff@physik.hu-berlin.de

Future space missions related to fundamental science, Earth observation or navigation and ranging require ultra-stable optical frequency references for the employed lasers. Setups based on saturation spectroscopy of molecular iodine are well known frequency reference for Nd:YAG lasers, of which space qualified versions are available.

With the goal of a space qualified iodine frequency reference with 10^{-15} stability at 6000 s, we have developed a compact ruggedized setup based on a 550 mm × 250 mm baseplate made of Clearceram-HS glass ceramic with ultra-low coefficient of thermal expansion (Fig. 1). The optical elements are joint to the baseplate using adhesive bonding technology with a space-qualified two-component epoxy. The spectroscopy setup features a 30 cm iodine cell used in triple pass configuration of the counter propagating pump- and probe beam, which are stabilized to 8 mW and 1 mW, respectively. Balanced detection provides an excellent signal to noise ratio of the modulation transfer spectroscopy signal. As laser source we employ a frequency doubled Nd:YAG laser. Frequency modulation of the pump beam is realized via an acousto-optic modulator, where residual amplitude modulation is detected and cancelled in quadrature detection to avoid lock point errors. The laser is stabilized to the a_{10} component of the transition R(56)32-0, and its frequency stability is determined from beat note measurements with a cavity stabilized laser. The frequency measurements show a short term stability of 8×10^{-15} at 1 s integration time averaging down to below 3×10^{-15} at 20 s (cf. Fig. 2).

In a current activity, an engineering model (EM) will be realized on a 380 mm × 180 mm baseplate and a special manufactured multipass cell of dimension 100 mm × 100 mm × 30 mm, which will undergo thermal cycling and vibrational tests.

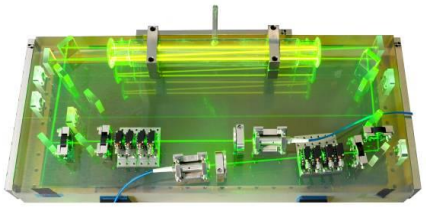

Fig. 170: Photograph of the elegant breadboard model of the iodine spectroscopy setup. Laser light is fibre-coupled to the setup with a triple-pass configuration of a 30 cm iodine absorption cell.

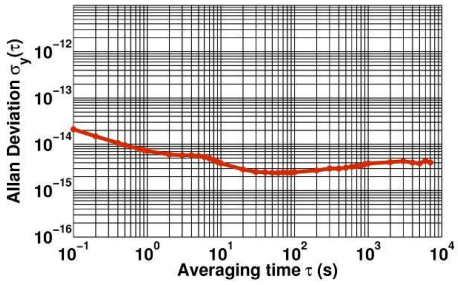

Fig. 2: Allan Deviation of the beat note between the elegant breadboard iodine reference and a cavity stabilized reference laser. A linear drift of 50 Hz/s, attributed to the reference cavity, was subtracted from the frequency time record.

IFCS-EFTF6-M1-2

A laser frequency stabilization unit for next-generation space atomic clocks

A. Nevsky[1], S. Alighanbari[1], Q.F. Chen[1], I. Ernsting[1], S. Vasilyev[1], S. Schiller[1], G. Barwood[2], P. Gill[2], N. Poli[3], M. Schioppo[3], G.M. Tino[3], U. Sterr[4]

[1]Institut für Experimentalphysik, Heinrich-Heine-Universität, Düsseldorf, Germany

[2] National Physical Laboratory, Teddington, Middlesex, UK

[3]Dipartimento di Fisica e Astronomia e LENS, Universita' di Firenze, Sesto Fiorentino, Italy

[4]Physikalisch-Technische Bundesanstalt, Braunschweig, Germany

E-mail: alexander.nevsky@uni-duesseldorf.de

A range of new applications in fundamental physics, in time and frequency metrology, and in geophysics will be enabled by ultra-precise atomic clocks in space, in part in conjunction with terrestrial clocks. The "Space Optical Clocks" project aims for operating an optical clock on the ISS toward the end of this decade. An EU-FP7 funded-consortium [1] is currently developing two transportable lattice clock demonstrators, based on strontium and ytterbium.

One unit of the modular strontium clock apparatus is a compact and reliable frequency stabilization system (FSS) for absolute frequency stabilization of several laser sources at distinctly different wavelengths, needed for cooling and manipulation of Sr atoms: 689 nm, 922 nm, 813 nm. The FSS setup is based on three low-to-medium-finesse optical cavities, embedded in the same ULE block housed in a small vacuum chamber. Waves from the lasers are led to the respective cavities using single-mode fibers and fiber combiners. The lasers are locked to the cavities using the Pound-Drever-Hall technique. For each laser, a waveguide electro-optic modulator (EOM) performs a double phase modulation generating two sideband triplets. The central line of one triplet is locked to the cavity. It can be frequency-tuned (here, over 600 MHz) relative to the carrier, allowing bridging the frequency gap between an ULE cavity mode and the atomic transition frequency. The whole optical setup (see picture) is assembled into a compact aluminum vacuum chamber with size of approx. 40 x 30 x 15 cm^3 plus a box containing the waveguide modulators (on top) and the compact, DDS-based control electronics subunit. Three external cavity diode lasers were simultaneously stabilized to the FSS, using independent EOMs. A fourth laser, the independently stabilized 698 nm clock laser, can also be coupled to the FSS. Its purpose is to measure and correct the drift of the FSS cavity with respect to the ultra-stable reference cavity. The linewidth and the absolute frequency stability of the stabilized lasers were characterized by means of a femtosecond frequency comb stabilized to a H-maser and a virtual beat with an ultra-stable Yb clock laser. The most critical laser, the 689 nm laser for cooling on the $^1S_0 \rightarrow {}^3P_1$ intercombination Sr transition, exhibits a linewidth of approximately 100 Hz at 1 s integration time (0.9 kHz at 70 s) and a drift smaller than 0.5 Hz/s. These values are mostly determined by the properties of the reference cavity and the environment, since for simplicity, compactness and weight reduction no means have been implemented for reducing the vibration sensitivity of the cavity.

The system has been successfully integrated into the Sr compact lattice optical clock at LENS (Firenze, Italy), achieving robust and stable operation, with 1.1×10^4 ^{88}Sr atoms in the lattice and clock transition spectroscopy with 23 Hz linewidth.

[1]www.soc2.eu; S. Schiller, *et al.*,"Towards Neutral-atom Space Optical Clocks (SOC2): Development of high-performance transportable and breadboard optical clocks and advanced subsystems", in: *Let's embrace space*, Vol. II, Ch. 45, ISBN 978-92-79-22207-8, doi:10.2769/31208

IFCS-EFTF6-M1-3

Laser dynamics effects on the systematics of large size laser gyroscopes

J. Belfi[1], A. Beghi[2,3], N. Beverini[1,4], B. Bouhadef[4],

D. Cuccato[2,3], A. Di Virgilio[4] and A. Ortolan[3]

[1]Dept. of Physics, University of Pisa, Largo Bruno Pontecorvo 3, Pisa, Italy
[2]Dept. of Information Engineering, University of Padova, Via Gradenigo 6/B, Padova, Italy
[3]INFN National Laboratories of Legnaro, Viale dell'Università 2, Legnaro, Padova, Italy
[4]INFN Section of Pisa, Largo Bruno Pontecorvo 3, Pisa, Italy

Email: belfi@df.unipi.it

Large frame ring laser gyroscopes provide precise measurements of local frame rotations induced by earthquakes, tides, local tilts of the terrestrial crust and even by the wobbling of the axis of the planet[521]. A ground based experiment aimed at measuring the Lense-Thirring effect with an array of laser gyroscopes has been recently proposed[522]. The project foresees the construction of a tri-axial gyroscope for the measurement of the Earth's rotation vector with a precision better than 10^{-9}. This goal requires a strict control of all the systematics connected to the geometrical scale factor and to the nonlinear dynamics of the laser. The complete identification of the laser parameters is then required for the absolute calibration of such detectors.

We present the results of comprehensive experimental tests of the Lamb's semiclassical theory of ring lasers obtained by operating the "G-Pisa" gyroscope with the laser plane oriented almost perpendicularly to the local North direction. In this configuration, the Earth's rotation contribution to the Sagnac frequency is less sensitive to the orientation error, and a more precise estimate of the systematics coming from the laser dynamics can be achieved. Cavity losses and the corresponding dissipative Lamb parameters are monitored by observing the single beams intensity modulation at the Sagnac frequency while the gain parameters are identified by a dedicated spectroscopic analysis of the plasma dispersion function. The adopted methods and the improvements of the ultimate performances of the G-Pisa apparatus, obtained with the application of a Kalman filter algorithm, will be detailed.

521 K. U. Schreiber et al., "How to Detect the Chandler and the Annual Wobble of the Earth with a Large Ring Laser Gyroscope", Phys. Rev. Lett. **107,** 173904 (2011).

522 F. Bosi , et al., "Measuring Gravito-magnetic Effects by Multi Ring-Laser Gyroscope", Phys. Rev. D **84**, 122002, (2011).

IFCS-EFTF6-M1-4
Gar-Wing Truong[1], James Anstie[1,2], Thomas Stace[3], **Andre Luiten[1,2]**
[1]School of Physics, The University of Western Australia, Perth, Western Australia, Australia, [2]School of Chemistry and Physics, and IPAS, The University of Adelaide, Adelaide, South Australia, Australia, [3]School of Physics, The University of Queensland, Brisbane, Queensland, Australia

Determination of the Boltzmann Constant using Laser Absorption Spectroscopy

G.-W. Truong[1], J.D. Anstie[1,2], T.M. Stace[3], and A.N. Luiten[1,2].
[1]School of Physics, University of WA, Nedlands, WA Australia
[2]School of Chemistry and Physics and Institute of Photonics & Advanced Sensing (IPAS), University of Adelaide, Adelaide SA, Australia.
[3]School of Physics, University of Queensland, St Lucia, QLD, Australia

Email: andre.luiten@adelaide.edu.au

The current CODATA value and its associated uncertainty for the Boltzmann constant, k_B, is primarily derived from a single acoustic measurement performed in 1988[1,2]. Since a call in 2005, there have been renewed efforts towards a redetermination of k_B in preparation for the redefinition of the kelvin[3]. Here, the unit of temperature is no longer tied to a particular state of matter, but instead, to an ensemble of fixed fundamental constants.

In this talk, we will present recent progress towards a redetermination of k_B using high-precision and high-accuracy Doppler-broadened spectroscopy of cesium atoms in a thermal vapour cell. By extracting the width of the Gaussian component of an isolated hyperfine absorption feature one can determine the translational thermal energy, k_BT, of the atomic vapour. By combining this with an independent measurement of temperature T, it is possible to determine the Boltzmann constant[4]. We will present a Boltzmann constant determination with an 8 ppm statistical uncertainty and discuss sources of systematic error.

Spectrometer: The probe laser at 894nm was offset-frequency locked to a stable master laser, providing a tunable, but stabilized optical frequency to probe the D1 transition. The spectrometer utilises a single-pass dual-beam topology, with one path detected immediately while the other is directed through a well-shielded, temperature-controlled cesium cell. We have shown that our spectrometer is capable of shot-noise limited precision[5].

Systematic Errors: Currently, the performance of our thermal enclosure is the principal limitation to achieving ppm-level accuracy. We will discuss the use of an advanced thermostat which can reduce temperature gradients to below 15μK – sufficient for a ppm-level retrieval of k_B. Whilst the compact, single-pass topology possible with the highly absorbing alkali metals is a distinct advantage, one must also be wary that the atomic population can easily be significantly perturbed away from thermal equilibrium by the probe source. We have observed and quantified an anomalous power broadening and a spatial beam profile distortion that can be attributed to optical pumping in the 3-level Λ system. Both of these can disturb the accuracy of the measurements.

[1] Moldover, M. R., et al. "Measurement of the universal gas constant R using a spherical acoustic resonator." *Physical review letters* 60.4 (1988): 249-252.
[2] Mohr, Peter J., Barry N. Taylor, and David B. Newell. "CODATA recommended values of the fundamental physical constants: 2006." *Reviews of Modern Physics* 80.2 (2008): 633.
[3] Fellmuth, Bernd, Ch Gaiser, and Joachim Fischer. "Determination of the Boltzmann constant—status and prospects." *Measurement Science and Technology* 17.10 (2006): R145.
[4] Bordé, Christian J. "Base units of the SI, fundamental constants and modern quantum physics."

Philosophical Transactions of the Royal Society A: Mathematical, Physical and Engineering Sciences 363.1834 (2005): 2177-2201.
[5] Truong, Gar-Wing, et al. "Absolute absorption line-shape measurements at the shot-noise limit." *Physical Review A* 86.3 (2012): 030501.

IFCS-EFTF6-M1-5

Hollow-Core Fibre Frequency Standards

C. Perrella[1,2], J. Anstie[1,2], P. Light[1,2], A. Lurie[1], T. Stace[3], F. Benabid[4] and A.N. Luiten[1,2].
[1]School of Chemistry and Physics and Institute of Photonics & Advanced Sensing (IPAS), University of Adelaide, Adelaide SA, Australia.
[2]School of Physics, University of WA, Nedlands, WA Australia
[3]School of Physics, University of Queensland, St Lucia, QLD, Australia
[4]GPPMM Group, Xlim Research Institute, CNRS, Universite de Limoges, France

Email: andre.luiten@adelaide.edu.au

A continuing challenge for the broader applicability of high precision frequency standards is the large size and fragility of the best examples. This talk presents our research aimed at developing new platforms for precision measurement based on compact and robust gas-filled hollow-core photonic crystal fibre (HC-PCF). We will address two particular examples: (i) iodine-filled fibre for delivering a flexible visible light standard suitable for length metrology; (ii) rubidium-filled fibre for a compact frequency standard based on a narrow two-photon transition.

(i) Iodine[523]: We have loaded a 50cm long hollow-core (~25µm core diameter) photonic-crystal fibre with ~5Pa of iodine vapour. By probing with counter-propagating and frequency-shifted 532nm beams, we see strong and clean Doppler-free resonances with a low-power linewidth of around 6MHz. This linewidth is dominantly set by transit-time effects across the fibre core. We use FM spectroscopy to lock the laser to one of these spectral lines and have achieved a fractional frequency stability of $2.3 \times 10^{-12}/\sqrt{\tau}$ where τ is the integration time of the measurement. This stability is consistent with photon shot-noise on the detected signal. We predict that with some improvements to the modulation scheme, together with lowering of the iodine pressure, it should be possible to improve this stability by a factor of 10.

(ii) Rubidium[524]*:* We have loaded a high density of Rb into 15cm of hollow-core optical fibre with a 35µm core diameter. We excite the two-photon resonance (5S to 5D) in Rubidium using two counter-propagating lasers at 780nm and 776nm. This dual colour excitation gives a much stronger transition than would be the case from a pure 778nm excitation. The high intensity conditions, together with the long length of the fibre, can result in substantial absorption of IR light (>80%). The observed two-photon linewidth is around 10MHz arising from three effects: transit time (5.6MHz), residual magnetic fields in the unshielded fibre (2.6MHz) and a residual Doppler effect (3.1MHz) arising from excitation by two different wavelengths. Frequency stabilization of the sum frequency of the two lasers is possible using modulation-transfer spectroscopy variant : we observe amplitude modulation on one colour transferred from frequency modulation on the other. The measured fractional frequency stability of the sum frequency was 9.8×10^{-12} at 1.3s integration time. This performance is limited by varying light shifts driven by alignment fluctuations. Were these to be suppressed the shot-noise floor corresponds to a level of 10^{-13} at 1s.

[523] Lurie et al, OPTICS LETTERS 36, 4776, (2011).; Lurie et al, OPTICS EXPRESS 20, 11906 (2012).

[524] C. Perrella et al. PHYSICAL REVIEW A 87, 013818 (2013); C. Perrella et al, Optics Letters, (2013), submitted

IFCS-EFTF6-M1-6

Towards a new clock laser system using a ceramic cavity and laser linewidth transfer technique

Kazumoto Hosaka[1], Hajime Inaba[1], Daisuke Akamatsu[1], Masami Yasuda[1], Jun Sugawara[2], Atsushi Onae[1], and Feng-Lei Hong[1]

[1] National Metrology Institute of Japan (NMIJ), AIST, Tsukuba, 305-8563, Japan

[2] Ceramics Division, Krosaki Harima Corporation, Kitakyushu City, 806-8586, Japan

Email: kazu.hosaka@aist.go.jp

Theoretical study shows that the frequency stabilities of ultra-stable lasers at a short averaging time are close to being limited by mechanical thermal fluctuations of the optical cavities[525]. A long spacer for the cavity should help to reduce the thermal noise relatively. However, a long cavity could be sensitive to the vibration. To surmount the problems, there is a need for a new material with high specific rigidity and very low thermal expansion at room temperature. We have applied an ultra low thermal expansion ceramic based on poly-crystalline cordierite ceramics ('NEXCERA' Krosaki Harima[2]), which has a Young's modulus of ~ 130 GPa and a Poisson's ratio of ~ 0.30, to an optical cavity spacer. To evaluate the thermal expansion coefficient of the ceramic, we produced an optical cavity consisting of two ULE mirrors in optical contact with a ceramic spacer. The length and diameter of the ceramic spacer were 75 and 25.4 mm, respectively. A Nd:YAG laser operated at 1064 nm was stabilised to the ceramic cavity and the resonant frequency of the cavity was measured by a fibre-based frequency comb system [3,4]. We found that the ceramic cavity had a zero cross temperature at 16.4 (1) °C where the thermal expansion coefficient crosses zero[5]. A finite element based analysis has been employed to calculate the ceramic cavity deformation when loaded. The response to the vertical acceleration is estimated from computations of the axial displacements at the centre of the mirror surface. A reduction in the response of the ceramic cavity to the vertical acceleration by a factor of 2 comparing with an ULE cavity has been shown (Fig. 1.). By combining the ceramic cavity with laser linewidth transfer technique using our high-speed controllable fibre-based frequency comb[3,4], clock lasers for Yb and Sr optical lattice clocks will be linewidth-narrowed and stabilised.

This research is supported by the MEXT/JSPS through its FIRST Program and Grants-in-Aid for Scientific Research Program (KAKENHI Grant Number: 22540415).

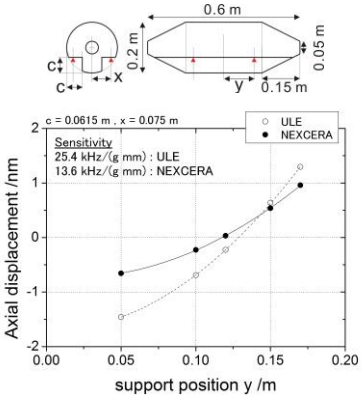

Fig. 171: A design of a long cavity and a calculated result of cavity length change under vertical acceleration as a function of the support position.

[1] K. Numata, *et. al.*, Phys. Rev. Lett., **93**, (2004) 250602.

[2] J. Sugawara, *et. al.*, Proceedings of ASPE 2010 Annual Meeting, **50**, (2010) 405.

[3] Y. Nakajima, *et. al.*, Opt. Express, **18**(2), (2010) 1667.

[4] K. Iwakuni, *et. al.*, Opt. Express, **20**, (2012) 13769.

[5] K Hosaka, *et. al.*, Jpn. J. Appl. Phys., **52**, (2013) 032402.

Modeling and Frequency Synthesis

CLUB H

Thursday, July 25 2013, 02:00 pm - 03:30 pm

Chair: **David Howe**
NIST

IFCS-EFTF2-M2-1

Physical model of phase noise in feedback oscillator

Xianhe Huang

School of Automation Engineering, University of Electronic Science & Technology of China, Chengdu, China
xianhehuang@uestc.edu.cn

Background: The phase noise of feedback oscillator is a key factor which limits the performance of electronic system.

Classical Leeson Model Analysis: When applying this model to design a feedback oscillator, one should know what key points should be paid more attention to? What drawbacks of this model also should be noted[1-4]. In this paper, determinants between loaded quality factor Q_L and equivalent parameters of a resonator and that of a oscillation circuit are tried to be revealed, influencing factors of noise factor F and corner frequency f_c are analyzed, and improvement measures are discussed as well.

Design examples and analysis:

Low phase noise quartz crystal BAW oscillator with AT-cut and SC-cut resonator[5].
Low phase noise oscillator with SAW resonator[6].
Low phase noise bulk wave oscillator with $LiTaO_3$ resonator[7].
LC/RC feedback oscillator.

Conclusion:

The loaded quality factor Q_L is a dynamic parameter.
The noise factor F is also a dynamic parameter.

Discussion:

Further studies about methods for improving the phase noise performance of the feedback oscillator.

References:

1. John R. Vig " Quartz Crystal Resonators and Oscillators for Frequency Control and Timing Applications - A Tutorial " http://www.ieee-uffc.org [Online]

2. Jeremy Everard "Low Phase Noise Signal Generation, Models and Theory, Oscillators and Their Key Elements, Fractional Regenerative Frequency Division, Teaching",2012 IEEE International Frequency Control Symposium

3. Michael Driscoll "Modeling Phase Noise in Multifunction Subassemblies" Frequency Control and the European Frequency and Time Forum (FCS), 2011 Joint Conference of the IEEE International

4. E. Rubiola and V. Giordano, "On the 1/f frequency noise in ultra-stable quartz oscillators", IEEE Trans. Ultrason. Ferroelectr. Freq. Control, vol. 54, no. 1, pp. 15-22, Jan. 2007.

5. Huang, Xianhe "The Design and Implementation of a 120-MHz Pierce Low-Phase-Noise Crystal Oscillator", IEEE Trans. Ultrason. Ferroelectr. Freq. Control, vol. 58, no. 7, pp. 1302-1306, 2011

6. Huang, Xianhe "Optimization and Realization of a 315-MHz Low-Phase-Noise Voltage-Controlled SAW Oscillator", IEEE Trans on Circuits and Systems II-Express Briefs, Vol: 59 no: 1 pp: 16-19, 2012

7. Huang, Xianhe "Design of a Wide-Tuning-Range Lithium Tantalate Low-Phase-Noise Voltage-Controlled Oscillator", IEEE Trans on Circuits and Systems II-Express Briefs, Vol: 60 no: 3

IFCS-EFTF2-M2-2

Design, Simulation and Test of an Oscillator Suitable for Wafer Level Evaluation of SAW Resonator Phase Noise

Dan Porga, Twinkle Shah, Dennis Thoma, Andrew Sawyer, Mike Driscoll (Consultant)

Phonon Corporation, Simsbury, CT, USA

Email: DanP@phonon.com

In a well-designed BAW or SAW oscillator, the primary contributor to near-carrier, flicker-of-frequency noise should be the resonator itself and not the sustaining stage amplifier. Determination of resonator short-term frequency stability (self-noise) at the wafer level is highly desirable from both the perspective of resonator selection prior to packaging and evaluation processing conditions resulting in low noise resonators. The objective of this work was to design a SAWR oscillator where both the flicker-of-PM noise contribution of the sustaining stage could be reliably determined. In addition, the oscillator design needed to be compatible with and tolerant of coaxial probe connections to on-wafer resonator arrays.

It was decided to design the oscillator using a 50 ohm sustaining stage amplifier. To this end, several candidate amplifiers were evaluated, including inexpensive, tape-and-reel type amplifiers containing darlington pair configurations with resistive feedback as well as SMP modular amplifiers. A novel method was used for very simple and accurate determination of amplifier flicker-of-PM white (additive) noise without the SAW resonator installed that consists of oscillator operation using an intentionally low delay (low Q) LC resonator or band-pass filter. The amplifier operating point (bias, excess gain, etc) is the same as with the SAWR installed, except the open loop white PM and 1/f PM noise is intentionally enhanced to quite high and easily measurable levels. We observed a reasonably large spread in 1/f PM noise for different model tape-and-reel amplifiers purchased from the same vendor. The same method was used in a discrete component sustaining stage, and in that case, resonator loading was both measured and successfully simulated via determination of the $1/2\pi\tau$ corner frequency in the phase noise.

The wafer probe oscillator was first evaluated using packaged resonators where the sustaining stage contribution towards oscillator near-carrier noise was 6-10dB below the best resonators. The oscillator was then installed in a wafer probe set-up, where extraordinary measures needed to be taken to reduce the effects of acoustic noise, electrical interference and vibration. The current status is that the results obtained for evaluation of packed and on-wafer devices are quite comparable.

Synthesis of Ultra-Stable Radio Frequency Signals From Independent Microwave Frequency Oscillators

John G. Hartnett[1,2], Stephen R. Parker[1], Eugene N. Ivanov[1], Nitin R. Nand[1]

[1]School of Physics, The University of Western Australia, Crawley, Australia
[2]Institute of Photonics and Advanced Sensing, School of Chemistry and Physics, University of Adelaide, Adelaide, Australia

Email: stephen.parker@uwa.edu.au

We present the design, implementation and evaluation of 10 MHz, 100 MHz and 1 GHz signals synthesized from two nominally identical 11.2 GHz Cryogenic Sapphire Oscillators (CSO). The fractional frequency stabilities of the CSOs for integration times below 5 seconds are comparable to the state-of-the-art performance of X-band signals generated by optical-comb division[526], while stability for integration times from 5 to 4000 seconds remains without peer. This translates in to low phase noise, high frequency stability performance of the generated RF signals, with applications in millimeter wave Very Long Baseline Interferometry.

Previous work reported on the synthesis of a 10 MHz and 100 MHz signal from a single CSO[527], we have now synthesized these signals independently from separate CSOs and directly compare them. We also generate a 1 GHz signal by phase locking a voltage controlled oscillator to a 1 GHz output derived from a CSO. Fractional frequency stabilities at 1 second integration time are 1×10^{-14}, 2×10^{-15} and 1.5×10^{-15} respectively for the 10 MHz, 100 MHz and 1 GHz signals (Fig. 1). Single sideband phase noise at 1 Hz offset is -134 dBc/Hz for the 10 MHz signal (≈12 dB lower than the best commercial 10 MHz quartz oscillator), -130 dBc/Hz for the 100 MHz signal (>25 dB lower than the best commercial 100 MHz quartz oscillator) and -112 dBc/Hz for the 1 GHz signals. Phase noise performance is limited by the frequency dividers and is surpassed only by signals synthesized using regenerative dividers[528]. Possibilities for improvement will be discussed.

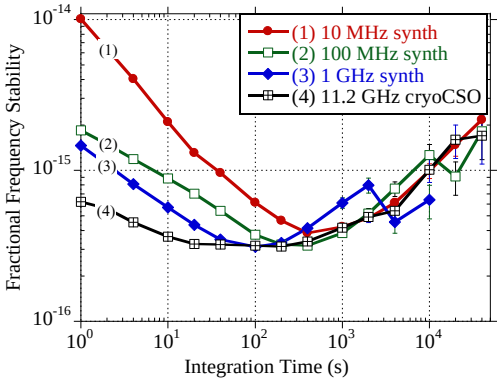

Fig. 172: Fractional frequency stability of 10 MHz (curve 1), 100 MHz (curve 2), 1 GHz (curve 3) signals and an 11.2 GHz CSO (curve 4).

[526] T.M. Fortier, M.S. Kirchner, F. Quinlan, J. Taylor, J.C. Bergquist, T.Rosenband, N. Lemke, A. Ludlow, Y. Jiang, C.W. Oates, and S.A. Diddams, "Generation of ultrastable microwaves via optical frequency division," Nature Photonics, vol. 5, pp. 425-429, 2011.

[527] N.R. Nand, J.G. Hartnett, E.N. Ivanov, G. Santarelli, "Ultra-stable very low-phase-noise signal source for Very Long Baseline Interferometry using a cryocooled sapphire oscillator," IEEE Trans on Micro. Theory & Tech., vol. 59, no. 11, pp. 2978 – 2986, 2011.

[528] A. Hati, C.W. Nelson, C. Barnes, D. Lirette, J.A. Desalvo, T. Fortier, F. Quinlan, A. Ludlow, T. Rosenband, S.A. Diddams, D.A. Howe, "Ultra-low-noise regenerative frequency divider for high-spectral-purity RF signal generation," Frequency Control Symposium (FCS), 2012 IEEE International , vol., no., pp.1-4, 21-24 May 2012.

IFCS-EFTF2-M2-4

The sampling theorem in Π and Λ digital frequency dividers

Claudio E. Calosso[1] and Enrico Rubiola[2]

[1]Division of Optics, INRIM, Torino, Italy
[2]Department of Time and Frequency, CNRS FEMTO-ST Institute, Besancon, France

Home page http://rubiola.org

Email: c.calosso@inrim.it and rubiola@femto-st.fr

The noise-free frequency divider can be assimilated to an ideal gearbox that divides the input frequency by d, transferring the total jitter δt from the input to the output. Accordingly, the phase-noise spectral density is ruled by $[S_\varphi(f)]_{out} = [S_\varphi(f)]_{in}/d^2$. So, a modulo-10 divider reduces the input phase noise by 20 dB.

In the classical (Π) digital divider (a chain of flip-flops), the output *white* noise is $[S_\varphi(f)]_{out} = [S_\varphi(f)]_{in}/d$. The denominator is d instead of d^2. So, a modulo-10 divider reduces the input noise by 10 dB instead of 20 dB. This unfortunate outcome is due to the sampling theorem applied to phase noise. In fact, the phase noise is sampled at the rising and falling edges of the square wave, which means at a sampling frequency $2\nu_{in}$ at the input, and $2\nu_{out}$ at the output. Owing to the Parseval theorem, the time fluctuation is $\langle(\delta t)^2\rangle = S_{\delta t}(f)\, B$, where B is the noise bandwidth, i.e., the Nyquist frequency. Down-sampling by a factor of d at the output, the spectrum of the time fluctuation scales up by a factor of d.

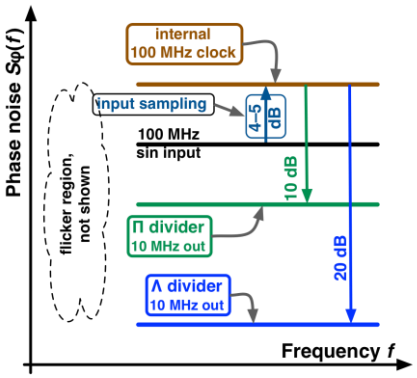

Fig. 173: Phase noise in noise-free modulo-10 Π and Λ dividers.

Our de-aliased (Λ) divider uses shift registers and a resistor network to generate a triangle-like waveform at frequency $\nu_{out} = \nu_{in}/d$, sampled at the full speed $2\nu_{in}$. Having removed the down-sampling phenomenon, the output noise is $[S_\varphi(f)]_{out} = [S_\varphi(f)]_{in}/d^2$, as in the ideal divider. The phase noise is equivalent to that of a noise-free DDS[529]. By contrast, the complexity of a Λ divider is a mere factor of 2–3 higher than that of a Π divider, and suitable to simple/cheap gate arrays.

The schemes are called Π divider (traditional) and Λ divider (de-aliased). The names follow the output waveform, as in the case of the weight function of the Π and Λ counters[530].

In a real divider, the input sampling, inherently, introduces noise. Additionally, the output stage can be a limiting factor because its phase noise adds up after scaling down the input noise. Flicker noise does not behave as described because the electrical power in higher-frequency aliases is low. However, we have good reasons believe that the flicker noise can be lower in Λ divider, as compared to the Π divider. This will discussed only after further experiments.

The article provides theory and experimental verification of the phase-noise aliasing, and demonstrates the virtues of the Λ divider.

---

[529] C. E. Calosso, Y. Gruson, E. Rubiola, "Phase noise in DDS," Proc. 2012 IFCS p. 777–782.

[530] E. Rubiola, "On the measurement of frequency and of its sample variance with high-resolution counters," Rev. Sci. Instrum. 76(5) 054703, May 2005.

IFCS-EFTF2-M2-5

Trim Effect Compensation Using an Artificial Neural Network

John Esterline
Engineering, Greenray Industries, Mechanicsburg, PA
Email: jesterline@greenrayindustries.com

Trim effect is a skewing of the frequency versus temperature performance of a crystal oscillator as the frequency is pulled (trimmed) away from the oscillator's nominal frequency. As TCXO (Temperature Compensated Crystal Oscillator) frequency versus temperature stabilities have improved to ppb (part per billion) levels trim effect has become more of a concern. Even though unwanted, the degradation of performance from trim effect is something generally accepted as a characteristic of TCXOs. This paper focuses on a method of compensating crystal oscillator trim effect. Through the use of an artificial neural network, trim effect compensation of AT cut crystal oscillators can be achieved with better than +/-15ppb stability over the industrial temperature range (-40 to +85 °C). This is more than a 10 fold improvement over the inherent trim effect found using state of the art polynomial function generator compensation, see Figure 1 below. The theory of this compensation method with be discussed, and data showing the results of trim effect compensation on actual oscillators will be presented.

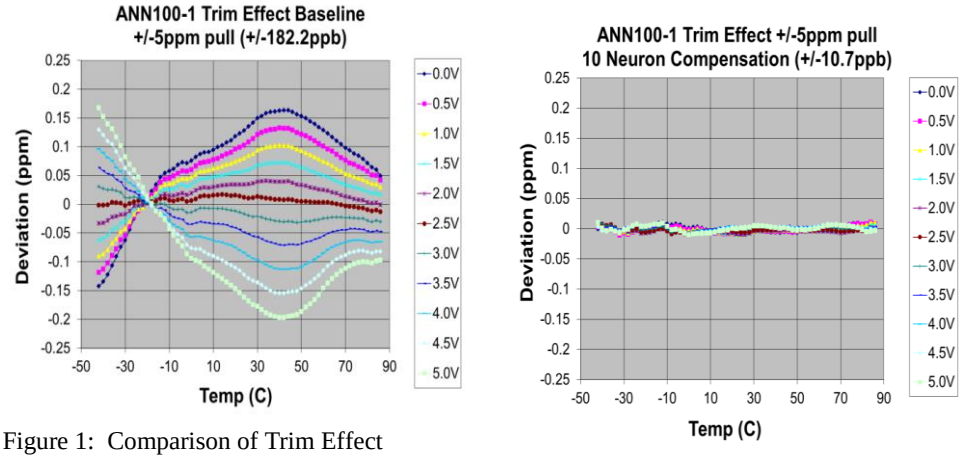

Figure 1: Comparison of Trim Effect uncompensated (left) versus compensated (right).

Novel Sensing Materials and Devices

CLUB D

Thursday, July 25 2013, 02:00 pm - 03:30 pm

Chair: **Fabien Josse**
Marquette University

IFCS-EFTF4-M3-1

Piezoelectric Acceleration Sensors Based on LGX and ReCOB Crystals for Application above 645 DegC

Yanqing Zheng[1], Xiaoniu Tu[1], Jianjun Chen[1], Pan Gao[1], Erwei Shi[1]

[1]Shanghai Institute of Ceramics, Chinese Academy of Sciences, Jiading, Shanghai/P. R. China

Email: zyq@mail.sic.ac.cn

Piezoelectric acceleration sensors that could stand environment temperature above 645ºC (1200ºF) are of great important to the field of vibration monitoring of aviation and aerospace engine. The traditional piezoelectric materials used in this area include lithium niobate crystal, bismuth layer structure system piezoelectric ceramics[531]. But the issue of the lower electric resistivity limits their application of temperature higher than 645 ºC. $GaPO_4$ crystal which is grown by hydrothermal method could be used up to 900 ºC. However, the difficulty in crystal growth of $GaPO_4$ crystal makes it very expensive and limits its application.

ReCOB (Re= La, Y, Sm, Nd, Lu) crystals and LGX crystals including LGT, LGN and LGS are piezoelectric crystals with high melting points above 1400ºC and without phase transition from room temperature to their melting points. All of these crystals can be grown by common Czochralski method up to 4 inches. They are all good candidates for high temperature application.

LGT, LGS, YCOB and SmCOB were grown with efforts to study the factors affecting the electric resistivity of each crystal and increase their electric resistivity under high temperature in our laboratory in recent years. LGS and YCOB with diameter of 4 inches, LGT of 3 inches and SmCOB of 2 inches were successfully grown and the basic physical properties and crystal quality were characterized. The rocking curve of high-resolution X-ray diffraction (HRXRD) of these crystals shown that they were of high quality. Piezoelectric acceleration sensors used the X-cut rings of 10 mm diameter based on these crystals were fabricated and tested. It was shown that our as-grown LGT crystal could be used up to 645 ºC with very steady sensitivity. YCOB and SmCOB crystals could be used to higher temperature up to 900 ºC after overcoming the issue of pyroelectric effect.

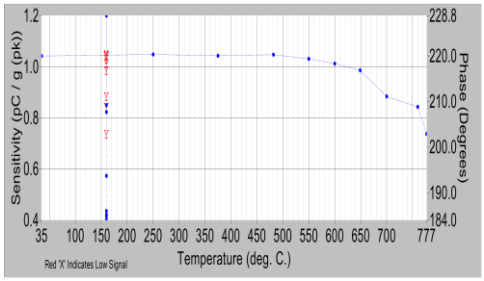

Fig. 174: The sensitivity vs temperature curve of the piezoelectric acceleration sensors based on LGT crystal grown in SICCAS .

[531] S.J. Zhang, X. N. Jiang, M. Lapsley, et al, "Piezoelectric acelerometers for utrahigh temperature aplication", Appl. Phys. Lett., vol. 96(1), p.013506, 2010.

IFCS-EFTF4-M3-2

Thin quartz layer transferred on silicon for SAW applications

S. Grousset[1], E. Augendre[1], T. Signamarcheix[1], T. Baron[2], E. Courjon[2], S. Ballandras[2]

[1]CEA, LETI, MINATEC Campus, 17 rue des Martyrs, 38054 GRENOBLE Cedex 9, France.
[2]FEMTO-ST, UMR 6174 CNRS-UFC-ENSMM-UTBM, Besançon, France.

Email: sebastien.grousset@cea.fr

Motivation

The transfer of piezoelectric material is of a great interest for the direct integration of Surface Acoustic Wave (SAW) devices on silicon wafers. This approach offers a lot of opportunities for the development of smart devices dedicated to sensing or integrated frequency sources. However, the bonding/thinning process must allow preserving SAW properties, comparable with devices built on single-crystal wafers.

Achievement

We present improved results on the development of single-crystal quartz layer transferred onto silicon through direct wafer bonding and thinning process. One-port SAW resonators have been built using a stepper-based industrial process. To overcome the Temperature Coefficient of Expansion (TCE) difference of dissimilar materials like quartz (13.2 ppm/°C) and silicon (2.3 ppm/°C), a low temperature direct wafer bonding process has been implemented. This process is performed at atmospheric pressure with low temperature annealing (<200°C). InfraRed (IR) imaging shows excellent bonding quality with no defects.

Results

Thin AT-cut quartz layers of about 100 µm were obtained after grinding and polishing process. While the thinning process of quartz is likely to be known for increasing crystal disorder and to induce some defects in the transferred layer[532], our quartz thin films are achieved without any damaged layer and with a crystal quality equivalent to bulk material. Aluminum electrodes were deposited on quartz to achieve SAW resonators. Figure 1 shows the resonators obtained on the hybrid quartz/silicon wafer. Inter Digital Transducers (IDT) were designed to generate Rayleigh waves at 430 MHz. The electrical response of a single-port SAW resonator is shown in figure 2 where the fundamental resonance exhibits a Q-factor of about 12500.

The developed process was applied to different quartz crystal orientations to satisfy a large variety of applications.

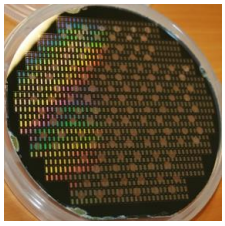

Fig. 1: SAW resonators on a 100mm hybrid wafer.

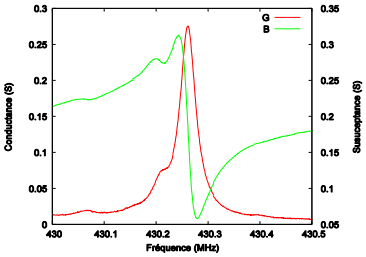

Fig. 2: Admittance of a SAW resonator.

[532] B. Imbert et al., "Thin film quartz layer reported on silicon," in *2011 Joint Conference of the IEEE International Frequency Control and the European Frequency and Time Forum (FCS) Proceedings*, 2011, pp. 1–4.

IFCS-EFTF4-M3-3

Acoustic properties of carbon nanotubes as high acoustic impedance electrode in BAW resonators

E. Iborra, L. García-Gancedo, S. Esconjáuregui, J. Sangrador, M. Clement, M. de Miguel-Ramos, J. Olivares, J. Capilla, A. J. Flewitt, W. I. Milne
GMME-CEMDATIC, ETSIT, Universidad Politécnica de Madrid, Spain
Electrical Engineering Division, Department of Engineering, University of Cambridge, UK

E-mail: eiborra@etsit.upm.es

Bulk acoustic wave (BAW) resonators can be used as gravimetric sensors by tracking the shift in the resonant frequency that takes place when the mass of the devices changes due to the adsorption of biological or chemical agents. To promote the adsorption of a specific agent the uppermost layer of the device has to be adequately functionalized. In addition, to increase the quality factor of the resonator, it is advisable to use a top electrode with an acoustic impedance as high as possible, which provides a larger confinement of the mechanical energy into the piezoelectric. At the same time, the weight of the top electrode should be kept as low as possible to avoid lowering the electromechanical coupling factor. Therefore, the ideal top electrode would be a highly conducting material, exhibiting low mass density and high acoustic velocity, which would double as an electrode and as a sensing layer. Because of their morphology, carbon nanotubes (CNT) have densities below 1 g/cm^3. They also exhibit low resistivity and very high elastic constants, which lead to a high propagation velocity. These features, together with the possibility of being functionalized and their exceptionally high surface to volume ratio, make CNT layers very good candidates as top electrode in gravimetric sensors based on BAW resonators. For designing purposes, a deep knowledge of the material properties is required. In this communication we present a study of the acoustic properties (sound velocity and acoustic impedance) of CNT layers by means of the characterization of BAW resonators using a CNT layer as top electrode.

BAW resonators consisting of a Mo/AlN/CNT piezoelectric sandwich were built on acoustic mirrors composed of Mo and SiO_2 alternating layers deposited on a silicon substrate. The CNT film used as top electrode was grown on a Ti layer by the pyrolithic decomposition of C_2H_2 diluted in NH_3 using Fe nanoparticles as catalytic agent. The frequency response of the resonators was assessed as a function of the thickness of the CNT electrodes, which varied from 0.5 µm to 10 µm. Apart from the resonant frequency corresponding to the longitudinal mode in the AlN, a λ/2-resonance is also excited into the CNT layer, whose frequency is related to the thickness and the sound velocity of the film. To derive the density, the sound velocity and the acoustic losses of the CNT layers, the frequency response of the resonators was fitted using the Mason's model; as inputs we used the values of the densities, the acoustic velocities and the losses of all the layers involved in the device (Mo, SiO_2, Ti and AlN) that had been accurately determined in previous works, as well as their thicknesses assessed by profilometry. We have obtained values of the mass density varying from 0.1 g/cm^3 to 0.5 g/cm^3 and sound velocities around 18000 m/s, which lead to acoustic impedances ranging from $1.8 \cdot 10^6$ $kg \cdot m^{-2} \cdot s^{-1}$ to $9 \cdot 10^6$ $kg \cdot m^{-2} \cdot s^{-1}$. When grown under specific conditions, CNT layers possess higher acoustic impedance and lower density than the metals commonly used as electrodes in BAW devices (Mo, Au, Cr, Ti, Zr, Ag, Pt, Al), which makes them suitable as low mass electrodes with high acoustic impedance and low series resistance. Raman spectroscopy, XPS, AFM and SEM characterization has been performed to determine the structure of the CNT layer.

Properties of Piezoelectric Single Crystals $Ca_3TaGa_3Si_2O_{14}$ at High-Temperature and High-Vacuum Conditions

Hongfei Zu[1], Huiyan Wu[1], Yinzhong Wang[1], Qing-Ming Wang[1]
Shujun Zhang[2], T.R. Shrout[2]
[1] Department of Mechanical Engineering & Materials Science, University of Pittsburgh, Pittsburgh, PA, USA, Email: qiw4@pitt.edu
[2]Materials Research Institute, The Pennsylvania State University, University Park, PA

High temperature sensors which could be applied safely and stably under harsh environments are of major importance to the aerospace and energy industries[1]. Recently, a kind of fully ordered langasite family crystals $Ca_3TaGa_3Si_2O_{14}$ (CTGS) have attracted considerable attention for high-temperature applications[2]. In this paper, Piezoelectric single crystals Ca_3TaGa_3- Si_2O_{14} (CTGS) were grown by the Czochralski pulling method along <100> direction and cut into lateral mode. The dielectric, elastic and piezoelectric properties of them were investigated as functions of temperature (up to 1073.15K) and pressure (up to E-7 torr). It was found that all the crystals exhibited pressure stability properties (up to E-7 torr) and temperature dependent characteristics (up to 1073.15K). Fig. 1 presents the resonant frequency as a function of temperature at different pressures, exhibiting linear temperature/frequency characteristics over a wide temperature range. According to our calculation, the dielectric permittivity $\varepsilon_{11}^T/\varepsilon_0$, elastic coefficient s_{11}^E and piezoelectric coefficient d_{11} were 17.66 (±3.75%), 8.83~9.29 (pm^2/N) and 3.77 (±2.11%) (pC/N), respectively. Fig. 2 gives the elastic constant (s_{11}^E, s_{22}^E) as a function of temperature at different pressures. The good properties make CTGS promising candidates for sensing applications at high-temperature and high-vacuum conditions.

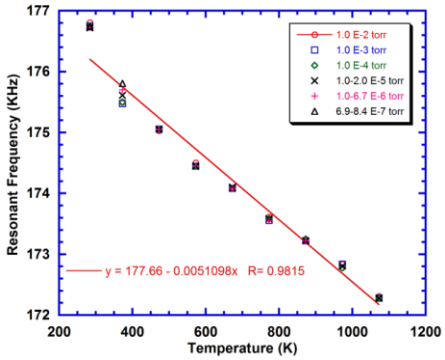

Fig. 175: Resonant frequency as a function of temperature for CTGS lateral mode crystal at different pressures.

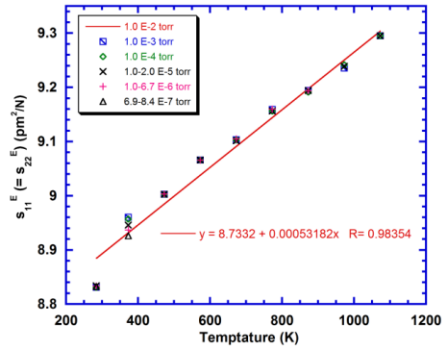

Fig. 2: Elastic constant variation as a function of temperature for CTGS lateral mode crystal at different pressures.

[1] Fapeng Yu, Shujun Zhang, Xian Zhao, Duorong Yuan, Lifeng Qin, Qing-ming Wang and Thomas R. Shrout, "Investigation of $Ca_3TaGa_3Si_2O_{14}$ piezoelectric crystals for high temperature sensors," Journal of applied physics 109, 114103, 2011.

[2] S. J. Zhang, Y. Q. Zheng, H. K. Kong. J. Xin, E. Frantz, and T. R. Shrout, "Characterization of high temperature piezoelectric crystals with an ordered langaste structure," J. Appl. Phys. 105, 114107, 2009.

IFCS-EFTF4-M3-5

High Overtone Bulk Acoustic resonators for high temperature sensing applications

[1]*Emilie Courjon,* [2]*Marc Loschonsky,* [1]*Bruno François,* [1]*Gilles Martin,* [1]*William Daniau,* [2]*Jean-Michel Friedt,* [2]*Brahim Belgacem,* [1]*Thomas Baron,* [3]*Leonhard Reindl,* [4]*Sylvain Ballandras*
FEMTO-ST, UMR 6174 CNRS-UFC-ENSMM-UTBM, Besançon France
SENSeOR, SAS TEMIS Innovation, Besançon – Mougins, France
IMTEK, Freiburg, Germany
frec|n|sys, Besançon France

The development of elastic wave sensors capable to be remotely interrogated without on-board energy has yield new markets rise. The corresponding users challenge these sensor for several extreme applications such as operation at temperature above 500°C. Although the use of Langasite was the most promising approach, Aluminum Nitride (AlN) based structures were also considered as a potential solution. It was demonstrated that high overtone bulk acoustic resonators (HBARs) can be applied for wireless sensing as an alternative to SAW resonators. As AlN is well-suited for such devices and exhibit a melting point in excess of 2000°C, the idea to exploit AlN-based HBAR for high temperature operation was considered in the present work.

AlN-based HBARs have been manufactured in a Sigma-Trikon sputtering machine, depositing 1µm thick layers onto a (111) Ti/Pt backside electrode deposited atop 530µm thick Sapphire and 400µm thick Silicon substrates. The classical figure of HBAR response was observed, with a frequency separation of about 8 to 9 MHz depending on the substrate and a maximum resonance of the layer alone near 2 GHz. The resonances between 400 and 500 MHz (close to the 434 MHz centered ISM band, Fig.1) have been focused for assessing the operation of the devices at temperature larger than 500°C.

These devices have been submitted to temperature cycles up to 600°C for 48 hours in an oven developed at IMTEK for calibrating acoustic devices, and their electrical response were monitored at various frequencies during the experiment. The observation of the device showed minimal deweting effects in form of single droplets atop the surface. The material lattice was found stable enough to withstand the temperature induced tensions as the thermal grooving and the resulting forming of droplets leaving micro cavities in the metallization layer is limited. The experiments then were extended successfully up to 800°C. The use of these HBAR for wireless applications will be tested in the near future.

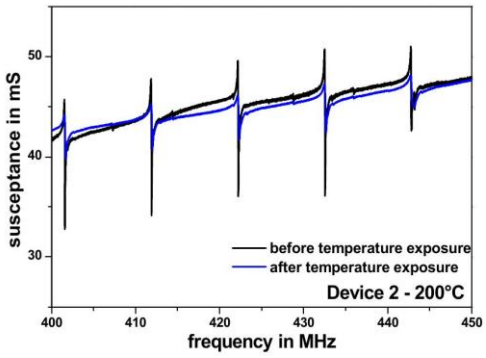

Fig. 2: Electrical response of a AlN/Sapphire HBAR before and after exposition to 600°C for 48 hours

IFCS-EFTF4-M3-6

Langatate Temperature-Compensated BAW Orientations Identified Using High-Temperature Constants

Peter Davulis, Mauricio Pereira da Cunha

Electrical and Computer Engineering Dept. University of Maine, Orono, ME, USA

Email: mdacunha@maine.edu

There is a growing demand for high-temperature (>200°C) sensors and frequency control devices. Langatate (LGT) crystal is a prime candidate substrate for surface acoustic wave (SAW) and bulk acoustic wave (BAW) devices to address high-temperature sensing applications due to demonstrated long-term harsh-environment operation and recently published acoustic wave constants up to 900°C. While prior work by the authors on LGT has focused on high-temperature SAW performance, LGT BAW devices capable of operating in harsh-environments enable additional applications such as deposition rate monitoring, gas, chemical, and physical sensors, and high-temperature timing devices.

In this work, LGT BAW orientations are investigated up to 900°C for temperature-compensated orientations targeting harsh-environment applications. The study utilizes recently published LGT elastic, piezoelectric, and dielectric constants extracted by the authors using resonant ultrasound spectroscopy (RUS) up to 900°C based on the resonances of bulk crystal samples. The constants were independently verified with high-temperature SAW measurements. Temperature-compensated LGT BAW orientations are investigated and discussed based on the analysis of the temperature coefficient of frequency (TCF), the turnover temperature (TCF=0) and the piezoelectric coupling for both thickness-field and lateral-field excitation of the three bulk wave modes.

A range of LGT BAW orientations are identified with turnover temperatures up to 550°C, which enable their use in high-temperature harsh-environment applications. Temperature-compensated orientations are uncovered for both the slow-shear (c) and fast-shear (b) modes and for both thickness-field and/or lateral-field coupling at high temperatures. The c-mode turnover temperatures are plotted in Fig. 1 against the angles φ and θ for the orientation Euler angles (φ, θ, 90°), BAW cut (YXwl) φ, θ. The identified temperature-compensated orientations are compared in the paper with plots of the piezoelectric coupling to determine select orientation regions with TCF=0 at 550°C and coupling up to 0.1 for thickness excitation or up to 0.14 for lateral excitation. Additionally, b-mode orientations were identified with turnover temperature up to 150°C. The data provided in the paper allows the selection of temperature-compensated LGT BAW orientations up to 550°C, considering different thickness and lateral field excitations values for a given sensor or frequency control application.

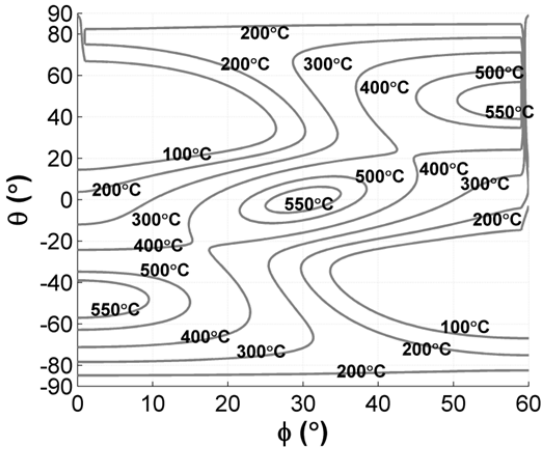

Fig. 176: Contour plot of LGT BAW c-mode turnover temperatures for Euler angles (φ, θ, 90°).

[i] A. Hati, C.W. Nelson, and D.A. Howe, "Vibration-induced PM Noise in Oscillators and its Suppression," *Aerial Vehicles*, Ch. 13, pp. 259-286, Jan. 2009.
[ii] Z. Wang, *et al.*, "Phase transitions of adsorbed atoms on the surface of a carbon nanotube", *Science*, vol. 327, pp. 552-555, Jan. 2010.
[iii] J. Lee, P. X.-L. Feng, "High frequency graphene nanomechanical resonators and transducers", *Proc. IEEE Inter. Freq. Contr. Symp. (IFCS2012)*, DOI: 10.1109/FCS.2012.6243742.
[iv] Q. H. Wang, *et al.*, *Nature Nanotechnology* **7**, 699-712 (2012).
[v] R. A. Barton, *et al.*, *J. Vac. Sci. Technol. B* **29**, 050801 (2011).
[vi] J. Lee, P. X.-L. Feng, *Proc. IEEE Inter. Freq. Contr. Symp. (IFCS2012)*, DOI: 10.1109/FCS.2012.6243742.
[vii] Hanne Martinussen et al. ''Wide frequency range measurements of absolute phase and amplitude of vibrations in micro- and nanostructures by optical interferometry'',OPT. EXPRESS, 15, 11370 (2007).
[viii] Ken-ya Hashimoto et al., ''A Laser Probe Based on a Sagnac Interferometer With Fast Mechanical Scan for RF Surface and Bulk Acoustic Wave Devices'', IEEE Ultrason., Ferroelectr., Freq. Control, vol. 58, p. 187-194, 2011.
[ix] Kimmo Kokkonen et al., ''Scanning heterodyne laser interferometer for phase-sensitive absolute amplitude measurements of surface vibrations'', Appl. Phys. Lett., vol. 92, 063502, 2008.
[x] J. P. Barrat and C. Cohen-Tannoudji. 1961, *Journal de Physique et le Radium*, **22**, 329–36

[xi] Itano W M, Lewis L L and Wineland D J,1982, *Phys. Rev. A*, **25**, 1233–5

[xii] Beloy K, Safronova U I and Derevianko A, 2006, *Phys. Rev. Lett.*, **97**, 040801

[xiii] Moreira, P.; Serrano, J.; Alvarez, P.; Darwazeh, I., "Distributing RF signals in an Ethernet network," Frequency Control Symposium (FCS), 2012 IEEE International , vol., no., pp.1,6, 21-24 May 2012
[xiv] A. Hati, C.W. Nelson, and D.A. Howe, "Vibration-induced PM Noise in Oscillators and its Suppression," *Aerial Vehicles*, Ch. 13, pp. 259-286, Jan. 2009.
[1] Yao Huang *et al.*, "Evaluation of the systematic shifts of a single-$^{40}Ca^{+}$-ion frequency standard", Phys. Rev. A 84, 053841 (2011).
[2] Yao Huang *et al.*, "Hertz-level measurement of the $^{40}Ca^{+}$ $4s\ ^2S_{1/2}$-$3d\ ^2D_{5/2}$ clock transition frequency with respect to the SI second through the Global Positioning System", Phys. Rev. A 85, 030503(R) (2012).
[xvi] A. L. J. Olsson, H. C. van der Mei, D. Johannsmann, H. J. Busscher, and P. K. Sharma, Analytical Chemistry **84**, 4504 (2012).
[xvii] C.Y. Chen, *et al.*, *Nature Nanotechnology* **4**, 861-867 (2009).
[xviii] J. Lee, P. X.-L. Feng, *Proc. IEEE Inter. Freq. Contr. Symp. (IFCS2012)*, DOI: 10.1109/FCS.2012.6243742.
[xix] V.Zholnerov, A.Besedina, G.Kazakov. Comparison of achievable performances as regards rubidium gas cell frequency standards with continuous and pulse laser pumping and with coherent population trapping//Proceedings of EFTF-IFCS 2009. P.587, Besançon, France, 2009.
[xx] E. Breschi, G.Kazakov, C. Schori, G. Di Domenico, G. Mileti, A. Litvinov, B. Matisov //Phys.Rev.A 82, 063810, 2010.
[xxi] A. Litvinov, G. Kazakov, B. Matisov, V. Romanenko, A. Romanenko, L. Yatsenko//J. Phys. B: At. Mol. Opt. Phys. 43, 215402-1-9, 2010.
[xxii] E. Breschi, G. Kazakov, R. Lammegger, G. Mileti, B. Matisov, and L. Windholz.//Phys. Rev. A 79, 063837,2009.
[xxiii] Spence D E, Kean P N, Sibbett W, "60-fsec pulse generation from a self mode locked Ti:sapphire laser", Opt. Lett., vol. 16, p. 42-44, 1991.
[xxiv] Wei Z Y, Kobayashi Y, Zhang Z G, et al, "generation of two-color femtosecond pulses by self-synchronization Ti:sapphire and Cr:forsterite lasers", Opt. Lett., vol. 26, p. 1806-1808, 2001.